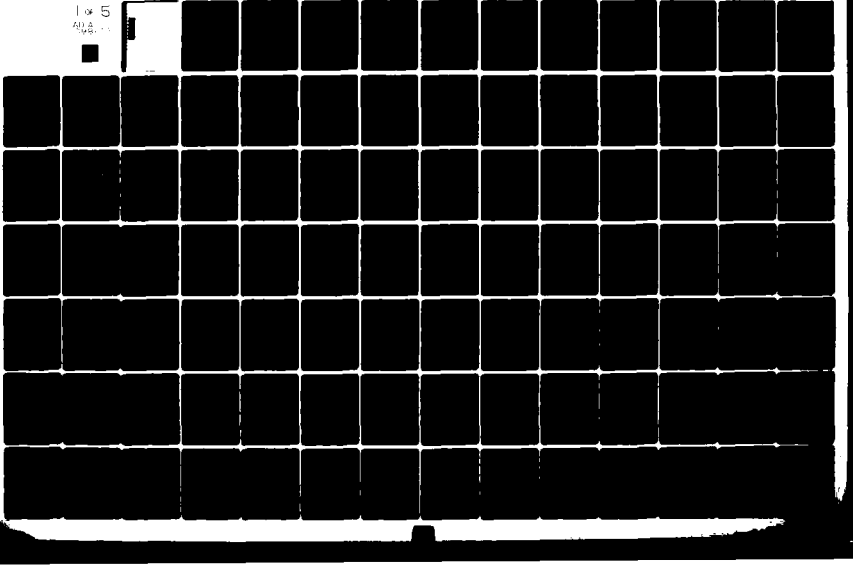
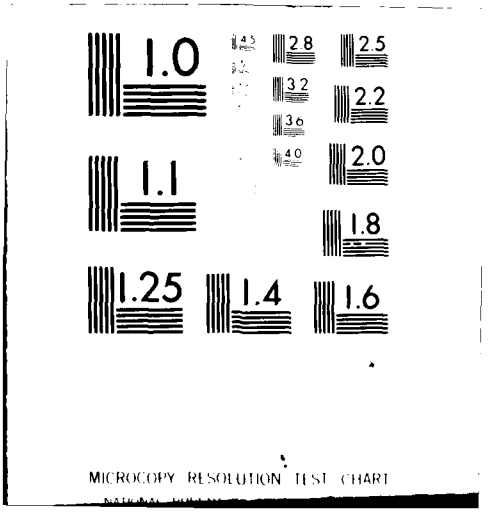
AD-A098 170 LAMONT-DOHERTY GEOLOGICAL OBSERVATORY PALISADES NY F/G 8/3
EDDIES OF THE WESTERN ARCTIC OCEAN - THEIR CHARACTERISTICS AND --ETC(U)
MAR 81 T O MANLEY N00014-76-C-0004
UNCLASSIFIED LDGO-CU-1-81 NL




1.0
2.8
2.5
3.2
2.2
3.6
4.0
2.0
1.1
1.8
1.25
1.4
1.6
MICROCOPY RESOLUTION TEST CHART

AD A098170

(1 D-4...1 thru

(11) L-450-CU-1-81, TR-1

(12)

(6) EDDIES OF THE WESTERN ARCTIC OCEAN - THEIR CHARACTERISTICS AND IMPORTANCE TO THE ENERGY, HEAT, AND SALT BALANCE

by

(12) 442

(10) Thomas Owen Manley

LAMONT-DOHERTY GEOLOGICAL OBSERVATORY
of Columbia University
Palisades, New York

(11) Mar[redacted]81

(1) DOCTORAL DISSERTATION

(2) SUPPORTING MATERIAL

(15) *Prepared for the Office of Naval Research under Contract N00014-76-C-0004*

Reproduction in whole or in part is permitted for any purpose of the United States Government. In citing this manuscript in a bibliography, the reference should be followed by the phrase: UNPUBLISHED MANUSCRIPT.

Approved for public release; distribution unlimited.

404497

ABSTRACT

Eddies of the Western Arctic Ocean - Their Characteristics and Importance to the Energy, Heat, and Salt Balance

Thomas Owen Manley

High speed transient undercurrents were first observed in the Arctic Ocean in 1937 however, it was not until 1974 that these high velocity jets were determined to be the instantaneous observations of small subsurface baroclinic eddies confined between the base of the mixed layer(50 m) and 300 meters. Typical dimensions of these eddies were estimated to be 10-20 km in diameter and roughly 200 meters in thickness.

With the undertaking of the main 1975-76 AIDJEX experiment located in the central Beaufort Sea, four manned camps collected for one year the largest and most complete set of oceanographic data within the Arctic Ocean to this date. During this time, a total of 146 separate crossings of eddies were observed. Using T-S signatures, 31 of the 146 crossings are found to represent duplicate crossings of 12 individual eddies, making a total of 127 separate eddies observed during the one year. On the basis of the AIDJEX data set, arctic eddies have been found to, 1) be prevalent in the Amerasia Basin and in particular the Beaufort Sea, 2) predominantly reside in the depth range of 50 to 300 meters although deeper eddies are also present, 3) contain more than half of the total amount of kinetic energy in the upper 200m of the Beaufort Sea, 4) transfer kinetic energy to the mean flow, 5) be predominately anticyclonic in their rotational tendency, 6) apparently originate north of Point Barrow, Alaska as a result of instability in the eastward flowing Alaskan Coastal Current although there are a few eddies in which T-S data may indicate the possibility of local origin, 7) transfer fresher, less saline water into the deep

Arctic Ocean from the Chukchi Sea, 8) transfer both warm and cold water into the deep Arctic Ocean in response to the seasonally changing shelf conditions, 9) translate in response to barotropic forcing over short time scales, although over longer time periods move with the mean geostrophic field, 10) decay in a clockwise pattern from their point of origin, which is consistent with the upper layer movement of the Beaufort Sea.

TABLE OF CONTENTS

	Page
Acknowledgements	iii
List of Tables	iv
List of Figures	v
Chapter 1 - Introduction	1
A) Research Objectives	1
B) Geographic Setting	4
C) Water Masses of the Arctic Ocean	8
D) General Circulation of the Arctic Ocean	18
E) Ice Cover	24
F) Volume, Heat, and Salt Transport for the Arctic Ocean	28
G) The AIDJEX Experiments	29
Chapter 2 - Eddies of the Oceans	40
A) Eddies of the Arctic Ocean	40
B) Eddies of the Other Oceans	55
C) Criteria for the Selection of Eddies	62
D) Classification of Eddies	67
E) Results and Statistics	70
F) Origin of the Arctic Eddies	84
1) local origin - atmospheric forcing	84
2) local origin - brine convection	95
3) distant origin	97
4) formation by cutoff of coastal current meanders	107
Chapter 3 - Kinetic Energy	111
A) Kinetic Energy of the Eddies and the Mean Flow	111
B) Monthly Kinetic Energy Variations and Eddy Decay	127
C) Transfer of Kinetic Energy by Eddies	135
Chapter 4 - Partition of Energy Within the Arctic Eddies	154
A) Background	154
B) Partition of Energy, a Simplified Theory for Geostrophic Flow	156
C) Kinetic and Available Potential Energy Models	160
1) Kinetic Energy Model	160
2) Available Potential Energy Model	162
D) Discussion	164
Chapter 5 - Estimates of the Importance of Heat, Salt, and Biomass Fluxes by Eddies	167
A) Background	167
B) Decay Within the Deep Ocean	168
1) question of preferential movement	168
2) mean conditions of the Beaufort Sea	170
C) Decay of Kinetic Energy Over Space and Time	174
D) Volume Transport	175
E) Salt Transport	177
F) Heat Transport	179
G) Biological Transport	188

Chapter 6 - Summary and Conclusion 197

Bibliography 203

Appendix 1 - Conversion table from AIDJEX days to calendar days 211

Appendix 2 - Additional Oceanographic AIDJEX Data

Acknowledgements

My sincere appreciation to professor Ken Hunkins. Because of his guidance and understanding, this study was both enjoyable and rewarding. I also wish to thank Ed Bauer and Bill Tiemann for their untiring efforts in the reduction of the AIDJEX STD and PCM data sets. A special thanks to Alan Thorndike for the time and help he gave to further reduce the AIDJEX satellite navigation data for current meter application.

To my wife Pat: there are seldom enough words to express my feelings for all of the sacrifices you have made and the continual support given to me during these years. A better friend I could have never hoped for.

Accession For
NTIS GRA&I
DTIC TAB
Unannounced
Justification
By
Distribution/
Availability Codes
Avail and/or
Dist Special
A

LIST OF TABLES

	Page
1. Annual mean water,salt, and heat budgets for the Arctic Ocean (adapted from Coachman and Greisman,1975).	27
2. Breakdown of number of STD and PCM stations at each of the manned camps along with starting and ending dates.	37
3. Eddies observed prior to 1975.	47
4. Total number of eddies separately classified by PCM and STD data at each of the camps.	67
5. Number of eddies tabulated under the classification system at each camp.	70
6. Monthly breakdown of number of eddies(E), distance traveled (km), and eddies per 100 kilometer(E/100). Parentheses indicate totals.	78
7. Number of eddies per month at each camp.	79
8. Eddy rotation statistics at each camp.	80
9. Maximum observed differences of temperature and salinity in the layer above and below the salinity inflection point. Tables a, b,c, and d represent Caribou, Blue Fox, Snowbird, and Big Bear respectively.	90
10. Integrated monthly averages of the different kinetic energy components(joules/m^2).	124
11. Percentage breakdown of the total observed kinetic energy for the 1972 main camp and all of the 1975-76 manned camps (joules per square meter).	134
12. Example of the removal of the smallest x and y intercamp distances for kinetic energy flux calculations.	145
13. Estimated geostrophic velocities using Newton's map of dynamic topography at the average monthly position of the camp.	148
14. Multiple observations of eddies.	172
15. Numbers of common and uncommon planktonic species observed during the the 150 -> 0 meter net hauls at camp Big Bear.	189

LIST OF FIGURES

Page

1. Beginning and ending positions of the four manned AIDJEX camps. Caribou(C), Blue Fox(F), Snowbird(S), and Big Bear(B). Subscripts of 1 and 2 imply the beginning and ending positions respectively. 3

2. Physiographic provinces of the Arctic Ocean(adapted from Johnson et al,1979). 5

3. Bathymetry of the Arctic Ocean and surrounding seas(adapted from Johnson et al,1979). 6

4. Typical profiles of temperature(T), salinity(S), and density(σ_t) taken a) in the Beaufort Sea during the main AIDJEX Experiment, b) in the eastern Arctic during the FRAM I Experiment. 9

5. Temperature - salinity (T-S) diagram showing the differences between the western Arctic(AIDJEX,Big Bear) and the eastern Arctic(FRAM I). 10

6. Map of the Arctic Ocean showing the operational areas for the 1975-76 AIDJEX and FRAM I experiments. 11

7. Vertical profiles of temperature(T), salinity(S), and density(σ_t) at Snowbird showing steps in the mixed layer on 4-July-75. 13

8. Vertical profiles of temperature(T), salinity(S), and density(σ_t) at Caribou taken on 4-July-75 with the mixed layer absent. 14

9. T-S diagram showing the decay of the Pacific Temperature Maximum from the beginning of the AIDJEX Experiment (June 1975) to the end of the program (April 1976). 15

10. Deep potential temperatures of the Amerasia and Eurasia Basins(Coachman,1968). 17

11. Mean dynamic topography and surface drift vectors for the Arctic Ocean(Coachman and Aagaard,1974). 19

12. Dynamic height anomalies of selected isobaric surfaces along an east-west(top) and north-south(bottom) section of the Beaufort Gyre(Newton,1973). 20

13. Surface dynamic topography in dynamic meters(30/500 db) (Newton,1973). 21

14. Circulation pattern of the Atlantic Water as inferred from percentage retention of temperature and time required for such movement in years(Coachman and Aagaard,1974). 23

15. General ice conditions for the Arctic Ocean and surrounding Seas(Sater,1969). 26

16. Configurations and locations of the AIDJEX pilot studies within the Beaufort Sea(redrawn from Newton,1973). 30

17. Beginning and ending positions of the AIDJEX 1975-76 manned camps superimposed on the mean dynamic topography(Newton, 1973) of the Beaufort Sea. Abbreviations are C(Caribou), F(Blue Fox), S(Snowbird), and B(Big Bear). Subscripts 1 and 2 indicate the beginning and ending positions of the camps respectively. 32

18. Detailed drift tracks of the four manned camps during the main AIDJEX project. Numbers at beginning and ending of drift track are days after December 31, 1974. a) Caribou, b) Blue Fox, c) Snowbird, and d) Big Bear. 33

19. Vertical current profiles of high speed undercurrents as observed from ice island T-3 during the summer of 1965 (Galt,1967). 42

20. Vertical profile of eddy observed at camp Caribou. Speed is the solid line and direction is the dashed line. 43

21. Vertical profile of eddy observed at camp Blue Fox. 44

22. Vertical profile of eddy observed at camp Big Bear. 45

23. Positions of all available historical high speed undercurrents Letters correspond to those indicated in Table 3. Dashed line indicates drift track of NP-1. Outlined sector which is north of Alaska represents the operational area of the 1975-76 AIDJEX Experiment. 46

24. Averaged (2 hr.) absolute currents at 150 m along the drift track of Brass Monkey (AIDJEX 1972). Outermost circle indicates extent of eddy. Inner circle represents current maximum. X's denote hydrographic stations(Newton,1973). 49

25. Vertical section of eddy seen in figure 20 showing isopycnals and isotachs of dynamically computed currents. Arrows indicate hydrographic stations(adapted from Newton,1973). 50

26. Cyclonic eddy observed at the AIDJEX 1972 main camp. Plan view of absolute currents at 125 m along with vertical sections of isohalines are shown. Vertical lines are hydrographic stations(adapted from Hunkins,1974). 51

27. Vertical profiles of a) velocity and b) temperature(T), salinity(S), and density(σ_t) for eddy observed at Snowbird. Solid line in velocity profile is absolute speed and dashed line is true direction. b) Solid and dashed lines denote conditions outside and within the eddy respectively. Note warm core at 175 m and inflection point in salinity at 125 m which corresponds to the depth of velocity maximum. 53

28. Positions of eddies(crosses) and variable currents(dots) observed in the worlds oceans.(Swallow,1976) 56

29. Diagram of ring formation from meander development(1a) to separation from the stream(1d). Solid lines represent the position of the 15 degree C isotherm at 200 m. Dashed lines represent the approximate limit of the Sargasso side of the Gulf Stream(Parker,1971). 59

30. Plot of isohalines versus time in days. STD station numbers are at bottom of the plot. 65

31. Deep event observed at Camp Caribou. 71

32. Deep event observed at Camp Snowbird. 72

33. Deep event observed at Camp Big Bear. 73

34. Number of eddies per month at each camp (labeled solid lines) and cumulative number for CB, BF, and SB in dashed line. 76

35. Number of eddies per 100 km of distance traveled along the drift track (labeled solid lines). Total camp average is dashed line. 77

36. Positions of eddies observed during the main AIDJEX experiment. Sector area is the same as in figure 6. 81

37. Total number of eddies observed as a function of depth. 83

38. Temperature and salinity characteristics of eddies observed by Newton et al(1974) during the 1972 AIDJEX Pilot Study superimposed on the average temperature-salinity envelope for the area of study(redrawn from Newton et al,1974). 88

39. Stick diagram showing the ice velocity and current velocity at four different depth levels from Camp Big Bear. Horizontal axis is time in days. 96

40. Current meter observations for Camp Snowbird at a depth of 130 m along its drift track. 99

41. Vertical cross section of the isohalines along the drift track of Snowbird corresponding to figure 39. 100

42. Vertical cross section of the isotherms along the drift track of Snowbird corresponding to figure 39. 101

43. T-S diagram of the Snowbird eddy seen in figures 41 and 42. The highly anomalous warm core of the eddy is seen between σ_t lines of 26.10 and 26.60. 102

44. T-S diagram of selected eddies observed at the various camps during the main AIDJEX experiment. T_F denotes the freezing point line. 103

45. T-S diagram of selected eddies along with the summer envelope of selected stations near the Alaskan Coastal Current north of Point Barrow. 106

46. Sketch indicating the two currents in the shear zone region north of Alaska. The main gyre current(dashed line) and the Alaskan Coastal Current(solid line). Arrows indicate the direction of movement. 108

47. Minimum monthly kinetic energy field observed during the main AIDJEX experiment. Solid line at left is mean kinetic energy dashed line is kinetic energy due to fluctuations away from the mean, and solid line to right is the total kinetic energy. 115

48. Maximum monthly kinetic energy field observed during the main AIDJEX experiment. 116

49. Caribou kinetic energy profile, 14-month mean. 118

50. Blue Fox kinetic energy profile, 14-month mean. 119

51. Snowbird kinetic energy profile, 14-month mean. 120

52. Big Bear kinetic energy profile, 7-month mean. 121

53. Ensemble mean kinetic energy (49 months). 122

54. AIDJEX 1972 main camp average of mean, fluctuating, and total kinetic energy(Hunkins,1974). 123

55. Individual camp plots showing the amount of vertically integrated barotropic(solid) and baroclinic(dashed) kinetic energy per month, through time. 129

56. Integrated baroclinic kinetic energy from 50 to 190 m plotted on the mean dynamic topography of the Beaufort Sea. 132

57. Mean positions for Camps Caribou(CB), Blue Fox(BF), and Snowbird(SB) during November 1975. 144

58. Eddy kinetic energy flux for June 1975. 148

59. Eddy kinetic energy flux for July 1975. 149

60. Eddy kinetic energy flux for August 1975. 150

61. Eddy kinetic energy flux for September 1975. 151

62. Theoretical partition of energy for geostrophic flows as a function of length(L). R_D is the internal Rossby radius of deformation. 159

63. Trajectories of eddies that were observed more than once during the main AIDJEX experiment. Heavy lines denote dynamic topography of the Beaufort Sea(figure 13). Identification numbers correspond to those in Table 6. 171

64. Temperature differences between individual eddies and local mean conditions as listed in Table 10. ΔT_1 and ΔT_2 define the upper and lower layers respectively. Dashed lines show

the 0.04 degree C limits of the background noise. 180

65. Horizontal balance of forces in a) geostrophic flow and, b) geostrophic flow modified by friction. Veering of the velocity vector for both anticyclonic and cyclonic flow are shown in (c) and (d) respectively. 183

66. Cross-section along the diameter of an a) anticyclonic and, b) cyclonic eddy suggesting the upper layer flow patterns. 184

67. Suggested decay patterns of thermal properties within the eddies for the upper($\Delta S_1, \Delta T_1$) and lower ($\Delta S_2, \Delta T_2$) cores. 186

68. Common species of copepods taken during the summer biological program at Camp Big Bear. Dates of actual observations are given at the bottom of the plot. 190

69. Common species of copepods taken during the summer biological program at Camp Big Bear. Dates of actual observations are given at the bottom of the plot. 191

70. Uncommon species of copepods taken during the summer biological program at Camp Big Bear. Dates of actual observations are given at the bottom of the plot. Horizontal bars indicate time periods during which eddies were observed at Big Bear. 192

71. T-S plot of the warm core eddy corresponding to the 6-17 June Big Bear eddy. 195

1. Introduction

A) Research Objectives

In the past few decades, mesoscale eddies resembling the weather patterns of the atmosphere have been found in all of the world's oceans(McWilliams,1977). Although the ocean eddies are similar in many ways to their atmospheric counterparts such as their shape, aspect ratio, geostrophic nature and high energy content, they also possess many dissimilarities. In general, the ocean eddies, when compared with the atmospheric high and low pressure systems are, 1) smaller, 2) possess one to two orders of magnitude more energy when compared to the surrounding mean, 3) move with a slower translational as well as rotational velocity, 4) have a longer life span, and 5) are more abundant.

Further research into these mesoscale currents have brought about a major reorganization in the concepts relating to the processes by which energy, momentum, heat, salt, biomass and chemical constituents are transferred within the oceans(McWilliams,1977; Richardson,1976; Wiebe,1976). In specific cases, both in the atmosphere and ocean, eddy motions have been shown to transfer momentum and energy to the mean flow which is contrary to the more familiar cascading processes whereby energy is transferred from larger to smaller scale motion finally to be dissipated into heat by viscous and molecular forces.

It was not until 1974 that eddies were documented to exist in the western Arctic Ocean(Hunkins,1974; Newton et al,1974). Because of the inaccessibility of the Arctic Ocean, relatively little information was collected on these features until the 1975-1976 Arctic Ice Dynamics Joint Experiment (AIDJEX) when four drifting manned camps were deployed on the permanent pack ice in the Central Beaufort Sea of the western Arctic(figure 1). This experiment provided the

largest and most detailed oceanographic data set to date in the Beaufort Sea. During this one year experiment, a total of 146 mesoscale eddies were observed at the four manned camps.

The purpose of the study is twofold - first, to provide observational as well as statistical information pertaining to eddies of the Arctic Ocean in order to give insight as to their general characteristics, locations, possible modes of origin, and subsequent decay within the Beaufort Sea. The second aim is to show the importance of the arctic eddies in the horizontal energy balance of the upper 200 m of the water column as well as the role that they take in the transfer of heat, salt and biomass into the Arctic Ocean.

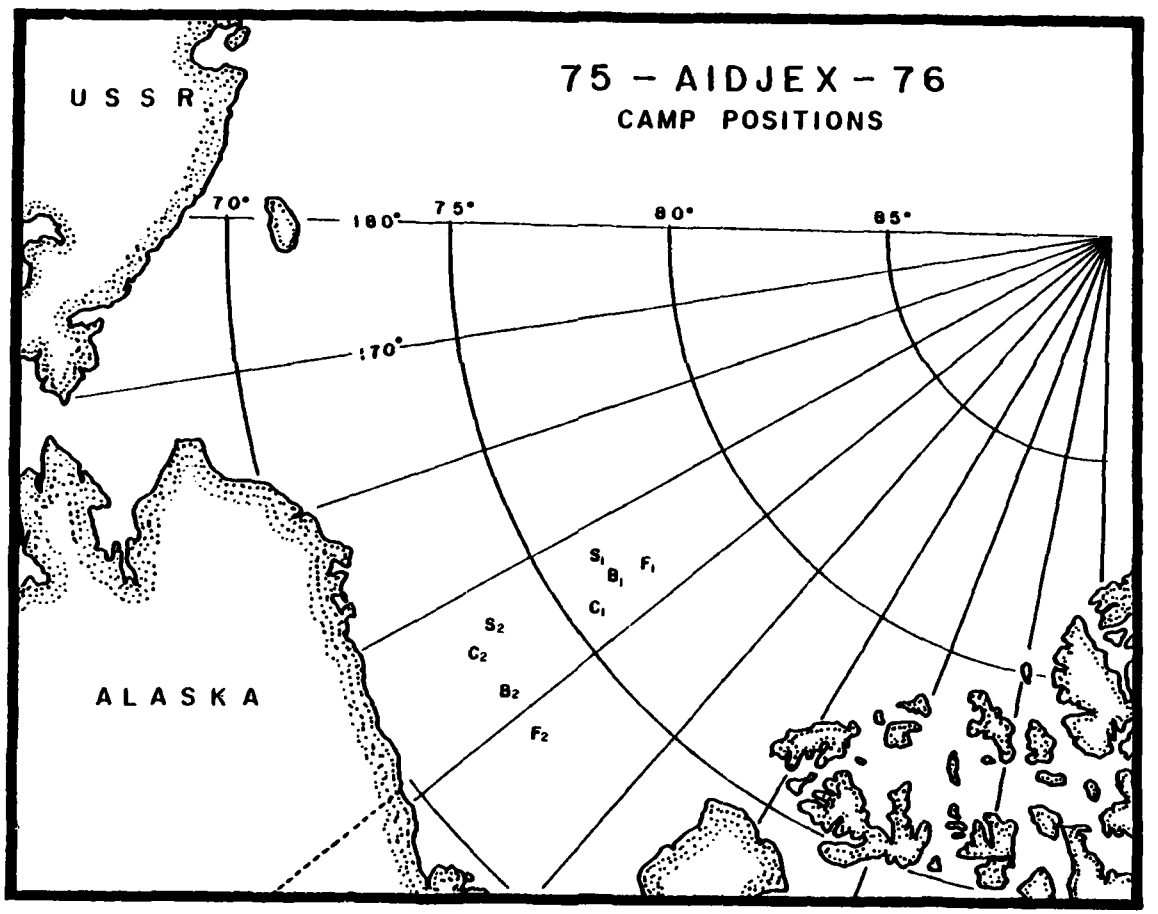


Figure 1. Beginning and ending positions of the four manned AIDJEX camps; Caribou(C), Blue Fox(F), Snowbird(S), and Big Bear(B). Subscripts of 1 and 2 imply the beginning and ending positions respectively.

B) Geographic Setting

The Arctic Ocean is bounded to the south by the land masses of Eurasia, Spitzbergen, Greenland, Canadian Archipelago, and North America. Terminology and bathymetry used in this work are based on the most recent bathymetric map of the Arctic Ocean(Johnson et al,1979). Figure 2 indicates the main physiographic provinces of the Arctic Ocean while the more detailed bottom topography is shown in figure 3.

In the western longitudes, the deep arctic basin is bounded by a continental shelf ranging from 50 to 200 km in width. In the eastern longitudes, however, a very broad continental shelf extends up to a maximum of some 1400 km, with the average width of 800-900 km. This broad shelf is associated with the Chukchi, East Siberian, Laptev, Kara and Barents Marginal Seas. The shelf itself is usually less than 100 meters below sea level with the exception of the Barents Sea which has a depth range of 100 to 500 meters. These marginal seas occupy nearly 36% of the area of the Arctic Ocean ,however they only contain 2% of the total volume of water(Coachman and Aagaard,1974).

Submarine canyons frequently indent the shelf areas and have been suggested as being a conduit through which intermediate or deep water may reach the surface as well as shelf water moving to greater depths (Mountain et al,1976; Garrison and Becker,1976). Two of the largest canyons are the St. Anna and the Vozonin troughs, both of which are in the Kara Sea.

The deep Arctic Ocean(greater than 500 m) is divided by the Lomonosov Ridge into two major basins(Beal et al, 1966), the Amerasia(western Arctic) and Eurasia(eastern Arctic) Basins. Each of these basins is further subdivided into two minor basins. In the Amerasia Basin these are the Canada and Makarov Basins and for the Eurasian Basin , the Amundsen and Nansen Basins. The Amundsen Basin is the deepest of the four with an average depth near 4200m. The next deepest are the Nansen and Canada Basins with average depths of



Figure 2. Physiographic provinces of the Arctic Ocean(adapted from Johnson et al,1979).

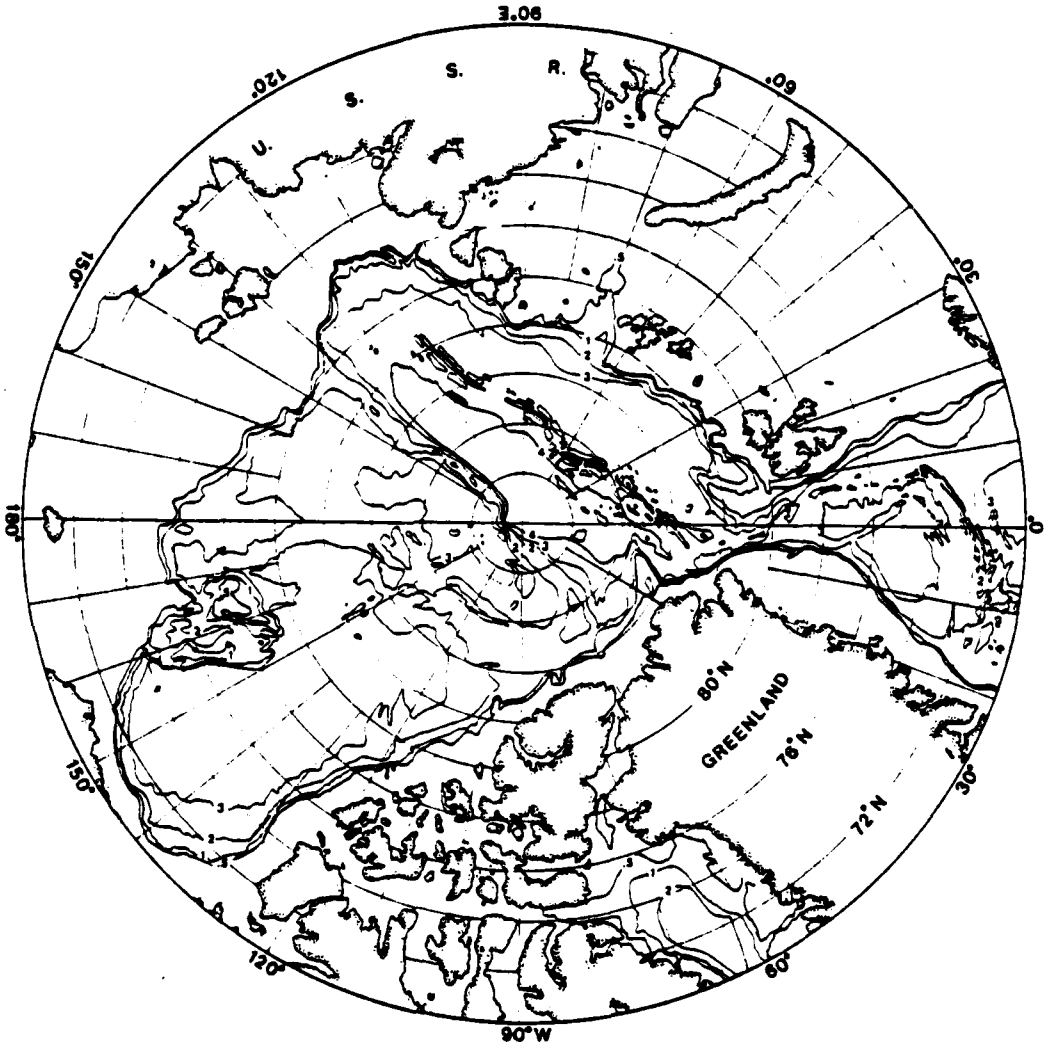


Figure 3. Bathymetry of the Arctic Ocean and surrounding seas(adapted from Johnson et al, 1979).

3500 meters. The shallowest is the Makarov Basin with an average depth of 3000 meters, although it does obtain a maximum depth of 4000 meters near the pole.

These basins are separated by topographic highs - the Arctic Mid- Ocean Ridge, the Lomonosov Ridge, and the Alpha-Mendeleyev Ridge Complex. The Lomonosov Ridge, shallowest of the ridges, plays an important part in the deep circulation of the Arctic Ocean. Although minimum depths of 800 meters are observed, the shallowest unbroken contour along the ridge is 2000 meters(figure 3). Estimated sill depth is between 1500 and 2000 meters.

The other major topographic high is the Chukchi Province which contains the following features: the Chukchi and Northwind Abyssal Plains, the Chukchi Plateau and the Northwind Ridge. Minimum depths of slightly less than 500 meters are recorded; however, in areal extent these features are minor compared to the Chukchi Province as a whole. Generally, depths are in excess of 1000 meters for this area. In the oceanic circulation of the Canada Basin, the Chukchi Province is believed to affect only the movement of the deeper layers.

C) Water Masses of the Arctic Ocean

Following the general classification of Coachman(1963), three distinct water masses are persistent throughout the Arctic Ocean. It is only in the subdivisions of the water masses that differences can be observed between the eastern and western Arctic Ocean. General profiles of temperature,salinity,and σ_t in the western and eastern Arctic are plotted in figure 4. σ_t is defined as $(\rho - 1.000) \times 10^3$. Corresponding T-S diagrams are shown in figure 5. Figure 4a shows data that was taken near the central part of the Beaufort Sea in the western Arctic Ocean during the main 1975-1976 AIDJEX Experiment while figure 4b depicts data that was taken during the 1979 FRAM 1 experiment in the eastern Arctic Ocean(Hunkins et al, 1979). The sectors of the Arctic Ocean occupied by the 1975-1976 AIDJEX and FRAM 1 Experiments are indicated in figure 6.

The major water masses and their subdivisions are listed below :

1) Surface water(Arctic Water) - Extends to a depth of 200 meters and is generally low in salinity with temperatures usually less than -1.0 degree C. Below the mixed layer lies a very steep pycnocline which is primarily determined by salinity. Temperatures at these latitudes are at or close to the freezing point and vary only slightly. As a result, density is controlled mainly by salinity. Subdivisions within this Surface Water are:

a) A mixed layer of relatively low salinity which varies both seasonally and spatially. During the winter months, the mixed layer is well established due to wind and ice stress near the surface but more predominantly due to brine convection during the freezing of open water to form sea ice. Spatial variations in the mixed layer salinity appear to increase monotonically from the coast of Alaska(27 ppt) to Franz-Joseph Land(approximately 33 ppt) neglecting near coastal areas. Temperatures in the mixed layer are at or very close to

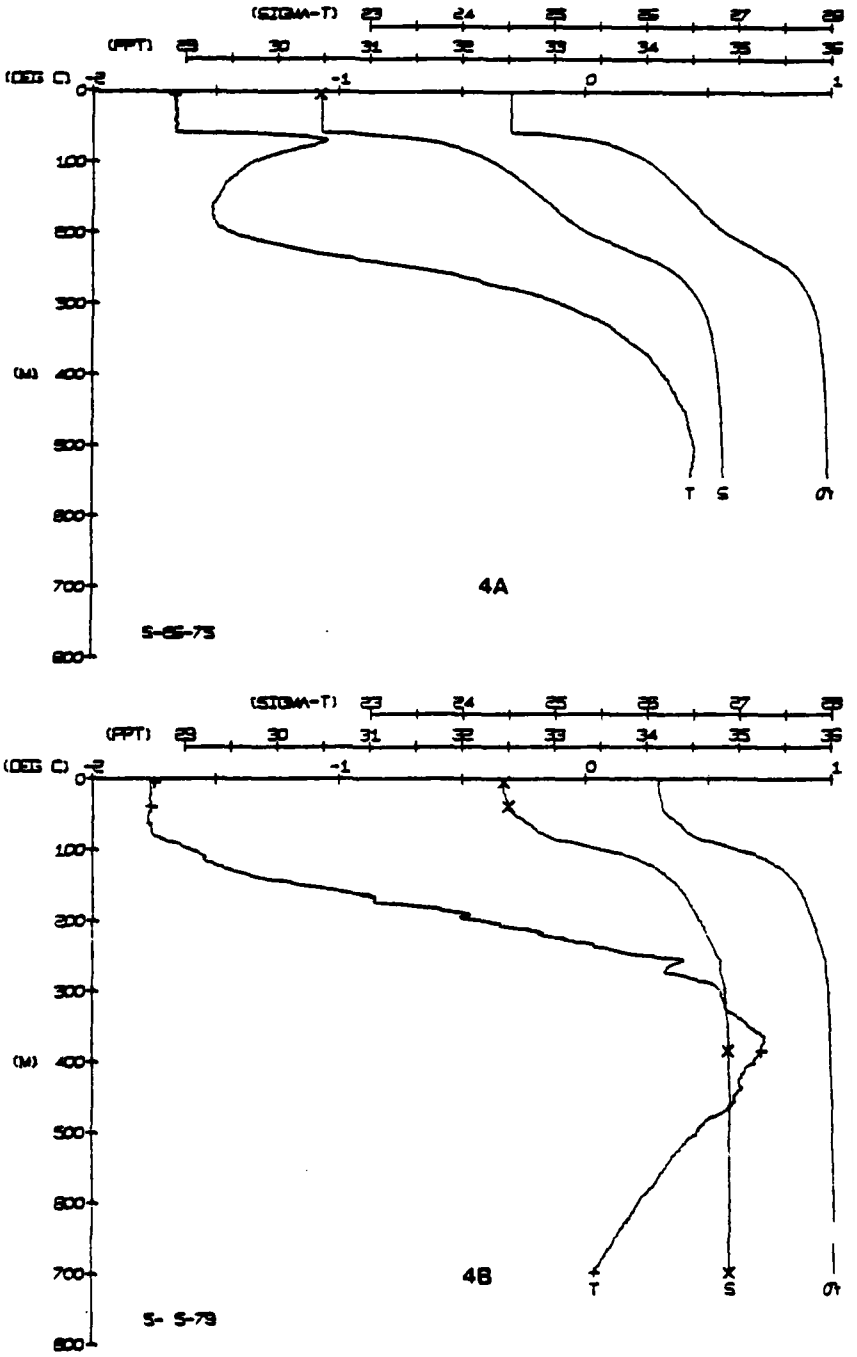


Figure 4. Typical profiles of temperature(T), salinity(S), and density(σ_t) taken a) in the Beaufort Sea during the main AIDJEX Experiment, b) in the eastern Arctic during the FRAM I Experiment.

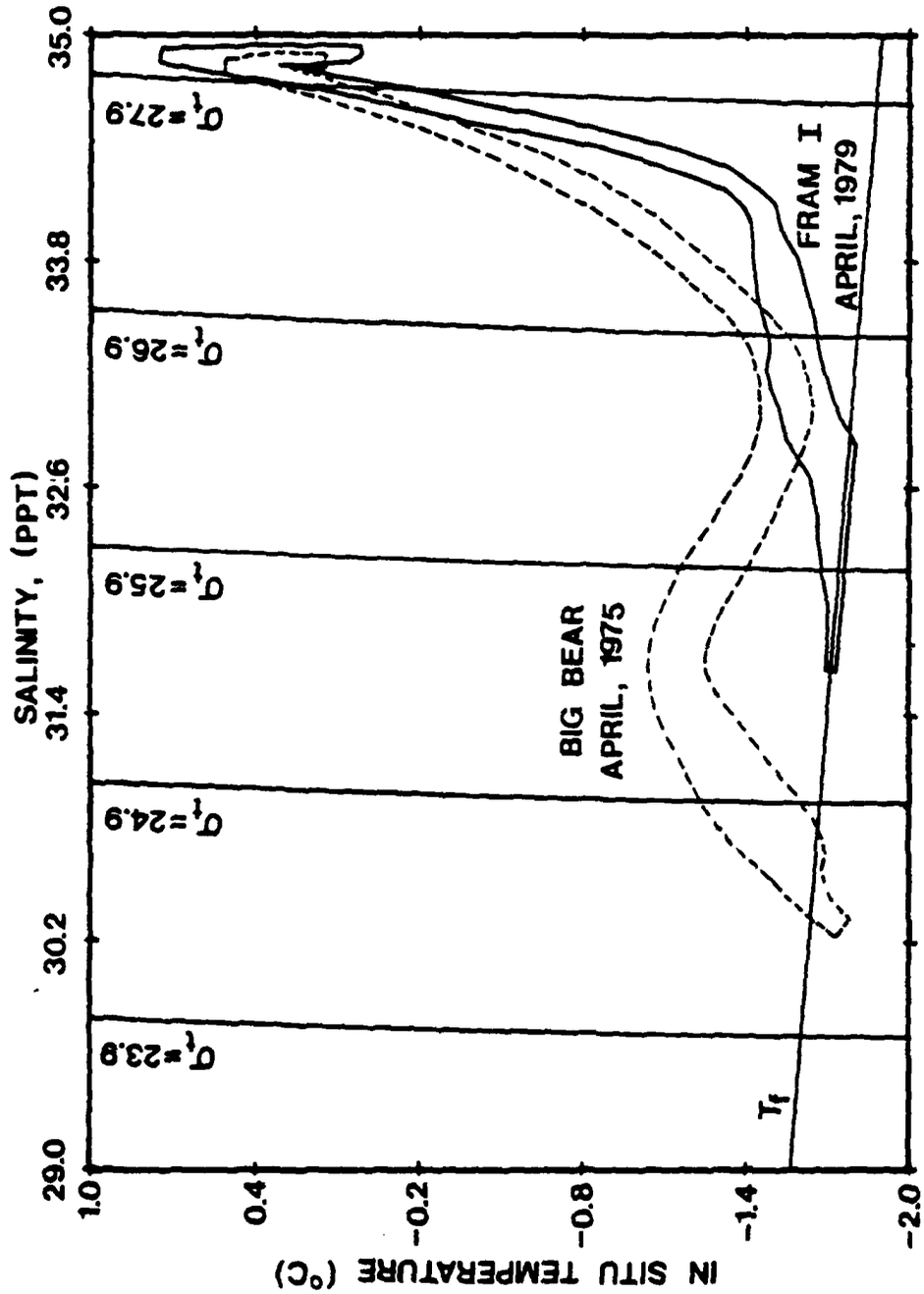


Figure 5. Temperature - salinity (T-S) diagram showing the differences between the western Arctic(AIDJEX,Big Bear) and the eastern Arctic(FRAM I).

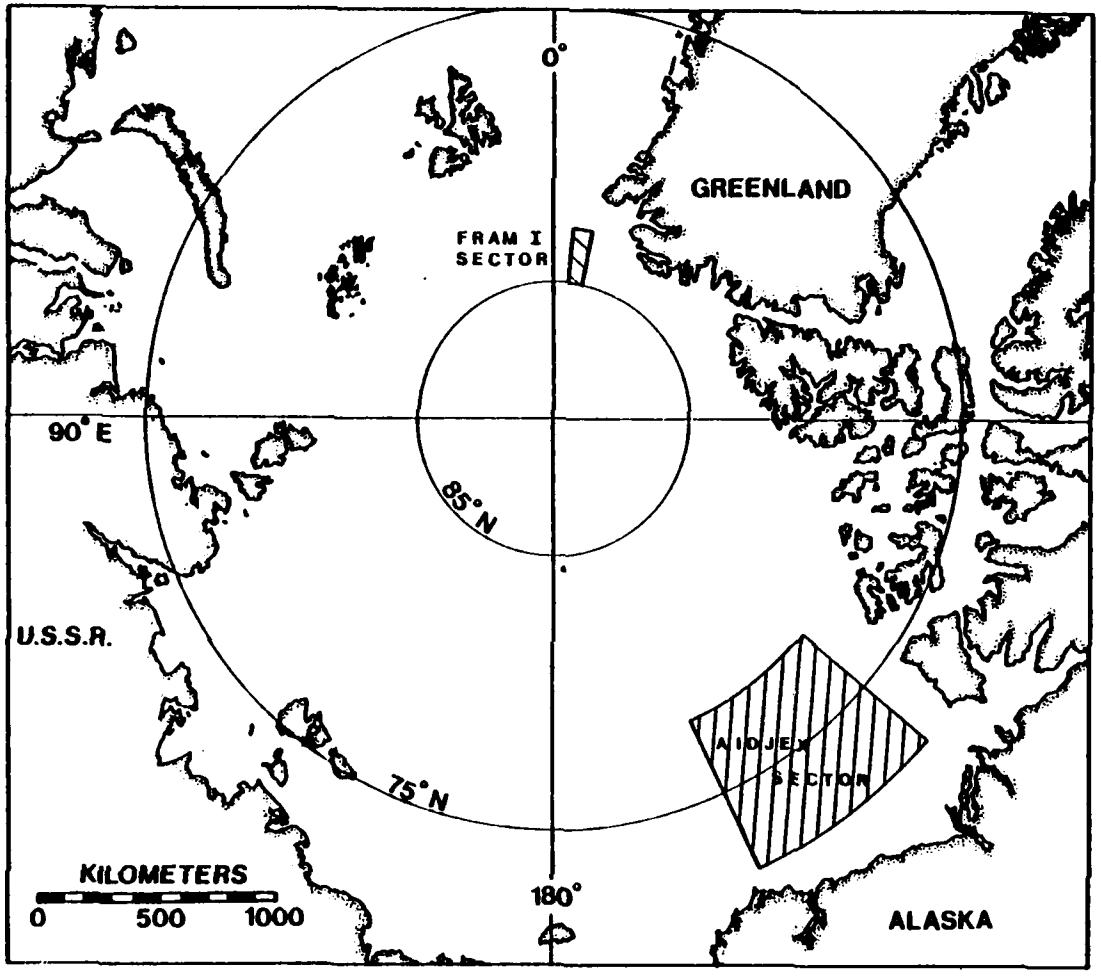


Figure 6. Map of the Arctic Ocean showing the operational areas for the 1975-76 AIDJEX and FRAM I experiments.

the freezing point. During the summer months, fresh water is added to the mixed layer via melting of the upper few feet of the permanent pack ice. Also, the winter mixed layer may be broken up into step like features due to episodic events of fresh water addition and mixing(figure 7) or may not exist at all(figure 8).

b) The Pacific summer water is marked by a shallow temperature maximum confined to a depth range of 50 to 130 m. The maximum temperature varies from 0 to -1.5 degrees C depending on the location in the western Arctic. The water has its origin from the Bering Sea as it enters through the Bering Straits and is further modified in the Chukchi Sea before being advected into the Arctic Ocean(Coachman and Aagaard;1974). This water loses its identifying characteristics as it moves out of the Chukchi Sea into the deep Arctic Ocean due to lateral and vertical diffusion of heat and is therefore not seen in the eastern Arctic Ocean. During AIDJEX a decrease of almost 0.5 degree C was observed in the Pacific T-max layer over the course of the experiment(figure 9).

c) Winter shelf water that has been advected along isopycnal surfaces and in the eastern Arctic occupies a layer from the base of the mixed layer to the upper reaches of the Atlantic water (figure 4b). In the western Arctic, this layer is directly under the Pacific T-max layer and is a local temperature minimum(approximately -1.5 degrees C) centered at approximately 175 meters (figure 4a).

2) The Atlantic layer extends from a depth of 200 to 900 meters. This water enters the Arctic Ocean via the Greenland-Spitzbergen passage. This layer has temperatures greater than 0 degrees C with a maximum temperature between 300 and 500 meters. In the upper section of this layer, salinity rapidly increases up to a depth of 300 meters where the vertical gradient in salinity is substantially reduced. Salinity values are close to 35 ppt at a depth

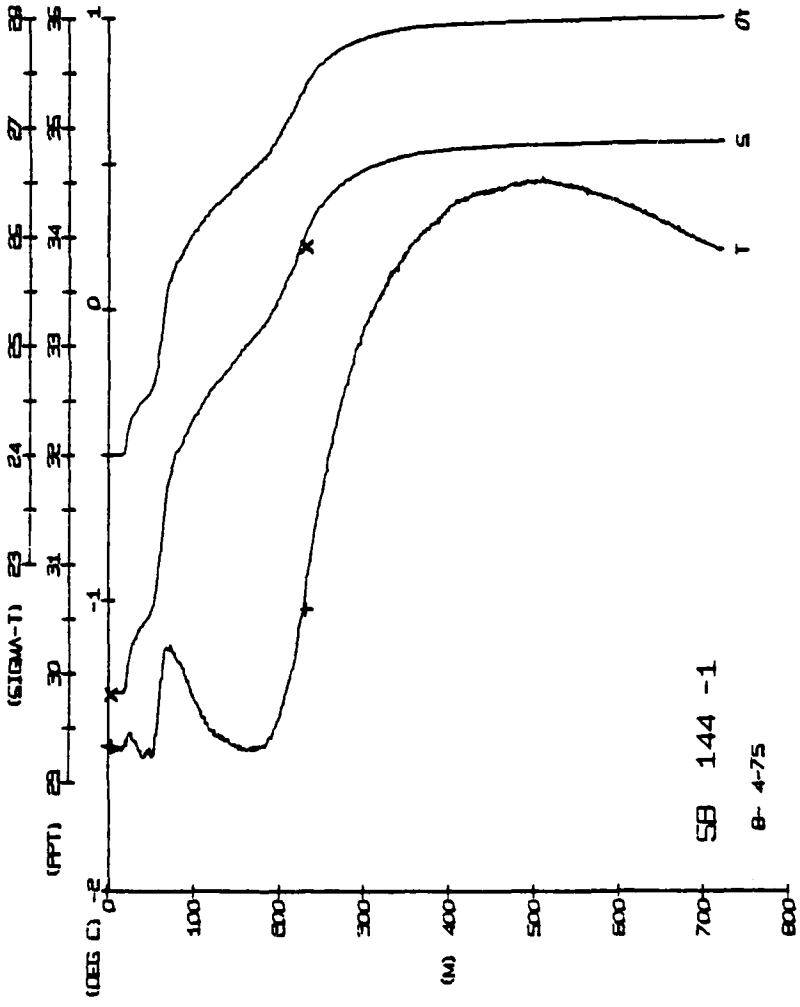


Figure 7. Vertical profiles of temperature(T), salinity(S), and density(σ_t) at Snowbird showing steps in the mixed layer on 4-July-75.

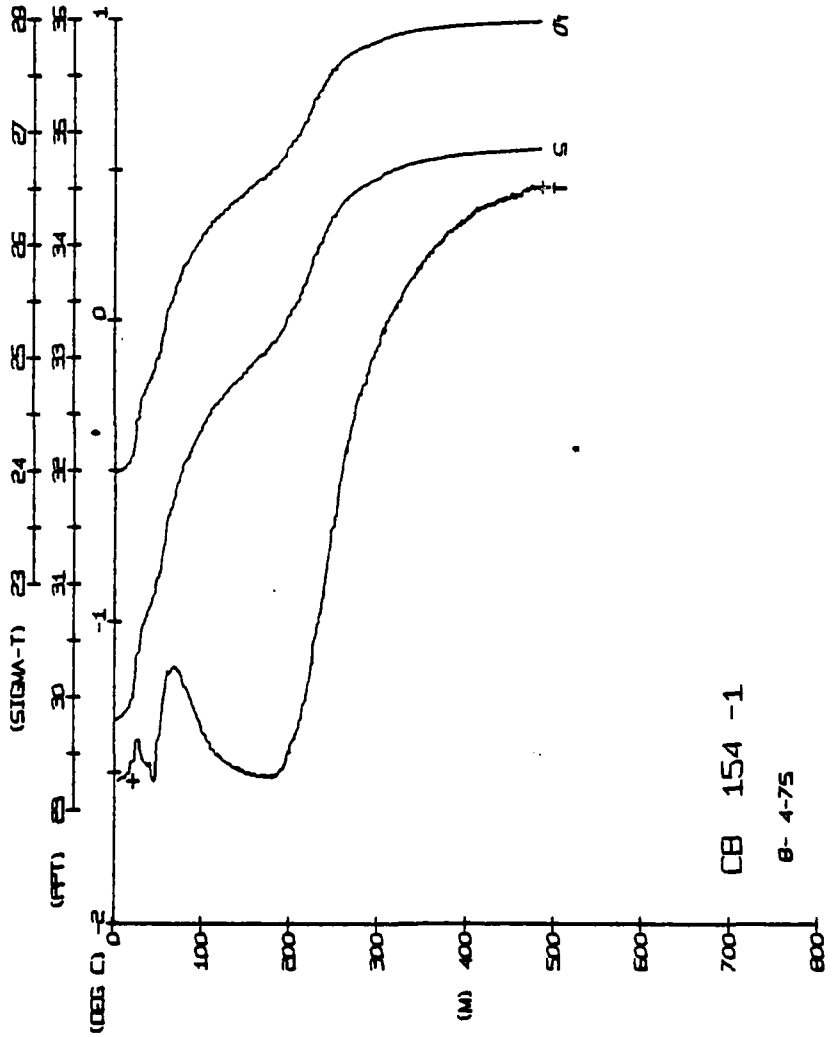


Figure 8. Vertical profiles of temperature(T), salinity(S), and density(σ_t) at Caribou taken on 4-July-75 with the mixed layer absent.

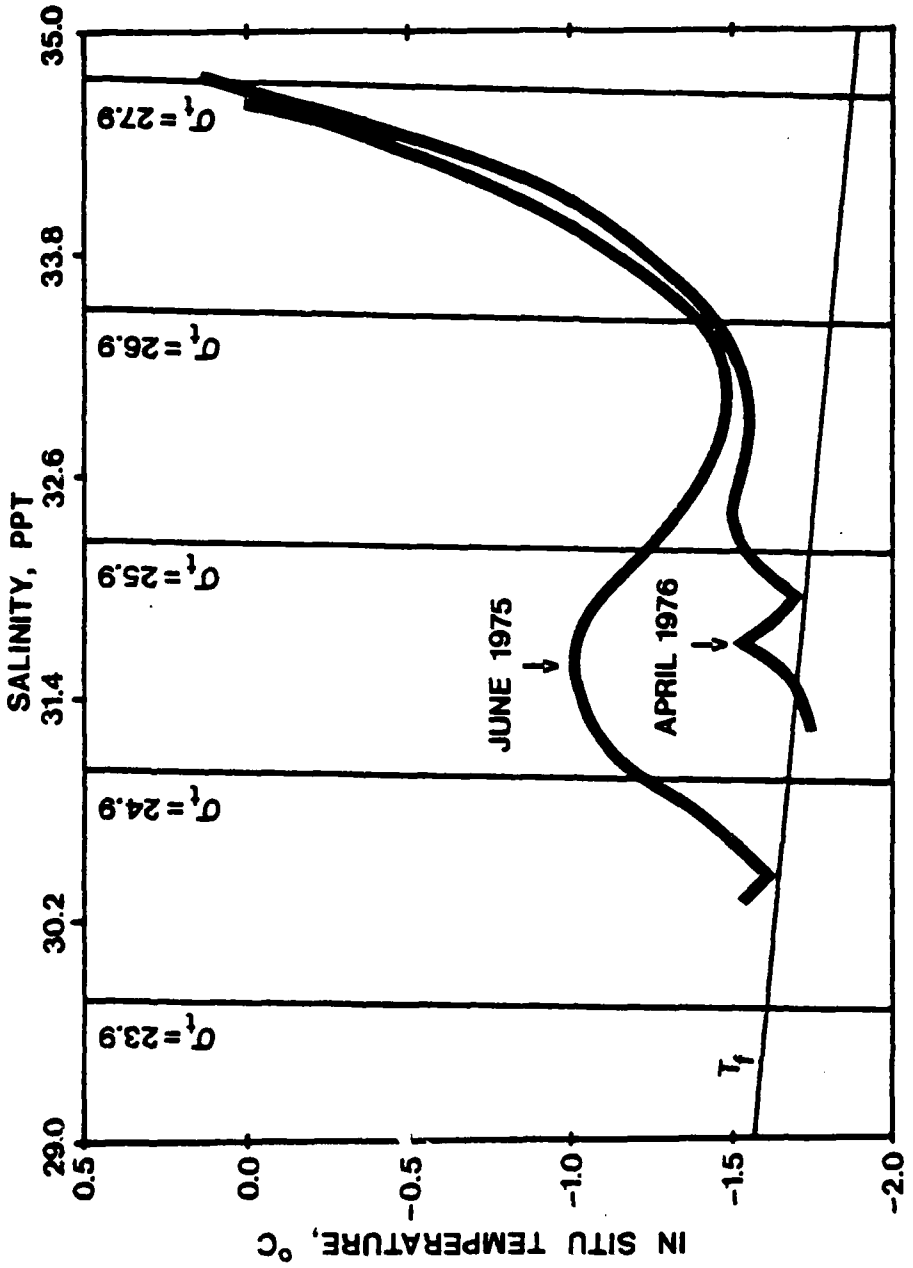


Figure 9. T-S diagram showing the decay of the Pacific Temperature Maximum from the beginning of the AIDJEX Experiment (June 1975) to the end of the program (April 1976).

of 900 meters irrespective of spatial position.

3) Bottom water which occupies the remaining water column is at potential temperatures less than 0 degrees C. The potential temperatures in the Canada and Makarov Basins(-0.5 degree C) are slightly warmer than the -0.9 degrees C. temperatures observed in the Amundsen and Nansen Basins(figure 10). This is due to the shallow sill depth of the Lomonosov Ridge which prevents water deeper than approximately 1550 meters in the Eurasian Basin from entering the Amerasian Basin.

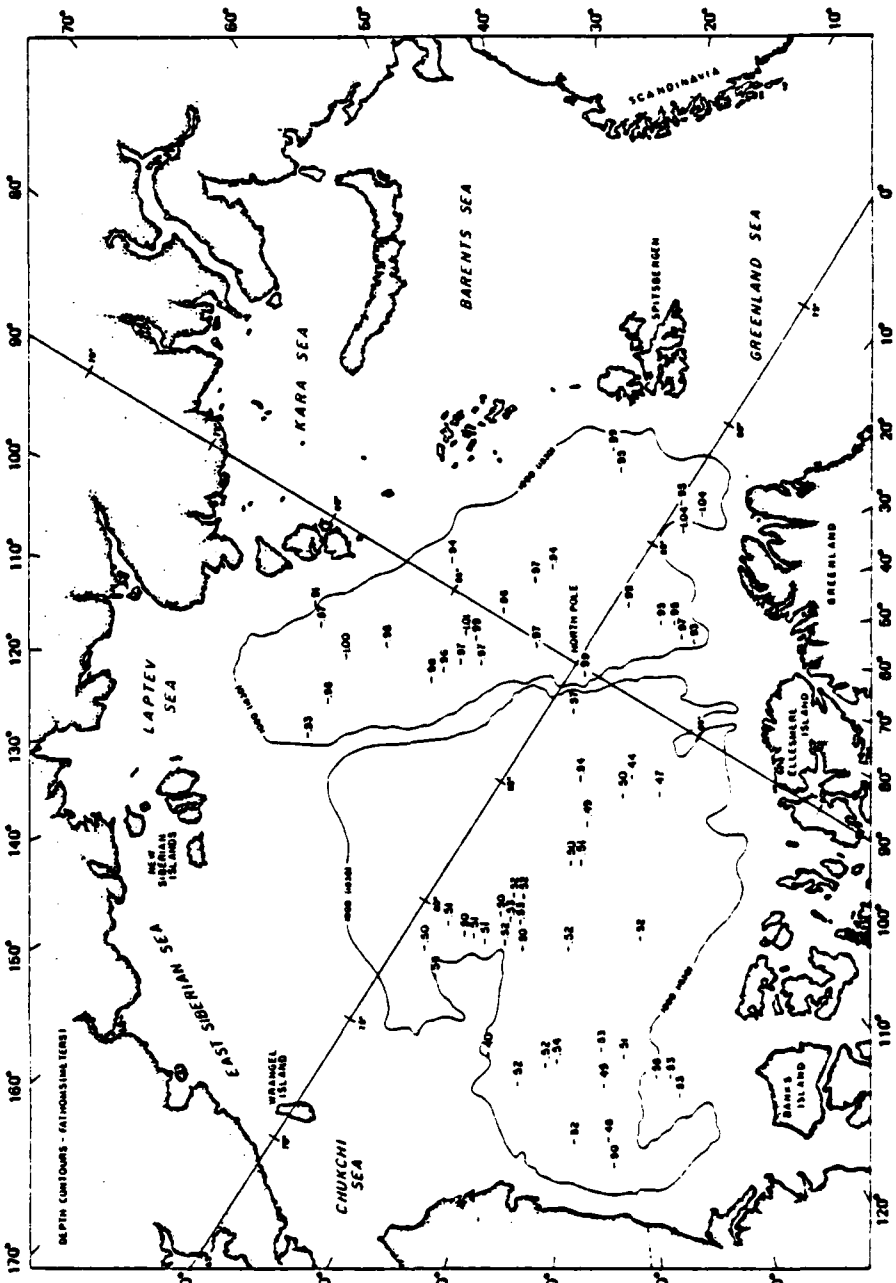


Figure 10. Deep potential temperatures of the Amerasia and Eurasia Basins(Coachman,1968).

D) General Circulation of the Arctic Ocean

The dynamic topography of the surface of the Arctic Ocean, using 1200 db as the reference level, is shown in figure 11. The major transport of surface water in the Arctic Ocean is from the Eurasian shelf to the Greenland-Spitzbergen Passage in the Transpolar Drift. Once past the Greenland Spitzberger Passage, transport out of the Arctic Ocean is along the coast of Greenland forming the East Greenland Current. Approximately 80% of the transport within the Beaufort Sea is located in the upper 300 meters of the water column(Newton,1973) and can be inferred by the elevated dynamic height surfaces relative to those below 500 meters in both the east-west and north-south sections(figure 12). More detailed work has been done on the upper layer dynamic topography of the Beaufort Sea by Newton (1973) who used a shallower zero reference level of 500 db thereby allowing the use of more historical data in the analysis(figure 13).

A large, rather slow moving clockwise gyre, known as the Beaufort Gyre(figure 2), is located in the Canada Basin and is apparently a result of a consistent high pressure system over the Beaufort Sea(Campbell,1965).

The Atlantic Layer circulation(figure 14), within the Arctic Ocean can be considered as a large cyclonic gyre. As the Atlantic Water is brought into the Arctic Ocean via the West Spitzbergen Current, it sinks to a core depth of 300-500 meters and flows parallel to the continental slope of the Barents and Kara Seas. This layer becomes broader after crossing over the Lomonosov Ridge still paralleling the Eurasian continental shelf. The return flow of the Atlantic layer is along the continental slopes of the Canadian Archipelago and Greenland where it leaves the Arctic Ocean as the lower part of the East Greenland Current. An anticyclonic feature in the flow of the Atlantic layer is observed directly north of Alaska and is believed to be a result of the interference of the flow pattern by the Chukchi Province(Coachman and Aagaard,1974) although it

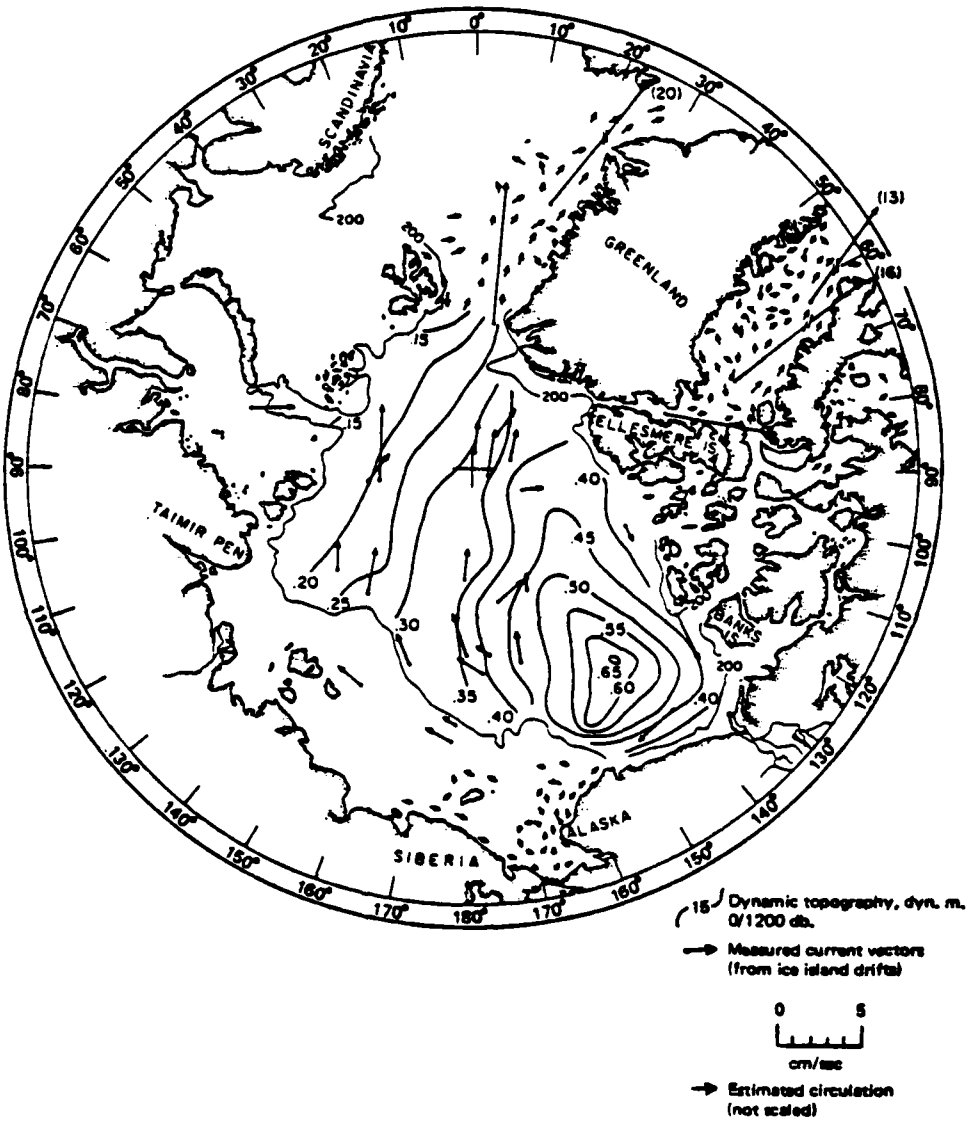


Figure 11. Mean dynamic topography and surface drift vectors for the Arctic Ocean(Coachman and Aagaard,1974).

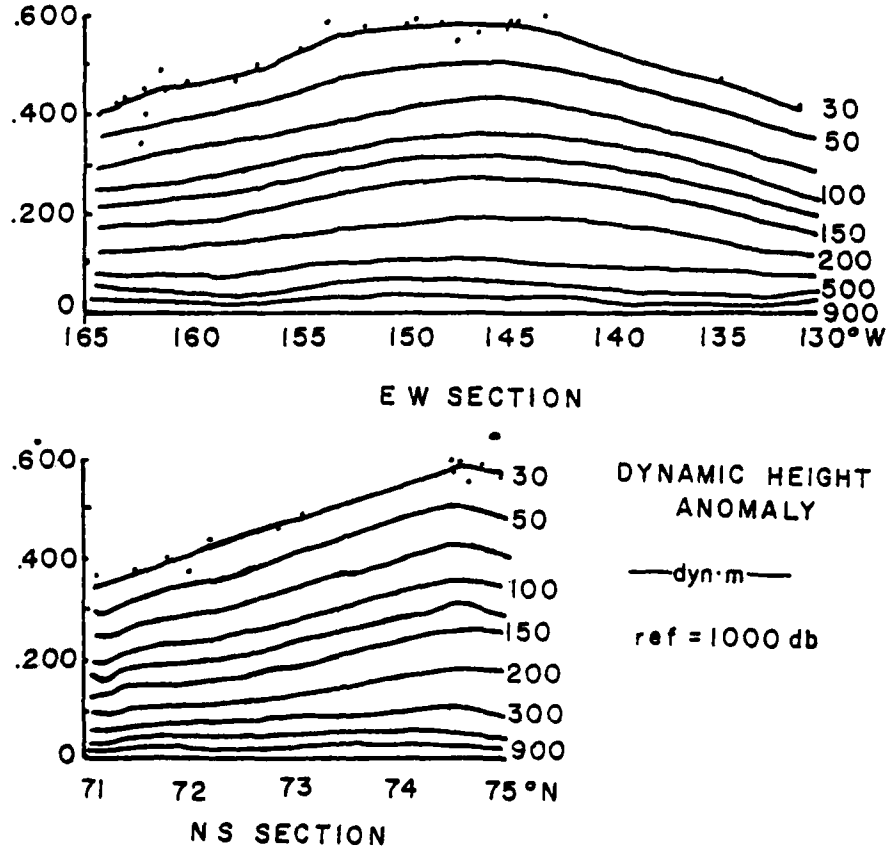


Figure 12. Dynamic height anomalies of selected isobaric surfaces along an east-west(top) and north-south(bottom) section of the Beaufort Gyre(Newton, 1973).

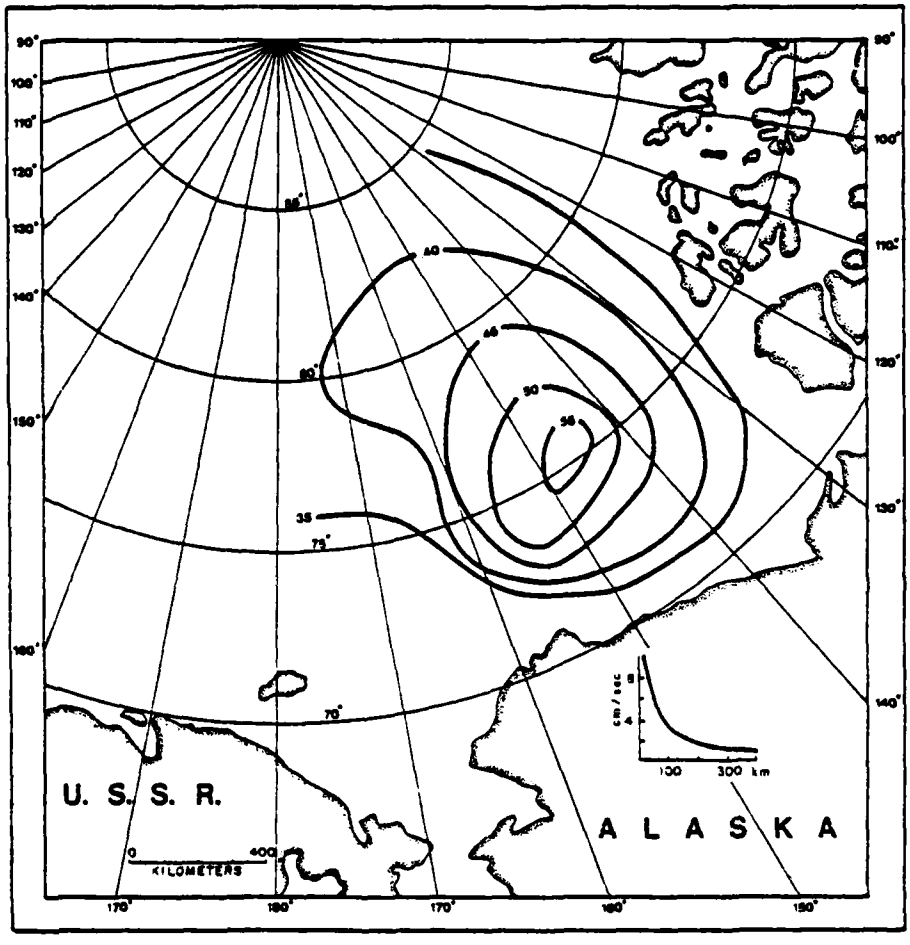


Figure 13. Surface dynamic topography in dynamic meters(30/500 db) (Newton,1973).

is still in question.

Bottom water movement is largely unknown because of the lack of a large number of direct current measurements. Potential temperatures are extremely uniform in the major basins(figure 10) and do not provide an opportunity to perform percentage retention characteristics of the core layer as was done for the Atlantic layer. Coachman and Aagaard(1974), however, suggest that the water column below 400 meters moves as a unit, with relatively slow speeds and without any significant vertical shear.

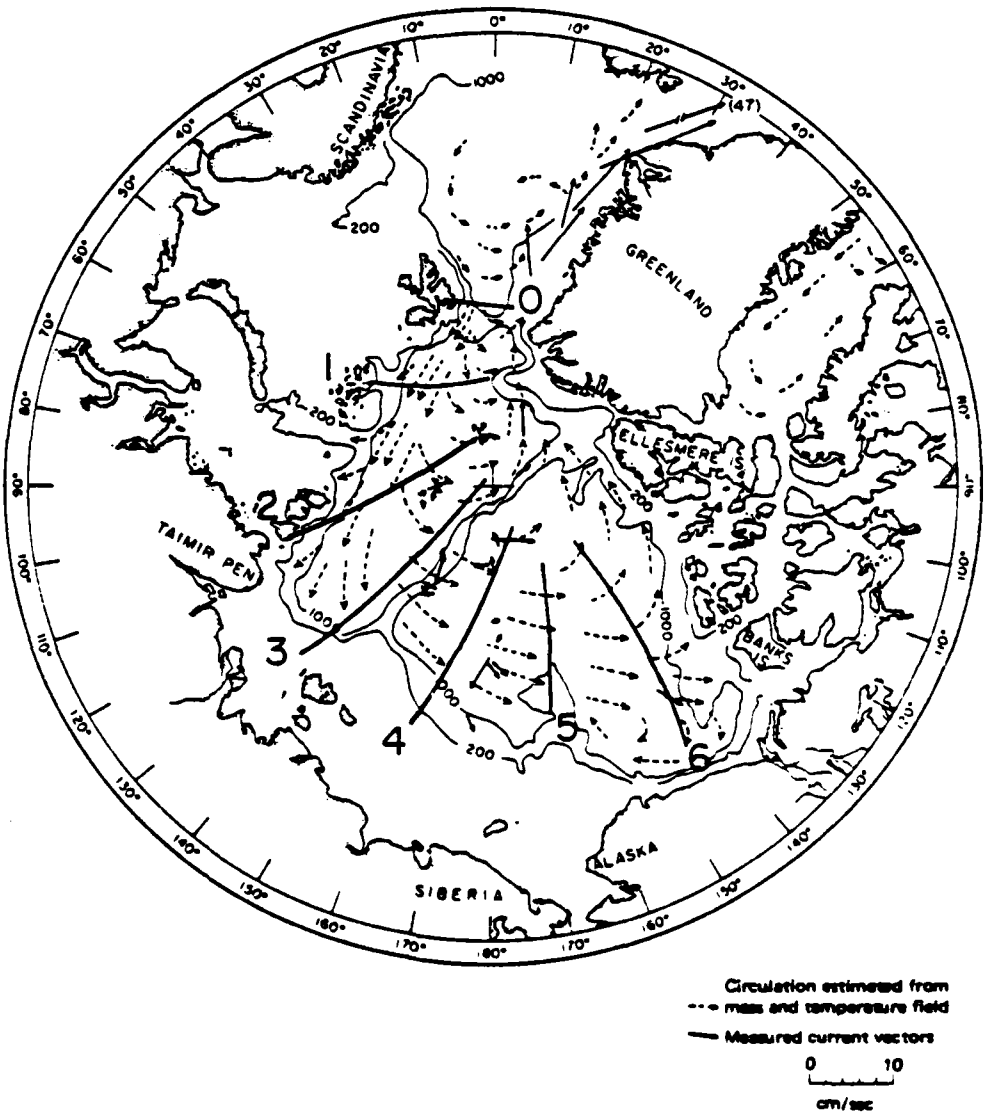


Figure 14. Circulation pattern of the Atlantic Water as inferred from percentage retention of temperature and time required for such movement in years (Coachman and Aagaard,1974).

E) Ice Cover

The polar oceans maintain a thin veneer of annually varying sea ice which is a direct response to the net loss of radiation to space at these high latitudes. Due to sea ice having a higher albedo(70-80%) than that of water(10-20%), it acts as a positive feedback mechanism to keep the polar oceans as heat sinks on a global scale. Opinions differ as to whether the ice cover of the polar oceans is stable or is capable of switching from no-ice to ice conditions with somewhat periodic regularity(Kellogg,1973). Recently, investigations of deep cores from the Arctic Ocean have led Herman and Hopkins(1980) to suggest that out of the past 4.5 million years, perennial sea ice has occupied the Arctic Ocean only within the past 700,000 years. Clark(1977), however, indicates that perennial sea ice has been in this region for the past 3-4 million years using data obtained from cores taken from ice island T-3.

The amount of ice cover and its associated thickness over a local region is very important for the determination of heat balance across the air-ice-water boundaries. Because of the very large temperature differences between the air-water boundary which is roughly 30-40 degree C., it may take as little as 2% of open water to dominate the heat balance in the colder months (Untersteiner,1976). Available data, however, does not show this to exist, thereby leaving the next most important terms of ice thickness and its associated areal extent to determine either a positive or negative heat flux(Maykut,1976).

The sea ice coverage is highly variable in the Arctic Ocean depending on the season. During the winter months the Arctic Ocean, including the marginal seas, is completely covered with sea ice that ranges in thickness from 1 to 3 meters. Sea ice may range in size from small blocks of rubble to uniform floes of ice up to a few kilometers in diameter. Adjacent floes are delineated from each other by the presense of narrow ribbons of open water(leads), or relatively thin ice(.1-.3 m in thickness), which is a result of rapid freezing of the

open water or zones of compression (pressure ridges).

During the summer months, most of the ice cover on the shelf areas melts leaving approximately 40% of the Arctic Ocean ice free(Untersteiner et al, 1976). In the deep Arctic Ocean, where the ice cover is perennial, the amount of open water may be as high as 20%. Due to the increased solar radiation, the upper .1 to .8 m of the permanent pack ice is melted forming small to large shallow depressions filled with fairly fresh water (melt pools). A map indicating the ice conditions of the winter and summer months for the Arctic Ocean as well as adjacent areas is shown in figure 15 (Sater, 1969).

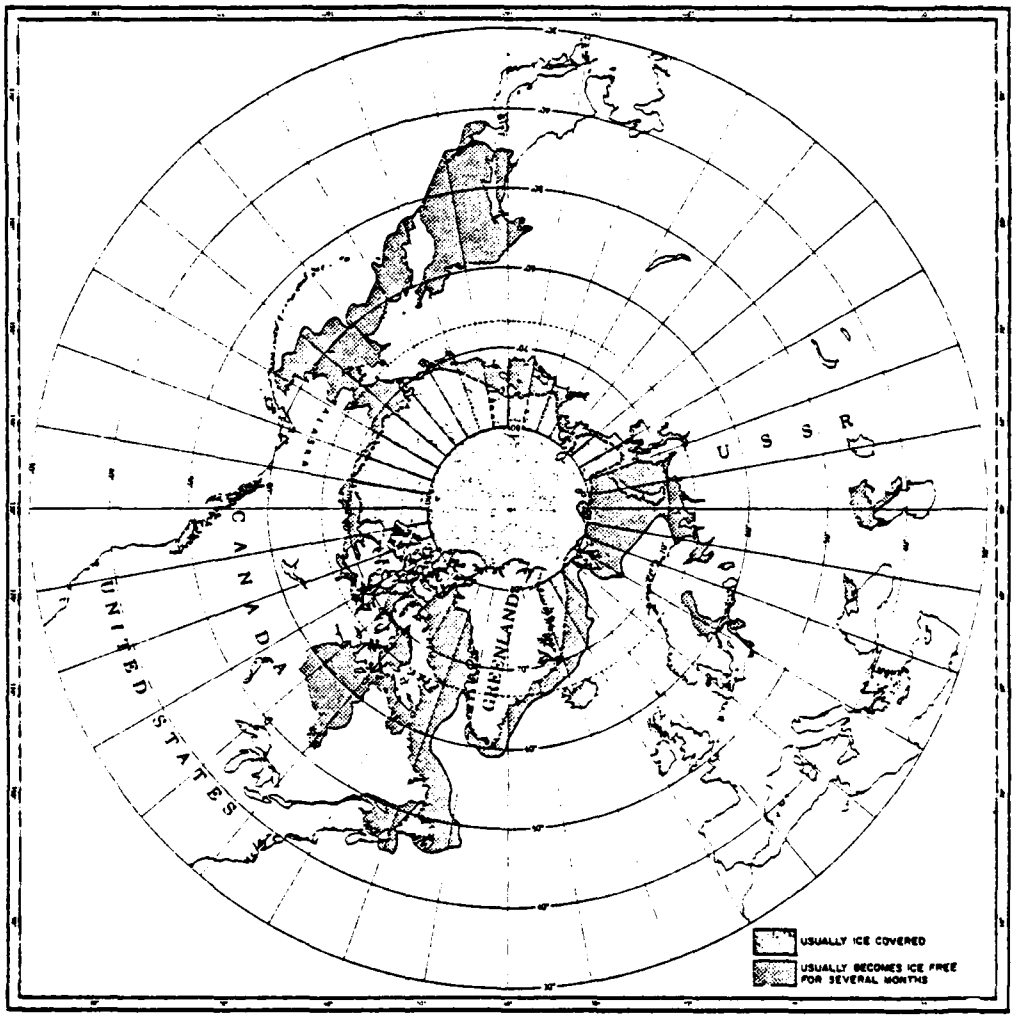


Figure 15. General ice conditions for the Arctic Ocean and surrounding Seas(Sater,1969).

Table 1 Annual mean water, salt, and heat budgets for the Arctic Ocean (adapted from Coachman and Greisman,1975).

Source	Volume Transport Sv	Heat Transport 10^9 kcal s^{-1}	Mean Temperature C	Salt Transport 10^3 metric tons s^{-1}	Mean Salinity ppt
Bering Strait					
Water	1.5	0.9	0.5	48.6	32.4
Ice	negligible	-0.4		negigible	
Arctic Archipelago	-2.1	1.3	-0.7	-71.8	34.2
East Greenland Current					
Polar Water	-1.8+	2.0	-1.2	-61.2	34.0
Atlantic Water	-5.3+	-3.2	0.5	-185.0	34.9
Ice	-0.1	8.0		-0.3	3.0
West Spitzbergen Current	7.1	16.3	2.2	248.9	35.0
Spitzbergen-FranzJosef Land	-0.1	-0.3	2.7	-3.5	34.9
FranzJosef Land-Novaya Zemlya#	0.7	0.7	0.9	24.3	34.7
Runoff	0.1	0.5	5.0	0.0	
Total Inflow	9.4		1.8	321.8	34.6
Total Outflow	-9.4		-0.1	-321.8	34.6
Total Advective Heat Gain		29.7			
Total Advective Heat Loss		-3.9			
Net Exchange	0.0	25.8		0.0	

F) Volume, Heat, and Salt Transport for the Arctic Ocean

There are three major passages through which the Arctic Ocean has direct communication with the adjacent oceans. The largest of these is between Greenland and Spitzbergen. Due to its relatively large width of 600 km and sill depth of 2600 m, a major exchange of water, heat and, salt between the Arctic and the rest of the oceans occurs here(Aagaard and Greisman,1975).

Volumetrically, outflow from the Arctic Ocean through the Canadian-Archipelago is the second largest, even though the depths are generally shallow (200m). The Nares Strait and Lancaster Sound are two of the largest passages in this area and are located near Baffin Bay.

The third most important passage is the Bering Strait located in the western Arctic between Alaska and Siberia, the strait itself is narrow (85 km) and shallow (50 m). Numerous investigations have compiled data on both the heat and volume transports through the Bering Strait; however, the most recent work has been done by Coachman et al(1975). Generally, the results state that volume transport can vary significantly over short periods in time from northward to southward flow. A long term average yields a northward flow into the Arctic Ocean with a transport that ranges from 1-2 million cubic meters per second.

A more detailed breakdown of volume, heat and salt transports for the Arctic Ocean are given in Table 1. The major impact of the work done by Aagaard and Greisman(1975) indicates that the transport of heat and water through the Greenland-Spitzbergen passage is larger than previously expected(Mosby,1962; Vowinckel and Orvig,1970). Also of importance is that sensible heat input by the West Spitzbergen Current and the export of ice via the East Greenland Current are the dominant terms in the heat balance in the Arctic Ocean.

G) The AIDJEX Experiments

The Arctic Ice Dynamics Joint Experiment (AIDJEX) consisted of three pilot projects and one major experiment in the Beaufort Sea from 1970 to 1976. The first three AIDJEX Experiments were of short duration (approximately 1 month from mid March to mid April) pilot studies during the years 1970, 1971, and 1972. The large scale main experiment was started in March of 1975 and continued until April of the following year.

The purpose of the oceanographic program during each of the pilot studies was to obtain and analyze hydrographic and current meter data taken on spatial scales of the intercamp separations(figure 16). The hydrographic data consisted of bottle casts with the exception of the 1972 Pilot study, where a Plessey 9040 STD was used at the main camp in conjunction with bottle casts (Amos, 1975; Hunkins, 1974). A minimum of two current meters were suspended at predetermined depths at each of the manned camps. In 1972, however, a hand lowered current meter was used to obtain a vertical profile of horizontal currents to a maximum depth of 170 meters at 10 meter intervals(Hunkins,1974). The positions of the three AIDJEX pilot studies are shown along with their spatial configuration in figure 16.

The main AIDJEX program (1975-1976) was designed to obtain data on the meso- and macroscale interactions of the wind-ice-water system in order to provide major improvements in the modeling of an ice-covered ocean(Untersteiner et al,1976). The major part of the experiment consisted of meteorological and oceanographic programs on four manned drifting ice camps in the Beaufort Sea. The manned camps were initially established in an array with three satellite camps forming a triangle centered around a larger main camp. Spacing between the satellite camps was nominally 100 km and the duration of the experiment was one year, April 1975 to April 1976. A map of the AIDJEX operational area is shown in figure 17, including the beginning

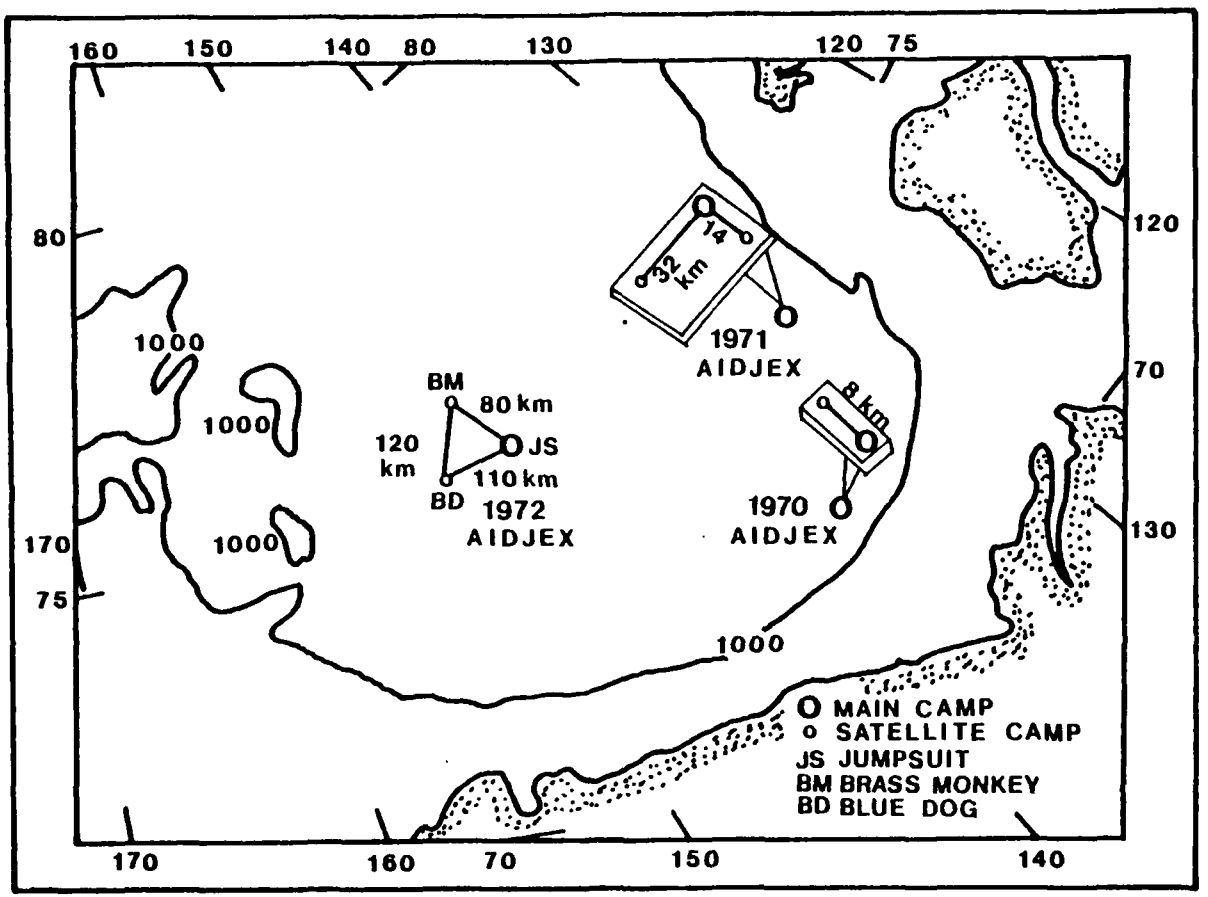


Figure 16. Configurations and locations of the AIDJEX pilot studies within the Beaufort Sea(redrawn from Newton,1973).

and ending positions of the manned camps superimposed on the dynamic topography of the Beaufort Sea. More detailed drift tracks of the individual stations are shown in figures 18a,b,c, and d.

The radio call signs of the satellite camps were Snowbird, Blue Fox, and Caribou. The main camp was known as Big Bear. During the course of the experiment, Big Bear was evacuated due to severe ice breakup during late September of 1975. Caribou then became the main camp for the duration of the experiment.

The meteorolgical program during the main AIDJEX experiment obtained estimates of the wind stress from the mean atmospheric pressure field. The observations of air temperature, wind speed, direction, and barometric pressure at the manned camps provided the basic information for computing air stress (Leavitt,1975). Remote buoys located in a circular array 200 km away from the manned camps provided the mean atmospheric pressure and temperature over a large sector of the Beaufort Sea. Air stress measurements were then related to the pressure fields in order to provide input to the AIDJEX model(Paulson and Bell, 1975).

Satellite positioning of the manned camps was used to provide accurate movement of the local ice field (position,velocity and acceleration) to determine its response to the driving forces of wind and water. At each of the manned camps, a Navy Navigation Satellite System (NAVSAT) was used to determine the position of the camp to within 40 meters. As many as 60 usable fixes were obtained during any one 24 hour period, the average being 25-30.

During the initial processing of the satellite navigation data(Thorndike and Cheung, 1977), energy at the inertial period for the Arctic Ocean(roughly 12 hours) was damped by approximately 50% due to the choice of a low covariance factor (Q=100) during Kalman filtering. For oceanographic investigations, the data set proved to be unacceptable, particularly in the summer months when

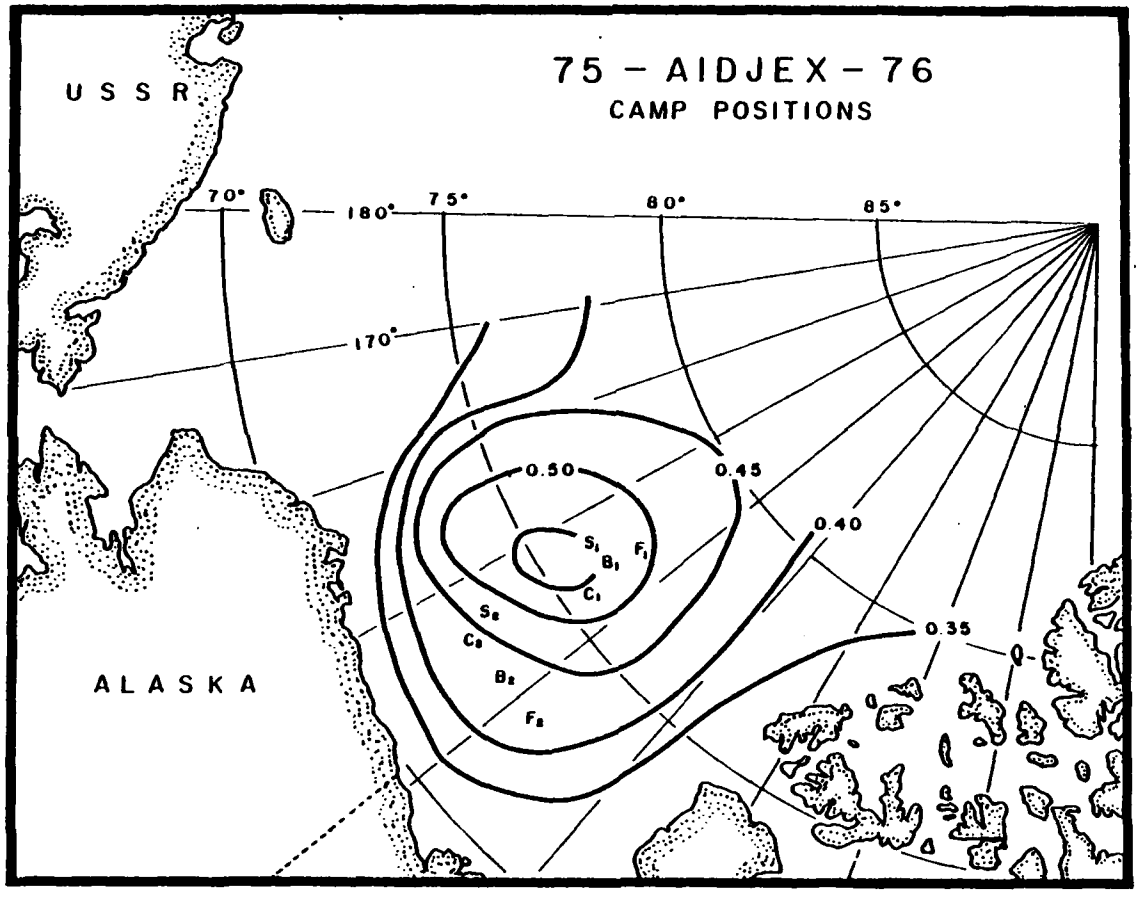


Figure 17. Beginning and ending positions of the AIDJEX 1975-76 manned camps superimposed on the mean dynamic topography(Newton, 1973) of the Beaufort Sea. Abbreviations are C(Caribou), F(Blue Fox), S(Snowbird), and B(Big Bear). Subscripts 1 and 2 indicate the beginning and ending positions of the camps respectively.

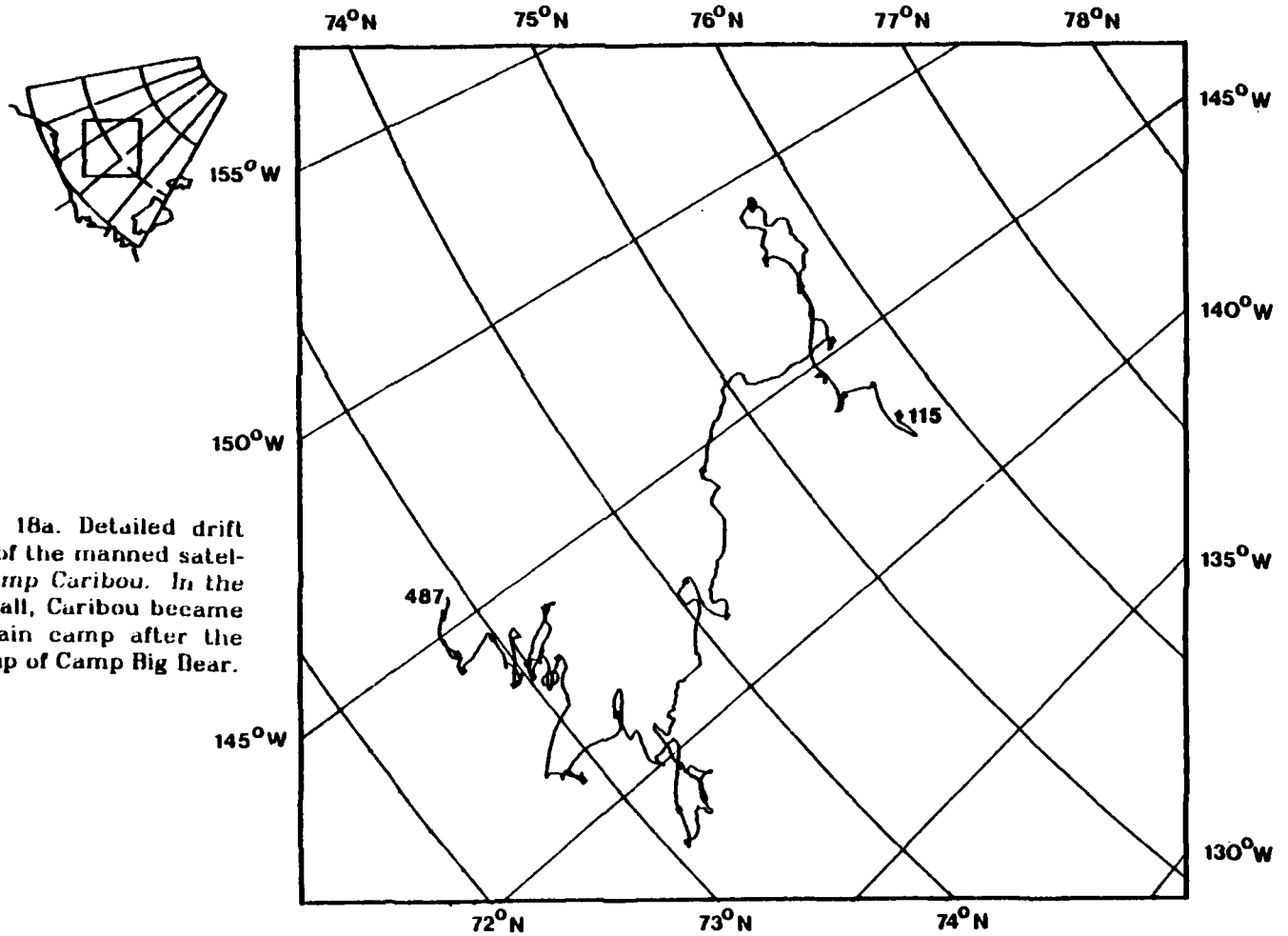
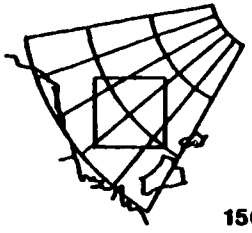


Figure 18a. Detailed drift track of the manned satellite *Camp Caribou*. In the early fall, Caribou became the main camp after the breakup of Camp Big Bear.



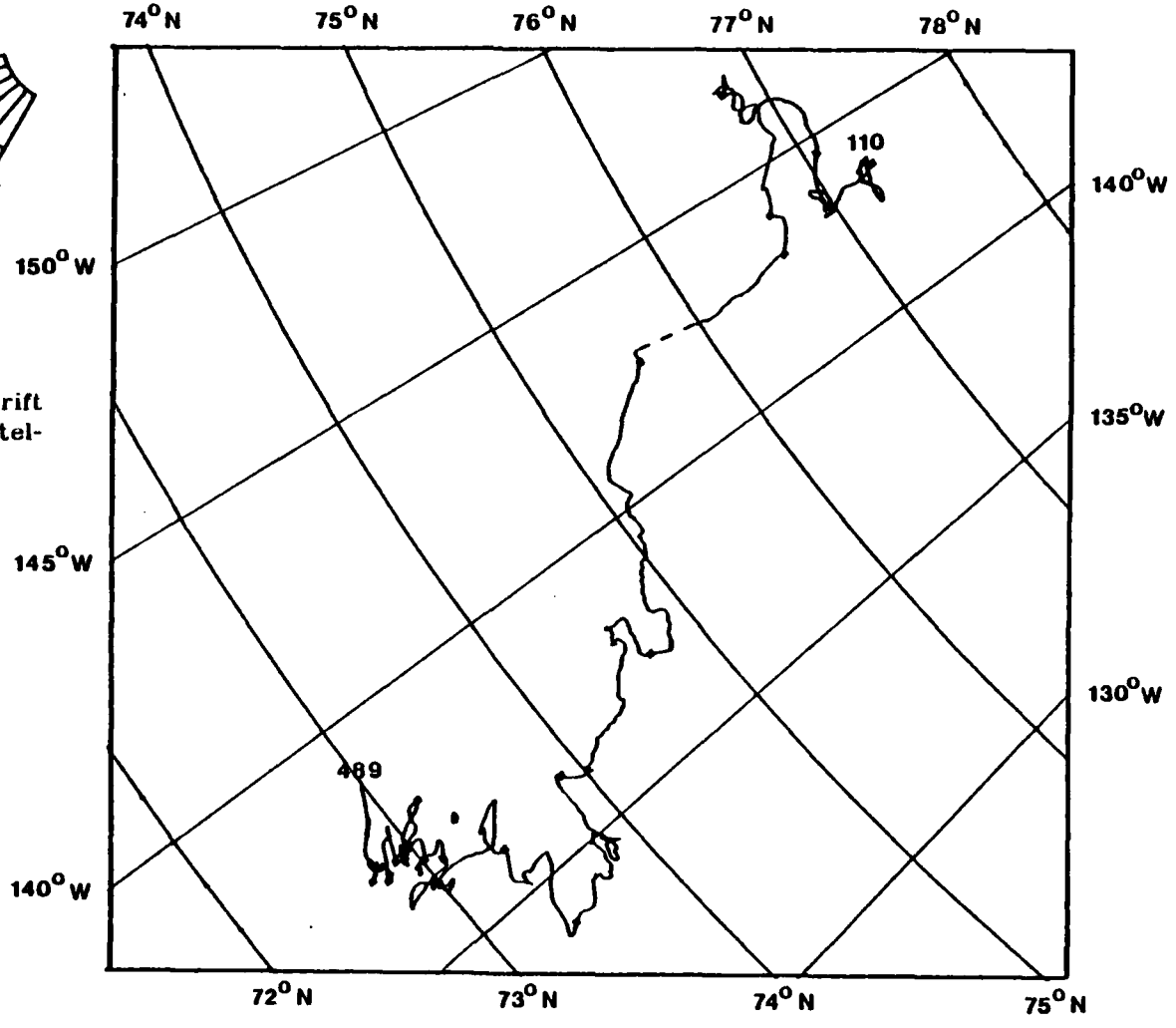


Figure 18b. Detailed drift track of the manned satellite Camp Blue Fox.

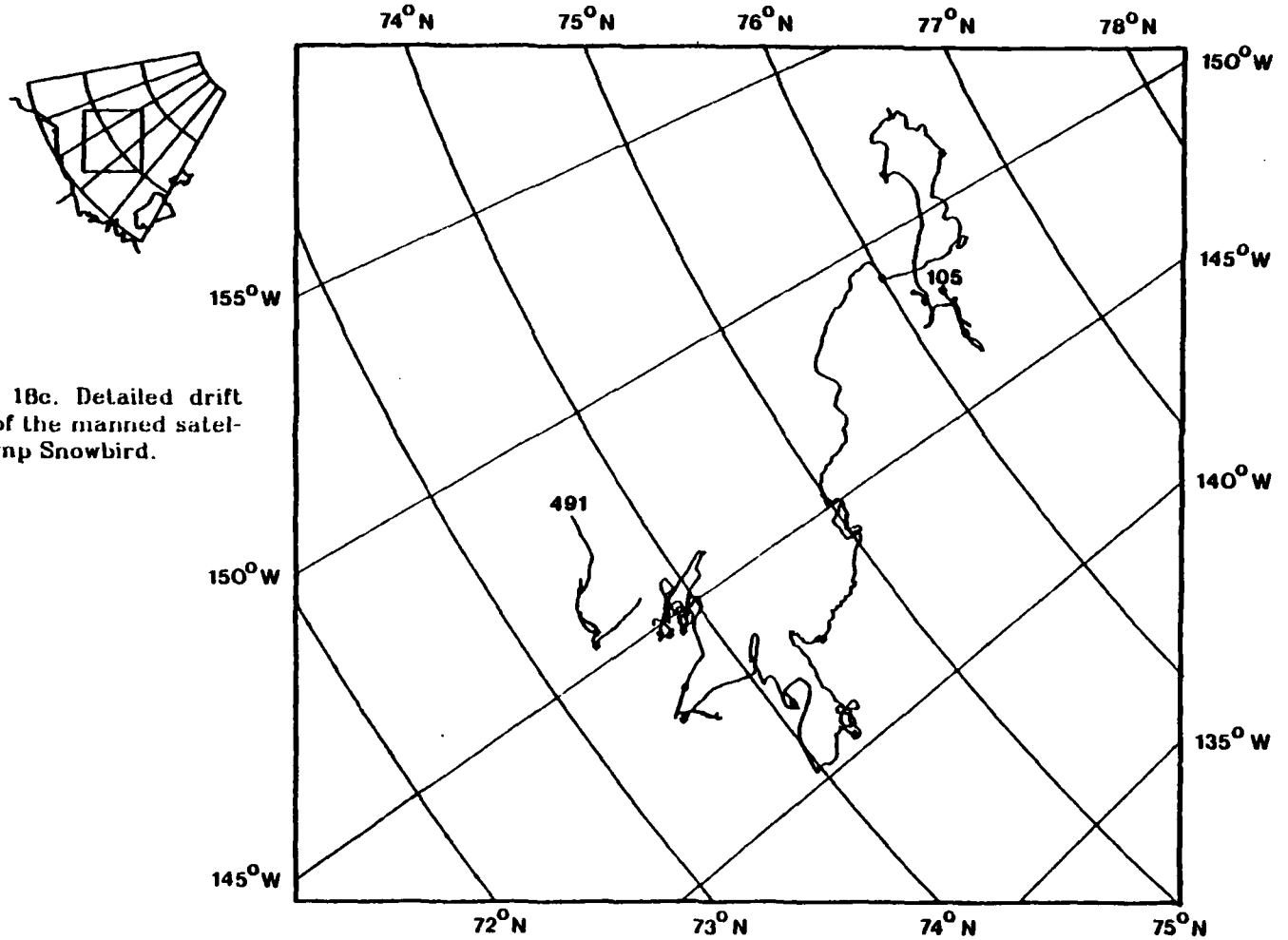
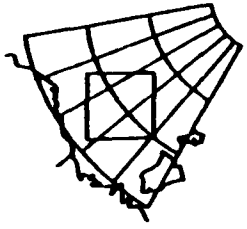


Figure 18c. Detailed drift track of the manned satellite Camp Snowbird.



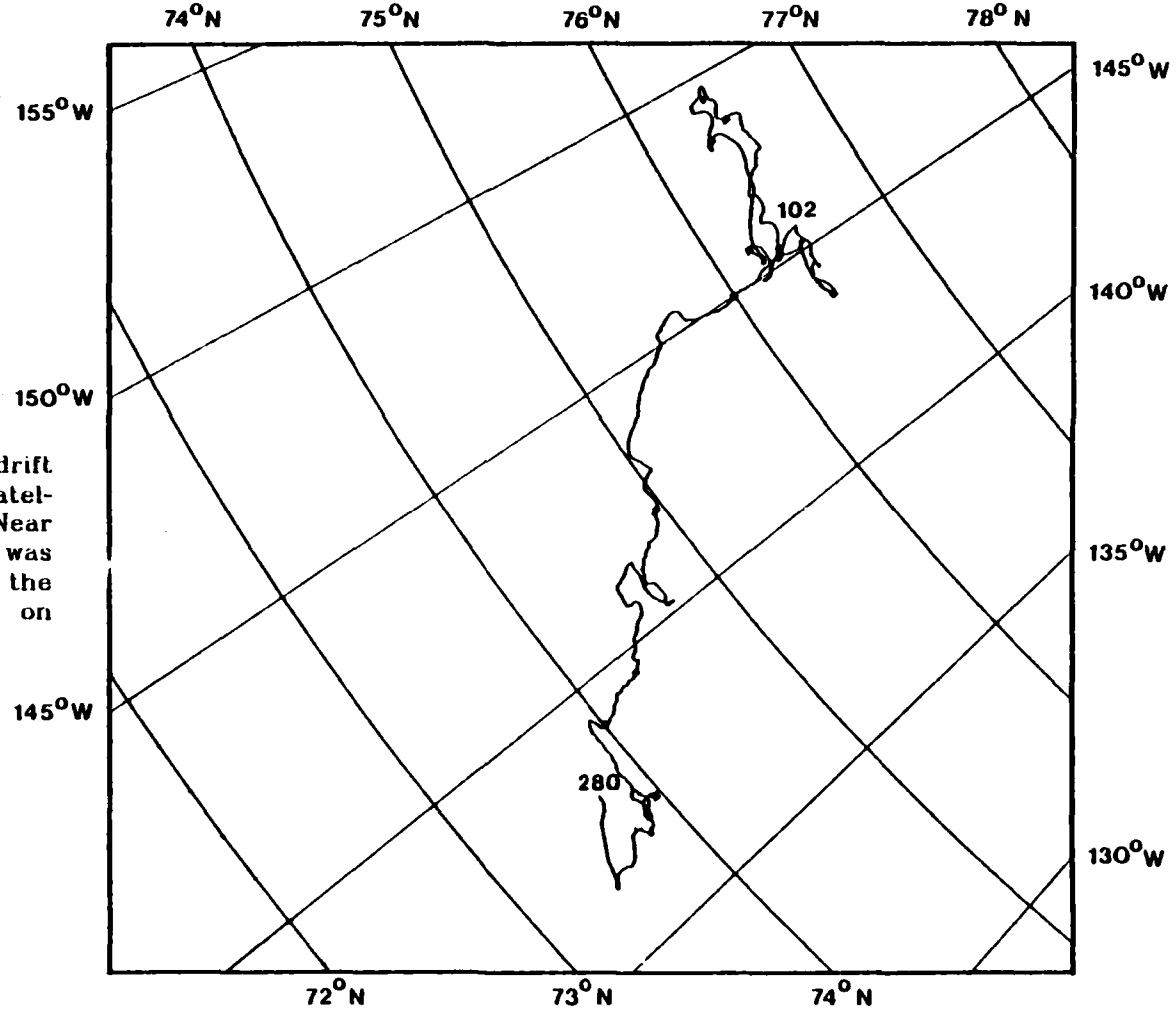


Figure 18d. Detailed drift track of the manned satellite Camp Big Bear. Near day 280, the camp was abandoned due to the breakup of the floe on which it resided.

TABLE - 2

CAMP	OCCUPATION DATE	EVACUATION DATE	TOTAL STATIONS TAKEN	PROFILING STATIONS	STATIONS REJECTED	TIME SERIES	STATIONS FROM MAG. TAPE	MANUALLY DIGITIZED STATIONS
STD	(14 MAY '75)	(25 APR '76)	852	416	30	406	245	171
CARIBOU	6 APR '75	7 MAY '76						
PCM	(5 AUG '75)	(22 APR '76)	404	395	232	9	0	163
STD	(10 MAY '75)	(20 APR '76)	520	310	10	200	16	294
BLUE FOX	5 APR '75	4 MAY '76						
PCM	(8 MAY '75)	(20 APR '76)	700	698	322	2	0	376
STD	(16 MAY '75)	(20 APR '76)	604	299	20	285	145	154
SNOWBIRD	4 APR '75	6 MAY '76						
PCM	(4 MAY '75)	(20 APR '76)	620	603	226	17	0	377
STD	(4 APR '75)	(1 OCT '75)	562	262	44	256	20	242
BIG BEAR	13 MAR '75	8 OCT '75						
PCM	(8 APR '75)	(1 OCT '75)	425	397	139	28	0	258

Note: 1) Paranthetical dates are those when PCM or STD data began or ended
2) "Digital stations" indicates profiling data taken from digitally recorded magnetic tape
3) "Manually digitized stations"
a) STD - profiling stations whose analog charts were manually digitized for computer reduction
b) PCM - stations that had sustained speeds of a few cm/sec and manually digitized for computer reduction

there was a significant amount of inertial motion. The position data was later refiltered(Thorndike and Manley,1980) to allow 99% of the inertial period to pass through the filter.

The oceanographic program was designed to observe the temperature, salinity and current structure of the upper ocean(above 800 m), thereby providing estimates of the momentum and stress balance between the ice and water(Hunkins, 1974b; Hunkins,1975; McPhee,1975)

At each of the manned camps, current meters of uniform type throughout the array were operated both in the planetary boundary layer and in the steep pycnocline below it. Instrumentation consisted of a TSK profiling current meter(PCM) and Hydro Products geodetic current meters. The Hydro Products meters were rigidly mounted to the ice at depths of 2 and 30 meters below ice base and were referred to as fixed mast current meters. Although not discussed here, the fixed mast data were reduced and were reported by the AIDJEX staff(1976) and later by McPhee(1978).

PCM casts were taken twice daily at all of the camps at approximately the same time. The profiling current meter consisted of a Savonius rotor, directional vane and pressure sensor. The PCM was raised and lowered at 5 m/min by an electric winch. The rate was chosen after experiments on the station to determine rotor response at different axial velocities. Current direction was referenced to an internal magnetic compass. The direction vane follower and compass were both sensed with photocells so that only bearing friction limited the compass, an important factor in the weak horizontal magnetic field at these latitudes. Speed, direction, and depth vs time were recorded on an analog chart as well as the AIDJEX digital data logging(DDL) system. Magnetic declination was measured one or more times each day on the surface in order to convert directions referenced to magnetic north to true north.

Salinity and temperature observations were also taken at each of the manned camps usually once daily to a depth of 750 meters with a Plessey model 9040 STD system. At the main camp two STD casts were taken daily as well as a weekly deep cast to 3000 meters. Reversing thermometers and salinity samples were taken at several depths in the water column at each of the camps in order to provide accurate sensor calibration. Salinity samples taken at the satellite camps were flown to the main camp where they were analyzed.

PCM and STD casts were not usually taken simultaneously at the satellite camps. This was due to having only one person responsible for the oceanographic program as well as the individual sensors being located in different areas of the camp. At the main camp, however, concurrent PCM and STD casts were normal because each instrument had an operator.

More information on the processing of the PCM data is given in the AIDJEX oceanographic report by Manley et al,1980a. Other technical reports pertaining to the PCM and STD data are in the process of publication(Manley et al,1980b,c,d; Bauer et al,1980a,b,c,d).

During the year-long experiment a total of 2084 PCM stations and 1391 vertical STD profiles were taken. Of these, 116 PCM and 1287 STD stations were used for the oceanographic data base. Stations were omitted for various reasons such as recording failures or lack of currents. Table 2 shows the breakdown of the PCM and STD stations for each camp as well as the occupation dates, which were obtained from A. Heiberg(personnel communication).

2. Eddies of the Oceans

A. Arctic Ocean

Eddies were only recently documented to exist within the Arctic Ocean (Newton,1973; Newton et al,1974; Hunkins,1974). Prior to this, eddies had been observed occasionally but were classified as transient high speed undercurrents, or counter currents. The first observation of such an event was made by Shirshov in 1937 while on the Russian North Pole-1(NP-1) Experiment(Belyakov,1972).

Relatively little was known about these events before 1974, although it was believed that they were generated locally within the deep ocean in response to atmospheric forcing (Shirshov as reported by Belyakov(1972), Browne and Crary, 1958) or by intense brine convection. On the basis of anomalous T-S properties within the eddies as compared to the surrounding mean conditions, Hunkins(1974) and Newton et al(1974) have suggested that distant origin is more probable. In the context of this study, distant origin implies an eddy origin in an area of the ocean not within the immediate vicinity of where it was observed.

It was found that spatially, the arctic eddies are confined to a narrow depth range extending from the base of the mixed layer(approximately 50 m) to roughly 300 m which comprises most of the pycnocline(figure 4). Vertical profiles of the horizontal velocity component through an eddy are generally parabolic with a maximum velocity centered at 100 to 150 meters. Velocities within the eddy are normally 2-12 times the long term mean currents of a few hundredths of a m/sec, and may attain speeds as high as .60 m/sec. An example of such an event was observed at ice island T-3 for a period of eight days during the summer of 1965(Galt,1967) and is shown in figure 19 by a series of profiles through time. Other examples of velocity profiles of some of the higher

speed eddies observed at three of the manned camps are shown in figures 20, 21 and 22.

Table 3 lists all the known eddies prior to 1975 along with dates, positions, references, and other associated information. Positions of the eddies are shown in figure 23 as code letters which refer back to Table 3. The eddy observed by Shirshov has an unknown position, but lies somewhere along the drift track of NP-1 which is shown as a dashed line.

Before the advent of small light-weight portable PCM and STD sensors capable of being transported by helicopter, positions where measurements were taken were completely dependent on the movement of the ice floe on which the camp was located. A vast majority of drift tracks that involve observations of an eddy are usually slow and have rather circuitous routes. When the drift track of the ice has a higher velocity than the translational movement of the eddy, observations tend to "freeze" the eddy in space. Data from such a drift track provide a clearer understanding of its two dimensional structure. Unfortunately, drift tracks that are linear and rapid are rare and if available are usually along a chord rather than the diameter of the eddy. Because of the unknown relative position that the observations have within the eddy, their structure is usually difficult to interpret. Of the eddies listed in Table 3, only 2 had passes through or very close to the diameter of the eddy. These eddies were from the 1972 AIDJEX pilot experiment and are associated with code letters j and k(Table 3).

Both cyclonic as well as anticyclonic eddies have been observed within the deep Arctic Ocean. Figures 24 and 25 show the best example of an anticyclonic eddy in both its horizontal current structure at a depth of 150 m and vertical density structure along the drift track of the ice camp Brass Monkey(Newton et al,1974). The anticyclonic rotation of the eddy is apparent from the direction of the velocity vectors(figure 24). Due to the rapid pass across the eddy's

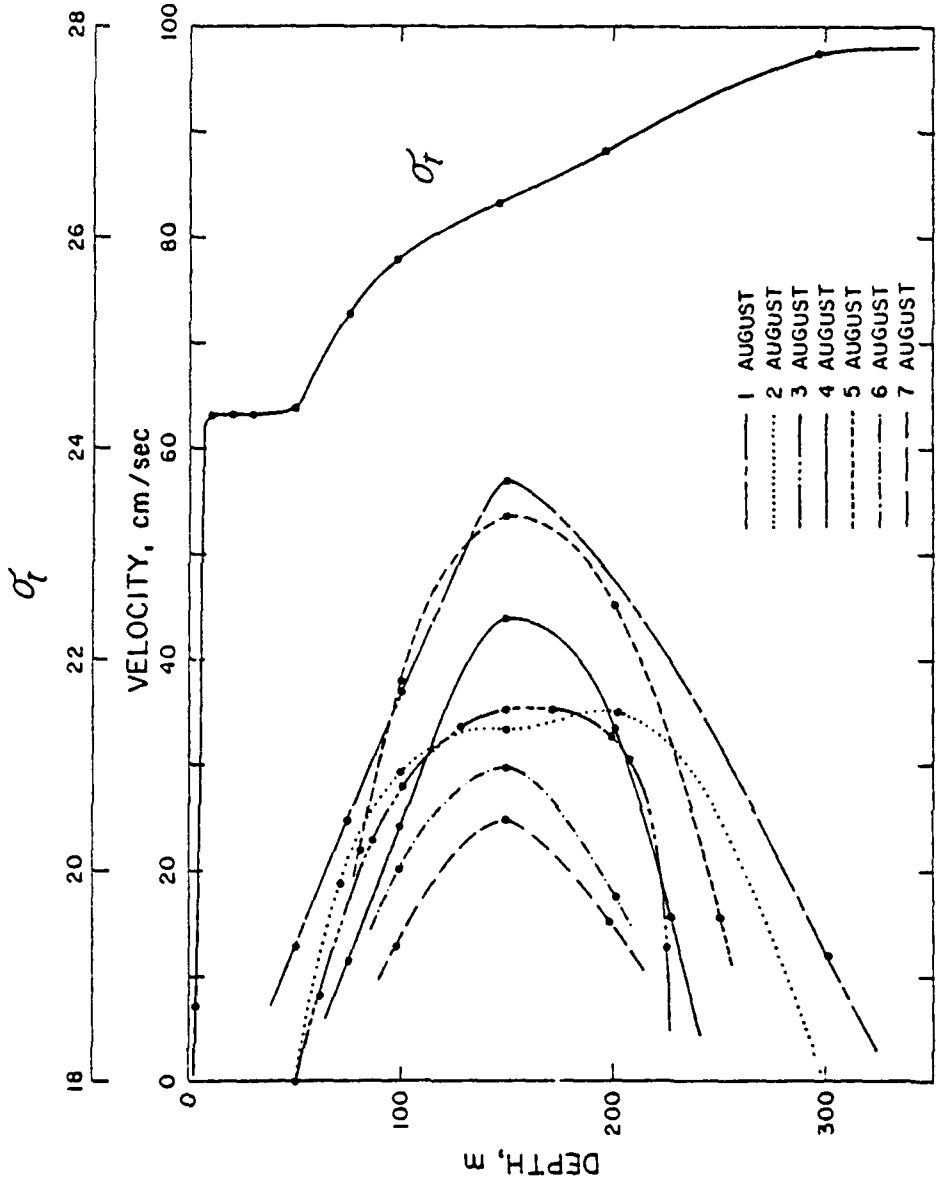


Figure 19. Vertical current profiles of high speed under-currents as observed from ice island T-3 during the summer of 1965 (Galt, 1967).

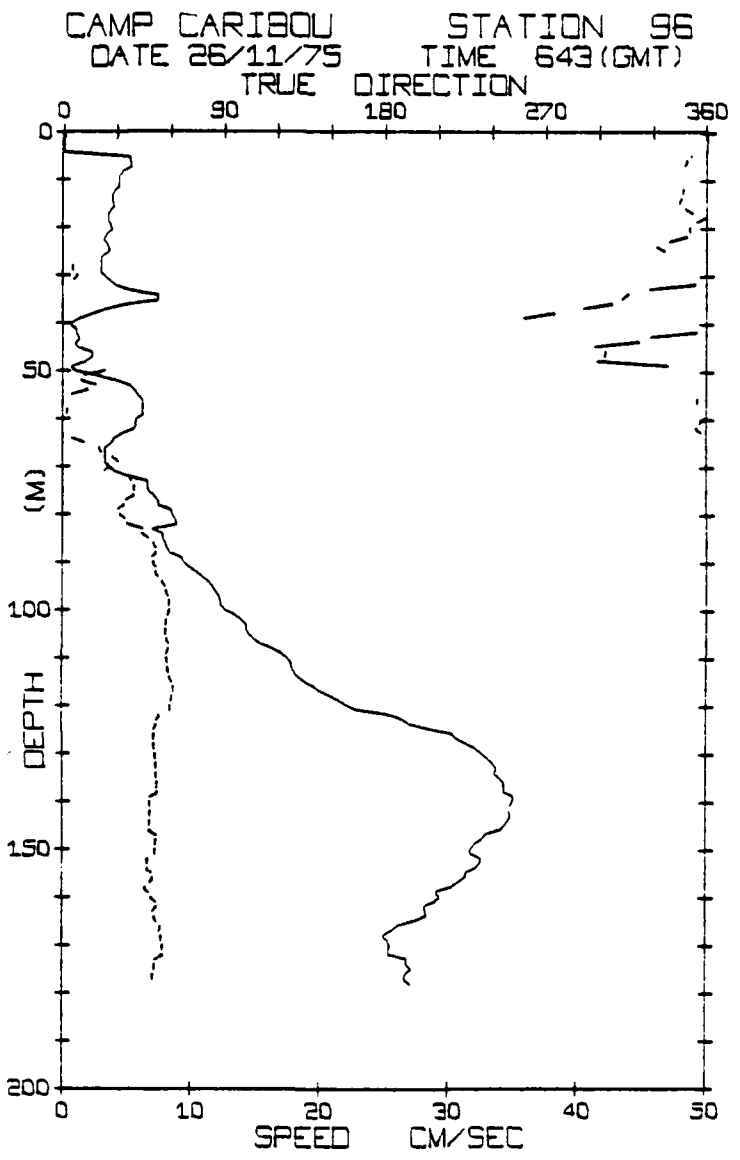


Figure 20. Vertical profile of eddy observed at camp Caribou. Speed is the solid line and direction is the dashed line.

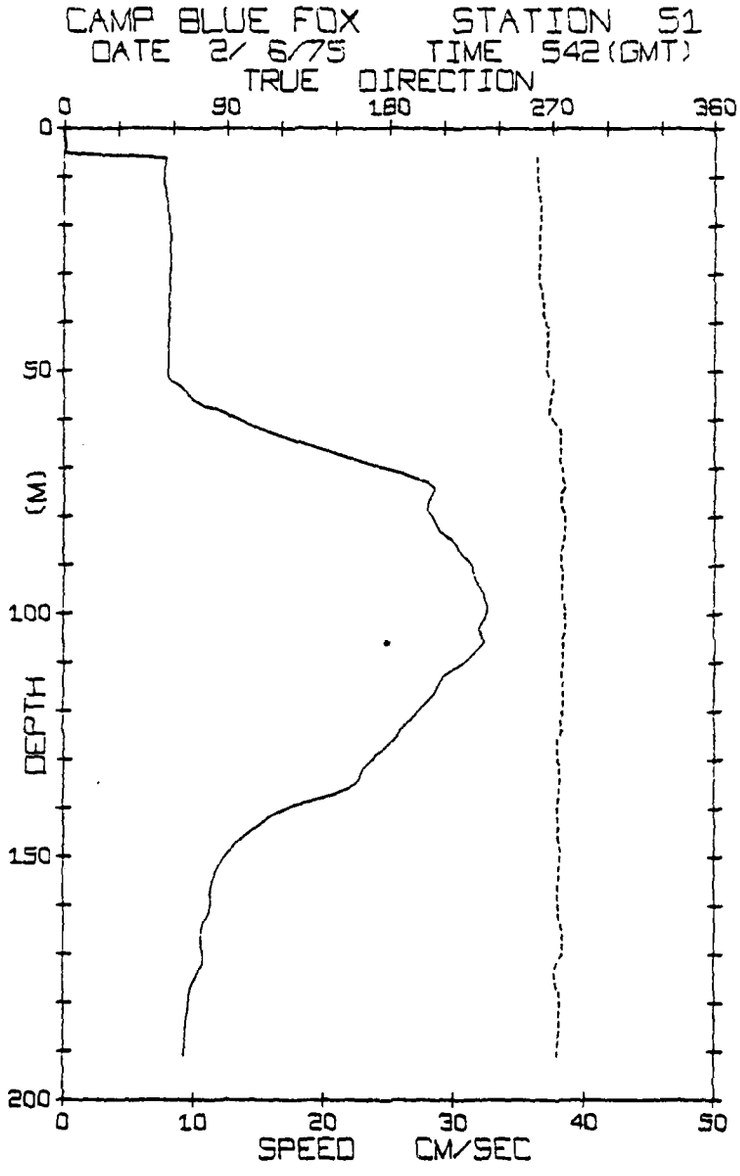


Figure 21. Vertical profile of eddy observed at camp Blue Fox.

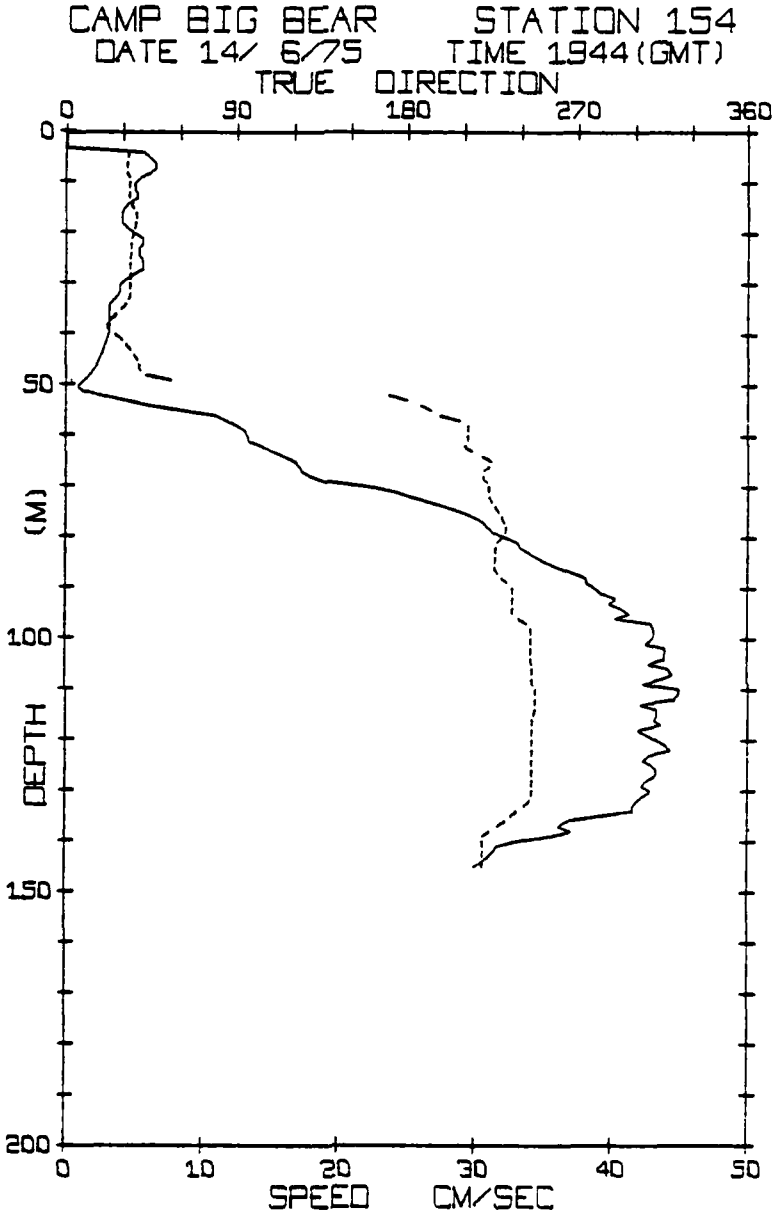


Figure 22. Vertical profile of eddy observed at camp Big Bear.

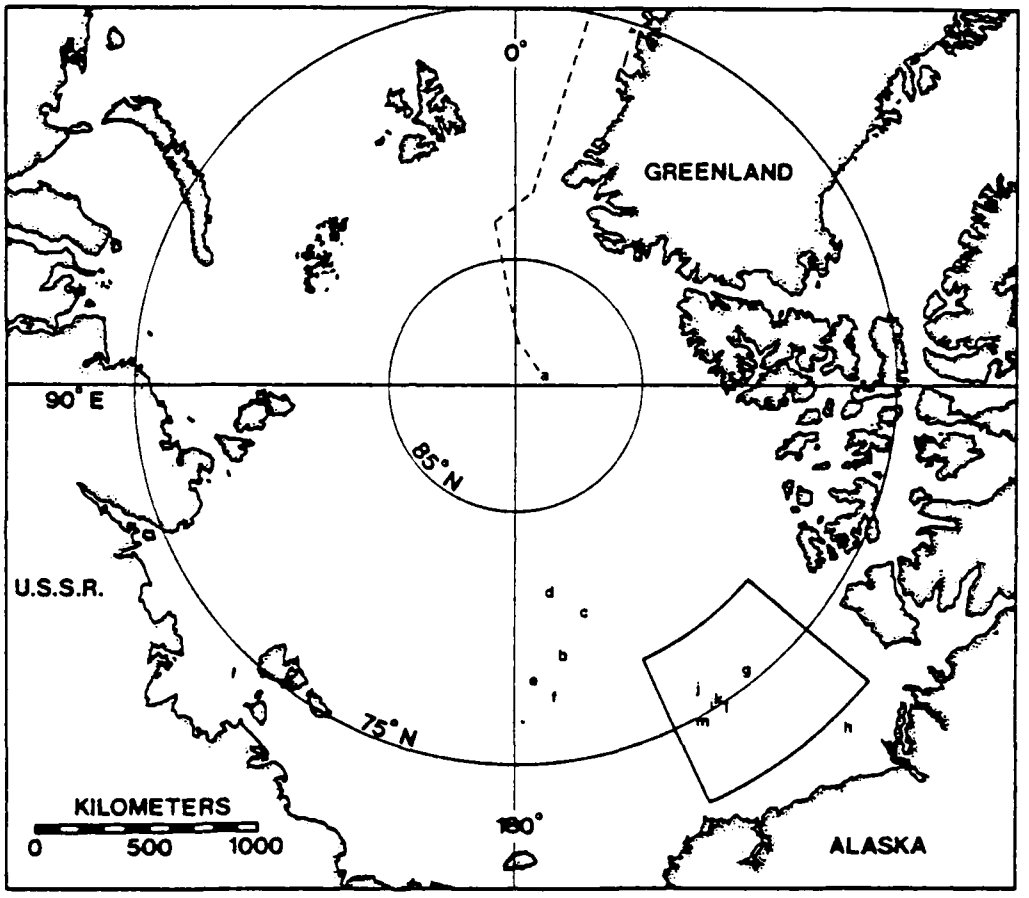


Figure 23. Positions of all available historical high speed undercurrents Letters correspond to those indicated in Table 3. Dashed line indicates drift track of NP-1. Outlined sector which is north of Alaska represents the operational area of the 1975-76 AIDJEX Experiment.

Table 3 Eddies observed in the Arctic prior to 1975

Experiment	Reference	Date	Rotation	Latitude	Longitude	Code
NP-1	Belyakov,1972	1937	--	along drift track		a
NP-2(ser.2)	Somov,1954-55	Aug 50	--	79 00'	170 00'	b
NP-2(ser.4)	Somov,1954-55	Jan 51	--	80 30'	163 00'	c
NP-2(ser.5)	Somov,1954-55	Mar 51	--	81 30'	171 30'	d
NP-8	Belyakov,1972	10 Sep 59	--	78 24'	176 30'	e
Np-8	Belyakov,1972	11 Jan 60	--	77 40'	173 00'	f
T-3	Galt,1967	1- 7 Aug 65	CW	75 30'	142 00'	g
AIDJEX 1970	Coachman and Newton,1972	Mar 70	CW	71 20'	136 30'	h
AIDJEX 1972	Hunkins;Newton et al,1974	13-18 Mar 72	CW	75 14'	147 56'	i
AIDJEX 1972	Newton et al,1974	23-28 Mar 72	CW	76 03'	150 05'	j
AIDJEX 1972	Hunkins,1974	27-28 Mar 72	CCW	75 03'	148 31'	k
AIDJEX 1972	Hunkins;Newton et al,1974	29 Mar-5 Apr 72	CW	75 01'	148 25'	l
AIDJEX 1972	Hunkins,1974	16-19 Apr 72	CCW	75 07'	151 04'	m

diameter and frequency of observations, evidence for solid body rotation(velocity proportional to radius) extending from the center to a maximum radius of 7 km as well as irrotational flow(velocity inversely proportional to radius) extending from 7 to 15 km was also shown to exist within the eddy field(Newton et al,1974).

The horizontal dimensions of the eddies agree roughly with the calculated internal Rossby radius of deformation , R_i , for a stratified fluid which is defined as

$$R_i = \frac{ND}{f} \tag{2.1}$$

where N is the average Brunt-Väisälä or buoyancy frequency over the depth D defined as:

$$N^2 = \frac{-g}{\rho}\frac{d\rho}{dz} \tag{2.2}$$

The Coriolis parameter f is defined as:

$$f = 2\omega\sin\Theta \tag{2.3}$$

where Θ is the latitude of the observation, and ω is the angular velocity of the earth.

The internal density structure of anticyclonic eddies is typical of the one shown in figure 25 where the isopycnals are displaced away from a centrally undisturbed isopycnal. In the case of cyclonic rotation ,the isopycnals are displaced towards a centrally undisturbed level. An example of a cyclonic eddy which was observed by Hunkins (1974) is shown in figure 26. The current vectors at a depth of 125 m along the drift track also indicate cyclonic rotation.

In both types of eddies, the lower half of the density structure represents the area of isostatic compensation for the anomalous upper layer. Without this compensation, the rotational velocity of the eddy would remain high throughout the depth of the water column until a horizontal boundary of some type was encountered. The depth at which compensation begins represents

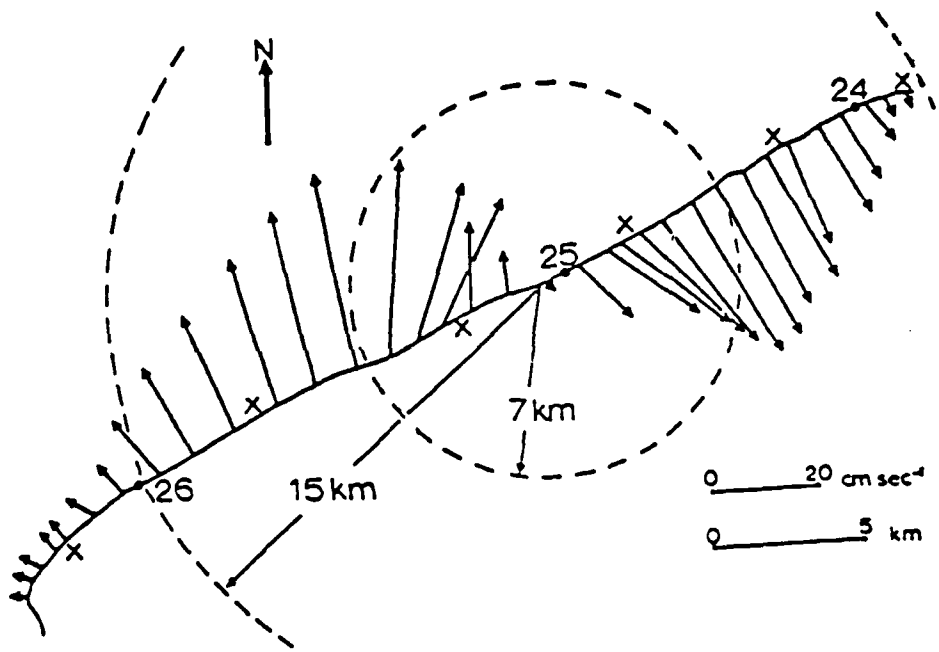


Figure 24. Averaged (2 hr.) absolute currents at 150 m. along the drift track of Brass Monkey (AIDJEX 1972). Outermost circle indicates extent of eddy. Inner circle represents current maximum. X's denote hydrographic stations(Newton, 1973).

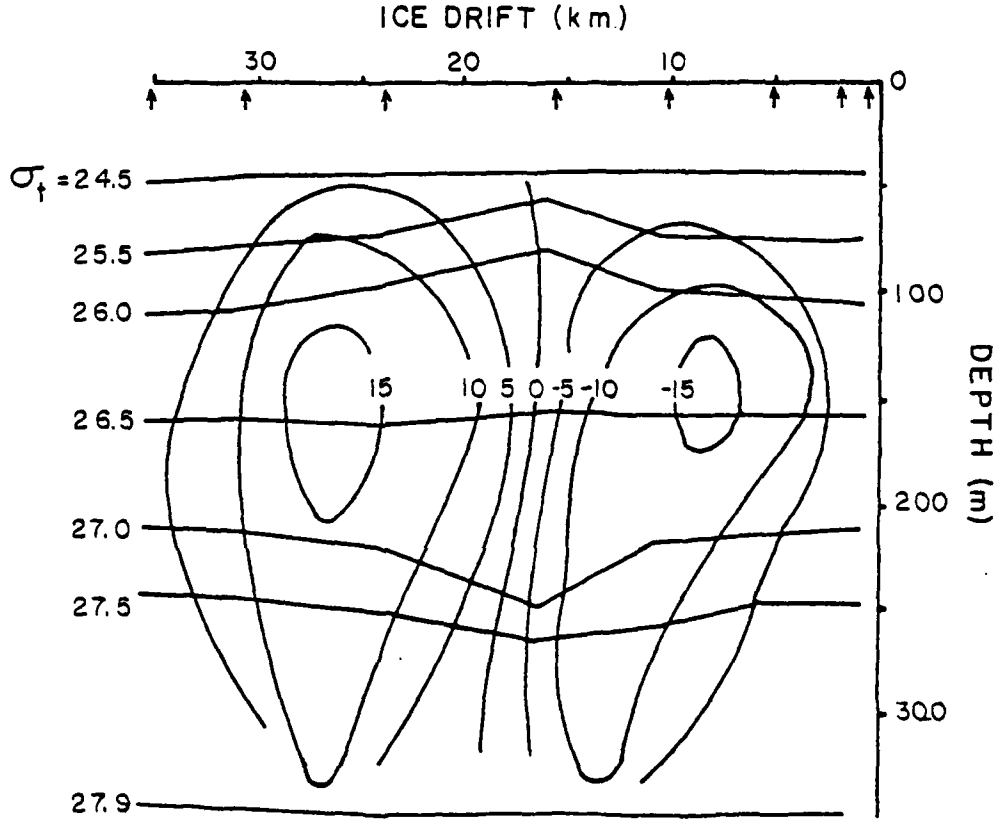


Figure 25. Vertical section of eddy seen in figure 20 showing isopycnals and isotachs of dynamically computed currents. Arrows indicate hydrographic stations(adapted from Newton, 1973).

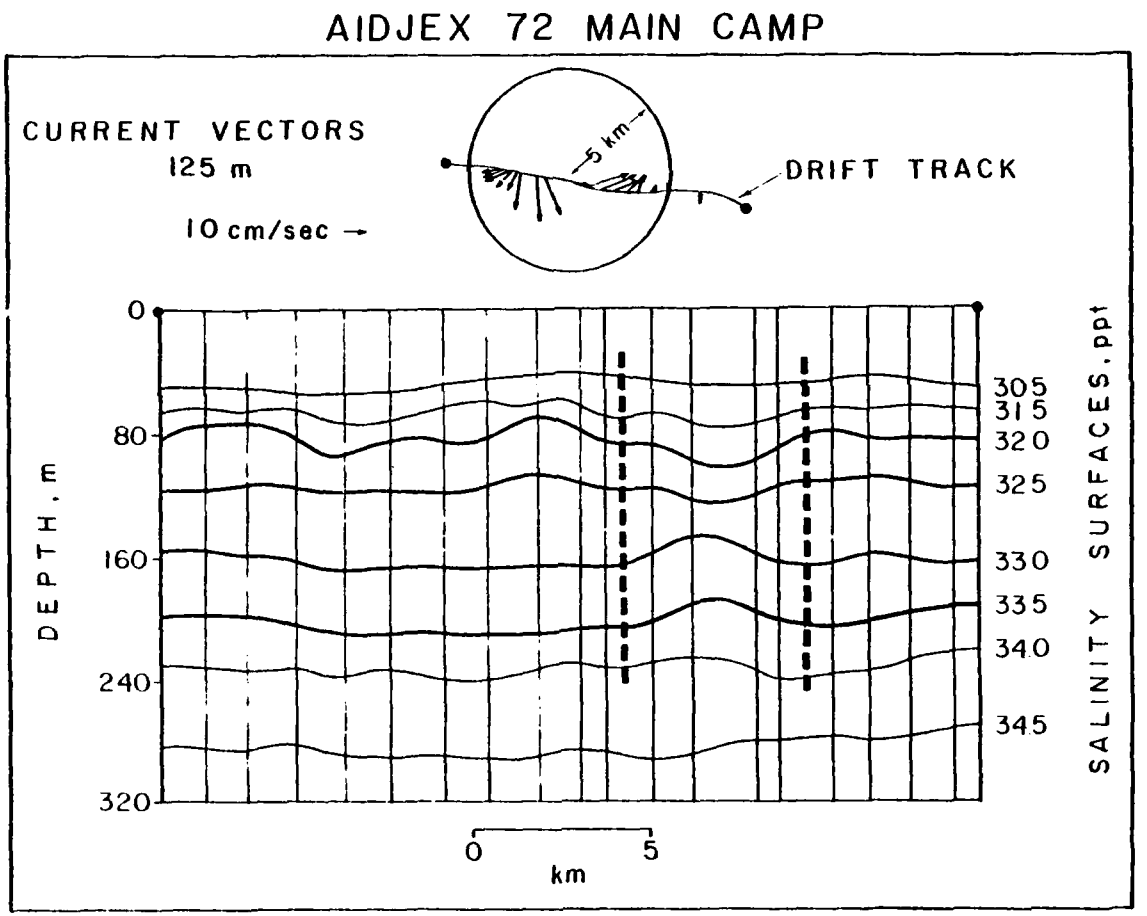


Figure 26. Cyclonic eddy observed at the AIDJEX 1972 main camp. Plan view of absolute currents at 125 m. along with vertical sections of isohalines are shown. Vertical lines are hydrographic stations(adapted from Hunkins,1974).

the observed as well as calculated depth of maximum velocity. A vertical velocity profile as well as T-S and σ_t profiles within and outside an eddy observed during the 1975-1976 AIDJEX Experiment(Camp Snowbird) is shown in figure 27. This eddy had a maximum observed velocity of .58 m/sec at a depth of 119 m. The crossover point at which compensation starts to take place is located at a depth of approximately 120 meters. Snowbird STD Station 32 indicates the density field near the center of the eddy, while Snowbird STD station 21 was observed outside the eddy and indicates the mean conditions.

In T-S space, the occurrences of eddies are more easily noted by their anomalous thermal properties within the narrow temperature range of the upper few hundred meters. In the case of the Snowbird eddy(figure 27), the most outstanding feature of STD station 32 is the warm 'core' centered at 150 meters.

Hunkins(1974) on the basis of four eddies, indicated a 1 to 1 ratio between anticyclonic and cyclonic rotation. Newton et al(1974) made a more extensive survey of past high speed currents on the basis of current meter data. His analysis showed 7 anticyclonic and 1 cyclonic(88% anticyclonic). Unfortunately, the reliance upon current meter data can provide misleading information on the rotation of an eddy if the drift track is erratic.

Using the data listed in Table 3, the rotation of the individual eddies was re-evaluated using only hydrographic data. This method is easier and more reliable requiring only two stations, one inside the eddy and the other representing the mean conditions. If the isopycnals within the eddy are displaced away or constricted towards a central density surface that is not perturbed then the eddy is either anticyclonic or cyclonic respectively. Eddies that were observed only by current meters or that had inadequate hydrographic coverage were removed from the analysis. The results from this analysis(Table 3) still indicate a predominance of anticyclonic eddies by a ratio

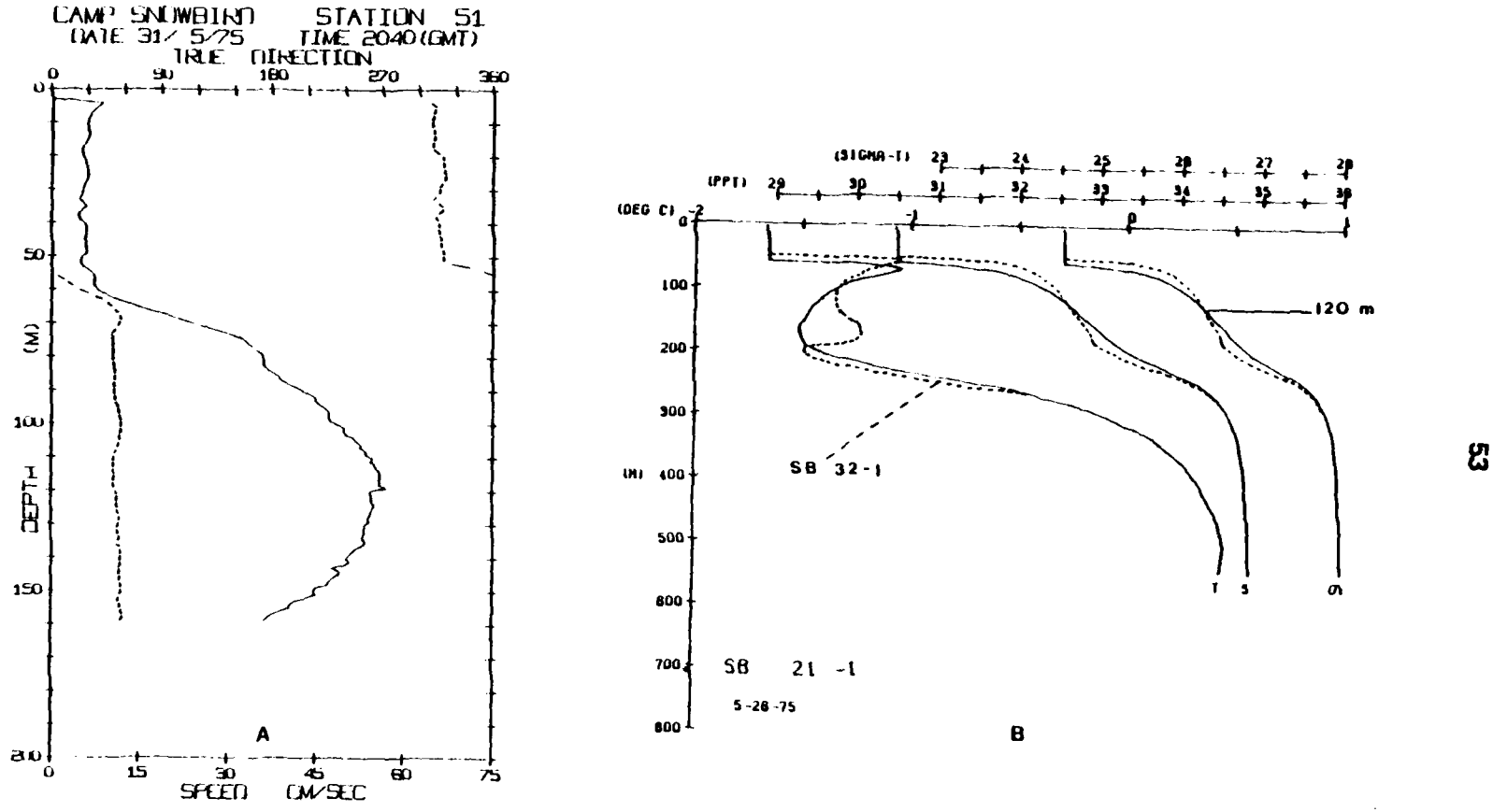


Figure 27. Vertical profiles of a) velocity and b) temperature(T), salinity(S), and density(σ_t) for eddy observed at Snowbird. Solid line in velocity profile is absolute speed and dashed line is true direction. b) Solid and dashed lines denote conditions outside and within the eddy respectively. Note warm core at 175 m. and inflection point in salinity at 125 m. which corresponds to the depth of velocity maximum.

of 5:2(71%).

Hunkins(1974) and Newton et al(1974) indicated that there was a possibility that the eddies observed during the 1972 AIDJEX Pilot Study may not have been formed from the local surroundings based on T-S data. Hunkins(1974) further suggested that baroclinic instability may play an important part in their production off the coast of Alaska. This was later reinforced by the work of Hart and Killworth(1976) which indicated that if baroclinic instability was the cause for the eddies observed in the Canada Basin, it must occur in shallower water and not in the open ocean. The relative merits of local and non-local origin will be discussed in more detail in a later section.

B. Eddies of the Other Oceans

The observation and understanding of mesoscale eddies has increased dramatically in the past several years. Reviews on mesoscale currents by the MODE group(1978), Robinson(1975), Koshlyakov and Monin(1978), McWilliams(1977), McLeish(1976), and McWilliams(1979) provide a great deal of information as well as further references on the mesoscale variability of the oceans.

A global picture of observations of surface as well as deep mesoscale eddies within the oceans as of 1976(Swallow) is shown in figure 28. The number of observations as well as the understanding of their importance in global circulation has rapidly progressed since the mid 1930's when Iselin(1936) observed an eddy north of the Gulf Stream.

More recently, eddies of the oceans have been likened to the atmospheric weather system possessing the familiar high(anticyclonic) and low(cyclonic) pressure systems(Hammond,1974). Using nondimensional comparison between the eddies of the ocean and atmosphere which takes into consideration the density difference between air and water, some of the more important similarities between the two systems are that - 1) Time and space scales are roughly equivalent assuming that the systems are governed by Rossby wave theory(McWilliams,1976). 2) They draw energy from the mean density distribution, transfer heat across large fronts, and transfer their kinetic energy back into the mean(Starr,1951; 1953; Webster,1961). 3) They posses higher energy than their respective mean flows. 4) They are nearly geostrophic and approximately circular. 5) They are widely distributed.

Dissimilarities between the two systems are also evident and indicate that the ocean eddies may play a major role in the general circulation as well as transfer of properties. Ocean eddies are dissimilar from their atmospheric counterparts in that: 1) They generally possess more energy(Hammond,1974). 2) They transfer(in addition to heat energy) salt, biomass, and other chemical

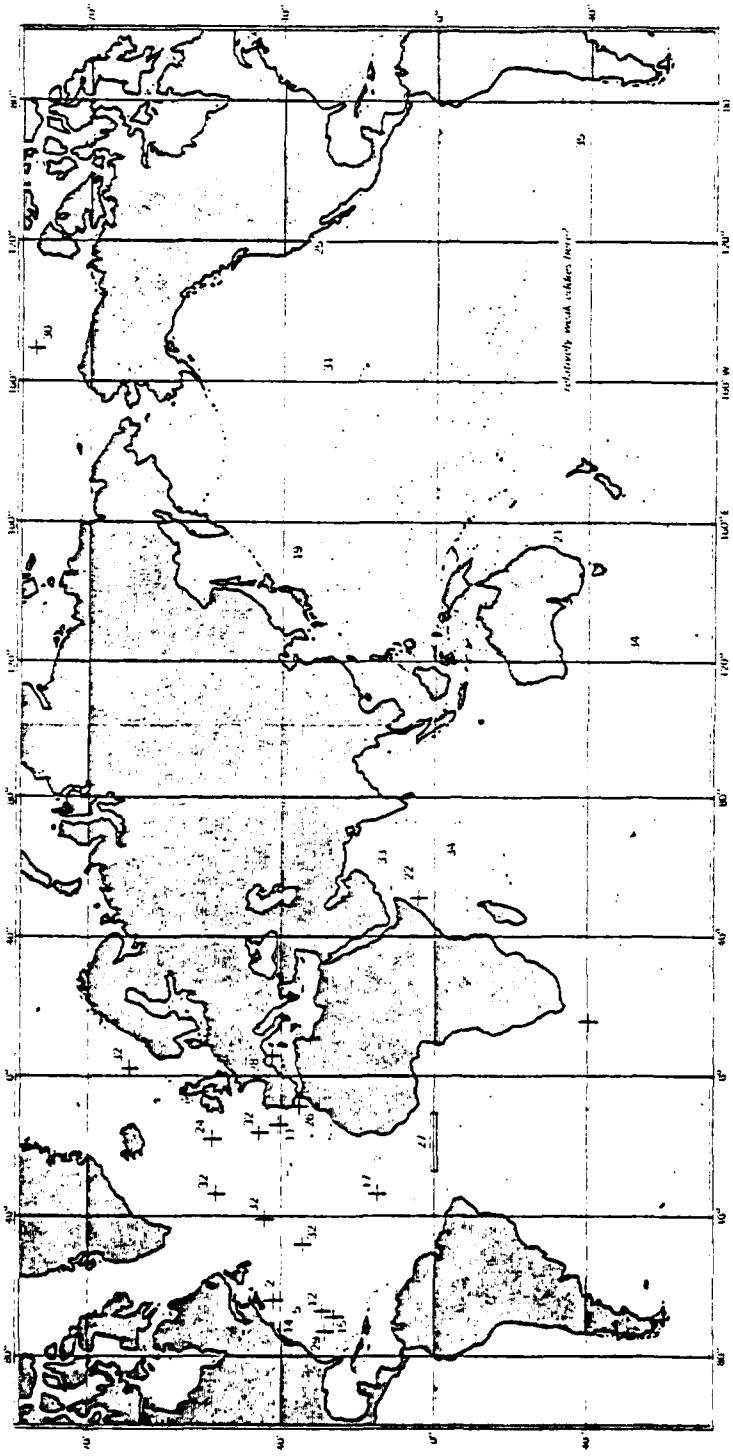


Figure 28. Positions of eddies(crosses) and variable currents(dots) observed in the worlds oceans.(Swallow, 1976)

constituents. 3) They move more slowly, usually passing over a given area in one to two months, as compared to one week for the synoptic pressure systems of the atmosphere. 4) They have a longer life expectancy, ranging from a few months to several(5 to 6) years.

Typical spatial scales of oceanic eddies vary from 10 to 300 km in diameter and a hundred to thousands of meters in thickness. Mid-latitude eddies are the largest with a typical aspect ratio(characteristic diameter divided by thickness) of 50:1 (200 km/4 km). Polar eddies such as the ones observed in the Arctic also have an aspect ratio of 50:1, however, are smaller with an average diameter of 10 km and thickness of 200 meters.

As previously mentioned, rotational velocities of the arctic eddies may be as high as .60 m/s. Mid-latitude eddies,however, may attain speeds reaching 1.50 to 2.00 m/sec, although mean speeds of .30 m/sec are more common. Being common features in the oceans, as well being more persistent and more energetic than their atmospheric counterparts, ocean eddies are now considered to play a major role in the dynamics of the general ocean circulation.

More detailed investigations of these mesoscale currents have been carried out in the North Atlantic with such large experiments as operation Cabot, (Fuglister and Worthington,1951), Polygon-70(Brekhovskikh, 1971; Fofonoff, 1976), MODE-1(MODE group, 1978), and Polymode (U.S.P.M.O.C.,1971). From the results obtained by the varying projects, two generally different types of eddies have emerged. The best understood of the two is the Gulf Stream Ring type. It originates in intense meandering and subsequent detachment of the closed meander associated with a western boundary current, such as the Gulf Stream or Kuroshio. The rings are classified as having three different water types within the local field of the eddy(Fuglister, 1971). Within the center of the ring is water of a type originating on the opposite side of the boundary current and is highly atypical of the surrounding conditions. The second water mass is

that of the boundary current itself which forms the rim of the eddy. The third water mass is the local surrounding water. An example of the formation of a Gulf Stream ring and the three differing water masses is shown in figure 29.

In the case of the Gulf Stream, anticyclonic rings that have broken off to the north or west of the Gulf Stream axis possess warmer more saline Sargasso Sea water in their core. Those that break off to the south or east are cyclonic and have cold less saline shelf water as their core.

Using an average of 13 rings per year formed by the Gulf Stream, Richardson(1976) estimated a cross-stream transport of 41 million cubic meters/sec which is approximately 30% of the Gulf Stream flow. Not only do Gulf Stream rings transport water across the Gulf Stream but also act as agents by which large volumes of water are transported to the South thereby augmenting the general return flow in the North Atlantic.

Gulf Stream Rings store approximately 95% of their energy as potential energy in the elevated thermal and salinity structures relative to the mean surrounding conditions (Parker,1971). The other 5% is accounted for by the kinetic energy(KE) of rotational movement. For a Bering Sea eddy, Kinder and Coachman(1977) estimated the relative importances of PE to KE to be 98.5 : 1.5 respectively. Using the amount of available potential energy stored within several Gulf Stream rings, Barrett(1971) was able to calculate an average decay rate of .005-.010 joules/m^2-sec for the Gulf Stream rings, indicating a life span of three to five years although it is more generally accepted to be one to two years due to re-entrainment of eddies back into the Gulf Stream(Richardson,1976).

In the Gulf Stream system, the warm core anticyclonic rings have a shorter life span of only 6 months because of their inevitable coalescing with the Gulf Stream along with their more restricted area of movement. Cyclonic rings also tend to coalesce with the Gulf Stream but usually after a longer

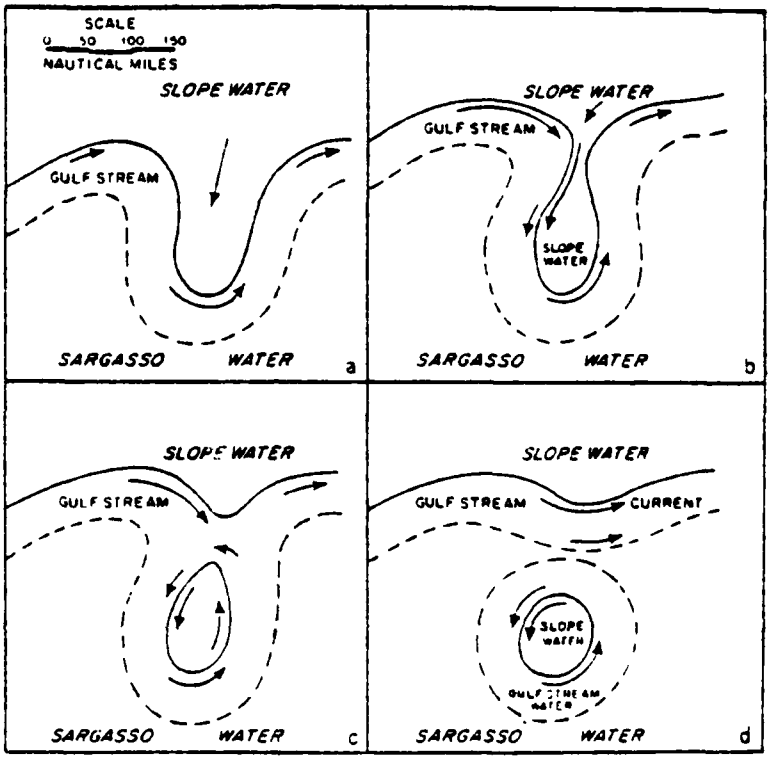


Figure 29. Diagram of ring formation from meander development(1a) to separation from the stream(1d). Solid lines represent the position of the 15 degree C isotherm at 200 m. Dashed lines represent the approximate limit of the Sargasso side of the Gulf Stream (Parker,1971).

period of time(1-2 years).

As previously mentioned, the amount of volume transport that the mesoscale rings provide across the Gulf Stream is relatively significant. Also of great importance is the role that they play in the transfer of energy, heat, salt, biomass, and other chemical constituents across what would normally be an impenetrable boundary current(Wiebe, 1976; Webster, 1961, 1964; Robinson, 1976).

The second type and least understood are the eddies observed in the central part of the oceans which are not of the ring class. Both cyclonic and anticyclonic eddies of this type are observed, however, their origin remains largely unknown. A typical example of such a feature would be the eddy which was observed during the Mid-Ocean Dynamics Experiment(MODE). The generating mechanism of baroclinic instability is the most attractive even though atmospheric forcing has been suggested (Philander,1978; Frankignoul and Muller,1979). The life span of these eddies is also unknown but is definitely greater than several months(Wunsch,1976).

Looking for the possibility of spatial variations of mesoscale features in the oceans, Dantzler(1976) and Wyrtki et al(1976) found that within the main gyres, there appear to be some areas that have high thermocline fluctuations and current velocities which are indicators of eddies. The areas possessing high amplitude fluctuations are near high intensity currents such as western boundary currents (Gulf Stream and Kuroshio) while lower amplitude oscillations are found near the centers of gyres and near weaker currents.

Eddies have also had a major impact on the ocean modeling of the global circulation even though in essence only a few of the essentials are known about them. Carl Wunsch(1976) summarized the topic well when he wrote:

> The notion of a slow, sluggish general ocean circulation driven directly by the climatological average winds and heating is gone forever. Most older models of

> **global circulation have been reduced to mathematical curiosities - interesting and useful as they were in their day, no one any longer believes that the oceans work like that.**

At the present level of understanding, mesoscale eddies appear to be ubiquitous features of the oceans. Their ability to transfer heat, salt, biomass, energy and other constituents along with a generally long life span gives them a special importance in the dynamics of the oceans. In a broad sense, there appear to be two major types of eddies - the rings which are formed from meandering of a high speed current such as the Gulf Stream or Kuroshio, and the eddies which are not of the ring class. Regardless of their nature or origin, relatively little is understood about them when compared to their atmospheric counterparts.

C. Criteria for the Selection of Eddies

During the 1975-1976 AIDJEX main experiment, approximately 3.5 years of manned-camp data were collected within a one year period. A total of 2084 profiling current meter stations and 1391 STD-CTD stations were obtained over this period of time. Even though the interstation spacing(100 km) was too large to map individual eddies in great detail, a number of anomalous events similar to that of previously documented eddies were observed. Due to the range in intensity of the anomalous events, criteria had to be found that would define the lowest acceptable limits for an anomalous feature to be classified as an eddy.

Both the profiling current meter data as well as the STD data were used in the search for observed eddies during the 1975-1976 main experiment. Initially, each data set was used independently of the other for the determination of these mesoscale features. Later the two separate findings would be combined together to provide a check between the different data sets. In this study, it is impossible to show all of the final PCM or STD data relating to these eddies, although a few of the better examples will be presented.

The criteria for the selection of eddies are based entirely on the previously documented eddies observed in the Arctic Ocean by Newton(1973), Hunkins(1974), and Newton et al(1974) and are as follows:

Profiling Current Meter Criteria

A) There must be a noticeable subsurface velocity maximum. The minimum acceptable speed of the eddy must be greater than .10 m/sec over the minimum velocity observed in the profile. This was done to remove the atmospherically-induced barotropic component of motion from the velocity profile to insure that only the eddy signature was analyzed. The barotropic component of motion can be considered a uniform flow field from the surface

to the bottom which is set up in response to the change in sea surface height due to changing atmospheric pressure or more importantly to winds.

B) The subsurface velocity maximum must be below the base of the mixed layer, thereby removing from consideration high speed events found in the mixed layer that are caused by wind and ice stress.

C) In order to define a continuous series of PCM stations observing the same eddy:

1) The subsurface velocity maximum must be observed at the same depth plus or minus 30 meters in all the profiles.

2) If the characteristic profile of the eddy is no longer seen in the PCM records after 25 hours from the time of the last observation, the series will be terminated at the time of the last observation. This will allow enough time for the ice camp to drift past the center of the eddy where currents are small or nonexistent.

3) If the eddy signature does reappear within 25 hours, the velocity maximum must be at the previous depth of plus or minus 30 meters.

4) In order to define the starting and ending dates for a particular eddy, other bounding PCM stations that had velocity maximums less than the accepted minimum were included in the eddy series provided that all of the above conditions could be met.

Salinity - Temperature Criteria

In the Arctic Ocean, salinity dominates the determination of σ_t; as a result, lines of constant salinity through time where used as the sole method for the determination of eddies. Figure 30 shows a typical example of a monthly plot of different isohalines plotted against depth and time used in the selection of eddies. The time base used during the AIDJEX Experiment and all subsequent publications as well as this study is known as the AIDJEX calendar.

This is a modified Julian Calendar with a starting date of January 1, 1975. Subsequent days are numbered sequentially to the 14th of May 1976(AIDJEX day 500). Appendix 1 is a conversion table that references AIDJEX days to the normal calendar days. The criteria for the determination of eddies based on STD data is given below:

A) The eddy must be compensated for, in salinity(density), at deeper levels.

B) The eddy may either be an expansion or constriction of the isohalines. An eddy must have at least one isohaline that has a vertical displacement of greater than or equal to 10 m with respect to the surrounding mean.

C) One station is enough to establish the presence of an eddy.

D) The beginning and ending limits of the eddy are determined subjectively when the data returns to the mean conditions.

E) In order for a series of STD stations to be considered as observing a single eddy;

1) No station within the series can be shown to have mean conditions which are determined subjectively.

2) If there is a break in the continuity of the data for any reason that is greater than 25 hours, the observation of the eddy is terminated. Any subsequent anomalous perturbations of the isohalines will then be classified a new eddy.

Criteria for the determination of the sense of rotation of an eddy

Sense of rotation of an eddy will be based entirely on the relative vertical displacement of the isohalines within the eddy as compared to the mean. The determination of rotation by PCM data becomes more and more ambiguous with an increasingly complicated drift track. It should be noted, however, that of the few cases where there was a clear definition of rotation by current meter

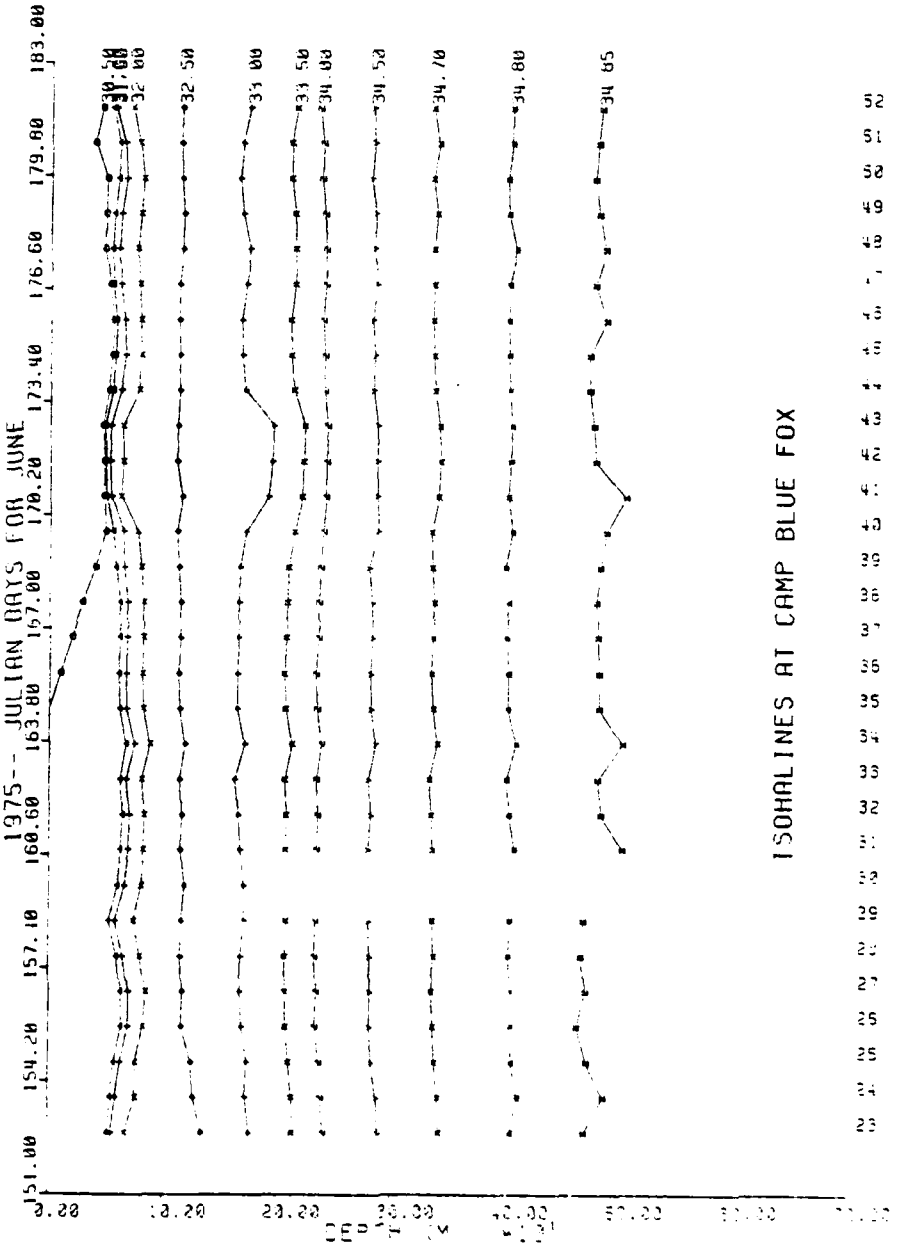


Figure 30. Plot of isohalines versus time in days. STD station numbers are at bottom of the plot.

data, there was no disagreement with the rotation obtained from STD data.

D. Classification of Eddies

Using the sets of criteria previously explained, the PCM and STD stations were grouped into observations consisting of one or more consecutive stations. The number of separately classified eddies for both the PCM and STD data are listed in Table 4 for each of the manned camps.

Table 4
Total number of PCM and STD eddies observed at each camp

CAMP	PCM EDDIES	STD EDDIES
Caribou	16	33
Blue Fox	42	30
Snowbird	36	35
Big Bear	22	22
Total	116	120

The observation of eddies by both PCM and STD are roughly comparable at all of the camps with the exception of Caribou which had a non-functional PCM directional sensor during the beginning of the project. With the break up and later evacuation of the main camp(Big Bear), the PCM that was operating at Big Bear was transferred to Caribou.

Separately classified eddies(PCM and STD) were then combined to provide a consistent picture of the number of individual eddies observed. Due to the sampling rate and the random down times of the sensors, as well as the relatively small horizontal scale of the eddies(10 km) , eight different correlations could be defined and are listed below.

Correlation Classification of Eddies

CLASS C(Correlated) eddies - Those eddys that were defined in both

the PCM and STD data at the same time and depth range.

CLASS P(PCM) eddies - PCM data provided the only indication of the eddy. STD was not functioning at the time or the nearest STD cast was too far away in either time or distance. Because of the small diameter of these eddies, it was felt that if a distance greater than 2 km(~25% radius) existed between the PCM and STD stations or a time difference greater than 2 hours, it was possible that the two stations may not be observing the same features and were therefore not forced to be correlated or uncorrelated.

CLASS S(STD) eddies - STD data provided the only indication of the eddy. PCM was not operating at the time or the nearest PCM cast was too far away in either time or distance. Eddies defined by STD may have also been too deep for the PCM to have observed. The PCM maximum depth was 200 m.

CLASS UP(uncorrelated PCM) eddy - PCM defined the eddy. However, STD provided no correlation. One or more STD stations were within the time and distance limits and showed no characteristics of an eddy signature.

CLASS US(uncorrelated STD) eddy - STD defined the eddy. One or more PCM stations were close enough in time and space to the STD data to have observed the same event, however, provided no substantiating evidence.

CLASS D(Deep) eddies - STD was the only instrument capable of observing these eddies. Only the upper portion of the eddy was observed. These eddies were anomalous in the isohaline field and required two consecutive STD stations to confirm the anomaly. The compensation of the features was not observed due to depth limitation of STD to 750 m. This is the only case where two consecutive STD stations are required to substantiate the eddy.

Although initially the criteria were explicit for the selection of eddies from both the PCM and STD data sets with respect to velocity and vertical

displacement of isohalines, correlation between the two data sets required a little more flexibility. These circumstances which occurred rarely were important for future statistical work and are described briefly in the following paragraphs.

The two different cases where this did occur were when either the STD or PCM data indicated an eddy but was not indicated by the other sensor. Upon closer examination of the other sensors data, an eddy was there; however, it was less than the required criteria described earlier. These stations were then incorporated into the data set of eddies and therefore appear not to have conformed with the initial criteria. These special cases were given the last two classifications of CPB and CSB which are explained below.

CLASS CPB(Correlated,PCM below criteria) - STD data defined the eddy. The PCM data did show a characteristic eddy signature; however, the maximum velocity was less than the minimum limits.

CLASS CSB(Correlated,STD below criteria) - PCM data defined the eddy. The STD data did show the characteristic vertical displacement of the isopycnals; however, the maximum displacement was below the minimum limits.

In physical reasoning, this was also acceptable, in that the eddies are small features with a diameter of approximately 10 km, and may not be mapped perfectly due to the time between successive observations and any time differences between stations of the two different sensors. Generally, there were two PCM casts for every one STD station except for the main camp where they were equal in number. If, in addition, the ice velocity was moderate to high(> .10 m/sec), one sensor may have picked up a good signature while hours later,the other sensor could have picked up a very weak signal or no signal at all.

E. Results and Statistics

Table 5 lists the results from the correlation of the two data sets.

Table 5
Number of eddies tabulated under the classification system at each of the manned camps.

	MANNED CAMPS				
CLASS	Caribou	Blue Fox	Snowbird	Big Bear	Total
C	11	22	22	13	68
CSB	3	4	7	4	18
CPB	0	0	2	0	2
P	2	18	5	5	28
S	18	5	3	4	30
UP	0	0	0	0	0
US	0	0	0	0	0
D	1	0	1	1	3
Total	35	47	40	27	149

The three deep eddies, which are shown between the heavy solid lines in figures 31,32, and 33, although classified, will not be considered in the statistical analysis of the eddies observed at the various camps. The reason for this choice is the unknown structure of these eddies. Even though the isohalines are appreciably displaced with respect to the mean surroundings ,(in what is considered to be the upper part of the eddy), information relating to the lower part of the eddy is lacking because no deep casts were taken during these time periods. Although conclusive proof cannot be shown to indicate that these deep events are truly eddies, there is no a priori reason for restricting the presence of eddies to the upper few hundred meters of the ocean. If they are, then compensation of the upper anomalous field may well extend down to 2000 meters.

It should also be stated that eddies are defined at all the camps by sequential observation through time. This classification system does not take

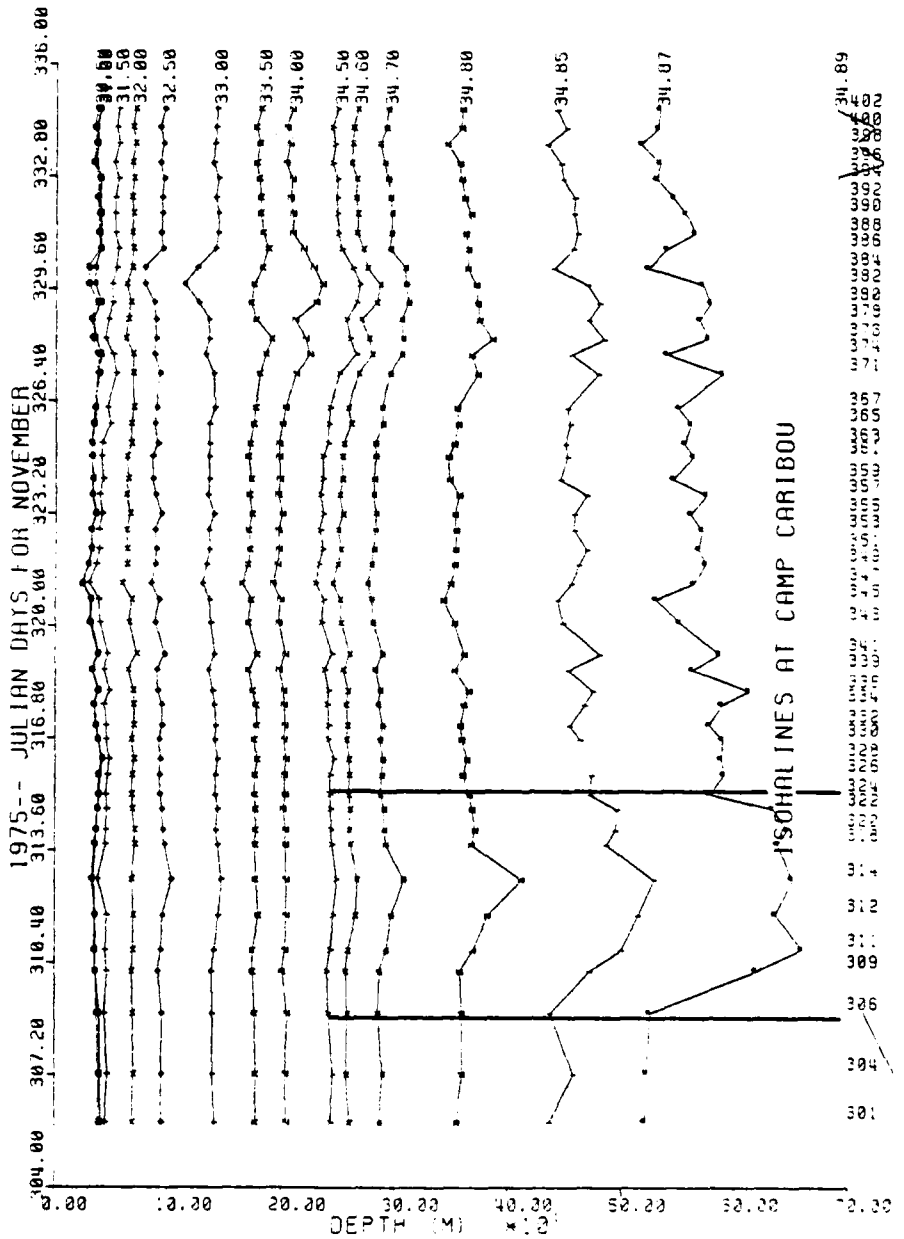


Figure 31. Deep event observed at Camp Caribou.

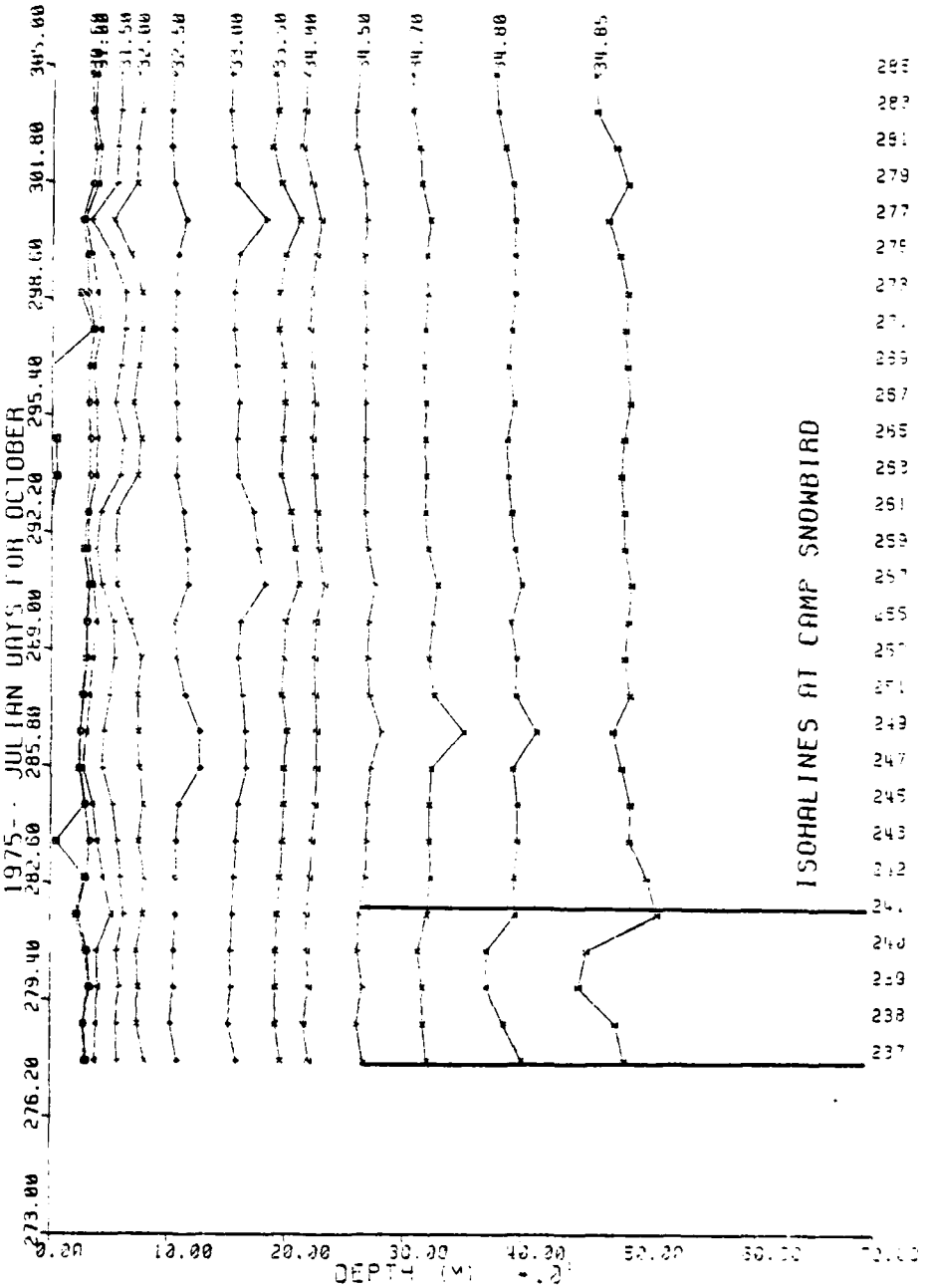


Figure 32. Deep event observed at Camp Snowbird.

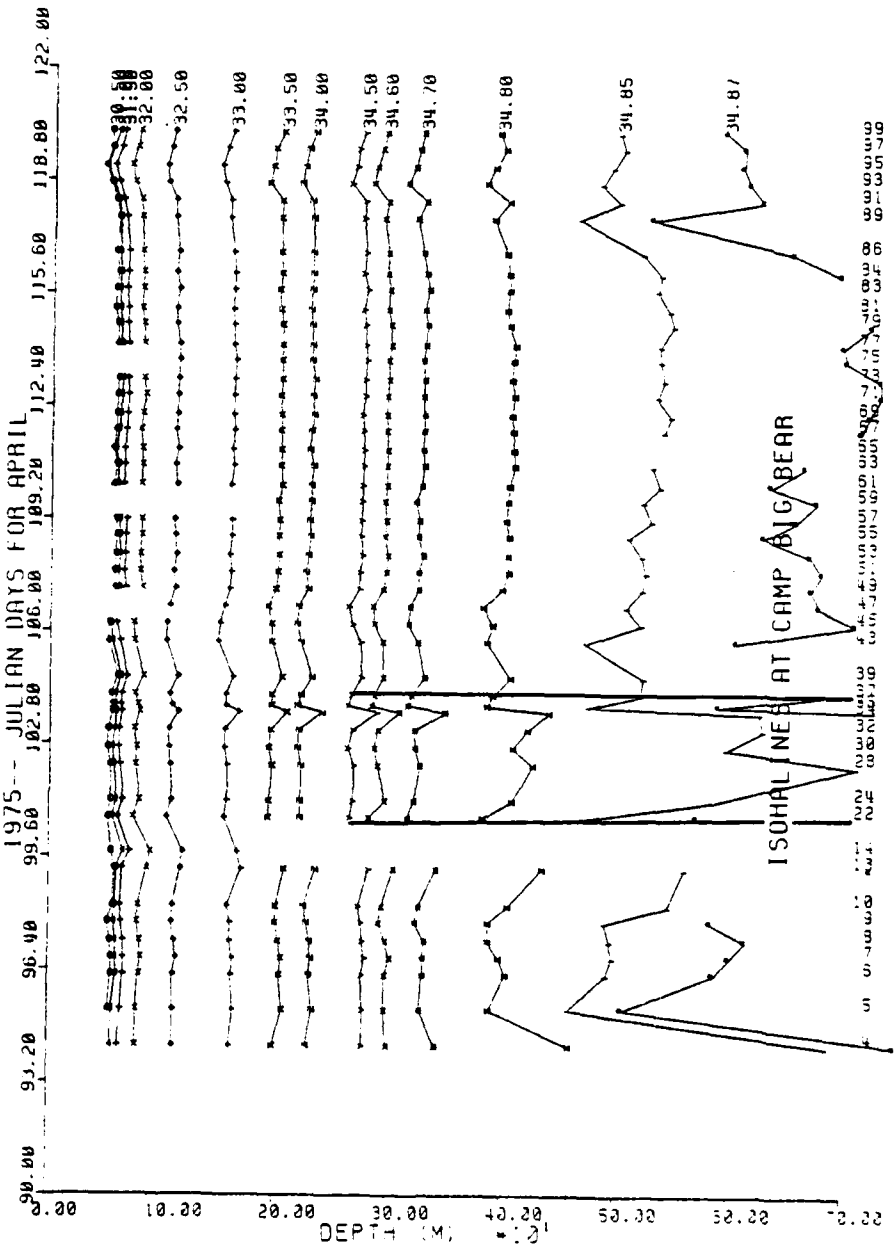


Figure 33. Deep event observed at Camp Big Bear.

into account that a particular eddy observed at ne camp could not have been observed one or more times at the same camp · at different camps. To study this problem, T-S signatures were used as a ıethod of "fingerprinting" by which an eddy may be classified as being obser :d more than once. Using this method, it became apparent that only eddies wi ı extremely unique T-S signatures could be used for tracing. Twelve eddies v :re observed more than once. Most of the duplicate observations were at the s ne camp where it was repeatedly seen within a short period of time. Other ddies spanned not only large periods of times but also were observed at c ferent camps. A total of 31 different observations comprised the 12 individ al eddies. The difference, 19 stations, would then bring down the total nu ber of individually observed eddies to 127. The duplicate observation of eddi s will be discussed more fully in chapter 5.

A number indicating the percentage of STD nd PCM data that were correlated out of the 146 separate eddies is difficult t give because a large number of the eddies, 59, were observed when the other instrument was not operating or had data that were too far apart in distanc or time. Of the 88 eddies in which both sensors were operating within the ıaximum allowable time and distance limits, none were shown to be uncor :lated. As mentioned before, the only event that was defined to be uncorrela d was done so because of the 8 day duration of the eddy, in which time, som indication should have been seen in the STD data. Including the uncorrela ed eddy a worst error of 1% would be indicated in the ability of the PCM and TD to correlate.

Eddies were observed throughout the expe ment on a somewhat regular basis. The only times in which eddies were not bserved for an entire month were February 1976 for Caribou, and March ar April 1976 for Blue Fox. All other months indicated a minimum of one edd observed at each camp, the maximum number of eddies observed being 11, which was at Blue Fox during

the month of September,1975. Figure 34 shows the number of eddies per month observed at each of the manned camps as well as the average and total number of eddies per month observed at Caribou, Blue Fox, and Snowbird. Eddies from Big Bear were removed from the cumulative total because it operated for only a part of the experiment.

An increase in the observation of eddies during the summer months is most likely a result of the increased movement of the pack ice when open water is more prevalent. In contrast to figure 34, figure 35 shows the number of eddies per 100 km traveled by each camp during a given month. As a result, the summer peak observance dropped dramatically. There is a constant level of about 2 eddies/100 km throughout the year. Table 6 lists the eddies observed and distance traveled per month at each of the camps. Partial months of observations were removed from this analysis.

Averaged over the duration of each of the camps, the number of observations of eddies per month ranged from a minimum of 3.0 at Caribou to a maximum of 4.4 at Big Bear. The average for all of the camps taken over the 40 months of observation was 3.6 eddies per month. This can be compared to the data of Hunkins(1974) who observed 4 eddies within a time span of 5 weeks and Newton et al(1974) who recorded 3 eddies over a period of 2 months. Table 7 lists the various camp averages of eddies per month as well as the total average taken over all 4 camps.

During the experiment, eddies were observed in 23% of the Profiling Current Meter stations and 30% of the STD stations. The average duration of each eddy was 1.7 days, the minimum being the observation by one station which lasts just a few hours. The maximum amount of time devoted to the continuous observation of an eddy was 10.0 days at camp Big Bear.

Of the eddies that were recorded by the PCM(<200 m), the maximum observed speed was .58 m/sec at camp Snowbird. The average velocity

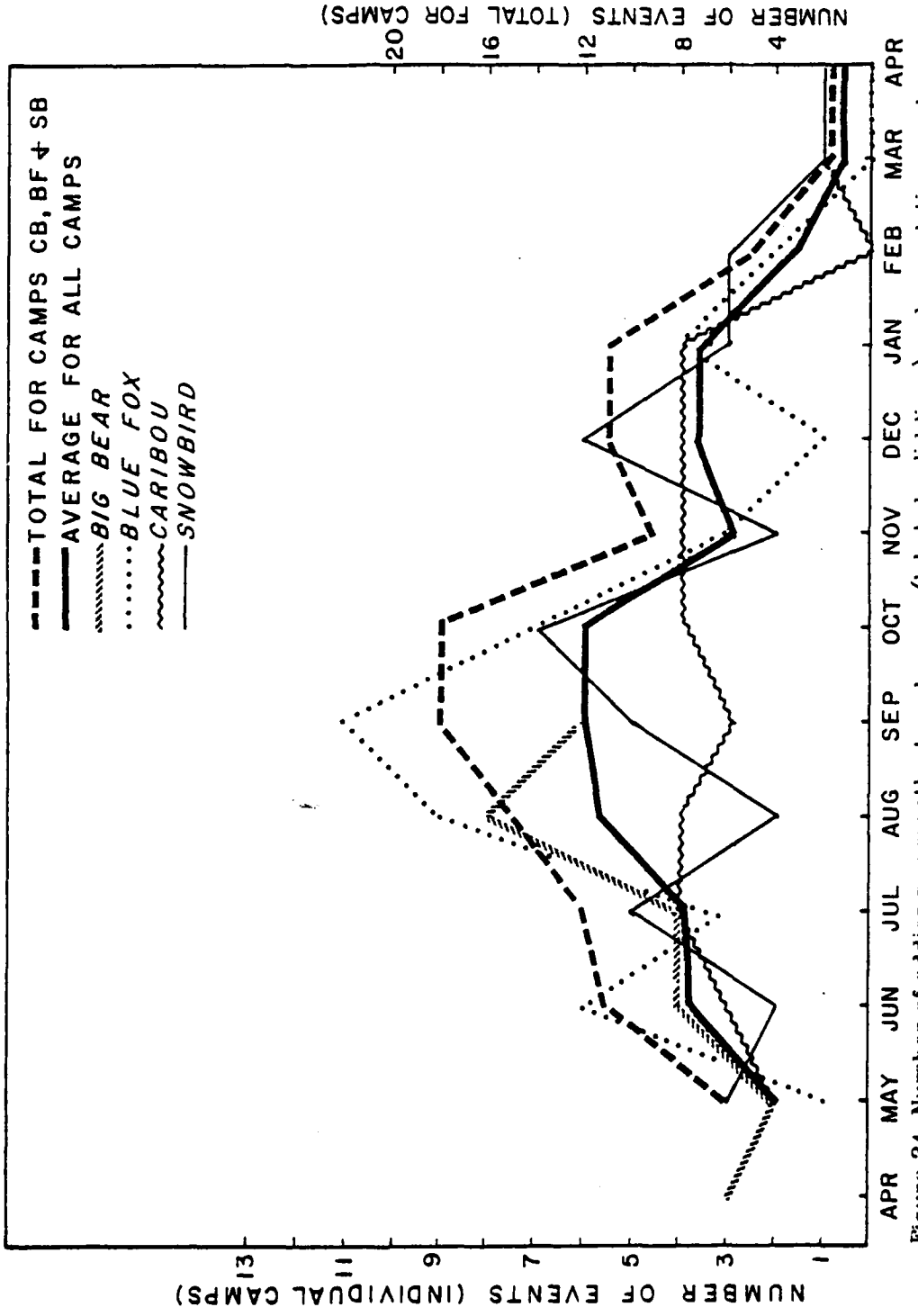


Figure 34. Number of eddies per month at each camp (labeled solid lines) and cumulative number for CB, BF, and SB in dashed line.

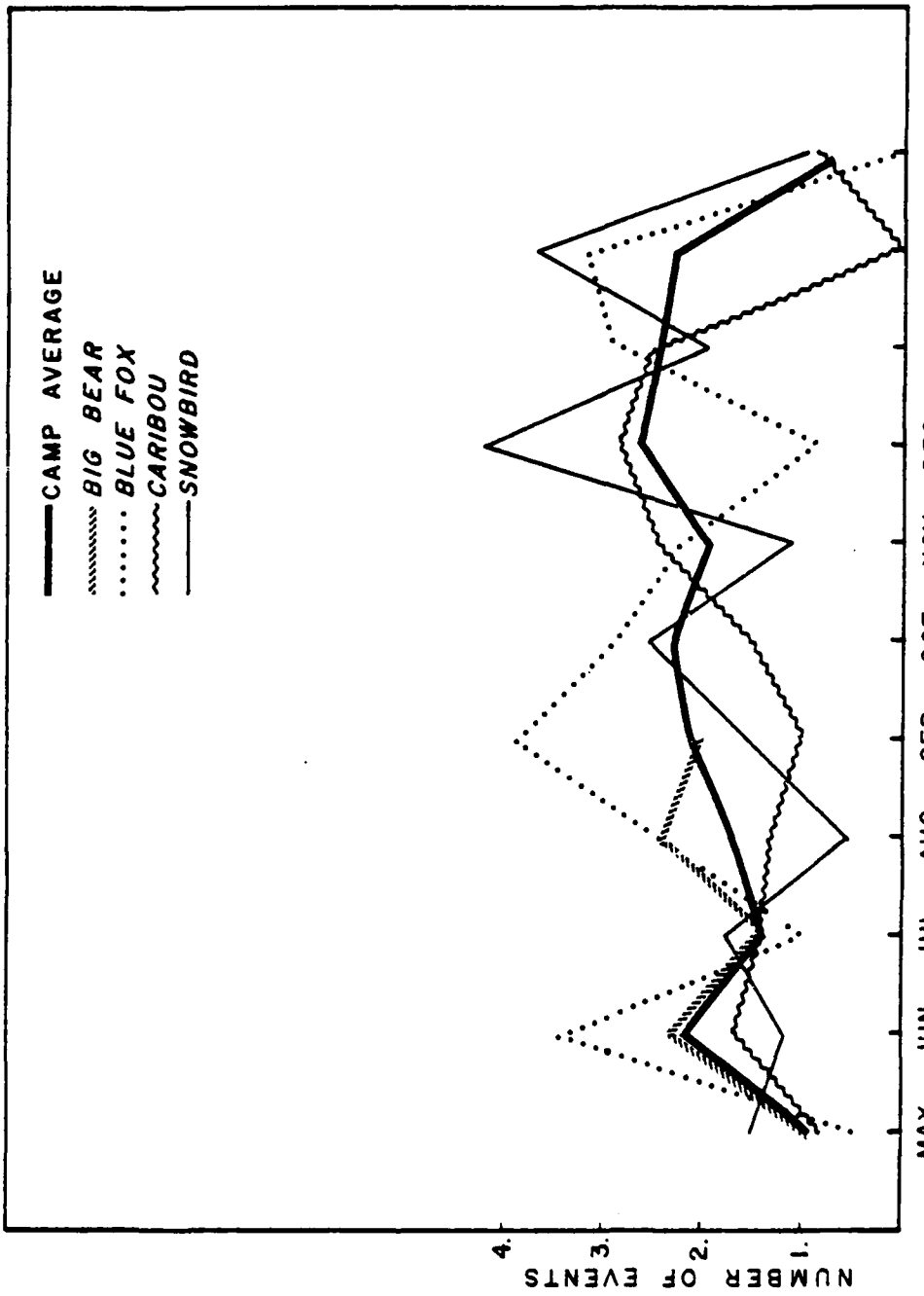


Figure 35. Number of eddies per 100 km of distance traveled along the drift track (labeled solid lines). Total camp average is dashed line.

Table 6 Monthly breakdown of the number of eddies(E), distance traveled(km), and eddies per 100 kilometers(E/100). Parentheses indicate totals.

	CARIBOU			BLUE FOX			SNOWBIRD			BIG BEAR		
	E	km	E/100	E	km	E/100	E	km	E/100	E	km	E/100
May-1975	2	205.8	0.80	1	182.7	0.55	3	200.3	1.50	2	196.7	1.02
June	3	177.2	1.69	6	172.5	3.48	2	170.0	1.18	4	173.5	2.31
July	4	277.2	1.44	3	292.9	1.02	5	284.4	1.76	4	291.0	1.37
August	4	301.0	1.33	9	362.8	2.48	2	347.0	0.58	8	333.7	2.40
September	3	293.9	1.02	11	283.2	3.88	5	322.9	1.55	6	294.4	2.04
October	4	261.2	1.53	7	244.2	2.87	7	271.9	2.57			
November	4	161.9	2.47	3	134.0	2.24	2	178.9	1.12			
December	4	141.9	2.82	1	119.6	0.84	6	141.7	4.23			
January-1976	4	159.3	2.51	4	140.0	2.86	3	151.7	1.98			
February	0	78.4	0.00	2	64.2	3.12	3	81.1	3.70			
March	1	107.9	0.93	0	61.6	0.00	1	105.2	0.95			
April	1	125.8	0.79	0	118.0	0.00	1	128.6	0.78			
AVERAGE---	(34	2291.5)	1.48	(47	2175.7)	2.16	(38	2383.7)	1.59	(24	1289.3)	1.86

Table 7
Number of eddies per month at each camp

Camp	Months of Observations	Number of Eddies	Eddies per Month
Caribou	11.4	34	3.0
Blue Fox	11.4	47	4.1
Snowbird	11.5	39	3.4
Big Bear	5.9	26	4.4
Total	40.2	146	3.6

maximum observed within an eddy for the entire experiment was .24 m/sec with a standard deviation of .10 m/sec. The depth of maximum velocity ranged from 31 to 200 meters with the average being 115 m.

The relative importance of anticyclonic and cyclonic eddies within the Arctic Ocean has been in question. As previously stated, estimates of the ratio of anticyclonic to cyclonic eddies varied from 1:1(Hunkins,1974) to 7:1 (Newton et al,1974) with the author's reevaluation of previous historical data being 5:2. During the 1975-1976 main AIDJEX Experiment, the sense of rotation was found to be dominantly anticyclonic(clockwise). Table 8 shows the rotation of the individual eddies at each of the camps based strictly on STD data. Those eddies that were classified as P, D, or UP are listed as having unknown rotation. Of the 98 individual eddies that were capable of being classified as to their rotation(duplicate observations removed), 97% or 95 of the 98 eddies were anticyclonic. A plot showing the positions of all of the eddies observed during the 1975-76 Experiment are shown in figure 36. Cyclonic eddies are circled.

This suggests a similar origin of these eddies. Because of this predominantly anticyclonic rotation, a swift current could be the source of the eddies within the Arctic Ocean and in particular the Beaufort Sea, as the Gulf Stream and Kuroshio are sources for the north Atlantic and Pacific. In contrast to that of the Gulf Stream, the current which is south of the observational site would

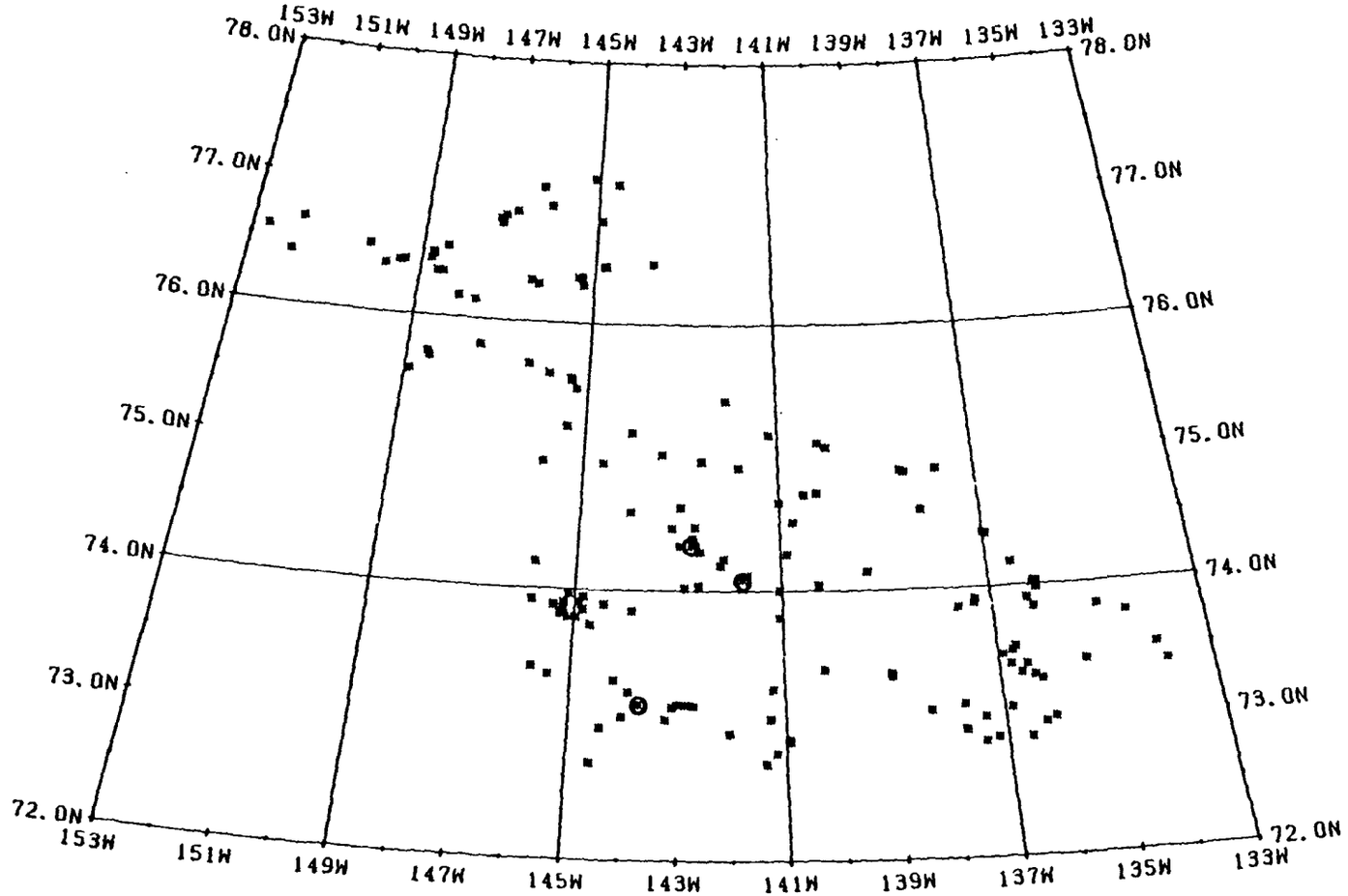


Figure 38. Positions of eddies observed during the main AIDJEX experiment. Sector area is the same as in figure 6.

Table 8
Sense of eddy rotation at each camp.

Camp	ROTATION Unknown	CW	CCW	Total	PERCENTAGE CW	CCW
Caribou	3	24	1	25	96	4
Blue Fox	17	28	0	28	100	0
Snowbird	6	25	2	27	93	7
Big Bear	6	18	0	18	100	0
Total	32	95	3	98	97	3

have to flow eastwards in order to produce the anticyclonic eddies that would be observed within the Arctic Ocean.

Prior to the 1975-76 AIDJEX Experiment, eddies of the Arctic Ocean were believed to be confined to the pycnocline region which lies between the mixed layer and 300 meters. The 1975-1976 AIDJEX data set indicates that a large majority of the eddies do reside within this depth range; however deeper eddies are observed. In several cases only the upper disturbance is shown by the STD data which goes to a depth of approximately 700 meters. A plot of the number of eddies observed within 50 meter intervals starting at 25 meters is shown in figure 37. Eddies are defined to be within a specific depth range provided that either the depth of maximum velocity within the eddy or the depth of the centrally neutral isopycnal(above and below which isopycnals are displaced vertically) is within the upper and lower limits of the given depth range.

As observed , a large majority of the eddies are centrally located within a depth range of 50 meters to 200 meters. In terms of water masses, this depth range is co-ocupied by the Pacific Water characterized by T-max and T-min layers which are believed to originate from Chukchi shelf waters. If the eddies are not formed locally within the Beaufort Sea, but rather advected into the Canada Basin from some distant origin as suggested by Hunkins(1974) and

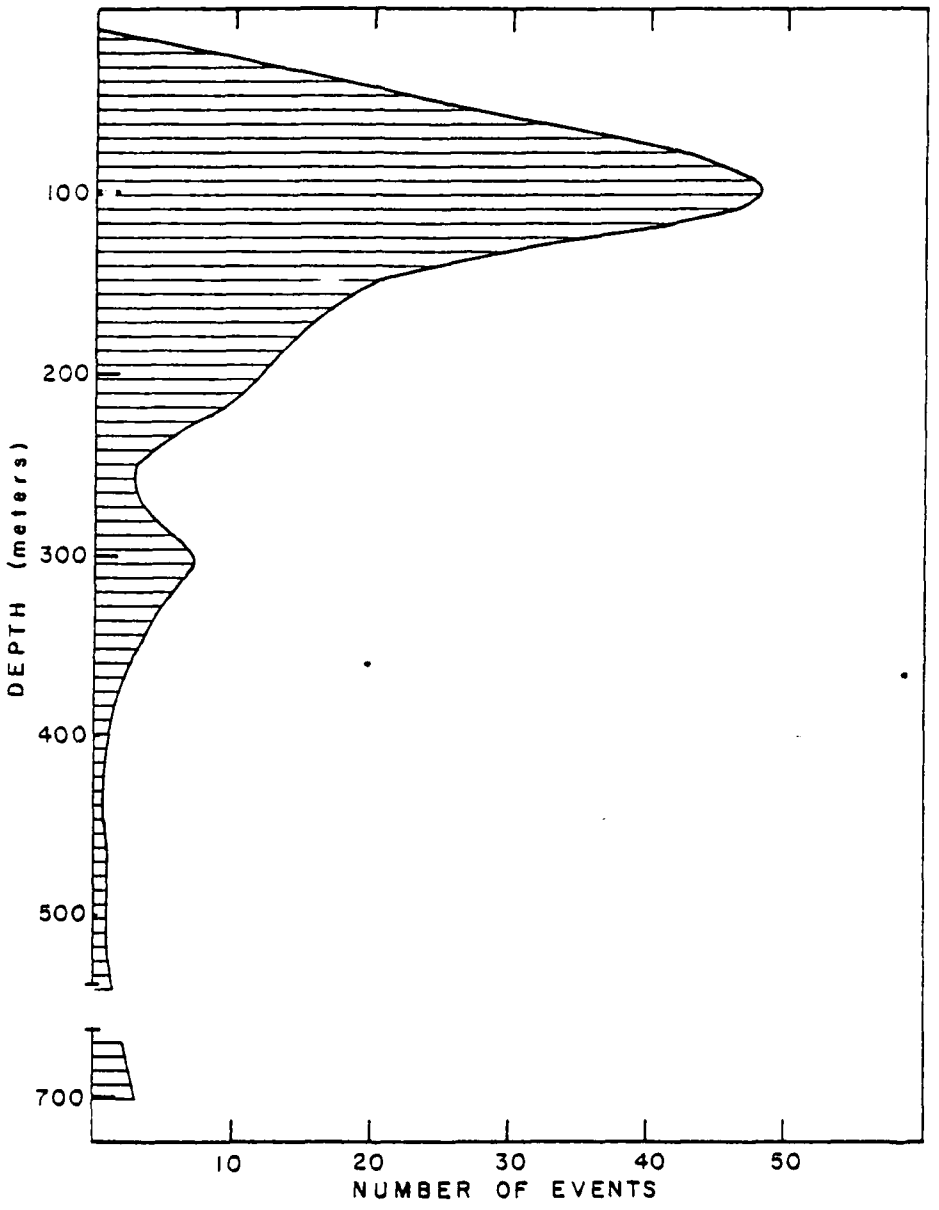
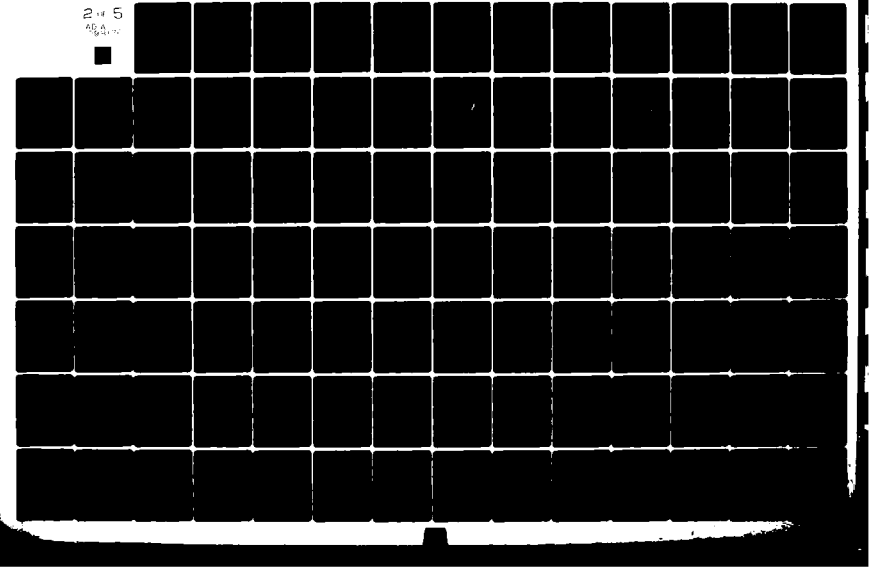


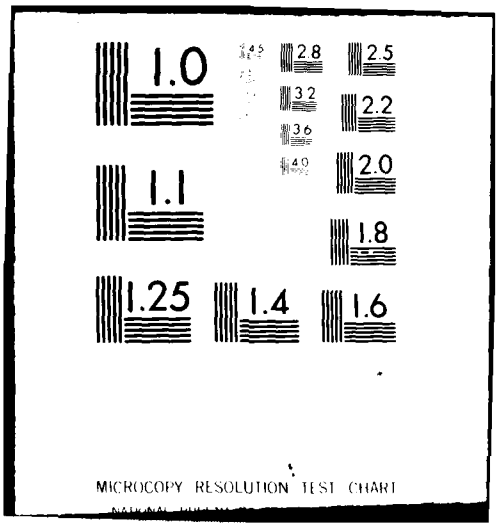
Figure 37. Total number of eddies observed as a function of depth.

Newton et al(1974), the Chukchi Sea and surrounding areas would be likely formational areas.

AD-A098 170 LAMONT-DOHERTY GEOLOGICAL OBSERVATORY PALISADES NY F/G 8/3
EDDIES OF THE WESTERN ARCTIC OCEAN - THEIR CHARACTERISTICS AND --ETC(U)
MAR 81 T O MANLEY N00014-76-C-0004
UNCLASSIFIED LDGO-CU-1-81 NL

2 of 5
AD A098170




1.0
2.8
2.5
3.2
2.2
3.6
4.0
2.0
1.1
1.8
1.25
1.4
1.6
MICROCOPY RESOLUTION TEST CHART

F. Origin of the Arctic Eddies

Historical data pertaining to eddies are rather limited(Table 3) and only hint as to possible mechanisms of their creation as well as their point of origin. In the light of the number of eddies observed during the main AIDJEX Experiment, new information will be provided that will help show the relative importance of the local and distant origin hypotheses.

Even though the data set does not allow for the observation of distant, in-place eddy formation, it does provide a unique data set to observe local formation, if any is present, over the total 3.5 years of manned-camp observations. Special characteristics of the eddies such as T-S properties, rotation, numbers and positions also indicate origins as well as possible mechanisms as to the origin and will be discussed later in greater detail.

The different suggestions as to the origin of the eddies and their respective formational mechanisms will be discussed in the next sections in more detail. Also to be discussed in these sections is how the data, both historical and current , bear out these hypotheses.

For the analysis of the eddies existing in the 75-76 AIDJEX data set, only those that were observed by the STD will be used. PCM data will be used but only if it is associated with STD data.

1) Local Origin; Atmospheric Forcing

Shirshov(as reported in Belyakov,1972) was the first to suggest that the high speed undercurrents in the Arctic Ocean were observations of "counter currents" which were set up as a compensating subsurface return flow resulting from a surface Ekman divergence. In response to the vertically displaced isopycnals, baroclinic flow would follow.

Browne and Crary(1958) also confirmed the role of local atmospheric forcing in producing counter currents at depths of approximately 150 meters while on Ice Island T-3. Unfortunately, they do not indicate absolute speeds of the observed counter currents and it is therefore difficult to say if a magnitude of .60 m/sec could by reached by this mechanism. More recently, other investigators(Chang and Anthes,1978), Frankignoul and Muller(1979), Harrison(1978), Leetmaa(1978), Longuet-Higgins (1975), Magaard(1977) and Philander(1978), have also suggested or studied the possibility of atmospheric forcing as the cause for the larger mid-ocean eddies. McWilliams (1979) indicates that if atmospheric forcing is indeed a cause of the mid-ocean eddies, it is a relatively minor one.

An immediate major drawback to the production of eddies by atmospheric forcing is that of scale. Synoptic weather patterns are on the order of 1000 kilometers, and wind-forced eddies would be expected to be on the same scale. The eddies of the Arctic, on the other hand, are two orders of magnitude smaller, making it unlikely that they are wind-forced.

Two other expected features of atmospheric forcing are also negative. The first is that since winds are fairly uniform over the Arctic Ocean, atmospheric forcing would imply a uniformity of eddies throughout the Arctic Ocean, and second, the T-S properties of the eddies themselves would not differ from the surrounding conditions. If the eddy is created locally within the ocean, then the resulting internal temperature and salinity field would show no anomaly with respect to the surroundings.

If the distribution of eddies within the Arctic Ocean is indicative of the frequency of observation within the various parts of the Arctic, then the historical data indicates the possibility of an asymmetry in the number of eddies observed throughout the Arctic Ocean, in that they are almost entirely confined to the Canada Basin. Of the 14 eddies that were observed within the

Arctic Ocean(Table 3) from 1937 to 1972, 13 were observed within the Canada Basin. The single eddy found outside the Canada Basin was observed by Shirshov in 1937 while on the Russian ice station North Pole-1(Belyakov,1972). Because of the difficulty in obtaining pre-war literature, the position of the eddy is unknown,however,the drift track of NP-1 is located within the Eurasian Basin of the eastern Arctic Ocean (figure 23). This asymmetry of the spatial observations of eddies is not an artifact of observations being taken only in the Canada Basin. From 1954 to 1970, there have been 19 Russian North Pole Exeriments, a majority of which have operated in both the Amerasia and Eurasia Basins. As reported in the available Russian literature, only 6 have been reported(Table 3), and all but one have been in the Canada Basin. Also of more recent note is the Fram I experiment which operated entirely within the Eurasian Basin(figure 6) for nearly six weeks. According to statistics from the 1975-76 AIDJEX experiment, roughly 5 eddies should have been encountered; however none were observed. Camp Iceman of the LOREX 1979 Experiment which operated over the Lomonosov Ridge for approximately six weeks also saw no signs of eddy signatures in the data taken(Pounder,1980).

Within the historical data there is very little information regarding the temperature and salinity structure of those eddies. Only during the 1972 AIDJEX pilot project were there enough detailed observations to indicate that these eddies were not created from the local surrounding conditions(Hunkins,1974; Newton et al,1974). Figure 38 shows the anomalous T-S field within the 3 eddies observed by Newton et al,1974) superimposed on the local T-S envelope of the 1972 AIDJEX Pilot Study area. The hatched areas indicate the envelope of the 60 m(on the left) and the 270 m(on the right) observations excluding the three eddies. No observations in T-S space showed that the eddy was similar to the surrounding mean, although it was suggested that in relation to the T-S envelope of the entire Beaufort Sea, the eddies would

not be indicated as anomalous. This indicates the possibility that the eddies may indeed be locally generated, but after their formation would move with the mean geostrophic field into areas of the Beaufort Sea where they would appear as anomalous structures.

Using only the eddies within the main AIDJEX data set that were classified according to T-S properties, maximum deviations in temperature and salinity were tabulated for each eddy with respect to a station outside the eddy representing the local surrounding mean conditions. Maximum deviations in salinity were calculated using levels of constant depth. Delta values were calculated using equation 2.3.

$$\Delta S = S_{eddy} - S_{mean} \qquad (2.3)$$

where:

ΔS is the salinity difference observed at depth D,

S_{eddy} is the salinity observed within the eddy at depth D, and

S_{mean} is the salinity observed at a selected station outside the eddy which best represents the local surrounding mean field.

Temperature deviations, however, were calculated along lines of constant salinity which are very close to lines of constant density. Delta values were calculated using an equation similar to that of 2.3 except that temperatures at a defined salinity (density) were used rather than a geometric depth. Temperature and salinity differences less than or equal to 0.04 degree C and 0.02 ppt respectively were considered to be within the average statistical error limits of the C/STD data at all of the camps. Statistically, some camps(depending on the processing and the sensor involved) had much better error limits. The above mentioned limits were chosen to represent the mean errors for two reasons - 1)Interpolation between data points was frequently used to provide estimates of ΔT and ΔS, which in itself produces errors and 2) Time lag between the eddy and mean stations may induce some subtle temperature or salinity differences. Also recorded, while using the ΔS analysis, was the depth of the

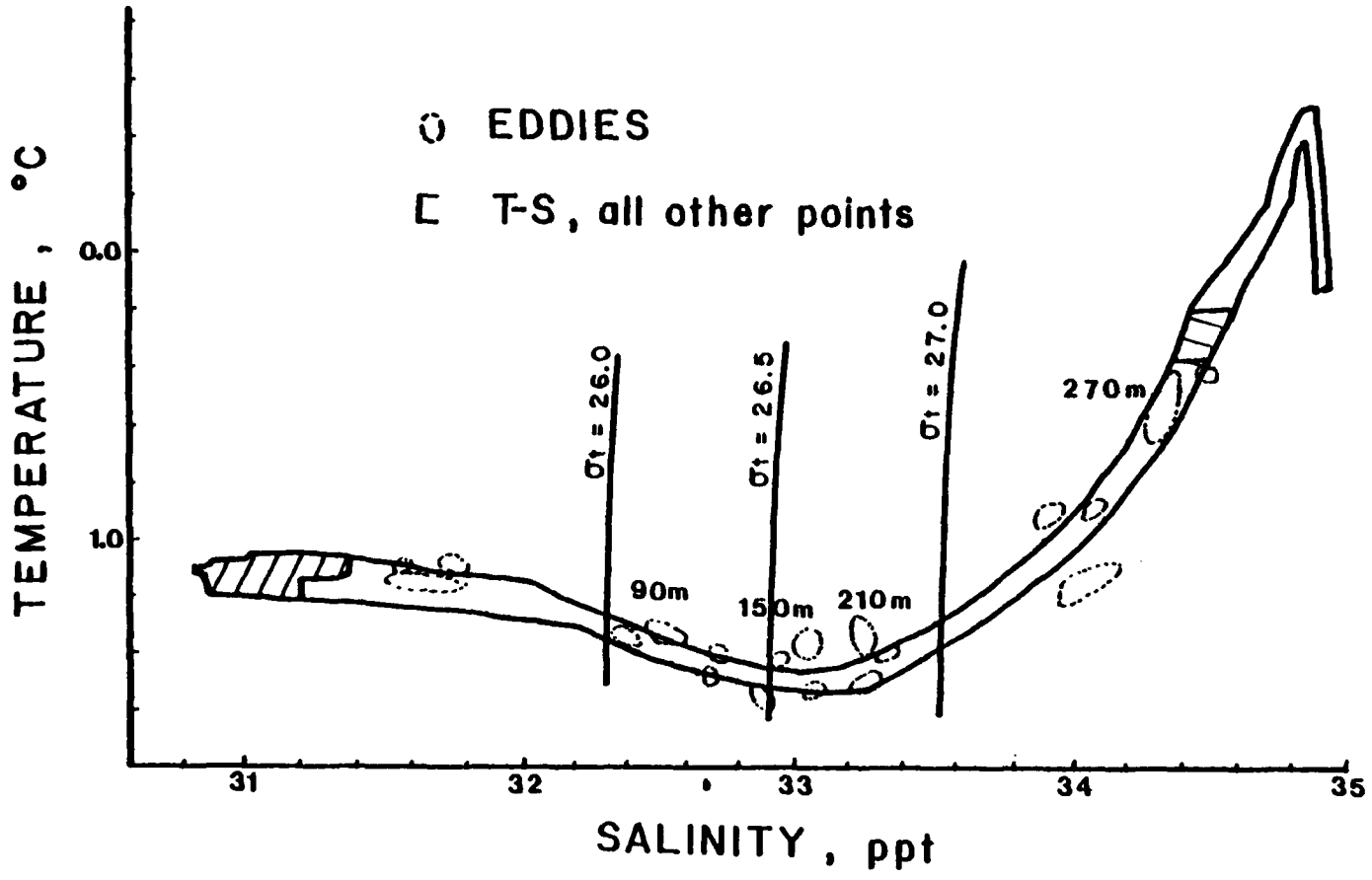


Figure 38. Temperature and salinity characteristics of eddies observed by Newton et al(1974) during the 1972 AIDJEX Pilot Study superimposed on the average temperature-salinity envelope for the area of study(redrawn from Newton et al,1974).

neutral salinity surface(salinity inflection point,figure 27), and the depth of the bottom of the eddy. The bottom of the eddy was defined as the depth at which differences in salinity were less than 0.02 ppt or where there was a local minimum in the ΔS values at a depth below the salinity inflection point.

Both temperature and salinity differences were calculated at roughly 5 meter intervals from the surface to approximately 700 meters. Because many of the eddies were observed to have differing thermal properties between the upper and lower half(figure 42; discussed in more detail in section 3. Distant Origin), maximum differences in temperature and salinity were calculated on a two-layer basis where the depth of the salinity inflection was defined to be the division mark. The resulting maximum deviations and the depths at which they were observed at are shown in Tables 9a,b,c,and d.

Data from Table 9 indicate 12 eddies that had temperature differences less than or equal to 0.04 degree C. Although the presence of these eddies does suggest that they are of local origin, another valid possibility is that they are eddies which are in the last stages of decay. If all 12 eddies were defined to represent local formation, this would account for only 9% of the 127 individual eddies during the main experiment(duplicate observations removed).

Table 9

Maximum observed differences of temperature and salinity in the layer above and below the salinity inflection point. Differences were calculated using the most anomalous STD station within the eddy and a station representing the local surrounding conditions. Temperature differences are computed along lines of constant density. Salinity differences are computed along lines of constant depth. STN is the station number representing the eddy. ΔT and $D_{\Delta T}$ are the maximum temperature difference and its corresponding depth respectively. ΔS and $D_{\Delta S}$ are the maximum salinity difference and its corresponding depth respectively. Infl is the depth of the salinity inflection point. D_{max} is maximum observed depth of the eddy. Tables 9a,b,c, and d correspond to camps Caribou, Blue Fox, Snowbird, and Big Bear respectively. Blanks imply temperature differences that were below the general background noise previously mentioned. Negative values imply eddy cores that are colder or less saline than the surrounding mean. Positive values imply eddy cores that are warmer or more saline that the mean.

Table 9a
Camp Caribou

	ABOVE INFLECTION					BELOW INFLECTION				
STN	ΔT	$D_{\Delta T}$	ΔS	$D_{\Delta S}$	Infl	ΔT	$D_{\Delta T}$	ΔS	$D_{\Delta S}$	D_{max}
27			1.00	55	95			-0.10	140	210
31			0.94	55	125	-0.07	145	-0.32	190	125
35			0.13	265	335	-0.10	405	-0.04	465	595
69			0.77	55	125			-0.18	170	265
93			1.19	60	120			-0.31	190	255
102			0.23	195	229	-0.10	286	-0.15	285	340+
124			0.72	55	115			-0.22	205	270
126	0.08	180	0.20	145	185	0.15	225	-0.50	245	405
140	-0.06	80	0.47	60	90	-0.06	115	-0.18	130	250
156			0.56	70	130	-0.07	200	-0.43	215	260
163	0.23	75	0.67	60	85			-0.22	115	185
187	0.05	105	0.47	55	115	0.05	130	-0.36	205	340
203			0.94	30	95	-0.15	140	-0.25	155	250
235	0.11	190	0.47	55	195	-0.31	275	-0.39	250	410
246	0.11	190	0.42	65	195	-0.25	271	-0.41	260	415
252	-0.18	115	0.62	60	120	-0.28	147	-0.35	180	220
271	-0.09	80	0.31	55	82	-0.16	100	-0.15	120	160
289	0.13	55	0.44	30	55	0.13	70	-0.34	80	120
300			0.04	140	305			-0.02	410	570
314	-0.08	51	1.16	35	87			-0.21	90	175
384	0.17	151	0.23	110	185	0.15	196	-0.33	220	305
432	0.13	151	0.35	65	177	0.13	225	-0.53	225	330
446	0.10	181	0.31	160	200	-0.08	235	-0.31	250	335
476	-0.05	185	-0.21	220	322			0.03	390	480
480	0.11	190	0.19	160	192	0.17	213	-0.32	220	310
500	0.11	150	0.24	120	192	0.14	220	-0.39	235	345
559	0.08	155	0.14	130	156	-0.11	220	-0.09	205	230
676			0.28	65	96	0.08	200	-0.14	135	290
804	0.05	185	0.11	180	195	0.05	213	-0.12	215	255

Table 9b
Camp Blue Fox

	ABOVE INFLECTION					BELOW INFLECTION				
STN	ΔT	$D_{\Delta T}$	ΔS	$D_{\Delta S}$	Infl	ΔT	$D_{\Delta T}$	ΔS	$D_{\Delta S}$	D_{max}
20	-0.12	215	0.20	180	219	-0.39	270	-0.24	265	445
23			1.25	60	102			-0.19	130	195
29			1.05	60	120			-0.04	160	200
43	-0.10	87	1.06	55	117	-0.07	157	-0.32	190	315
48			0.32	55	97			-0.11	205	275
54	0.05	75	1.14	60	115	-0.06	120	-0.25	160	240
57	-0.05	50	0.09	10	60	-0.13	70	-0.30	65	90
82			0.61	25	56	-0.26	75	-0.30	75	115
86	-0.14	135	0.22	75	140	-0.20	160	-0.32	205	295
96			0.72	25	65	-0.10	75	-0.23	95	290
100			0.99	25	57	-0.27	75	-0.30	70	110
102	0.06	90	0.47	55	97	0.08	128	-0.23	150	325
114			0.52	25	44	-0.28	75	-0.30	80	140
124	-0.08	70	0.37	45	102			-0.11	155	210
130			0.24	40	57	-0.37	75	-0.40	80	240
140			0.33	40	60	-0.31	71	-0.21	70	105
142			0.20	55	107	-0.05	206	-0.12	175	220
180			0.80	35	60	-0.17	70	-0.25	80	150
208	0.10	62	0.45	55	102	-0.19	141	-0.32	160	320
228	0.11	70	0.18	55	90	-0.09	127	-0.25	140	250
238	0.11	176	0.24	70	192	0.14	230	-0.38	250	410
246	0.09	71	0.24	75	89	-0.06	190	-0.17	145	220
272			0.63	35	40	-0.11	46	-0.30	85	160
290	0.06	200	0.13	215	296			-0.03	365	465
324	0.06	71	0.22	75	91	-0.18	110	-0.22	125	200
338			0.04	220	275			-0.05	320	395
378	-0.11	186	0.18	200	235			-0.05	255	350
382			0.08	195	247			-0.04	280	315

Table 9c
Camp Snowbird

	ABOVE INFLECTION					BELOW INFLECTION				
STN	ΔT	$D_{\Delta T}$	ΔS	$D_{\Delta S}$	Infl	ΔT	$D_{\Delta T}$	ΔS	$D_{\Delta S}$	D_{max}
3	-0.07	155	0.64	60	160	-0.16	190	-0.31	230	355
19			0.55	60	157	-0.05	185	-0.07	222	305
32	0.07	120	1.11	55	122	0.26	170	-0.30	215	360
66			0.35	55	127	0.26	195	-0.13	230	305
86	-0.10	480	0.12	235	500			-0.16	580	700+
94			0.68	65	127			-0.29	197	290
104			0.04	175	197			-0.14	255	312
112	-0.05	255	0.12	230	287	0.07	435	-0.04	405	590
122	0.05	256	0.29	215	295	0.06	345	-0.06	380	700+
136			0.44	75	134	-0.09	187	-0.43	220	335
184			0.91	55	110	-0.06	162	-0.24	185	270
196			0.15	45	59	-0.17	70	-0.13	70	85
206			0.50	25	54	-0.40	70	-0.36	75	100
234	-0.06	100	0.33	45	102	-0.11	145	-0.18	150	215
241			0.79	25	34	-0.10	65	-0.39	55	115
247	-0.20	50	0.44	50	75	0.06	87	-0.26	115	285
249			-0.06	320	440	-0.09	526	0.01	560	615+
259	0.16	70	0.66	55	100	-0.06	220	-0.24	155	245
277	0.18	70	0.69	50	94	-0.09	235	-0.43	210	235
328			0.16	55	82	-0.10	200	-0.16	110	325
334	0.06	121	0.31	65	145	-0.07	225	-0.25	200	260
348	0.30	105	0.56	60	107	0.38	115	-0.38	200	300
354			0.14	175	190	-0.08	240	-0.20	210	255
378	0.05	78	0.51	55	86	-0.11	186	-0.20	120	185
392	0.08	70	0.69	45	86			-0.14	115	135
412	0.25	105	0.46	55	109	0.30	120	-0.22	180	265
422	-0.07	105	0.33	70	110	-0.17	151	-0.17	162	242
482	0.05	92	0.32	75	147			-0.06	165	185
492			0.70	45	87			-0.06	135	190
521			0.36	35	46	-0.05	70	-0.26	85	135

Table 9d
Camp Big Bear

	ABOVE INFLECTION					BELOW INFLECTION				
STN	T	$D_{\Delta T}$	S	$D_{\Delta S}$	Infl	T	$D_{\Delta T}$	S	$D_{\Delta S}$	D_{max}
4	0.07	267	0.12	225	275	0.17	506	-0.06	560	700+
105			1.08	55	152	-0.05	255	-0.25	225	372
255	0.27	143	1.28	60	120	-0.17	245	-0.51	215	375
281	0.29	126	1.15	60	135	-0.08	220	-0.45	225	365
349			0.33	230	332	0.08	490	-0.04	415	685
357	-0.08	290	0.23	205	355	-0.11	690	-0.04	660	700+
427	0.05	71	1.12	60	122	-0.05	300	-0.38	190	350
436	-0.06	176	0.76	70	196			-0.40	245	305
451	-0.15	70	0.81	35	75	-0.28	80	-0.21	90	100
457	0.10	73	0.70	70	109	0.06	113	-0.26	140	190
469	-0.05	81	0.31	55	132			-0.09	230	245
477			0.79	25	54	-0.13	71	-0.22	75	140
491	-0.07	70	0.19	70	95			-0.15	160	210
513	0.06	71	0.38	50	136			-0.35	200	290
530	-0.15	115	0.55	60	117	-0.17	146	-0.22	165	210
562	0.12	70	0.24	70	87	-0.08	110	-0.16	130	185
590	0.05	170	0.28	65	97			-0.10	130	182

Casual examination of the eddy and ice velocity data does not show any obvious correlation between the two. Spectral analysis of the data was not useful in that the PCM data were not taken at regular intervals in space or time, and hence it would have been difficult to extract any meaning. A typical example of the comparison between ice velocity and the currents at four different levels within the upper 200 meters is shown in figure 39. The eddy was observed at Big Bear between AIDJEX days 157 and 169 starting at 50 meters and extending to depths greater than 200 meters. The velocities observed within the eddy field are substantially higher than ice velocities and bear no correlation with them.

In general, the arctic eddies show themselves to be transient features with little correlation with the wind even though there is some indication that a few of the eddies may have local origin.

2) Local Origin; Brine Convection

Another method for local generation of eddies is intense haline convection during the winter caused by the rapid growth of sea ice from open water. It is believed that the resulting brine convection would perturb the upper part of the pycnocline, creating a horizontal flow centered around the disturbance.

The major fault with this mechanism is that of scale, but in the opposite sense to that of atmospheric forcing. Leads within the permanent pack ice region of the Arctic Ocean are generally on the order of 100 meters or less in width and 10 to 100 times as long. Any feature created on this space scale would be two orders of magnitude smaller than the typical diameter of an eddy which is 10 km.

Brine convection within the open Arctic Ocean has also not been shown to exist below a depth of 50 to 60 meters which is the maximum limit attained by the mixed layer during the main AIDJEX Experiment. Therefore, if brine

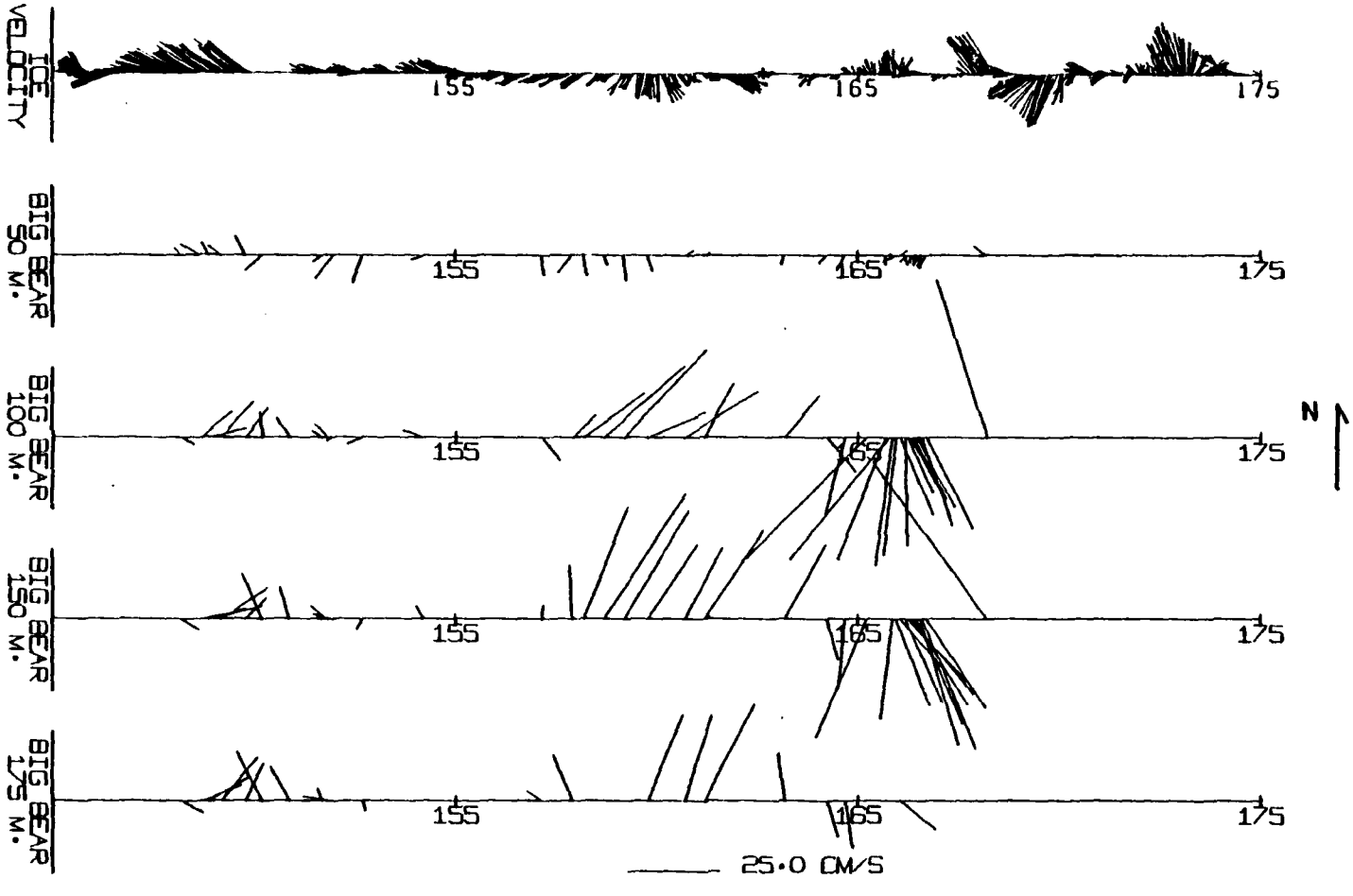


Figure 39. Stick diagram showing the ice velocity and current velocity at four different depth levels from Camp Big Bear. Horizontal axis is time in days.

convection were considered to be a valid mechanism, only shallow(< 70 m), small diameter features with cold cores would be observed. Although a few of the eddies within the main AIDJEX data set do comply with two out of the three criteria(shallow, cold), their actual diameter is unknown.

If the eddies do originate by brine convection, there should be a seasonal variation. Freezing of open water would be at its maximum during the beginning of the winter season, and as a consequence the production rate of eddies by brine convection should rise dramatically. During the remainder of the winter and early spring, production rates would drop significantly. In the summer, when open water does not freeze, the production rate would go to zero. The observation of the number of eddies observed per 100 km traveled during any given month(figure 35) does not show this pattern to exist, but rather a general constant observation rate of nearly 2 eddies/100 km.

In summary, intense brine convection has several major discrepancies pertaining to the production of eddies. The first is that features produced by such a mechanism would be 2 to 3 orders of magnitude smaller than the typical diameter of an eddy. Second, brine convection has not been shown to extend deep enough to account for eddies greater than 50 to 60 meters. Third, brine convection can only account for cold anomalous temperatures near the freezing point. Warm core eddies can not be produced by such a mechanism. Fourth, the beginning of the winter months should be the maximum production rate of brine induced eddies; however, the number of observed eddies per month does not support this. In effect, the role that this mechanism plays in the production of eddies can be considered extremely minor.

3) Distant Origins

Distant origin of the arctic eddies, suggested by both Hunkins (1974), Newton et al(1974) and Dixit(1978), was based on the anomalous T-S

characteristics of eddies relative to their surroundings(figures 38). As previously indicated, 91% of the eddies observed during the main experiment were anomalous to their surroundings. This implies without question that the vast majority of arctic eddies are created in an area or areas that have temperature and salinity characteristics which are different from those in the area where the eddy was found.

One of the best examples of an eddy observed during the main AIDJEX Experiment was taken at camp Snowbird and has previously been discussed by Dixit(1978). Figure 40 shows the current vectors at 130 meters superimposed on the drift track of the camp. This eddy also had the highest recorded velocity of .58 m/sec. The diameter of the dashed circle is 15 km and does not imply the diameter of the eddy but rather a reference by which the diameter may be estimated. Anticyclonic rotation is apparent.

Figure 41 shows the structure of the salinity field along the drift track during the same Snowbird eddy shown in figure 40. The characteristic movement of the isohalines away from a centrally neutral surface (32.6 ppt) indicates anticyclonic rotation. Figure 42 shows the thermal structure of the same eddy. Notice that the anomalously warm water resides in the lower half of the eddy, while there is almost no thermal anomaly in the upper layer. The reason for this type of apparent multilayer thermal structure within the eddies is most likely a result of the decay mechanism and will be discussed in a later section.

The T-S plot of the Snowbird eddy with respect to the mean conditions outside the eddy is shown in figure 43. The internal core of the eddy is highly anomalous with respect to the surrounding mean, 0.26 degrees C warmer than the corresponding temperature at the same density level. A group of selected eddies from the 1975-1976 data set are also shown in figure 44.

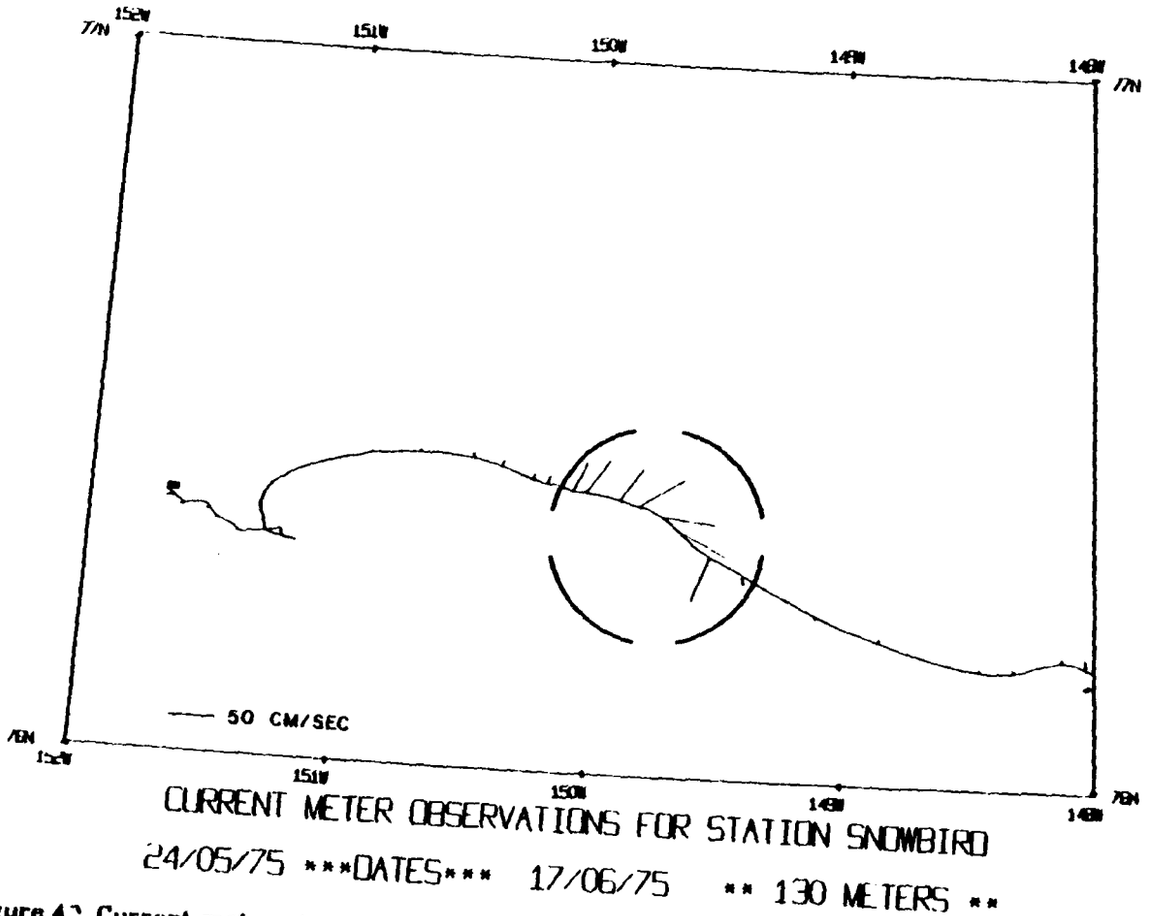


Figure 4?. Current meter observations for Camp Snowbird at a depth of 130 m. along its drift track.

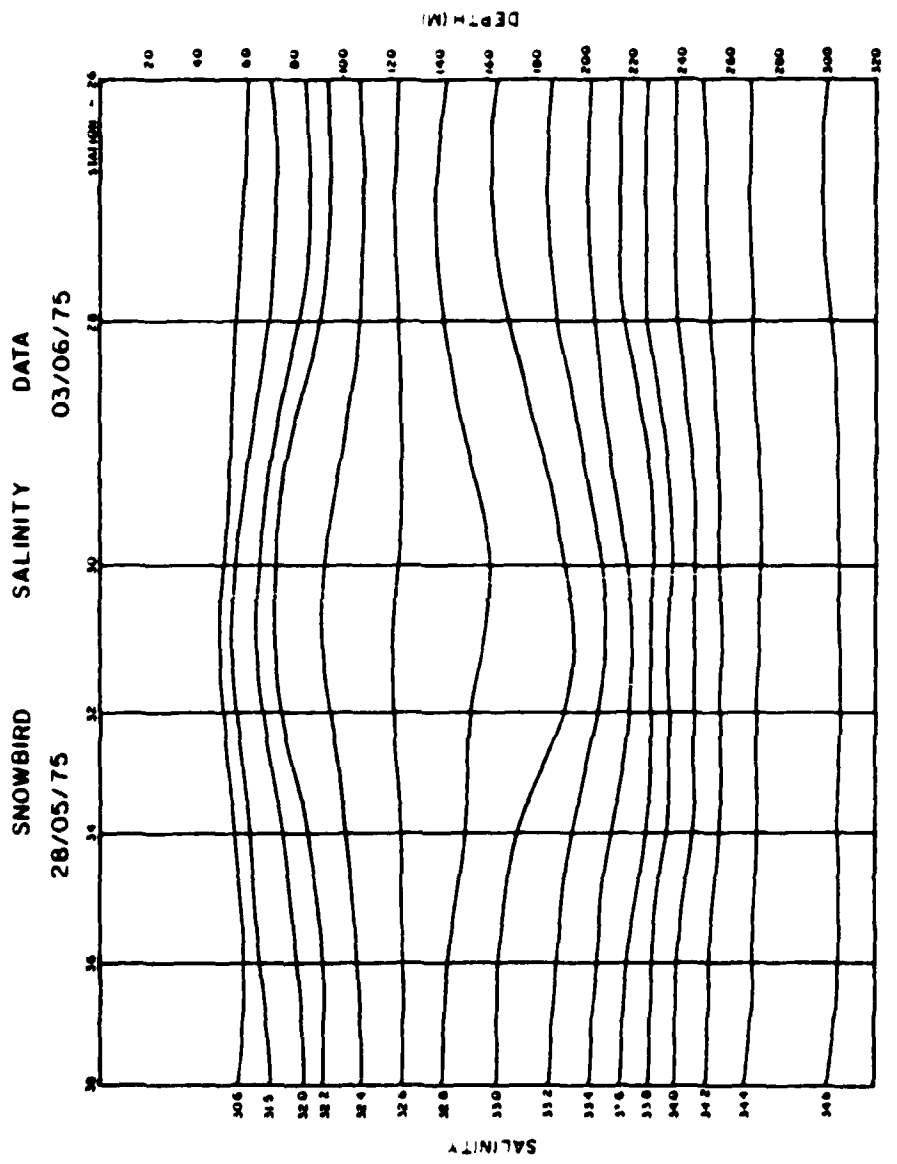


Figure 41 Vertical cross section of the isohalines along the drift track of Snowbird corresponding to figure 39.

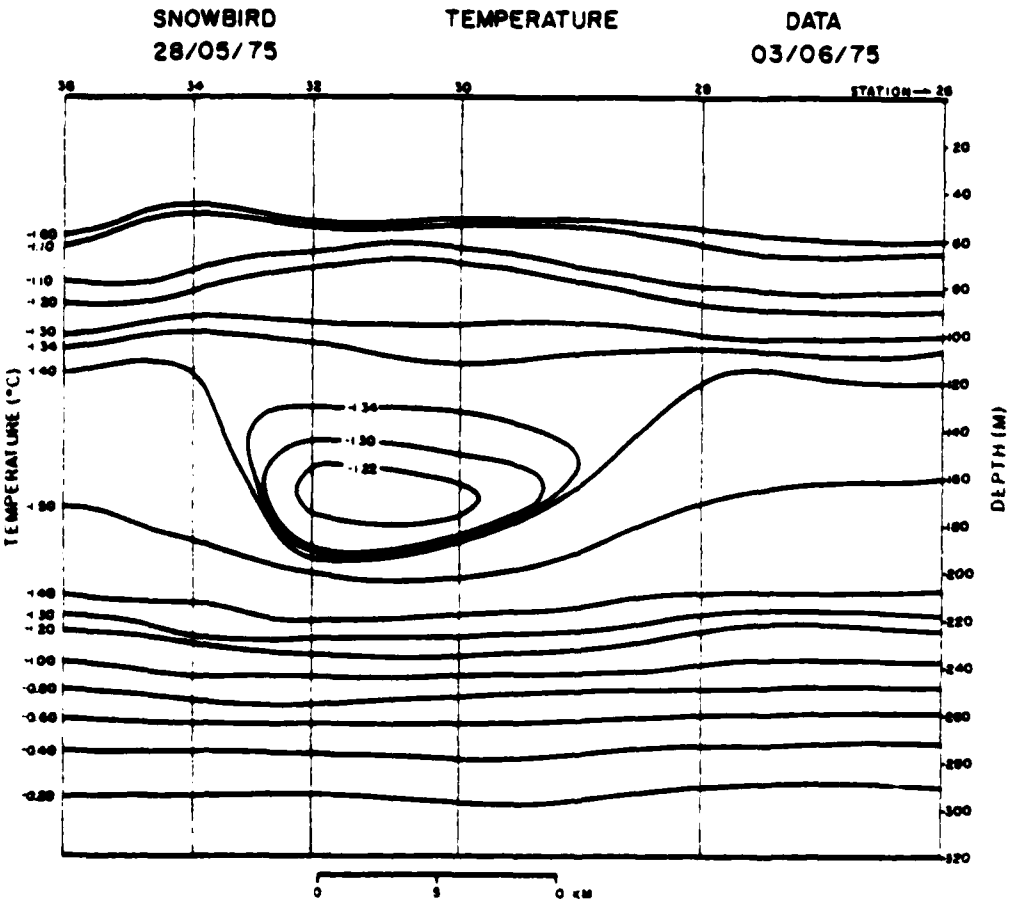


Figure 42. Vertical cross section of the isotherms along the drift track of Snowbird corresponding to figure 39.

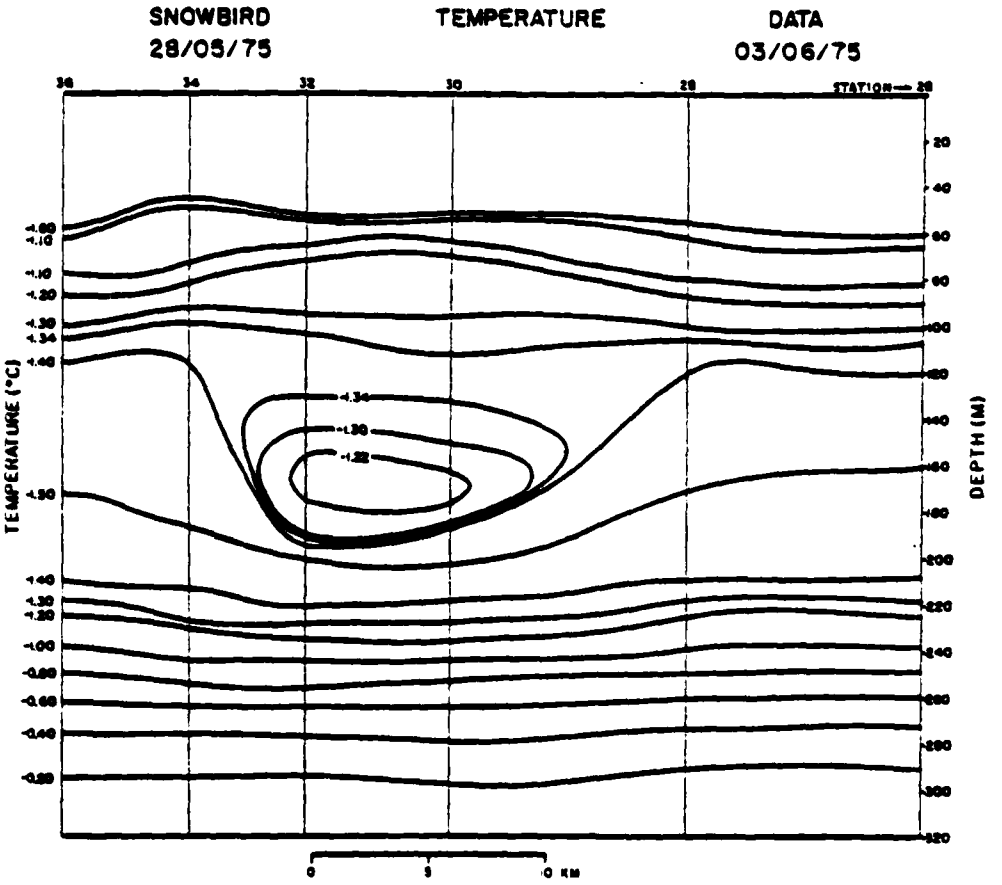


Figure 42. Vertical cross section of the isotherms along the drift track of Snowbird corresponding to figure 39.

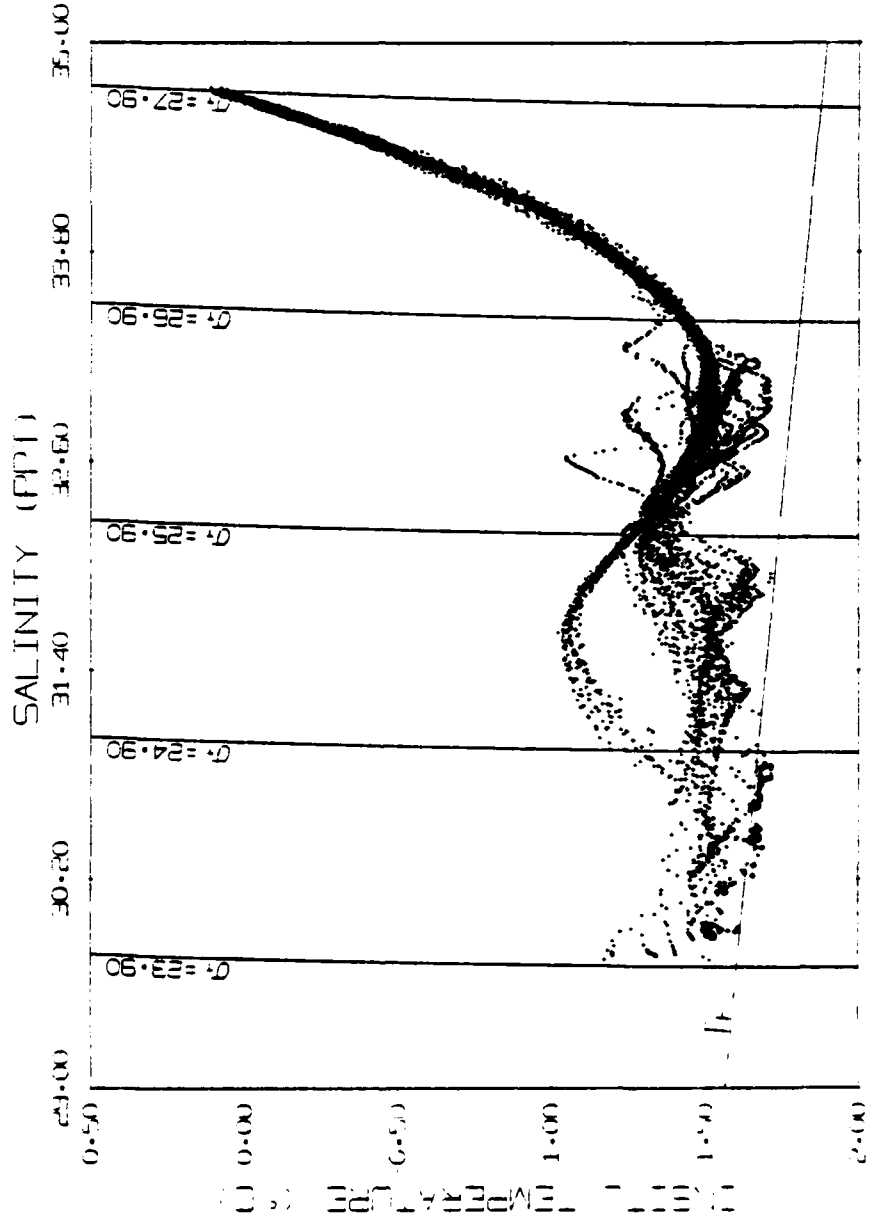


Figure 44. T-S diagram of selected eddies observed at the various camps during the main AIDJEX experiment. T_f denotes the freezing point line.

On the basis of baroclinic instability, Hunkins(1974) suggested that the central Beaufort Sea was not an optimal area for the generation of eddies due to the very low vertical shears and extremely long growth rates of approximately one month. Observations suggest that the flow field is more baroclinically unstable and had faster e-folding times of a few days near the current axis north of Point Barrow, Alaska(Hunkins,1974). Hart and Killworth(1976) also reinforced this hypothesis, but stated explicitly that the origin of eddies would be more likely in shallow depths of the continental shelves or near slope areas.

Hunkins(personal communication) has completed more work on the baroclinic instability near Point Barrow, as well as in the major frontal zone between Spitzbergen and Greenland. Results indicate that over the slope region in the Point Barrow vicinity, e- folding times of the fastest growing wavelength(eddy diameter 60 km) would be on the order of two weeks. The STD profiles used in the calculation of geostrophic shear were located on the continental slope in water depths ranging from 500 to 1500 m. In the frontal region of the eastern Arctic between Greenland and Spitzbergen, where warmer, more saline Atlantic Water flows into the Arctic Ocean as the West Spitzbergen Current, and cooler, less saline water flows out as the East Greenland Current, the fastest growing wavelength was of a smaller scale(eddy diameter of 25 km) with roughly the same e-folding time as north of Point Barrow.

Using T-S data for the eddies observed in the Beaufort Sea during the 75-76 AIDJEX Experiment, a composite set of profiles was made possessing the maximum anomalies. Available data from ship cruises within the Chukchi and East Siberian Seas as well as the surrounding coastal regions of Alaska during the summer and early fall were used to see if there was any correlation with the eddies of the Arctic.

From the shelf-slope data, the range in temperature and salinity is more than enough to provide the typical core characteristics within the arctic

eddies. During the summer months, temperatures at the surface may be as high as 12 degree C, while at the bottom they may be at or close to the freezing point. During the winter months when there is ice covering all of the shelf, temperatures throughout the water column are very close to the freezing point.

In the particular set of data taken during the October 1-5, 1984 Northwind cruise(Cook,1986) along the shelf and slope break north of Alaska, the envelope of selected stations corresponded remarkably well to the maximum and minimum temperatures of the selected eddies shown in figure 44. Figure 45 shows the T-S envelope of the data taken near the Alaskan Coastal Current North of Point Barrow. This ,however, indicates only summer conditions where surface waters become very warm. During the transition to winter conditions, this envelope would migrate towards colder temperatures finally becoming almost synonymous with the freezing line(T_F).

The warm and cold cores of the eddies seen within the Arctic Ocean can be accounted for by the changing thermohaline conditions of the shelf water throughout the year. For example, a typical cold core eddy would form during the late fall, winter or early spring when the entire water column is close to the freezing point. Warm core eddies, however, must be created within the summer months when temperatures on the shelf or near the shelf have sufficiently high temperatures to appear anomalous to the mean conditions of the Arctic Ocean.

Temperature may be an excellent indicator of shelf conditions; however, salinity controls the density of the water masses and hence determines the level at which intruded water will lie. According to data collected within the shelf areas of the Chukchi Sea and Alaskan Shelf areas, salinities range from a few ppt in the surface during the summer when melting of shelf ice and continental runoff are prevalent, to 34.99 ppt(Aagaard and Tripp,1978; SCOR,1979). Salinities of 34.99 ppt are extremely high and are also very rare for shelf conditions and represent a density high enough to sink to the bottom of the Arctic

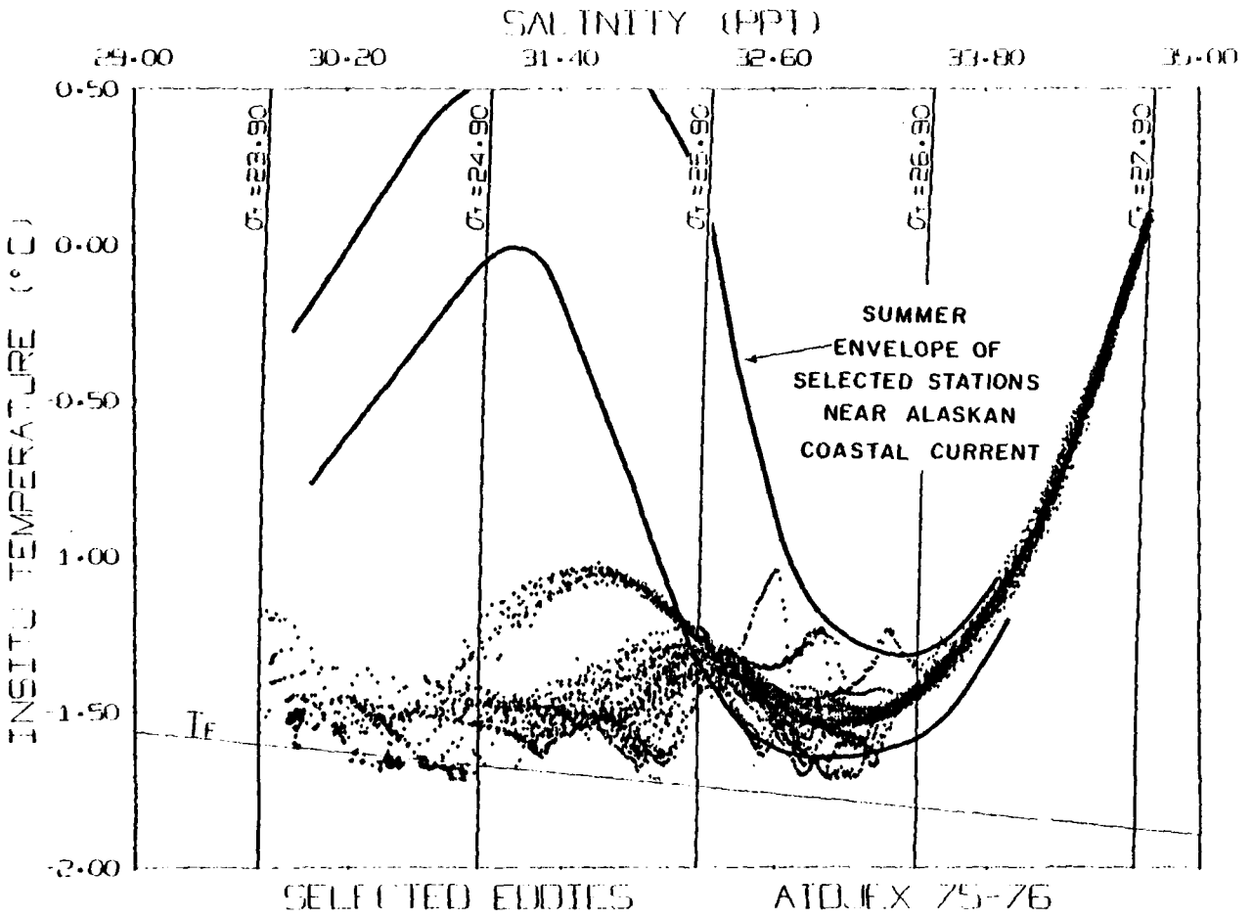


Figure 45. T-S diagram of selected eddies along with the summer envelope of selected stations near the Alaskan Coastal Current north of Point Barrow.

Ocean.

In general, the density of shelf water from the Chukchi Sea falls between 25.00 and 26.70 σ_t units. In the Canada Basin the range in density corresponds in depth to the Pacific T-max centered at approximately 75 meters and the Pacific T-min centered at 180 meters (figure 4). These depth ranges also correspond to the depth ranges of maximum observation of eddies(figure 37). Deep eddies can be accounted for by the extremely high winter salinities on the shelf, although these will undoubtedly be fewer in number.

4) Formation by Cutoff of Coastal Current Meanders

Shelf water conditions represent an attractive source for the varying thermal characteristics of the eddies cores as well as the correct densities at which a majority of eddies are observed. Presumably they are generated in baroclinically or barotropically unstable areas, the most likely area being the intense shear zone region associated with the eastward moving Alaskan Coastal Current and the westward moving Beaufort Sea circulation(figure 46). Both of these areas have reasonably high velocities, although the Alaskan Coastal Current is by far the swiftest with speeds up to 1.0 m/sec(Paquette and Bourke,1974). Based on dynamic calculations, speeds near the edge of the gyre are usually less than .10 m/sec.

Although both currents are part of a general horizontal shear in this region, eddy rotation depends on the direction of travel that the current takes. Since the number of anticyclonic eddies observed within the Beaufort Sea is indicative of the consistency of the mechanism creating these eddies, an unstable eastward flowing current would be by far the most dominant producer of mesoscale eddies. In the case where instability is prominent at the edge of the gyre, any wave-like disturbance that would be advected into the central

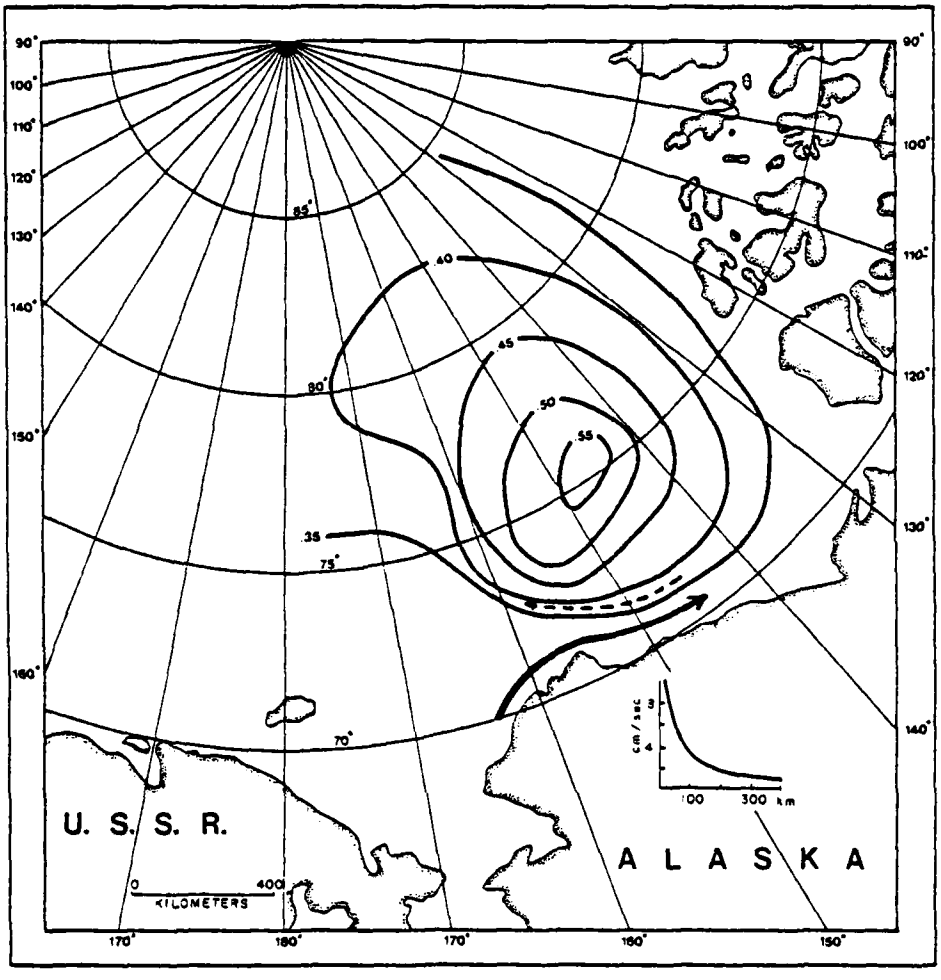


Figure 46. Sketch indicating the two currents in the shear zone region north of Alaska. The main gyre current(dashed line) and the Alaskan Coastal Current(solid line). Arrows indicate the direction of movement.

Beaufort from this westward moving current would have to be cyclonic. In the case of a meandering of the Alaskan Coastal Current, any breakoff on the side of the Beaufort Sea would be anticyclonic. Therefore, in the area of the Beaufort Sea region, the Alaskan Coastal Current appears to be the strongest possibility.

Work done on the Alaskan Coastal Current(Paquette and Bourke,1974; Hufford,1973) has shown it to extend as far east as 152 degrees west longitude along the continental shelf and shelf-slope areas. The assumption that the Alaskan Coastal Current may be the unstable front from which eddies are created is also in agreement with Hart and Killworth(1976). Although baroclinic instability may play an important role in the production of eddies, it should also be noted that for narrow currents, such as the Alaskan Coastal Current(Paquette and Bourke,1974), barotropic instability may become more important than baroclinic instability.

If it can be assumed that 1) anomalous eddies observed within the Beaufort Sea region are indeed spun off the Alaskan Coastal Current, 2) the active length of the Alaskan Coastal Current is 400 km, and 3) that 10 eddies with an initial radius of 7 km can be formed per week(e-folding time of 2-3 days), then roughly 500 eddies would be formed per year. In order to provide a comparison for this number, there should be some agreement with the 115 anomalous eddies observed within the Beaufort Sea region during the AIDJEX Experiment.

Assuming that the drift track of each camp represents an area of the Beaufort Sea equal to the length of the drift track multiplied by a representative width equal to 20 km, then the total area covered by all of the camps is equal to 160,000 km^2. An estimate of the total area encompassed by the Beaufort Sea yields 600,000 km^2. Assuming that the areal density of eddies within this region is constant, then at any given time there should be about 450

individual eddies within the Beaufort Sea which is in rough agreement with the estimate of the number of eddies spun off of the Alaskan Coastal Current.

One other possible source of arctic eddies should be briefly mentioned although there is only a small amount of information to suggest it. Investigations have already shown that the Barrow Canyon acts as a conduit by which shelf water as well as Atlantic Water of the Beaufort Sea may move down or up respectively(Mountain et al,1976; Garrison and Becker 1976), most likely in response to atmospheric forcing. Current meter data in the Barrow Canyon have measured speeds as high as .50 m/sec from the shelf to the Arctic Ocean which may indicate that a significant volume of water may be injected into the ocean in a short period of time. If the implacement of shelf water is rapid enough, baroclinic flow would be set up by the injected water mass. Assuming a cross-sectional area of the Barrow Canyon of 2.4×10^6 m^2 and a constant velocity of water down the canyon of .50 m/sec, it would take 7 hours of flow to equal the volume of a single eddy. This is not an unreasonable injection time; however, this is only a postulate and more detailed work as well as modeling must be done on this question.

3. Kinetic Energy

A) Kinetic Energy of the Eddies and Mean Flow

As previously mentioned, the number of eddies within the Beaufort Sea observed during the main AIDJEX Experiment, show them to be a widespread phenomena. Since their rotational velocities are an order of magnitude greater than the mean flow , it would be expected that they would dominate the kinetic energy balance of the upper two to three hundred meters.

To calculate the relative importance of the mean and time dependent (fluctuating) components, instantaneous measurements of the velocity (u and v) can be decomposed as follows:

$$u = \overline{u} + u'$$

$$v = \overline{v} + v' \tag{3.1}$$

where u and v are the observed east and north components of velocity respectively. Superscript bars($\overline{u}$) imply time averages, primes(u') imply the instantaneous deviations away from the time means.

By definition, kinetic energy is equal to $0.5m\,v^2$, thus kinetic energy per unit volume for the mean and time dependent terms can be written in the following way:

$$KE_{total} = 0.5\rho\left[u^2 + v^2\right]$$

$$= 0.5\rho\left[\left[\overline{u} + u'\right]^2 + \left[\overline{v} + v'\right]^2\right] \tag{3.2}$$

$$= 0.5\rho\left[\left[\overline{u}^2 + 2\overline{u}u' + u'^2\right] + \left[\overline{v}^2 + 2\overline{v}v' + v'^2\right]\right]$$

where ρ is the density of the fluid.

By taking the time average of (3.2) we have

$$KE_{total} = 0.5\rho\left[\overline{u}^2 + \overline{v}^2 + \overline{2\overline{u}u'} + \overline{2\overline{v}v'} + \overline{u'u'} + \overline{v'v'}\right] \tag{3.3}$$

The terms $\overline{\overline{u}u'}$ and $\overline{\overline{v}v'}$ are defined to be zero as demonstrated in the following short proof:

By definition

$$u'_i = u_i - \overline{u}$$

$$= u_i - \frac{1}{N}\sum_{j=1}^{N} u_j$$

By taking an arbitrary time average

$$\overline{u'_i} = \overline{\left\{u_i - \frac{1}{N}\sum_{j=1}^{N} u_j\right\}}$$

$$\frac{1}{n}\sum_{i=1}^{n} u'_i = \frac{1}{n}\sum_{i=1}^{n}\left\{u_i - \frac{1}{N}\sum_{j=1}^{N} u_j\right\}$$

$$= \frac{1}{n}\sum_{i=1}^{n} u_i - \frac{1}{n}\sum_{i=1}^{n}\left[\frac{1}{N}\sum_{j=1}^{N} u_j\right]$$

$$= \frac{1}{n}\sum_{i=1}^{n} u_i - \frac{n}{n}\left[\frac{1}{N}\sum_{j=1}^{N} u_j\right]$$

$$= \frac{1}{n}\sum_{i=1}^{n} u_i - \frac{1}{N}\sum_{j=1}^{N} u_j$$

If the arbitrary time average defined for $\overline{u'_i}$ is for the exact time period as that defined for $\overline{u}$, then $n = N$ and $j = i$. Therefore

$$\overline{u'_i} = \frac{1}{N}\sum_{i=1}^{N} u'_i = \frac{1}{N}\sum_{i=1}^{N} u_i - \frac{1}{N}\sum_{i=1}^{N} u_i = 0$$

Terms such as $\overline{\overline{u}u'} = \overline{\overline{u}v'} = \overline{\overline{w}v'} = \ldots = 0$

It is more intuitively obvious that the time average of a mean is the mean. As seen in the above proof, it can therefore be removed from the second order time averaging. It then follows that:

$$\overline{\bar{u}u'} = \bar{u}\cdot\overline{u'} = 0$$

By removing the terms $\overline{\bar{u}u'}$ and $\overline{\bar{v}v'}$, equation 3.3 can be rewritten in the following way.

$$KE_{total} = 0.5\rho\left[\bar{u}^2 + \bar{v}^2\right] + 0.5\rho\left[\overline{u'u'} + \overline{v'v'}\right] \qquad (3.4)$$

$$= \quad K.E._{mean} \quad + \quad K.E._{tdm}$$

where:

$K.E._{mean}$ is the kinetic energy resulting from the mean flow field

$K.E._{tdm}$ is the kinetic energy resulting from the time dependent motion.

The density , ρ , can be considered to be unity in the cgs system. In the processing of the original PCM data recorded on analog charts, only those stations that had relative speeds greater than the threshold velocity of the sensor (.05 m/s) were manually digitized for further computer reduction. Stations that were not digitized indicated that the water column, to a depth of 200 meters, was moving uniformly, plus or minus .05 m/sec, with the ice. In terms of absolute velocity, the water column was moving with the velocity of the ice, within the resolution of the PCM. This type of uniform velocity field extending to great depths is known as a barotropic current and is a result of the tilting of the sea surface.

During the computation of kinetic energy, all current meter profiles were used. If the station was not digitized, the ice velocity at the time of the

observation was taken as the absolute velocity of the current in the upper 200 m.

Kinetic energy of the mean and time dependent motion were calculated at one-meter intervals to a maximum depth of 200 meters. Monthly and yearly kinetic energies were calculated for each camp. In the special case of Big Bear, a six month average was made. An ensemble average covering 3.5 years of station data was also calculated to provide the general conditions of the Beaufort Sea.

Two examples of monthly kinetic energy plots which indicate the minimum and maximum values calculated during the AIDJEX 75-76 Experiment, are shown in figures 47 and 48 respectively. Monthly mean kinetic energy is shown by the solid line on the left. The kinetic energy due to the fluctuating or time dependent motion is indicated by the dashed line. The total amount of kinetic energy (sum of mean and fluctuating) is the solid line to the right. Factors such as the depth of the eddies, the number of observations made within the eddy, the type of pass made through the eddy and its age, all play an important part in the amount of energy observed during any given month. It is believed, however, that the rotational velocity of the eddy and the frequency of observations are the most important of the several factors when attaching significance to the monthly data. The number of PCM stations per month remained fairly constant. However during the summer months, the camps traveled farther , thereby increasing the number of eddies observed during the month as shown in figure 34. The relative amount of kinetic energy of the summer data , is in some cases less than the winter data. This is most likely a problem dealing with the probability in encountering random events.

Although the two monthly plots, figures 47 and 48, show an order of magnitude difference in the maximum amount of kinetic energy observed, longer time averages of the data show less relative differences. Averages of kinetic

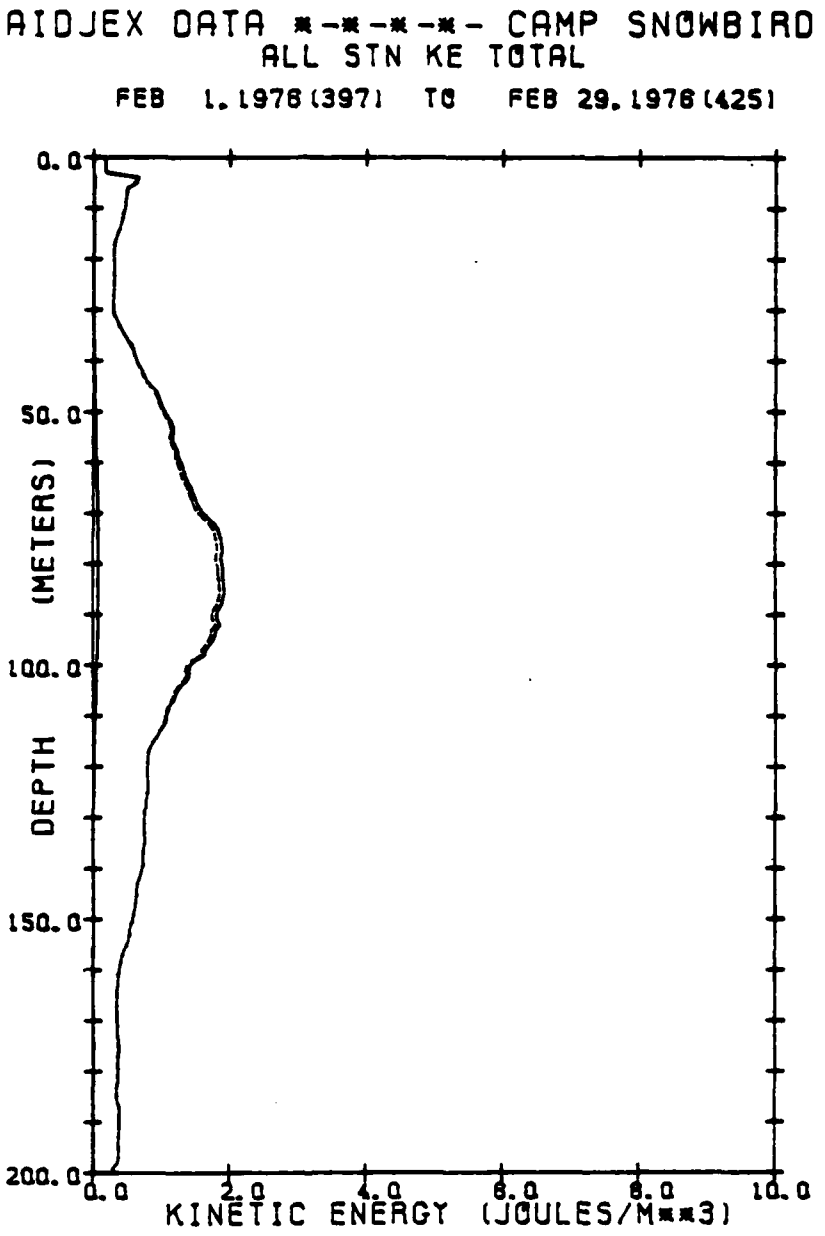


Figure 47. Minimum monthly kinetic energy field observed during the main AIDJEX experiment. Solid line at left is mean kinetic energy dashed line is kinetic energy due to fluctuations away from the mean, and solid line to right is the total kinetic energy.

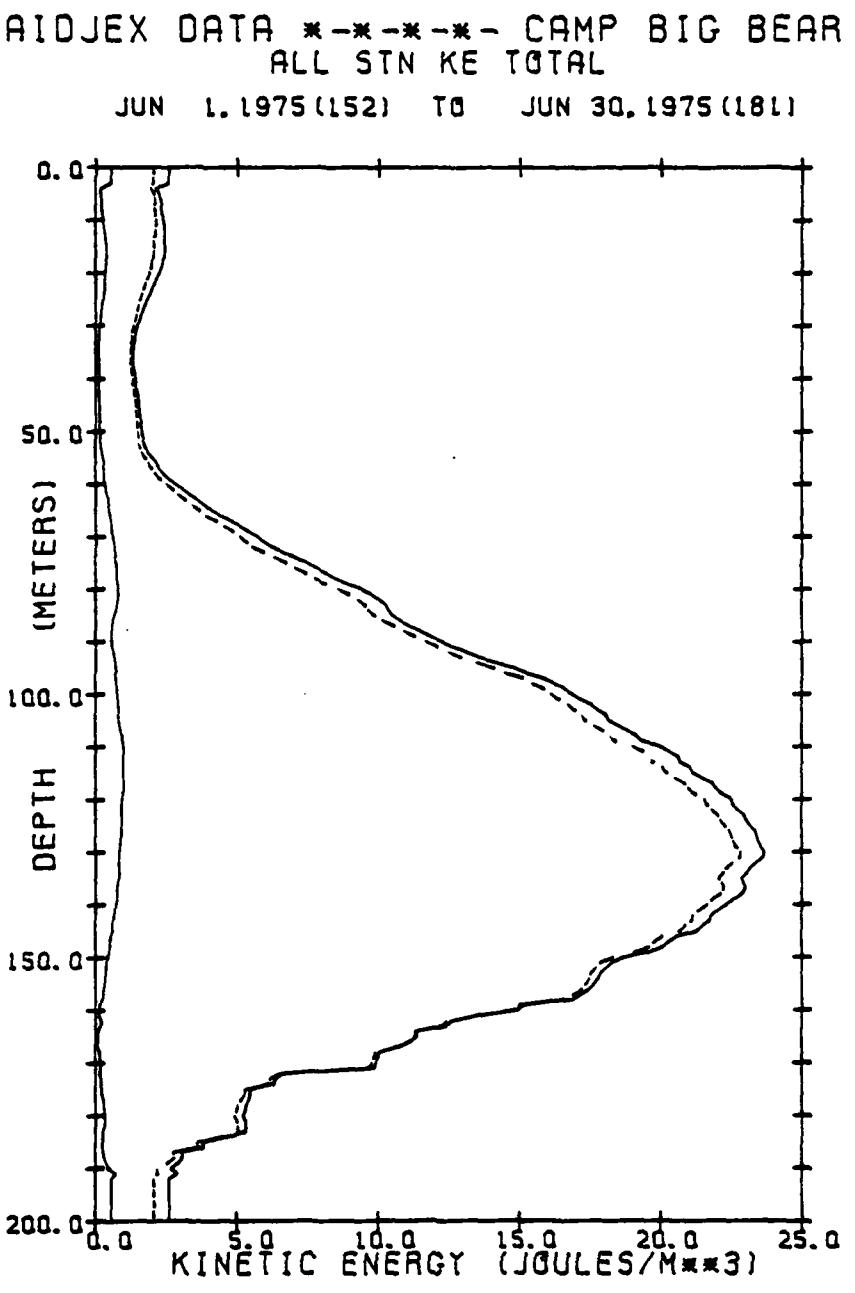


Figure 48. Maximum monthly kinetic energy field observed during the main AIDJEX experiment.

energy taken over the duration of the individual camps are shown in figures 49,50,51, and 52 for comparison. These diagrams correspond in format to that of figure 47 where the left solid line is the mean kinetic energy, the dashed line is the fluctuating kinetic energy and the total kinetic energy is the right solid line. Figure 53 shows the total intercamp kinetic energy over the 3.5 year average. For this ensemble mean there is a peak in eddy energy at 120 meters. This implies that even though eddies are observed from the base of the mixed layer to depths greater than 700 meters, the dominance of the eddy kinetic energy clearly resides in the depth level from 50 to 190 meters. Mean kinetic energies of the main experiment are insignificant, so that the line defining the mean and the base line coincide in some cases.

At the main camp during the 1972 pilot experiment, hourly mean data from 10 mast mounted current meters spaced every 10 meters in depth to a maximum of 100 meters were used to calculate kinetic energy(Hunkins,1974). The length of the data set was from 29 March, 1972 to 25 April, 1972. The results obtained from this data set are shown in figure 54. Even though the period over which the data was analyzed was short and the depth of observation did not extend down to the depth of maximum velocity of the eddies, several important findings were made. The first is that the kinetic energy field in the upper 100 meters in the section of the Beaufort Sea occupied by the pilot experiment was dominated by the time dependent motion. Kinetic energy due to the mean flow was generally an order of magnitude less than the kinetic energy supplied by the fluctuations.

The second finding was that the kinetic energy of the time dependent motion is divided into two separate and distinct depth levels. The first is a low energy peak extending from the surface to approximately 10 meters and is the result of energy put into the mixed layer by wind and ice stress. The second, more dominant peak extends from the base of the mixed layer (approximately

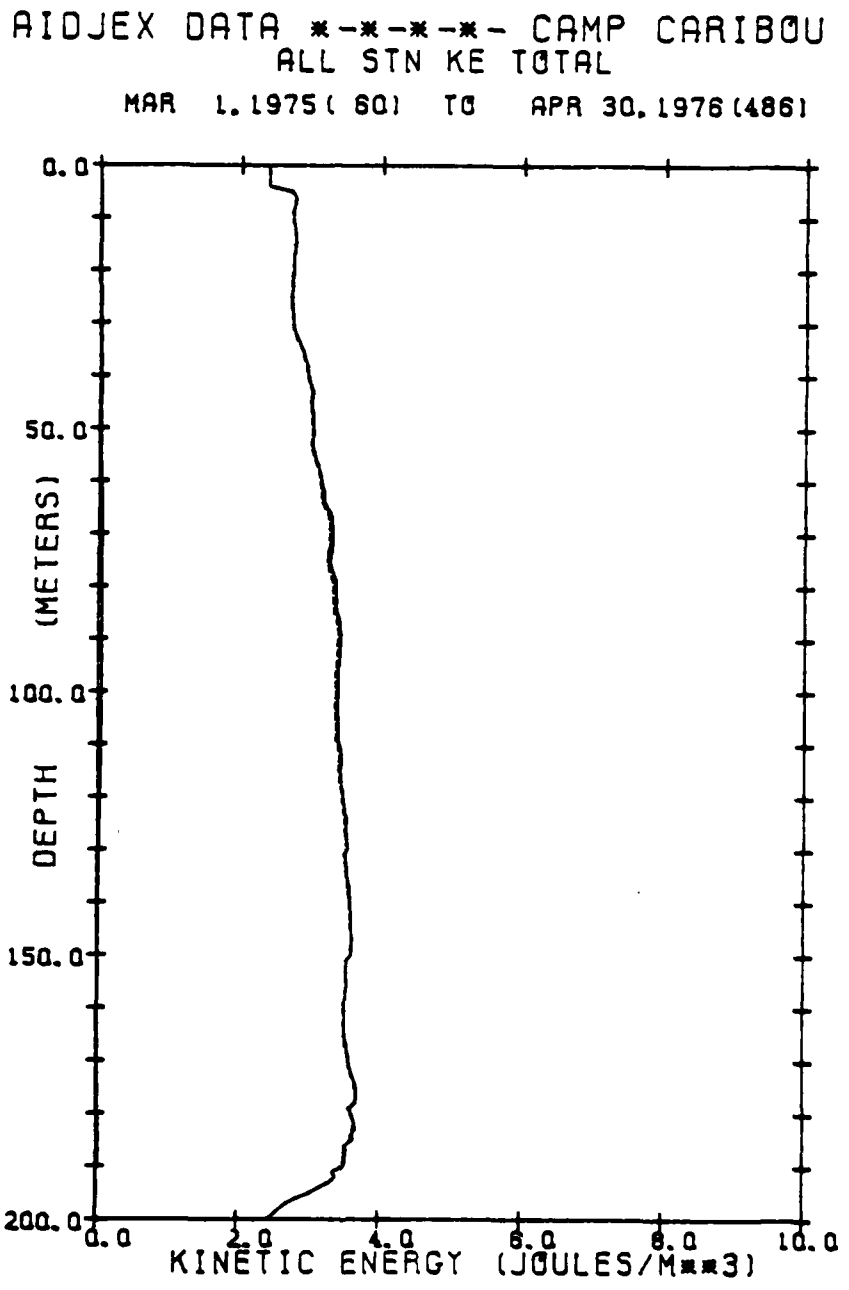


Figure 49. Caribou kinetic energy profile, 14-month mean.

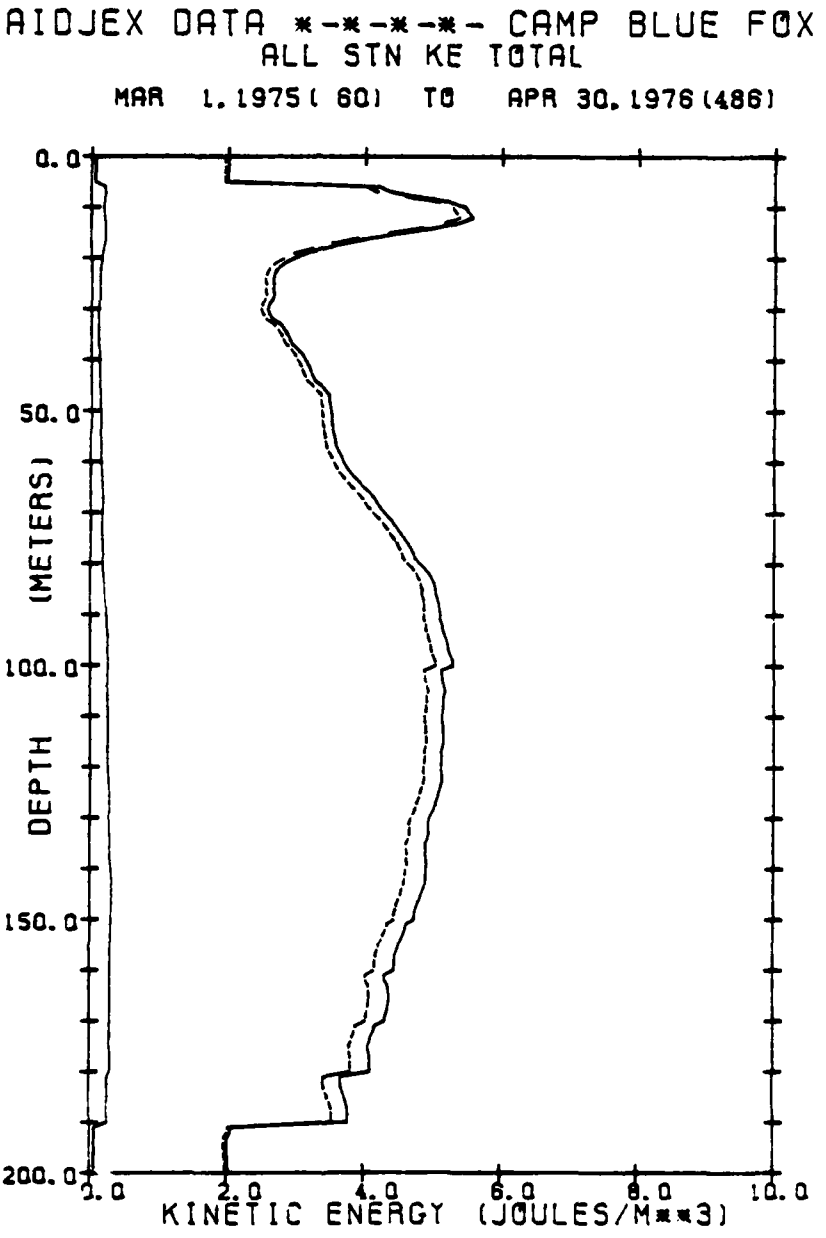


Figure 50. Blue Fox kinetic energy profile, 14-month mean.

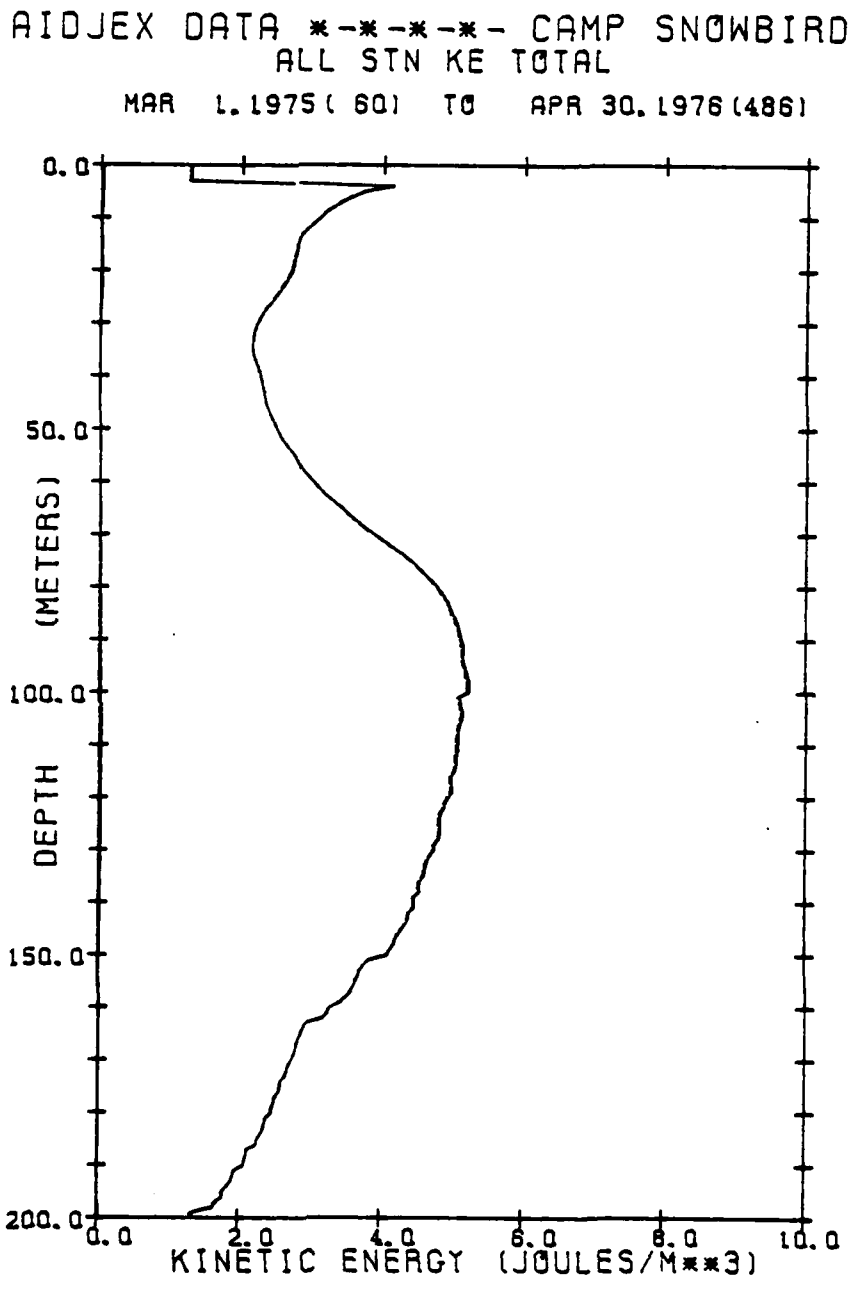


Figure 51. Snowbird kinetic energy profile, 14-month mean.

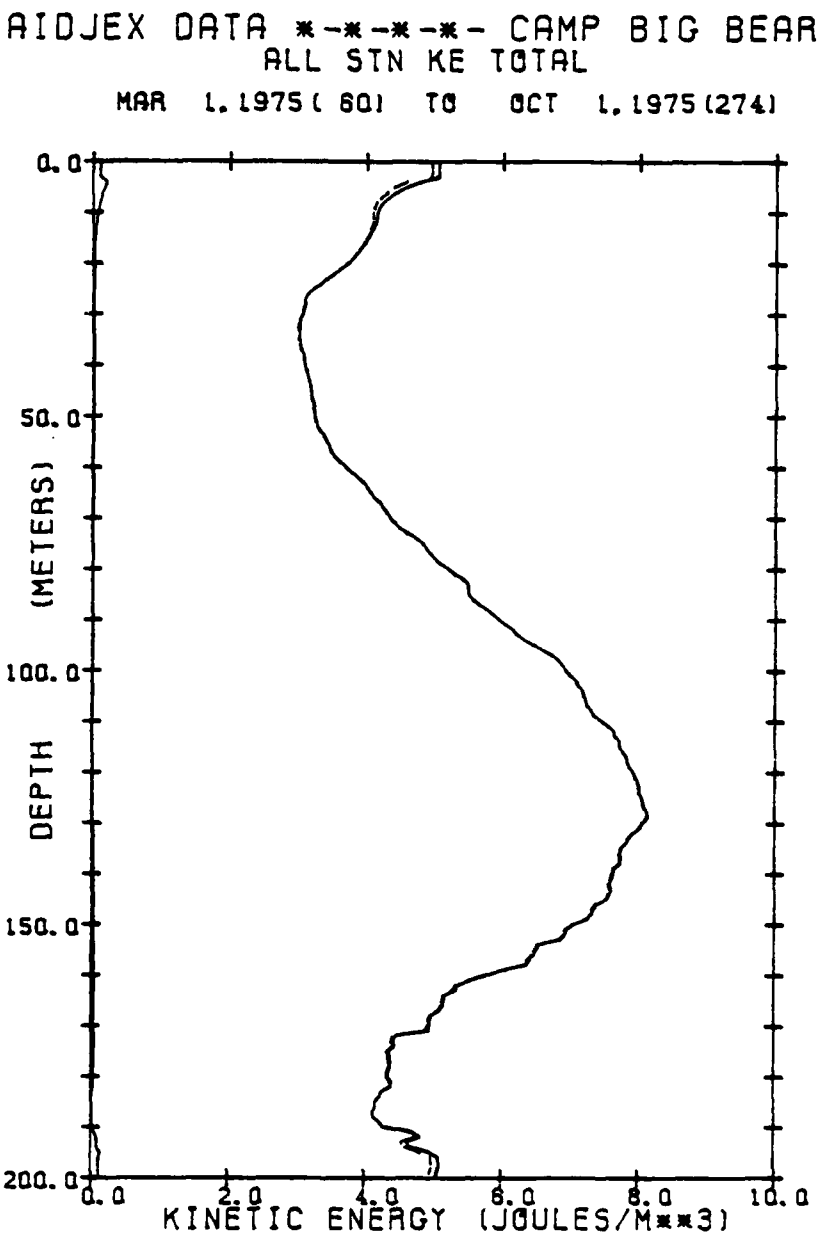


Figure 52. Big Bear kinetic energy profile, 7-month mean.

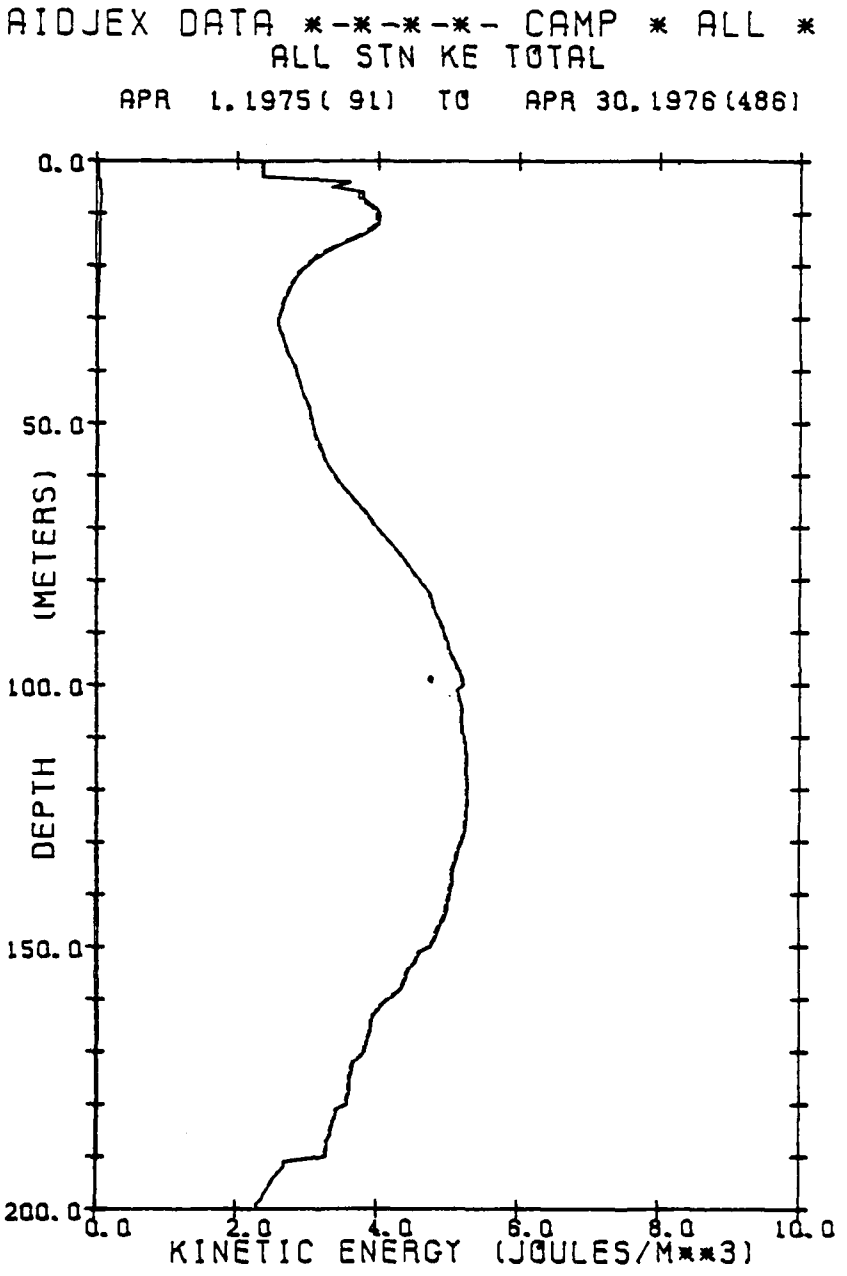


Figure 53. Ensemble mean kinetic energy (49 months).

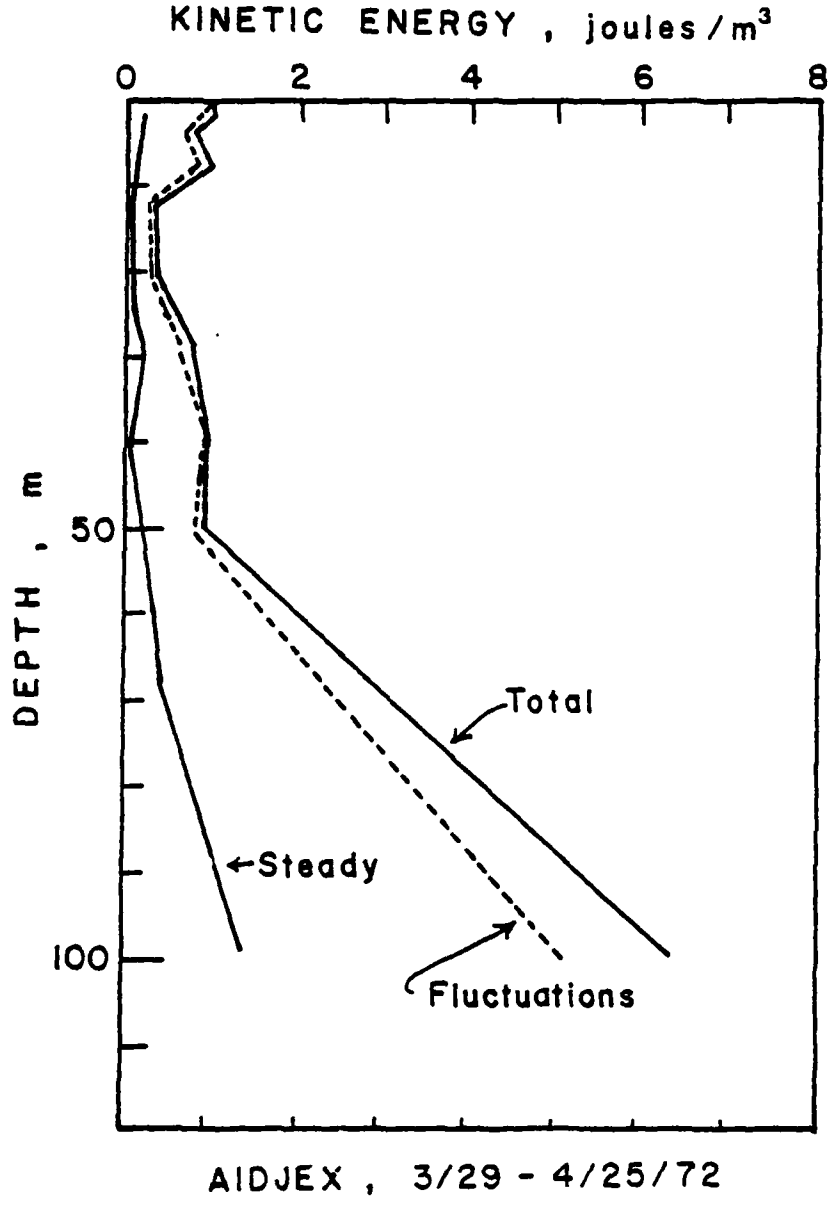


Figure 54. AIDJEX 1972 main camp average of mean, fluctuating, and total kinetic energy(Hunkins,1974).

50 meters) to the maximum depth limitation of the data set. Although this broad high energy area never reached a peak, on the basis of deeper current profiles, it was inferred that the eddies which existed within the depth span of 50 to 300 meters are the major source of kinetic energy in the upper part of the water column.

As compared with the 1972 data(figure 54), the 1975-76 data indicates that over 95% of the kinetic energy observed is confined to the fluctuating terms. On the basis of the data contained in figures 49 to 54, a percentage breakdown of the components of maximum observed kinetic energy at the various camps in the mixed layer (<50m) and below (eddy), was tabulated and is listed in Table 10.

A comparison of all figures shows that 1) mean kinetic energy is the smallest component providing less than 6 percent of the total kinetic energy, 2) time dependent motion supplies the major amount of kinetic energy and 3) the time dependent motion can be broken up into two vertically separate components which are the wind-ice stress components near the surface and the

Table 10

Percentage breakdown of the total observed kinetic energy for the 1972 main camp and all of the 1975-76 manned camps.

Camp	** MIXED LAYER **			***** EDDY *****		
	Depth m.	Mean %	Fluct. %	Depth m.	Mean %	Fluct. %
Main 1972	10	10	90	100	22	78
AIDJEX 75-76						
Caribou	12	2	98	128	1	99
Blue Fox	13	3	97	100	5	95
Snowbird	5	1	99	98	1	99
Big Bear	5	4	96	130	1	99
Average	9	4	96	111	6	94

eddy component at deeper levels.

Several new results can be seen from the 1975-1976 data. The first is that the shallow energy peak extends to a deeper level than it did in the 1972 data and corresponds well with the concept that frictional effects of wind or ice-induced energy are confined to a layer approximately 20 meters thick (Hunkins, 1966).

A second new result is that the eddies give up some of their kinetic energy to the base of the mixed layer. During nine out of the 12 months, the base of the mixed layer is approximately 50 meters. Over 90% of the eddies observed by the PCM during this period had their starting depth at the base of the mixed layer. A typical example of this is seen in figure 24 which shows the initial increase in velocity at 60 m. On the basis of an STD cast on the same day, the base of the mixed layer was at the same depth.

The mixed layer tends to appear as a buffer between the stress applied by the wind-driven ice at the surface, and the stress supplied by the eddy at its base. It has been observed(Hunkins,1966) and confirmed by the main AIDJEX data set that the effective Ekman layer depth in the Arctic during the summer at least is approximately 20 meters in depth. Therefore energy obtained in the mixed layer below this depth must have been put in by eddies. The 1972 AIDJEX data(figure 54), showed hints of this effect but was at too coarse a depth interval and possibly over too short a time period. The 1975-1976 AIDJEX data shows a minimum in kinetic energy at 30 m with a gradual increase with depth(figure 53).

The general mechanics would be similar to that of ice stressing the water except for two major differences, 1) the ice would have a larger surface roughness by way of ridge keels in order to help transmit stress, and 2) the ice is usually in constant motion and at all times puts in energy into the upper layer. The eddies, however, are transient features that can affect only a part of the

horizontal surface at the base of the mixed layer and for only short periods of time. Eddy stress at the base of the mixed layer may not be as large as that of the wind and ice stress; however, data suggest that eddies do provide some input of kinetic energy into the base of the mixed layer.

B) Monthly Kinetic Energy Variations and Eddy Decay

Variations in kinetic energy from month to month do occur(figures 47 and 48). These observed variations throughout time may be the result of a decay of the eddy field or a nonuniform distribution of eddies throughout space, or both. On the basis of the number of eddies observed per 100 kilometers per month(figure 35), the possibility of having a nonuniform field of eddies is not evident throughout the AIDJEX 1975-76 sector. The first possibility, that of eddy decay, intuitively as well as physically appears to be more plausible. It has been shown that in the Atlantic, there is on the average, a fairly constant number of Gulf Stream Rings within a given sector of the Sargasso Sea. Decay of these rings begins immediately after separation with the Gulf Stream(Barrett,1971). If eddies are advected into the Beaufort Sea north of Point Barrow, then a decrease in the amount of kinetic energy along the mean circulation path of the gyre should be observed.

To observe this, estimates have to be made as to the kinetic energy resulting solely from the eddies. Dividing the time dependent motion term of kinetic energy into two parts, we have

$$KE_{tdm} = KE_{bc} + KE_{bt} + KE_{x}$$

where:

KE_{tdm} has been previously defined in equation 3.4

KE_{bc} is the kinetic energy of the mesoscale baroclinic eddies

KE_{bt} is the kinetic energy resulting from all other time dependent motion other than mesoscale eddies. This would consist of tides, internal waves, inertial and barotropic motions.

KE_{x} is the kinetic energy resulting from the cross terms of the baroclinic eddy motion, and other time dependent motion as well as the mean field.

If the observations and resulting calculations of kinetic energy are restricted to depth ranges outside the observed eddy field, then by definition

$$KE_{bc} = KE_{z} = 0$$

Then, for kinetic energy calculations outside the direct influence of eddies

$$KE_{tdm} = KE_{bt}$$

Although the term KE_{bt} is an accumulation of energy from a variety of motions, the barotropic component of motion is the largest. This type of motion occupies more than 50% of the profiling current meter data with peak velocities greater than .30 m/sec. Other motion generated by internal waves, tides and inertial motion in the Arctic Ocean are small when compared to the barotropic motion.

For the purpose of this study, the energy associated with the barotropic motion throughout the upper 200 m will be defined as the minimum kinetic energy due to the time dependent motion found outside the depth range of eddies, integrated over the two hundred meters. The depth range in which eddies are found depends on the time interval over which the averaging is done as well as the number and strength of the eddies observed during that time period. The remaining kinetic energy in the water column will then approximate the energy of the mesoscale eddies.

Table 11 lists the various vertically integrated kinetic energy components of the time dependent motion. Figures 55a and 55b show the barotropic(solid line) and baroclinic (dashed line) energy as given in Table 11. The monthly average of baroclinic and barotropic energy for all of the camps is shown in figure 55c. The integrated monthly baroclinic kinetic energy is also plotted at its geographic position within the Beaufort Sea(figure 56).

The baroclinic component of the eddy kinetic energy is seen to decay along the direction of mean flow as distance from the source region increases. Although the slope of the line defining the decrease in baroclinic kinetic energy

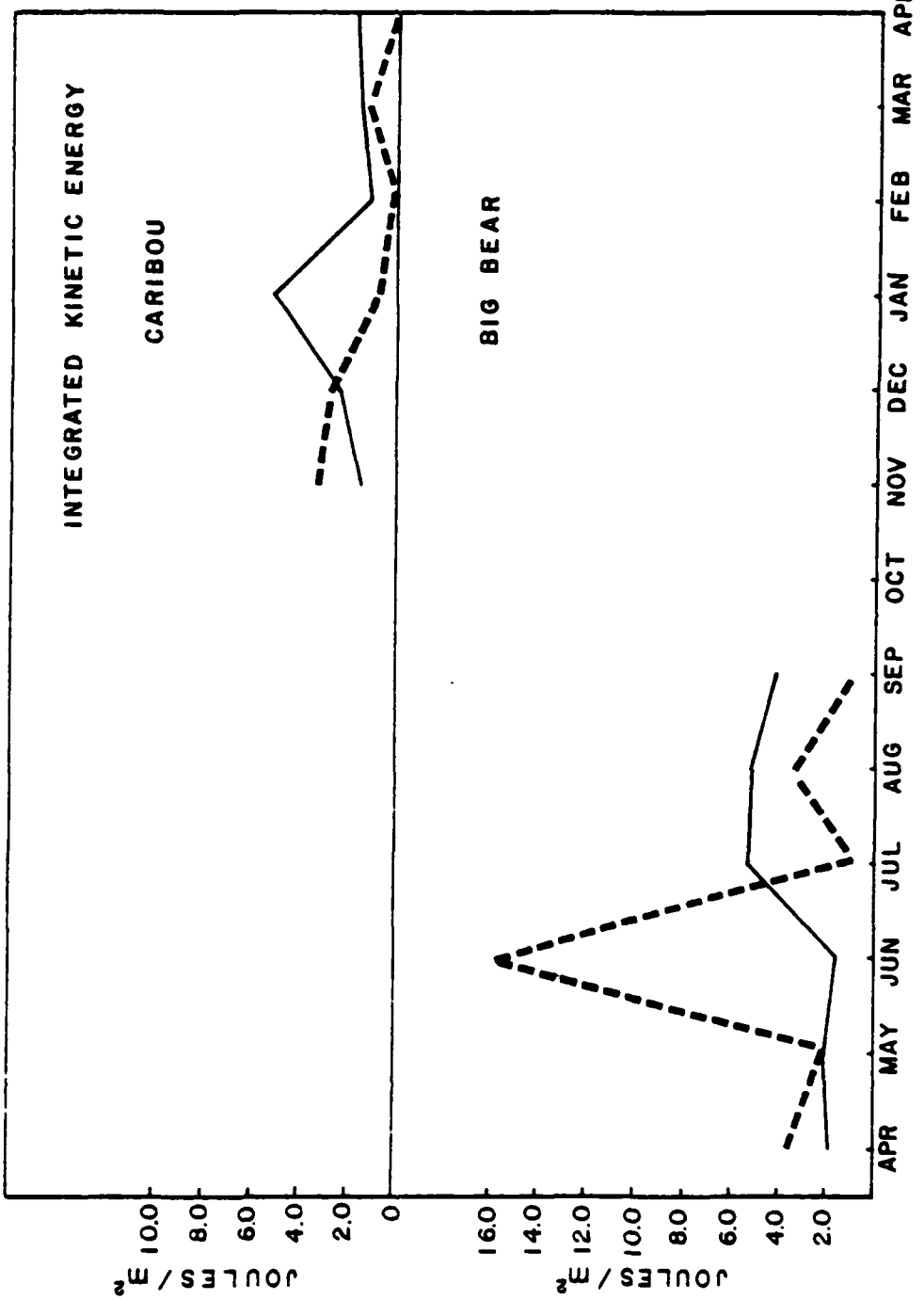


Figure 55a. Individual camp plots showing the amount of vertically integrated barotropic(solid) and baroclinic(dashed) kinetic energy per month, through time.

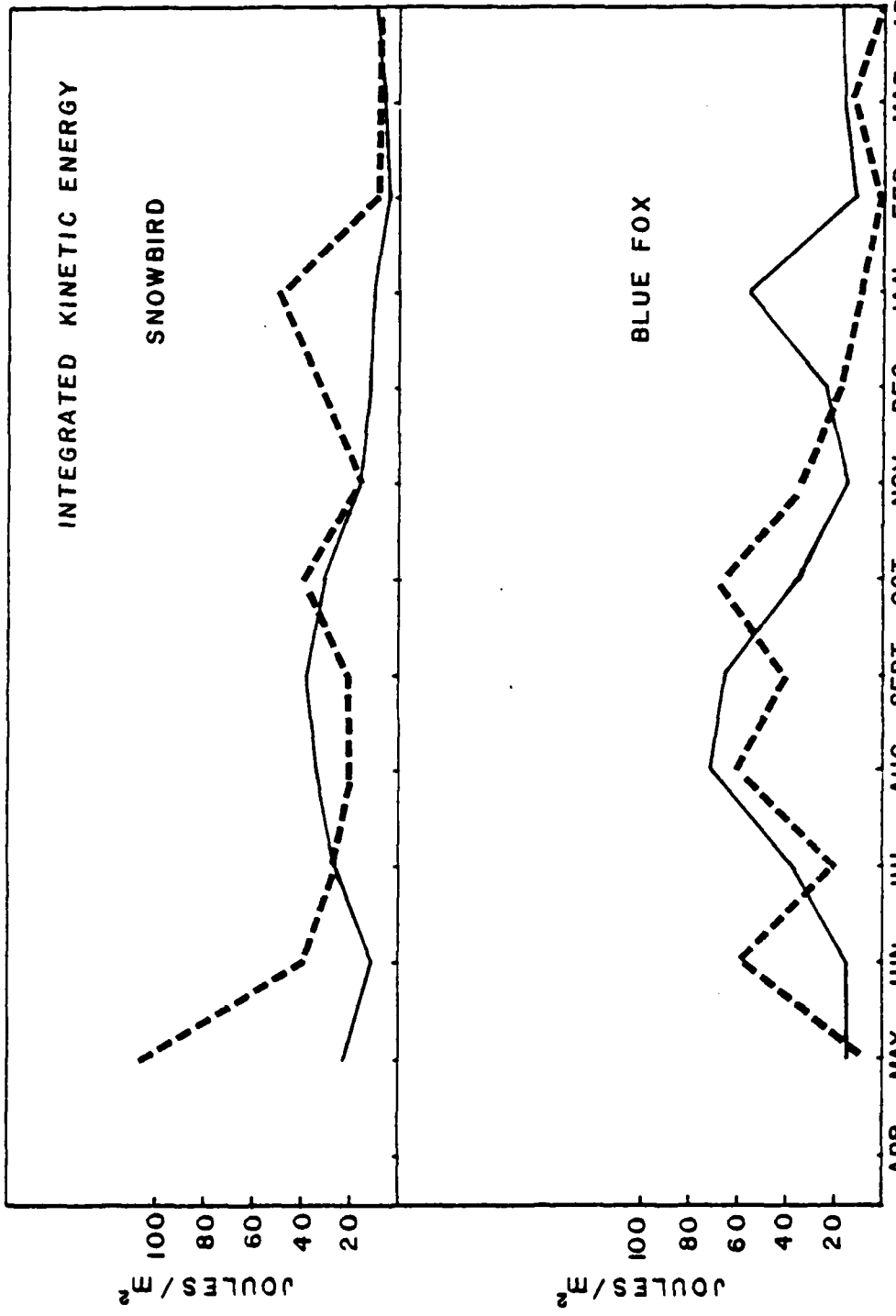


Figure 55b. Individual camp plots showing the amount of vertically integrated barotropic(solid) and baroclinic(dashed) kinetic energy per month, through time.

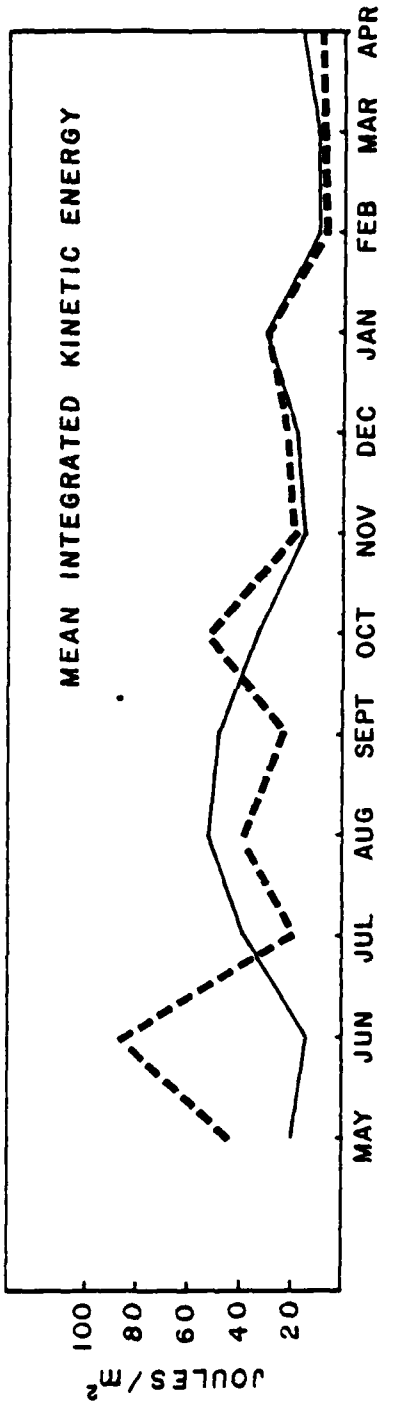


Figure 55c. Camp average of the vertically integrated barotropic(solid) and baroclinic(dashed) kinetic energy per month, through time.

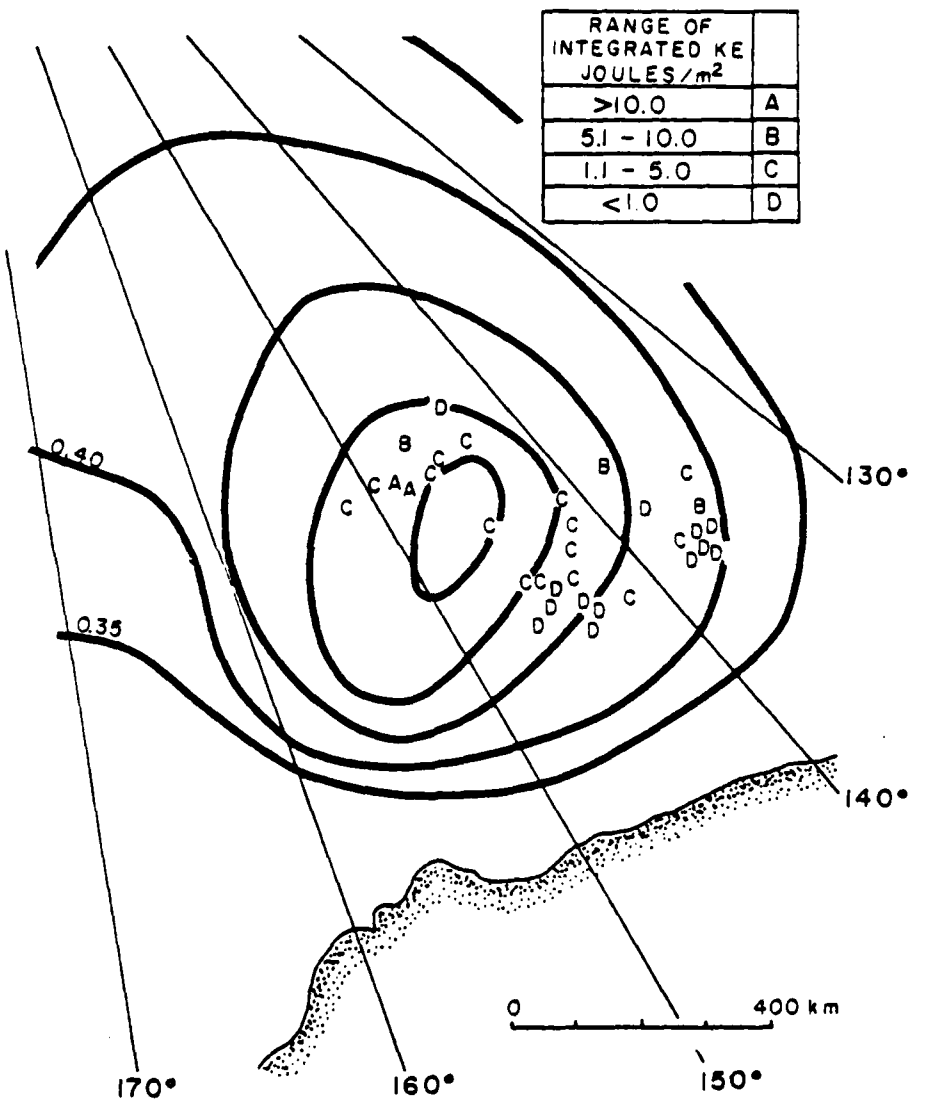


Figure 56. Integrated baroclinic kinetic energy from 50 to 190 m. plotted on the mean dynamic topography of the Beaufort Sea.

through time is only slightly negative(figure 55c), it does show a trend of decay through time. Spatially, this general decay scheme can also be seen even though there are a few points that appear higher as well as lower than what is observed within a particular region(figure 56).

Table 11

Integrated monthly averages of the different components of kinetic energy (joules/ m^2).

Month	Camp	Mean	Fluctuating	Barotropic	Baroclinic
Apr-1975	Big Bear	0.8	55.1	19.6	35.5
May-1975	Blue Fox	1.0	25.6	16.2	9.4
	Snowbird	2.9	129.6	23.3	106.3
	Big Bear	1.3	41.4	21.3	20.1
Jun-1975	Blue Fox	0.7	73.3	14.8	58.5
	Snowbird	4.9	48.9	10.5	38.4
	Big Bear	7.8	177.2	17.0	160.2
Jul-1975	Blue Fox	20.0	57.0	37.2	19.8
	Snowbird	7.3	51.7	26.4	25.3
	Big Bear	10.1	63.6	52.8	10.8
Aug-1975	Blue Fox	24.0	130.8	70.7	60.1
	Snowbird	16.3	55.0	33.7	21.3
	Big Bear	3.1	86.3	52.3	34.0
Sep-1975	Blue Fox	20.9	107.4	64.8	42.6
	Snowbird	2.0	59.1	37.9	21.3
	Big Bear	2.0	51.8	42.1	9.7
Oct-1975	Blue Fox	14.9	101.8	35.2	66.6
	Snowbird	1.7	69.0	31.4	37.6
Nov-1975	Caribou	1.4	47.9	15.3	32.6
	Blue Fox	1.0	20.1	12.8	7.2
	Snowbird	0.9	33.3	16.3	17.0
Dec-1975	Caribou	6.8	50.2	22.9	27.3
	Blue Fox	1.2	29.1	19.2	9.9
	Snowbird	1.5	43.1	11.8	31.3
Jan-1976	Caribou	7.8	59.1	51.5	7.6
	Blue Fox	3.4	58.2	28.7	29.5
	Snowbird	3.2	58.7	10.0	48.7
Feb-1976	Caribou	0.2	12.7	11.3	1.4
	Blue Fox	1.6	18.3	11.5	6.8
	Snowbird	0.4	13.6	4.0	9.6
Mar-1976	Caribou	7.1	28.3	15.8	12.4
	Blue Fox	0.8	10.6	8.2	2.4
	Snowbird	3.3	14.4	6.2	8.2
Apr-1976	Caribou	0.2	18.6	16.9	1.6
	Blue Fox	0.7	25.0	20.3	4.6
	Snowbird	3.9	18.3	9.5	8.8

C) Transfer of Kinetic Energy by Eddies

In the generally accepted sense of frictional flow, energy dissipation follows a normal "cascading" in which the mean flow loses energy to intermediate scale features which in turn lose energy to smaller scale features finally to be dissipated into heat by molecular and viscous forces(Rossby,1936; Stommel,1958; von Arx,1954). Recently there is an increasing amount of evidence supporting the transfer of energy from the large scale eddies to the mean flow of which the first conclusive work was done by Starr(1953) for the earth's atmosphere. Starr concluded that the transfer of atmospheric eddy kinetic energy was large enough to replenish the mean kinetic energy of the atmosphere in approximately two weeks. The term negative viscosity was used by Starr(1968) to classify this mechanism as being the reverse of the normal dissipative regime. A recent planetary example of this was seen in Voyager's satellite imagery of Jupiter's turbulent atmosphere(Beebe et al,1980) where large scale eddies were supplying kinetic energy to the mean flow.

In the field of oceanography, meanders in the Florida Strait and Onslow Bay were analyzed by Webster(1961) using current meter data obtained from geomagnetic electro-kinetograph(GEK) measurements. The horizontal eddy kinetic energy resulting from the meanders was shown to supply kinetic energy to the mean northward flow of the Gulf Stream in both locations. Because of the rather uniform direction of the Gulf Stream at these sites, the general kinetic energy equation was able to be simplified to only one term which indicated the flux of kinetic energy between the mean and eddy motion. This term was calculated to be positive in a majority of the sections across the Gulf Stream. Near the continental edge of the Florida Current, however, Lee(1975) calculated that energy flux provided by the eddies spun off in this region was in the normal dissipative sense.

Using the same concept, Hunkins(1974) calculated the relative direction of kinetic energy transfer between the mean flow and the eddies, observed during the 1972 AIDJEX pilot study. The data consisted of 10 one-month time series, each taken from one of 10 mast mounted current meters that had a vertical spacing of 10 meters. The time series were made up of hourly means. Even though Hunkins states that the results are only tentative due to the short duration data set and the problems relating to statistical significance, eight out of the ten depth levels were found to be negative. This indicated that the flux of kinetic energy was in a normal dissipative sense, that is, from the mean flow to the eddy field. To study this problem of energy flux in general terms and for the Arctic Ocean in particular, some mention of the governing equations and assumptions will be given.

The decomposition of field parameters such as density(ρ), pressure(P), and velocity(V) into mean and fluctuations away from the mean (commonly called time dependent motion) can be written in the following way:

$$\begin{aligned} \rho &= \overline{\rho} + \rho' \\ P &= \overline{P} + P' \\ \vec{V} &= u\vec{i} + v\vec{j} + w\vec{k} \end{aligned} \tag{3.5}$$

where: $u = \overline{u} + u'$

$v = \overline{v} + v'$

$w = \overline{w} + w'$

The parameter on the left of the equals sign is the instantaneous measured value.

The coordinate system used in this analysis is cartesian, the positive x-axis directed eastwards, the positive y-axis directed northwards, and the z-axis directed positive downwards. The speeds u, v, and w correspond to the positive x,y, and z axis respectively.

Before deriving the kinetic energy equation, the relative importance of the mean and fluctuating terms will help simplify the original set of equations. Since the main purpose of the study concerns itself with eddies in particular, the mean and fluctuating components of density, pressure and velocity, for one of the strongest eddies observed during the main experiment (Snowbird, days 150 to 155) are given below.

Parameter	Units	Mean	Fluctuating
Density	$g/(cm^3)$	1.02660	0.002
Pressure	decibars	160.0	3.0
Velocity	cm/sec	5.	55.

The time dependent terms for density and pressure are at least two orders of magnitude less than the means and can be considered negligible. The only term that may be kept as a decomposition is the velocity, where in this case as well as other observed eddies, the fluctuations can be as high as one order of magnitude greater than the mean velocity field.

Another parameter that will be excluded is the vertical component of velocity(w). Realistically, this assumption will not alter the results of the analysis because of the very slow assumed vertical velocities.

The original field parameters can then be written in the following form:

$$\begin{aligned} \rho &= \overline{\rho} \\ P &= \overline{P} \\ \vec{V} &= u\vec{i} + v\vec{j} \end{aligned} \tag{3.6}$$

The two-dimensional horizontal momentum equations are as follows, where it is understood that ∇ defines the horizontal gradient only -

$$\frac{\partial \rho u}{\partial t} + \vec{V}\cdot\nabla\rho u = \rho f v - \frac{\partial P}{\partial x} - D_x \tag{3.7}$$

$$\frac{\partial \rho v}{\partial t} + \vec{V}\cdot\nabla\rho v = -\rho f u - \frac{\partial P}{\partial y} - D_y \tag{3.8}$$

where:
D_x and D_y are the dissipative forces in the x and y directions respectively.

With the use of the continuity equation (3.9), equations (3.7) and (3.8) can be rewritten in terms of momentum flux.

$$\frac{\partial \rho}{\partial t} + \nabla\cdot\rho\vec{V} = 0 \tag{3.9}$$

$$\frac{\partial \rho u}{\partial t} + \nabla\cdot\rho u\vec{V} = \rho f v - \frac{\partial P}{\partial x} - D_x \tag{3.10}$$

$$\frac{\partial \rho v}{\partial t} + \nabla\cdot\rho v\vec{V} = -\rho f u - \frac{\partial P}{\partial x} - D_y \tag{3.11}$$

With the use of equation in (3.6) and the definition of the time average as follows -

$$\overline{x} = \frac{1}{T}\int_{\frac{-T}{2}}^{\frac{T}{2}} x\,dt = \frac{1}{N}\sum_{i=a}^{b} x_i \tag{3.12}$$

where :

1) time of observation at $x_a = \frac{-T}{2}$

2) time of observation at $x_b = \frac{T}{2}$

The time average of equations (3.10) and (3.11) can then be rewritten as:

$$\frac{\partial}{\partial t}\left\{\overline{\rho\left[\overline{u}+u'\right]}\right\} + \frac{\partial}{\partial x}\left\{\overline{\rho\left[\overline{u}+u'\right]\left[\overline{u}+u'\right]}\right\} +$$

$$\frac{\partial}{\partial y}\left\{\overline{\rho\left[\overline{u}+u'\right]\left[\overline{v}+v'\right]}\right\} = -f\left\{\overline{\rho\left[\overline{v}+v'\right]}\right\} - \frac{\partial \overline{P}}{\partial x} - \overline{D_x} \tag{3.13}$$

$$\frac{\partial}{\partial t}\left\{\rho\left[\overline{v}+v'\right]\right\} + \frac{\partial}{\partial x}\overline{\left\{\rho\left[\overline{v}+v'\right]\left[\overline{u}+u'\right]\right\}} +$$

$$\frac{\partial}{\partial y}\overline{\left\{\rho\left[\overline{v}+v'\right]\left[\overline{v}+v'\right]\right\}} = -f\left\{\rho\left[\overline{u}+u'\right]\right\} - \frac{\partial \overline{P}}{\partial y} - \overline{D_y} \qquad (3.14)$$

By the use of the time averaging axioms stated previously, equations (3.13) and (3.14) may be simplified to -

$$\frac{\partial \rho\overline{u}}{\partial t} + \nabla\cdot\rho\overline{u}\overline{\vec{V}} + \nabla\cdot\overline{\rho u'\vec{V}'} = f\overline{\rho v} - \frac{\partial \overline{P}}{\partial x} - \overline{D_x} \qquad (3.15)$$

$$\frac{\partial \rho\overline{v}}{\partial t} + \nabla\cdot\rho\overline{v}\overline{\vec{V}} + \nabla\cdot\overline{\rho v'\vec{V}'} = f\overline{\rho u} - \frac{\partial \overline{P}}{\partial y} - \overline{D_y} \qquad (3.16)$$

Multiplying equations (3.15) and (3.16) by $\overline{u}$ and $\overline{v}$ respectively we have -

$$\overline{u}\frac{\partial \rho\overline{u}}{\partial t} + \overline{u}\nabla\cdot\rho\overline{u}\overline{\vec{V}} + \overline{u}\nabla\cdot\rho u'\vec{V}' = \overline{u}f\overline{\rho v} - \overline{u}\frac{\partial \overline{P}}{\partial x} - \overline{uD_x} \qquad (3.17)$$

$$\overline{v}\frac{\partial \rho\overline{v}}{\partial t} + \overline{v}\nabla\cdot\rho\overline{v}\overline{\vec{V}} + \overline{v}\nabla\cdot\rho v'\vec{V}' = -\overline{v}f\overline{\rho u} - \overline{v}\frac{\partial \overline{P}}{\partial y} - \overline{vD_y} \qquad (3.18)$$

The Coriolis terms may be removed by the addition of equations (3.17) and (3.18) yielding -

$$\overline{u}\frac{\partial \rho\overline{u}}{\partial t} + \overline{v}\frac{\partial \rho\overline{v}}{\partial t} + \overline{u}\nabla\cdot\rho\overline{u}\overline{\vec{V}} + \overline{v}\nabla\cdot\rho\overline{v}\overline{\vec{V}} + \overline{u}\nabla\cdot\overline{\rho u'\vec{V}'} + \overline{v}\nabla\cdot\overline{\rho v'\vec{V}'} \qquad (3.19)$$

$$= -\overline{u}\frac{\partial \overline{P}}{\partial x} - \overline{v}\frac{\partial \overline{P}}{\partial y} - \overline{uD_x} - \overline{vD_y}$$

The following steps will simplify and combine terms to obtain an equation stating the balance of kinetic energy for the mean and fluctuating flows.

$$\tfrac{1}{2}\frac{\partial \rho\overline{u}^2}{\partial t} + \tfrac{1}{2}\frac{\partial \rho\overline{v}^2}{\partial t} + \overline{u}^2\nabla\cdot\rho\overline{\vec{V}} + \overline{v}^2\nabla\cdot\rho\overline{\vec{V}} +$$

$$\overline{u}\overline{\vec{V}}\cdot\nabla\rho\overline{u} + \overline{v}\overline{\vec{V}}\cdot\nabla\rho\overline{v} + \overline{u}\nabla\cdot\overline{\rho u'\vec{V}'} + \qquad (3.20)$$

$$\overline{\vec{v}}\cdot\overline{\rho v'\vec{V}'} = -\overline{\vec{V}}\cdot\nabla\overline{P} - \overline{uD_x} - \overline{vD_y}$$

Using the time averaged continuity equation, which is

$$\nabla\cdot\overline{\rho\vec{V}} = \nabla\cdot\rho\overline{\vec{V}} = 0$$

equation (3.20) can be written as

$$\frac{\partial}{\partial t}\left[\tfrac{1}{2}\rho\left(\overline{u}^2 + \overline{v}^2\right)\right] + \overline{u}\overline{\vec{V}}\cdot\nabla\rho\overline{u} + \overline{v}\overline{\vec{V}}\cdot\nabla\rho\overline{v} +$$

$$\overline{u}\overline{v}\cdot\overline{\rho u'\vec{V}'} + \overline{v}\overline{v}\cdot\overline{\rho v'\vec{V}'} = -\overline{\vec{V}}\cdot\nabla\overline{P} - d$$

where:

d is the dissipative force, $\overline{uD_x} - \overline{vD_y}$

The above equation can be further simplified to

$$\frac{\partial}{\partial t}\left[\tfrac{1}{2}\rho\left(\overline{u}^2 + \overline{v}^2\right)\right] + \overline{\vec{V}}\cdot\nabla\left[\tfrac{1}{2}\rho\left(\overline{u}^2 + \overline{v}^2\right)\right] +$$

$$\overline{u}\overline{v}\cdot\overline{\rho u'\vec{V}'} + \overline{v}\overline{v}\cdot\overline{\rho v'\vec{V}'} = -\overline{\vec{V}}\cdot\nabla\overline{P} - d \qquad (3.21)$$

By defining the mean kinetic energy to be as follows

$$\overline{K} \equiv \tfrac{1}{2}\left\{\overline{u}^2 + \overline{v}^2\right\}$$

and by substituting into equation (3.21), we have

$$\partial\frac{\rho\overline{K}}{\partial t} + \overline{\vec{V}}\cdot\nabla\rho\overline{K} + \overline{u}\overline{v}\cdot\overline{\rho u'\vec{V}'} + \overline{v}\overline{v}\cdot\overline{\rho v'\vec{V}'} = -\overline{\vec{V}}\cdot\nabla\overline{P} - d$$

As previously explained, ρ (density) can be used as a time average mean with no time dependent fluctuations. It can further be considered to be constant throughout the Beaufort Sea for any one chosen depth level without any noticeable effects on the results. In further considerations of density, ρ will be defined as 1000 kg per cubic meter. ρ may then be removed from the left hand side of the equation to leave

$$\frac{\partial \overline{K}}{\partial t} + \overline{\vec{V}}\cdot\nabla\overline{K} + \overline{u\nabla}\cdot\overline{u'\vec{V}'} + \overline{v\nabla}\cdot\overline{v'\vec{V}'} = -\left\{\frac{\overline{\vec{V}}}{\rho}\right\}\cdot\nabla\overline{P} - \frac{d}{\rho} \qquad (3.22)$$

By definition, $\frac{\partial \overline{K}}{\partial t} = 0$ and equation (3.22) may be rewritten as :

$$\overline{\vec{V}}\cdot\nabla\overline{K} + \overline{u\nabla}\cdot\overline{u'\vec{V}'} + \overline{v\nabla}\cdot\overline{v'\vec{V}'} = \left\{\frac{\overline{\vec{V}}}{\rho}\right\}\cdot\nabla\overline{P} - \frac{d}{\rho} \qquad (3.23)$$

Each of the terms of the equation are dimensionally equal to kinetic energy per unit time and mass, and represent an average kinetic energy of the flow field over the time interval used to provide the average. One could integrate equation 3.23 with respect to time to provide the total amount of kinetic energy expended or gained for a particular time interval. This can be written as

$$\int \overline{\vec{V}}\cdot\nabla\overline{K}dt + \int \overline{u\nabla}\cdot\overline{u'\vec{V}'}dt + \int \overline{v\nabla}\cdot\overline{v'\vec{V}'}dt = -\int\left\{\frac{\overline{\vec{V}}}{\rho}\right\}\cdot\nabla\overline{P}dt - \int\left\{\frac{d}{\rho}\right\}dt \qquad (3.24)$$

Looking at the terms individually -

$\int \overline{\vec{V}}\cdot\nabla\overline{K}dt$ represents the total amount of kinetic energy due to the mean velocity field within a specified depth range.

$-\int\left\{\frac{\overline{\vec{V}}}{\rho}\right\}\cdot\nabla\overline{P}dt$ represents the total amount of available kinetic energy due to the mean pressure field within a specified depth range.

$-\int\frac{d}{\rho}dt$ is the total amount of kinetic energy due to the dissipative forces.

The terms $\int\left\{\overline{u\nabla}\cdot\overline{u'\vec{V}'} + \overline{v\nabla}\cdot\overline{v'\vec{V}'}\right\}dt$ can be expanded to form

$$\int\left[\overline{u}\frac{\partial\overline{u'u'}}{\partial x} + \overline{u}\frac{\partial\overline{u'v'}}{\partial y} + \overline{v}\frac{\partial\overline{u'v'}}{\partial x} + \overline{v}\frac{\partial\overline{v'v'}}{\partial y}\right]dt \qquad (3.25)$$

A further expansion of the above terms can be done using the definition that $\frac{\partial AB}{\partial x} \equiv A\frac{\partial B}{\partial x} + B\frac{\partial A}{\partial x}$. The terms in 3.25 can be rewritten as:

$$\int\left[\frac{\partial}{\partial x}\left[\overline{u}\left[\overline{u'u'}\right]\right] - \overline{u'v'}\frac{\partial \overline{u}}{\partial x} - \overline{u'v'}\frac{\partial \overline{u}}{\partial y}\right] dt +$$

$$\int\left[\frac{\partial}{\partial y}\left[\overline{u}\left[\overline{u'v'}\right]\right] + \frac{\partial}{\partial x}\left[\overline{v}\left[\overline{u'v'}\right]\right] - \overline{u'v'}\frac{\partial \overline{v}}{\partial x}\right] dt +$$

$$\int\left[\frac{\partial}{\partial y}\left[\overline{v}\left[\overline{v'v'}\right]\right] - \overline{v'v'}\frac{\partial \overline{v}}{\partial y}\right] dt$$

Regrouping the terms we have

$$\int\left[\frac{\partial}{\partial x}\left[\overline{u}\left[\overline{u'u'}\right]\right] + \frac{\partial}{\partial x}\left[\overline{v}\left[\overline{u'v'}\right]\right] + \frac{\partial}{\partial y}\left[\overline{u}\left[\overline{u'v'}\right]\right] + \frac{\partial}{\partial x}\left[\overline{v}\left[\overline{v'v'}\right]\right]\right] dt + \qquad (3.26a)$$

$$\int\left[\overline{u'u'}\frac{\partial \overline{u}}{\partial x} + \overline{u'v'}\frac{\partial \overline{u}}{\partial x} + \overline{u'v'}\frac{\partial \overline{u}}{\partial y} + \overline{v'v'}\frac{\partial \overline{v}}{\partial y}\right] dt \qquad (3.26b)$$

The terms in 3.26a represent the advection of mean kinetic energy carried by the turbulence while the terms in equation 3.26b represent the increase in mean kinetic energy at the expense of the horizontal turbulence(Webster, 1961).

Rewriting the complete horizontal equation of kinetic energy with the above mentioned divisions we have

$$\int\left[\overline{u}\frac{\partial \overline{K}}{\partial x} + \overline{v}\frac{\partial \overline{K}}{\partial y}\right] dt +$$

$$\int\left[\frac{\overline{u}}{\rho}\frac{\partial \overline{P}}{\partial x} + \frac{\overline{v}}{\rho}\frac{\partial \overline{P}}{\partial y}\right] dt +$$

$$\int\left[\frac{d}{\rho}\right] dt +$$

$$\int \left[\frac{\partial}{\partial x} \left\{ \overline{u} \left\{ \overline{u'u'} \right\} \right\} + \frac{\partial}{\partial x} \left\{ \overline{v} \left\{ \overline{u'v'} \right\} \right\} + \frac{\partial}{\partial y} \left\{ \overline{u} \left\{ \overline{u'v'} \right\} \right\} + \frac{\partial}{\partial y} \left\{ \overline{v} \left\{ \overline{v'v'} \right\} \right\} \right] dt +$$

$$\int \left[\overline{u'u'} \frac{\partial \overline{u}}{\partial x} + \overline{u'v'} \frac{\partial \overline{v}}{\partial x} + \overline{u'v'} \frac{\partial \overline{u}}{\partial y} + \overline{v'v'} \frac{\partial \overline{v}}{\partial y} \right] dt = 0 \qquad (3.27)$$

The PCM data sets at each camp during the main AIDJEX experiment were broken up into monthly segments. In each segment, the following values were tabulated at one meter intervals from the surface to 200 meters:

$$\overline{u}, \overline{v}, \overline{K}, \overline{u'u'}, \overline{u'v'}, \overline{v'v'}$$

The average position for the camp during the month as it drifted in response to the prevailing winds and ocean currents was also calculated. Five meter layer averages of the above quantities were then made for all the segments. Then for any one layer, say the 8 to 12 meter layer (denoted as the 10 meter averaged layer), gradients were calculated using the distance between the average monthly position of the camps in question.

During the experiment, three camps were used in the analysis for any one month. The month of October 1975 was removed from the analysis because only two camps were actively taking PCM stations. This was a result of the breakup of Big Bear and the subsequent evacuation to Camp Caribou which lasted from late September 1975 to the end of October 1975. During this time period, very few PCM or STD stations were taken at either camp.

In order to avoid gradients that did not represent mean changes over long distances, the shortest intercamp distances in both the x and y gradients were removed from consideration. An example of intercamp distance rejection can be seen for the month of November 1975, when Caribou, Blue Fox and Snowbird were used as the three operational camps. Their average position for this month is shown in figure 57. Table 12 shows the x and y intercamp distance in kilometers.

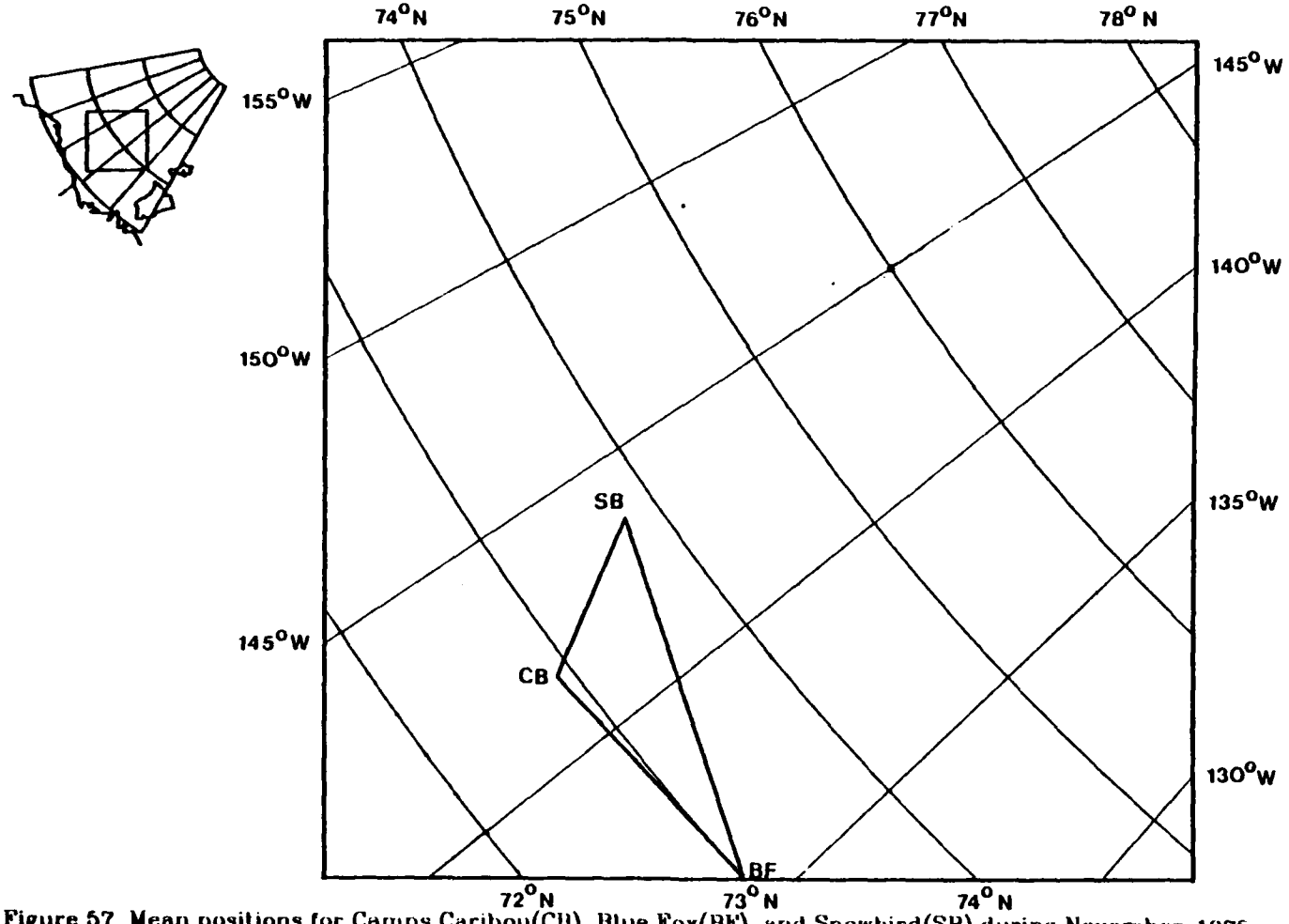


Figure 57. Mean positions for Camps Caribou(CB), Blue Fox(BF), and Snowbird(SB) during November 1975.

Table 12

Data for the Month of November 1975
Camps Used in the Analysis were Caribou, Blue Fox, and Snowbird

	AVERAGE POSITION		INTER-CAMP DISTANCE (km)		
Camp	Latitude degrees N.	Longitude degrees W.	**-**	X(km)	Y(km)
Caribou	72.936989	-141.794449	CB-BF	176.5	4.6
Blue Fox	72.978043	-136.402390	BF-SB	229.7	79.5
Snowbird	73.690811	-143.436279	CB-SB	53.8	84.1

CB-SB inter-camp values removed from calculations because of minimum x dist.
CB-BF inter-camp values removed from calculations because of minimum y dist.

The intercamp distances between Caribou and Blue Fox as well as Caribou and Snowbird were removed because of the short distance in the y and x directions respectively. The gradients that were finally calculated used the intercamp data from Caribou-Blue Fox and Blue Fox-Snowbird in the x direction and Blue Fox-Snowbird and Caribou-Snowbird in the y direction.

Due to the low statistical significance in the determination of a low amplitude mean (few cm/sec) from a short record consisting of high amplitude fluctuations, PCM data was not used for the calculation of mean velocities. As a result, the mean dynamic topography of the Beaufort Sea(figure 13) was used to calculate the components of $\overline{u}$ and $\overline{v}$ at the average monthly position of the camps. Gradients were then calculated for the camps as previously described. Table 13 indicates the mean geostrophic velocities as calculated from the dynamic topography of the 30 decibar level relative to the 500 decibar level (30/500 db) of the Beaufort Sea. Because of the curvature of the dynamic contours and the sometimes large intercamp distances involved, individual gradients would sometimes vary in sign between the camps for a particular month. To circumvent this, only those months when the intercamp gradients were identical in sign were included in the analysis. Using this criterion, only

four of the eleven months were used in the kinetic energy flux analysis. The four months were June, July, August and September of 1975.

The average eddy kinetic energy flux data as calculated for each camp at 5 meter intervals(10 to 190 meters for the months of June to September 1975)

Table 13

Estimated surface geostrophic velocities using Newton's(1973) maps of dynamic topography at the average monthly positions of the camps.

Month	Camp	$\overline{U_g}$	$\overline{V_g}$
May-1975	Blue Fox	1.5	-1.7
	Snowbird	2.2	1.3
	Big Bear	3.2	0.2
Jun-1975	Blue Fox	2.5	0.0
	Snowbird	1.8	1.5
	Big Bear	2.1	1.4
Jul-1975	Blue Fox	3.4	-3.3
	Snowbird	2.1	1.4
	Big Bear	2.5	0.6
Aug-1975	Blue Fox	-1.9	-3.0
	Snowbird	-4.0	-1.9
	Big Bear	-2.1	-3.3
Sep-1975	Blue Fox	-1.0	-2.4
	Snowbird	-2.8	-1.7
	Big Bear	-1.5	-2.1
Oct-1975	Blue Fox	-1.3	-2.2
	Snowbird	-3.0	-1.3
Nov-1975	Caribou	-2.1	-0.7
	Blue Fox	-1.1	-2.1
	Snowbird	-3.1	-0.9
Dec-1975	Caribou	-2.8	-0.5
	Blue Fox	-1.4	-2.2
	Snowbird	-3.6	-1.5
Jan-1976	Caribou	-2.8	-0.6
	Blue Fox	-1.7	-1.6
	Snowbird	-3.7	-1.5
Feb-1976	Caribou	-2.2	-0.5
	Blue Fox	-1.2	-1.9
	Snowbird	-3.4	-1.2
Mar-1976	Caribou	-2.2	-0.5
	Blue Fox	-1.5	-1.7
	Snowbird	-3.7	-0.8
Apr-1976	Caribou	-2.3	-0.5
	Blue Fox	-1.4	-1.8
	Snowbird	-3.7	-0.7

are shown in figures 58,59,60, and 61. These plots represent the sum of the eddy kinetic energy terms listed in equation 3.26a and 3.26b without the integration being done. Positive values indicate the transfer of eddy kinetic energy to the mean field, i.e. - counter gradient. Negative values indicate the normal dissipative regime in the cascading of energy from large to smaller features.

June of 1975 was the only month which showed the flux of eddy kinetic energy to be largely positive. The other three months indicate the transfer of eddy kinetic energy in a down-gradient sense.

During the month of June 1975, the monthly average of the fluctuating kinetic energy terms at each of the camps showed a dominant eddy signature. Kinetic energy increased below the base of the mixed layer and reached a maximum value between 100 and 150 meters, after which it decreased with depth. This is also reflected in the eddy kinetic energy flux shown in figure 58 by the broad peaks at mid-depth for each of the camps. Big Bear does show a negative flux in certain depth regions; however, from 100 to 130 meters where eddy kinetic energy was the largest, there is a positive flux. Data pertaining to the flux of kinetic energy during the months of July, August, and September are shown in figures 59,60, and 61 respectively.

Although data show fluxes from the eddies to the mean flow, this does not invalidate the assumption that $\frac{\partial \overline{K}}{\partial t} = 0$. During the one month time period that the data was averaged, only the bottom two lines of equation 3.27 were calculated. Energy provided in the top 3 terms would then provide the energy necessary to balance the system.

The amount of barotropic component within the fluctuating part of the kinetic energy was significantly less in June than the months of July , August, and September. In June, the barotropic component at each of the camps

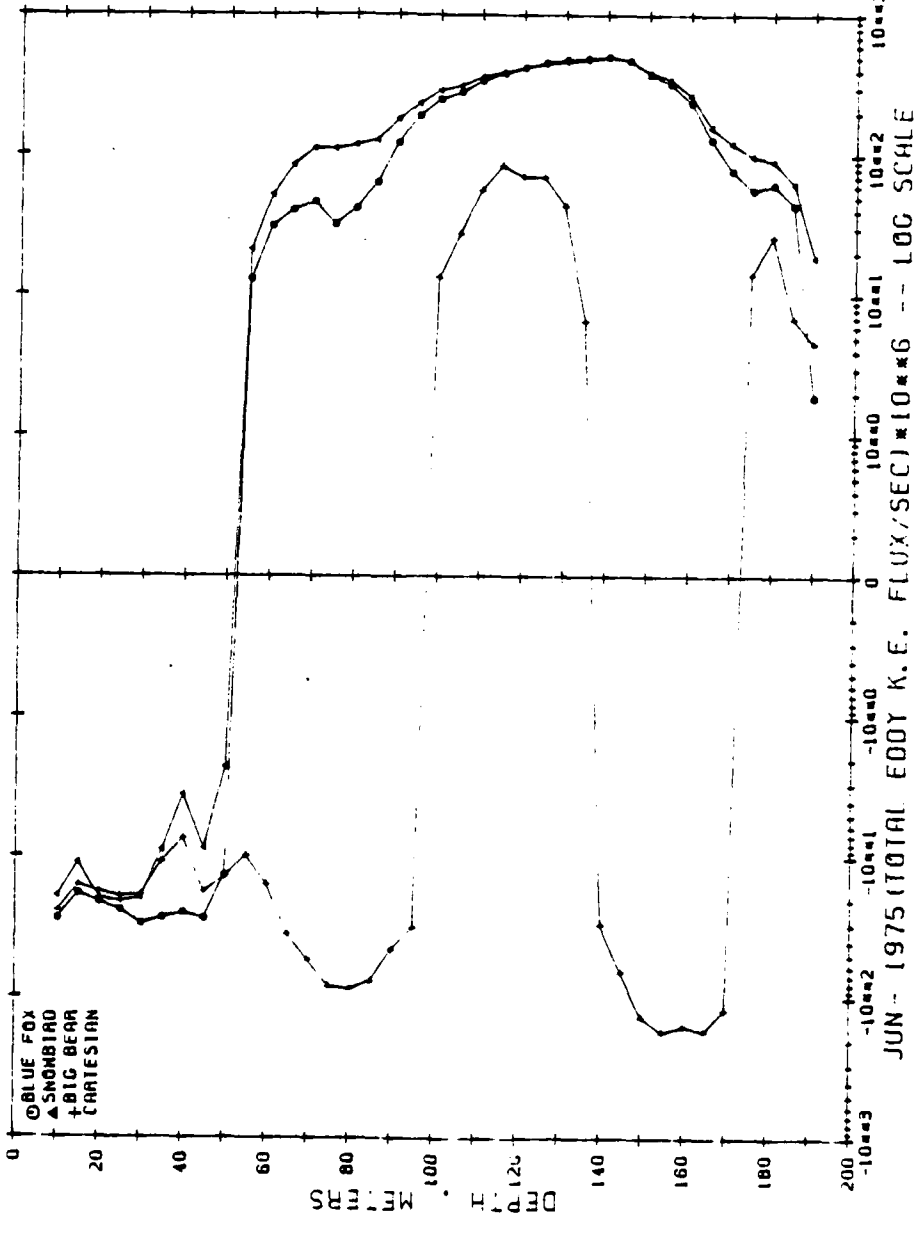


Figure 58. Eddy kinetic energy flux for June 1975.

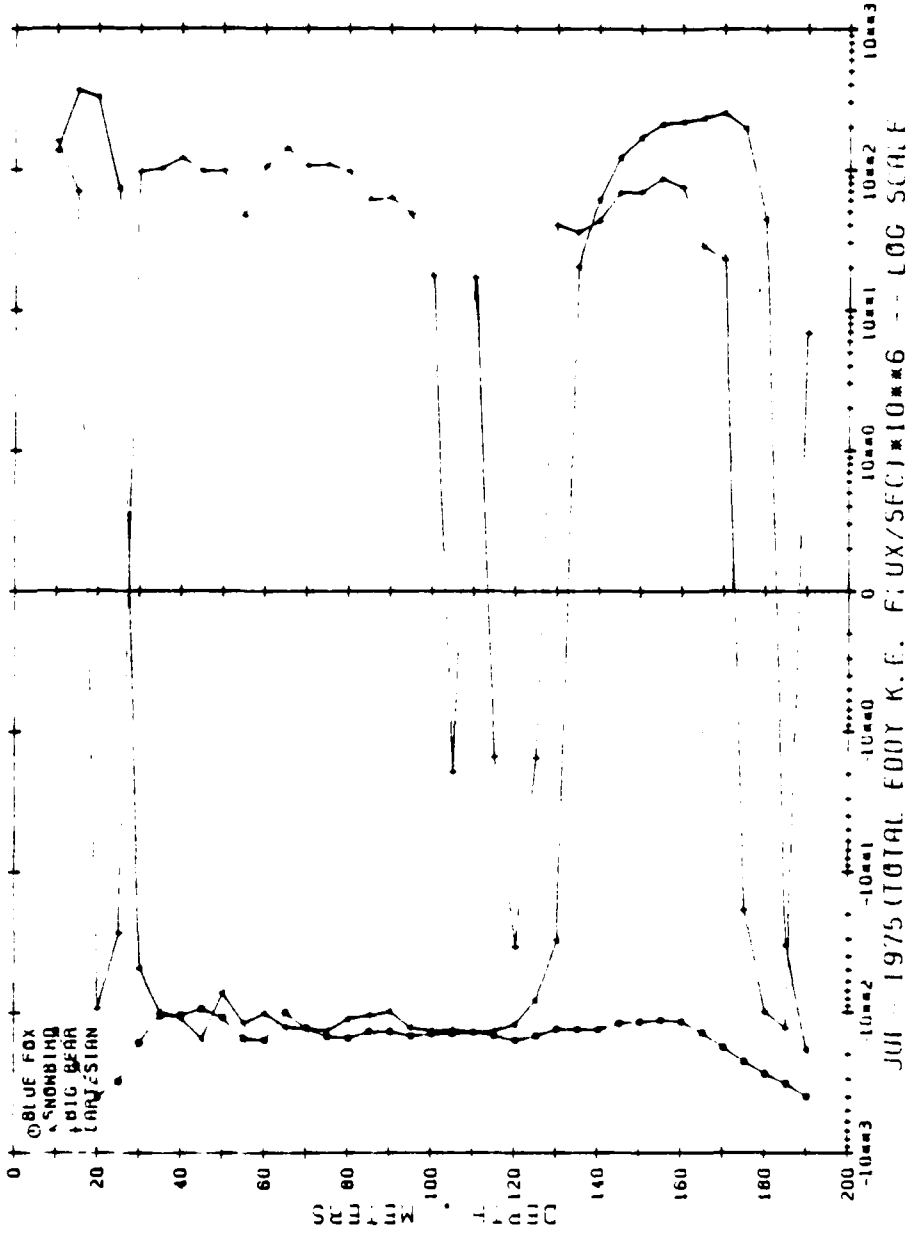


Figure 59. Eddy kinetic energy flux for July 1975.

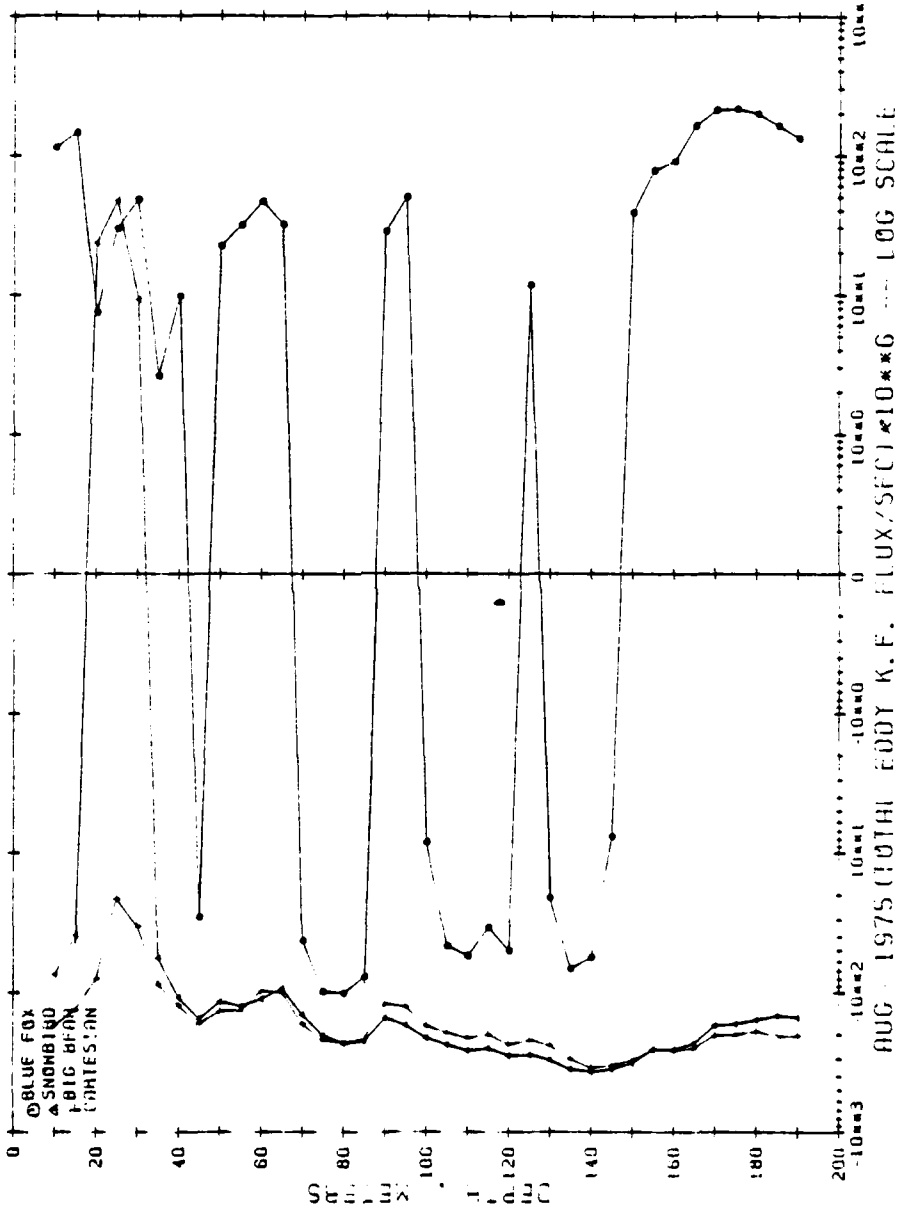


Figure 60. Eddy kinetic energy flux for August 1975.

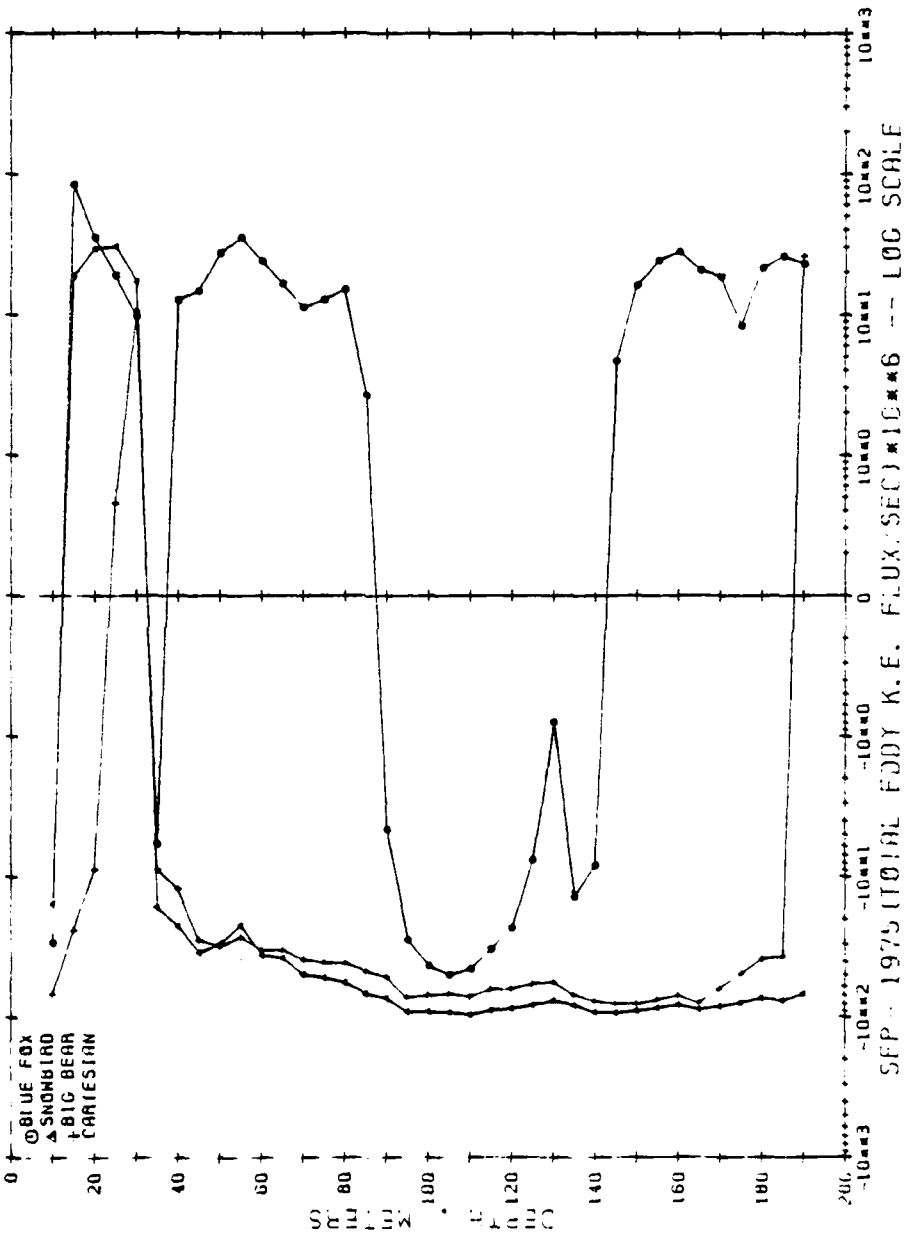


Figure 61. Eddy kinetic energy flux for September 1975.

ranged from less than 10% to 20% of the fluctuating component. In the other months the barotropic component tended to dominate the fluctuating part of the kinetic energy as seen in Table 10. A corresponding plot of Table 10 is shown in figures 55a and 55b. This agrees well with the positional data during the months of July, August, and September, when the camps moved rather large distances. During these high drift months, the barotropic component of the fluctuating kinetic energy varied from approximately 40% to 60% with very little baroclinic eddy kinetic energy observed, as in contrast to the month of June 1975.

In the final analysis, two separate mechanisms can be seen to operate within the Beaufort Sea area. The first is the barotropic component which is strongly dominant during July, August, and September and the second is that of the eddy(baroclinic) field which is strongly dominant over the barotropic component during the month of June. The barotropic component appears to provide kinetic energy to, as well as remove kinetic energy from, the mean field depending on the orientation of the barotropic currents to the mean dynamic topography. This even suggests the well known fact that the long term atmospheric forcing in this part of the Canadian Basin resulted in the formation of the dynamic topography of the Beaufort Sea. It is not unrealistic to expect that the barotropic component which is a result of the atmospheric systems would also be responsible for maintaining the mean kinetic energy field of the Beaufort Sea.

During June 1975, the baroclinic eddy field dominated strongly over the barotropic field and suggested a counter gradient flow of kinetic energy from the mesoscale eddies to the mean field. This is not in agreement with Hunkins(1974) who showed a normal dissipative regime. This may be explained in the difference of terms used in the respective analyses. Hunkins(1974) used only one of the eight eddy flux terms in the same manner as that of Web-

ster(1961), while this procedure used all of the terms in 3.26a and 3.26b.

4. Partition of Energy Within the Arctic Eddies

A) Background

Relatively little is known about the relationship between the two different energy fields existing within the mesoscale eddies of the Arctic Ocean. As previously discussed, the kinetic energy of the eddies almost completely dominates the kinetic energy field of the upper 200 meters of the western Arctic Ocean.

The mechanism that provides the eddy kinetic energy, in this case, is a conversion of potential energy stored in the anomalous density structure of the eddy which is a result of the temperature and salinity anomalies. It is important to understand the relationship between the available potential energy and the kinetic energy field of an eddy for several reasons. The first is to understand if mesoscale eddies of the Arctic approximate a theoretical concept pertaining to the partition of energy and second, to suggest an approximate life span.

Using Lorenz'(1955) original definition of available potential energy (APE), Barrett(1971) calculated the energy stored within two newly formed Gulf Stream rings as well as two other Gulf Stream rings that were in a more advanced stage of decay. Estimates of the loss rate of APE was .005-.010 joules/m^2-sec.

Estimates for the life span of an arctic eddy have been suggested by Hunkins(1974) and more recently(personal communication) to be several months to a year. Unfortunately, actual detailed analysis of the data does not provide this answer for several reasons -

1) The same eddy must be crossed at two different time periods

2) the crossing of the eddy must be along the diameter with a representative number of stations. Even this is a minimum requirement because as to this

date, eddies of the Arctic have had no three dimensional coverage to insure radial symmetry. Investigations pertaining to the physical dimensions of eddies in the other oceans have shown them to range from circular to elliptical.

With the AIDJEX data set, as well as previous historical data, eddies have been observed along the somewhat erratic drift track of the ice camp. Only recently have reliable small portable sensors been developed to study mesoscale features of the Arctic Ocean using helicopters or small planes as transportation. A study of this type within the Beaufort Sea would advance the understanding of these features in several areas, particularly their movement, decay and life span.

B) Partition of Energy - A Simplified Theory for Geostrophic Flow

The anomaly of potential energy per unit mass coming from the vertical displacement ,Δz, of a given σ_t surface from its normal mean level (Ebbesmeyer and Taft,1979), is defined as

$$APE = 0.5N^2\Delta z^2 \tag{4.1}$$

where N is the corresponding Brunt-Väisälä or buoyancy frequency associated with a specified σ_t layer and is defined in equation 4.2

$$N^2 = \frac{g}{\rho_0}\frac{d\rho}{dz} \tag{4.2}$$

where:

g is the gravitational acceleration,
ρ_0 is the mean density,
$d\rho$ is the change in density over a finite change in depth(dz)

Eddy kinetic energy anomaly per unit mass is defined as

$$AKE = \tfrac{1}{2}\Delta v^2 \tag{4.3}$$

where:

Δv is the velocity difference of two points on a horizontal plane a given distance apart.

For a geostrophic current in a stratified ocean where the y-axis is aligned in the direction of flow(u = 0), the following must be true:

$$\frac{dP}{dx} = \rho f v \tag{4.4}$$

$$\frac{dP}{dz} = \rho g \tag{4.5}$$

where:

P is pressure
f is the Coriolis parameter($2\omega\sin\theta$), ω being the angular velocity of the earth ($7.29 \times 10^{-5} sec^{-1}$).

Cross differentiation of equation(4.1) and(4.2) with respect to z and x respectively and subsequent substitution yields

$$\frac{\partial v}{\partial z} = \frac{g}{\rho f}\frac{\partial \rho}{\partial x} - \frac{v}{\rho}\frac{\partial \rho}{\partial z} \tag{4.6}$$

In the high latitudes of the Arctic, both the mean and eddy kinetic energy fields can be defined. On the basis of order of magnitude calculations for both fields, it can be shown that the first term on the right hand side of equation(4.6) is approximately 2 orders of magnitude greater than the second term. Equation(4.6) may then be rewritten to include only the most important term.

$$\frac{\partial v}{\partial z} = \left\{\frac{g}{\rho f}\right\}\frac{\partial \rho}{\partial x} \tag{4.7}$$

The above equation is the oceanographic analog to the meteorologist's thermal wind equation(Hess,1959). In finite difference form, equation (4.7) can be rewritten as

$$\frac{\Delta v}{\Delta z} = \frac{g}{\rho f}\frac{\Delta \rho}{L} \tag{4.8}$$

where:

L is the characteristic length of the density disturbance corresponding to $\Delta\rho$.

Combining equation(4.2) with equation(4.8) we have

$$\frac{\Delta v}{\Delta z} = \frac{N^2 \Delta z}{fL} \tag{4.9}$$

or in terms of the kinetic energy anomaly(A.K.E.)

$$\left\{\frac{\Delta v}{\Delta z}\right\}^2 = \frac{N^4 \Delta z^2}{f^2 L^2} \tag{4.10}$$

By defining the ratio of AKE to APE to be

$$\frac{AKE}{APE} = \frac{\frac{1}{2}\Delta v^2}{\frac{1}{2}N^2\Delta z^2} = \left\{\frac{\Delta v}{\Delta z}\right\}^2 N^{-2} \tag{4.11}$$

equation(4.10) may be written as

$$\frac{AKE}{APE} = \frac{N^2\Delta z^2}{f^2L^2} \tag{4.12}$$

By then defining the Rossby radius of deformation(R_d) to be

$$R_d = \frac{N\Delta z}{f} \tag{4.13}$$

equation(4.12) can be written as

$$\frac{AKE}{APE} = \left\{\frac{R_d}{L}\right\}^2 \tag{4.14}$$

The corresponding graph of such a relation is shown in figure 62. Geostrophic flows that are of the order of the Rossby radius, as are the eddies of the Arctic(Hunkins,1974;Newton et al,1974), should have an equal partition of energy. Those features with longer length scales will have a larger store of APE than KE by approximately the ratio of $1 + \frac{\Delta L}{R_d}$ where ΔL is defined to be:

$$\Delta L = L - R_d \tag{4.15}$$

The APE/KE ratio for length scales less than R_d is not described by this relation which assumes geostrophy. In the case of small features such as gravity waves, the partition of energy is equal.

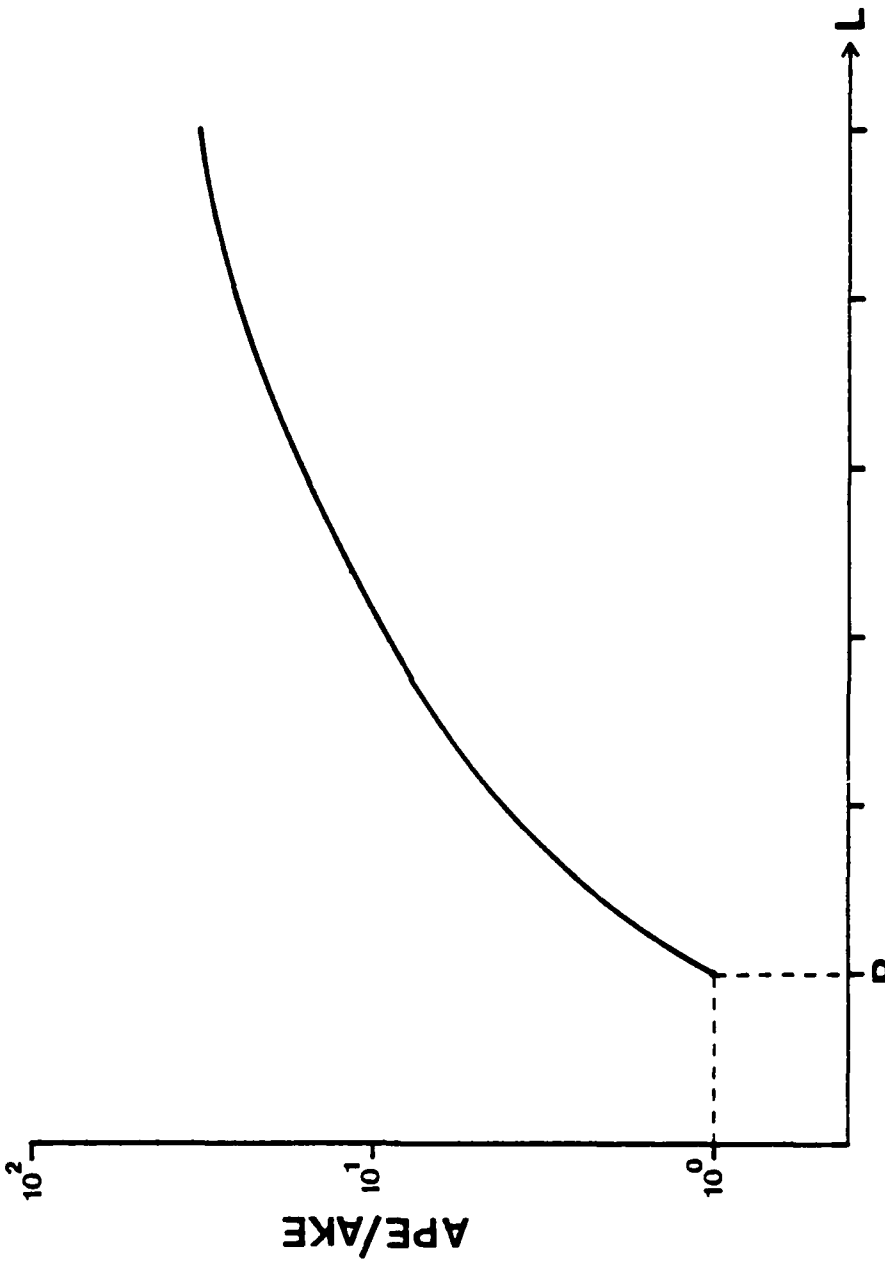


Figure 62. Theoretical partition of energy for geostrophic flows as a function of length(L). R_D is the internal Rossby radius of deformation.

C) Kinetic and Available Potential Energy Models

Kinetic energy as well as available potential energy were calculated for a simplified model using data from the eddy observed during the 1972 AIDJEX pilot study at Camp Brass Monkey(figure 24). This eddy was used because of the exceptional pass across its diameter as well as the amount of current meter and hydrographic data taken. Available kinetic energy and available potential energy were modeled separately and then later compared.

In order to calculate the partition of energy, several assumptions were made. These assumptions are 1) the eddy is circular, and 2) 150 meters is the depth of current maximum. Based on observational data the eddy can be considered to be confined between the depth range of 50 to 250 m.

A cylindrical coordinate system was used, the origin placed at the center of the eddy. The r-axis defines radial distance away from the center of the eddy in meters, and the z-axis (+ downwards) defines distance in meters away from the depth of maximum velocity(150 m).

1) Kinetic Energy Model

Horizontal velocities along the radius of the eddy are divided into a rotational flow where velocity is proportional to r and a flow where velocity is inversely proportional to r^2 . For the eddy which is being modeled, rotational flow is valid within the range of 0 to 7000 meters. Flow where velocity is inversely proportional to r^2 is defined for distances greater than 7000 m. At the depth of maximum velocity, horizontal velocities, V_0, can be written in the following manner:

$$V_0 = \begin{cases} Ar & \text{if } 0 \leq r \leq 7000 \\ AR^3r^{-2} & \text{if } r > 7000 \end{cases} \tag{4.16}$$

where:

A = constant

r = distance away from center (m)

R = critical radius or the maximum radius at which solid body rotation exists

Based on previous observation of eddies, the vertical profile of horizontal velocity is defined as a parabola whose maximum velocity is given by equation 4.16.

$$V = V_0\left[1 - Bz^2\right] \tag{4.17}$$

where:

V is horizontal velocity (m/sec)

V_0 is horizontal velocity at depth of maximum velocity(equation 4.16)

B is a constant

Z is the relative vertical depth (m), 0 is defined as the depth of maximum velocity.

Because the eddy is defined to be symmetric about the vertical axis, equation 4.17 represents the velocity within the eddy at any given point. Kinetic energy per unit volume, KE, at any point within the eddy may then be defined using equation 4.17.

$$KE = 0.5\rho V_0^2\left[1 - Bz^2\right]^2 \tag{4.18}$$

Total kinetic energy, KE_T, can then be calculated by integrating over the eddy in the following manner:

$$KE_T = \int_0^R \int_0^{2\pi} \int_{-B^{-\frac{1}{2}}}^{B^{-\frac{1}{2}}} 0.5\rho\left[A^2r^2\right]\left[1 - Bz^2\right]^2 \, dz \, d\theta \, dr \; +$$

$$\int_R^{\infty} \int_0^{2\pi} \int_{-B^{-\frac{1}{2}}}^{B^{-\frac{1}{2}}} 0.5\rho\left[A^2R^6r^{-2}\right]\left[1 - Bz^2\right]^2 \, dz \, d\theta \, dr \qquad (4.19)$$

For the eddy observed during the 1972 AIDJEX pilot study(figure 24), the values of the various constants are defined as follows:

$$A = 5\text{x}10^{-5}\ \text{sec}^{-1}$$
$$R = 7\text{x}10^{3}\ \text{m}$$
$$B = 1\text{x}10^{-4}\ \text{m}^{-2}$$

Calculating equation 4.19 with the above constants yields:

$$KE_T = 1.51 \times 10^{12}\ \text{joules}$$

2) Available Potential Energy Model

Using the definition of potential energy anomaly as defined by Fofonoff(1962),

$$PEA = \frac{1}{g}\int_0^P P\delta dP \qquad (4.20)$$

where:
δ is the specific volume anomaly

The largest value of available potential energy for an individual station was $2.5\text{x}10^4$ joules/m^2 which was calculated approximately 2000 m from the defined center of the eddy. If it is assumed that this value represents the APE at the center of the eddy, then the following equation would define the available potential energy of the eddy as a function of radius from its center.

$$APE = Ce^{-\frac{r}{D}^2} \tag{4.22}$$

Integrating over the eddy, the total available potential energy (APE_T) can then be defined as

$$APE_T = \int_0^{\infty} \int_0^{2\pi r} Ce^{-\frac{r}{D}^2} \, d\theta \, dr \tag{4.23}$$

Coefficients used for equation 4.23 were

$$C = 2.5 \times 10^4 \text{ joules}/m^2$$
$$D = 2.2 \times 10^3 \text{ m}$$

Evaluating 4.23, we have

$$APE_T = 3.8 \times 10^{11} \text{ Joules}$$

D) Discussion

Using the results from the kinetic energy model, the ratio of KE_T to APE_T is

$$\frac{KE_T}{APE_T} = \frac{1.5x10^{12}}{3.8x10^{11}} = 3.97$$

As indicated by the partition of energy, the eddies of the Arctic Ocean are in close agreement with the theoretical result of 1.0. Although no error limits for the models are given, the least accurate was that of the available potential energy. This was a result of the few hydrographic stations taken(which was more than that taken in other eddies). Calculated potential energy anomalies in various parts of the eddy showed no smooth decay with increasing distance away from the center of the eddy. Within the errors of the calculations, it is believed that the models represent a good approximation to that of the typical arctic eddy.

As previously mentioned, the actual calculation of loss of APE in one of the arctic eddies using the AIDJEX data set cannot be done. This does not preclude using estimates of the loss of energy(APE) by the Gulf Stream rings with an estimate of the total APE of the eddy just discussed. Barrett(1971), using 4 different Gulf Stream rings, two newly formed and two in a later stage of decay, calculated a rate of energy transformation (from APE to KE) of .005-.010 joules/m^2-sec. For the Gulf Stream rings, this energy transformation rate would imply a lifetime of three to five years before the anomalous field of the eddy would be reduced to the background noise level.

If a decay rate of .005 joules/ m^2-sec. were used with the assumption that decay is linear through time, the arctic eddy used in the previous model would decay within two months. Although the eddy used in this calculation displayed peak velocities that were half that of the Snowbird eddy(figures 40-43), the residence time of the eddy is not unreasonable within an order of magnitude. Using potential energy anomalies from higher velocity eddies, life expectancies

may be within the range of six months to a year. Based on a theory of frictional dissipation against the base of the ice and mixed layer, Hunkins (unpublished manuscript), calculated a life expectancy of an arctic eddy to be in the range of several months to a year.

Light on this question is given by the multiple observations of eddies based on T-S signatures(Table 14). Eddy number 4 was observed over a period of 5.5 months. Prior to its observation, it was unknown how much time this particular eddy had already spent within the Beaufort Sea. If it can be assumed that its origin was located in the region around Point Barrow and that it did travel in response to the mean geostrophic field(.05 m/sec), then its age at the first sighting would have been close to 8 months. Total time would then be 13.5 months, with the last observation still not showing the T-S anomaly being reduced to the background noise of the mean conditions.

Even though the eddies of the Beaufort Sea occupy only 25% of the volume of the upper 300 m, their total energy content is comparable to that of the mean kinetic energy of the entire ocean.

Previously it was estimated that 450 eddies could be observed within the areal extent of the Beaufort Sea(600,000 km^2) at any given point in time. Using the value obtained from the kinetic energy model of $1.5x10^{12}$ joules for a typical eddy, 450 eddies would comprise a total eddy kinetic energy of $6.8x10^{14}$ joules. This number, however, is restricted to the upper 300 m of the water column.

If a constant mean velocity of .05 m/sec is used for the upper 300 m and .01 m/sec for the remainder of the water column to a depth of 4000 m, then the total amount of mean kinetic energy contained within the Beaufort Sea would be $3.4x10^{14}$ joules of which $2.3x10^{14}$ joules were calculated for the upper 300 m.

Within order of magnitude calculations, the amount of energy stored within the eddies is comparable to that of the mean energy stored within the Beaufort Sea. With respect to the upper layer mean kinetic energy, eddy energy is only slightly larger by a factor of 3 and can not be considered a meaningful difference.

This estimate of the partition of kinetic energy due to the mesoscale eddies and that of the mean flow does not agree with the results obtained from the profiling current meter data(figure 53) which show mesoscale eddy kinetic energy to be an order of magnitude greater than the mean field. There may be several reasons for this difference such as the observed data being overly dominated by mesoscale eddy activity, or the number of eddies within the AIDJEX sector being underestimated. What may be interpreted, however, is that 50% to 90% of the total kinetic energy within the Beaufort Sea is a result of mesoscale eddies.

5. Estimates of the Importance of Heat,Salt and Biomass Fluxes by Eddies

A) Background

Fluxes of heat, salt, momentum and available potential energy have been calculated across various fronts in differing parts of the oceans. Oort(1964) showed that the meanders associated with the Gulf Stream near Onslow Bay were transporting heat from the shelf to the deep ocean against the gradient, i.e. from cold to warm. The estimated amount of heat transport across the Gulf Stream front was approximately 5% that of the total northward heat flux for the entire North Atlantic.

Bryden(1978) also calculated the poleward flux of heat across the polar front in the Drake Passage and found that low frequency motion (<1 cpd) could account for enough heat transport to equal the loss of heat to the atmosphere from the ocean surrounding the Antarctic continent.

The calculation of fluxes across fronts have several inherent difficulties associated with them. The first and foremost is whether these low frequency motions carrying the heat and salt, transfer all or only a fraction of the total amount available. The second problem is if the area of interpretation is truly representative of the mean transfer rates of heat, salt or other constituents.

In the case of the AIDJEX data set it is impossible to calculate directly the amount of heat or salt across the active front producing these eddies because no long duration data set is available within this area. Other information relating to estimates of heat, salt and biomass flux can, on the basis of the AIDJEX data set, be presented. First, however, some background must be developed upon which to build further conclusions.

B) Decay Within the Deep Ocean

Contrary to the generally accepted life history of Gulf Stream rings, which are capable of transferring only a portion of their total anomalous field to their surroundings because of eventual entrainment with the Gulf Stream, it is believed that a large majority of eddies of the Arctic decay entirely within the confines of the deep ocean.

It is not suggested that all of the eddies produced in this region never coalesce with the front, but rather those eddies that are found a great distance away from the generating area are advected with the general flow field, and therefore would not be reabsorbed back into the generating area. This statement is based on several observations which will be listed in more detail below.

1) Question of Preferential Movement

Gulf Stream rings do not move with the clockwise mean circulation of the Sargasso Sea but rather move consistently southwestward. This preferential movement of cyclonic Gulf Stream rings was discussed by Warren(1967) who showed possibilities for this drift as a result of the beta effect(latitudinal change in the Coriolis force), asymmetries in the ring, and bottom topography.

For the arctic eddies, only one parameter - the beta effect - may play an important role. Steering by bottom topography has no effect on the shallow eddies of the Arctic except when contact of continental shelf is made. The horizontal asymmetry of the eddies is completely unknown; however, on the basis of the beta effect argument, this asymmetry may be of little importance.

The equation used to define the beta effect on the radius of curvature for a particle moving within a ring is written as:

$$K_t - K_0 + \frac{\beta y}{v} = 0 \qquad (5.1)$$

and was initially derived by Whipple(1917) to define the movement of water parcels undergoing horizontal oscillations centered about the equator;
where:

v is an undefined velocity on a non-divergent isopycnal surface.

β (beta) has the following relation, $f = f_0 + \beta y$, where f_0 is the Coriolis parameter at the center of the ring. y is the North-South distance from the center of the ring(positive is North)

K_t is the horizontal component of curvature for the particle trajectory (positive for cyclonic curvature, negative for anticyclonic curvature)

K_0 is the reference horizontal radius of curvature

From this equation, it can be seen that for a cyclonic eddy as beta increases towards the north, the curvature must become larger and as beta decreases to the south, the curvature must become smaller. This change in the radius of curvature as the particle moves around the eddy defines a path which steadily translates the particle westward. The same preferential movement is also true for anticyclonic eddies in that the northward radius of curvature is smaller and to the south, the radius of curvature becomes larger.

For a Gulf Stream ring possessing a diameter of 200 kilometers and centered at a latitude of 45 degrees, there would be a 4% change in the Coriolis parameter. For an arctic eddy whose typical diameter is 10 km, the corresponding change in the Coriolis parameter at a latitude of 75 degrees north would be three orders of magnitude less than that of the Gulf Stream ring. On the basis of these calculations, it appears that this effect is most likely insignificant.

As previously indicated in chapter 2, several of the eddies were observed more than once at the same camp or different camps based on T-S data. Specifically 31 of the 146 individual crossings were shown to be the observation of 12 different eddies at various times and are listed in Table 14. Most of the duplicate observations were recrossings of the same eddy; two eddies however, were observed by different camps with the longest time difference between observations of six months. A list of these individual eddies and the observa-

tions that define them by STD station numbers as well as their respective dates, are shown in Table 14. Figure 63 indicates the directions of travel taken by the 12 eddies superimposed on the mean dynamic topography of the Beaufort Sea. As can by seen, many of the eddies travel along paths that are not in agreement with the mean flow field such as eddy numbers 1, 5, 6, 10, and 12(figure 63). It is believed that these movements over short periods of time are the result of the instantaneous and highly variable barotropic wind driven currents. Over the long term mean of many months to years, it is expected that this motion would also conform to the general clockwise circulation pattern of the Beaufort Sea. The only eddy observed over such a long term period (6 months) is eddy number 4 and it does approximate the general clockwise movement of the mean field in the Beaufort Sea.

2) Mean conditions of the Beaufort Sea

A clear majority of the observed eddies within the Beaufort Sea lie principally within the 50 to 300 meter depth range. As shown in figure 12, the major circulation of the Beaufort Sea is also almost entirely confined to the upper 300 meters of the water column(Newton,1973).

It appears that eddies within the Beaufort Sea move, over a long period of time, with the mean clockwise circulation pattern. If on the other hand, the mesoscale eddies are found outside the general surface circulation pattern of the Beaufort Sea, as suggested by historical data, i.e. to the west, then their movement would generally correspond with the Transpolar Drift, finally exiting via the East Greenland Current.

Using a dissipative frictional regime for the decay of eddies, Hunkins (unpublished manuscript) suggested that the 1/e decay time for a typical eddy would be on the order of several months. This would put an upper limit on the estimate of the life of an eddy to be less than one year. Using duplicate

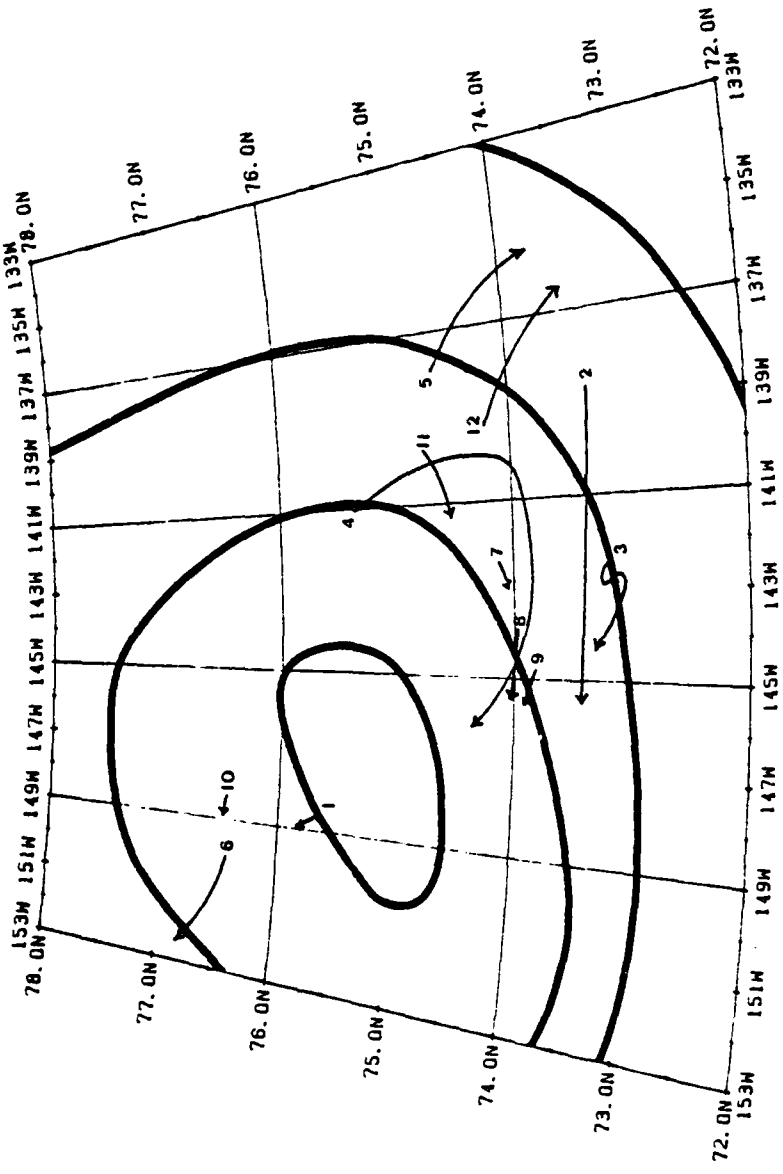


Figure 63. Trajectories of eddies that were observed more than once during the main AIDJEX experiment. Heavy lines denote dynamic topography of the Beaufort Sea(figure 13). Identification numbers correspond to those in Table 6.

Table 14
Multiple observations of eddies.

Eddy Number	Camp	STD Station	Date
1	Caribou	69	17-Jun-75
	Caribou	93	29-Jun-75
2	Caribou	235	15-Sep-75
	Caribou	248	21-Sep-75
	Snowbird	590	17-Apr-76
3	Caribou	384	28-Nov-75
	Caribou	432	8-Dec-75
	Caribou	448	23-Dec-75
	Caribou	480	4-Jan-76
	Caribou	500	9-Jan-76
4	Blue Fox	86	2-Aug-75
	Snowbird	234	25-Sep-75
	Snowbird	422	14-Jan-76
5	Blue Fox	114	23-Aug-75
	Blue Fox	130	31-Aug-75
	Blue Fox	140	5-Sep-75
6	Snowbird	32	31-May-75
	Snowbird	94	1-Jul-75
7	Snowbird	259	18-Oct-75
	Snowbird	277	27-Oct-75
8	Snowbird	334	25-Nov-75
	Snowbird	348	1-Dec-75
	Snowbird	412	8-Jan-76
9	Snowbird	376	20-Dec-75
	Snowbird	392	29-Dec-75
10	Big Bear	255	9-Jun-75
	Big Bear	281	16-Jun-75
11	Big Bear	469	14-Aug-75
	Big Bear	491	20-Aug-75
12	Big Bear	530	1-Sep-75
	Big Bear	562	1-Oct-75

observational data of eddies(table 8), the longest individual eddy that was observed more than once spanned a time period of 5.5 months. In that time period the eddy(eddy 4,figure 63) moved in fairly close agreement with the general circulation of the Beaufort Sea.

If such an eddy were advected into the Beaufort Gyre from the source region of the Alaskan Coastal Current, and did move on a long term basis, in response to the mean surface geostrophic velocity field, it could travel roughly 1600 km in 5.5 months using an estimate of .05 m/sec as a mean drift rate.

This distance would take an eddy generated near Point Barrow nearly 3/4 of the distance around the Beaufort Gyre if its movement was entirely confined to the 0.45 dynamic height contour(figure 17).

If the eddy was in the region of the Transpolar Drift, which is out of the influence of the Beaufort Gyre, it would probably not be able to cross the pole which is approximately 2500 km from Point Barrow. According to surface maps showing drift tracks of past manned ice camps in this area, the maximum distance that could be traveled would be close to 80 degrees north latitude. Arlis II made such a drift track; however, its starting position was some 300 km north of Point Barrow. After one year from its starting position, Arlis II was close to 81 degrees north latitude and 163 degrees east longitude. These arguments suggest that if the eddies are placed within the deep Arctic Ocean, their general movement is in accordance with the short term barotropic field and over a longer period, in accordance with the mean current field at the depth of the eddy. In response to these mean currents, the eddies would be continuously displaced from the area of origin and would decay entirely within the deep ocean.

C) Decay of Kinetic Energy over space and time.

It has already been indicated that during the main AIDJEX Experiment, averaged monthly integrated baroclinic kinetic energy dropped two orders of magnitude as the manned camps drifted in general agreement with the Beaufort Gyre. The maximum was observed during the month of June 1975 at Big Bear(figure 48) and the minimum was in February 1976 at Snowbird. Averaging the integrated baroclinic kinetic energy over the number of camps per month also yields a decreasing trend in the observed baroclinic component through time. The data agree well with the assumption that (baroclinic)eddy kinetic energy as well as T-S properties should decrease in magnitude as one moves clockwise within the gyre.

The decrease in T-S properties within the eddies, on the other hand, is not so easily shown to have decay properties in the clockwise direction of the gyre in comparison with the background energy of the mean field. This is due to the lack of the ability to observe the same eddy(or eddies) over long periods of time as well as making sure that the data were collected in the same part of the eddy.

D) Volume Transport

The relative importance that the arctic eddies have in the volume transport across the shelf with respect to other areas within the Arctic will indicate whether these features represent a significant mechanism by which heat, salt and biomass can be transferred. Although the initial structure of an eddy has not been documented, inferences can be made based on historical data within the Arctic and eddies actively observed during formation in other oceans.

In the particular case of Gulf Stream rings, initial shape after formation is oblate to circular(figure 29), extending to the bottom of the ocean with a velocity maximum at or near the surface. The properties of the newly formed rings are uniformly colder and less saline(cyclonic rings), or warmer and more saline(anticyclonic rings) than the new surrounding mean conditions. If it can be considered that the eddies observed within the Arctic are spun off near a frontal area associated with high currents such as the Alaskan Coastal Current, then it is not unrealistic to expect a similar process in their formation.

If an assumption is made that the initial shape of an arctic eddy is nearly cylindrical, extending from the surface to a depth of 200 meters, an estimate of the volume transport can be provided. If the eddy is lens shaped(which they are shown to be within the central Beaufort), then the estimates based on a simple cylinder will be approximately 15% too high.

It has been suggested by Parker(1971) that the Gulf Stream rings decay more rapidly in a vertical sense rather than horizontally because of the extremely large horizontal gradients required to do the latter. If this argument is suggestive of the dynamics of the arctic eddies, then the typical eddy diameter observed within the Beaufort Sea should not differ significantly with its original diameter after formation. The only pass along the diameter of an anticyclonic eddy was discussed by Newton et al(1974) and shows the part in solid body rotation to be approximately 10 km in diameter.

The mean salinity of water flowing through the Bering Strait is 32.4 ppt(Table 1). Eddies plotted on the T-S diagram of figure 44 indicate a visual average near 32 ppt. If the cross-shelf volume transport of the eddies ranges from 30% to 100% that of the Bering Strait inflow, eddies would transport from 1.4 to 4.5 x 10^4 metric tons of salt per sec into the Beaufort Sea.

The net effect of the salinity flux due to the eddies is that of maintaining an input of fresher, less saline shelf water into the Arctic Ocean in conjunction with the input of shelf water via direct advection processes(SCOR,1979).

E) Salt Transport

In the western Arctic, the water that is advected into the Arctic Ocean from the shelf regions of the Chukchi Sea normally ranges from <31 ppt to 33 ppt and -1.0 to 10.0 degrees C. in the summer months to 32 to 34 ppt and -1.5 to -1.7 degrees C. in the winter. Upon being advected into the Arctic Ocean, this water sinks along lines of constant density until reaching its stable depth below the mixed layer and above the Atlantic layer. These differing conditions in the summer and winter shelf water correspond to the layers occupied by the Pacific T-maximum and T-minimum within the Canada Basin.

The eddies of the Arctic Ocean, because of their composition of shelf water, will also move in the same manner to reach the approximate depth level at which they are stable. This is also in agreement with the concept that the entire structure of the eddy will translate as a column(Warren,1967). Since each season represents a differing water column with respect to salinity as well as temperature, each individual eddy may vary slightly in its stable depth within the Beaufort Sea. Usually this will represent a depth range from about 50 meters to 300 meters. Shelf water has been documented to have salinities as high as 34.99(Aagaard and Tripp,1978; SCOR,1979) and therefore densities similar to the bottom of the Arctic Ocean. It is therefore believed that the deeper eddies that were observed only by STD data with depths greater than 300 to 700 meters may have been a result of formation during conditions of active brine convection from early to late fall.

This mechanism of isopycnal sinking of the eddy would also account for the subsurface velocity maximum. An alternate method(Hunkins, unpublished manuscript) using frictional dissipation between the base of the ice(or mixed layer) and an eddy with a velocity maximum at the surface would, within a few months, dissipate the the upper part of the eddy leaving a subsurface velocity maximum.

Using this estimate of 7 km for the initial radius of formation, an arctic eddy would have a volume of 1.57 X 10^9 m^3 . Comparing this with the average transport of water through the Bering Strait(Table 1) of 1.5 X 10^6 m^3/sec , a typical eddy would comprise 5.7 hours of flow. If the eddies were solely required to transport the same annual flow of water through the Bering Strait across the shelf-slope boundary, nearly 1500 would have to be formed per year. This estimate of eddy production is not unrealistic with that calculated for the number of eddies created from the meandering of the Alaskan Coastal Current, and possibly the additional production of eddies by rapid implacement of shelf water into the deep Arctic Ocean via submarine canyons. On the basis of these assumptions, eddies may represent a volume transport across the shelf ranging from 30% to 100% that of the Bering Straits inflow.

F) Heat Transport

The amount of heat transported from the shelf to the Arctic Ocean by the eddies is extremely difficult to determine due to the constantly changing thermal conditions of the water which defines their internal cores. Depending directly on the season of the year, the vertical temperature structure of the shelf water may be relatively warm with the exception of relict near freezing winter water at the bottom during the summer, to near freezing isothermal conditions from the surface to the bottom during the winter.

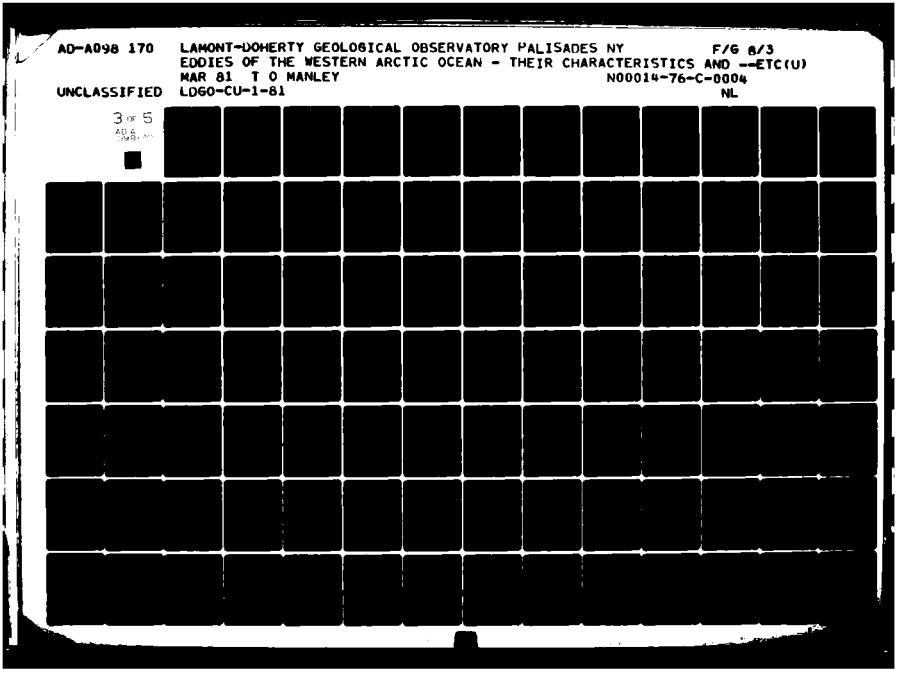
As previously mentioned, the vertical thermal properties within the cores of individual eddies were not consistently either warm or cold , but rather appeared to have a bi-level structure. The horizontal plane that defined the division of the two separate levels was constantly found at or very close to the depth of the salinity inflection(figure 27). The maximum temperature differences along lines of constant salinity(density) in the upper($\Delta T1$) and lower($\Delta T2$) half of the eddy as compared to a station representing the local mean conditions are shown in figure 64. Temperature differences of $\leq$ 0.04 degree C. are considered to be representative of the surrounding noise and are indicated by the dashed vertical and horizontal lines. Data falling within the dashed lines were automatically placed on or immediately surrounding the the axis(0.0 degree C. difference) for clarity.

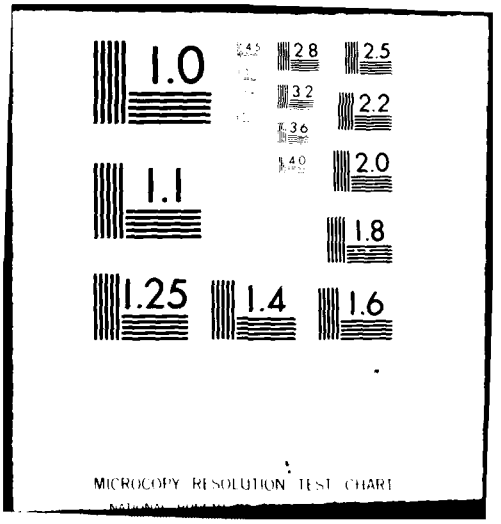
The cores of the eddies predominantly show only three of the four possible cases for upper and lower thermal differences. These cases are -- 1)totally warmer core(warm over warm) 2)totally colder core(cold over cold) and 3) warm over cold. The fourth case, cold over warm, is only observed twice during the AIDJEX main experiment and is also in accordance with conditions on the shelf.

Cases (1) and (2) indicate the time of formation as maximum summer and winter conditions respectively. Case (3) would represent the several months of

AD-A098 170 LAMONT-DOHERTY GEOLOGICAL OBSERVATORY PALISADES NY F/G 8/3
EDDIES OF THE WESTERN ARCTIC OCEAN - THEIR CHARACTERISTICS AND --ETC(U)
MAR 81 T O MANLEY N00014-76-C-0004
UNCLASSIFIED LDGO-CU-1-81 NL

3 OF 5
AD A
098170




1.0
2.8
2.5
3.2
2.2
3.6
4.0
2.0
1.1
1.8
1.25
1.4
1.6
MICROCOPY RESOLUTION TEST CHART

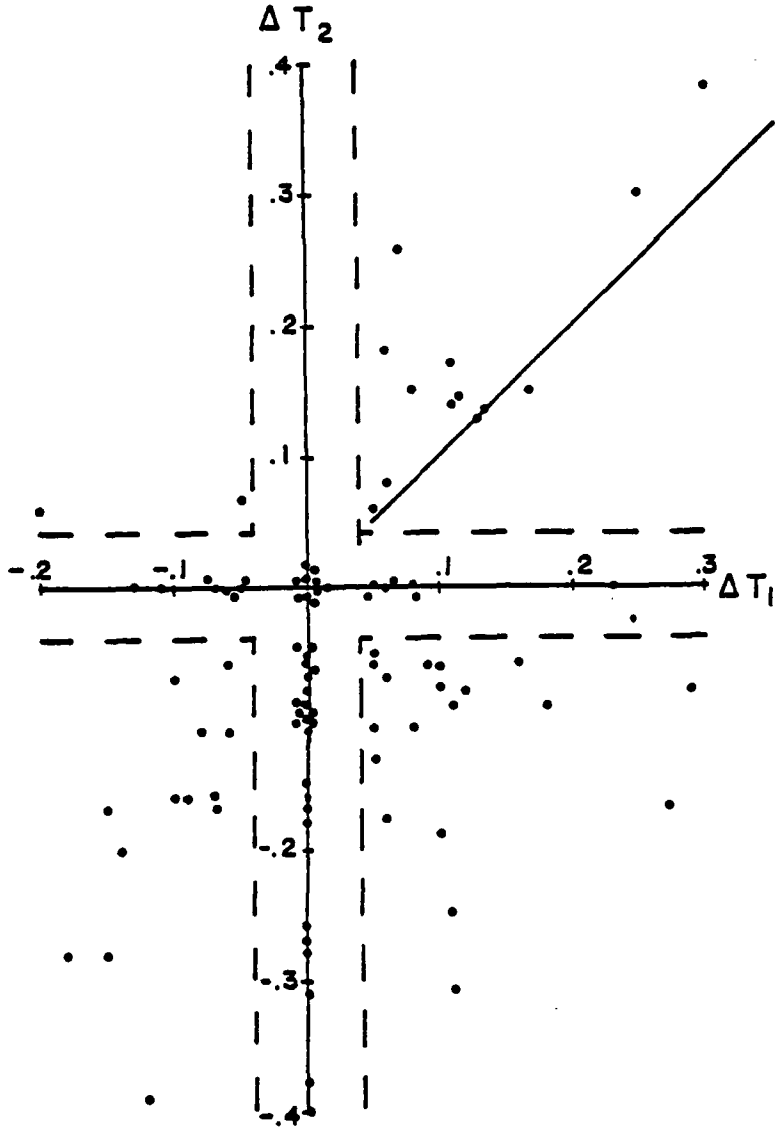


Figure 64. Temperature differences between individual eddies and local mean conditions as listed in Table 10. ΔT_1 and ΔT_2 define the upper and lower layers respectively. Dashed lines show the 0.04 degree C limits of the background noise.

transition between the winter and summer during the spring when the warmer fresher water overlies the colder relict winter conditions. Case (4), however, represents the rapid transition from summer to winter when active and vigorous mixing is accomplished with the onset of sea ice formation and resulting brine convection on the shelf. Although it is possible to have the thermal stratification as shown in case (4), it is known that the normal duration of the transition period is shorter than case (3).

Another observation that can be made from figure 64 is that of a possible decay mechanism which operates outside of the normal diffusive regime. As seen in quadrant 1, which represents the summer case, all but one of the eddies show a definite shift towards the ΔT2 axis. This implies that there is a consistently cooler upper layer with respect to the lower part of the core. Although this type of thermal structure may indeed represent shelf thermal structure, it is highly unlikely that all of the observed eddies would display this layering.

If a diffusive regime is assumed to act uniformly throughout the eddy, then there should be a fairly constant and uniform decrease in the upper and lower core temperatures through time. If the thermal structure of the eddy was viewed at different times, the relative temperature difference between the upper and lower core would remain the same. As a result, there should be more observations of eddies with a warmer core relative to the lower core; this, however, is just the opposite of what is indicated by the data. For the summer data, this disparity of what was expected and what is observed may be the result of a more rapid decay of the upper core in relation to the lower core. A typical example of this type of thermal structure within the eddy is shown in figure 42.

A simple frictional model would explain this type of accelerated upper thermal core decay relative to the lower core. The eddies have already been

shown to be nearly geostrophic in nature(Hunkins,1974; Newton et al,1974). Without the effect of friction, the resultant velocity field within the eddy will be normal to the pressure gradient(figure 65a). When friction modifies the geostrophic balance of forces, the net result will be a slight veering of the velocity vector producing a small cross isobar flow(figure 65b). The frictionally induced velocity change for the anticyclonic and cyclonic cases are shown in figure 65c and 65d respectively. For the anticlonic case(figure 65c), there is a net transport of water away from the center of the eddy near the frictional boundary. The opposite is true for the cyclonic case. Since mass has to be conserved, a compensating return flow must also occur with consequent secondary flow across isopycnal surfaces.

In the case of the eddies observed within the Arctic Ocean, frictional effects would become important in the uppermost part of the eddy which is in contact with the base of the ice or the base of the mixed layer. The magnitude of the frictional term would be larger in the case of ice friction, but the mixed layer, because of its very low stratification, would also be important.

The return flow within the cyclonic and anticyclonic eddies would most likely be on a horizontal density surface where the least amount of work is required for water to enter the field of the eddy. The depth of this horizontal plane corresponds with the point of salinity inflection within the eddy(figure 27). The general flow pattern depicting the forced frictional flow at the surface and return flow at depth for an anticyclonic and cyclonic eddy is shown in figure 66a and b. Theoretical implications (Hunkins, personal communication) suggest that this type of frictional coupling between the base of the ice or mixed layer can be responsible for changing a surface velocity maximum to a mid-depth velocity maximum in a time span of a few months.

In summary, it is believed that the original upper layer properties of the eddy are removed more rapidly than the lower layer via a frictionally induced

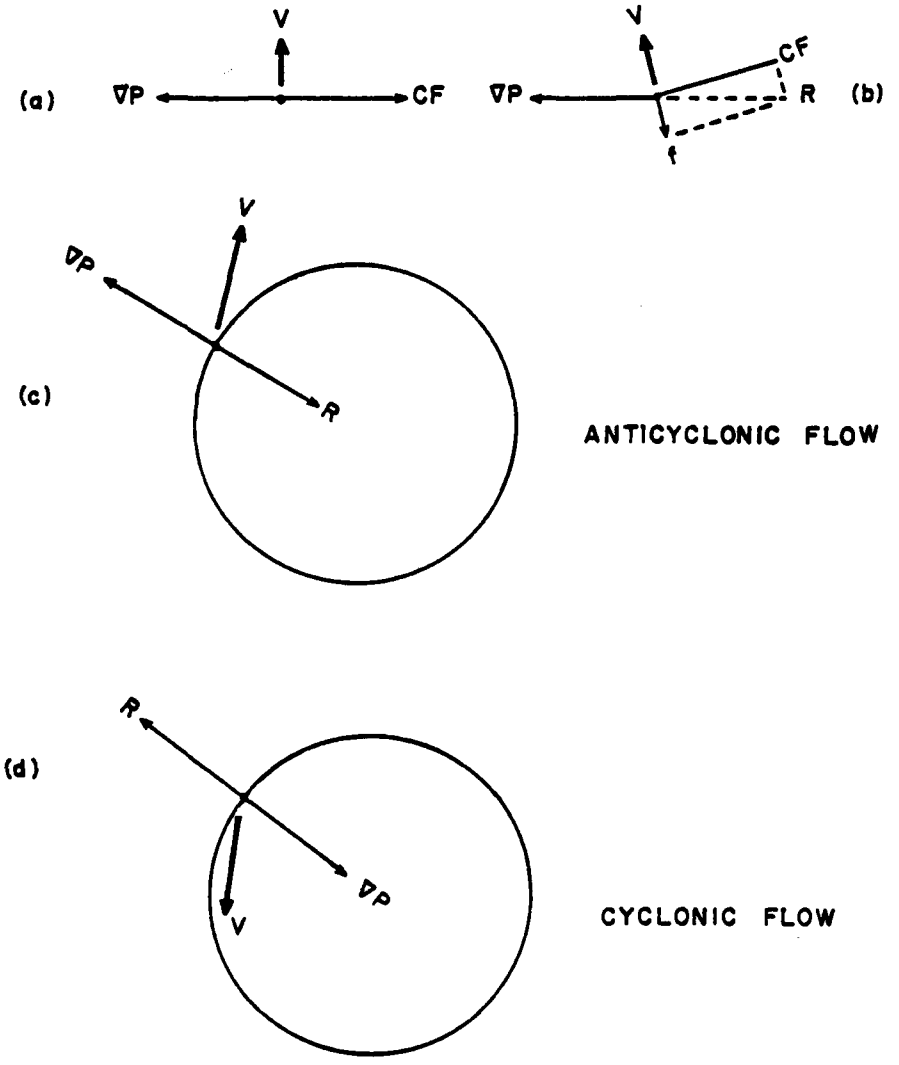


Figure 65. Horizontal balance of forces in a) geostrophic flow and, b) geostrophic flow modified by friction. Veering of the velocity vector for both anticyclonic and cyclonic flow are show in (c) and (d) respectively.

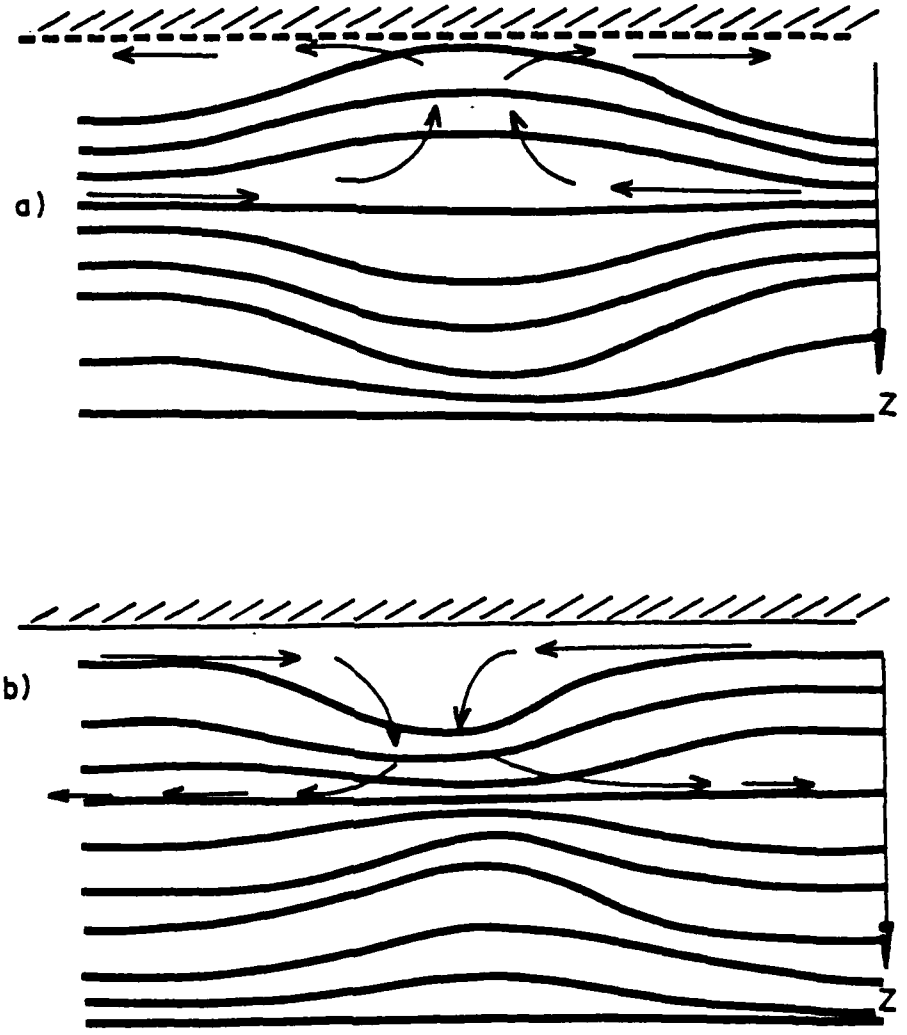


Figure 68. Cross-section along the diameter of an a) anticyclonic and, b) cyclonic eddy suggesting the upper layer flow patterns.

divergence at the surface and a compensating return flow at mid depth. This return flow replaces the upper layer anomalies with the local surrounding water. On the ΔT1 , ΔT2 coordinate system, this process suggests a rapid ΔT1 decay towards the background conditions due to advection and a much slower decay in the lower layer because of the lack of frictional effects and consequently a dominance of the diffusive regime. Once the upper layer has been reduced to the background noise of the surrounding mean, the lower half of the eddy will then decay along the ΔT2 axis. This type of process is shown in figure 87. The heavy arrows indicate a rapid advection-diffusion mechanism while the thinner arrows(parallel to the ΔT_2 axis) indicate the slower diffusive regime.

This process suggests that the eddies have a positive feedback mechanism that keeps the upper layer isopycnals in their original configuration. Also of major importance is that the eddies may also serve as a mechanism which enhances vertical mixing within the upper 200 meters of the water column below the base of the mixed layer.

The flux of heat carried by the eddies from the shelf to the deep ocean will depend largely on whether or not the observed data represents the original structure within the eddies. The upper layers can be considered unknown when temperature differences(away from the mean) are less than 0.05 degrees C.. Looking outside the 0.04 degree boundaries in figure 84, the upper layer thermal properties are largely dominated by warmer water in a ratio of 2.6:1. The lower thermal structure of eddies is almost completely dominated by colder water with a ratio of 2.8:1. This in itself is not unexpected, since the lower part of the shelf water is characteristic of winter conditions for a majority of the year. Qualitatively, what may be indicated is that the eddies duplicate the transfer of warm summer water into the region of the Pacific T-max layer and cold water into the region of the Pacific T-min layer. Their ability to transfer

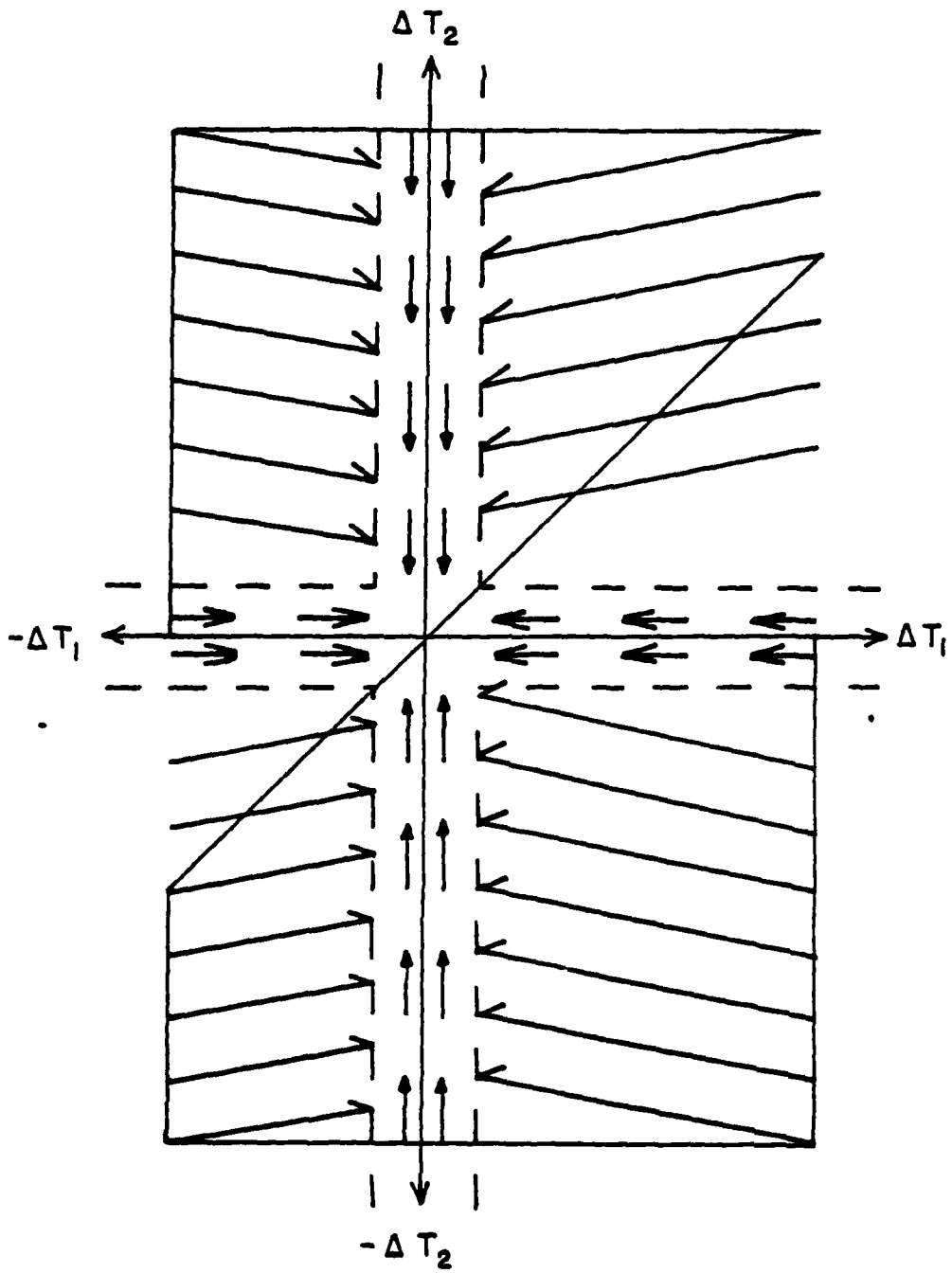


Figure 67. Suggested decay patterns of thermal properties within the eddies for the upper($\Delta S_1, \Delta T_1$) and lower ($\Delta S_2, \Delta T_2$) cores.

the anomalous water further than normal advection processes is quite evident by their anomalous characteristics when compared to the surrounding conditions.

G) Biological Transport

Previous work pertaining to the Gulf Stream Rings(Wiebe,1976a,b,c) suggests that eddies provide an important transfer mechanism of biomass across a front that would normally be impenetrable to planktonic and larger less mobile animals or plants. It is not the intention of the author to present as detailed an analysis as that of Wiebe, but rather to see if possible correlations do exist between the measurements of different species taken during net hauls and the presence of eddies.

During the summer of 1975, biological measurements consisting of plankton net hauls, chlorophyll a, and nitrate determinations were taken at camp Big Bear by C. Pautzke, Jerry Hornof and Kevin Wyman. The net hauls were taken using a 1 meter diameter ring net with a mesh size of 73 microns at regular intervals with wire out depths of 50, 100, and 150 m.

Copepods were classified by Pautzke(1980 and unpublished data) as commonly or uncommonly observed within the Beaufort Sea. Table 15 lists both the common and uncommon varieties as to species and the number observed during each net haul. Figures 68 and 69 show plots of the common species through time. Figure 70 indicates the number of uncommon species along with the time periods in which eddies were observed at camp Big Bear. Eddy observation time periods are shown as horizontal bars near the base of the figure. Only two out of the several eddies at camp Big Bear had coincident times when the net hauls were being taken. The corresponding dates for the eddies were the 7th of June and the 13th of September.

During the net hauls of 7 Jun, 1975, there was a significant deviation in the numbers of uncommon species observed. This occurred with the copepod *Scolecithricella minor* which peaked at 125. During the remainder of the experiment, the mean for this particular copepod was a little over 3. All of the other species listed in Table 16 show either general means or a long period variation

Table 16 Numbers of common and uncommom planktonic species observed during the 150- 0 meter net hauls at camp Big Bear(from Pautzke,1980).

Common Species	07 Jun	24 Jun	12 Jul	30 Jul	17 Aug	04 Sep	13 Sep	28 Sep
Calanus hyperboreus	81	114	164	158	307	491	539	235
Calanus glacialis	9	24	73	54	32	17	59	69
Euchaeta glacialis	23	20	35	81	54	20	28	14
Metridia longa	49	43	121	29	79	105	133	120
Microcalanus pygmaeus	3875	5750	15875	20875	24750	24250	30000	18250
Oithona similis	3125	2125	7500	5125	3250	3250	7750	14250
Oncaea borealis	2750	1750	3625	8500	9000	7250	8500	7750
Uncommon Species								
Scolecithricella minor	125	11		2	1	7		1
scaphocalanus magnus		1	4	6	5	4	3	7
Heterorhabdus norvegicus			2		2		1	2
Heterorhabdus compactus			4	2	1			
Chiridius obtusifrons			5	6	4	5	1	3
Temorites brevis				1				
Gaidius brevispinus				1	1			
Derjuginia tolli				4		2	3	8
Aetidiopsis Multiserrata								1
Eddy observed at Big Bear	Yes	No	No	No	No	No	Yes	No

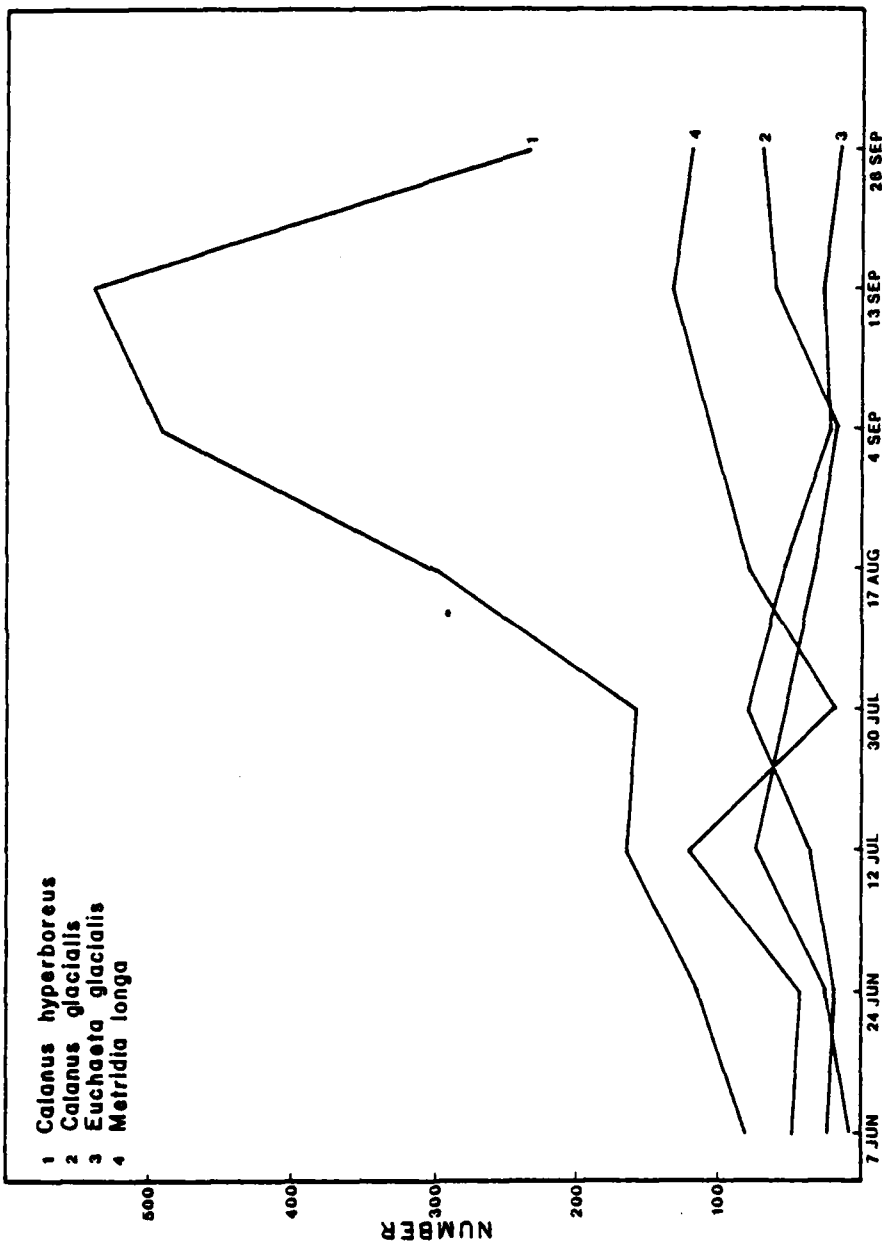


Figure 68. Common species of copepods taken during the summer biological program at Camp Big Bear. Dates of actual observations are given at the bottom of the plot.

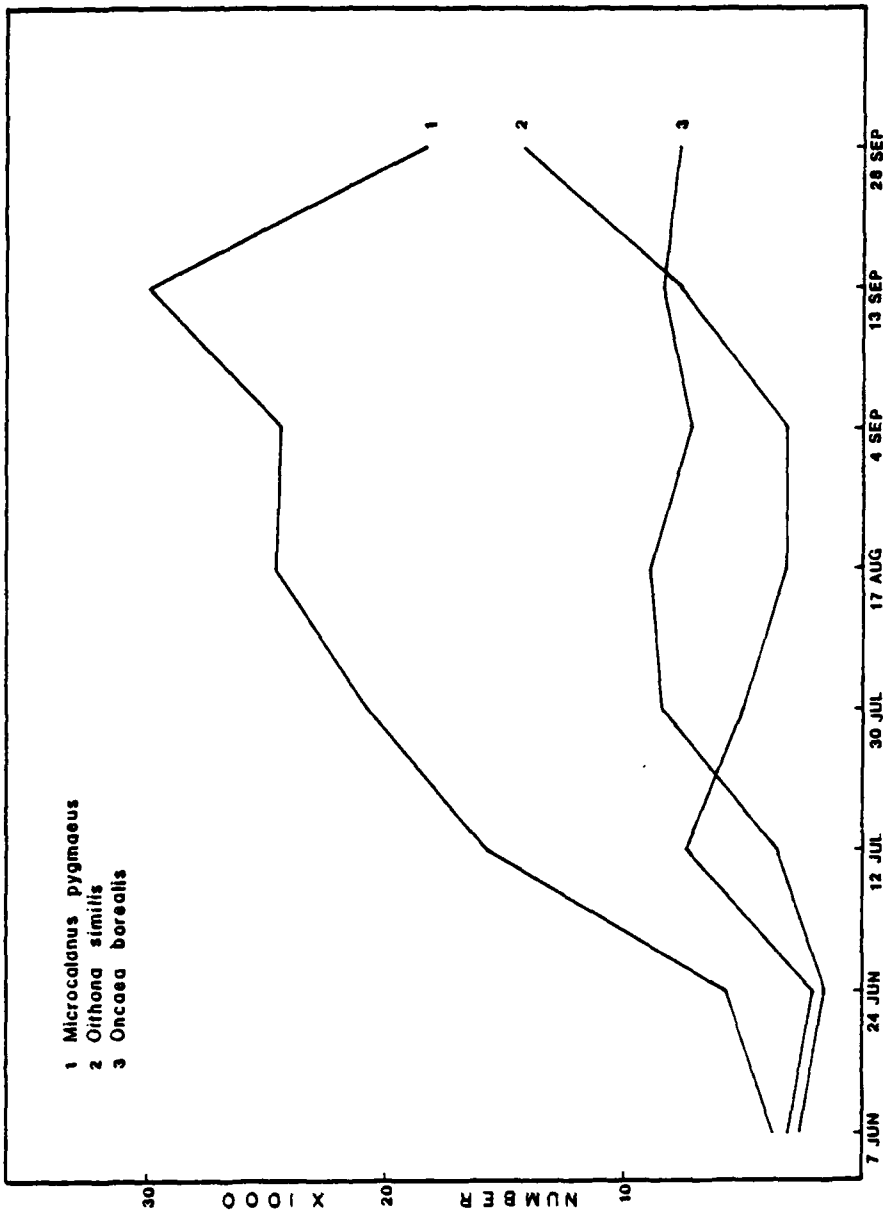


Figure 69. Common species of copepods taken during the summer biological program at Camp Big Bear. Dates of actual observations are given at the bottom of the plot.

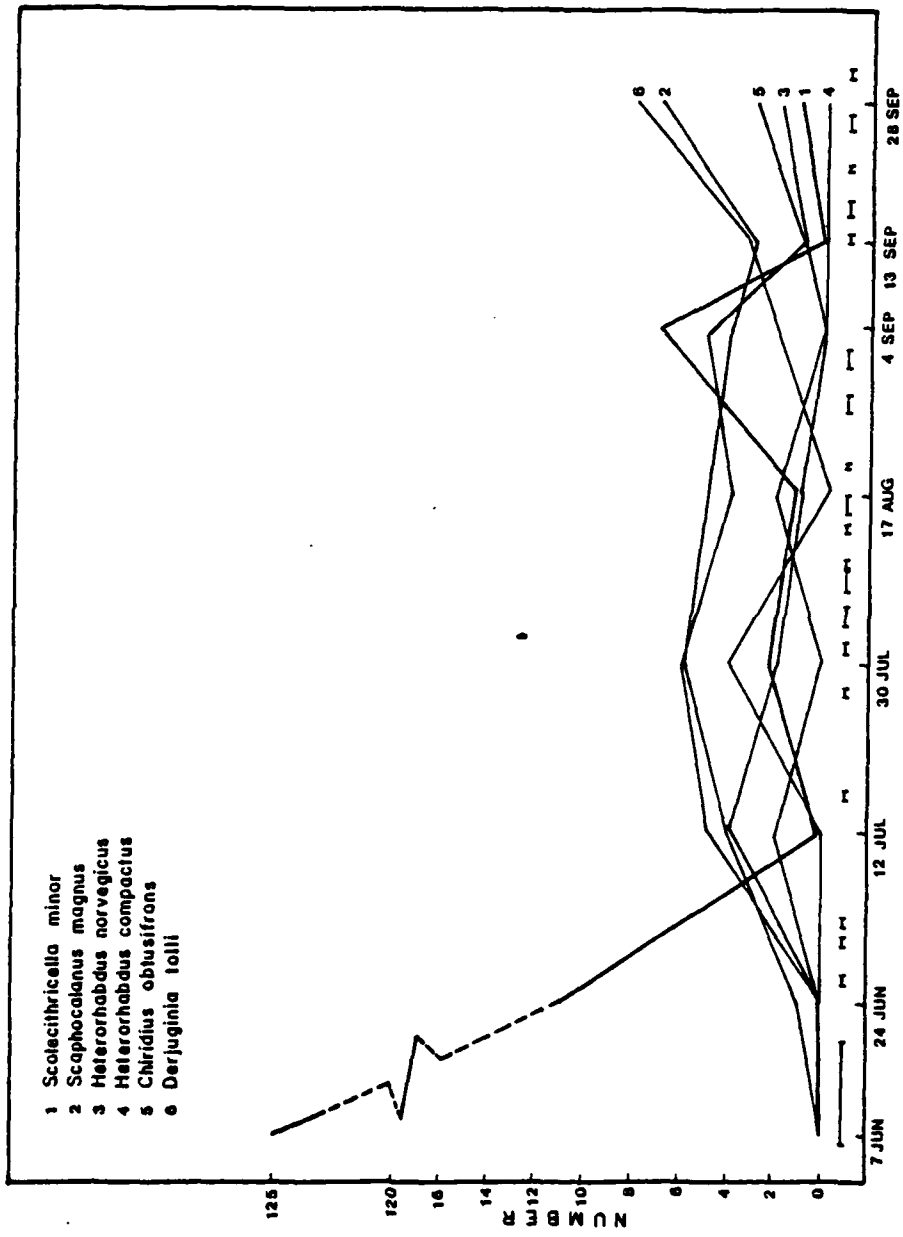


Figure 70. Uncommon species of copepods taken during the summer biological program at Camp Big Bear. Dates of actual observations are given at the bottom of the plot. Horizontal bars indicate time periods during which eddies were observed at Big Bear.

in number which do not correspond with the transient, short duration events(few days) of eddies.

Previous investigations relating to *S. minor* (Tidmarsh,1973; Brodsky,1950; Minoda,1971; Shih and Laubitz,1978; Hughes,1968) generally indicate that this species of copepod is found in higher abundance above 200 meters within the Arctic Ocean and closely neighboring areas, although it has been found in deeper waters. Hughes(1968), while on ice island T3 during the summer of 1966 and winter of 1967, observed a minimum of *S. minor* for the time period of June-July(1966) with a subsequent steady increase up to a high of 58(per net haul) during February(1967). The results of Hughes indicate an increase in population over a long period of time and does not indicate the possible presence of eddies.

The other correlation date between the observation of an eddy and a net haul was on the 13th of September. At this particular time, no major deviations were seen in the populations of the various species, either common or uncommon. The lack of deviations within the various species may be due to one or a combination of several reasons: 1) the net haul was taken near the edge of the eddy where maximum anomalous conditions do not exist, 2) the eddy may have been in a later stage of its life cycle and therefore any major anomalous properties would have been absent, and 3) at the time of initial formation for the eddy, the shelf conditions may have had a totally different standing crop of planktonic species that would not appear as abnormal to the Beaufort Sea Community.

When the two different eddies are compared to note any major differences that would account for the different observations, several conclusions were formulated. The first is that the June 7 eddy was one of the highest velocity eddies existing in all of the historical data with a maximum speed of .57 m/sec. The September 13 eddy, however, was of a much lower velocity indicating that the

observations were along the edge of a stronger eddy or the eddy was in a later stage of decay. The persistence of observations between the two eddies was also markedly different. The June 20 eddy was observed continuously for 10 days while the other eddy was observed for only a half of a day.

Unfortunately, STD data were not available for the September 13 eddy, although the June 20 eddy had excellent coverage. As shown in figure 71, the June 20 eddy was an extremely anomalous event in both the upper and lower layer thermal differences which were +0.26 and -0.17 degrees respectively. Not only are spring or summer conditions implied for the formation of the eddy, but due to its large upper layer anomaly, young age is also implied. Biological observations did not start prior to the 7th of June and as a result, the peak in *S. minor* can not definitely be considered to be a result of eddy transport. Other explanations for this high peak could be due to a high standing crop prior to the first observation or a simple vertical migration.

Although the habits of *S. minor* are not well understood for the Arctic Ocean, it is strongly felt that the above explanations do not play an important role for the June 7 eddy. Both of the explanations do not take into account that a mass of highly anomalous water comprising some 16 cubic kilometers was physically displacing the normal Beaufort Sea community. If *S. minor* was not taken from the eddy, the species had to be residing entirely within the upper 40 meters of the water column. If this were true, one would then expect a moderate number of observations for nearly all the net hauls taken subsequently. This, however, is not observed and therefore strongly suggests that *S. minor* was indeed residing within the eddy of June 7.

This fairly warm upper layer core tends also to support the abundance of *S. minor* which must have been resident on the shelf in the late spring or summer. The September 13 eddy may have been much older, in which case the upper core properties would have been removed by the advection process

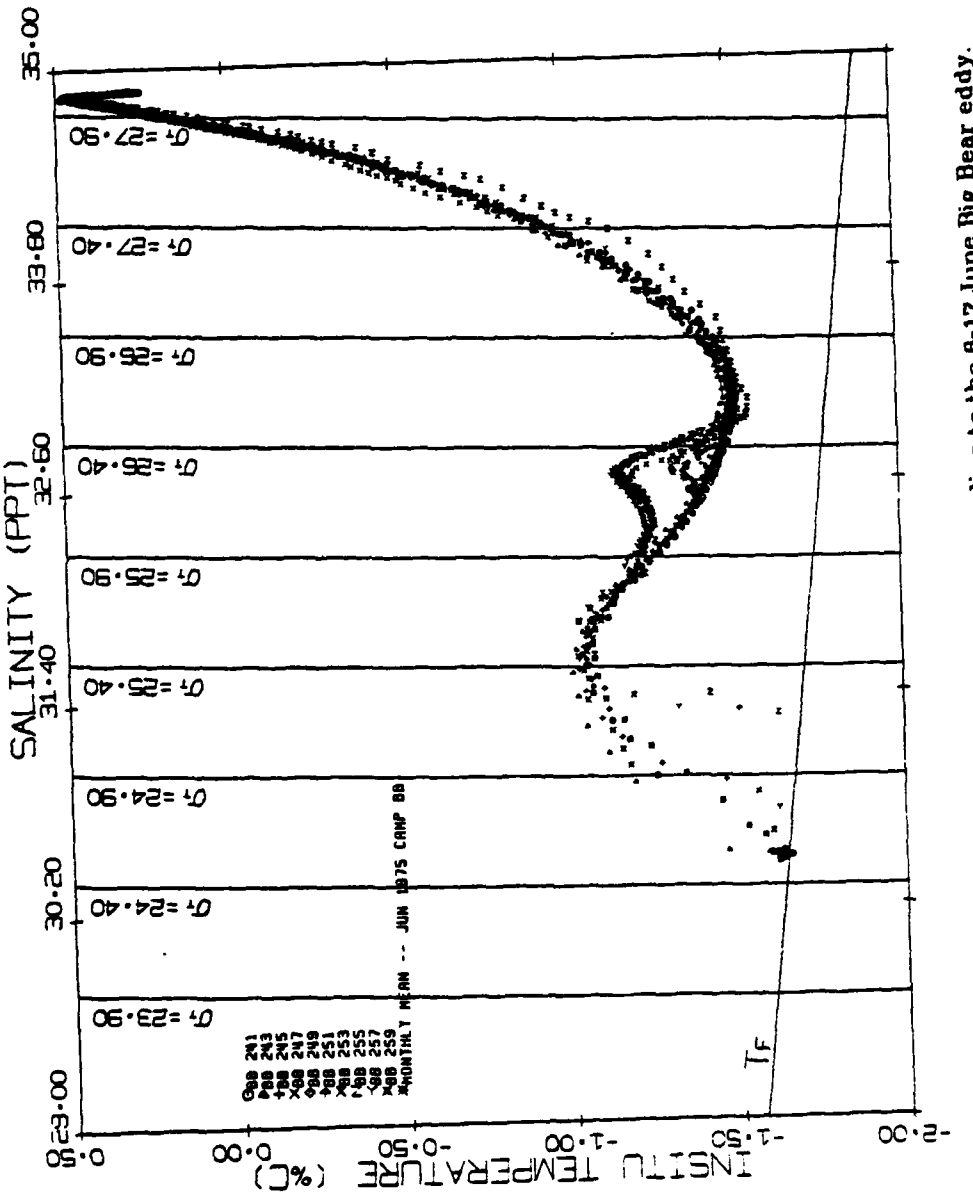


Figure 71. T-S plot of the warm core eddy corresponding to the 8-17 June Big Bear eddy.

previously discussed. When observations are then made in the upper core, no major anomalies would exist in temperature or biomass.

It is therefore believed that eddies of the Arctic Ocean operate in a similar manner to that of the Gulf Stream rings by transferring biomass across the shelf-slope front. Anomalies of the various species within the eddy as compared to the Beaufort Sea, however, will be strongly dependent on 1) the season in which the eddy was created, and 2) at what time the observations were made within the eddy after its formation.

6. Summary and Conclusions

Mesoscale eddies within the world's oceans play an important role in the transport of energy, salt, heat, and other constituents such as biomass and chemical tracers across large scale fronts that would normally be impenetrable. They are common features that are found in every ocean, but much is still unknown about them.

Due to the inaccessibility of the permanent pack ice zones of the Arctic Ocean, mesoscale eddies were not documented to exist within this region until 1974(Hunkins,1974; Newton et al;1974). Historical data at that time indicated that eddies had been observed but that they were believed to be broad linear features that were created in response to local atmospheric forcing (Shirshov,as reported in Belyakov,1972). On the basis of these studies and the present work, new information has been gathered on the characteristics of the arctic eddies.

When compared to the mid-latitude eddies which are typically on the order of 100-200 km in diameter and 2-4 km in thickness, the Arctic eddies were an order of magnitude smaller. Typical eddy diameter and thickness are 10 km and 200 m respectively. One difference was that the arctic eddies had a subsurface velocity maximum. Speeds within the arctic eddies are typically .20-.30 m/sec although they may be as high as .60 m/sec.

Very little was known about the eddies of the Arctic pertaining to their life span, decay mechanisms, origin, horizontal and vertical spatial density and variability, rotational characteristics, energetics, and transport capabilities. On the basis of available temperature, salinity, and current data at that time, it did appear that the eddies were of distant origin and that they dominated the kinetic energy balance in the upper 100 meters of the water column.

Using the STD and PCM data sets obtained from the four drifting manned camps located in the Beaufort Sea during the 1975-76 AIDJEX Experiment,

enough information was available to answer some of the questions and to speculate on some of the others.

Origin

The origin of the eddies within the Arctic Ocean remains an open question. Hypotheses range from local atmospheric forcing and intense brine convection to a formation at a baroclinically or barotropically unstable front.

Local atmospheric forcing was originally considered as the generation mechanism of the so called 'transient undercurrents', or 'counter currents'. However, there are several faults with this concept such as scale and spatial variability. The one suggestive piece of evidence is the observation of eddies that are similar to the surrounding conditions within the Beaufort Sea. They can also be interpreted as distantly generated eddies in an advanced state of decay. Unfortunately, there is no way to discriminate between the two at this time.

Intense brine convection caused by the rapid formation of sea ice was also ruled out as a possible mechanism because scale and seasonal occurrence do not support this process.

Hunkins(1974) suggested that baroclinic instability on the Alaskan slope near Point Barrow was a possible mechanism for the production of eddies. Data from ship cruises in the Chukchi Sea and the Alaskan shelf-slope regions were used to find possible correlations with the T-S signatures of eddies within the Beaufort Sea. Agreement between the two data sets was most conclusive directly north of Point Barrow.

Because of the predominance of anticyclonic eddies within the Beaufort Sea, the eastward flowing Alaskan Coastal Current appears to be the major source region from which the eddies are spun off in a similar manner to that of

the Gulf Stream rings. It is further suggested that in the case of the Alaskan Coastal Current, barotropic instability may also play an important part in the formation of eddies. The other possibility concerning mechanisms that can produce eddies is the rapid implacement of shelf water into the Beaufort Sea via submarine canyons. This mechanism is tentative and requires further evaluation.

Cross Shelf Transports of the Eddies

With the assumption that as many as 500 eddies may be spun off the Alaskan Coastal Current during a year(e-folding time of 2-3 days), the corresponding volume and salt transport into the deep ocean from the shelf would be 30% of the Bering Strait's input. Temperature flux is more difficult to estimate, but does suggest a transport of heat that maintains the thermal regime of the Beaufort Sea from 50 to 300 m.

Also suggestive of the eddy flux regime is that of the transport of biomass across the shelf-slope front into the Beaufort Sea. Although the data that suggests this transfer mechanism is far from being conclusive, future work should be done to either prove or disprove this process within the Arctic Ocean.

Spatial Density and Variability

The arctic eddies appear to be predominantly confined to the Amerasia Basin and more specifically, to the Beaufort Sea. They are undoubtedly ubiquitous within this region with an estimated horizontal density of one every 1000 km^2. During the main AIDJEX Experiment, 146 separate crossings over eddies were made. A clear majority were observed in a depth range from 50 to 300 meters, although eddies deeper than previously thought to exist were also observed. Both cyclonic and anticyclonic eddies are known to exist in the Arctic Ocean. Prior to 1975, statistics on the ratio of anticyclonic to cyclonic

eddies ranged from 1:1 to 7:1. Subsequent information shows that there is a clear dominance(97%) of anticyclonic eddies within the Beaufort Sea.

Kinetics

The eddies of the Arctic Ocean tend to dominate the kinetic energy balance of the upper 200 meters of the water column. Using profiling current meter data, eddy kinetic energy was calculated to be an order of magnitude larger than that of the mean field at a depth of 115 m. When a simplified model was used to estimate the total amount of kinetic energy due to the mean field as well as the eddies within the AIDJEX sector to a depth of 4000 m, their respective energies were approximately equal.

Of the thirteen months of data, only four months were able to be used in the kinetic energy flux analysis. Data within this particular time period suggest that the flux of baroclinic kinetic energy was in a counter-gradient direction indicating a transfer from the eddies to the mean field. The barotropic field was also shown to play an important role in the direction of kinetic energy flux depending on its relation to the mean geostrophic field.

Data from a simplified model further suggested that there is an equal partition between the available potential and kinetic energy of the eddies.

Internal Structure of the Eddies

Two different layers were found to exist within the eddies based on thermal contrasts with the surrounding conditions. The division between the upper and lower layers consistently agreed in depth with the salinity inflection point within the eddy.

An advection-diffusion mechanism set up in the upper part of the eddy by frictionally induced divergence at the base of the mixed layer or the ice

rapidly leads to decay of the upper core layer, while the lower core would decay much more slowly in response to an entirely diffusive regime.

Summary

Briefly, the upper several hundred meters of the western Arctic Ocean can no longer be viewed as a sluggish moving mass of water with slowly changing temperature and salinity, but rather a region with considerable variability on horizontal scales of tens of kilometers. This variability is primarily due to the presence of anticyclonic mesoscale eddies located in the depth range of 50 to 300 meters.

The interaction of these eddies with the mean conditions of the Beaufort Sea is complex and not completely understood. Their importance to the kinetic energy balance has been documented here. It is believed that these features transfer kinetic energy to the mean field in a "negative viscosity" manner rather than the normal dissipative sense. Because of their ubiquitous nature within this region and their high velocities, observational data indicate that they dominate the balance of kinetic energy within the upper 200 meters.

The origin of the arctic eddies is believed to be in the vicinity of the Alaskan shelf-slope region near Point Barrow based on T-S properties. The most probable mechanism for the creation of the eddies is that of barotropic or baroclinic instability of the eastward flowing Alaskan Coastal Current.

Estimated volume and salt transport of the eddies over a given period in time may be considered significant to that of the inflow of water through the Bering Straits. It is also believed that they decay entirely within the Arctic Ocean, thereby effectively transfering all of their heat, salt, biomass and other chemical constituents across the front north of Point Barrow, Alaska.

Simplified models of the available potential and kinetic energy contained within a typical arctic eddy indicate that the eddies obey the equal partition of energy theory for geostrophic flows which are close to the Rossby radius of deformation. Using decay rates of available potential energy calculated for the Gulf Stream rings, typical life spans of the Arctic eddies may range from a few months to a year.

Bibliography

Aagaard, K. and P. Greisman (1975) Toward new mass and heat budgets for the Arctic Ocean. *J. Geophys. Res., 80* (27): 3821-3827.

Aagaard, K. and R. B. Tripp (1978). Saline water in the northern Alaskan shelves. *EOS, 59* : 1091.

AIDJEX Staff (1976) First data report. *AIDJEX Bulletin, 32,* 71 pp.

Amos, A.F. (1975) Physical oceanography from the Arctic Pack ice. Project AIDJEX STD Programs. In *Proc. Plessey 3rd S/T/D Conference, Feb. 12-14, 1975.* San Diego, Calif. , 125-142.

Antonov, V.S. (1968) The nature of water and ice movement in the Arctic Ocean (in Russian). *Tr. Arktiki Antarktiki Nauch. Issled. Inst. 285* : 154-182.

Barret, J.R. (1971) Available potential energy of Gulf Stream Rings. *Deep-Sea Reasearch, 18* : 1221-1231.

Bauer, E.,K. Hunkins,T. O. Manley, and W. Tiemann (1980a) *Arctic Ice Dynamics Joint Experiment 1975-1976 Physical Oceanography Data Report, STD Data - Camp Caribou,* Volume 1, CU-8-80, Technical Report No. 8, Lamont-Doherty Geol. Obs. of Columbia Univ., Palisades, N.Y.

Bauer, E.,K. Hunkins,T. O. Manley, and W. Tiemann (1980b) *Arctic Ice Dynamics Joint Experiment 1975-1976 Physical Oceanography Data Report, STD Data - Camp Blue Fox,* Volume 2, CU-9-80, Technical Report No. 9, Lamont-Doherty Geol. Obs. of Columbia Univ., Palisades, N.Y.

Bauer, E.,K. Hunkins,T. O. Manley, and W. Tiemann (1980c) *Arctic Ice Dynamics Joint Experiment 1975-1976 Physical Oceanography Data Report, STD Data - Camp Snowbird,* Volume 3, CU-10-80, Technical Report No. 10, Lamont-Doherty Geol. Obs. of Columbia Univ., Palisades, N.Y.

Bauer, E.,K. Hunkins,T. O. Manley, and W. Tiemann (1980d) *Arctic Ice Dynamics Joint Experiment 1975-1976 Physical Oceanography Data Report, STD Data - Camp Big Bear,* Volume 4, CU-11-80, Technical Report No. 11, Lamont-Doherty Geol. Obs. of Columbia Univ., Palisades, N.Y.

Beal, M.A., F. Edvalson, K. Hunkins, A. Molloy and N. Ostenso (1966) The floor of the Arctic Ocean: Geographic names. *Arctic 19* (3): 214-219.

Beebe, R.E., et al (1980) Measurements and wind vectors, eddy momentum transports and energy conversions in Jupiter's atmosphere from Voyager I images. *Geophysical Research Letters 7* (1): 1-4

Belyakov, L.N. (1972) Triggering mechanism of deep episodic currents in the Arctic Basin (in Russian). *Problemy Arktiki i Antarktiki. 39* : 25-32.

Brekhovskikh, L.M., K.N. Federov, L.M. Fomin, M.N. Koshlyakov, and A.D. Yamplosky (1971). Large-scale multi-buoy experiment in the tropical atlantic. *Deep-Sea Res., 18* : 1189-1206.

Brodsky, K.A., (1950) Calanoida of the far-eastern seas of the U.S.S.R. and the polar basin. Publ. Zool. Inst. (Acad. Sci.). U.S.S.R. 35. 441 pp. (Translated by Israel Program for Sci. Translations, 1967).

Browne, I.M. and A.P. Crary (1958) The movement of ice in the Arctic Ocean. In *Arctic Sea Ice*, Publ. 598, National Academy of Sciences, Washington, D.C. 191-207.

Bryden, H.L. (1978) Poleward heat flux and conversion of APE in Drake Passage. *J. Marine Res., 37* (1): 1-22.

Campbell, W.J. (1965) The wind driven circulation of ice and water in a Polar Ocean. *J. Geophys. Res., 79* (14): 3279-3301.

Chang, S.W. and R.A. Anthes (1978) Numerical Simulations of the Oceans nonlinear, baroclinic response to translating hurricanes. *Journal of Physical Oceanography, 8* : 468 - 480.

Clark, D.L. (1977) Climatic factors of the late Mesozoic and Cenozoic Arctic Ocean. *Polar Oceans*, M. J. Dunbar, ed. Arctic Inst. of North America. , 603-615.

Coachman, L.K. (1963) Water masses of the Arctic. In: *Proceedings of the Arctic Basin Symposium, October ,1962.* Washington,D.C., Arctic Institute of North America: 143-172.

Coachman, L.K. (1968) Physical oceanography of the Arctic Ocean:1965. In *Arctic Drifting Stations*. J.E. Sater, Coord., Washington, D.C., pp 255-280.

Coachman, L.K. and J.L.Newton (1972) Water and ice motion in the Beaufort Sea. Spring 1970. *AIDJEX Bulletin, 12* : 61-91.

Coachman, L.K. and K. Aagaard, (1974) Physical oceanography of the Arctic and Subarctic seas. In *Marine Geology and Oceanography of the Arctic Seas.* Chapt. 1.: 1-92., Springer, N.Y.

Coachman, L.K., Aagaard, K. and Tripp, R.b. (1975) *The Bering Strait: The Regional and Physical Oceanography.* Univ. Washington Press., Seattle Washington. 172 pp.

Cook, G. (1966) *Oceanographic data, Arctic Ocean(Beaufort Sea) October 1964.* Technical report. NUWS consecutive number 417.

DeLeeuw. M.M. (1967) New Canadian bathymetric chart of the the western Arctic Ocean, north of 72 degrees. *Deep-Sea Research 14* (5): 489-504.

Dantzler, H.L. (1976) Geographic variations in intensity of the North Atlantic and North Pacific Oceanic eddy fields. *Deep-Sea Research 23* : 783-794.

Ebbesmeyer C.C. and B.A. Taft (1979) Variability of potential energy, dynamic height, and salinity in the pycnocline of the western North Atlantic. *Journal of Physical Oceanography, 9* : 1073-1089.

Fofonoff, N.P. (1962) Dynamics of ocean currents. In *The Sea*, M.N.Hill, ed. 1(3): 323-395. McGraw Hill.

Fofonoff, N. (1976) Polygon - 70 . *Oceanus, 19* (3): 40-44 , M. H. McLeish, ed.

Frankignoul, C. and P. Muller (1979) Quasi geostrophic response of an infinite beta-plane ocean to stochastic forcing by the atmosphere. *Journal of Physical Oceanography, 9* (1): 104-127.

Fuglister, F.C. and L.V. Worthington (1951) Some results of a multiple ship survey of the Gulf Stream. *Tellus, 3* (1): 1-14.

Fuglister, F.C. (1971) *Studies in physical oceanography, A Tribute to Georg Wüst on his 80th Birthday.* A.Gordon, ed. Gordon and Breach.

Galt, J.A. (1967) Current measurements in the Canada Basin of the Arctic Ocean, Summer 1965. Univ. Wash. Tech. Report No. 184: 17pp.

Garrison, G.R. and P. Becker (1976) The Barrow submarine canyon: a drain for the Chukchi Sea. *J. Geophys. Res., 81* (24): 4445-4453.

Hammond, A.L. (1974) Undersea storms: Experiments in the Atlantic. *Science 185* : 244-247.

Harrison, D.E. (1978) On the equilibrium linear basin response to fluctuating winds and mesoscale mo- tions in the oceans. *J. Geophys. Res., 84* (C3): 1221-1224.

Hart, J.E. and P.D. Killworth (1976) Open ocean baroclinic instability in the Arctic. *Deep-Sea Research 23* : 637-645.

Herman, Y. and D.M. Hopkins (1980) Arctic Ocean climate in the late Cenozoic time. *Science 209* : 557-562.

Hess, S.L. (1959) *Introduction to Theoretical Meteorology,* Holt, Rinehart and Winston, N.Y., N.Y. 363pp.

Holton, J.R. (1973) *An Introduction to Dynamic Meteorology.* Academic Press, N.Y., N.Y. 319pp.

Hufford, G.L. (1973) Warm water advection in the southern Beaufort Sea, August-September 1971. *J. Geophys. Res., 78* (15): 2702-2707.

Hughes, K.H. (1968) Seasonal vertical distributions of Copepods in the arctic water in the Canadian Basin of the North Polar sea. Masters Thesis, Univ. Wash., Seattle, Washington.

Hunkins, K.L. (1966) Ekman drift currents in the Arctic Ocean. *Deep-Sea Research 13* : 607-620.

Hunkins, K.L. (1974) Subsurface eddies in the Arctic Ocean. *Deep-Sea Research 21* : 1071-1033.

Hunkins K.L. (1974b) An estimate of the internal wave drag on pack ice. *AIDJEX Bulletin 26* : 141-162.

Hunkins, K.L. (1975) The oceanic boundary layer and stress beneath a drifting floe. *J. Geophys. Res., 80* (24): 3425-3434.

Hunkins, K.L., T. Manley and W. Tiemann (1979) *Observations of position, ocean depth, ice rotation, magnetic declination and gravity taken at the FRAM I drifting ice station.* Technical Report No. 1, CU-1-79. LDGO.

Iselin, C., O'D. (1936) A study of the western circula- tion of the Western North Atlantic. *Papers of Physical Oceanography and Meteorology, 4* : 1-101.

Johnson, G.L., Monahan, D., G. Grönlie, and L. Sobczak (1979) General bathymetric chart of the oceans (GEBCO) Published by the Canadian Hydrographic Service, Ottawa, Canada.

Kellogg, W.W. (1973) Climate feedback mechanisms invol- ving the polar regions. In *Climate of the Arctic*, G.Weller and S.A. Bowling , eds. Twenty fourth Alaska Science Conference, Univ. Alaska, Fairbanks, Alaska. Geophysical Institute: 111-116.

Kinder, T. H. and L.K. Coachman (1977) Observation of a bathymetrically trapped current ring. *Journal of Physical Oceanography, 7* : 948-952.

Koshlyakov, M.N. and A.S. Monin (1978) Synoptic eddies in the ocean. *Annual Reviews of Earth and Planetary Science, 6* 495-523.

Leavitt, E. (1975) Determination of air stress from AIDJEX surface layer data. *AIDJEX Bulletin 28* : 11-20.

Lee, T.N. (1975) Florida current spin off eddies. *Deep-Sea Research 22* : 753-765.

Leetmaa, A. (1978) Fluctuating winds, an energy source for mesoscale motions. *J. Geophys. Res., 83* (C1): 427-430.

Leming, T.D. (1972) Eddies west of the southern Antilles. In *In: Symposium of investigations and resources of the Caribbean Sea and adjacent regions (Proceedings)*, Unipub.,N.Y., 516 pp.

Longuet-Higgins, M.S. (1975) The response of a stratified ocean to stationary or moving wind systems. *Deep-Sea Research 12* : 923-973.

Lorenz, E.N. (1955) Available potential energy and the maintenance of the general circulation. *Tellus, 7* (2): 157-167.

McLeish, W.H.(ed.) (1976) Ocean Eddies. *Oceanus, 19* (3). The Woods Hole Oceanographic Institution , Woods Hole, Mass.

McPhee, M.G. (1975) The effect of ice motion on the mixed layer under the Arctic pack ice. *AIDJEX Bulletin, 30* : 1-29.

McPhee, M.G. (1978) AIDJEX oceanographic data report. *AIDJEX Bulletin, 39* : 33-78.

McWilliams, J.C. (1977) On the large scale circulation of the ocean: A discussion for the unfamiliar. In *Oceanic Sound Scattering Prediction*. Anderson, N.R.and B.J. Zahuranec (eds.) Plenum Press.

McWilliams, J.C. (1979) A review of research on mesoscale ocean currents. *Reviews of Geophysics and Space Physics, 17* (7): 1548-1558.

Magaard, L. (1977) On the generation of baroclinic Rossby Waves in the ocean by meteorological forces. *Journal of Physical Oceanography, 7* : 359-364.

Maksimov, I.V. (1945) Determining the relative volume of the annual flow of Pacific waters into the Arctic Ocean through the Bering Strait(in Russian). *Problemy Arktiki i Antarktiki 2* : 51-58.

Manley, T.O., K.L. Hunkins and W. Tiemann (1980a) *Arctic Ice Dynamics Joint Experiment 1975-1976, Physical Oceanography Data Report, Profiling Current Meter Data,Camp Caribou* , Volume 1, CU-4-80. Technical Report No. 4, Lamont-Doherty Geological Observatory, Palisades,N.Y.

Manley, T.O., K.L. Hunkins and W. Tiemann (1980b) *Arctic Ice Dynamics Joint Experiment 1975-1976, Physical Oceanography Data Report, Profiling Current Meter Data,Camp Blue Fox* , Volume 2, CU-5-80. Technical Report No. 5, Lamont-Doherty Geological Observatory, Palisades,N.Y.

Manley, T.O., K.L. Hunkins and W. Tiemann (1980c) *Arctic Ice Dynamics Joint Experiment 1975-1976, Physical Oceanography Data Report, Profiling Current Meter Data,Camp Snowbird* , Volume 3, CU-6-80. Technical Report No. 6, Lamont-Doherty Geological Observatory, Palisades,N.Y.

Manley, T.O., K.L. Hunkins and W. Tiemann (1980d) *Arctic Ice Dynamics Joint Experiment 1975-1976, Physical Oceanography Data Report, Profiling Current Meter Data,Camp Big Bear* , Volume 4, CU-7-80. Technical Report No. 7, Lamont-Doherty Geological Observatory, Palisades,N.Y.

Minoda, T. (1971) Pelagic copepoda in the Bering Sea and the Northwestern North Pacific with special ref- erence to their vertical distribution. *Memories of the Faculty of Fisheries. 18* (1/2): 1-74. Hokkaido Univ.

Maykut, G.A. (1976) Energy exchange over young sea ice in the Central Arctic. *AIDJEX Bulletin 31* : 45-74.

Mode Group (Baker, D.J., Jr., et al)(1978) The mid-ocean dynamics experiment. *Deep-Sea Research, 25* : 859-910.

Mosby,H. (1962) Water, salt and heat balance of the North Polar sea and of the Norwegian sea. *Geophysical Publication, 24* : 289-313.

Mountain, D.G., L.K. Coachman and K. Aagaard (1976) On the flow through Barrow Canyon. *Journal of Physical Oceanography, 6* (4): 461-470.

Newton, J. (1973) The Canada Basin: mean circulation and intermediate-scale flow features. Doctoral dissertation, Univ. Wash., Seattle, Wash.; 158pp.

Newton, J.L., K. Aagaard and L.K. Coachman. (1974) Baroclinic eddies in the Arctic Ocean. *Deep-Sea Research 21* : 707-719.

Oort, A. (1964) Computations of the eddy heat and density transports across the Gulf Stream. *Tellus, 16* (1): 55-63.

Paquette, R.G. and R.H. Bourke (1974) Observations on the coastal current of arctic Alaska. *J. Marine Res., 32* (2):195-207.

Parker, C.E. (1971) Gulf Stream rings in the Sargasso Sea. *Deep-Sea Research 18* : 981-993.

Paulson, C.A. and D.L. Bell. (1975) Meteorological observations during the AIDJEX Main Experiment. *AIDJEX Bulletin, 28* : 1-10.

Pautzke, C., (1979). Phytoplankton primary production below the Arctic Ocean pack ice: an ecosystem analysis. Doctoral Dissertation, Univ. of Washington, Seattle,Wash., 180pp.

Philander, G. (1978) Forced oceanic waves. *Reviews Geophysics and Space Physics, 16* : 15-46.

Pounder, E.R., (1980). Physical oceanography in the central Arctic(Abstract). Presented paper. *EOS, 61* (17), p. 278 (0-243).

Richardson, P. (1976) Gulf Stream rings. *Oceanus, 19* (3): 65-68.

Robinson, A.R. (1975) The variability of ocean currents. *Reviews Geophysics and Space Physics, 13* (3): 598-601.

Robinson, A.R. (1976) Eddies and ocean circulation. *Oceanus, 19* 19(3): 2-17.

Rossby, C. and G. Rossby. (1936) Dynamics of steady ocean currents in the light of experimental fluid mechanics. *Papers in Physical Oceanography and Meteorology, 5* (1): 1-43.

Stater, J.E. (1969) *The Arctic Basin.* The Arctic Inst. of N. America. Wash. D.C., 337pp.

Saunders, P.M. (1971) Anticyclonic eddies formed from shoreward meanders of the Gulf Stream. *Deep-Sea Research 18* : 1207-1219.

SCOR (1979) *Arctic ocean heat budget.* Report no. 52 of the Geophysical Institute, Division of Oceanography, Univ. of Bergen, Bergen, Norway.

Shih, C.T. and D.R. Laubitz (1978) Zooplankton distributions in the Eastern Beaufort Sea and the North- west Passage. *Astarte, 11* : 45-54.

Somov, M.M. (ed.)(1954-55) Observational data of the Scientific Research drifting Station of 1950- 51. Leningrad: *Morskoi Transport, Vol 1,* (2), 48-170 , 180-403 (translated) .

Starr, V.P. and White, R.M. (1951) A Hemispherical study of the atmospheric angular momentum balance. *Quart. J. Roy. Meteorol. Soc., 77* : 215-225.

Starr, V.P. (1953) Note concerning the nature of the large scale eddies in the atmosphere. *Tellus, 5* :494-498.

Starr, V.P. (1954) Commentaries concerning research of the general circulation. *Tellus, 6* : 268-272.

Starr, V.P. (1968) *Physics of Negative Viscosity Phenomena.* McGraw-Hill, 256 pp.

Stommel, H.M. (1958) *The Gulf Stream.* Berkley, USA, Univ. of Calif. Press. 202pp.

Swallow, J.C. (1976) Variable currents in mid-ocean. *Oceanus, 19* (3): 18-25 , M. H. McLeish, ed.

Thorndike, A.S., D.A. Rothrook, G.A. Maykut, and R. Colony (1975) Ice thickness distribution of sea ice. *J. Geophys. Res., 80* (33): 4501-4513.

Thorndike, A.S.and J.Y. Cheung (1977) AIDJEX Measurements of the sea ice motion, 11 April 1975 to 14 May 1976. *AIDJEX Bulletin 35* : 149pp.

Thorndike, A.S. and T.O. Manley (1980a) *Updated satellite positions for the AIDJEX manned camps, April 11, 1975 to October 17, 1975.* Technical Report No. 9, CU-9-80. Lamont-Doherty Geol. Obs. of Columbia Univ., Palisades, N.Y.

Thorndike, A.S. and T.O. Manley (1980b) *Updated satellite positions for the AIDJEX manned camps, October 17, 1975 to May 4, 1975.* Technical Report No. 9, CU-9-80. Lamont-Doherty Geol. Obs. of Columbia Univ., Palisades, N.Y.

Tidmarsh, W.G. (1973) *The Copepoda (Calanoida, Cyclopoida of Northern Baffin Bay and Southern Nares Strait: Their distribution and aspects of their biology.* Technical Report; The Arctic Instit. of North America.

Timofeyev, V.T. (1963) Interaction of the waters from the Arctic with those from the Atlantic and Pacific (in Russian). *Okeanologiya, 3* (4): 569-578.

Thompson, B.J. and G.A. Gotthardt (1971) Life cycle of a north atlantic eddy. *Transactions ACU. 52* (4): 421.

Turner, J.S. (1973) *Buoyancy Effects in Fluids.* G. K. Batchelor and J.W. Miles (eds.) Cambridge Univ. Press. 367pp.

Untersteiner, N., Hunkins, K.L., and B.M.buck (1976) Arctic science: Current knowledge and future thrusts. *Science, Technology and the Modern Navy,* Dept. of Navy, ONR, Arlington, Va. 277-297.

U.S.P.M.O.C. (United States POLYMODE Organizing Committee. (1977) *Theory and modeling of ocean eddies: Contribution of the U.S. delegation to the YALTA Polymode theoretical Institute.* (P.Rhines, ed.) Dept. of Meteorology, MIT.

von Arx, W.S. (1954) Measurements of the oceanic circulation in temperate and tropical latitudes. *Oceanographic Instrumentation,* National Research Council(US) Publ.no. 309: 13-35.

Vowinckel, E. and S. Orvig (1962) Water balance and heat flux of the Arctic Ocean. Arctic, 15: 205-223. *Arctic, 15* : 205-223.

Vowinckel, E. and S. Orvig. (1970) The climate of the North Polar Basin. In *Climates of the North Regions,* Chapt. 3: 129-252. Elsevier, N.Y.

Warren, B.A. (1967) Notes on translatory movement of rings of current with application to Gulf Stream eddies. *Deep-Sea Research 14* : 505-524.

Webster, F. (1961a) A description of Gulf Stream meanders off Onslow Bay. *Deep-Sea Research 8* : 130-143.

Webster, F. (1961b) The effects of meanders on the Kinetic energy balance of the Gulf Stream. *Tellus, 13* : 392-401.

Webster, F. (1964) Measurements of eddy fluxes of momentum in the surface layer of the Gulf Stream. *Tellus, 17* : 240-245.

Wiebe, P.H. (1976) The biology of cold core rings. *Oceanus, 19* (3): 69-76 , M. H. McLeish, ed.

Wiebe, P.H., E.M. Hulburt, E.J. Carpenter, A.E. John, G.P. Knapp III, S.H. Boyd, P.D. Ortner, and J.L. Cox (1976b) Gulf Stream cold core rings: large scale interaction sites for open ocean plankton communities. *Deep-Sea Research 23* : 695-710.

Wiebe, P.H. and P. Ortner (1976c) Biological evidence supporting the advective character of cold core rings. *Polymode News 8* : 3-6.

Whipple, F.J.W. (1917) The motion of a particle on the surface of a smooth rotating globe. *Phil. Mag., 33* (198): 457-471.

Wunsch, C. (1976) The mid-ocean dynamics experiment - 1. *Oceanus, 19* (3): 45-53 , M. H. McLeish, ed.

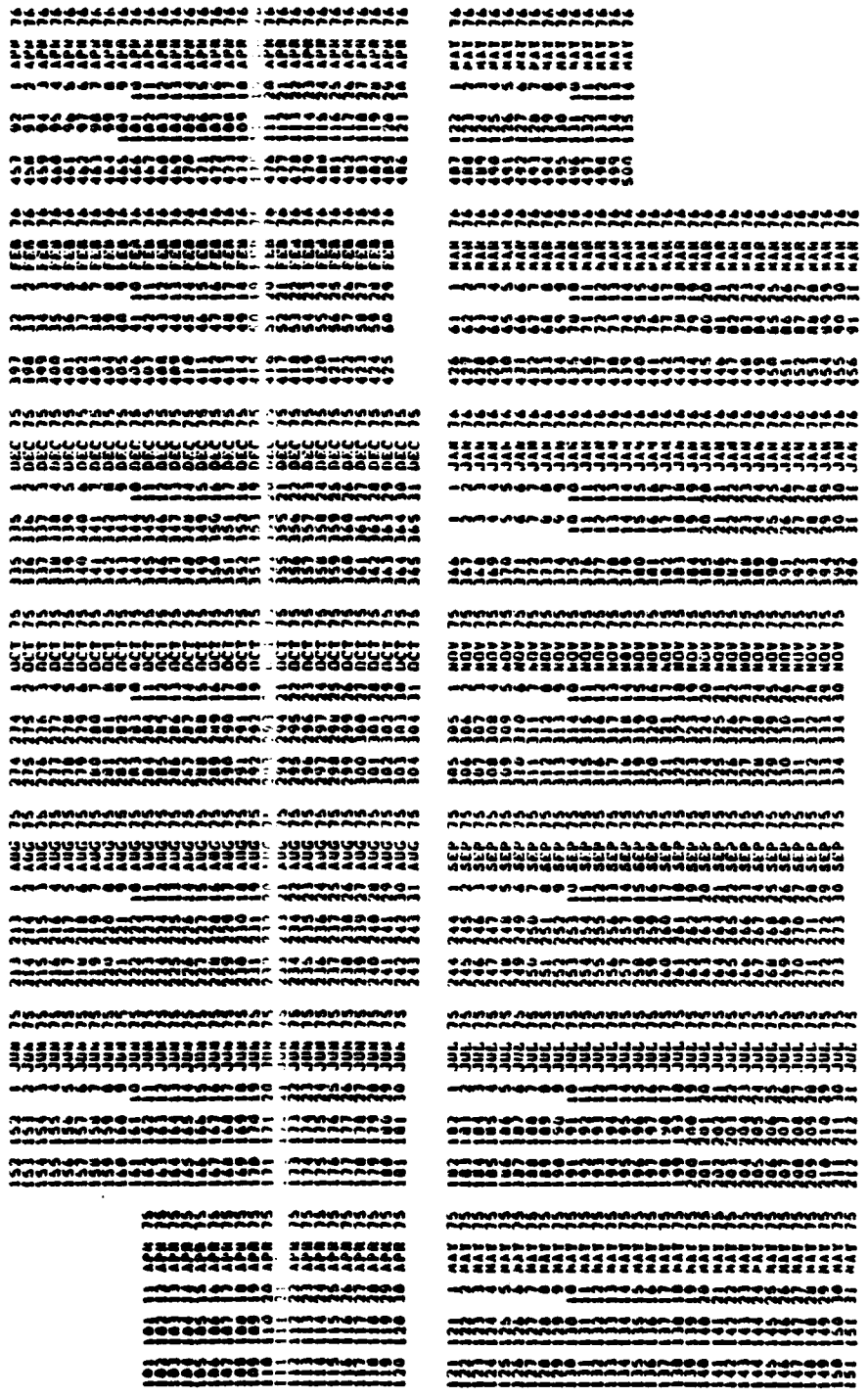
Wyrtki, K., L. Magaard, and J. Hager (1976) Eddy energy in the oceans. *J. Geophys. Res., 81* (15): 2641-2646.

Appendix 1

Conversion Table for AIDJEX Days to Calendar Days

For the main experiment, AIDJEX adopted a convention of numbering days consecutively, beginning with day 1(1 January, 1975) and ending with day 500(14 May, 1976).

In the conversion table, the first column is the AIDJEX day. The second column is the corresponding day of 1975 or 1976. The third entry is the calendar date.



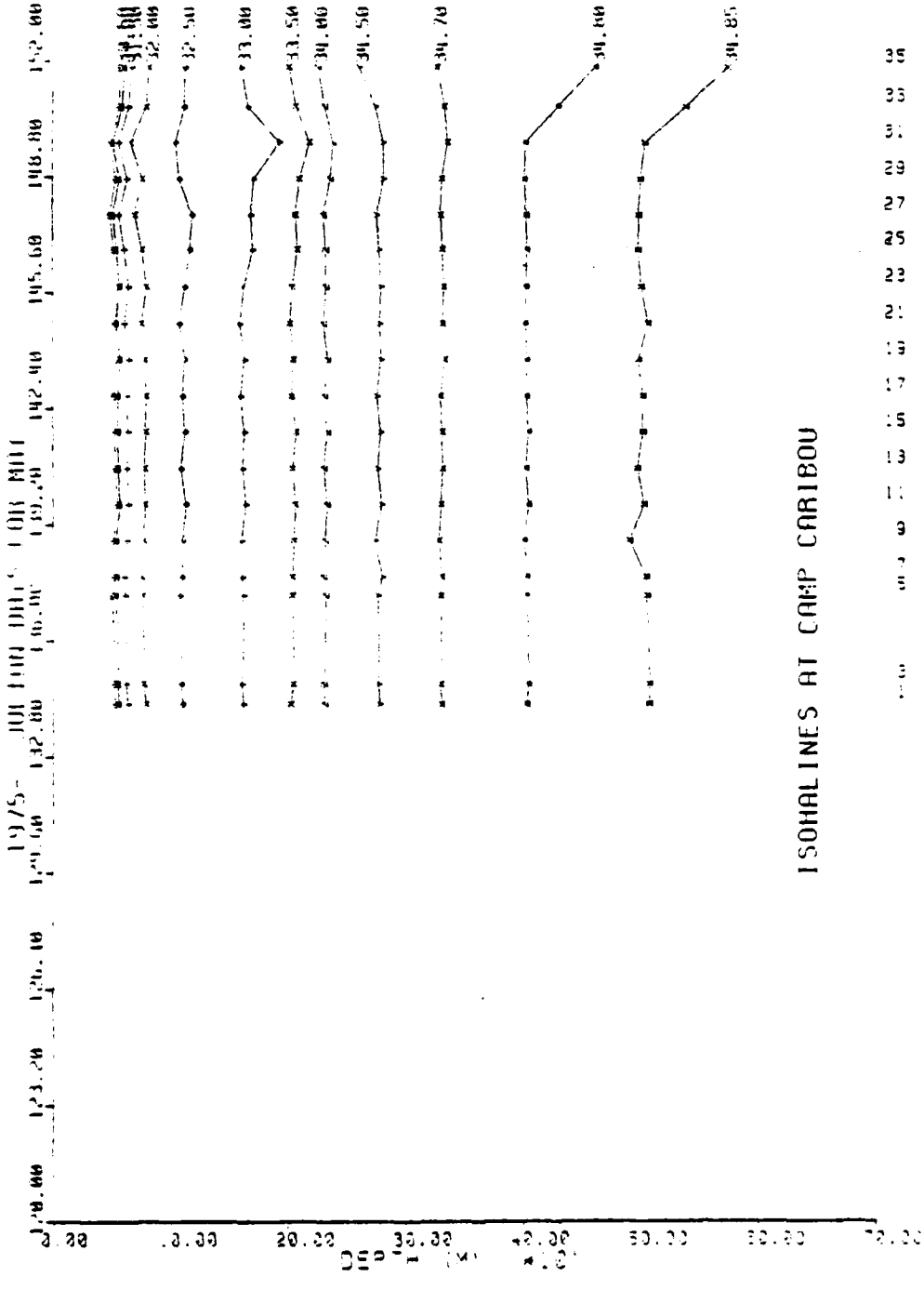
APPENDIX II

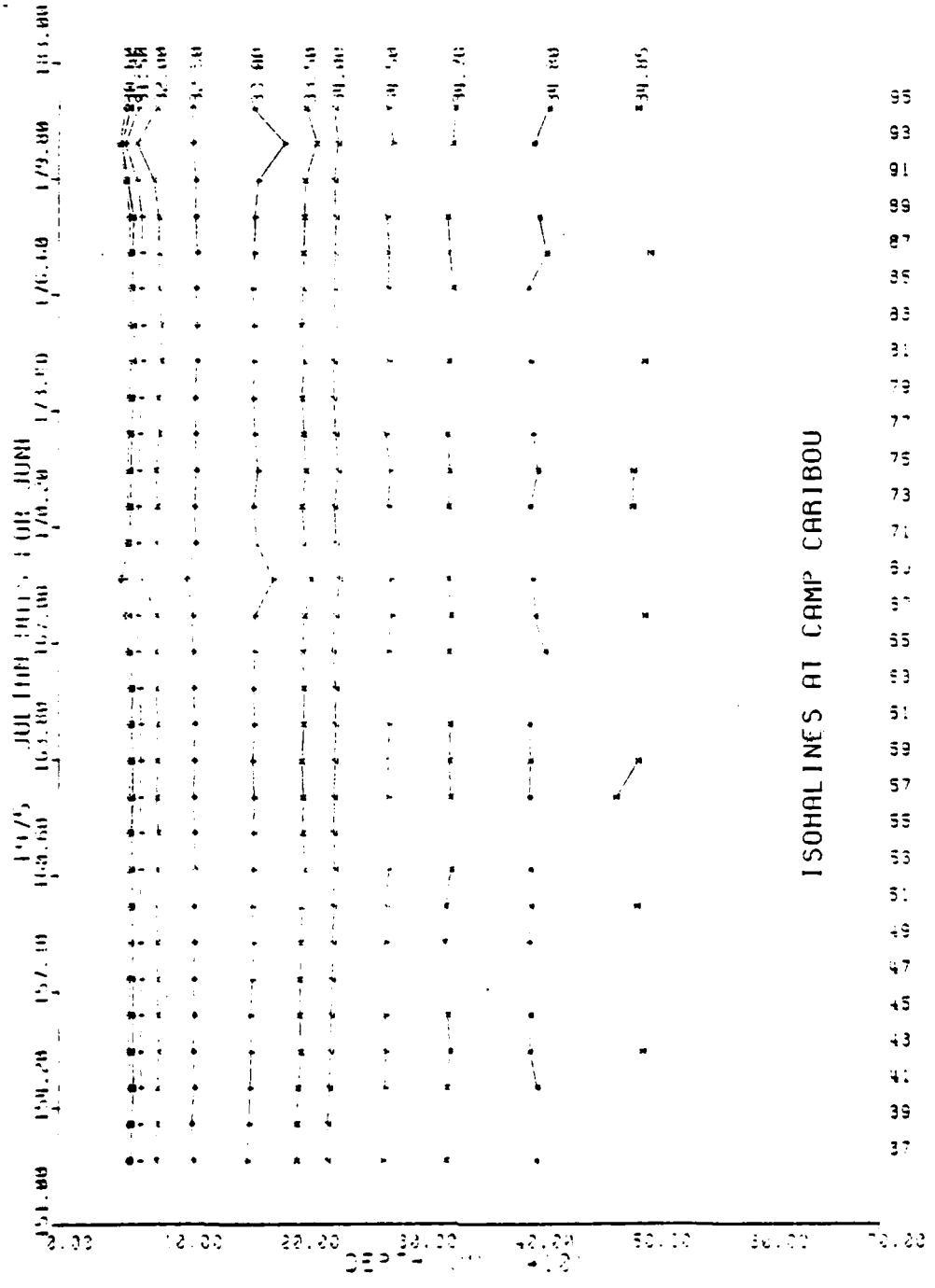
Additional AIDJEX Oceanographic Data

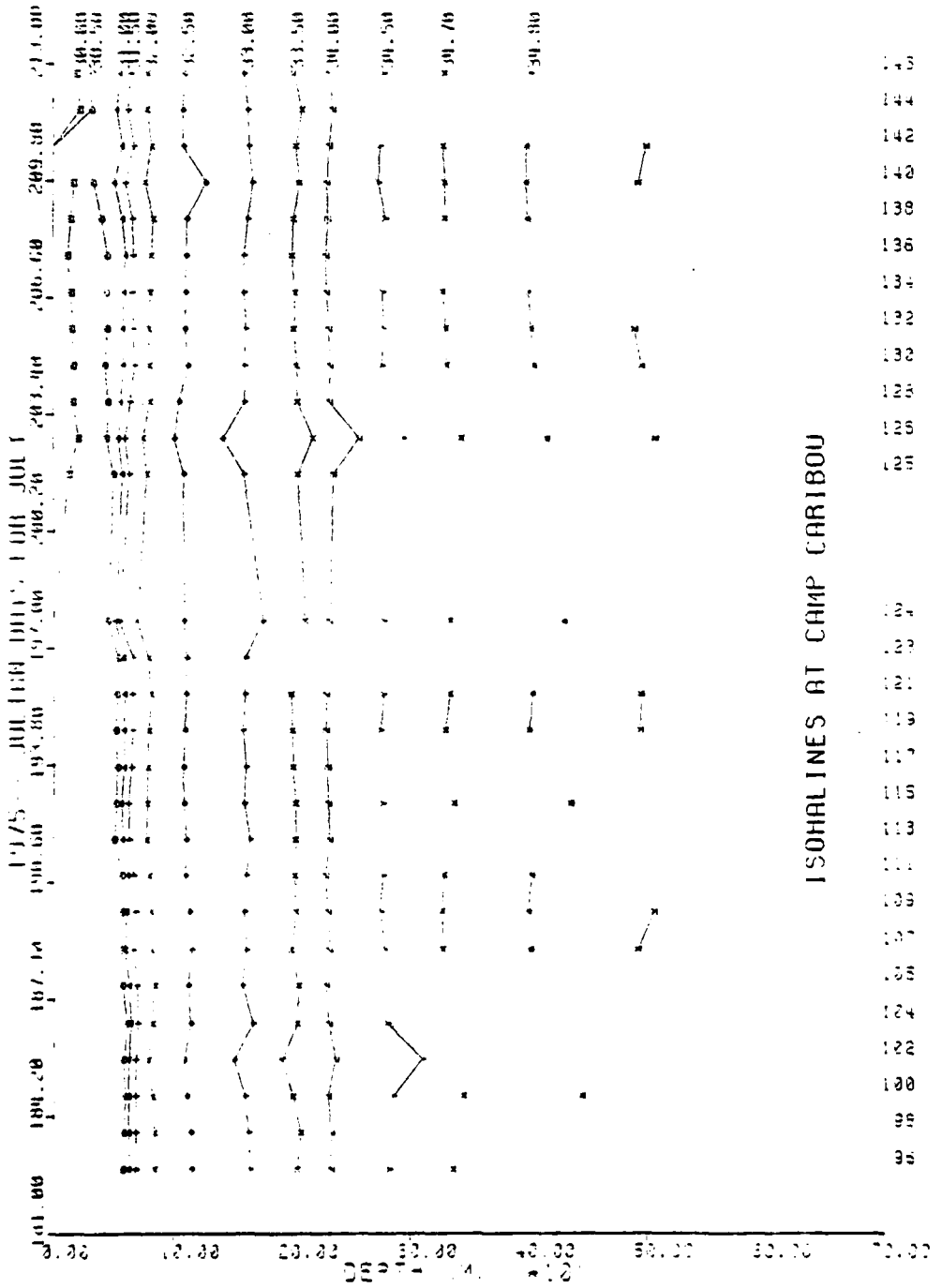
	Page
Section 1 Isohaline Levels versus Time	214
a. Camp Caribou	215
b. Camp Bluefox	227
c. Camp Snowbird	240
d. Camp Big Bear	252
Section 2 Temperature-salinity Diagrams for Observed Eddies	259
a. Camp Caribou	260
b. Camp Bluefox	295
c. Camp Snowbird	328
d. Camp Big Bear	364
Section 3 Listing of Eddies Observed during AIDJEX	385
Section 4 Monthly Mean Kinetic Energy	390
a. Camp Caribou	391
b. Camp Bluefox	397
c. Camp Snowbird	409
d. Camp Big Bear	421

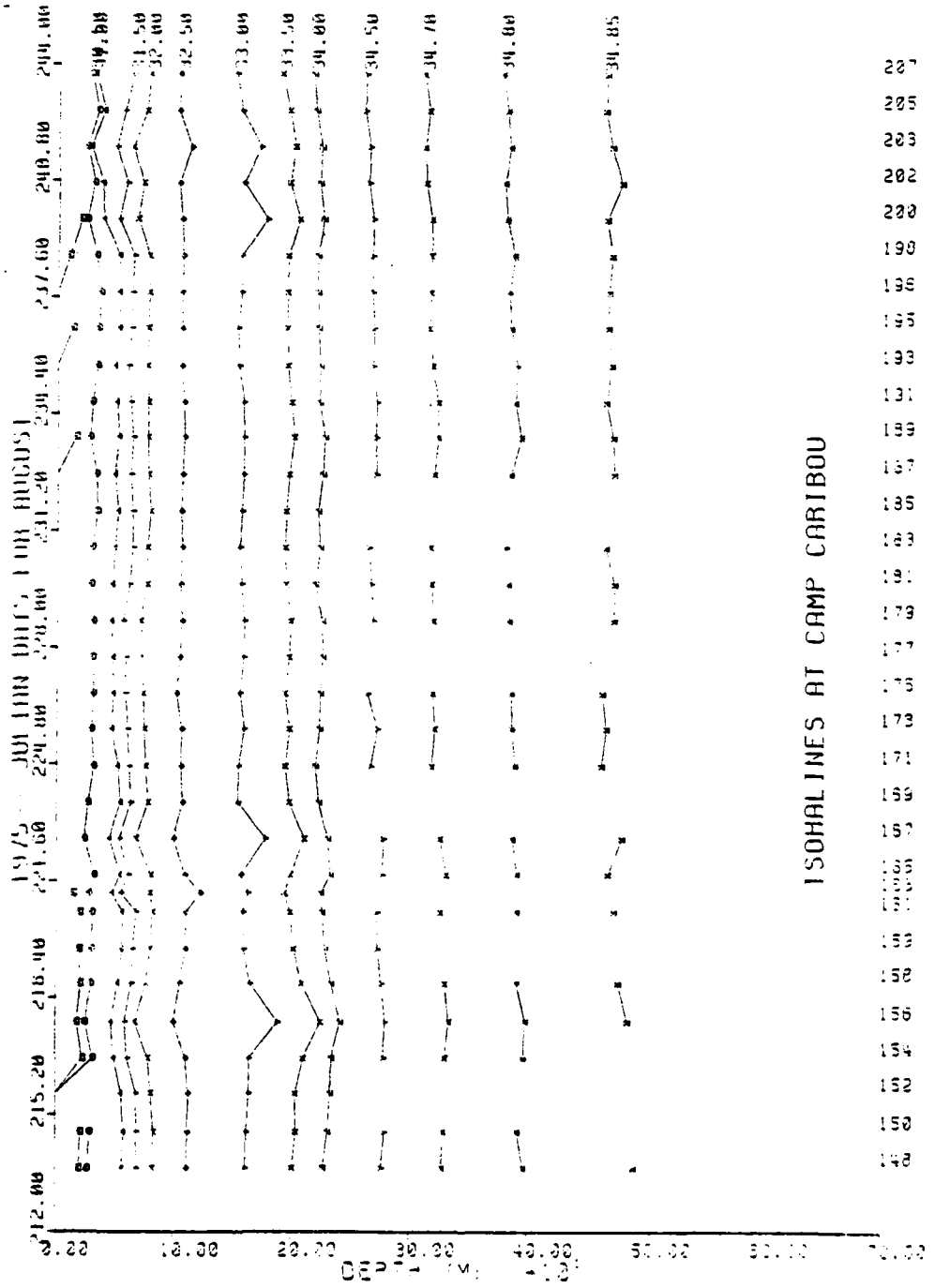
Section 1

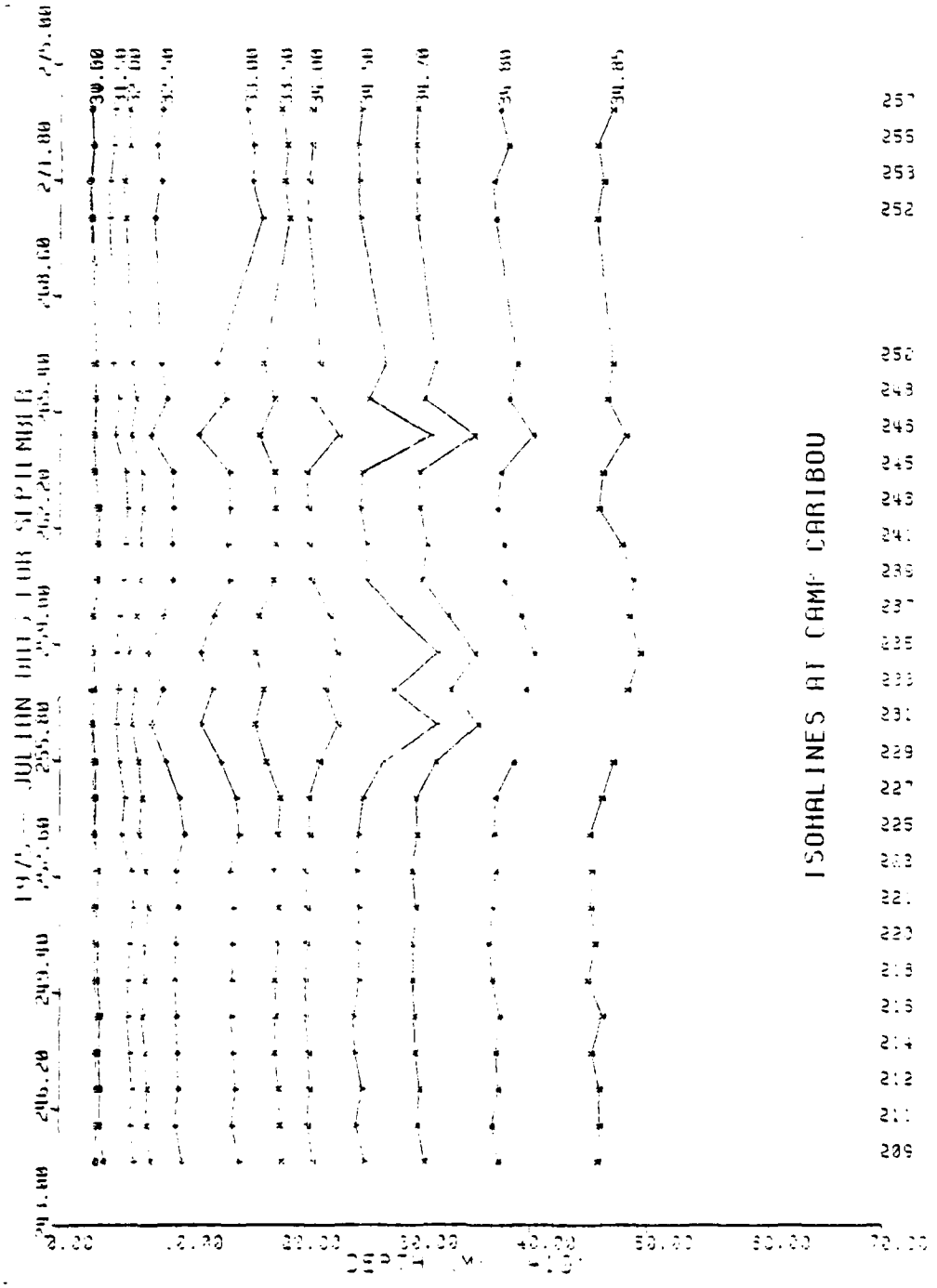
Isohaline Levels versus Time

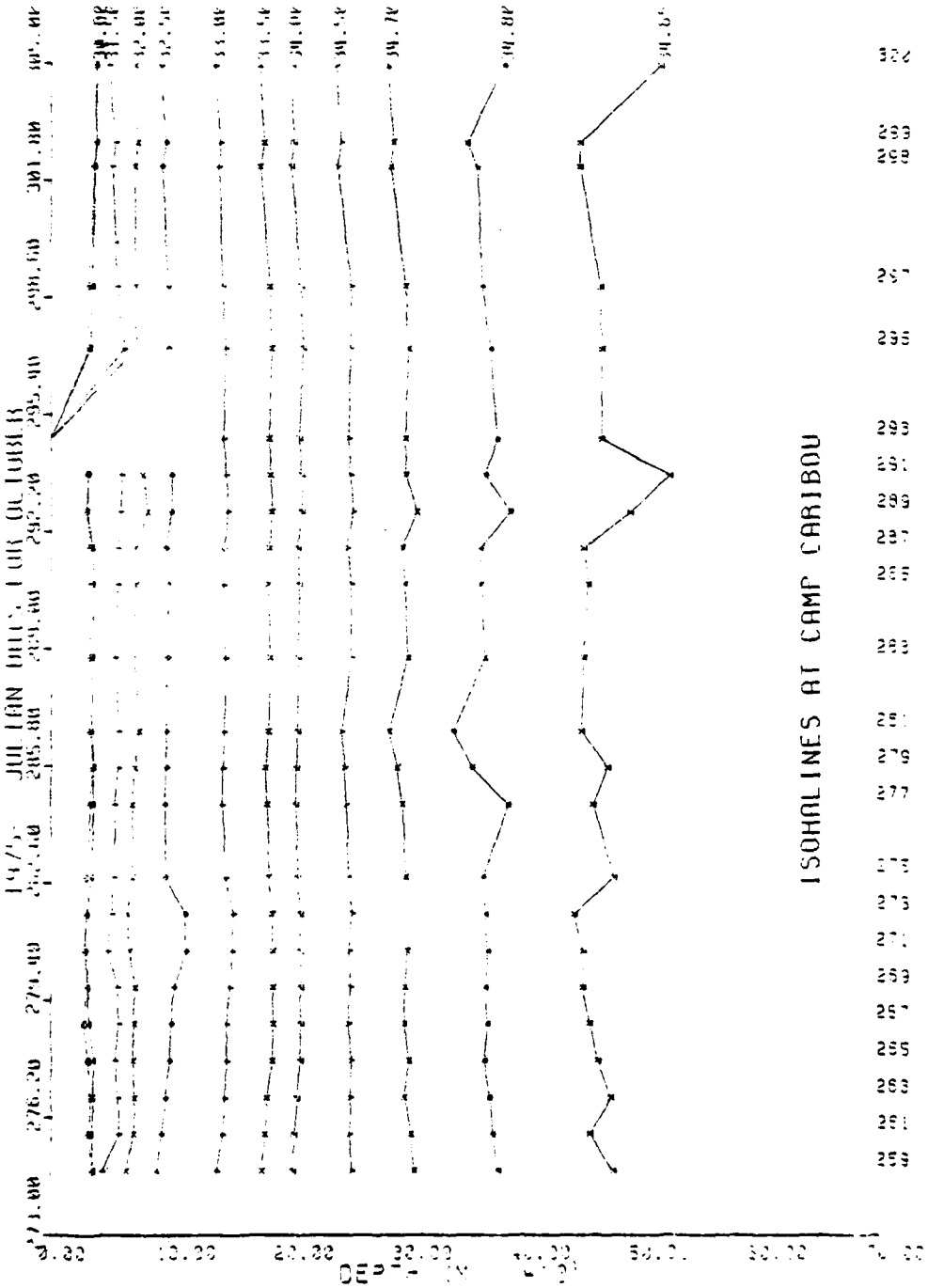

ISOHALINES AT CAMP CARIBOU

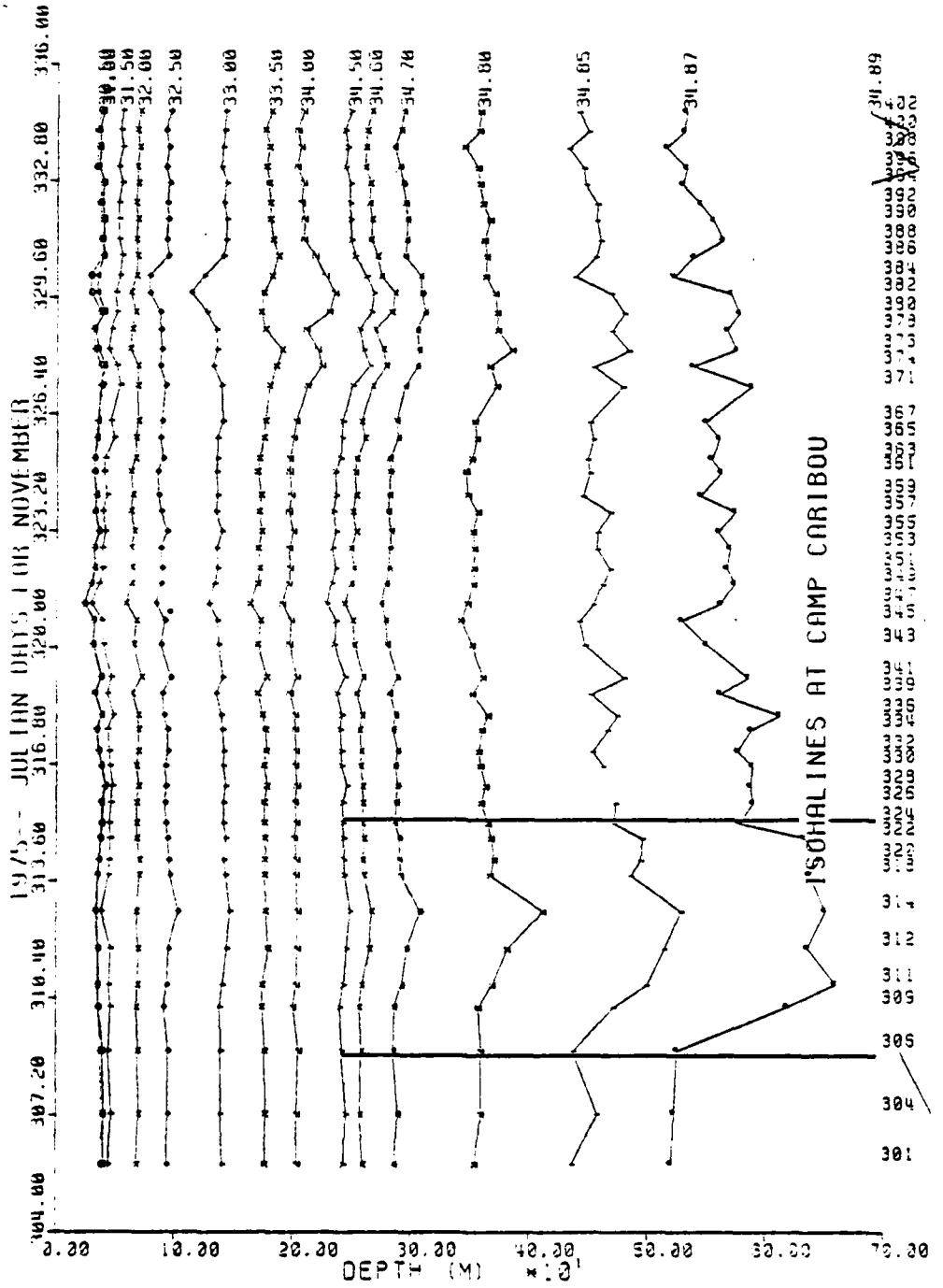

ISOHALINES AT CAMP CARIBOU

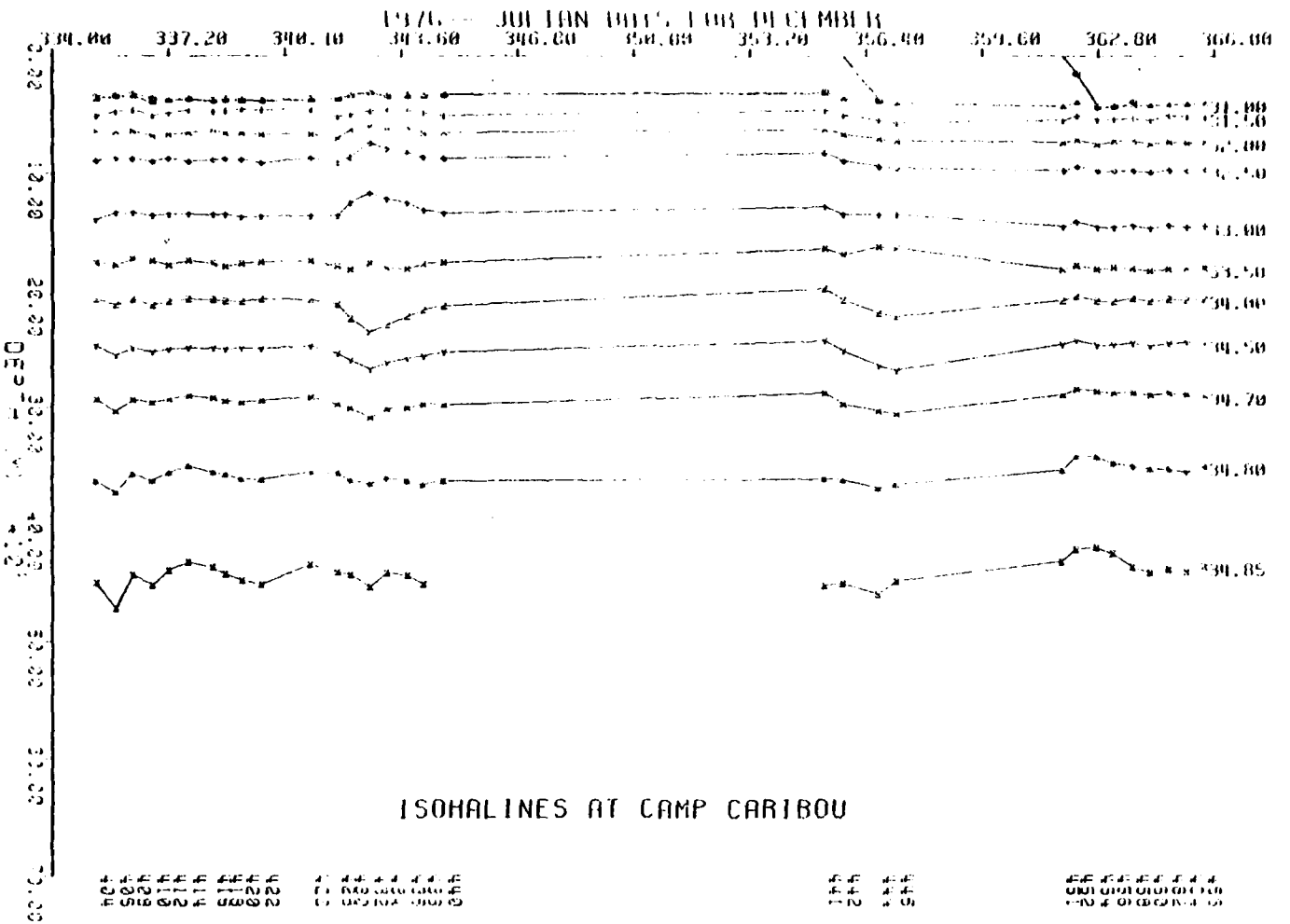

ISOHALINES AT CAMP CARIBOU


ISOHALINES AT CAMP CARIBOU
DEPTH (M)
0.00
10.00
20.00
30.00
40.00
50.00
60.00
70.00

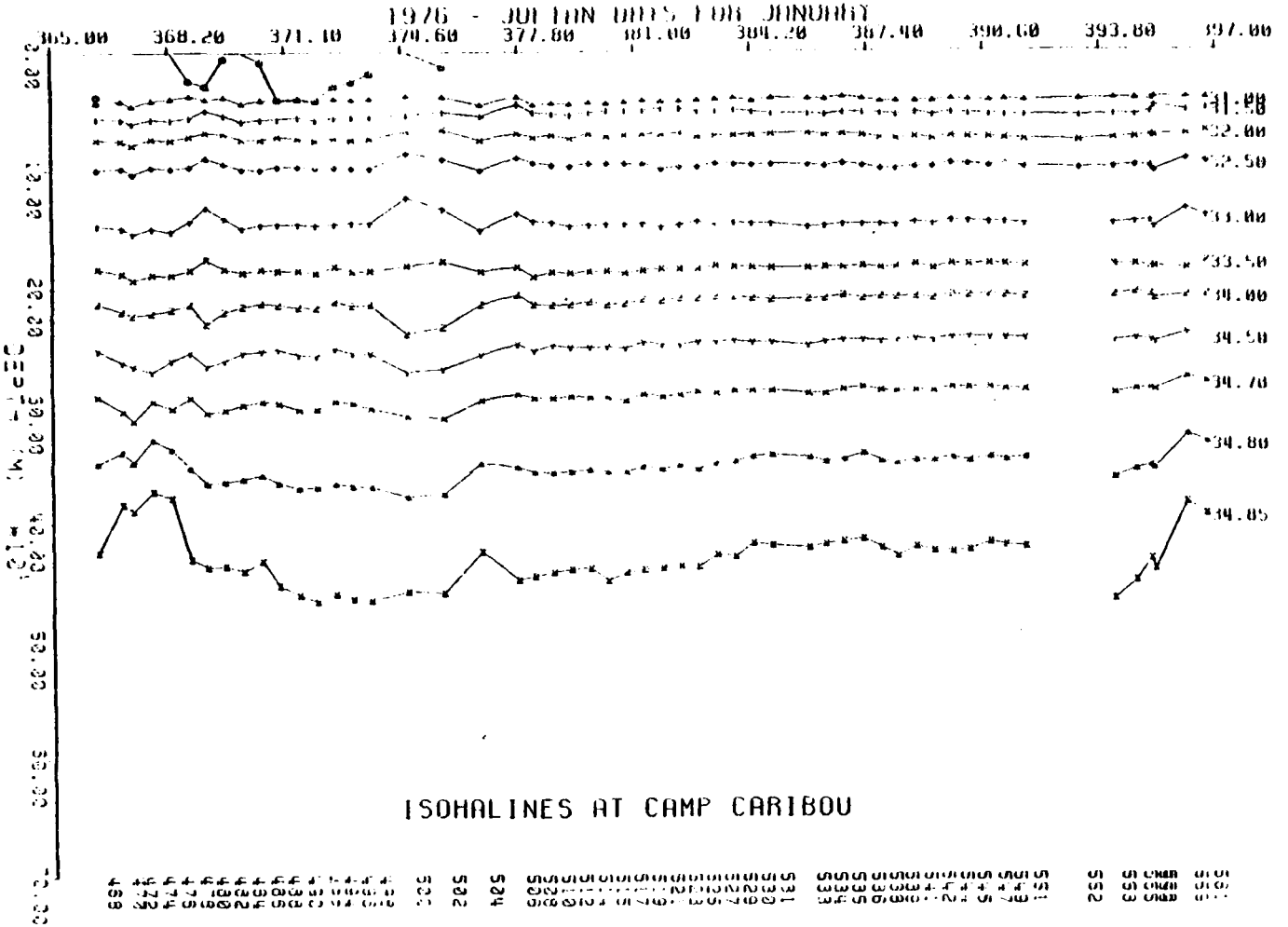

ISOHALINES AT CAMP CARIBOU
JULIAN DATE
DEPTH M


ISOHALINES AT CAMP CARIBOU

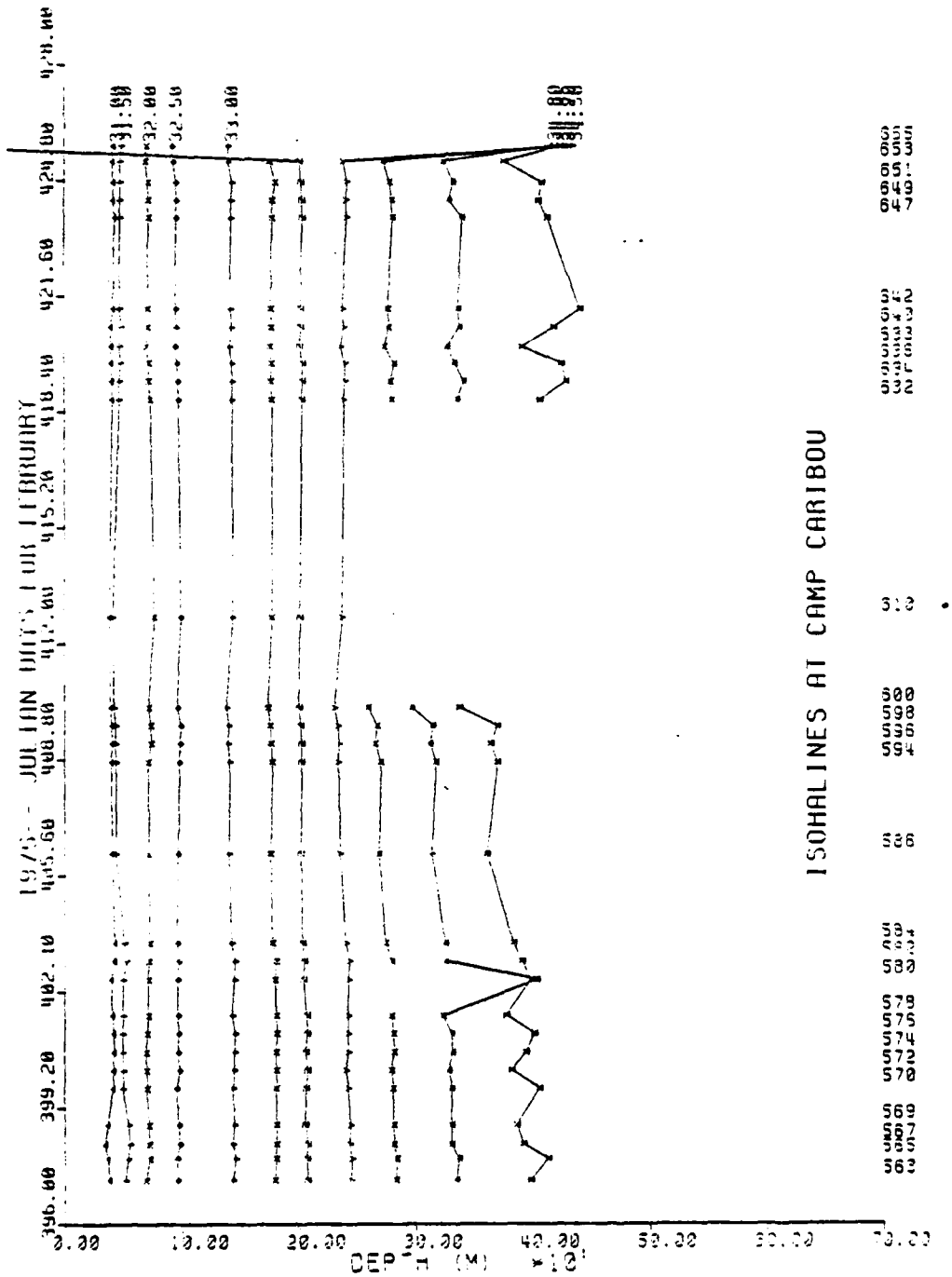

ISOHALINES AT CAMP CARIBOU
DEPTH (M)
JULIAN DAYS FOR NOVEMBER
31.89
31.87
34.85
34.80
34.70
34.60
34.50
33.50
33.00
32.50
32.00
31.50
31.00

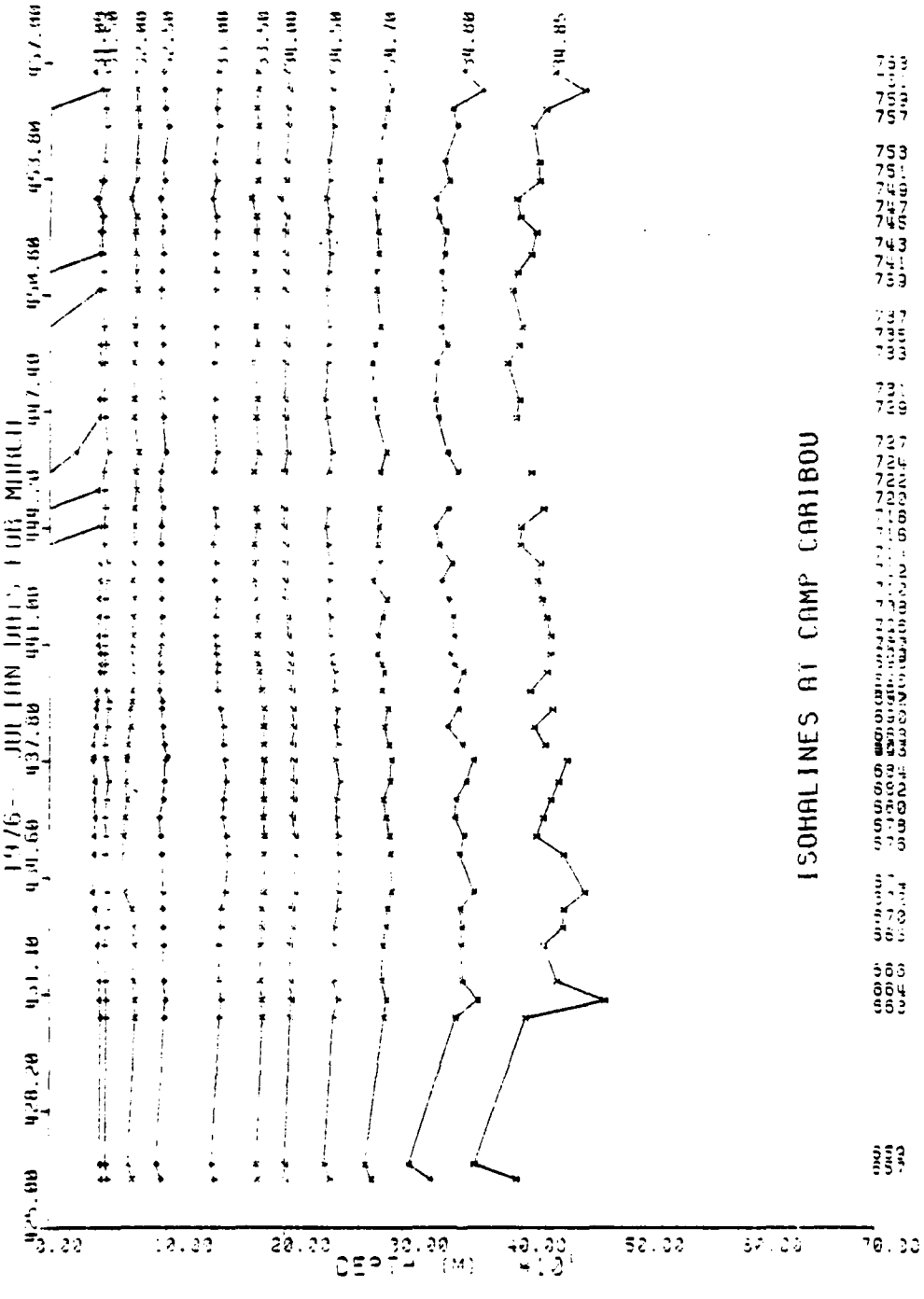


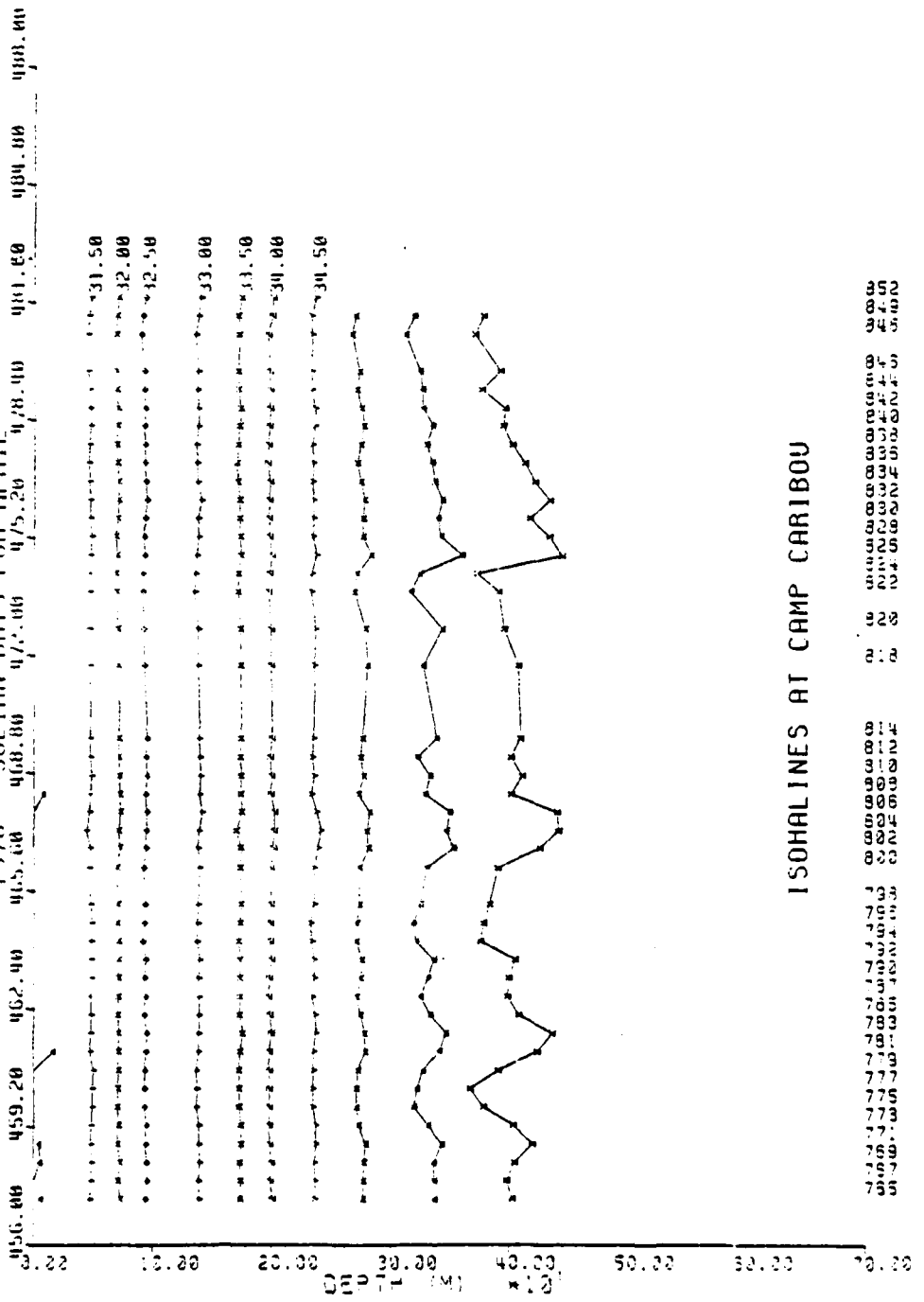
ISOHALINES AT CAMP CARIBOU

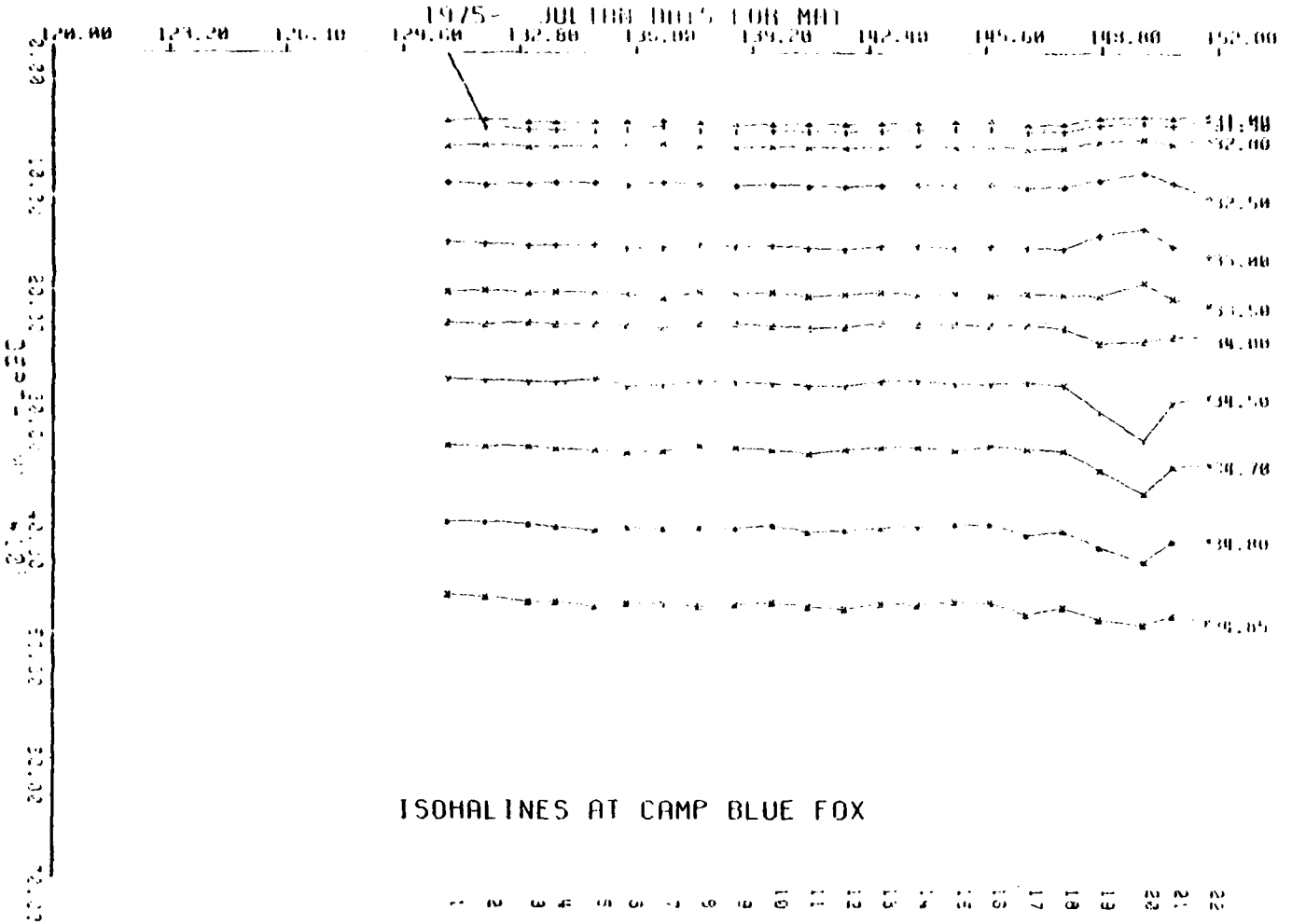


ISOHALINES AT CAMP CARIBOU

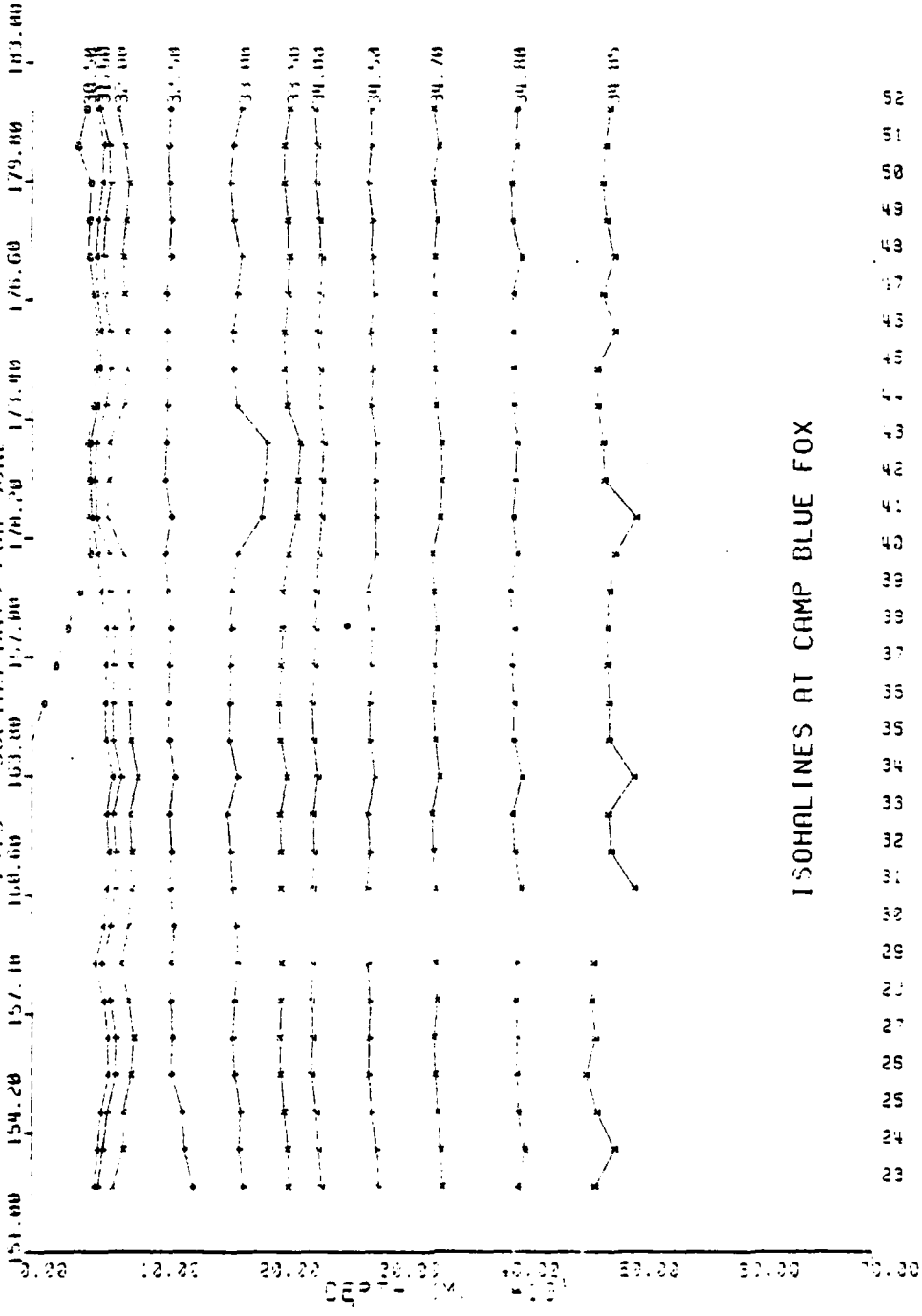

ISOHALINES AT CAMP CARIBOU
JULIAN DATES FOR FEBRUARY
DEPTH (M) *10
0.00
10.00
20.00
30.00
40.00
50.00
60.00
70.00
396.00
399.20
402.10
405.60
408.80
412.00
415.20
418.40
421.60
424.80
428.00
31.00
32.00
32.50
33.00
31.50
563
567
569
570
572
574
576
578
580
582
584
586
594
596
598
600
647
649
651
653
655

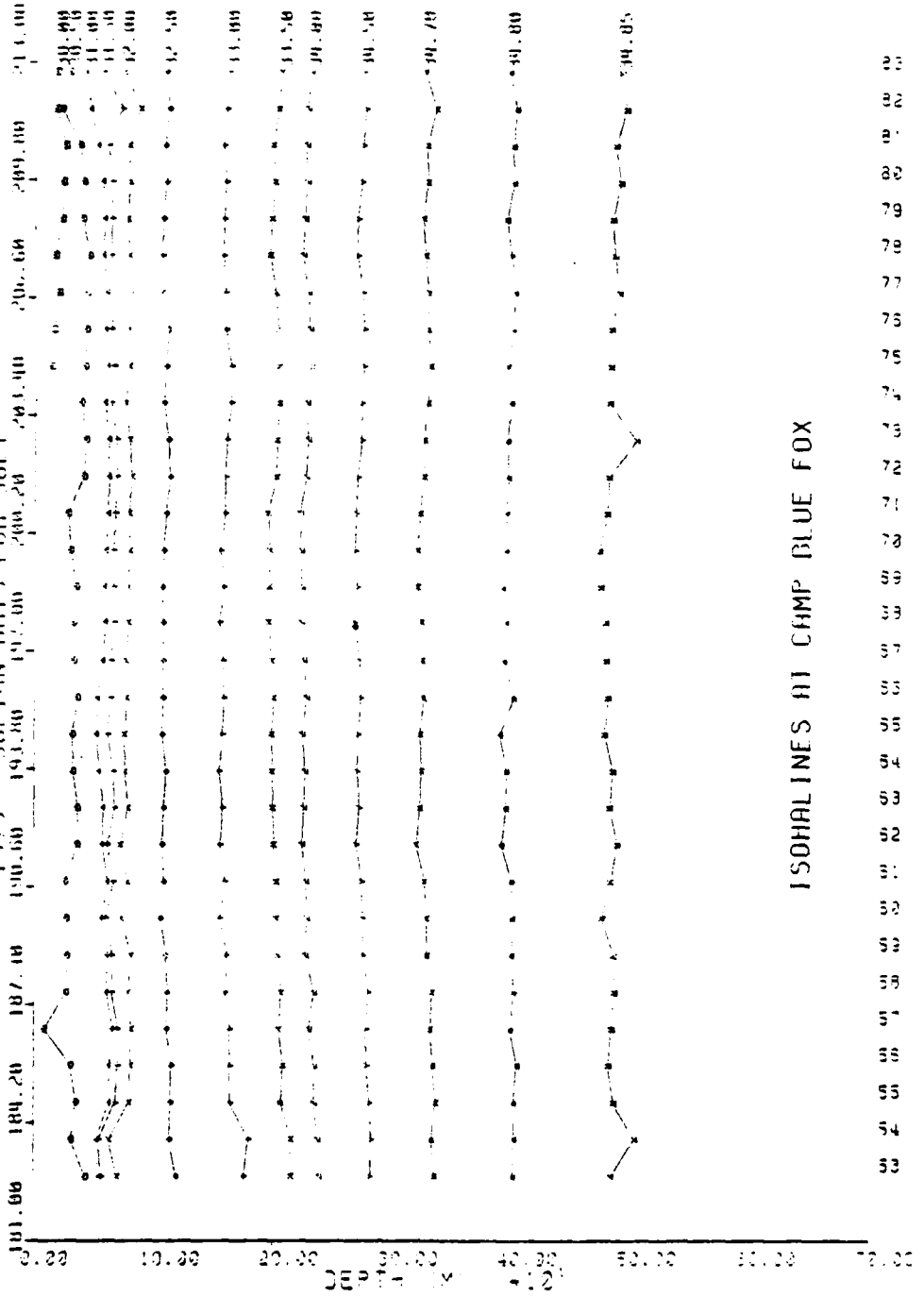

ISOHALINES AT CAMP CARIBOU
DEPTH (M)
0.00
10.00
20.00
30.00
40.00
50.00
60.00
70.00

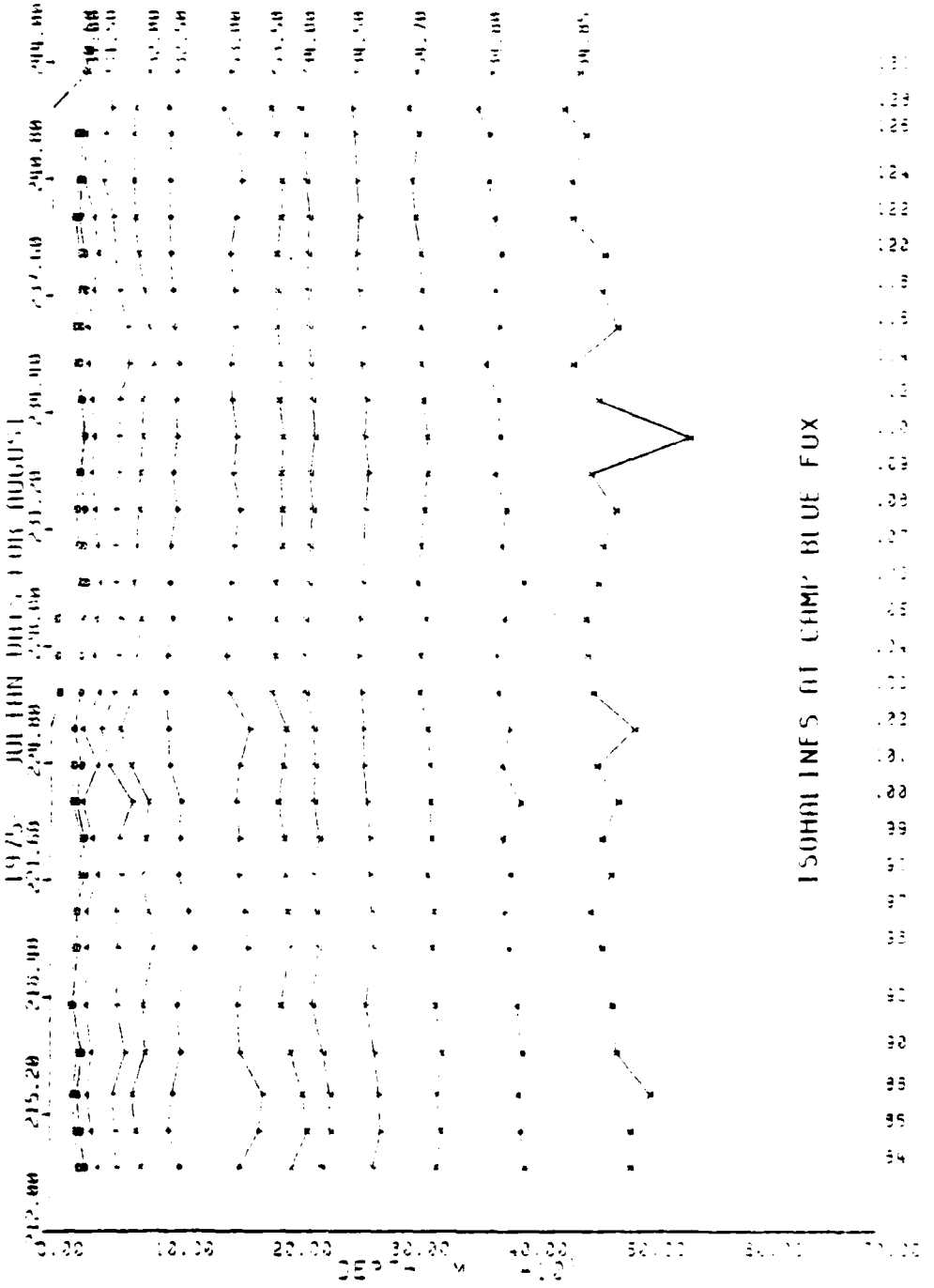

ISOHALINES AT CAMP CARIBOU
DEPTH (M)
0.00
10.00
20.00
30.00
40.00
50.00
60.00
70.00
456.00
459.20
462.40
465.60
468.80
472.00
475.20
478.40
481.60
484.80
488.00
31.50
32.00
32.50
33.00
33.50
34.00
34.50

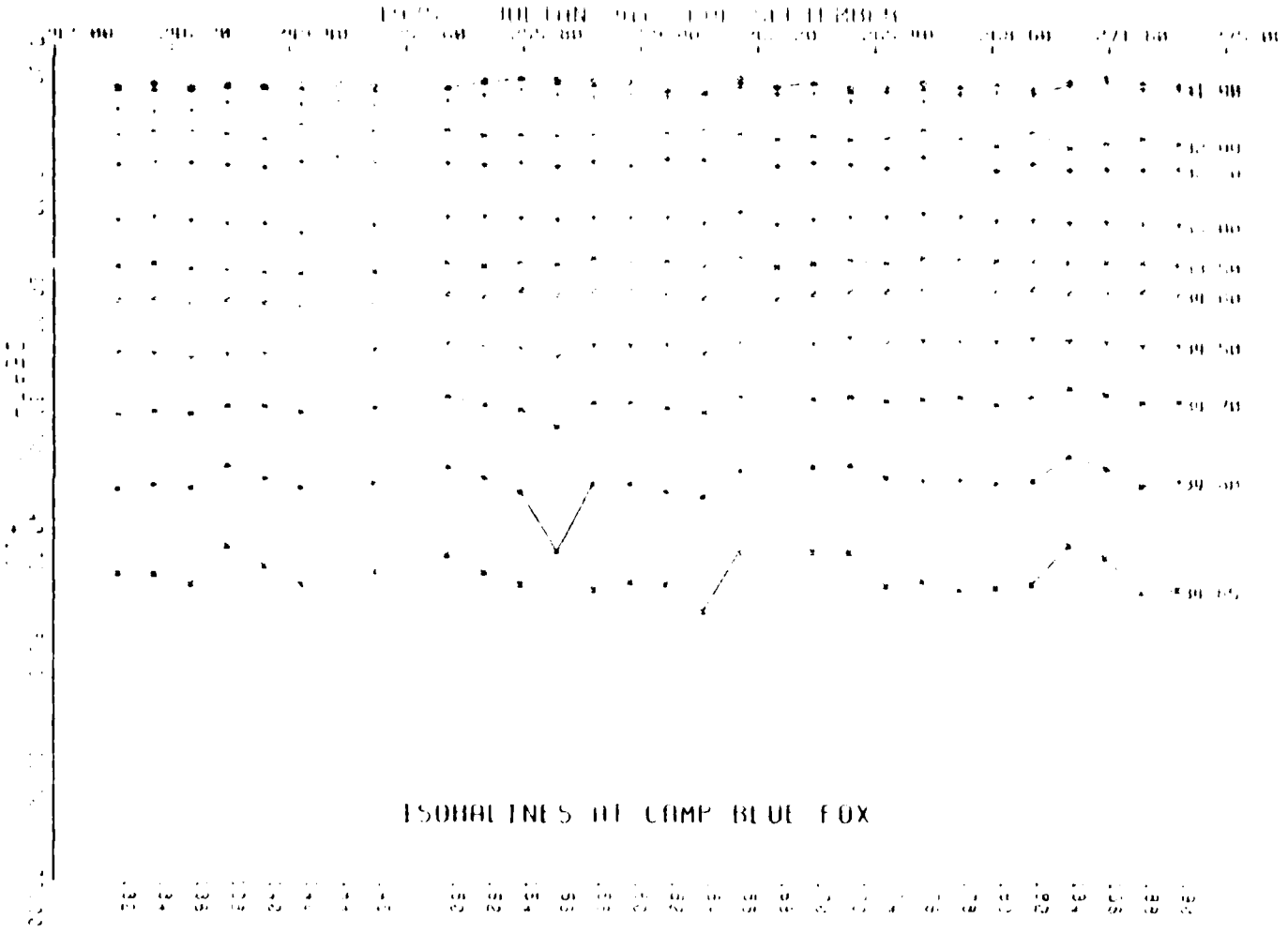


ISOHALINES AT CAMP BLUE FOX

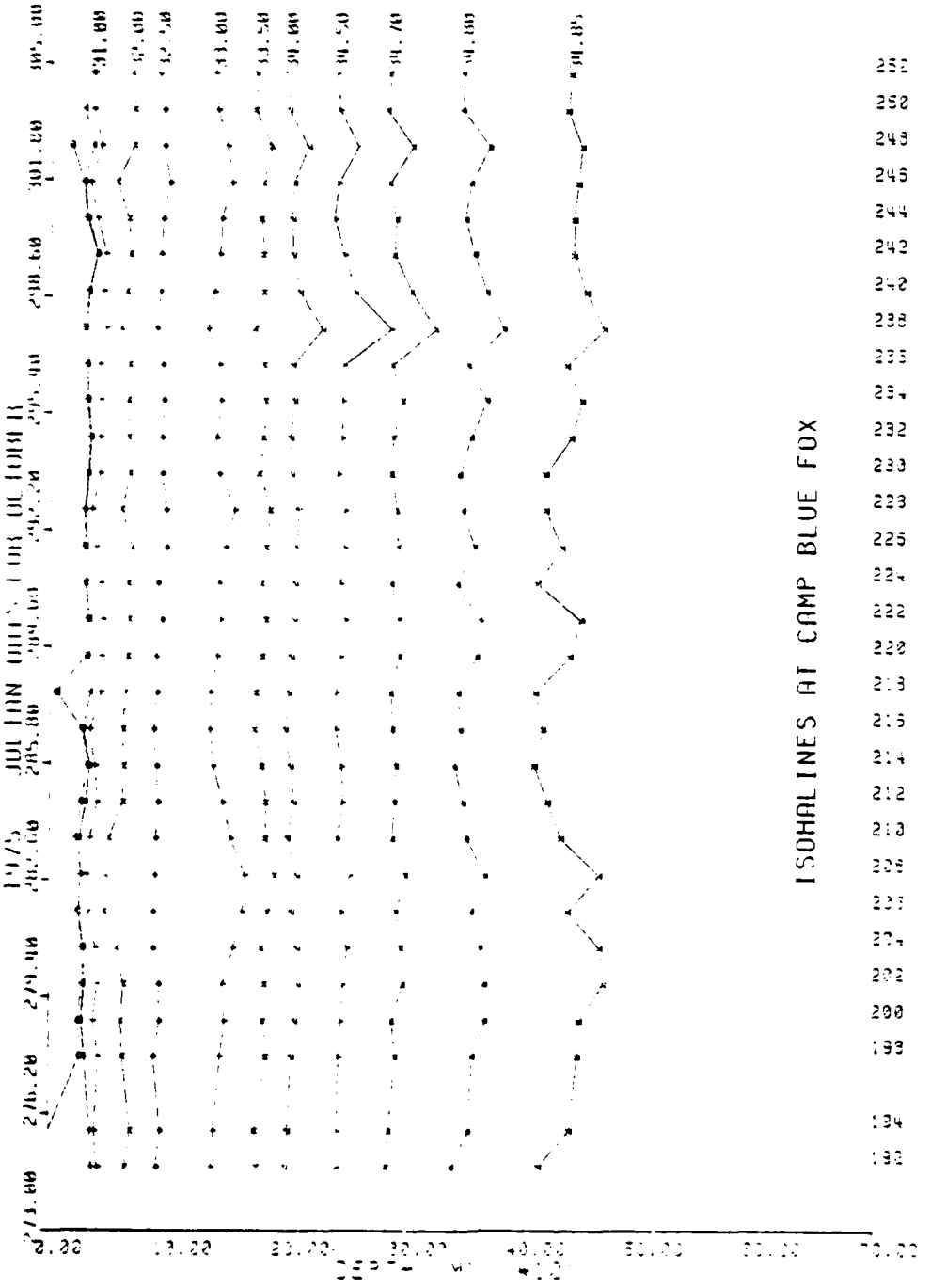

ISOHALINES AT CAMP BLUE FOX

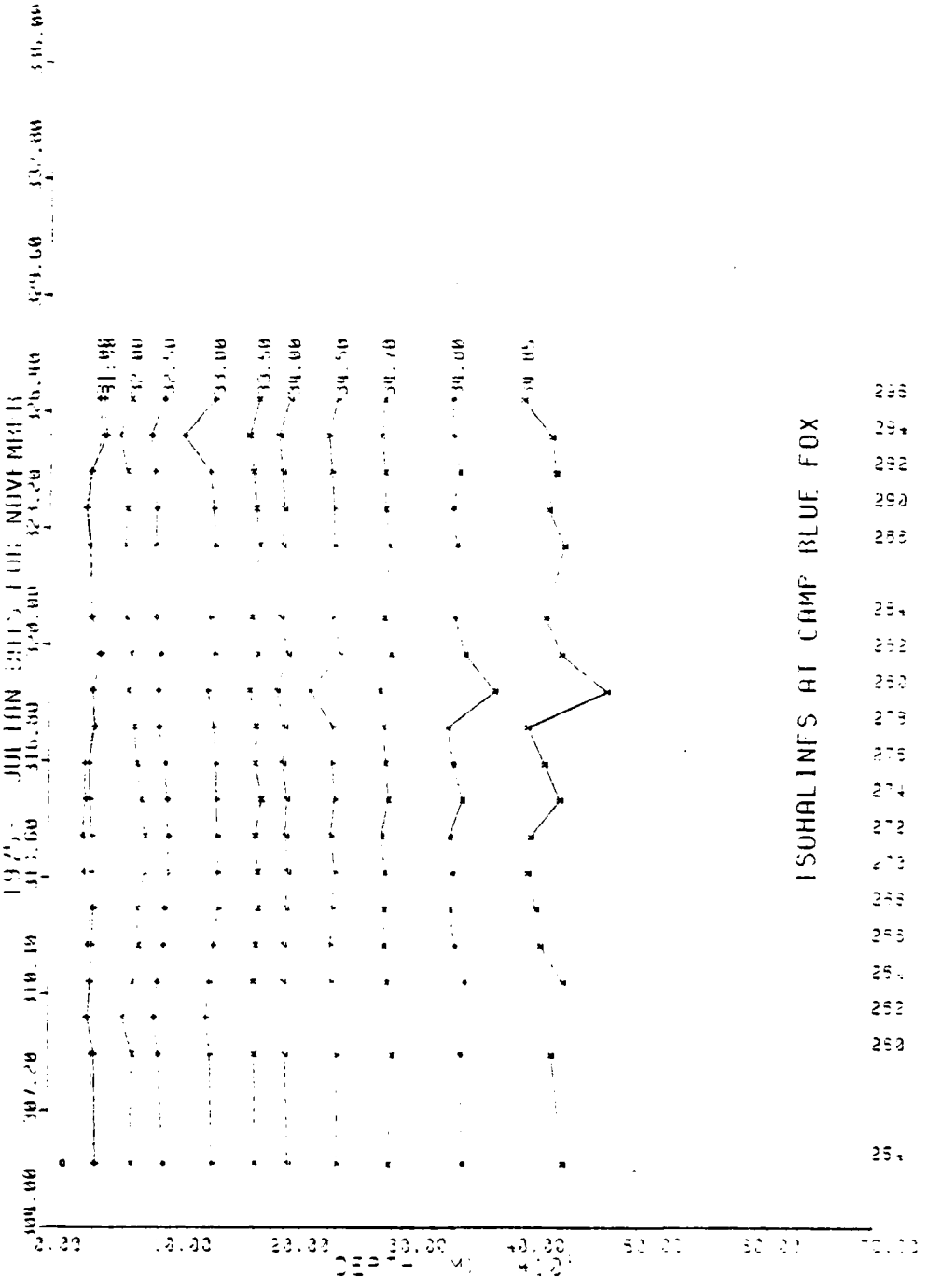

ISOHALINES AT CAMP BLUE FOX
DEPTH - M

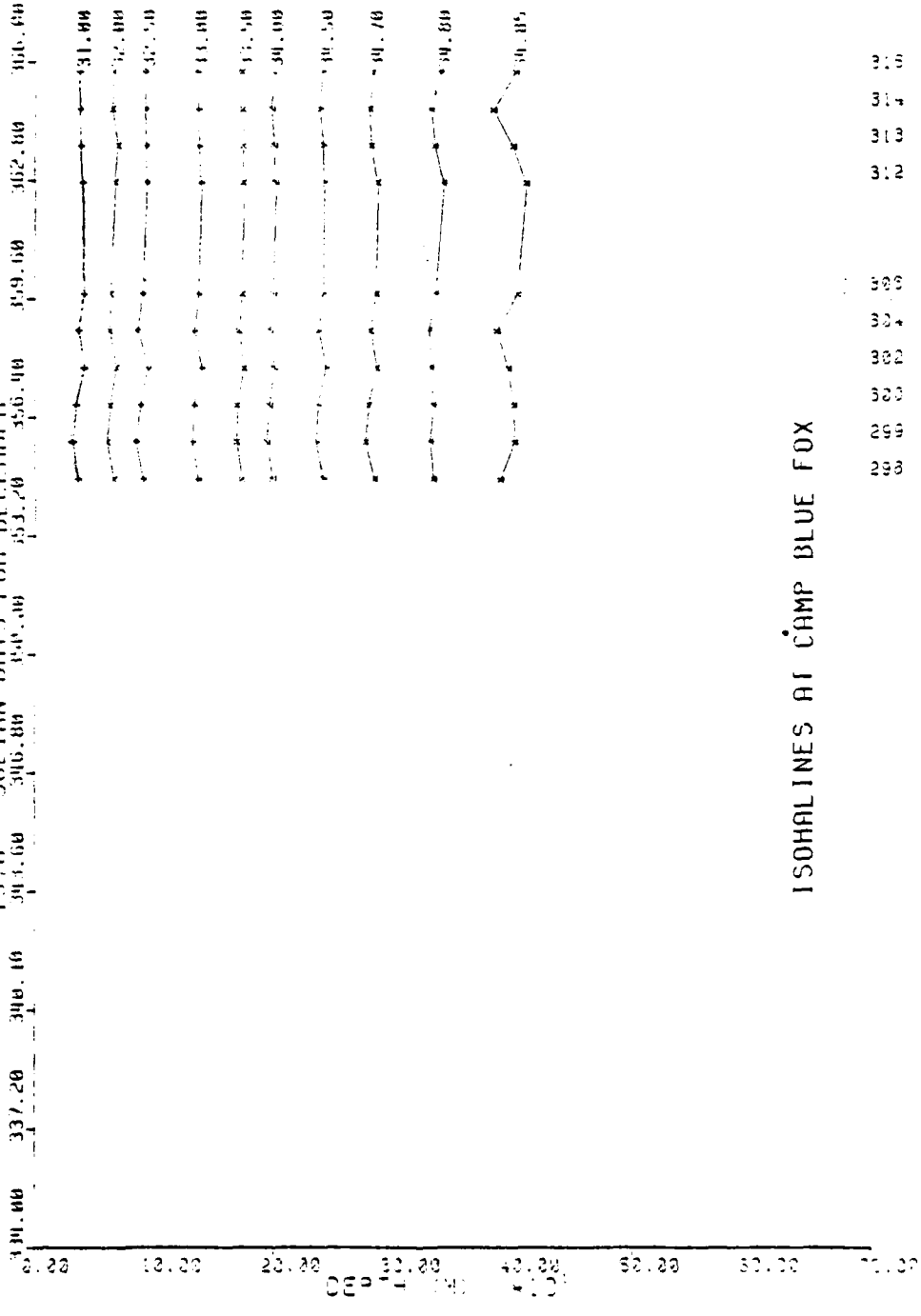

ISOHALINES OF CHMP BLUE FUX

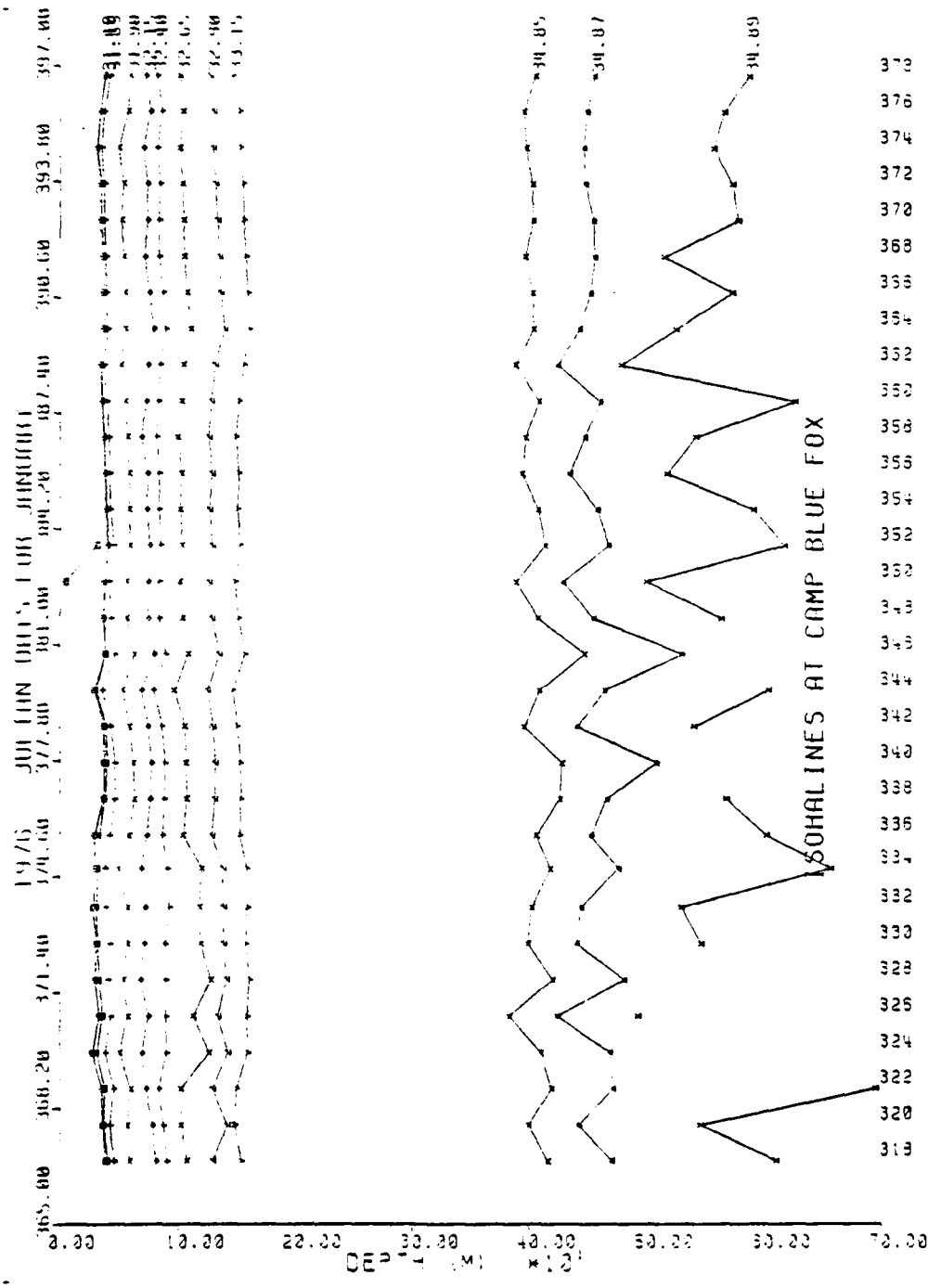


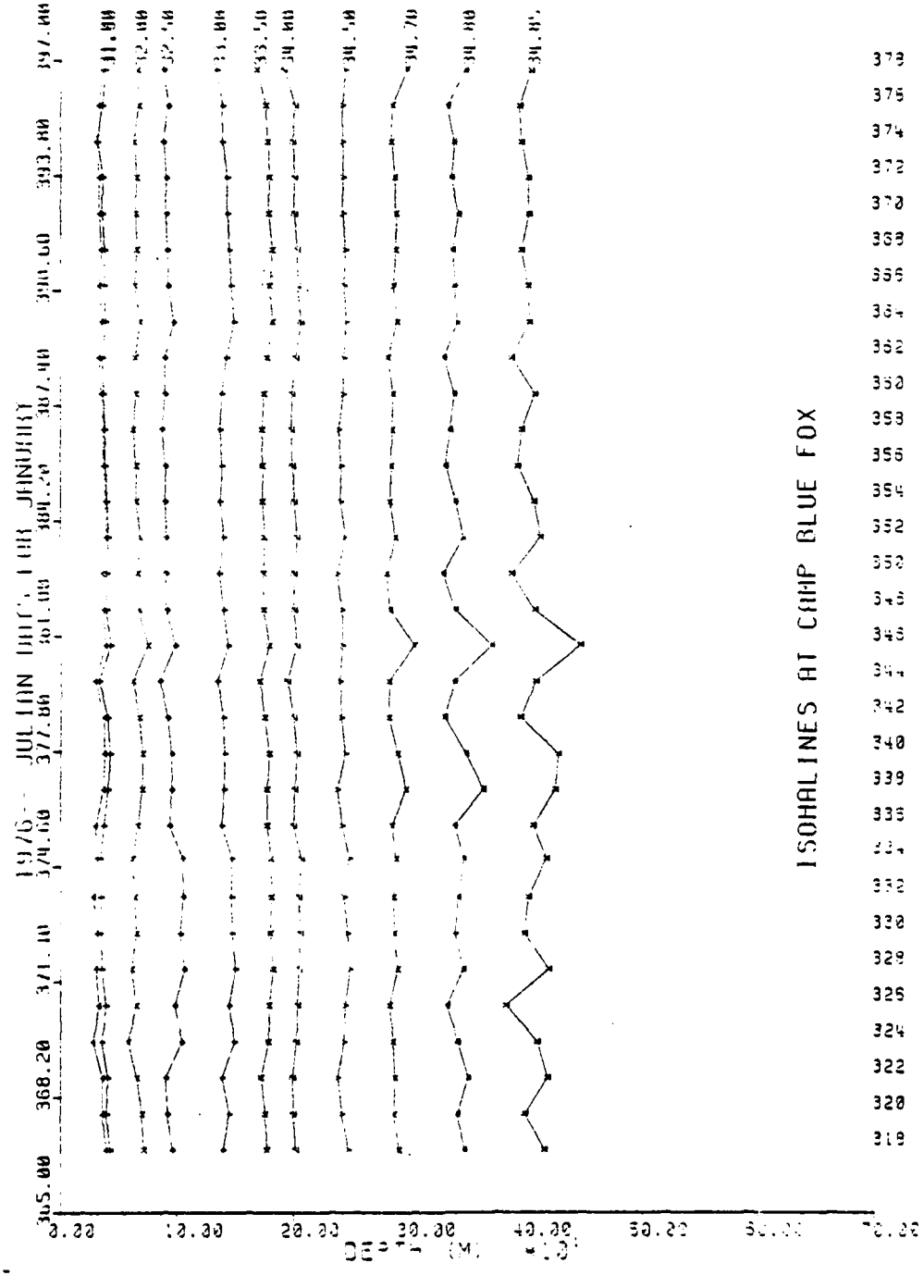
ISOBATHES AT CAMP BLUE FOX

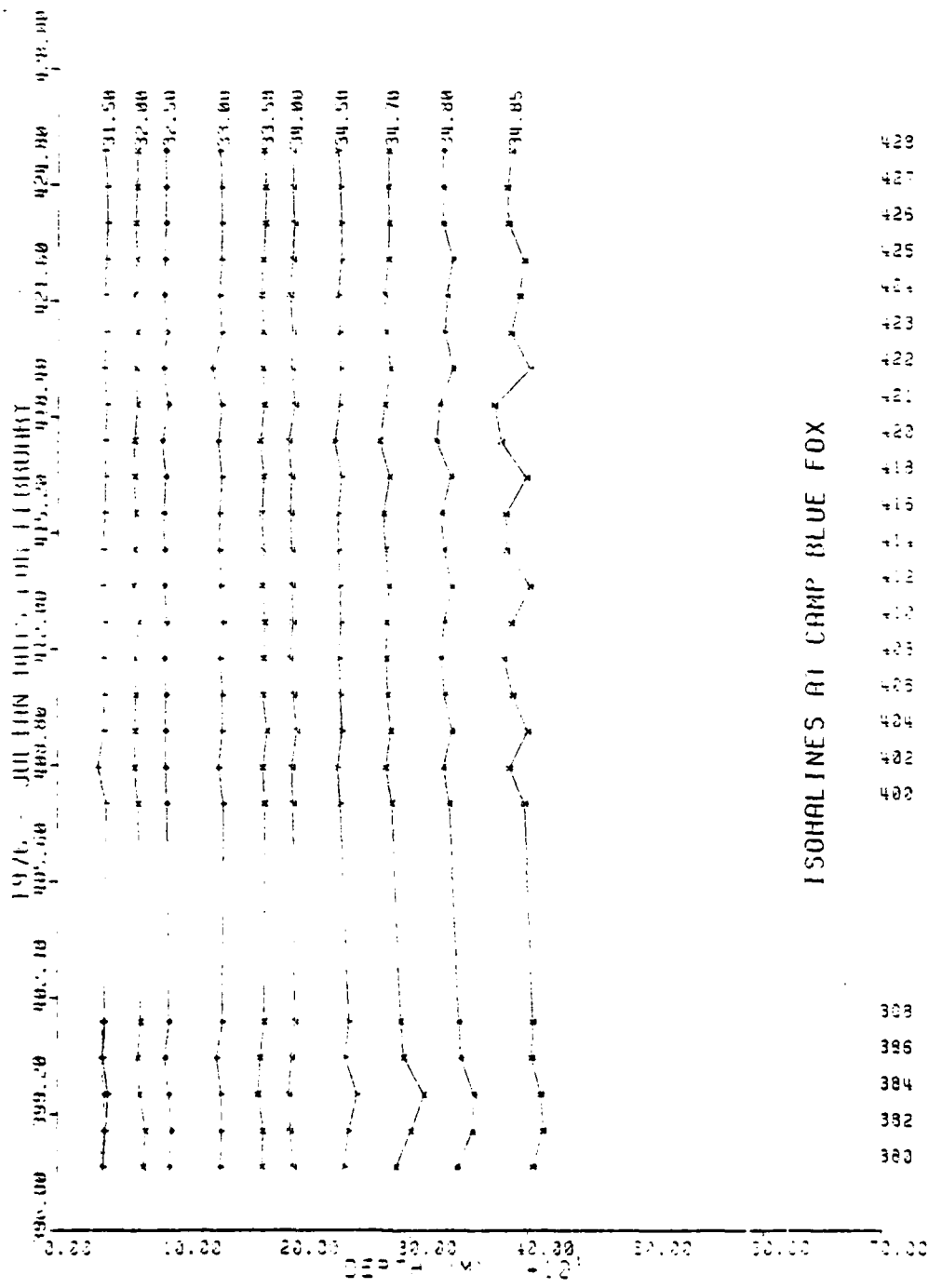

ISOHALINES AT CAMP BLUE FOX

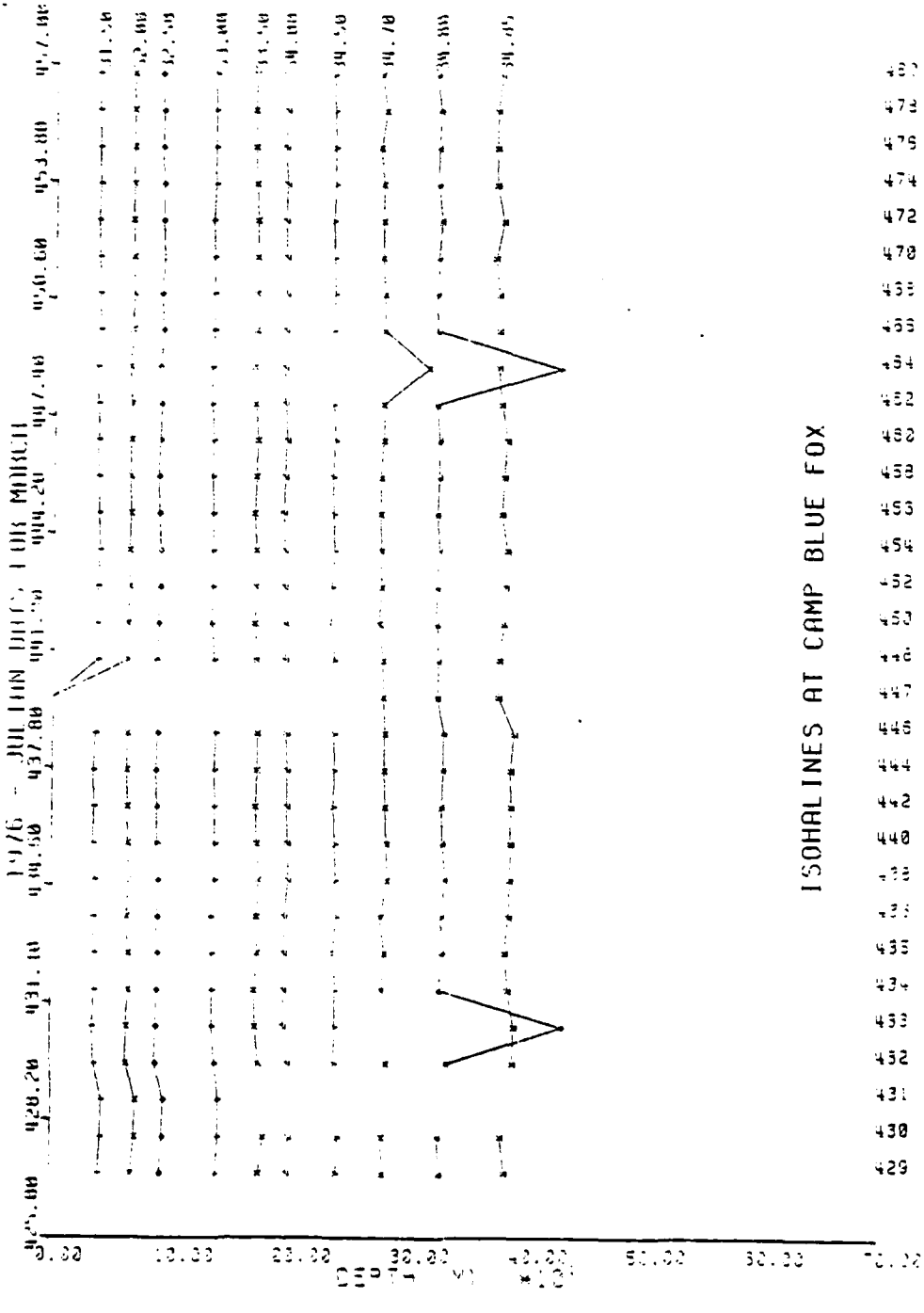

ISOHALINES AT CAMP BLUE FOX

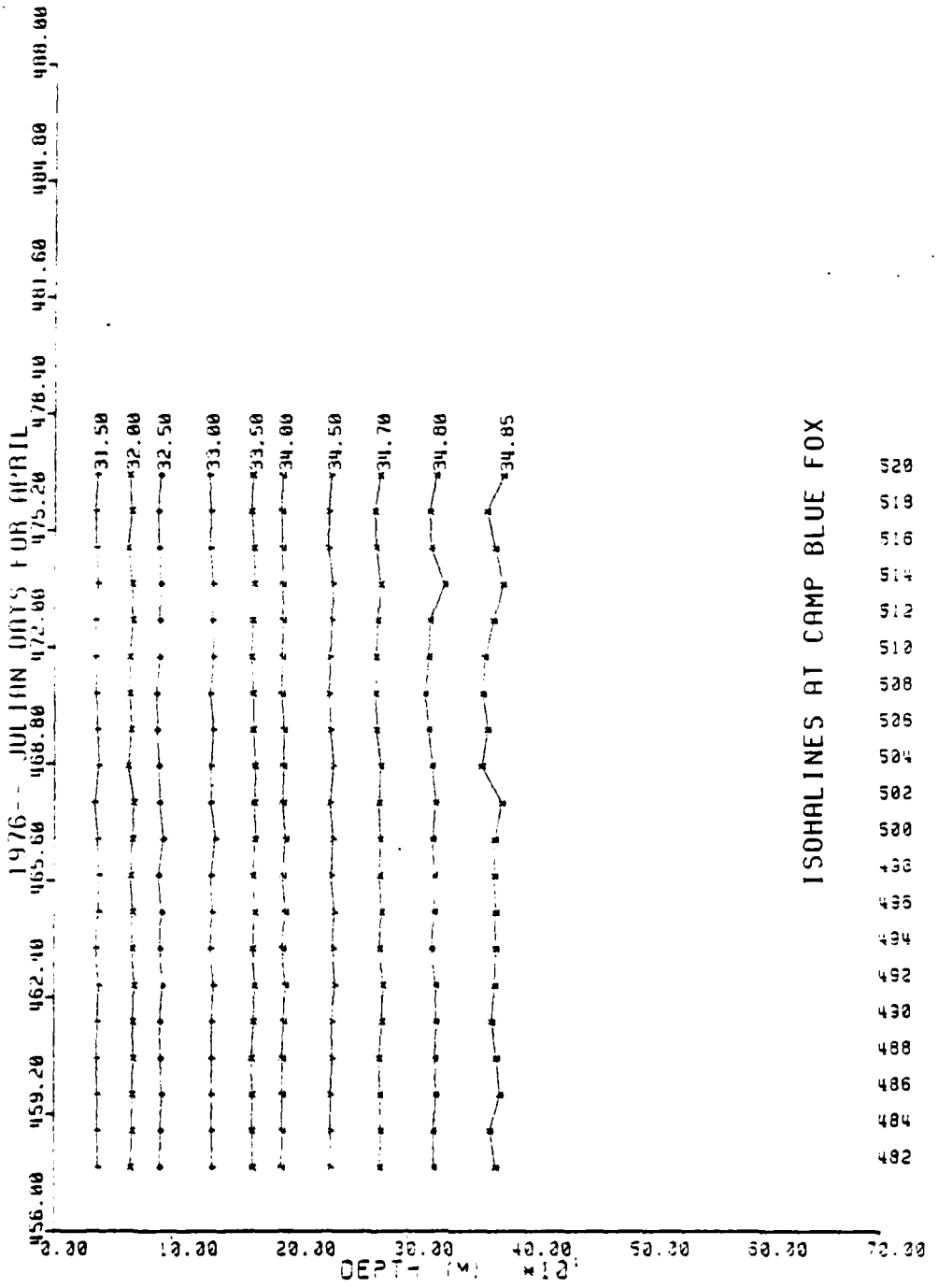

ISOHALINES AT CAMP BLUE FOX
316
314
312
310
308
306
304
302
300
298
0.00
10.00
20.00
30.00
40.00
50.00
60.00
70.00

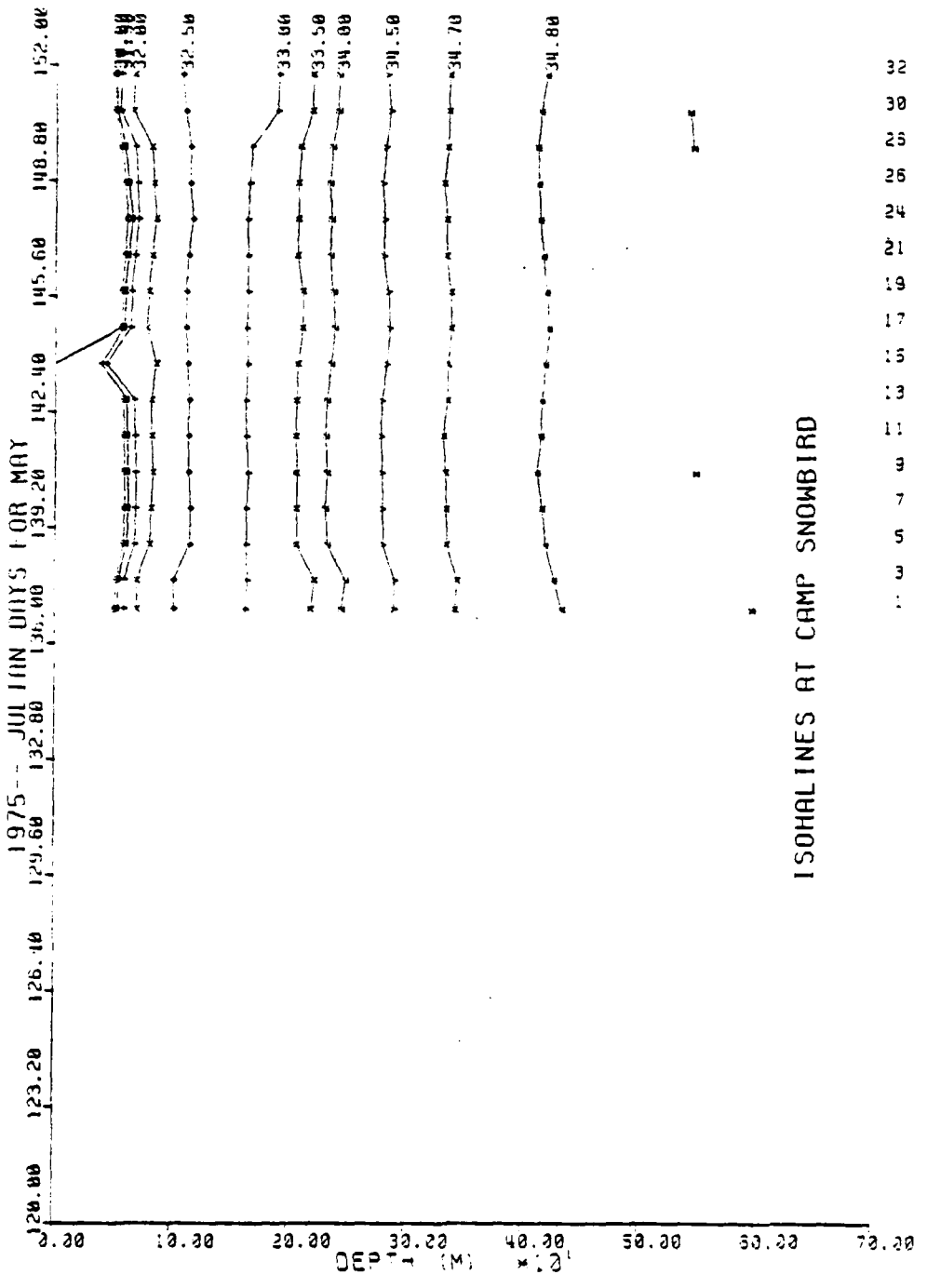

ISOHALINES AT CAMP BLUE FOX
DEPTH (M)

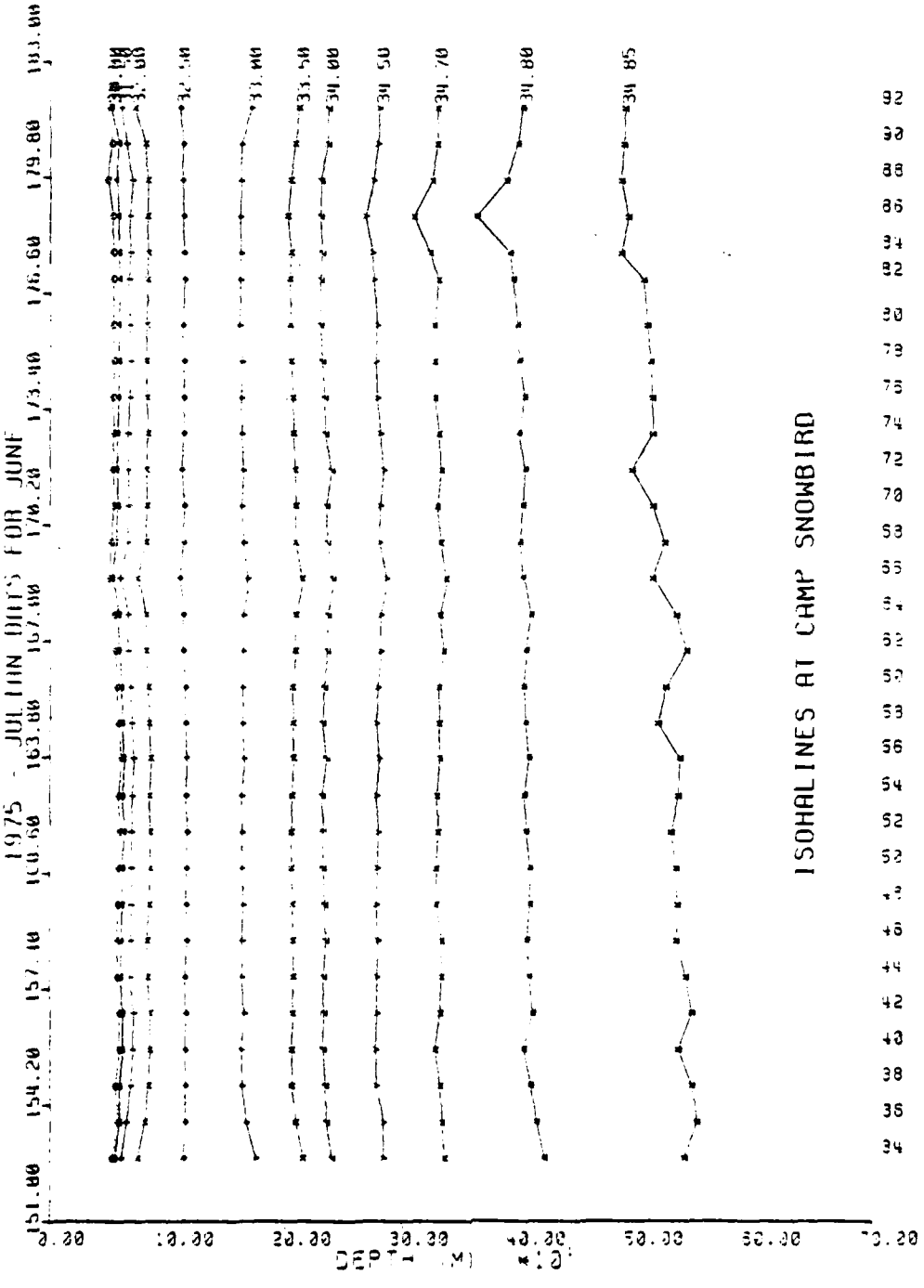

ISOHALINES AT CAMP BLUE FOX
1976 JULIAN DATE, 1 HR JANUARY
365.00
368.20
371.40
374.60
377.80
381.00
384.20
387.40
390.60
393.80
397.00
0.00
10.00
20.00
30.00
40.00
50.00
60.00
70.00
DEPTH (M)

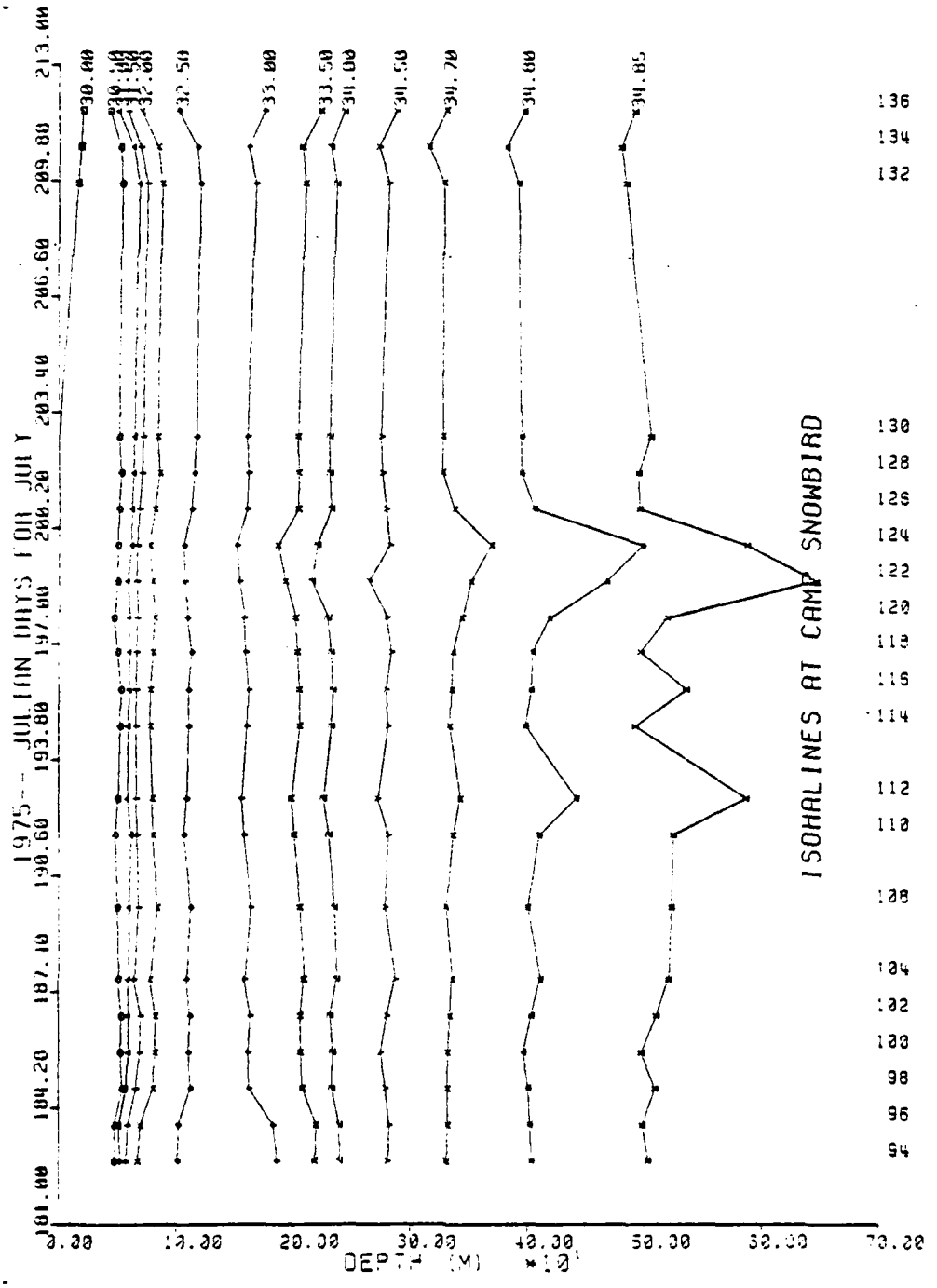

ISOHALINES AT CAMP BLUE FOX
428
427
426
425
424
423
422
421
420
418
416
414
412
410
408
406
404
402
400
398
396
394
392
390
0.00
10.00
20.00
30.00
40.00
50.00
60.00
70.00

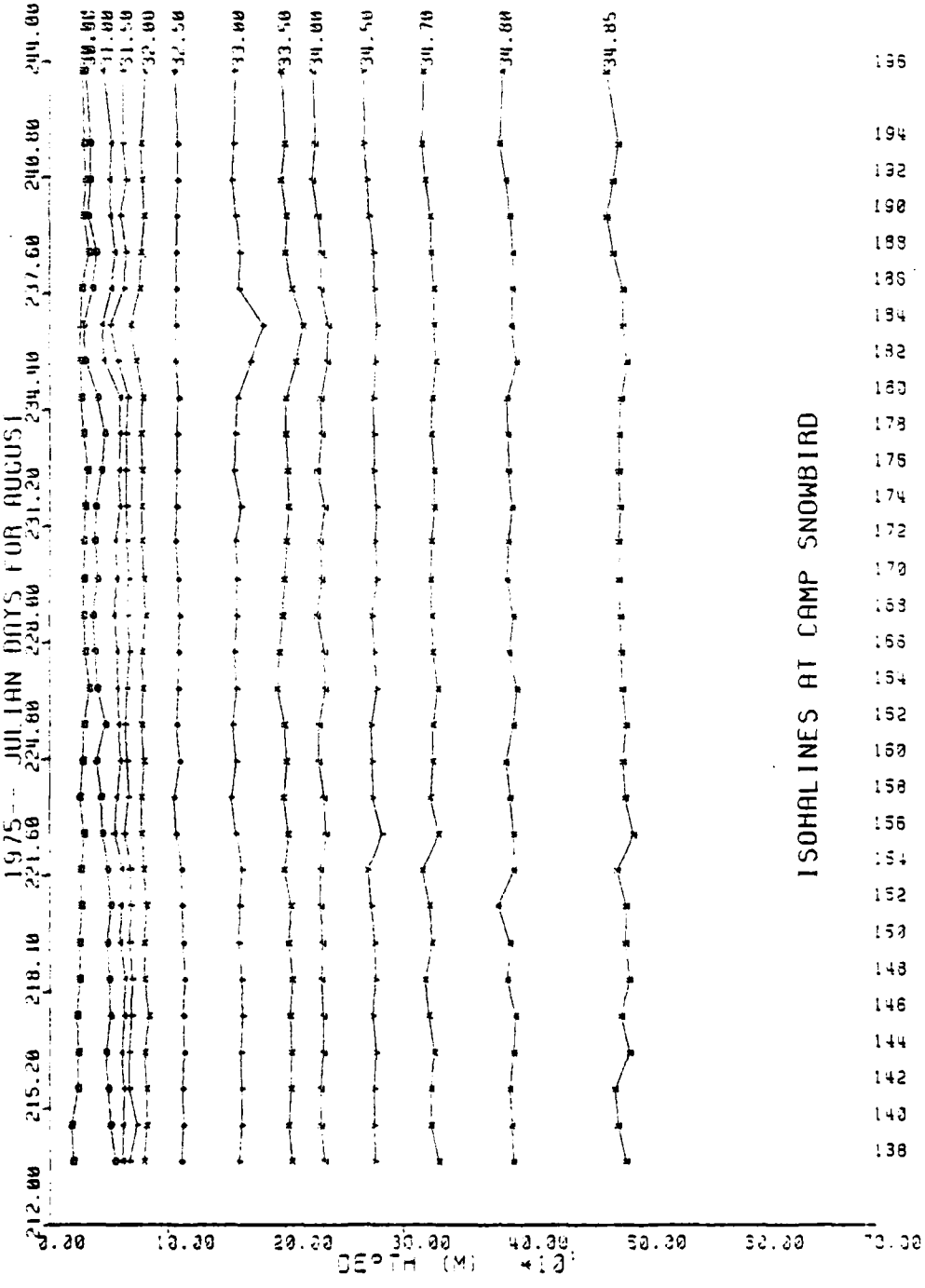

ISOHALINES AT CAMP BLUE FOX
0.00
10.00
20.00
30.00
40.00
50.00
60.00
70.00
DEPTH (M)
473
475
474
472
470
468
466
464
462
460
458
456
454
452
450
448
447
446
444
442
440
438
436
434
433
432
431
430
429

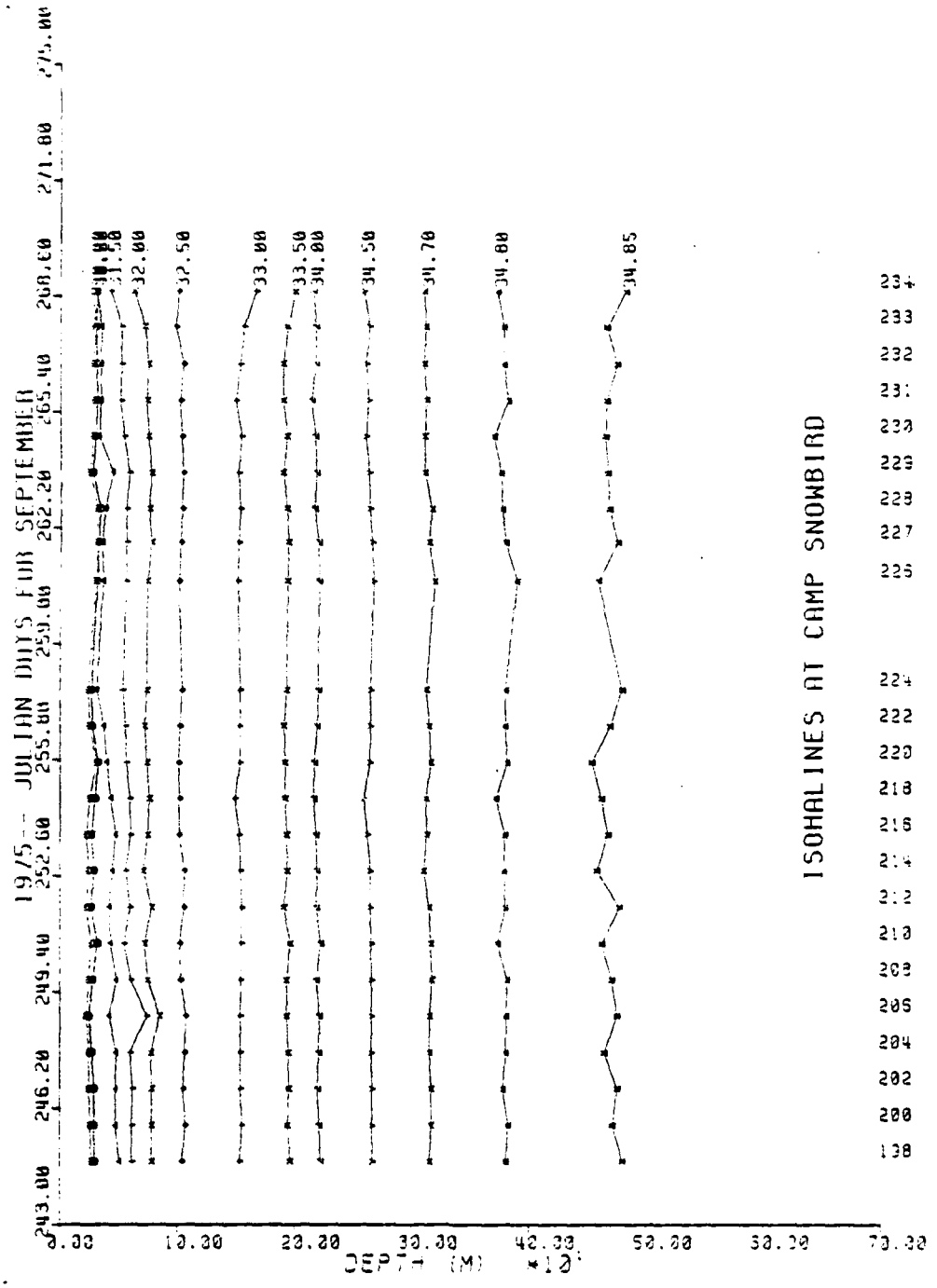

ISOHALINES AT CAMP BLUE FOX
1976- JULIAN DAYS FOR APRIL
456.00 459.20 462.40 465.60 468.80 472.00 475.20 478.40 481.60 484.00 488.00
31.50
32.00
32.50
33.00
33.50
34.00
34.50
34.70
34.80
34.85
520 518 516 514 512 510 508 506 504 502 500 498 496 494 492 490 488 486 484 482
2.00 10.00 20.00 30.00 40.00 50.00 60.00 70.00
DEPTH (M) x10²

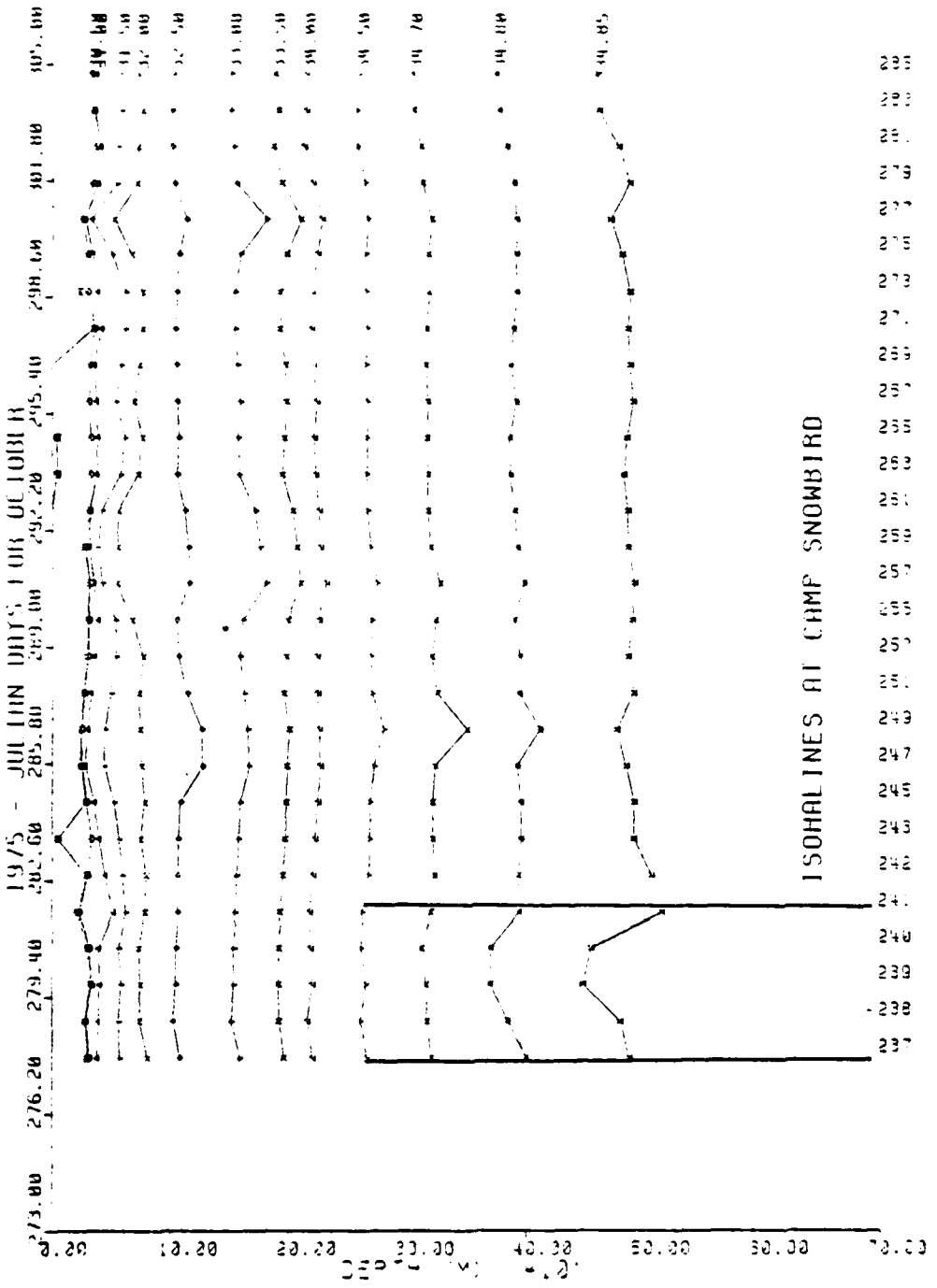

ISOHALINES AT CAMP SNOWBIRD
1975 - JULIAN DAYS FOR MAY
120.00
123.20
126.40
129.60
132.80
136.00
139.20
142.40
145.60
148.80
152.00
32.50
33.00
33.50
34.00
34.50
34.70
34.80
32
30
28
26
24
22
19
17
15
13
11
9
7
5
3
1
0.00
10.00
20.00
30.00
40.00
50.00
60.00
70.00
DEPTH (M) x10¹

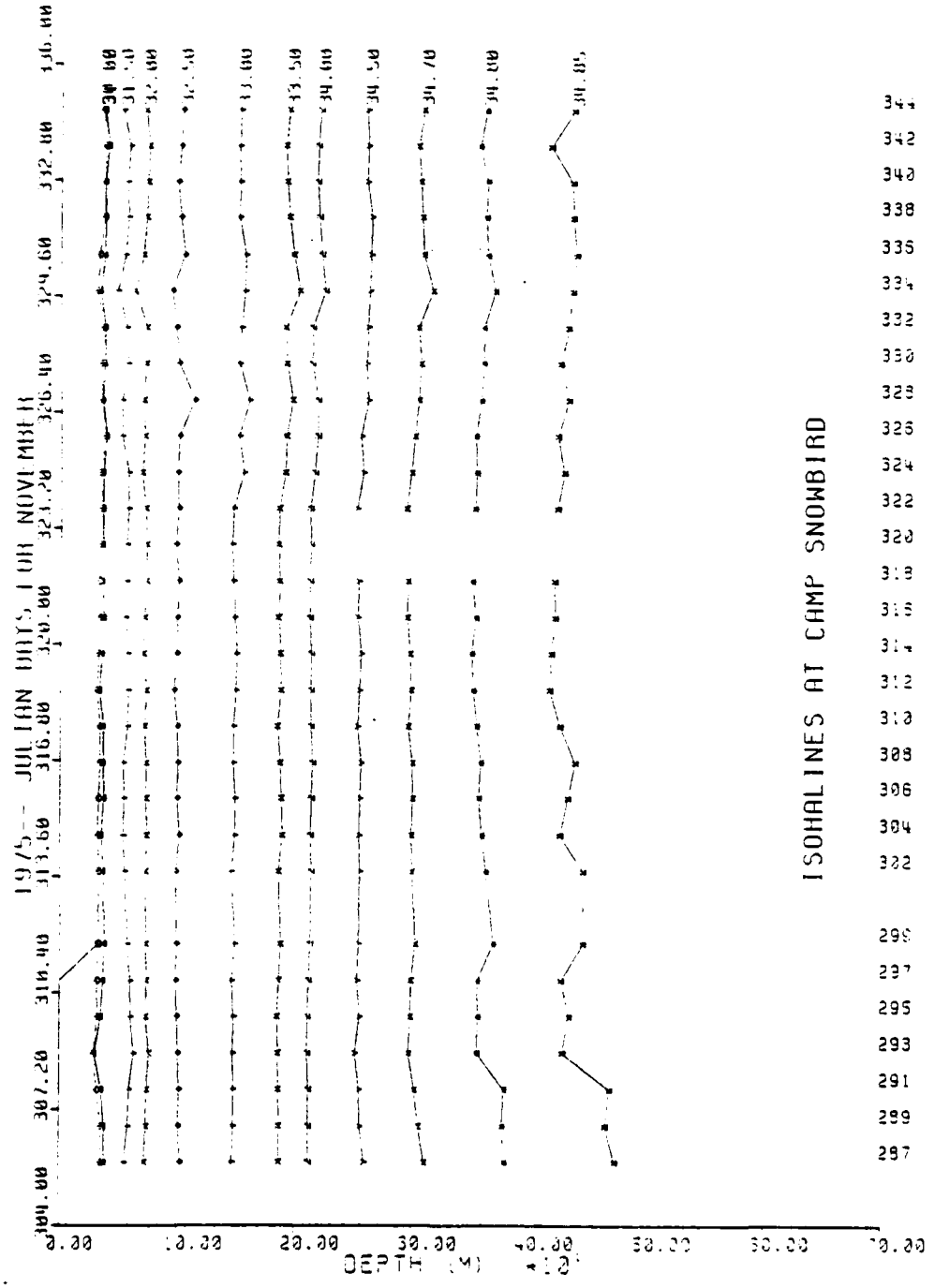

ISOHALINES AT CAMP SNOWBIRD
1975 - JULIAN DATES FOR JUNE
151.00
154.20
157.40
160.60
163.80
167.00
170.20
173.40
176.60
179.80
183.00
92
90
88
86
84
82
80
78
76
74
72
70
68
66
64
62
60
58
56
54
52
50
48
46
44
42
40
38
36
34
31.00
31.50
31.80
32.00
32.50
33.50
34.00
34.50
34.70
34.80
34.85
0.00
10.00
20.00
30.00
40.00
50.00
60.00
70.20
DEPTH (M)

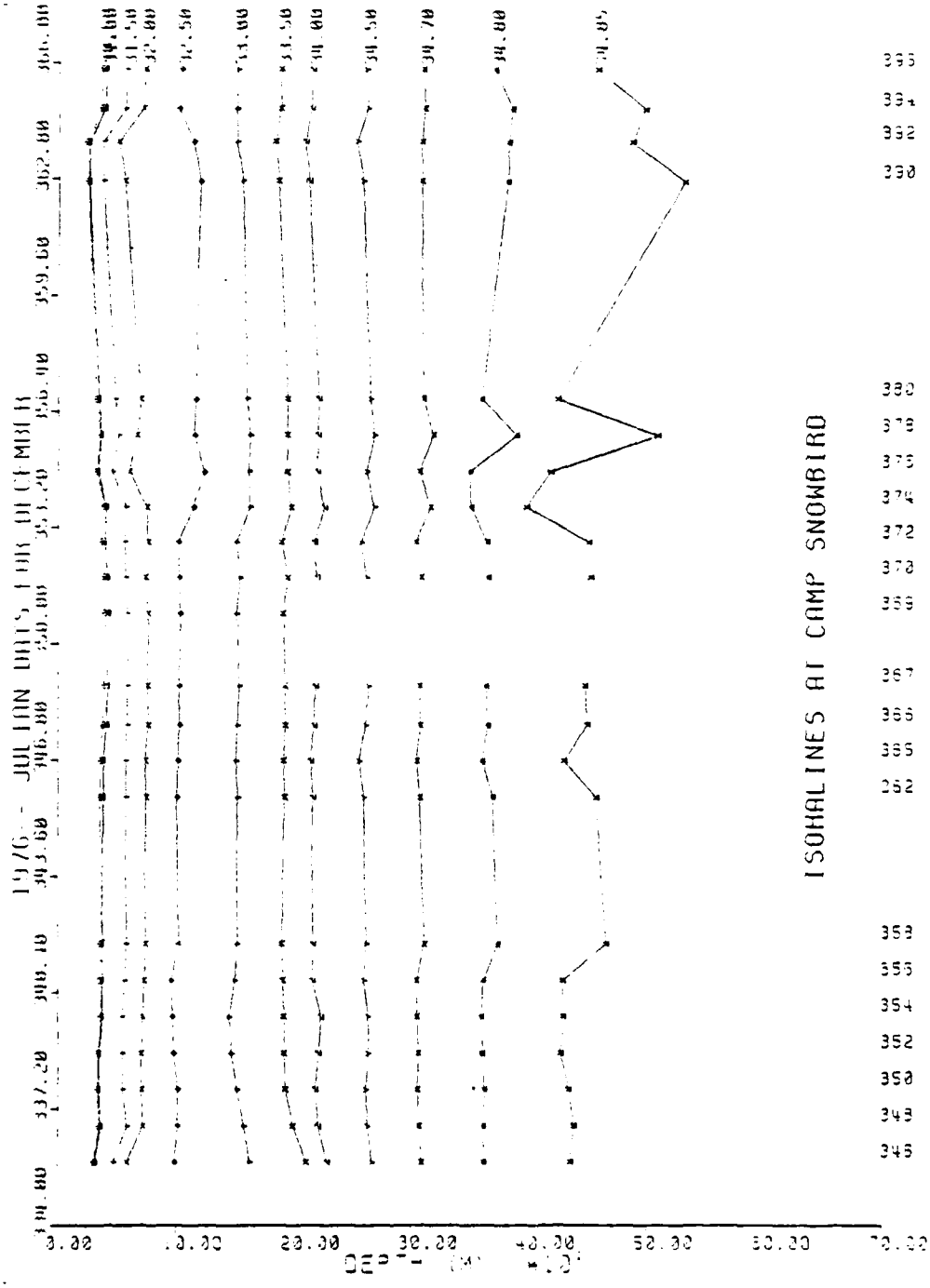

ISOHALINES AT CAMP SNOWBIRD
1975 -- JULIAN DAYS FOR JULY
181.00
184.20
187.40
190.60
193.80
197.00
200.20
203.40
206.60
209.80
213.00
0.00
10.00
20.00
30.00
40.00
50.00
60.00
70.00
DEPTH (M) *10¹
136
134
132
130
128
126
124
122
120
118
116
114
112
110
108
104
102
100
98
96
94

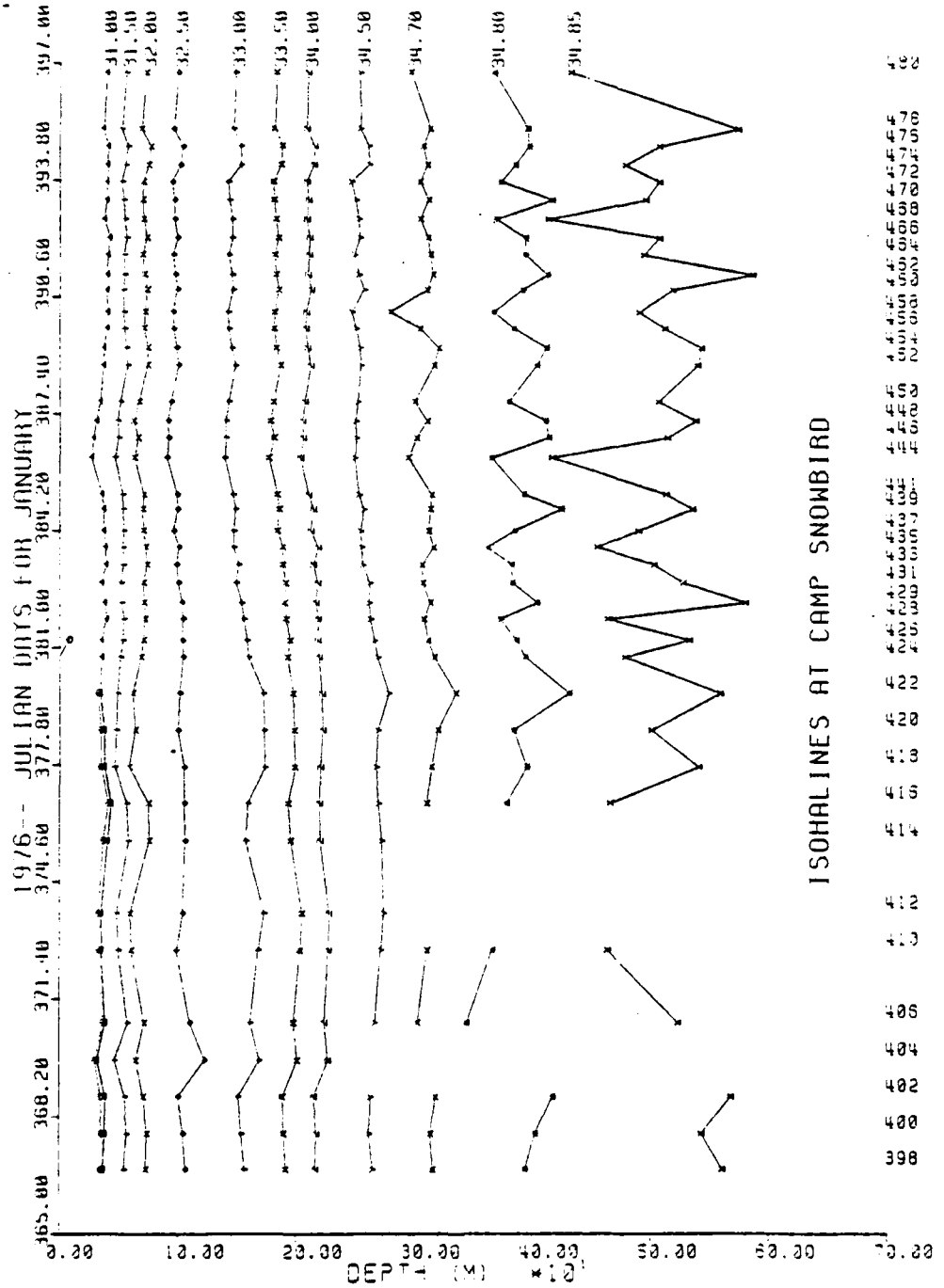

ISOHALINES AT CAMP SNOWBIRD
1975 - JULIAN DAYS FOR AUGUST
DEPTH (M) *10
0.00
10.00
20.00
30.00
40.00
50.00
60.00
70.00
212.00
215.20
218.40
221.60
224.80
228.00
231.20
234.40
237.60
240.80
244.00
138
140
142
144
146
148
150
152
154
156
158
160
162
164
166
168
170
172
174
176
178
180
182
184
186
188
190
192
194
196
30.85
30.70
30.60
30.50
31.00
31.50
32.00
32.50
33.00
33.50
34.00
34.50

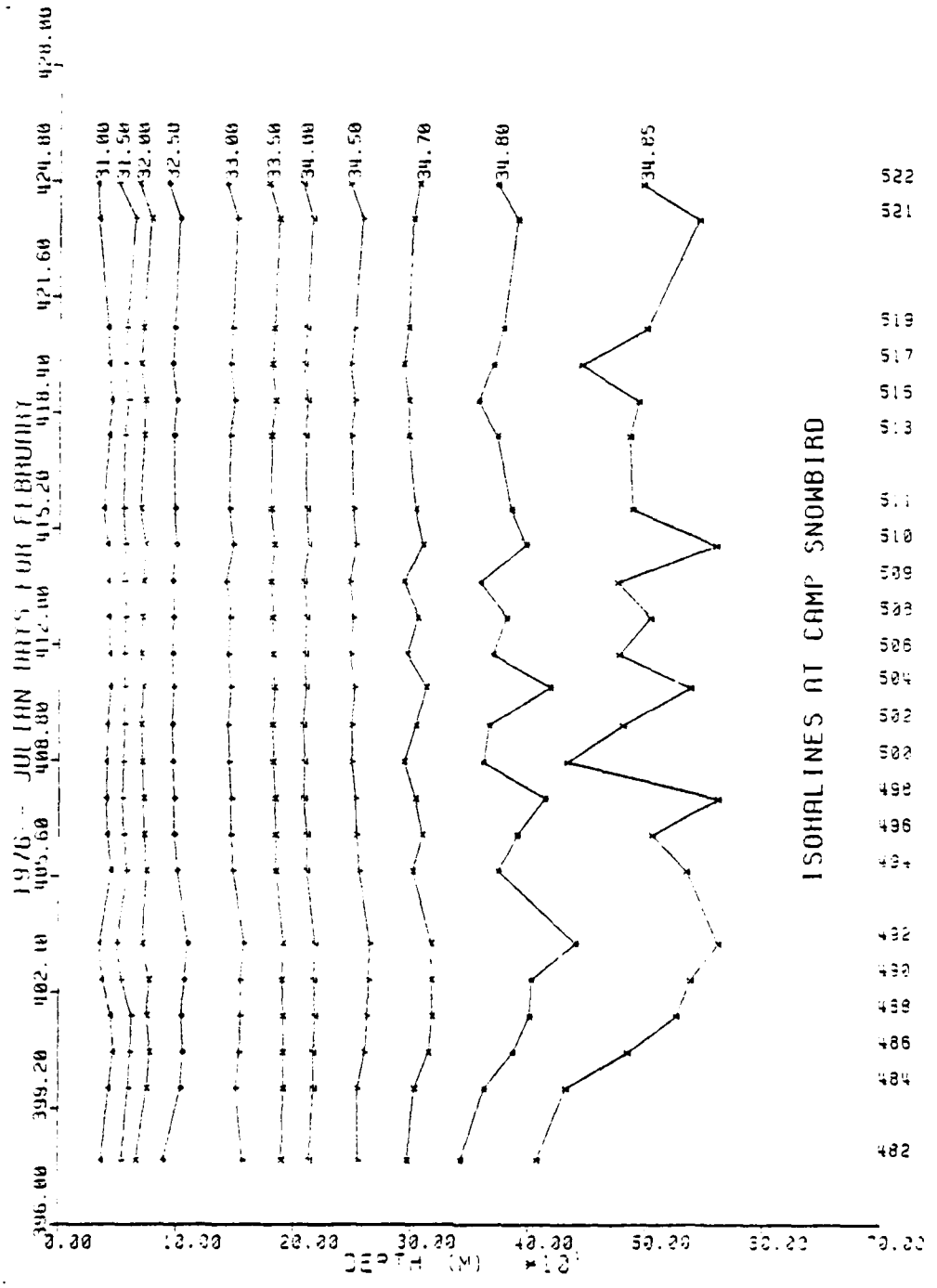

1975 - JULIAN DAYS FOR SEPTEMBER
243.00
246.20
249.40
252.60
255.80
259.00
262.20
265.40
268.60
271.80
ISOHALINES AT CAMP SNOWBIRD
DEPTH (M) *10
0.00
10.00
20.00
30.00
40.00
50.00
60.00
70.00
32.00
32.50
33.00
33.50
34.00
34.50
34.70
34.80
34.85

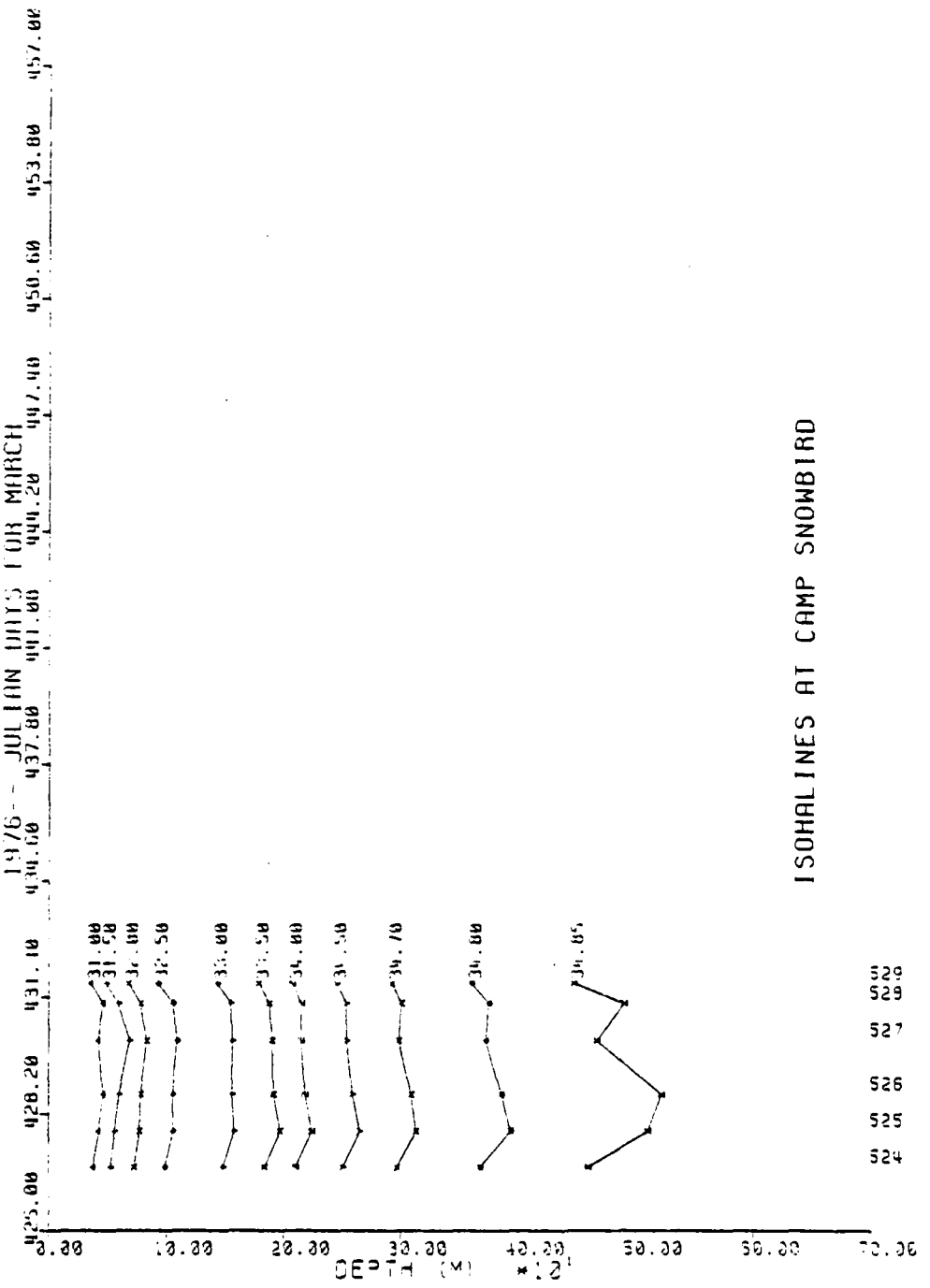

ISOHALINES AT CAMP SNOWBIRD
0.00
10.00
20.00
30.00
40.00
50.00
60.00
70.00


ISOHALINES AT CAMP SNOWBIRD
DEPTH (M) *10
0.00
10.00
20.00
30.00
40.00
50.00
60.00
70.00

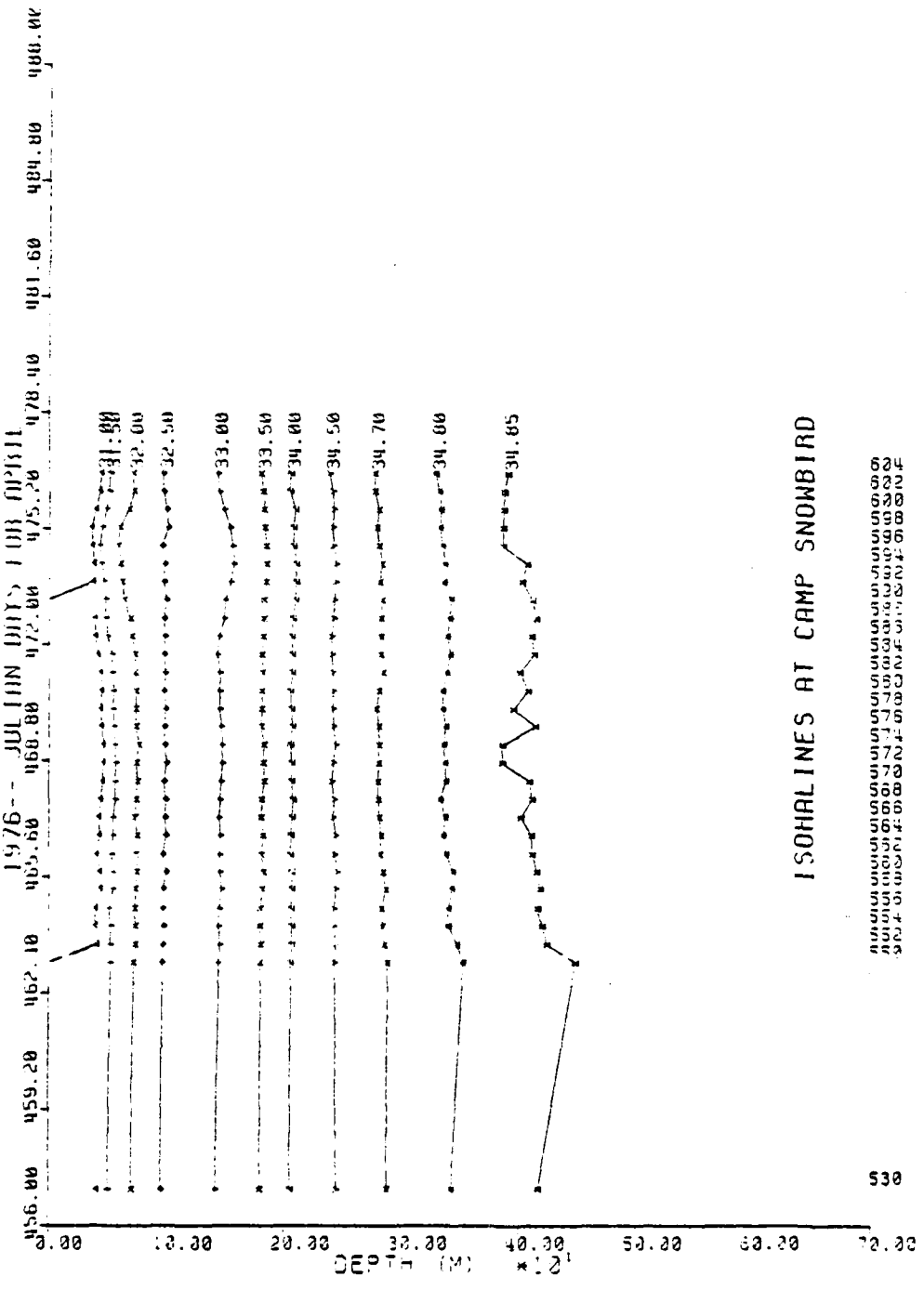

ISOHALINES AT CAMP SNOWBIRD
DEPTH (M)
0.00
10.00
20.00
30.00
40.00
50.00
60.00
70.00

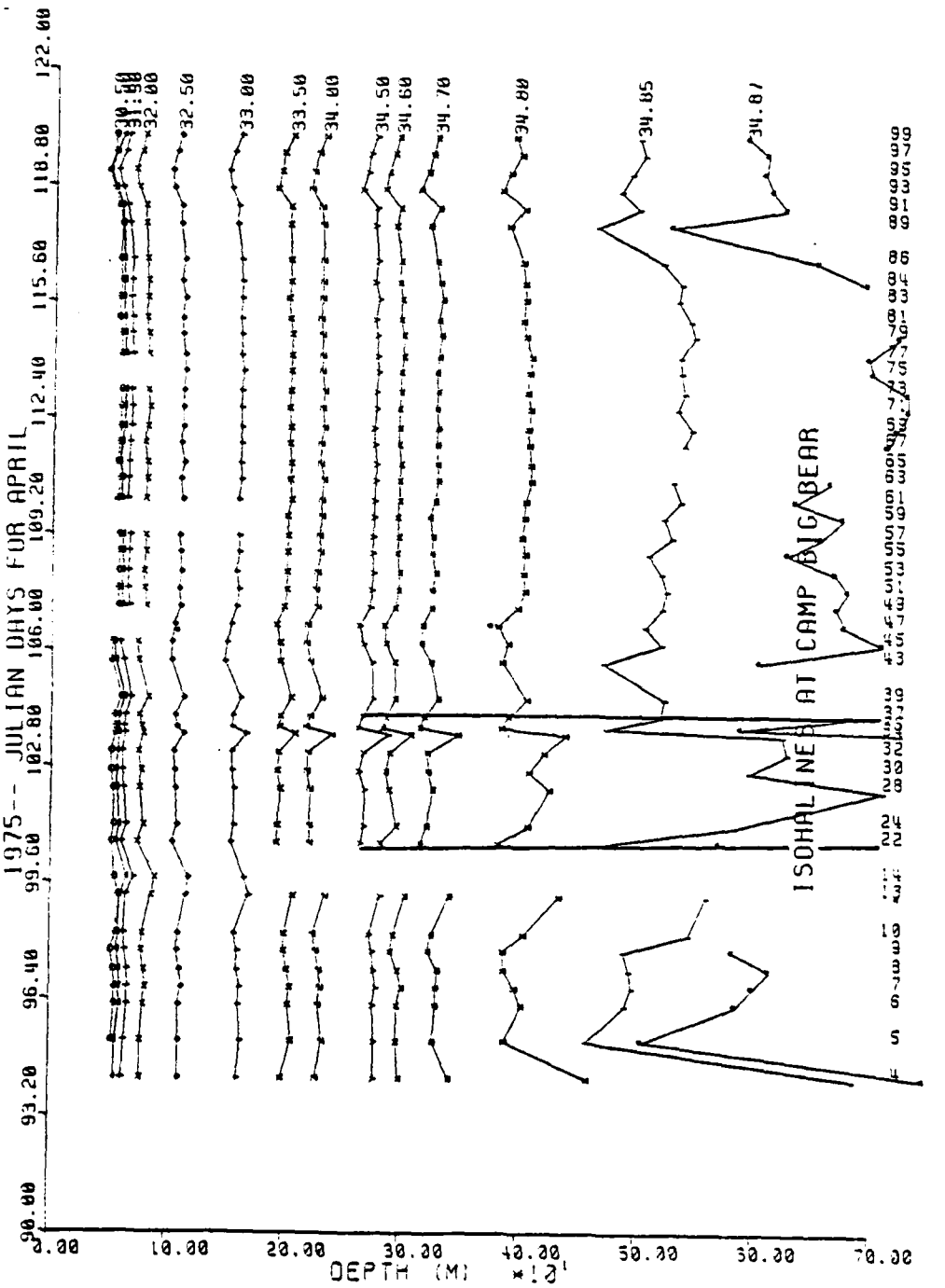

1976 - JULIAN DAYS FOR JANUARY
365.00
368.20
371.40
374.60
377.80
381.00
384.20
387.40
390.60
393.80
397.00
ISOHALINES AT CAMP SNOWBIRD
DEPTH (M) *10
0.00
10.00
20.00
30.00
40.00
50.00
60.00
70.00
398
400
402
404
406
414
416
418
420
422
*31.00
*31.50
*32.00
*32.50
*33.00
*33.50
*34.00
*34.50
*34.70
*34.80
*34.85

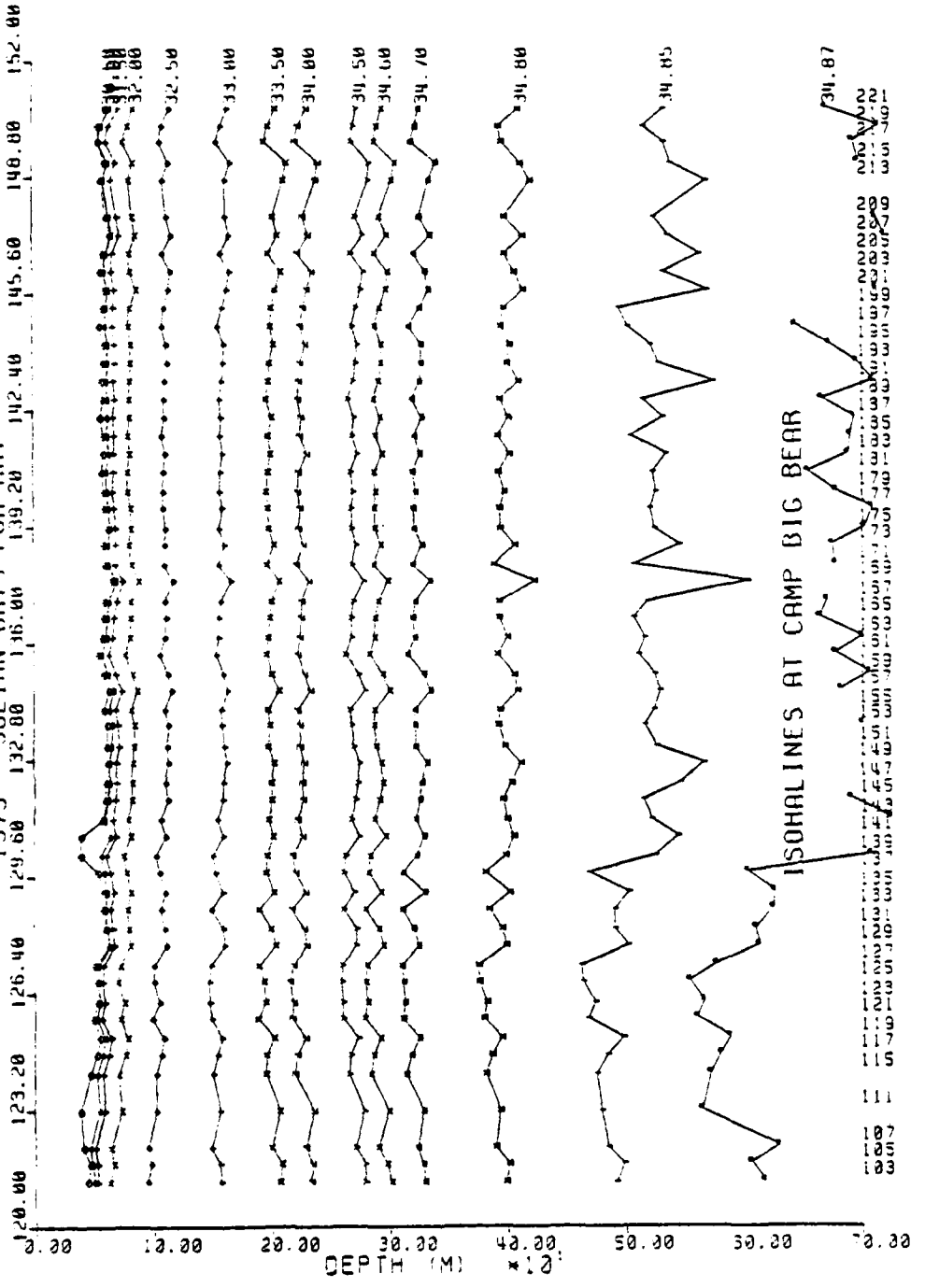

ISOHALINES AT CAMP SNOWBIRD
DEPTH (M)
0.00
10.00
20.00
30.00
40.00
50.00
60.00
70.00
31.00
31.50
32.00
32.50
33.00
33.50
34.00
34.50
34.70
34.80
34.85

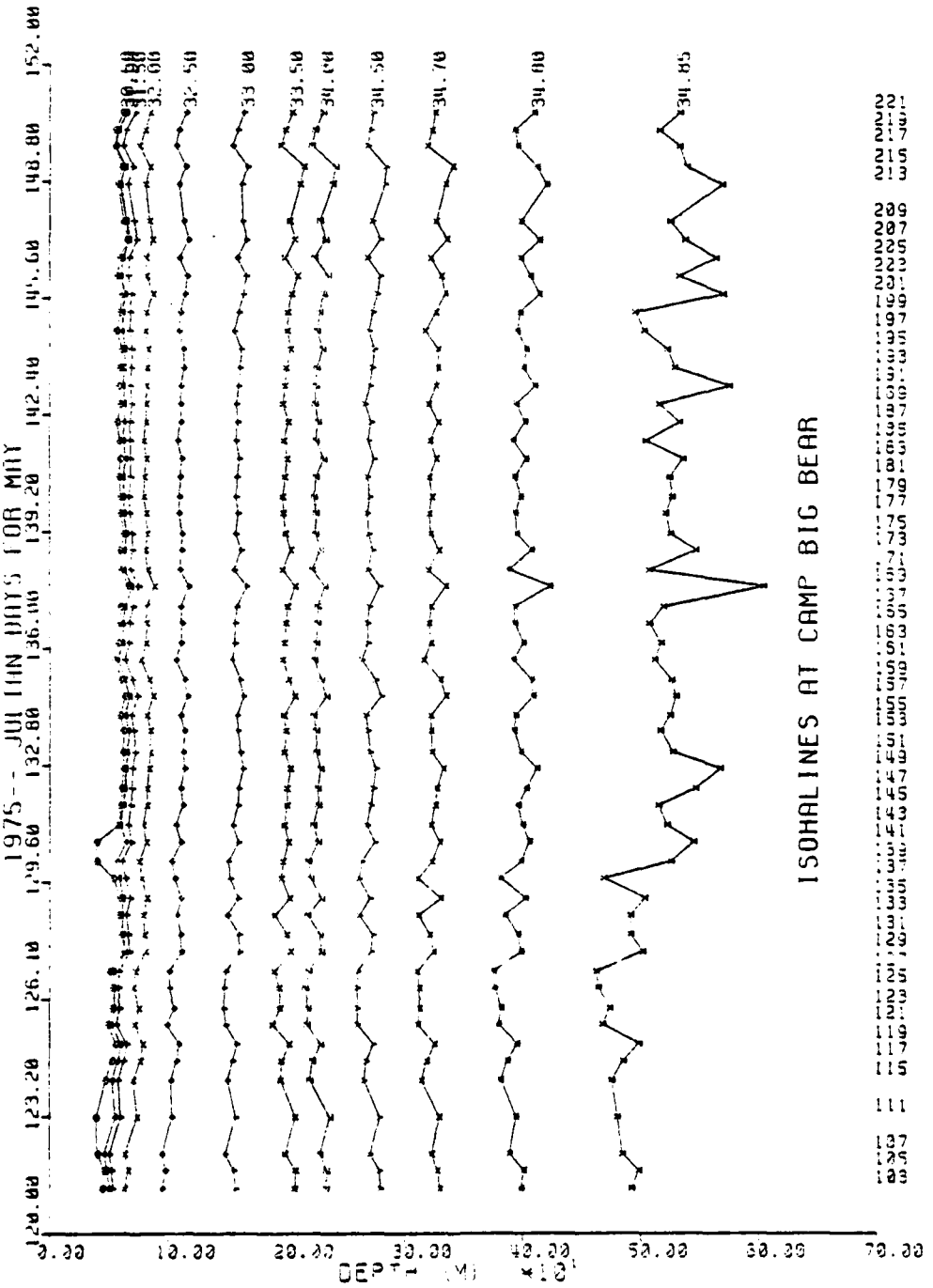


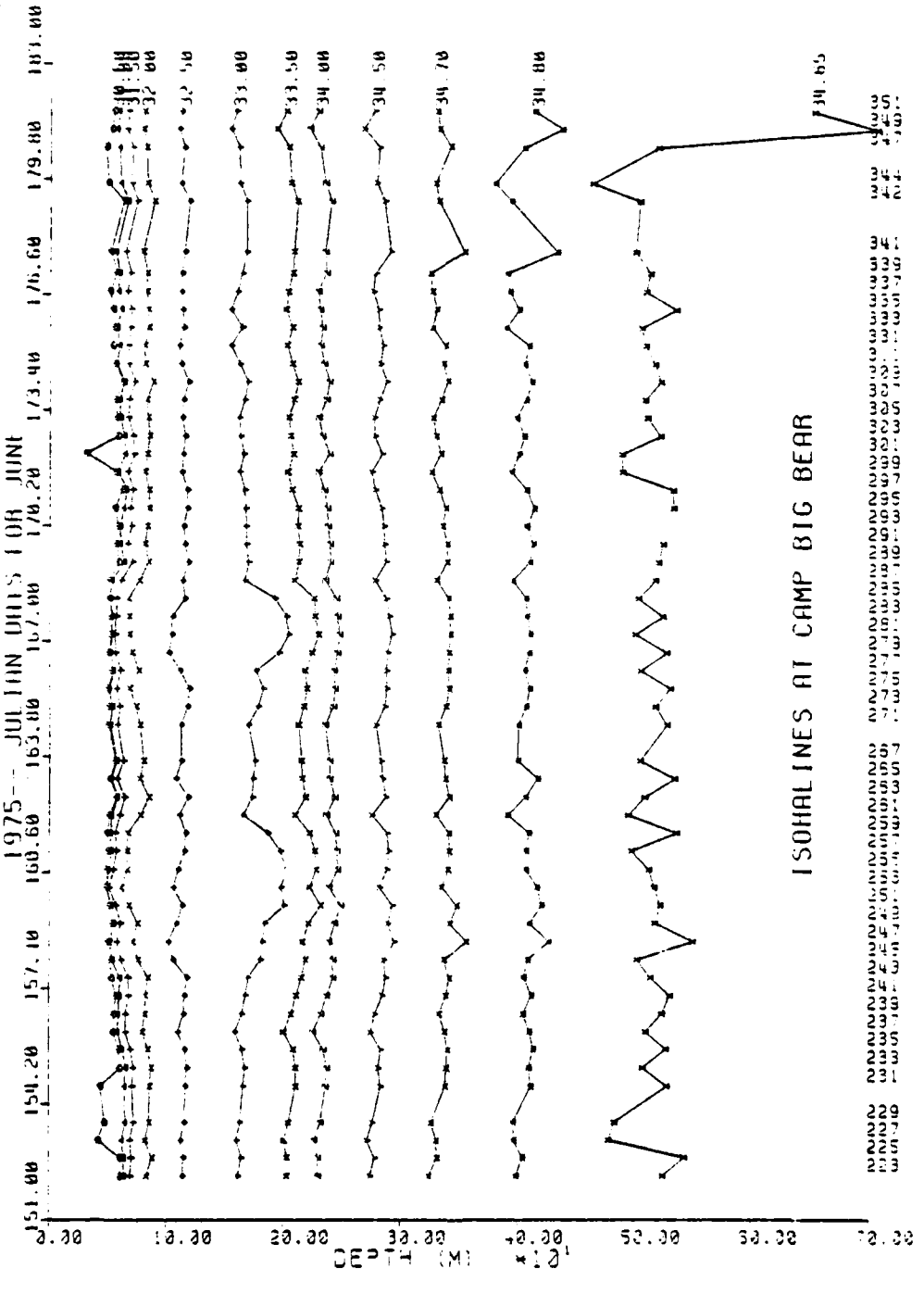
ISOHALINES AT CAMP SNOWBIRD

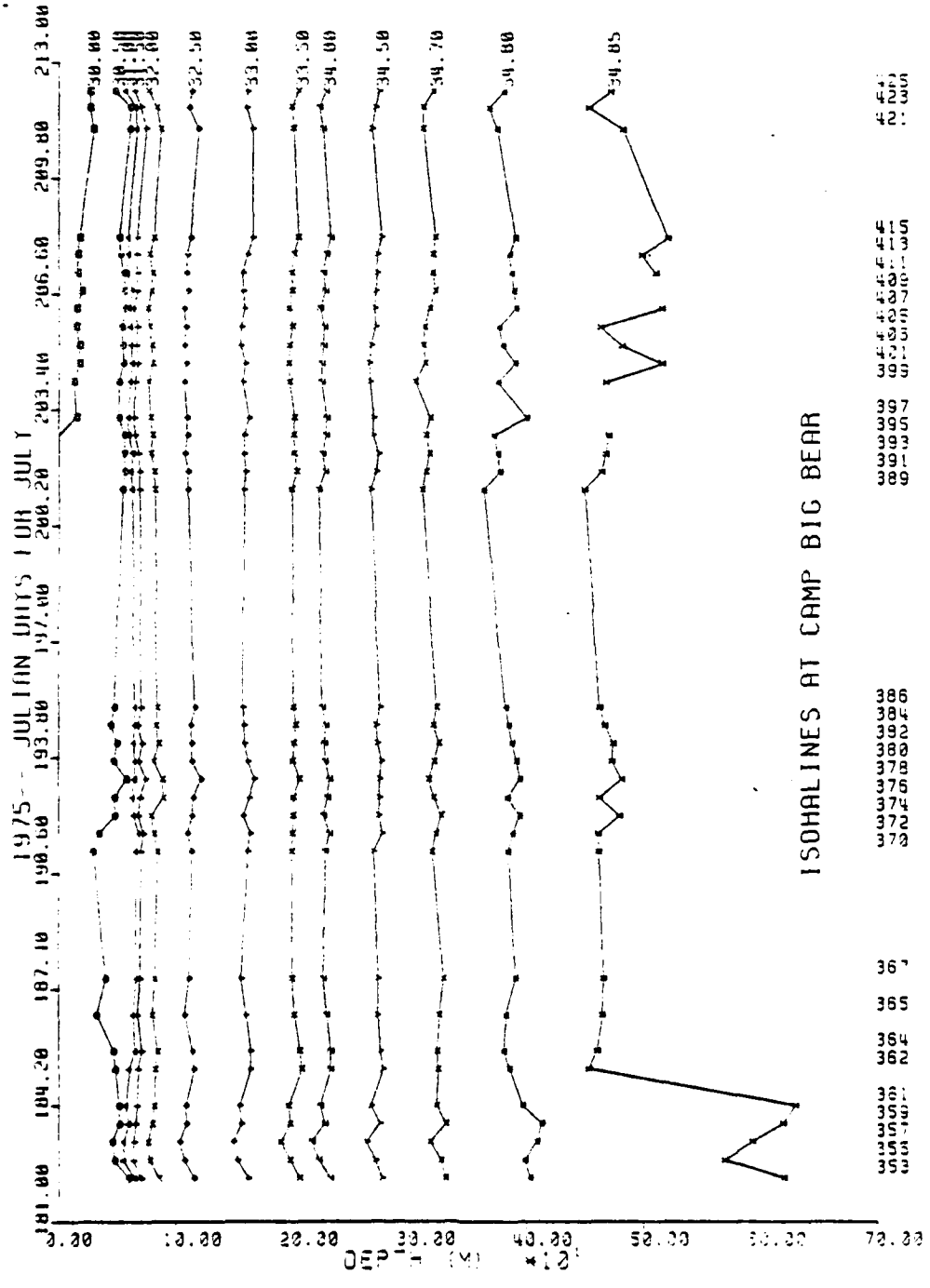

ISOHALINES AT CAMP SNOWBIRD
1976 - JULIAN DAYS 1 TO 366
456.00
459.20
462.40
465.60
468.80
472.00
475.20
478.40
481.60
484.80
488.00
530
624
622
620
598
596
576
572
570
568
566
34.85
34.00
34.70
34.50
34.00
33.50
33.00
32.50
0.00
10.00
20.00
30.00
40.00
50.00
60.00
70.00
DEPTH (M) *10¹

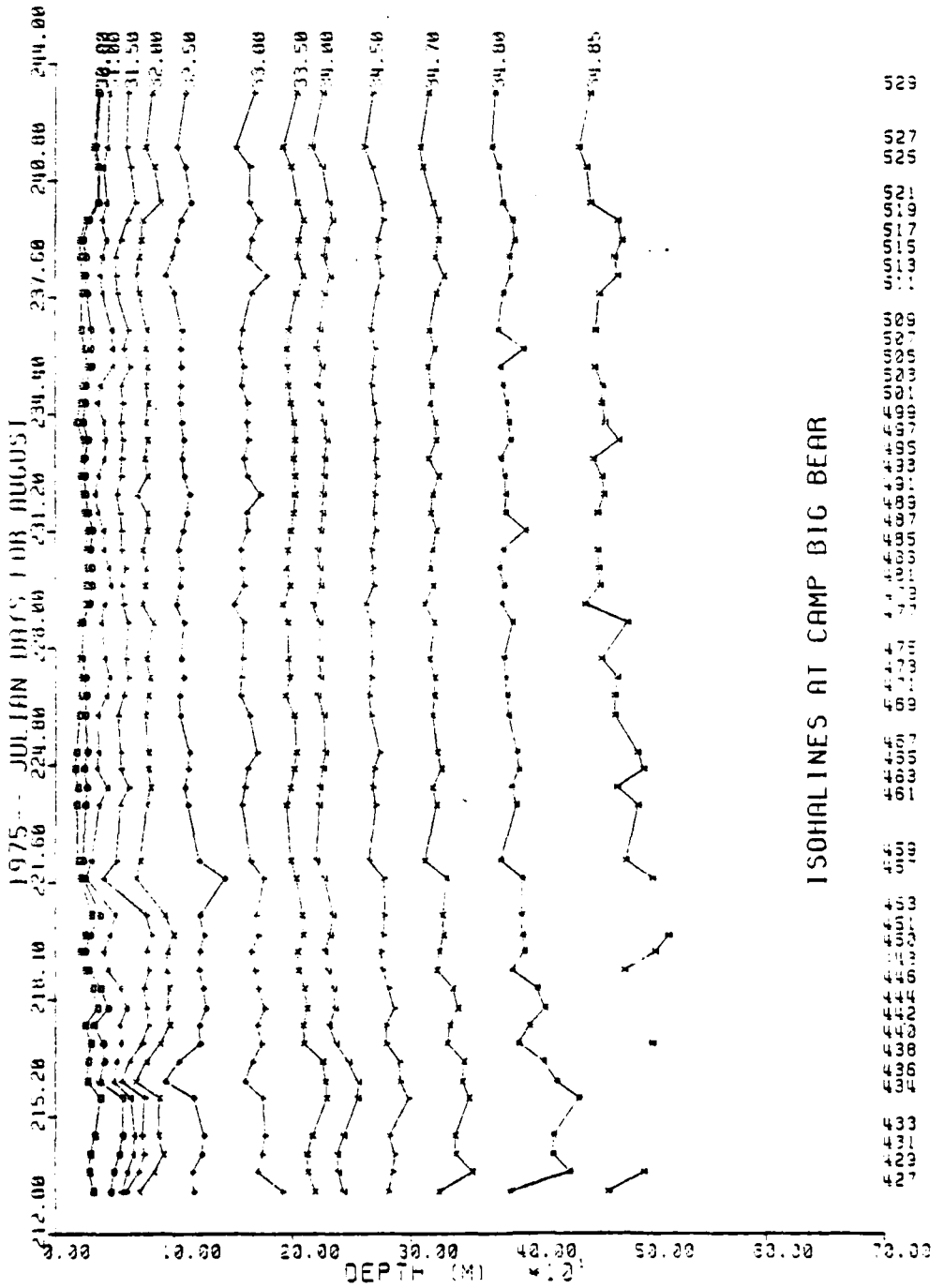

1975-- JULIAN DAYS FOR APRIL
90.00
93.20
96.40
99.60
102.80
106.00
109.20
112.40
115.60
118.80
122.00
2.00
10.00
20.00
30.00
40.00
50.00
60.00
70.00
DEPTH (M)
32.50
33.00
33.50
34.00
34.50
34.60
34.70
34.80
34.85
34.87
ISOHAL NEAR AT CAMP BIG BEAR

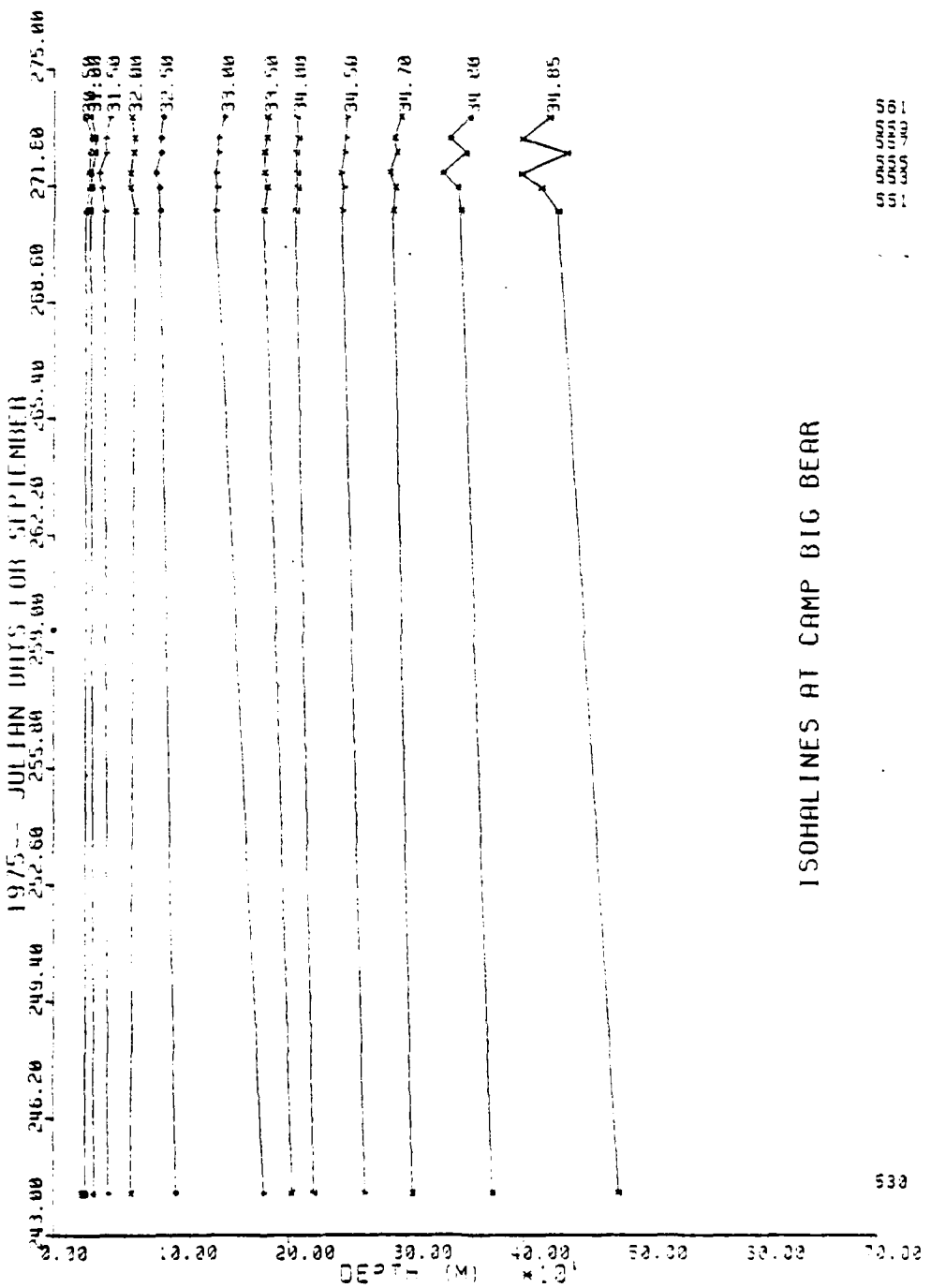

1975 - JULIAN DAYS FOR MAY
120.00 123.20 126.40 129.60 132.80 136.00 139.20 142.40 145.60 148.80 152.00
ISOHALINES AT CAMP BIG BEAR
0.00 10.00 20.00 30.00 40.00 50.00 60.00 70.00
DEPTH (M) *10


1975 - JUL 11th DAYS FOR MAY
120.00
123.20
126.40
129.60
132.80
136.00
139.20
142.40
145.60
148.80
152.00
0.00
10.00
20.00
30.00
40.00
50.00
60.00
70.00
DEPTH (M) X10
33.00
33.50
34.00
34.50
34.70
34.80
34.85
ISOHALINES AT CAMP BIG BEAR


1975-- JULIAN DAYS FOR JUNE
151.00
154.20
157.40
160.60
163.80
167.00
170.20
173.40
176.60
179.80
183.00
0.00
10.00
20.00
30.00
40.00
50.00
60.00
70.00
DEPTH (M) *10¹
ISOHALINES AT CAMP BIG BEAR

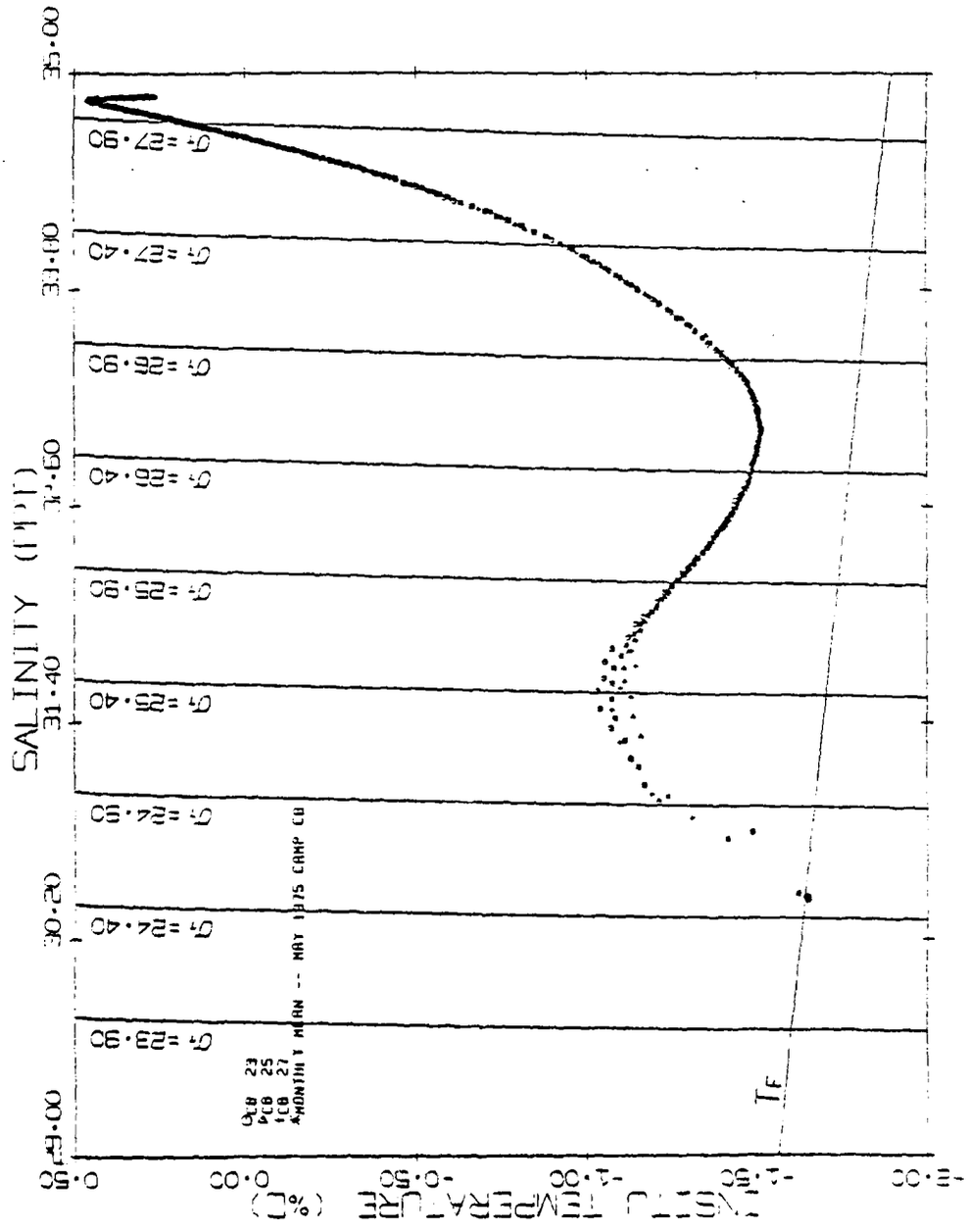

ISOHALINES AT CAMP BIG BEAR
1975 - JULIAN DAYS FOR JULY
DEPTH (M) *10
181.00
187.10
193.20
199.30
203.40
206.60
209.80
213.00
0.00
10.00
20.00
30.00
40.00
50.00
70.00
386
384
382
380
378
376
374
372
370
365
364
362
359
397
395
393
389
34.85
34.80
34.70
34.50
34.00
33.50
33.00
32.50
30.00

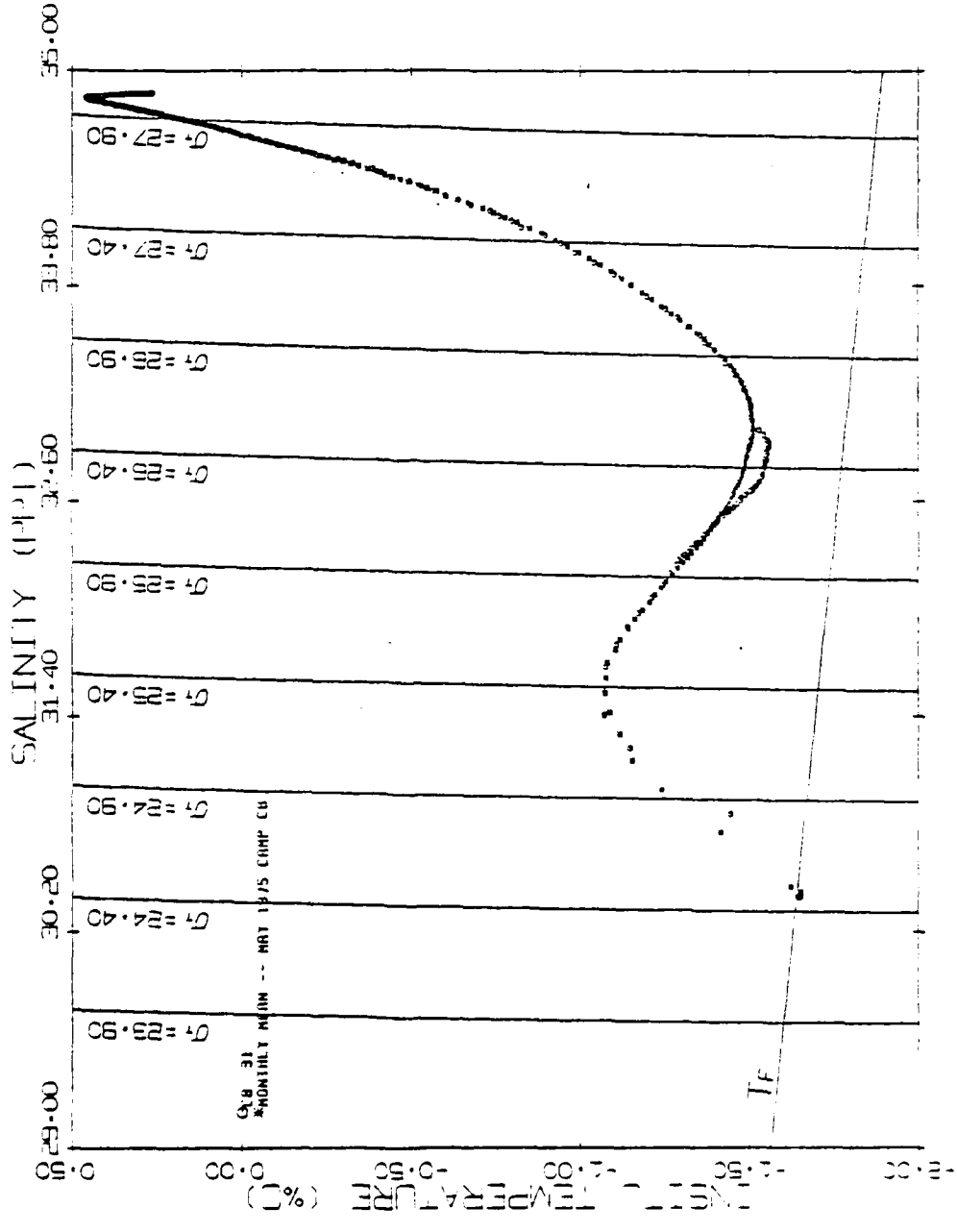

1975 -- JULIAN DAYS FOR AUGUST
212.00
215.20
218.10
221.60
224.80
228.00
231.20
234.40
237.60
240.80
244.00
ISOHALINES AT CAMP BIG BEAR
0.00
10.00
20.00
30.00
40.00
50.00
60.00
70.00
DEPTH (M)

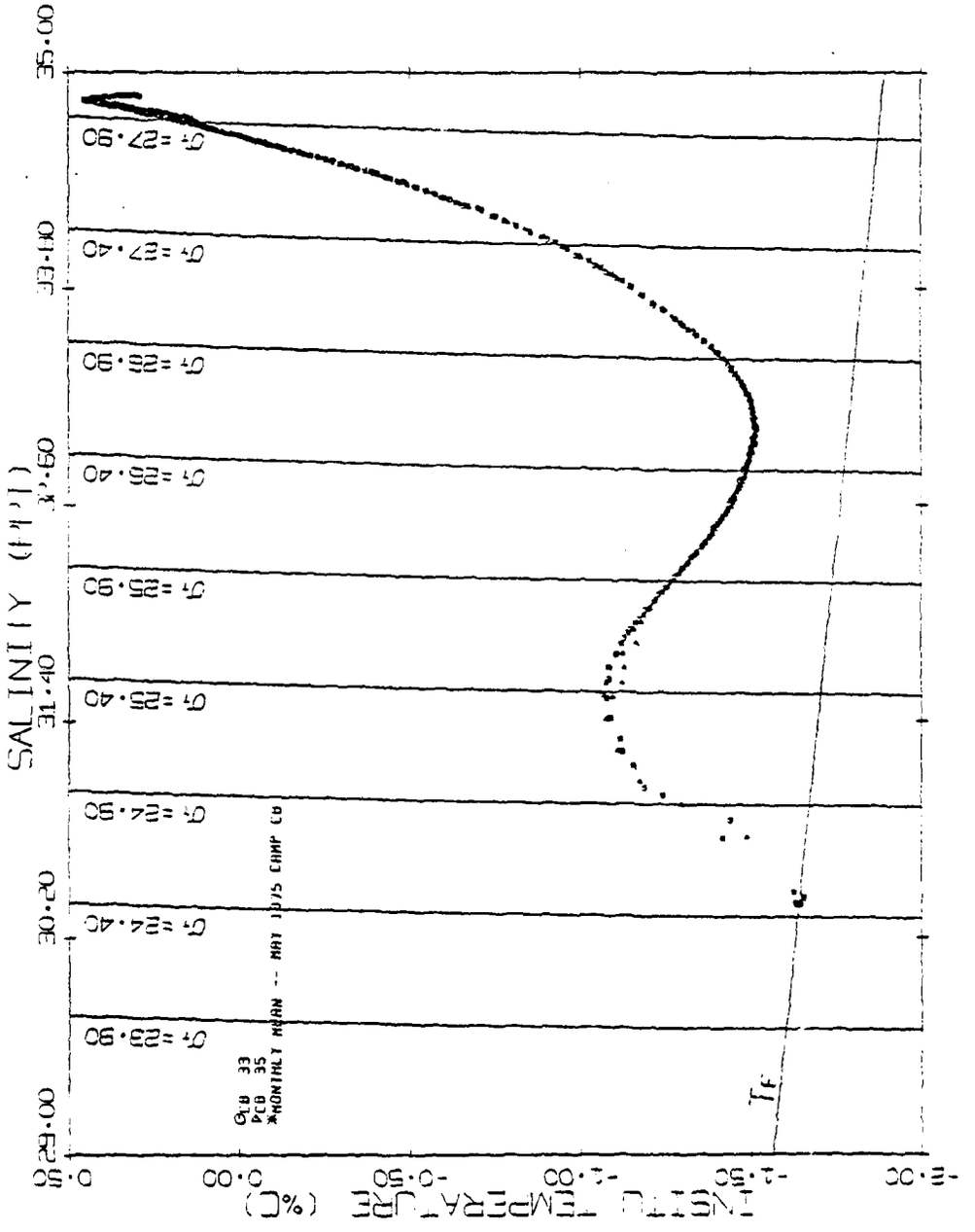

ISOHALINES AT CAMP BIG BEAR
1975 JULIAN DAYS FOR SEPTEMBER
243.00
246.20
249.40
252.60
255.80
259.00
262.20
265.40
268.60
271.60
275.00
30.50
31.00
32.00
33.00
33.50
34.00
34.50
34.70
34.80
34.85
530
0.00
10.00
20.00
30.00
40.00
50.00
60.00
70.00
DEPTH (M) x10¹

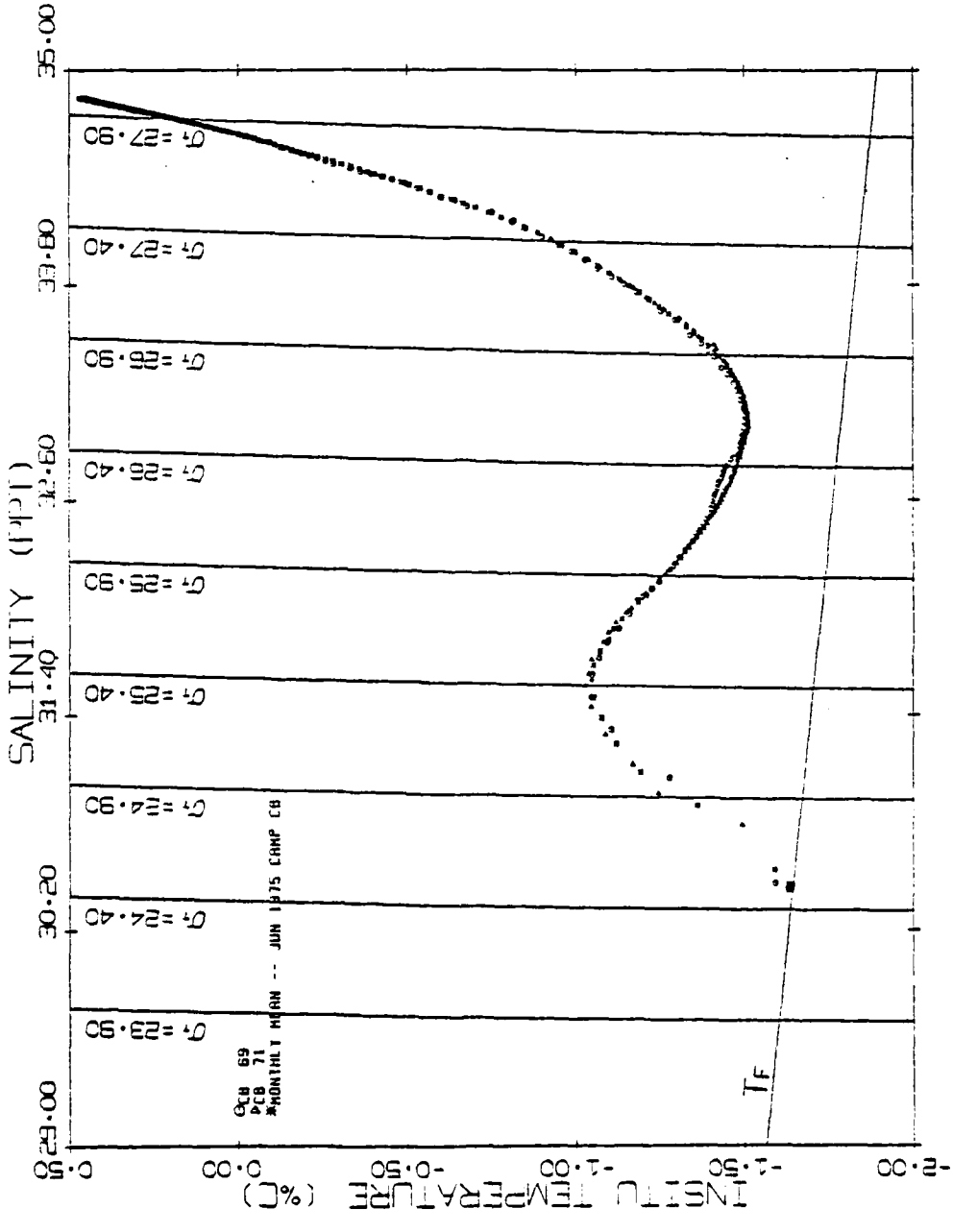
Section 2

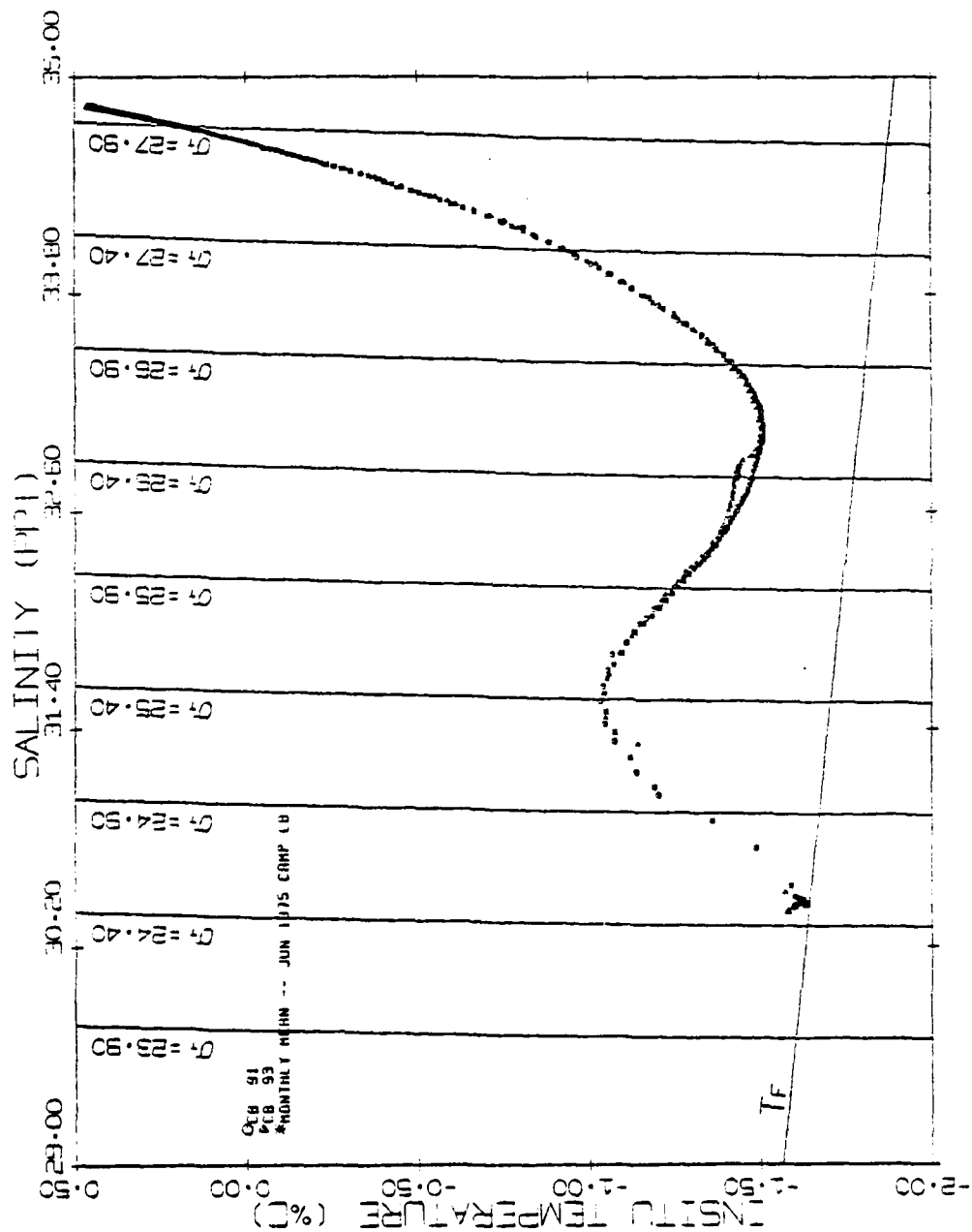
Temperature-salinity Diagrams for Observed Eddies

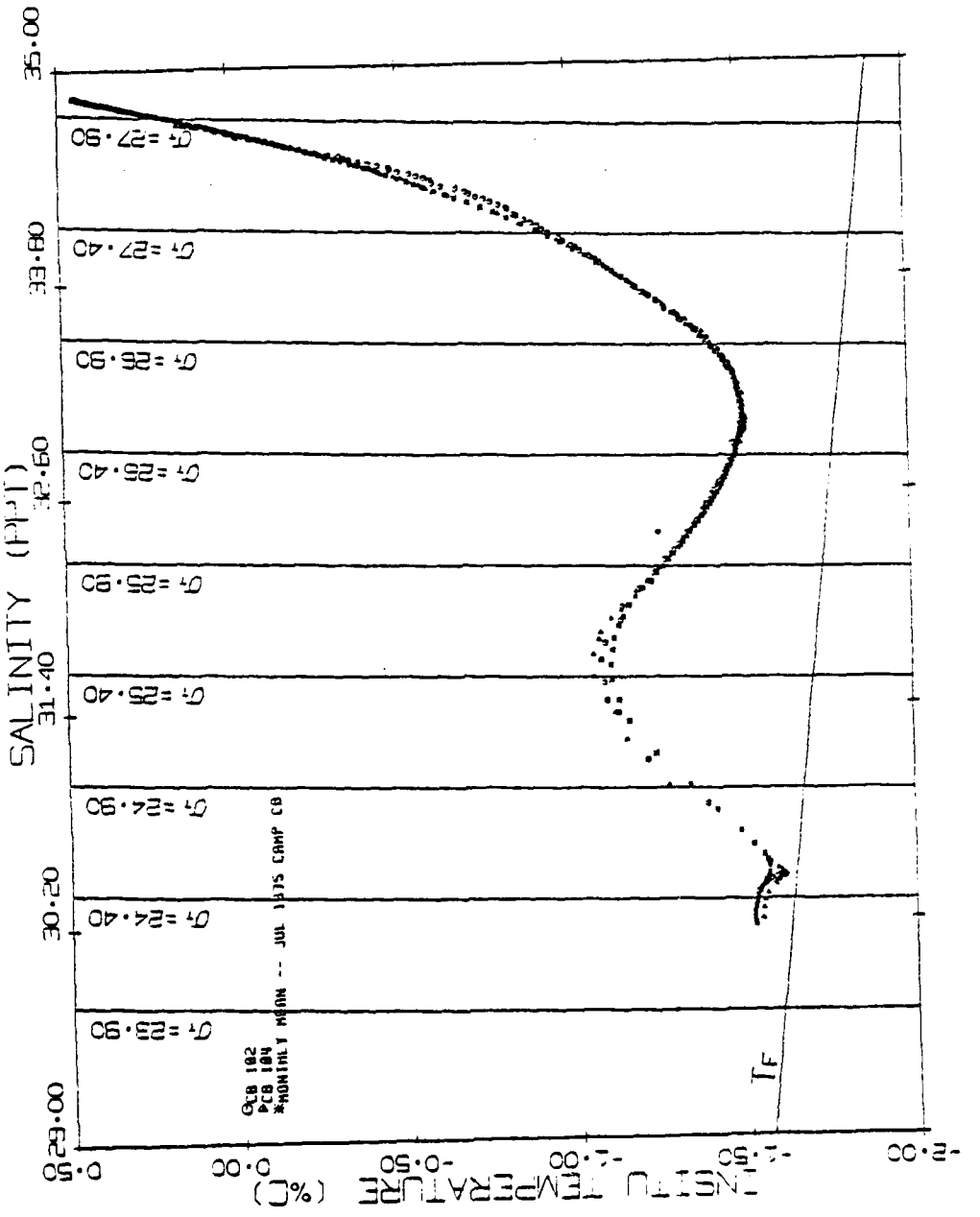

SALINITY (PPT)
POTENTIAL TEMPERATURE (°C)
σt =27.90
σt =27.40
σt =26.90
σt =26.40
σt =25.90
σt =25.40
σt =24.90
σt =24.40
σt =23.90
T_F
OCB 23
PCB 25
ICB 27
MONTHLY MEAN -- MAY 1975 CAMP CB

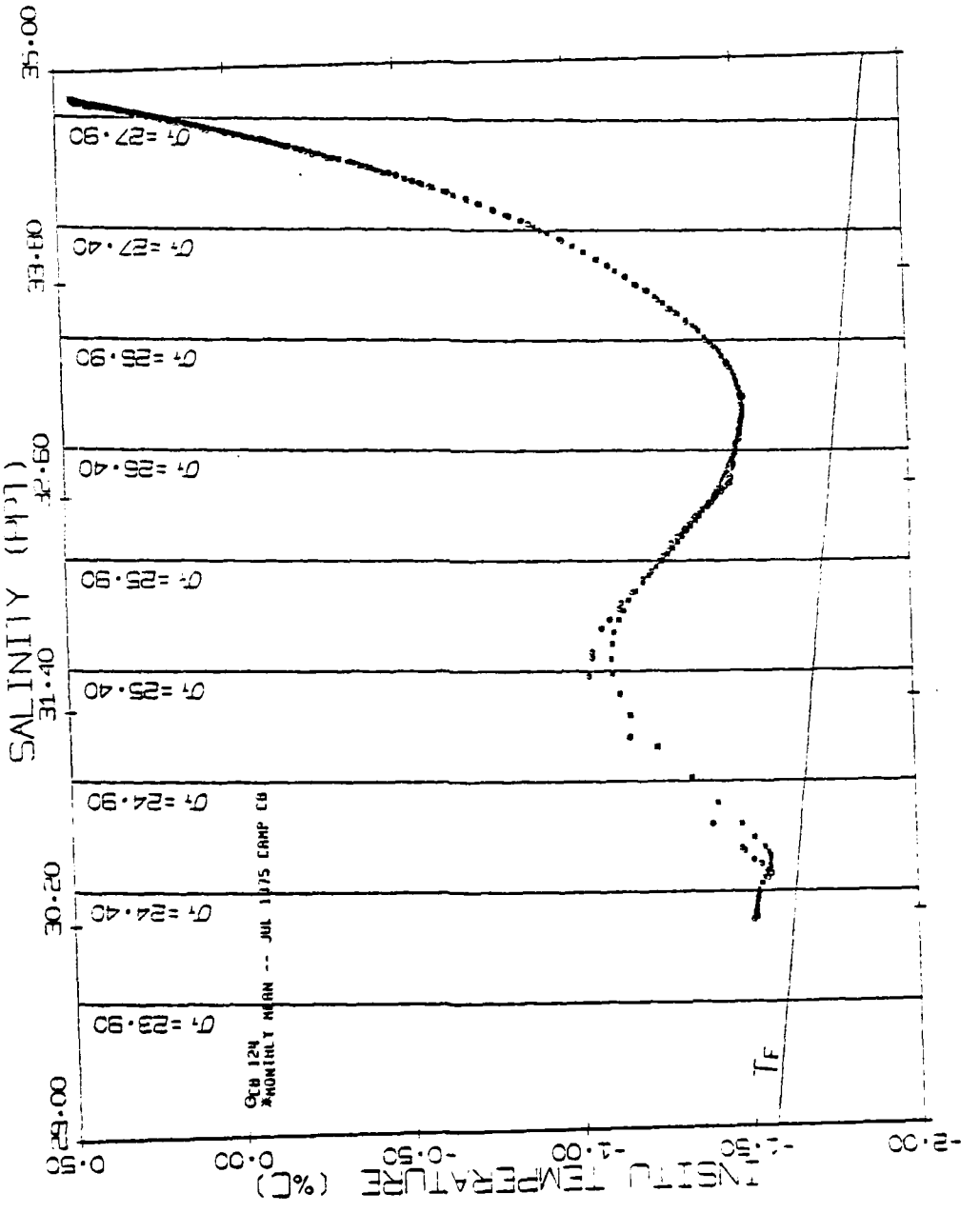

SALINITY (PPT)
35.00
34.80
34.60
34.40
34.20
34.00
σt =27.90
σt =27.40
σt =26.90
σt =26.40
σt =25.90
σt =25.40
σt =24.90
σt =24.40
σt =23.90
T_F
-2.00
-1.50
-1.00
-0.50
0.00
0.50

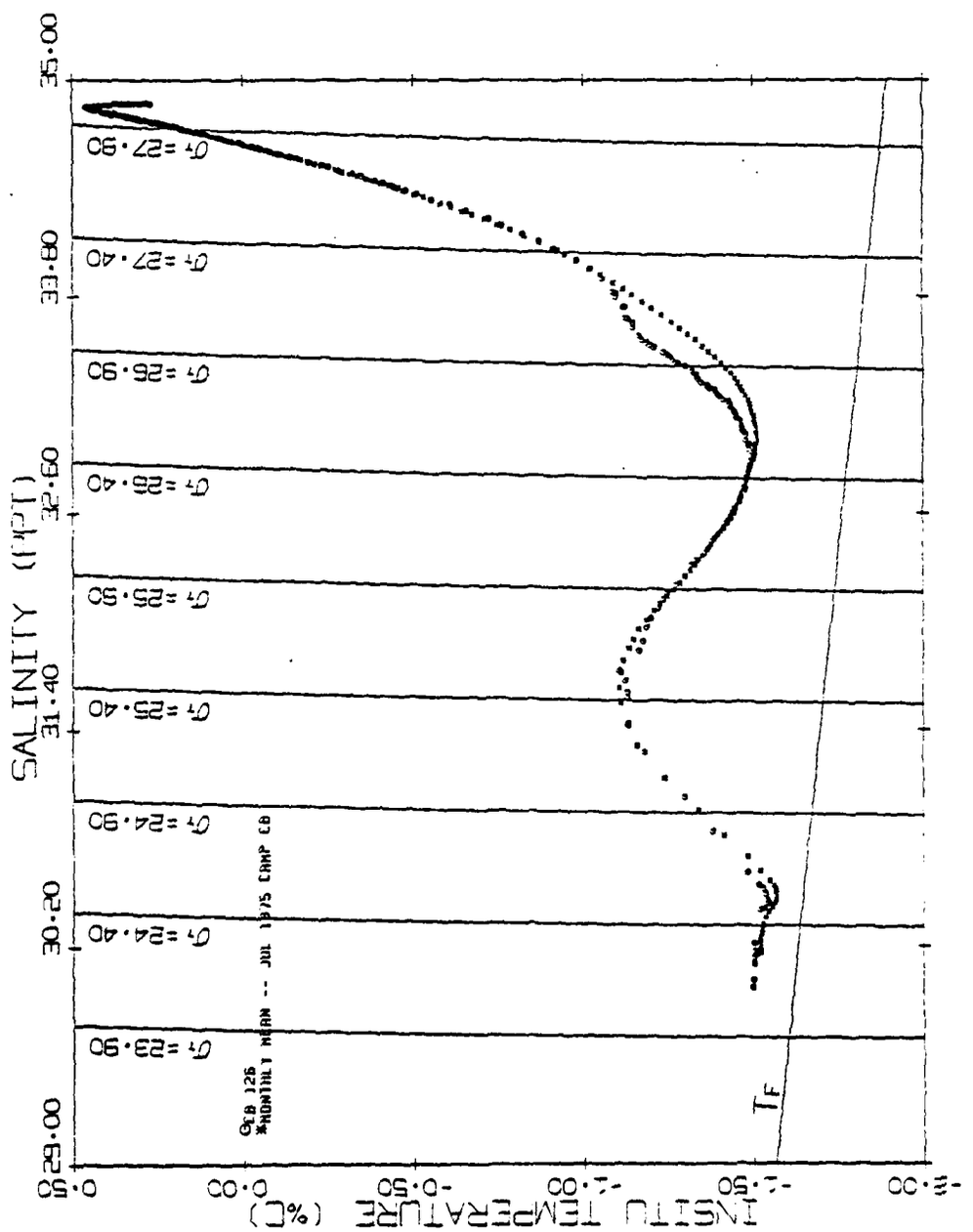

SALINITY (ppt)
35.00
34.60
34.20
33.80
33.40
σt =27.80
σt =27.40
σt =26.80
σt =26.40
σt =25.80
σt =25.40
σt =24.80
σt =24.40
σt =23.80
CTD 33
PCB 35
*MONTHLY MEAN -- MAY 1975 CAMP CB
POTENTIAL TEMPERATURE (°C)
0.50
0.00
-0.50
-1.00
-1.50
-2.00
T_f

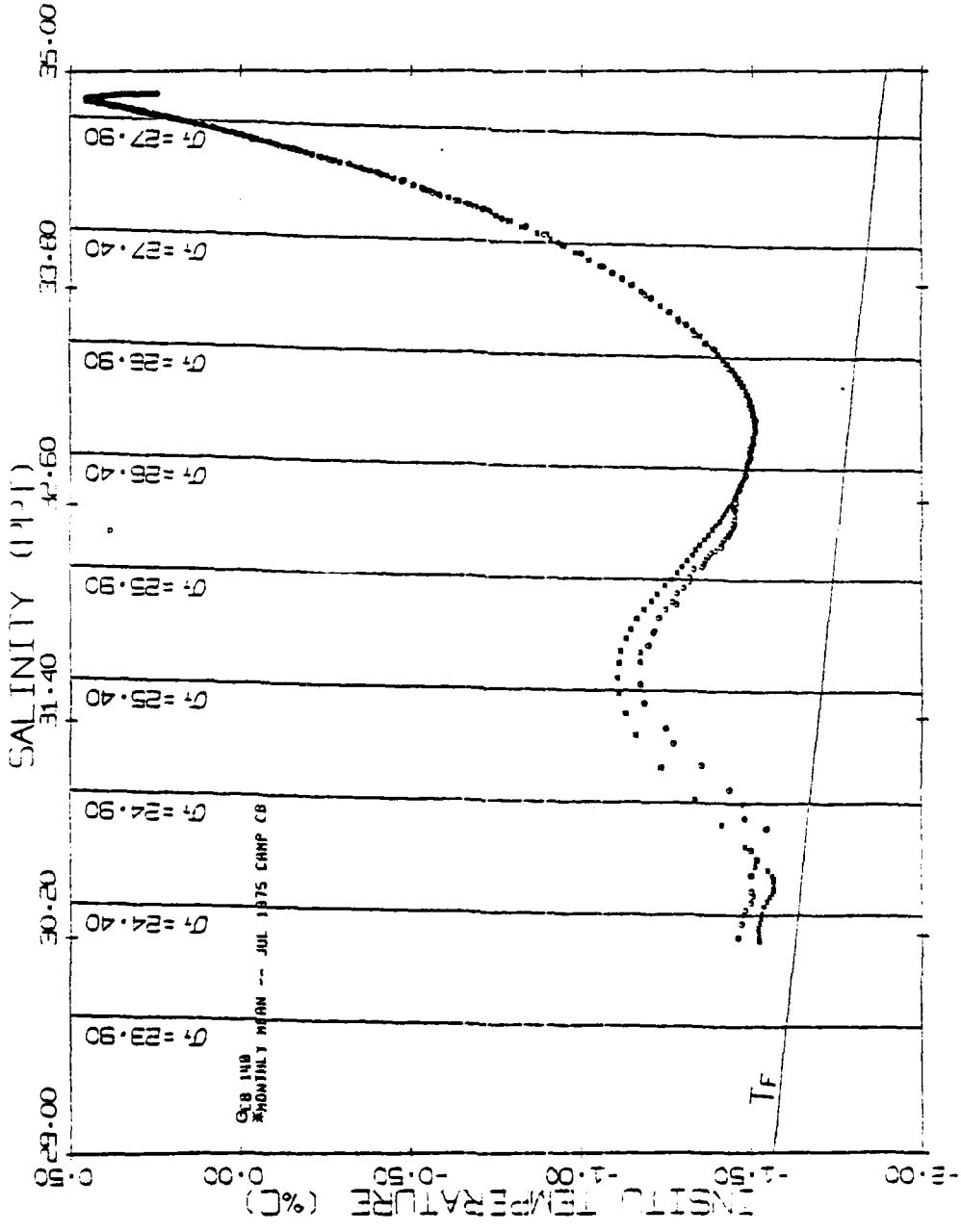

SALINITY (PPT)
35.00
33.80
32.60
31.40
30.20
29.00
σt =27.90
σt =27.40
σt =26.90
σt =26.40
σt =25.90
σt =25.40
σt =24.90
σt =24.40
σt =23.90
TF
0.50
0.00
-0.50
-1.00
-1.50
-2.00
INSITU TEMPERATURE (°C)
CTD 69
PCB 71
*MONTHLY MEAN -- JUN 1975 CAMP CB

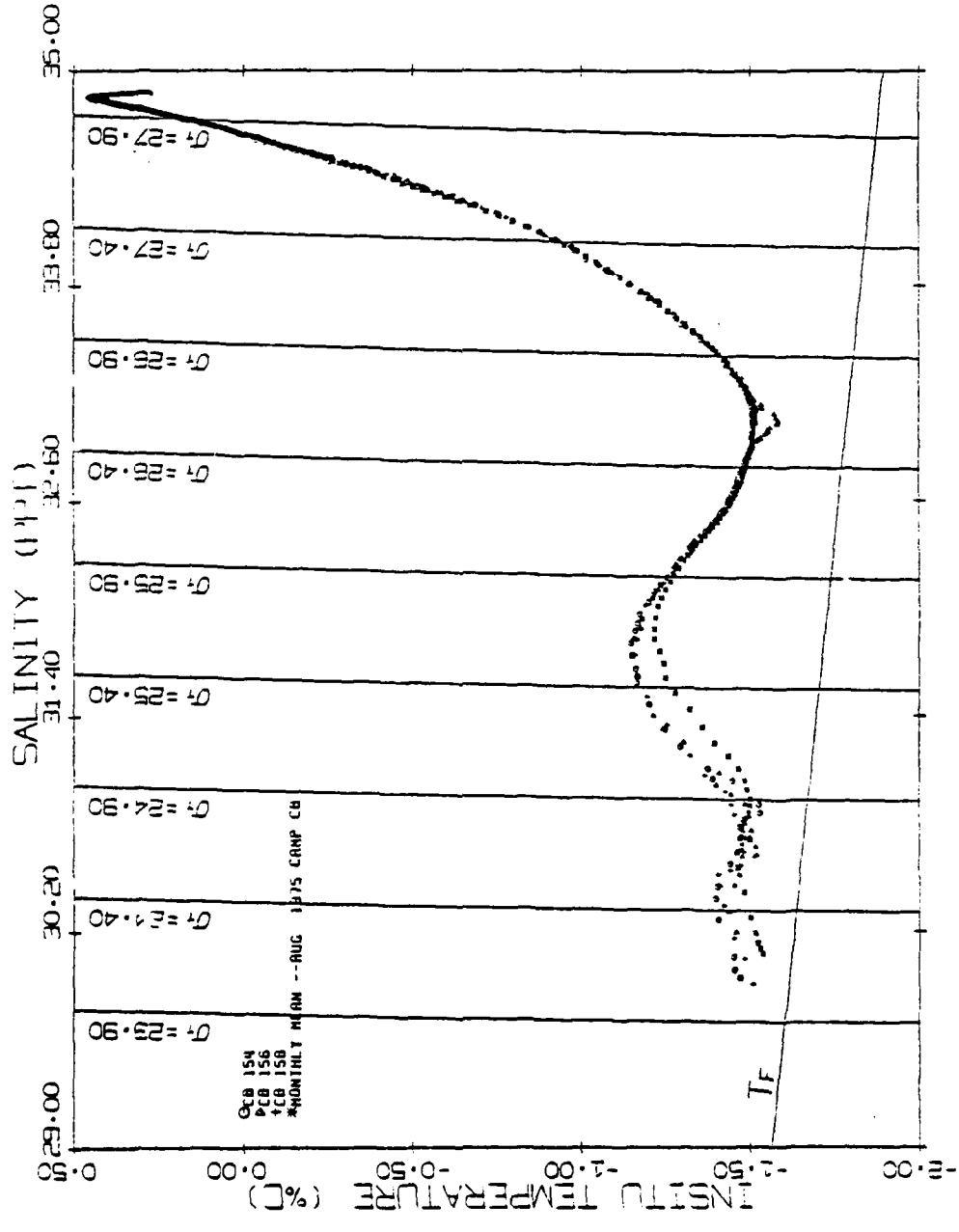

SALINITY (PPT)
POTENTIAL TEMPERATURE (°C)
σt =27.90
σt =27.40
σt =26.90
σt =26.40
σt =25.90
σt =25.40
σt =24.90
σt =24.40
σt =23.90
T_F
OCT 91
FEB 93
*MONTHLY MEAN -- JUN 1975 CRNF LB

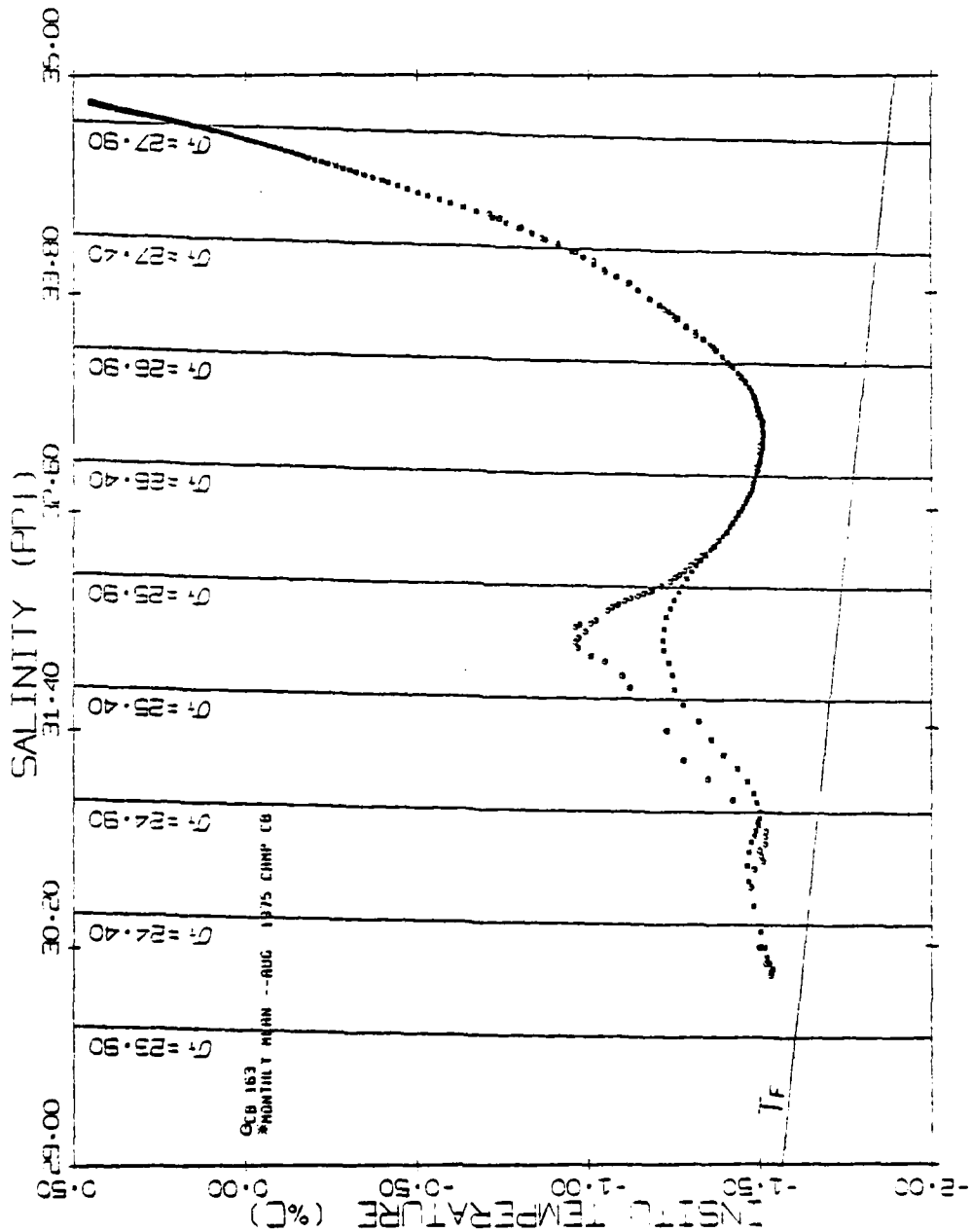

SALINITY (PPT)
POTENTIAL TEMPERATURE (°C)
35.00
33.80
32.60
31.40
30.20
29.00
0.50
0.00
-0.50
-1.00
-1.50
-2.00
σt =27.90
σt =27.40
σt =26.90
σt =25.40
σt =25.90
σt =25.40
σt =24.90
σt =24.40
σt =23.90
TF
CTD 182
PCB 184
*MONTHLY MEAN -- JUL 1975 CAMP CB

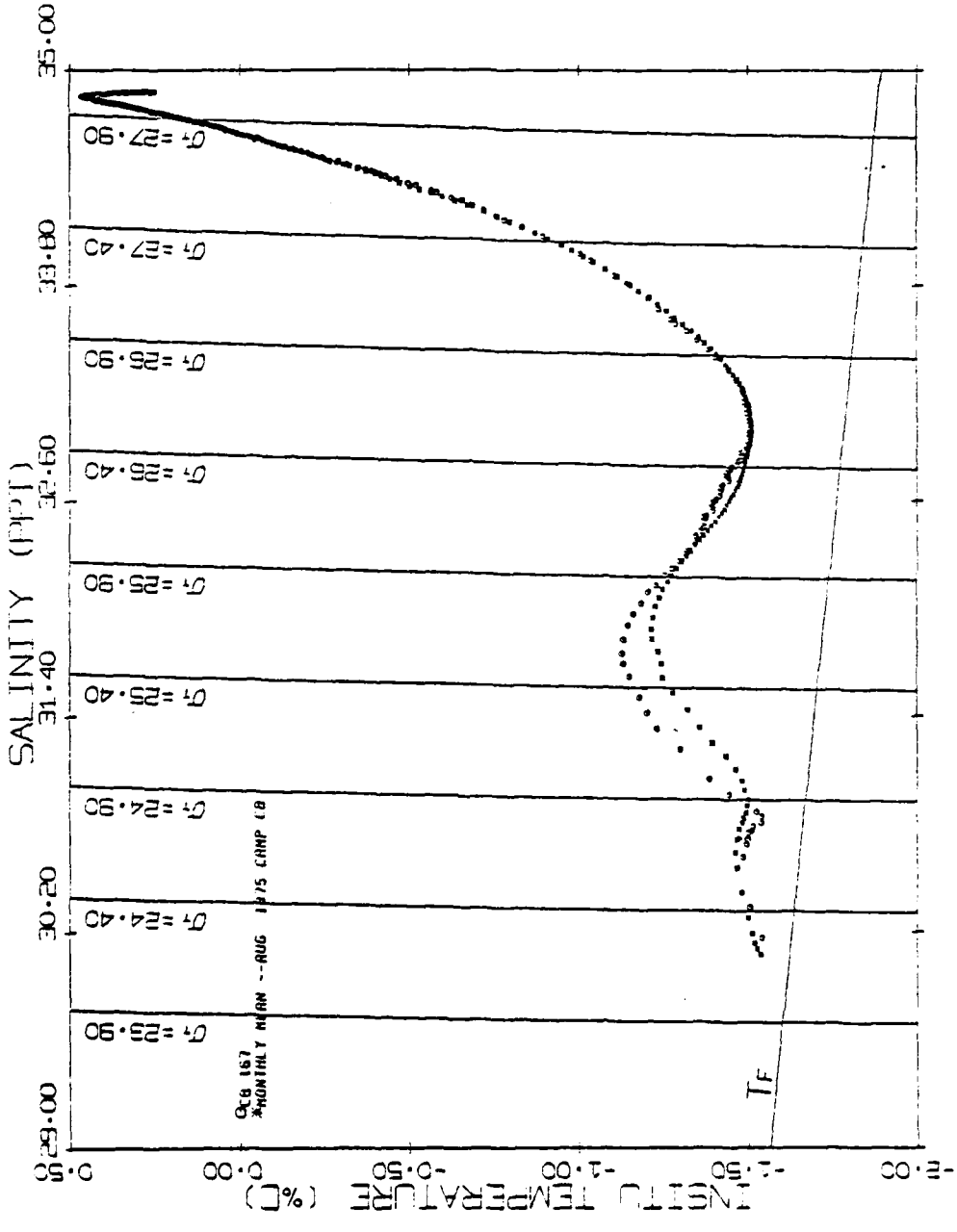

SALINITY (PPT)
35.00
33.80
32.60
31.40
30.20
29.00
σt =27.90
σt =27.40
σt =26.90
σt =26.40
σt =25.90
σt =25.40
σt =24.90
σt =24.40
σt =23.90
Qtr 124
*MONTHLY MEAN -- JUL 1975 CAMP CB
T_F
POTENTIAL TEMPERATURE (°C)
0.50
0.00
-0.50
-1.00
-1.50
-2.00

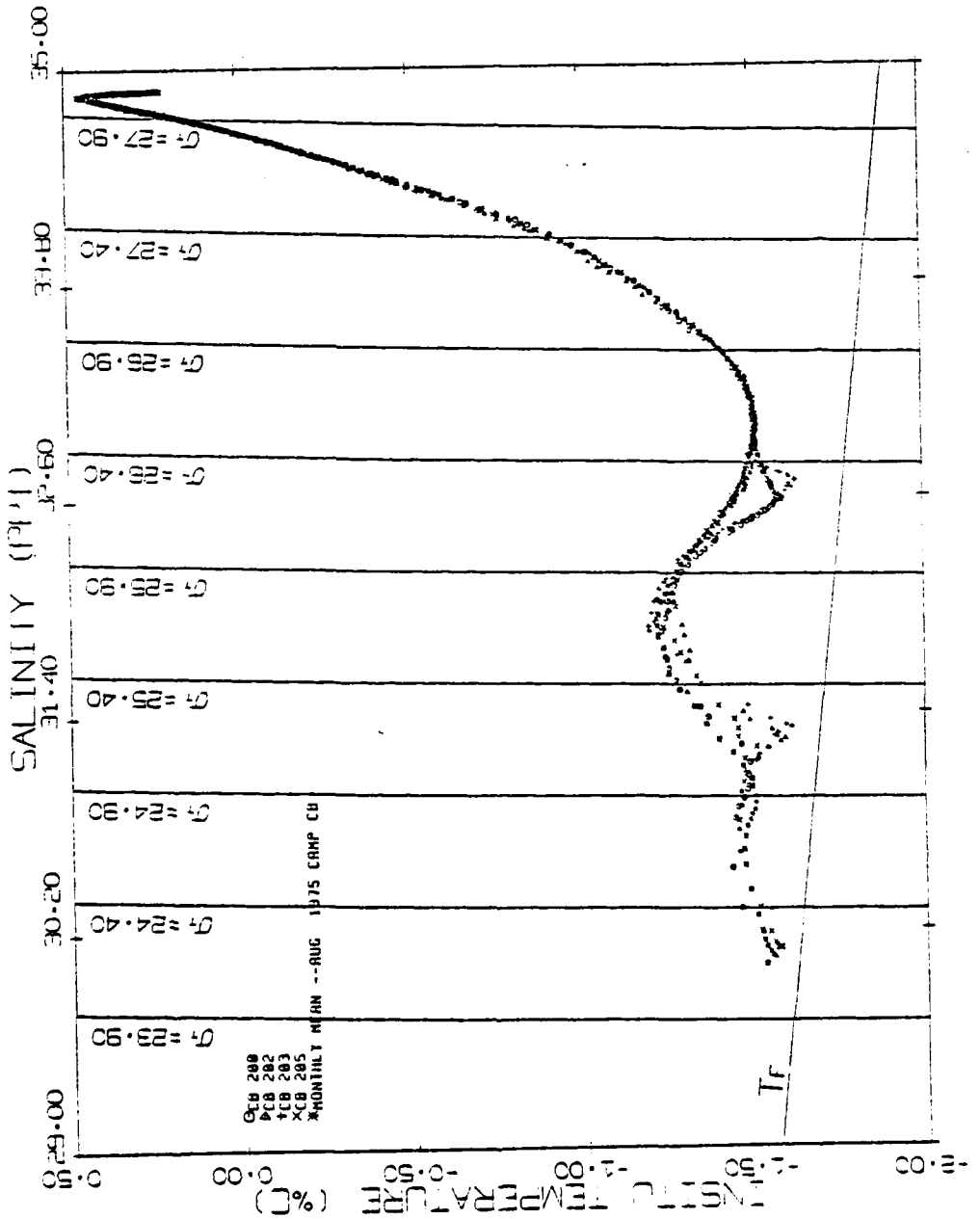

SALINITY (ppt)
INSITU TEMPERATURE (°C)
35.00
33.80
32.60
31.40
30.20
29.00
0.50
0.00
-0.50
-1.00
-1.50
-2.00
σt =27.90
σt =27.40
σt =26.90
σt =26.40
σt =25.90
σt =25.40
σt =24.90
σt =24.40
σt =23.90
CTD 126
*MONTHLY MEAN -- JUL 1975 CAMP CB
T_F

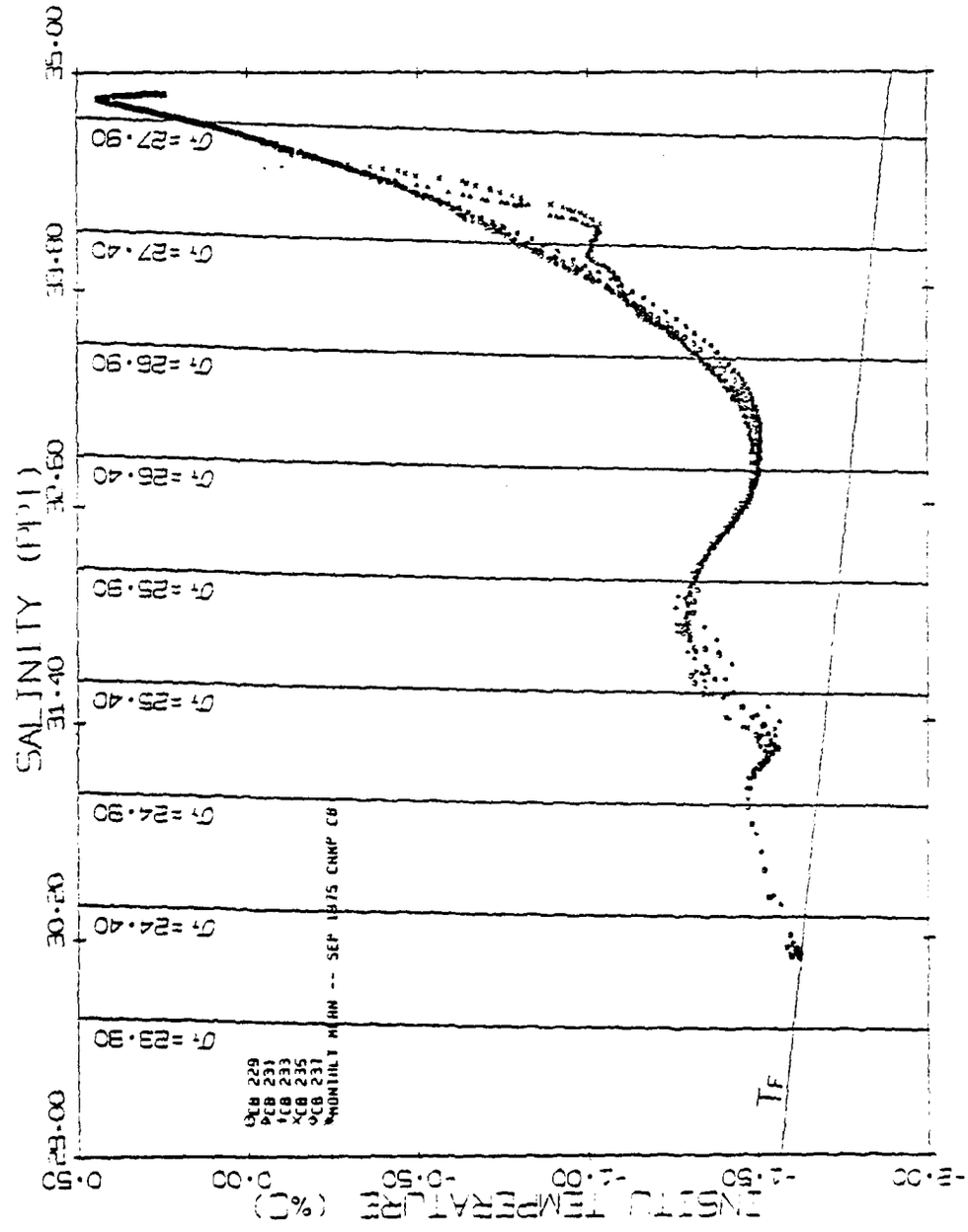

SALINITY (ppt)
35.00
33.80
32.60
31.40
30.20
29.00
σt =27.90
σt =27.40
σt =26.90
σt =26.40
σt =25.90
σt =25.40
σt =24.90
σt =24.40
σt =23.90
Tf
Qrs 148
*MONTHLY MEAN -- JUL 1975 CAMP C8
INSITU TEMPERATURE (°C)
0.50
0.00
-0.50
-1.00
-1.50
-2.00

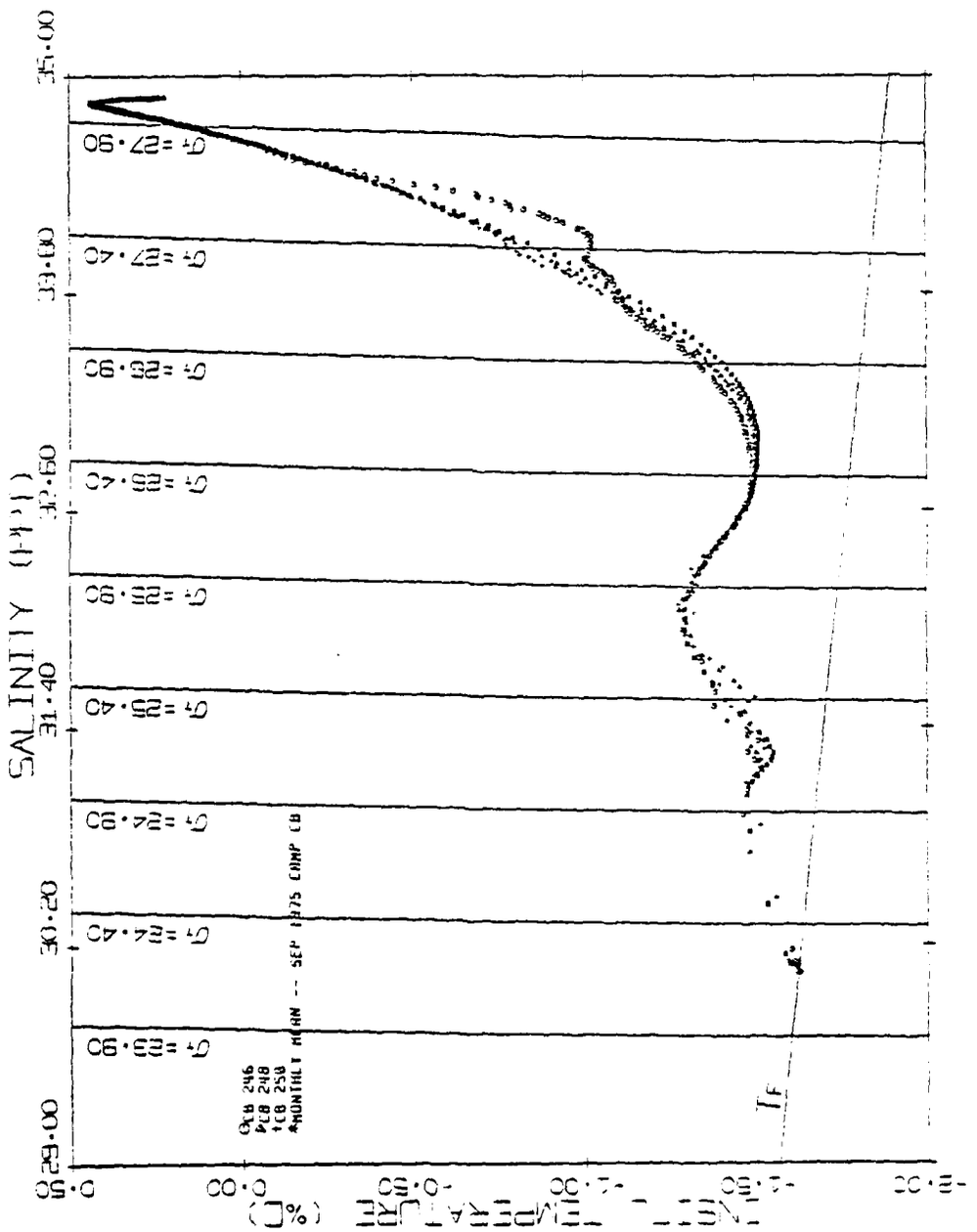

INSITU TEMPERATURE (°C)
SALINITY (PPT)
σt =27.90
σt =27.40
σt =26.90
σt =26.40
σt =25.90
σt =25.40
σt =24.90
σt =24.40
σt =23.90
T_F
PCB 154
PCB 156
TCB 158
*MONTHLY MEAN --AUG 1975 CAMP CB

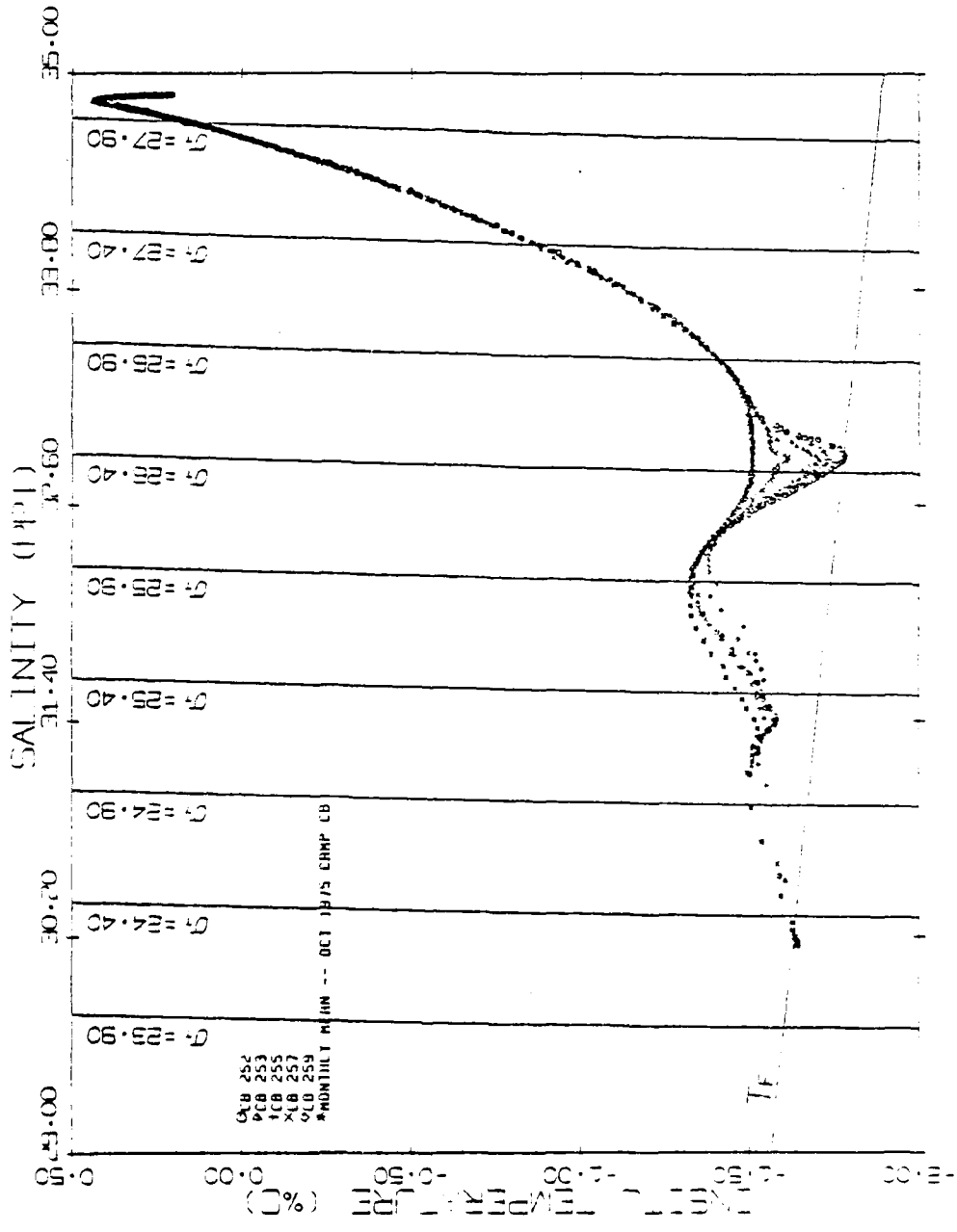

SALINITY (PPT)
POTENTIAL TEMPERATURE (°C)
σt =27.90
σt =27.40
σt =26.90
σt =26.40
σt =25.90
σt =25.40
σt =24.90
σt =24.40
σt =25.90
OCB 163
*MONTHLY MEAN --AUG
CHMP CB
TF

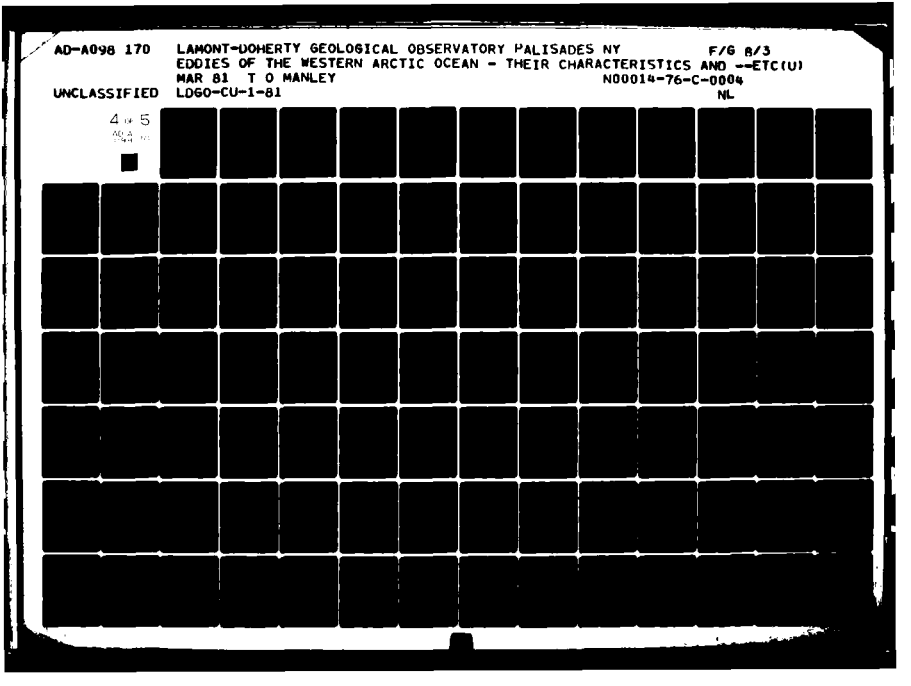

SALINITY (PPT)
35.00
33.80
32.60
31.40
30.20
29.00
σt =27.90
σt =27.40
σt =26.90
σt =26.40
σt =25.90
σt =25.40
σt =24.90
σt =24.40
σt =23.90
Oct 167
*MONTHLY MEAN --RUG 1975 CAMP 18
T_F
INSITU TEMPERATURE (°C)
0.50
0.00
-0.50
-1.00
-1.50
-2.00

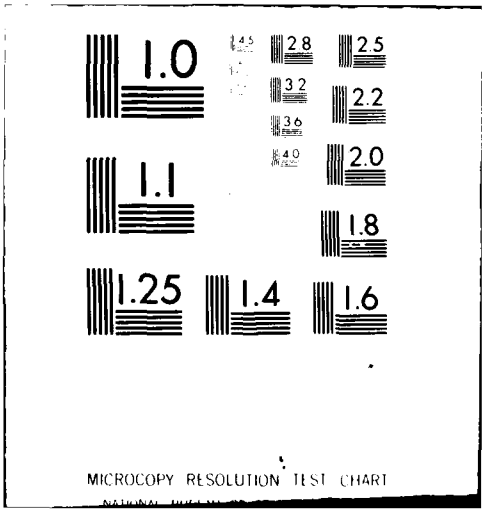

SALINITY (PPT)
POTENTIAL TEMPERATURE (°C)
σt =27.90
σt =27.40
σt =26.90
σt =26.40
σt =25.90
σt =25.40
σt =24.90
σt =24.40
σt =23.90
Tf
Orb 280
Pcb 282
+cb 283
Xcb 285
*MONTHLY MEAN --AUG 1975 CAMP CB

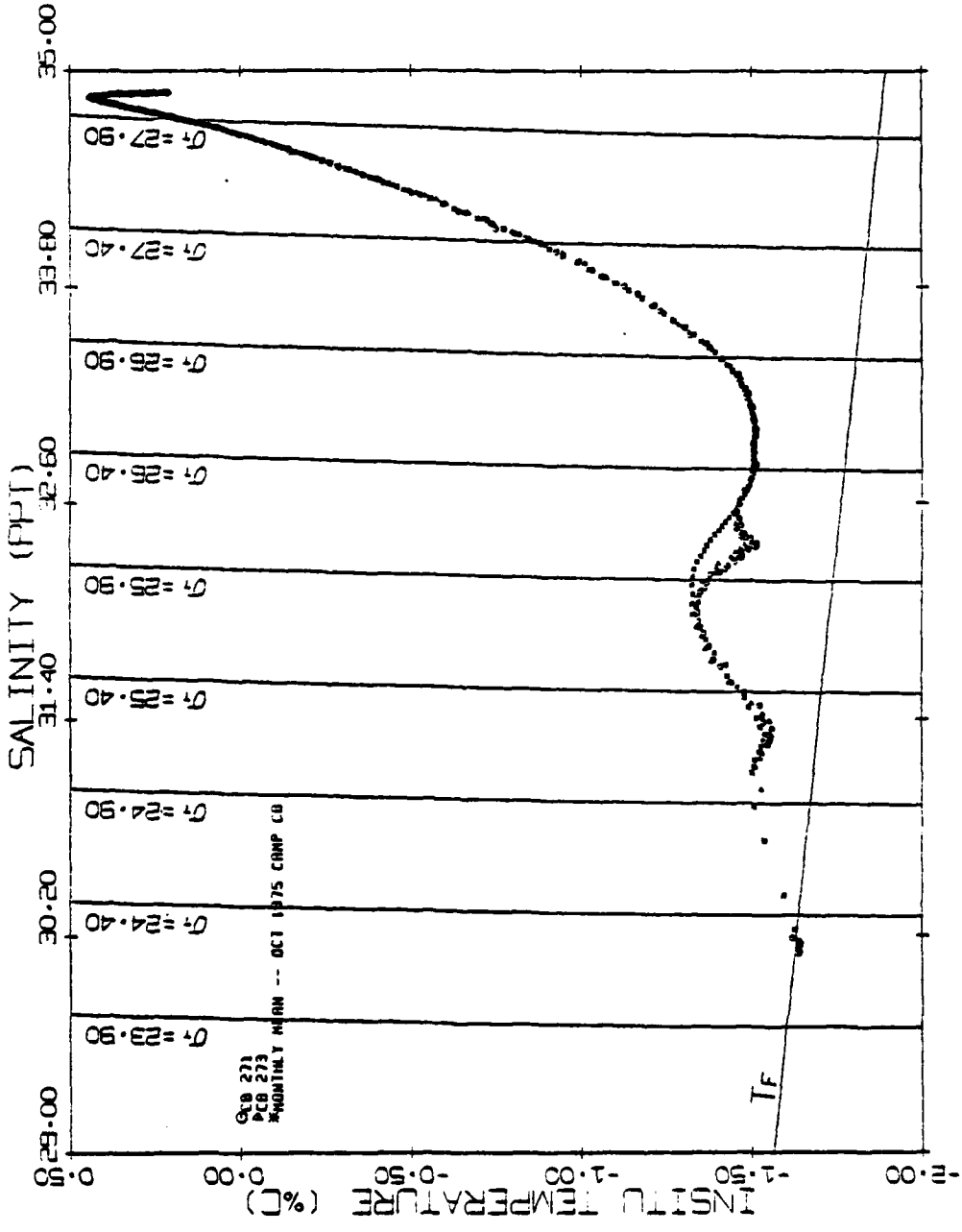

SALINITY (PPT)
35.00
33.00
32.60
31.40
30.20
29.00
σt =27.80
σt =27.40
σt =26.80
σt =26.40
σt =25.80
σt =25.40
σt =24.80
σt =24.40
σt =23.80
0.50
0.00
-0.50
-1.00
-1.50
-2.00
INSITU TEMPERATURE (°C)
Tf
MONTHLY MEAN -- SEP 1975 CNMP CR
PCB 229
PCB 231
PCB 233
PCB 235
PCB 237

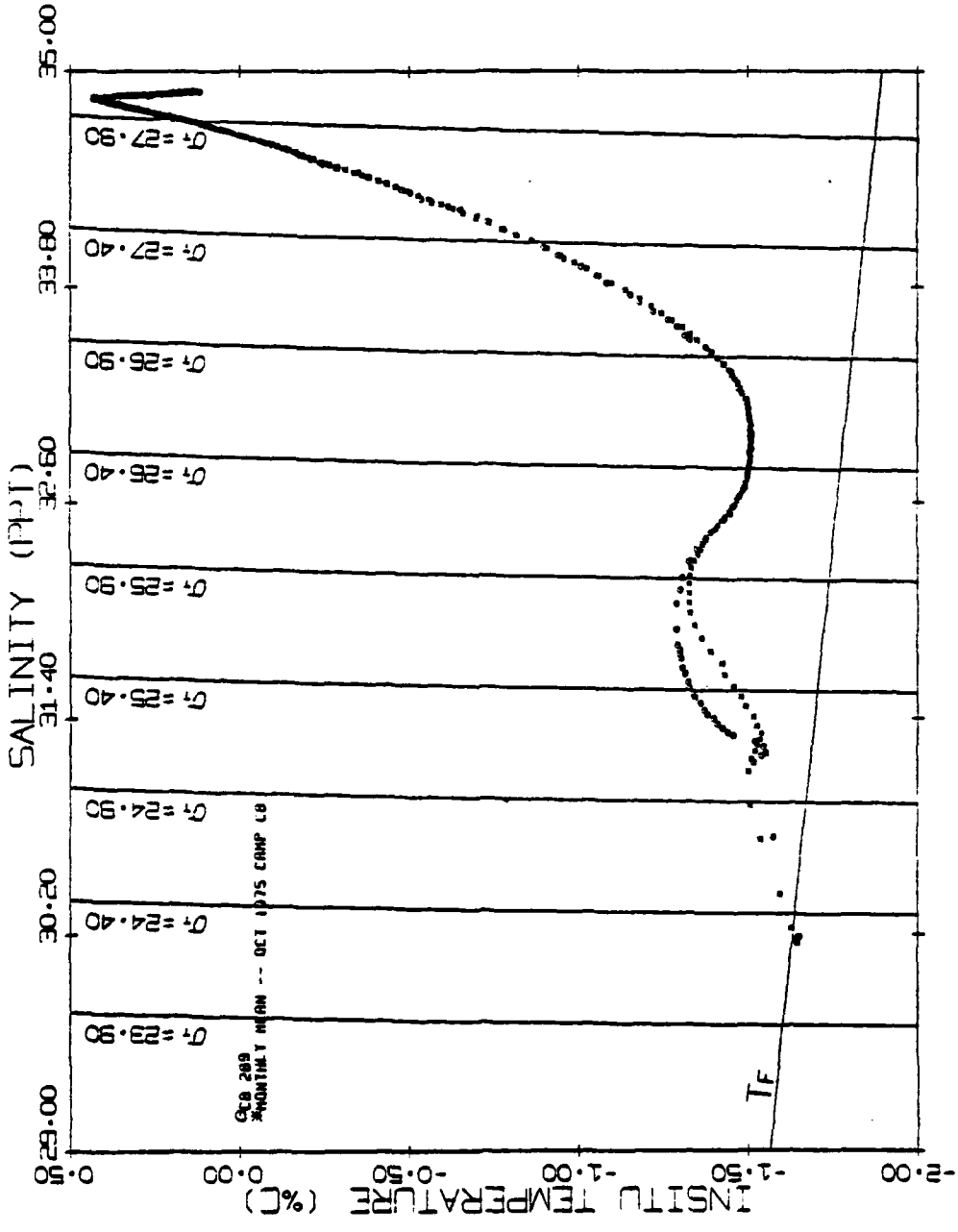

SALINITY (PPT)
35.00
30.80
30.60
30.40
30.20
30.00
σt =27.90
σt =27.40
σt =26.90
σt =26.40
σt =25.90
σt =25.40
σt =24.90
σt =24.40
σt =23.90
0.00
-0.50
-1.00
-1.50
-2.00
-2.50
-3.00
(°C)
Tf
Cruise 246
PCB 248
PCB 250
*MONTHLY MEAN -- SEP 1975 CAMP CB

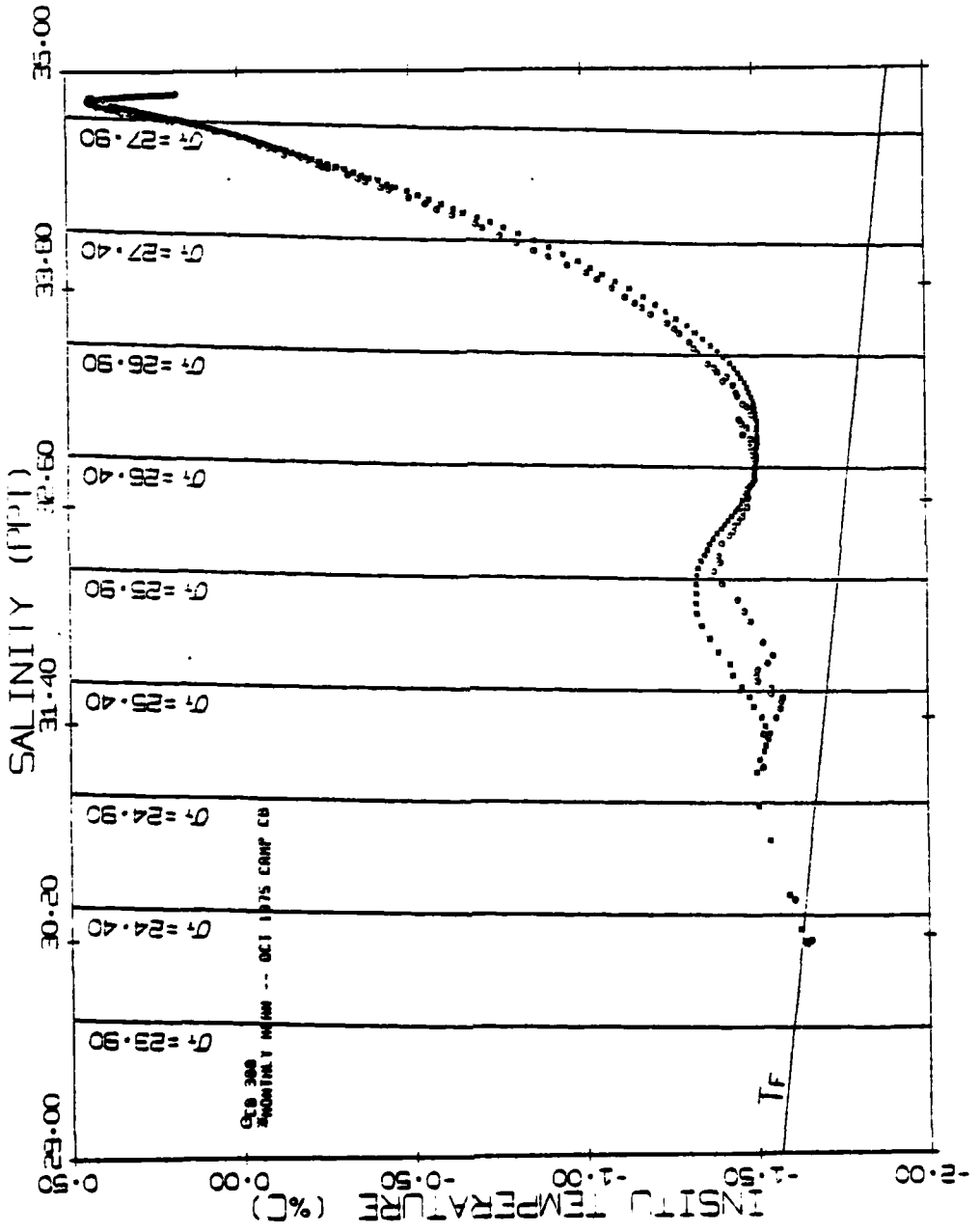

SALINITY (PPT)
POTENTIAL TEMPERATURE (°C)
σt =27.90
σt =27.40
σt =26.90
σt =26.40
σt =25.90
σt =25.40
σt =24.90
σt =24.40
σt =23.90
35.00
33.00
31.40
30.20
29.00
0.00
-0.30
-0.60
-0.90
-1.20
-1.50
-1.80
OCB 252
PCB 253
QCB 255
XCB 257
VCB 259
*MONTHLY MEAN -- OCT 1973 CAMP CB

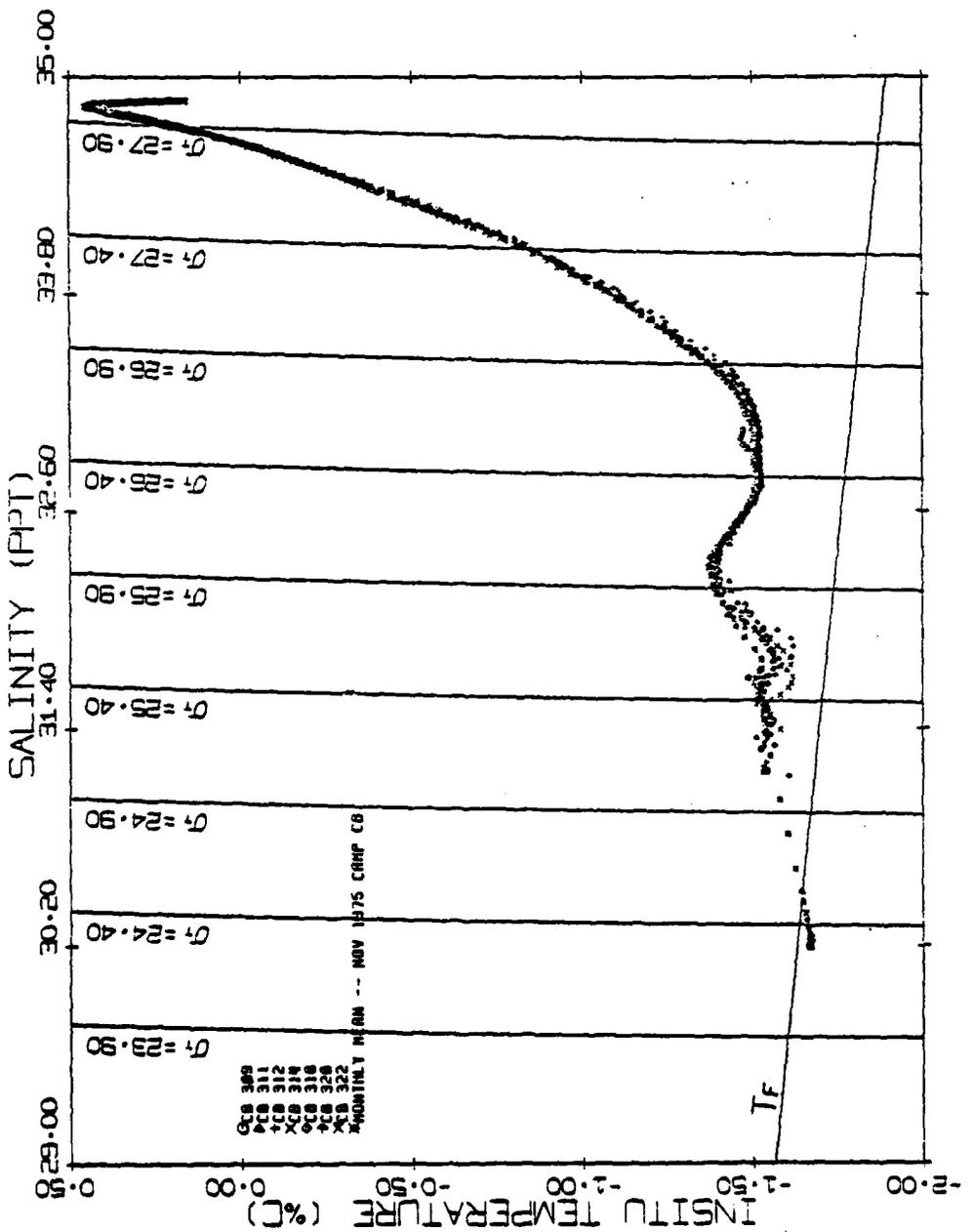

AD-A098 170
LAMONT-DOHERTY GEOLOGICAL OBSERVATORY PALISADES NY
F/G 8/3
EDDIES OF THE WESTERN ARCTIC OCEAN - THEIR CHARACTERISTICS AND --ETC(U)
MAR 81 T O MANLEY
N00014-76-C-0004
UNCLASSIFIED
LDGO-CU-1-81
NL
4 OF 5
AD A

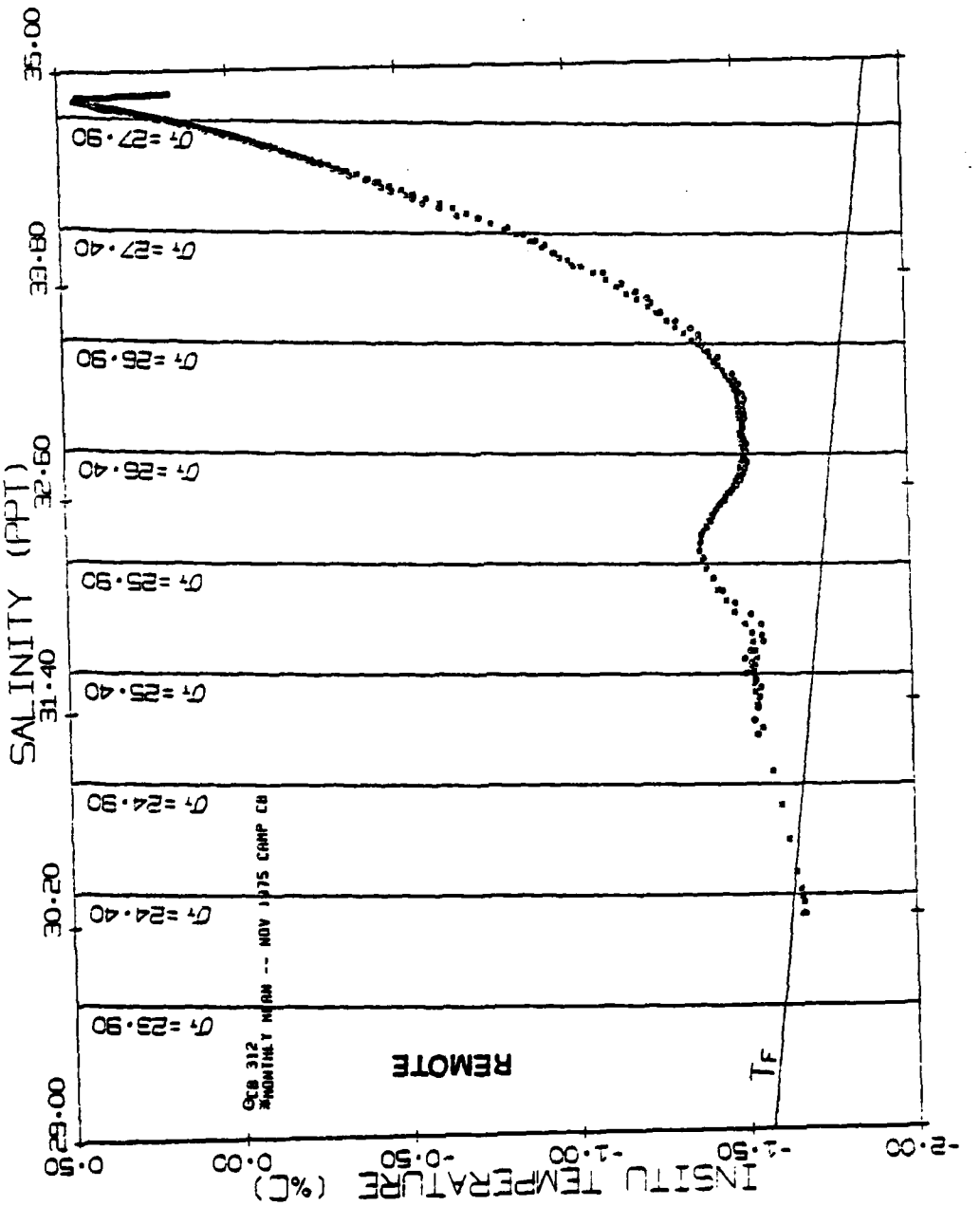

1.0
1.1
1.25
1.4
1.6
1.8
2.0
2.2
2.5
2.8
3.2
3.6
4.0
MICROCOPY RESOLUTION TEST CHART

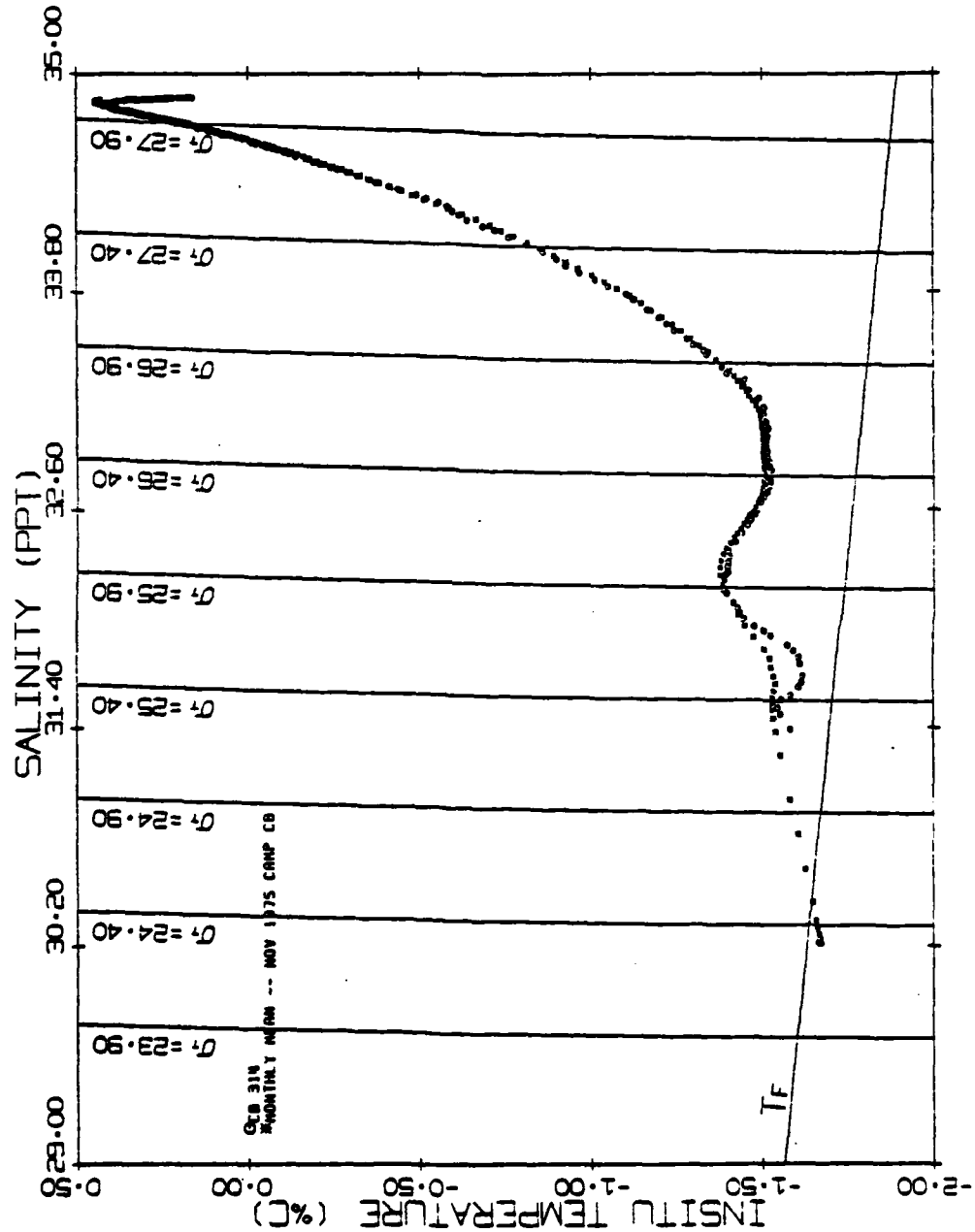

SALINITY (PPT)
35.00
33.80
32.60
31.40
30.20
29.00
σt =27.90
σt =27.40
σt =26.90
σt =26.40
σt =25.90
σt =25.40
σt =24.90
σt =24.40
σt =23.90
OCT 1975 CORP CD
MONTHLY MEAN
PCB 223
PCB 221
INSITU TEMPERATURE (°C)
0.50
0.00
-0.50
-1.00
-1.50
-2.00
T_F

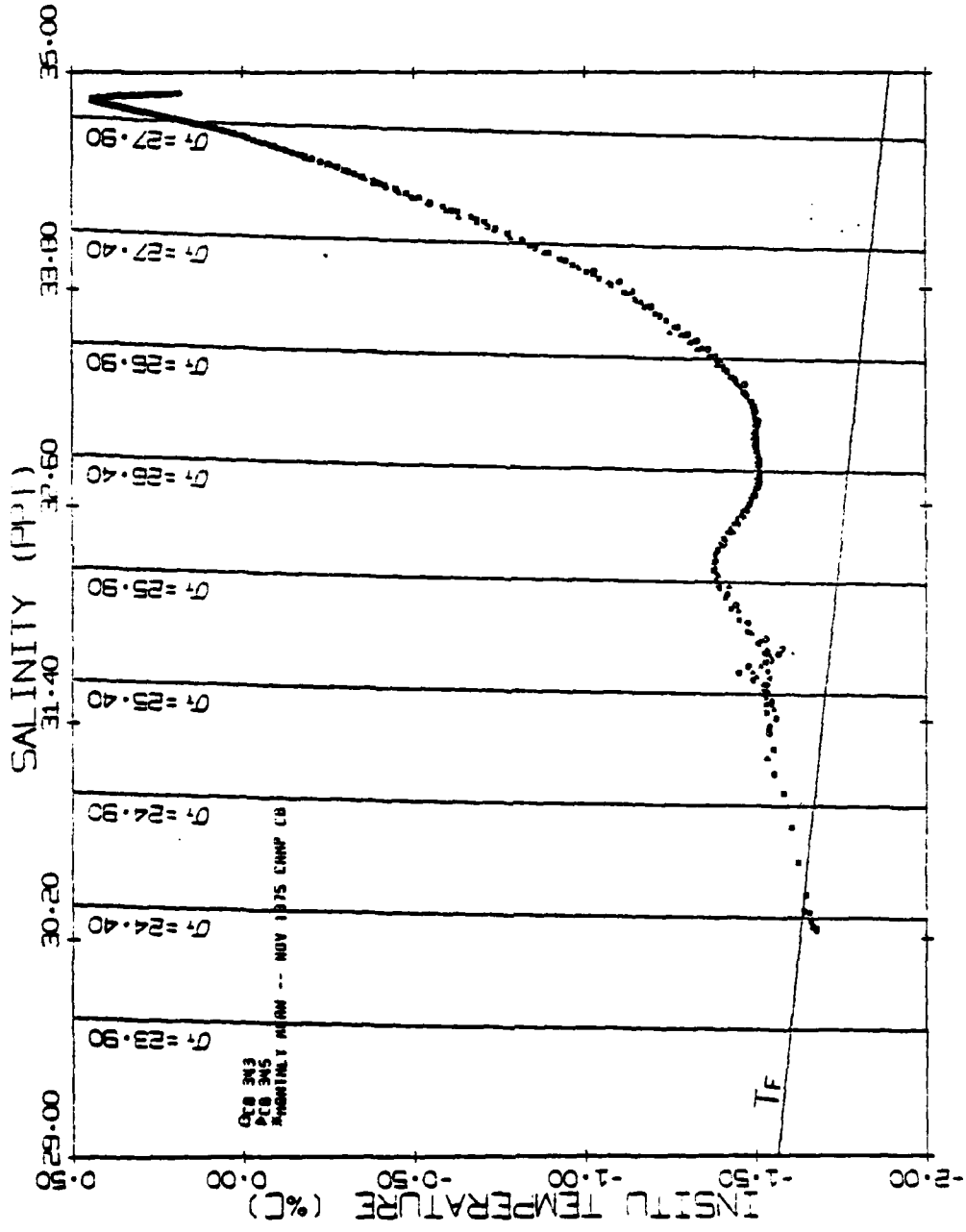

SALINITY (PPT)
35.00
33.80
32.60
31.40
30.20
29.00
σt =27.90
σt =27.40
σt =26.90
σt =26.40
σt =25.90
σt =25.40
σt =24.90
σt =24.40
σt =23.90
Stn 289
*MONTHLY MEAN -- OCT 1975 CAMP LB
T_F
0.50
0.00
-0.50
-1.00
-1.50
-2.00
INSITU TEMPERATURE (°C)

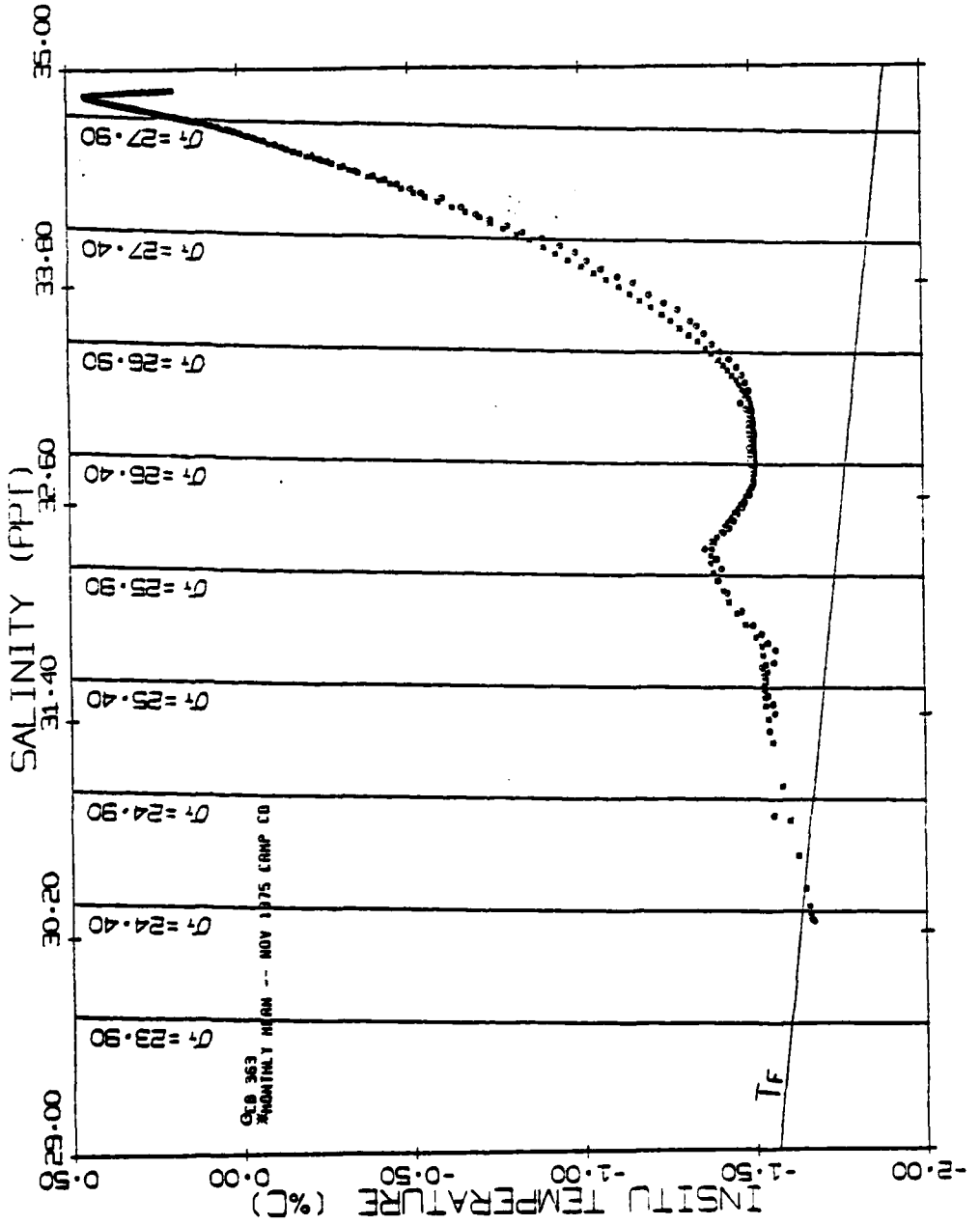

SALINITY (PPT)
INSITU TEMPERATURE (°C)
35.00
30.80
30.60
30.40
30.20
30.00
29.80
29.50
0.00
-0.50
-1.00
-1.50
-2.00
σt =27.90
σt =27.40
σt =26.90
σt =26.40
σt =25.90
σt =25.40
σt =24.90
σt =24.40
σt =23.90
T_F

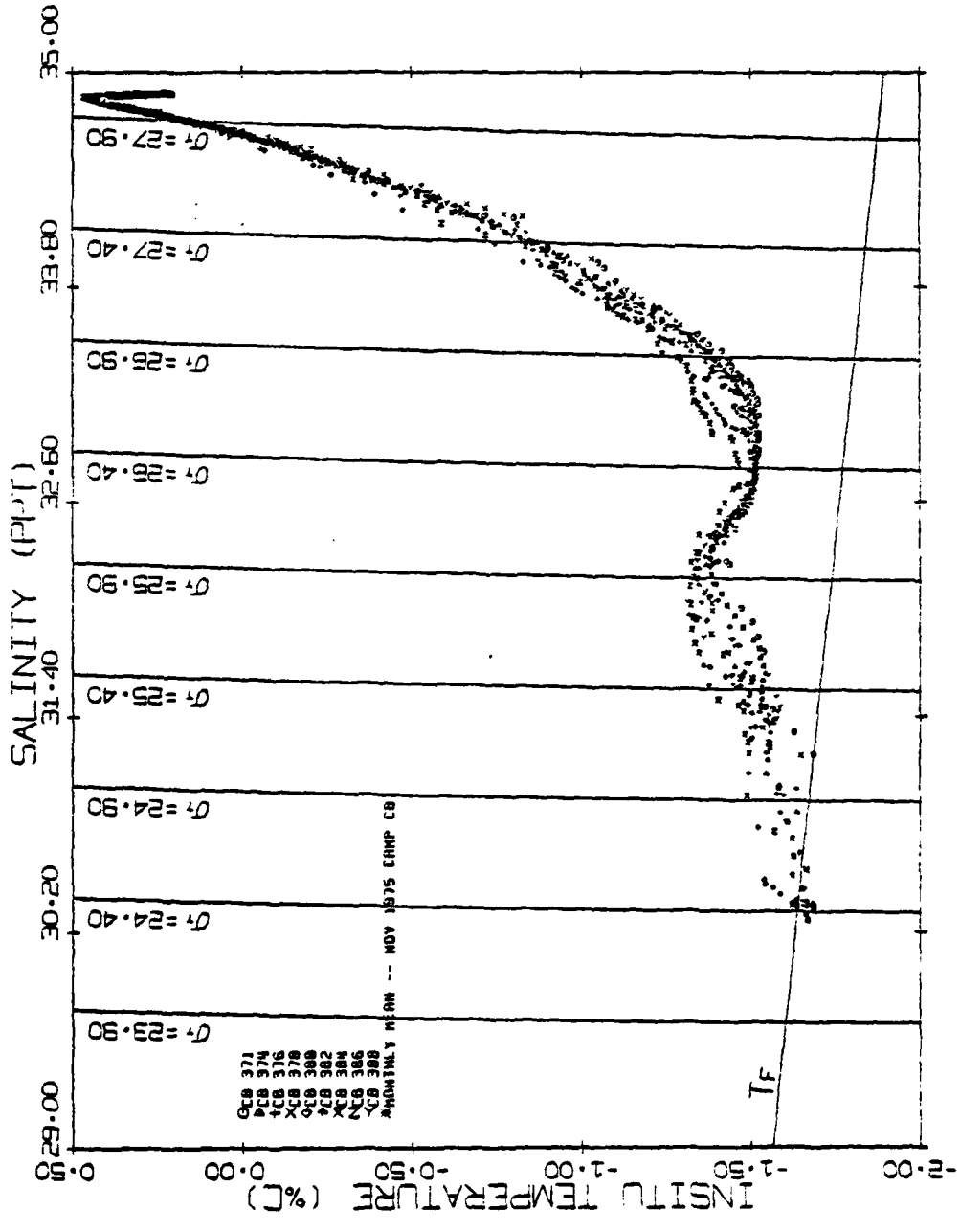

IN SITU TEMPERATURE (°C)
0.50
0.00
-0.50
-1.00
-1.50
-2.00
SALINITY (PPT)
29.00
30.20
31.40
32.60
33.80
35.00
σt =23.90
σt =24.40
σt =24.90
σt =25.40
σt =25.90
σt =26.40
σt =26.90
σt =27.40
σt =27.90
T_F
CB 309
CB 311
CB 312
CB 314
CB 318
CB 320
CB 322
MONTHLY MEAN -- NOV 1975 CRMP C6

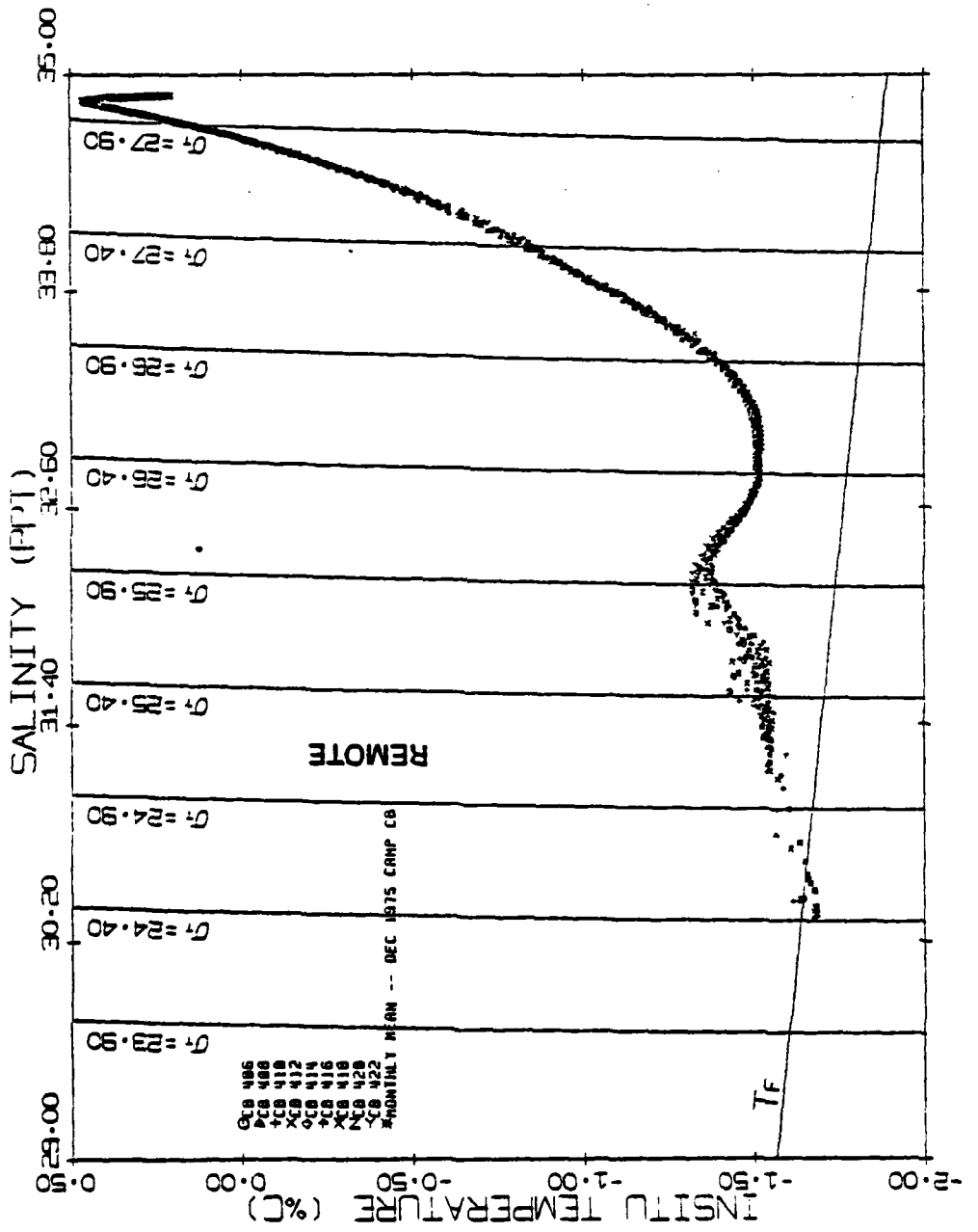

SALINITY (PPT)
35.00
33.80
32.60
31.40
30.20
29.00
σ_t =27.90
σ_t =27.40
σ_t =26.90
σ_t =26.40
σ_t =25.90
σ_t =25.40
σ_t =24.90
σ_t =24.40
σ_t =23.90
REMOTE
T_F
0.50
0.03
-0.50
-1.00
-1.50
-2.00
IN SITU TEMPERATURE (°C)

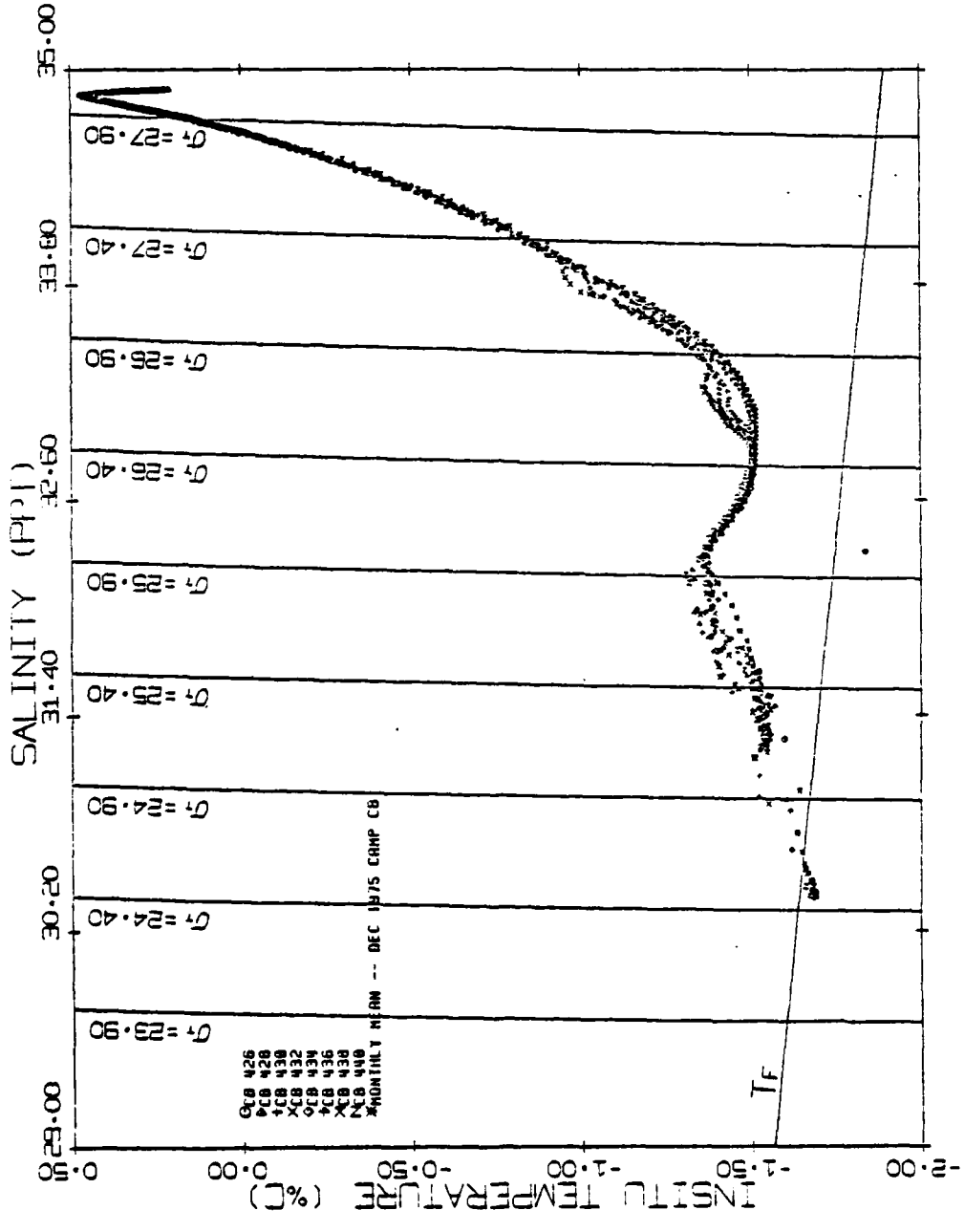

SALINITY (PPT)
35.00
33.80
32.60
31.40
30.20
29.00
σt =27.90
σt =27.40
σt =26.90
σt =26.40
σt =25.90
σt =25.40
σt =24.90
σt =24.40
σt =23.90
TF
0.50
0.00
-0.50
-1.00
-1.50
-2.00
INSITU TEMPERATURE (°C)

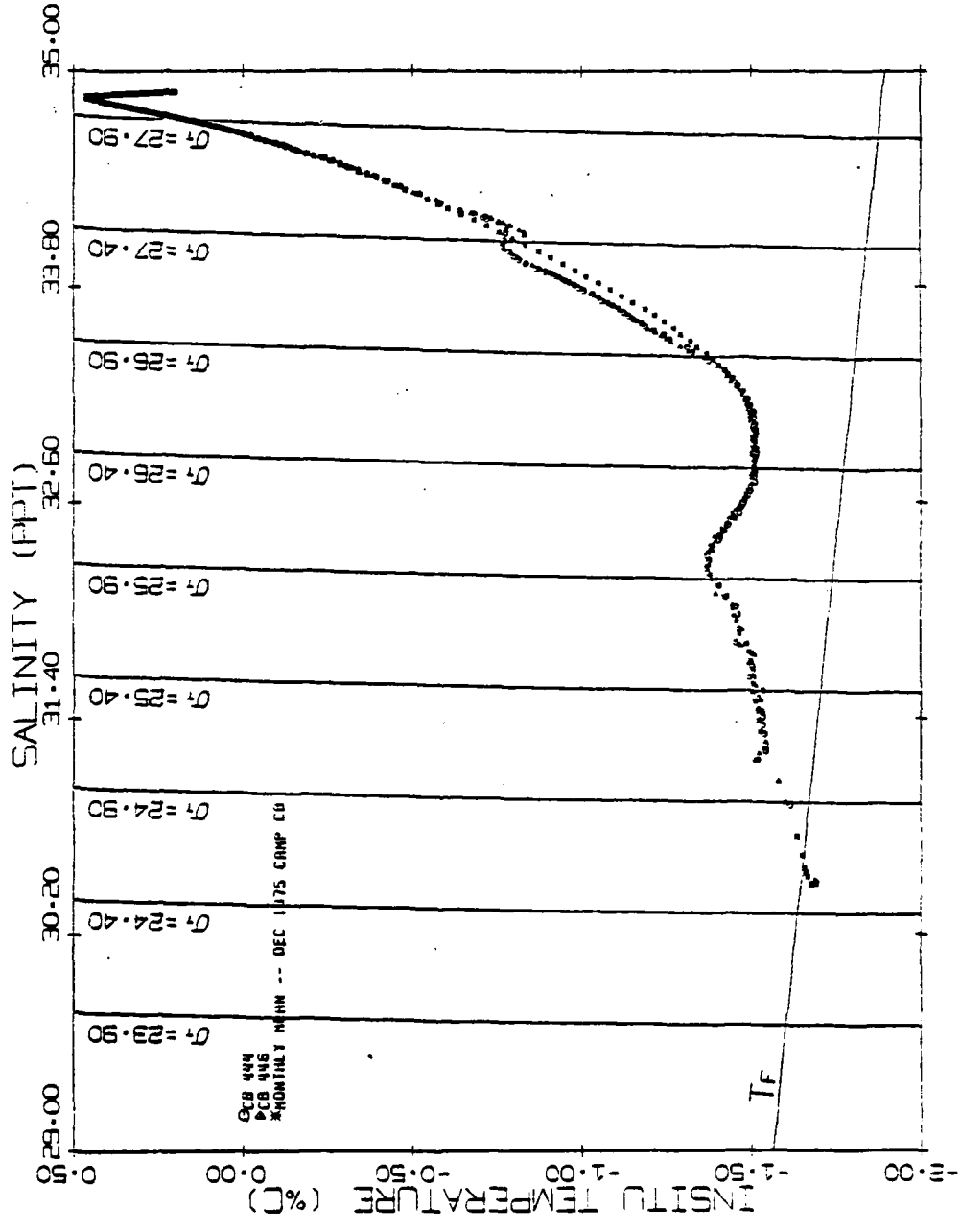

SALINITY (PPT)
35.00
33.30
32.60
31.40
30.20
29.00
σt =27.90
σt =27.40
σt =26.90
σt =26.40
σt =25.90
σt =25.40
σt =24.90
σt =24.40
σt =23.90
IN SITU TEMPERATURE (°C)
0.50
0.00
-0.50
-1.00
-1.50
-2.00
T_F

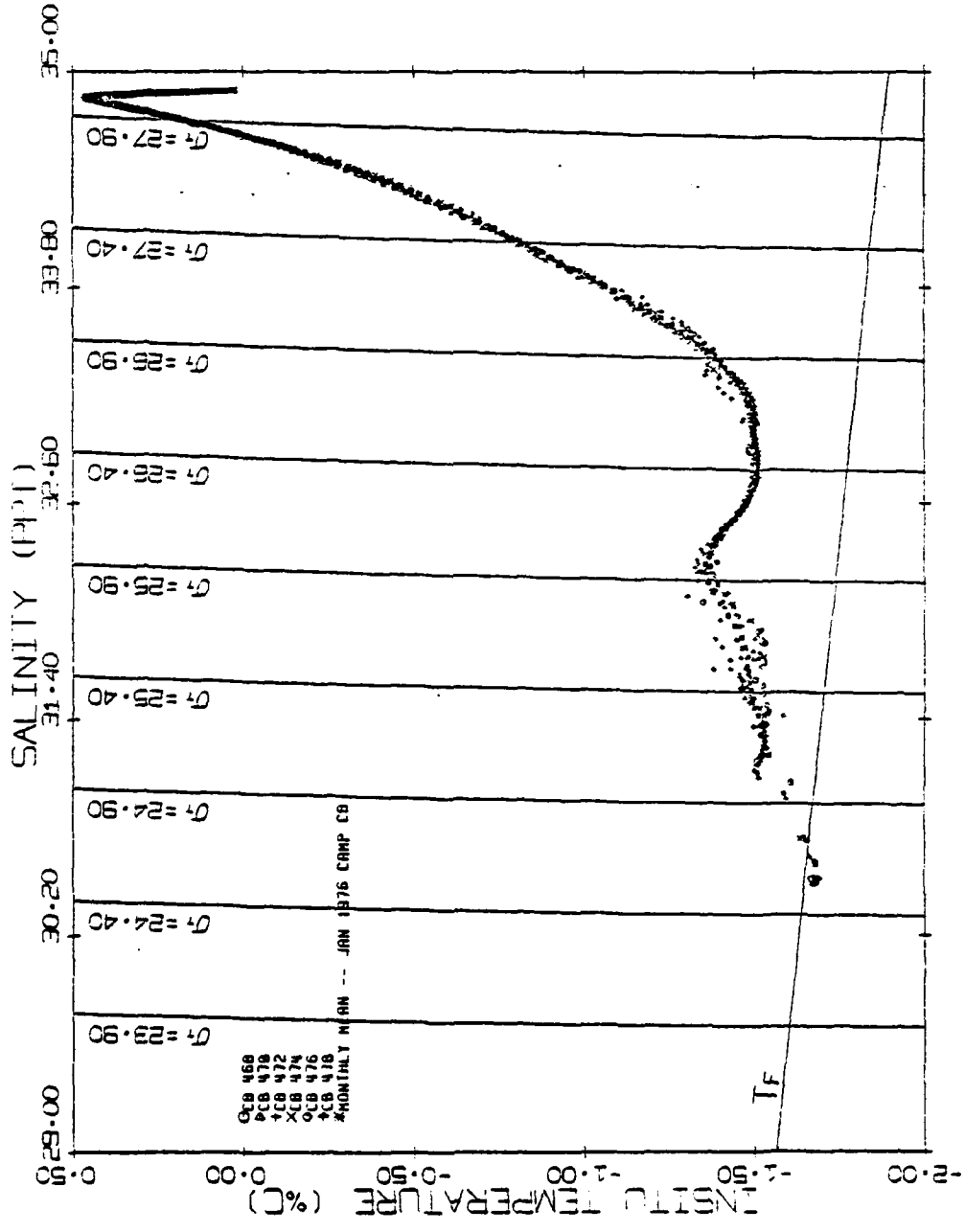

SALINITY (PPT)
35.00
33.80
32.60
31.40
30.20
29.00
σt =27.90
σt =27.40
σt =26.90
σt =26.40
σt =25.90
σt =25.40
σt =24.90
σt =24.40
σt =23.90
Tf
0.50
0.00
-0.50
-1.00
-1.50
-2.00
INSITU TEMPERATURE (°C)
CTD 363
MONTHLY MEAN -- NOV 1975 CRNP CO

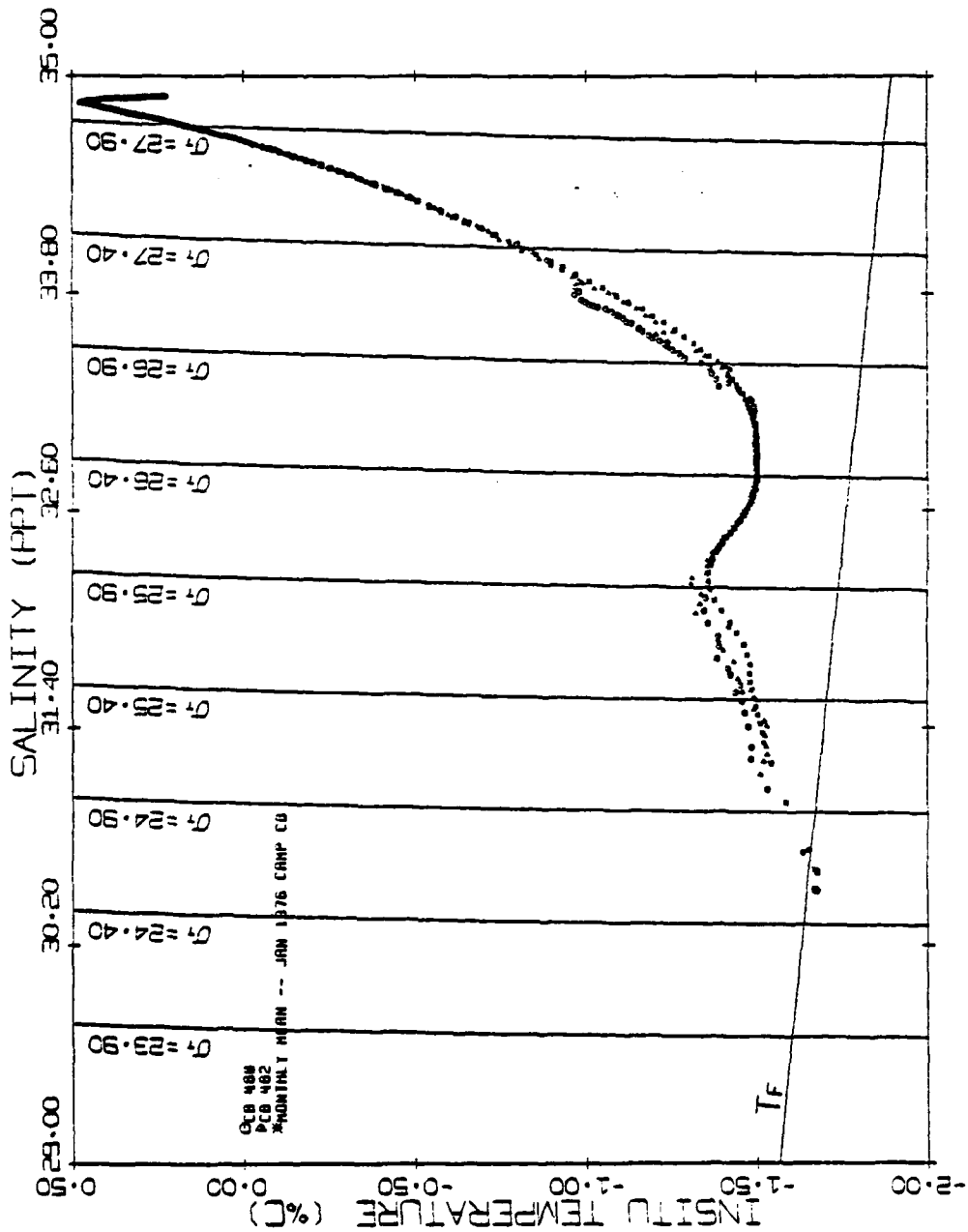

SALINITY (PPT)
35.00
33.80
32.60
31.40
30.20
29.00
INSITU TEMPERATURE (°C)
0.50
0.00
-0.50
-1.00
-1.50
-2.00
σt =27.90
σt =27.40
σt =26.90
σt =26.40
σt =25.90
σt =25.40
σt =24.90
σt =24.40
σt =23.90
T_F
CTD 371
CTD 374
CTD 376
CTD 378
CTD 380
CTD 382
CTD 384
CTD 386
CTD 388
MONTHLY MEAN -- NOV 1975 CAMP CB

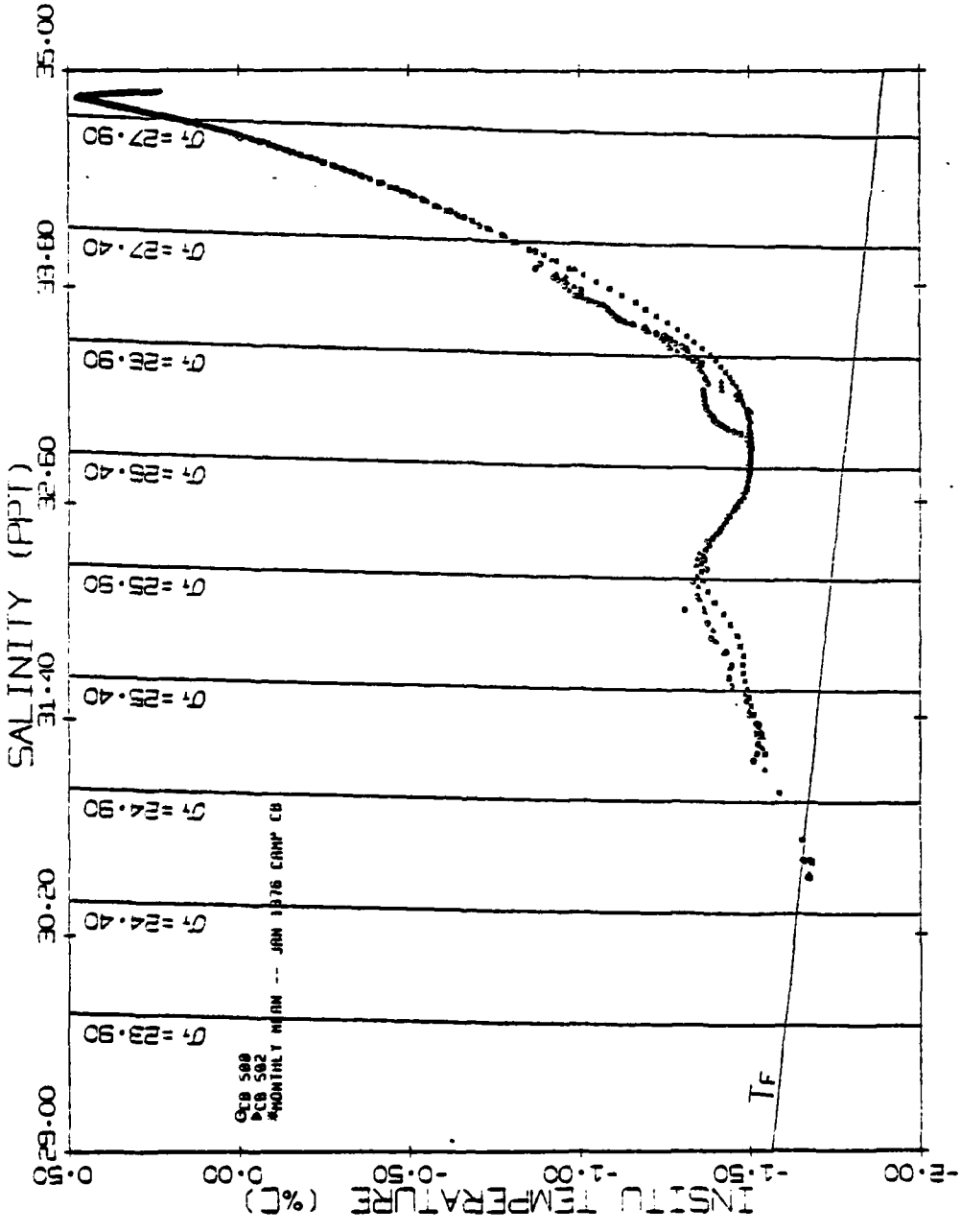

INSITU TEMPERATURE (°C)
0.50
0.00
-0.50
-1.00
-1.50
-2.00
SALINITY (PPT)
29.00
30.20
31.40
32.60
33.80
35.00
σt =23.90
σt =24.40
σt =24.90
σt =25.40
σt =25.90
σt =26.40
σt =26.90
σt =27.40
σt =27.90
REMOTE
Tf
*MONTHLY MEAN -- DEC 1975 CAMP CB

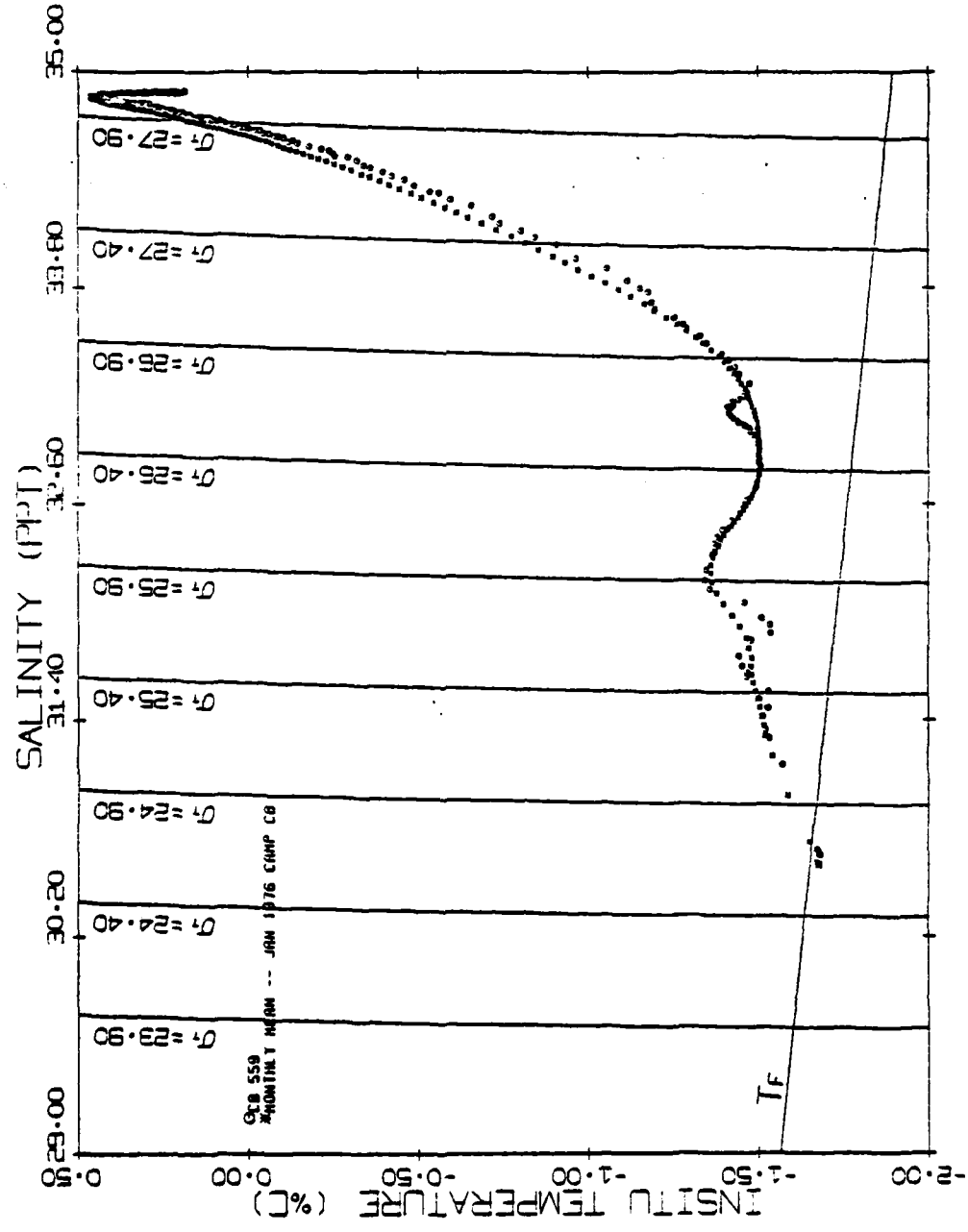

SALINITY (PPT)
INSITU TEMPERATURE (°C)
35.00
33.80
32.60
31.40
30.20
29.00
0.50
0.00
-0.50
-1.00
-1.50
-2.00
σt =27.90
σt =27.40
σt =26.90
σt =26.40
σt =25.90
σt =25.40
σt =24.90
σt =24.40
σt =23.90
T_F
CTD 426
CTD 428
CTD 430
CTD 432
CTD 434
CTD 436
CTD 438
CTD 440
MONTHLY MEAN -- DEC 1975 CAMP CB

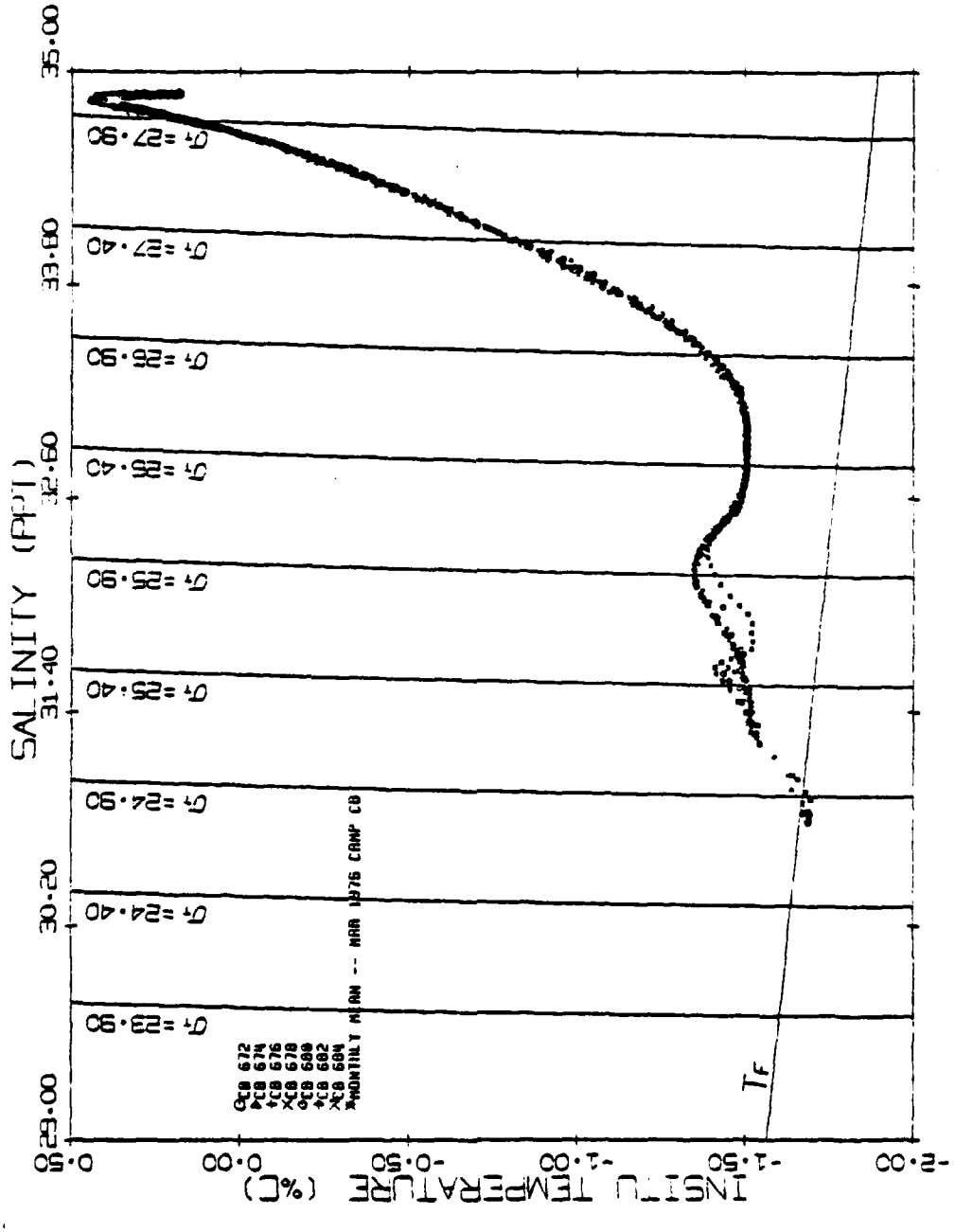

35.00
33.80
32.60
31.40
30.20
29.00
SALINITY (PPT)
σt =27.90
σt =27.40
σt =26.90
σt =26.40
σt =25.90
σt =25.40
σt =24.90
σt =24.40
σt =23.90
0.50
0.00
-0.50
-1.00
-1.50
-2.00
INSITU TEMPERATURE (°C)
T_F
PCB 444
PCB 446
*MONTHLY MEAN -- DEC 1975 CAMP CO

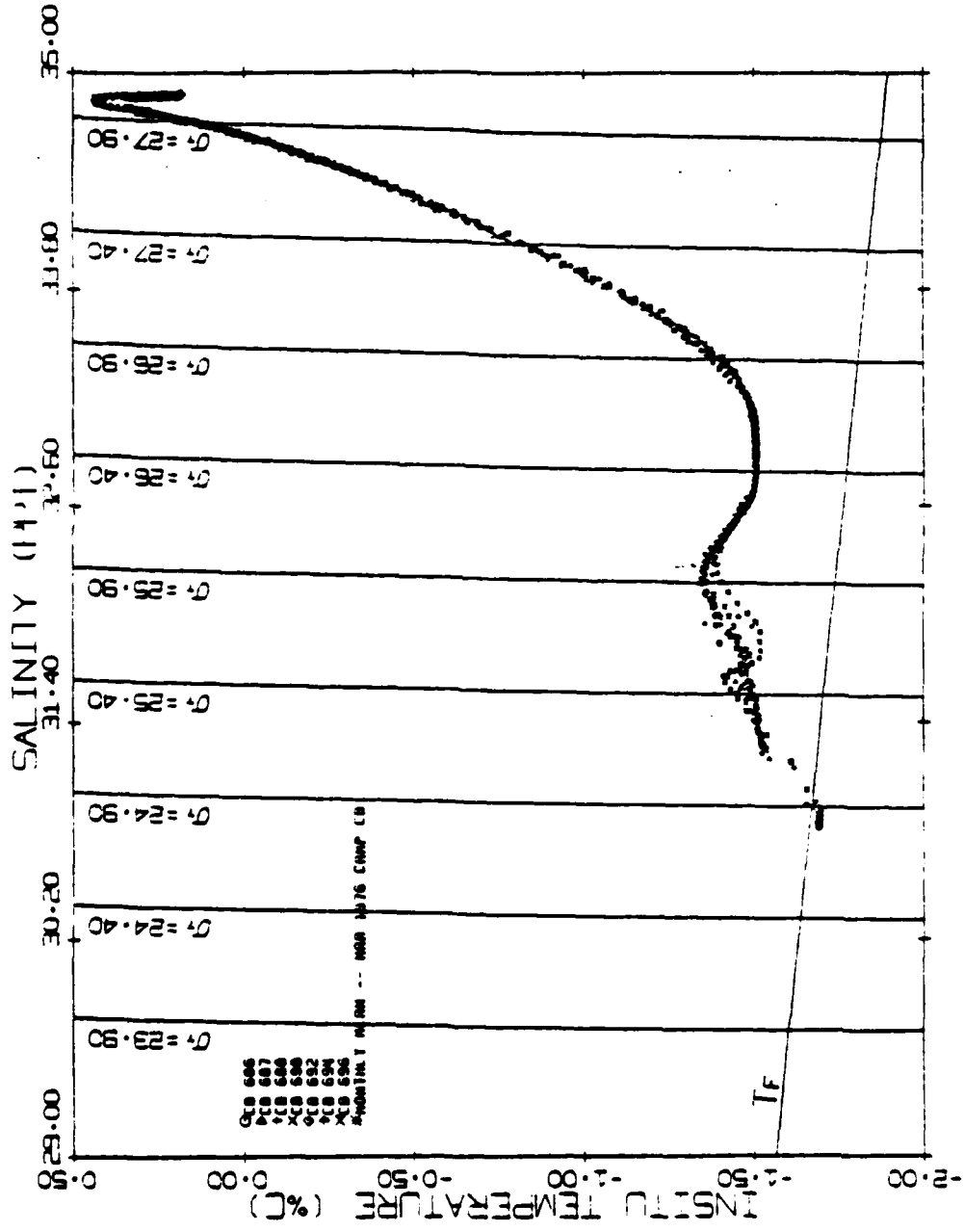

SALINITY (PPT)
29.00
30.20
31.40
32.60
33.80
35.00
σt =23.90
σt =24.40
σt =24.90
σt =25.40
σt =25.90
σt =26.40
σt =26.90
σt =27.40
σt =27.90
IN SITU TEMPERATURE (°C)
0.50
0.00
-0.50
-1.00
-1.50
-2.00
Tf
CB 468
CB 470
CB 472
CB 474
CB 476
CB 478
MONTHLY MEAN -- JAN 1976 CAMP CB

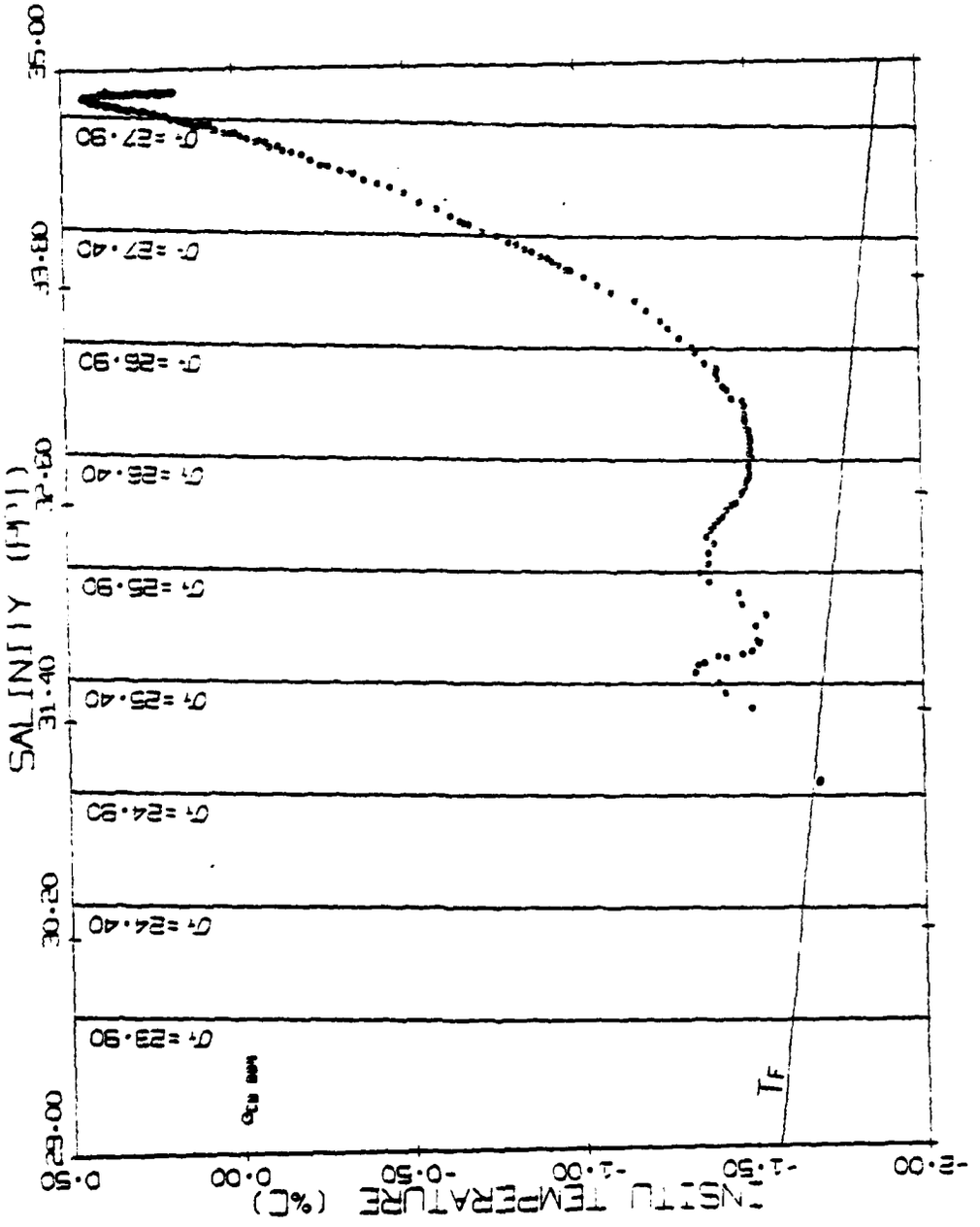

35.00
33.80
32.60
31.40
30.20
29.00
SALINITY (PPT)
0.50
0.00
-0.50
-1.00
-1.50
-2.00
IN SITU TEMPERATURE (°C)
σt =27.90
σt =27.40
σt =26.90
σt =26.40
σt =25.90
σt =25.40
σt =24.90
σt =24.40
σt =23.90
T_F
QCB 488
PCB 482
*MONTHLY MEAN -- JAN 1976 CAMP CO

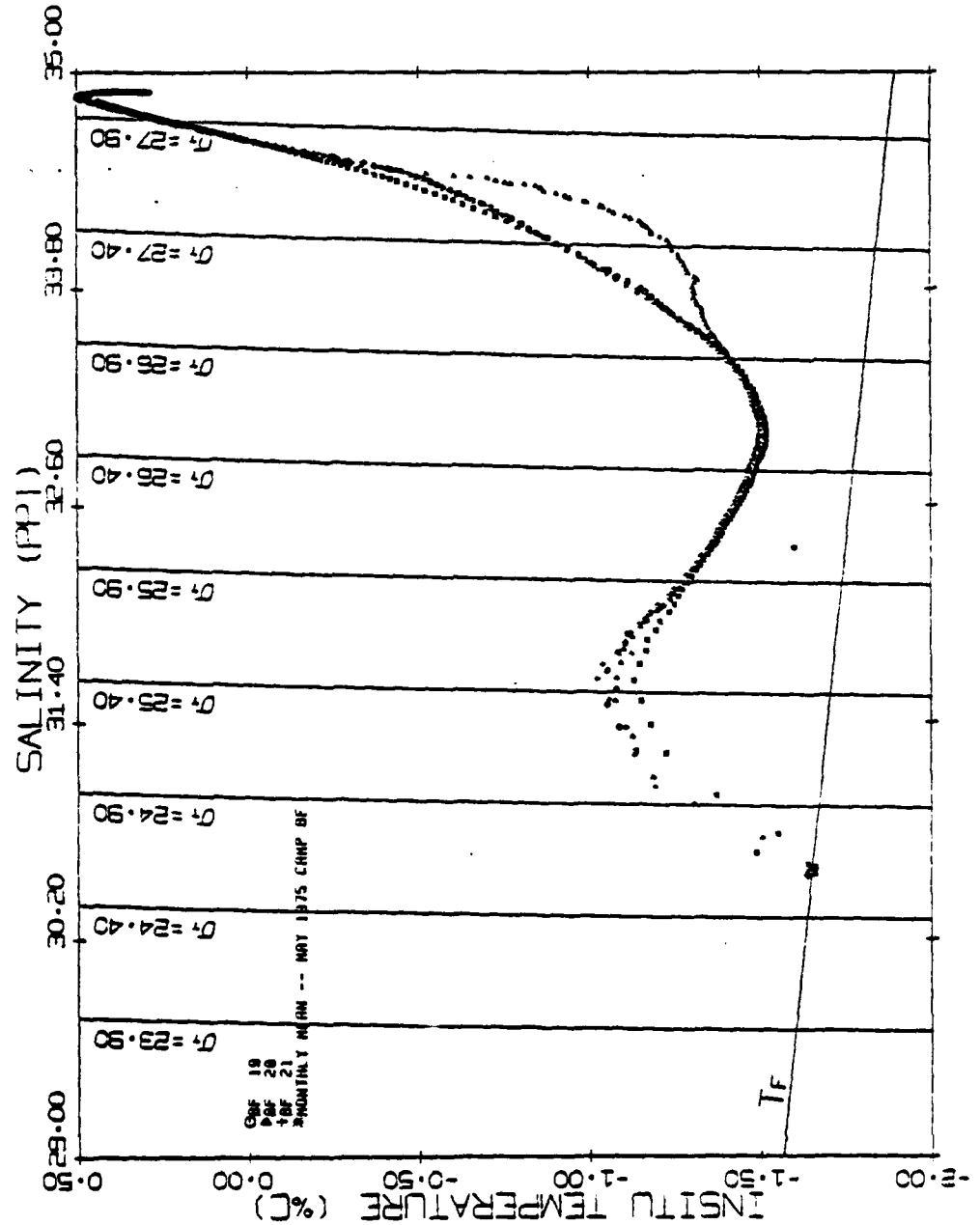

SALINITY (PPT)
35.00
33.80
32.60
31.40
30.20
29.00
σt =27.90
σt =27.40
σt =26.90
σt =26.40
σt =25.90
σt =25.40
σt =24.90
σt =24.40
σt =23.90
TF
INSITU TEMPERATURE (°C)
0.50
0.00
-0.50
-1.00
-1.50
-2.00
PCB 589
PCB 582
*MONTHLY MEAN -- JAN 1976 CAMP CB

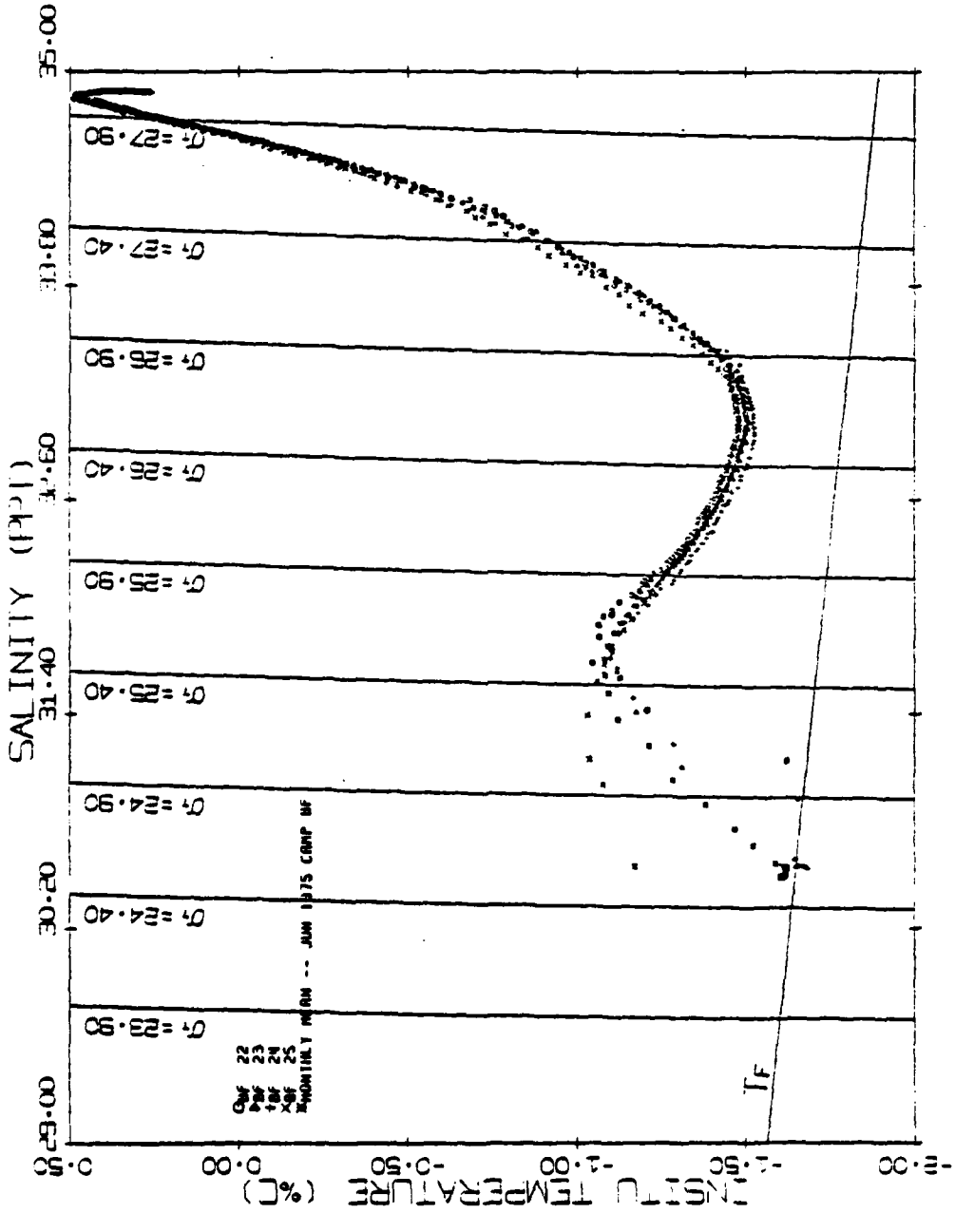

SALINITY (PPT)
INSITU TEMPERATURE (°C)
35.00
33.60
32.60
31.40
30.20
29.00
0.50
0.00
-0.50
-1.00
-1.50
-2.00
σt =27.90
σt =27.40
σt =26.90
σt =26.40
σt =25.90
σt =25.40
σt =24.90
σt =24.40
σt =23.90
CTD 559
MONTHLY MEAN -- JAN 1976 CAMP C8
T_F

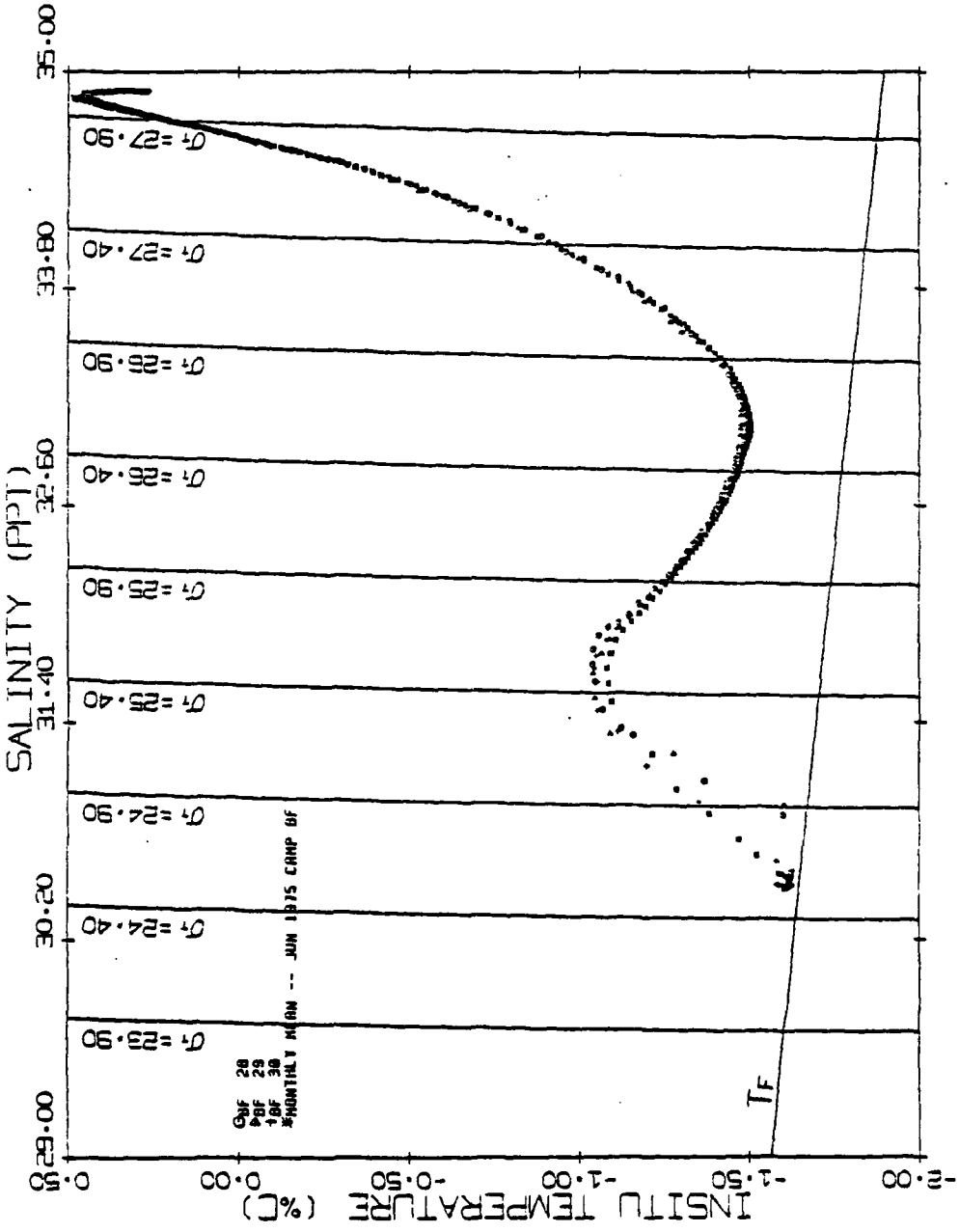

SALINITY (PPT)
35.00
33.80
32.60
31.40
30.20
29.00
σt =27.90
σt =27.40
σt =26.90
σt =26.40
σt =25.90
σt =25.40
σt =24.90
σt =24.40
σt =23.90
INSITU TEMPERATURE (°C)
0.50
0.00
-0.50
-1.00
-1.50
-2.00
Tf
MONTHLY MEAN -- MAR 1976 CRNF CB
CTD 632
CTD 674
CTD 676
CTD 678
CTD 680
CTD 682
CTD 684

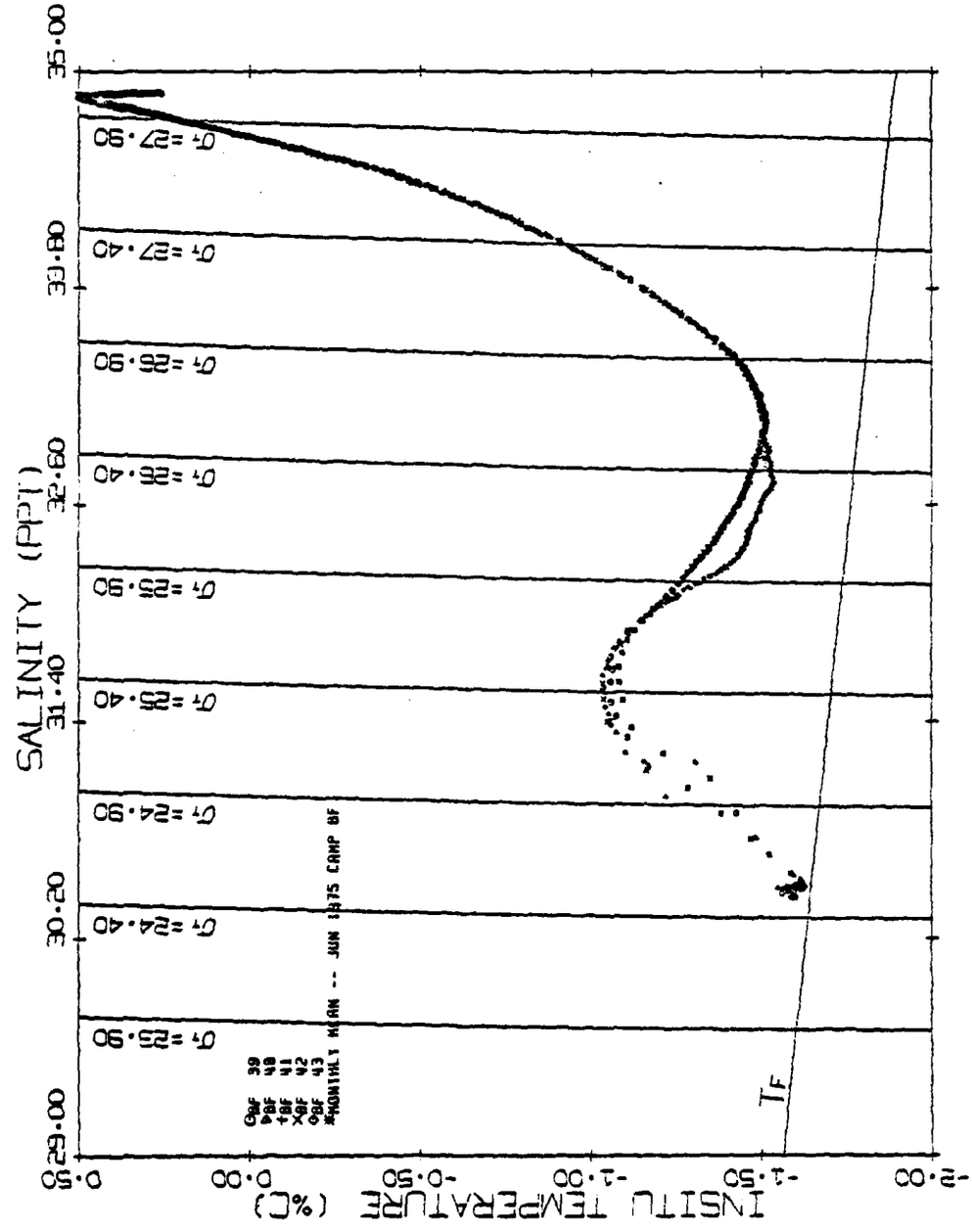

SALINITY (PPT)
35.00
33.80
32.60
31.40
30.20
29.00
σt = 27.90
σt = 27.40
σt = 26.90
σt = 26.40
σt = 25.90
σt = 25.40
σt = 24.90
σt = 24.40
σt = 23.90
T_F
0.50
0.00
-0.50
-1.00
-1.50
-2.00
INSITU TEMPERATURE (°C)

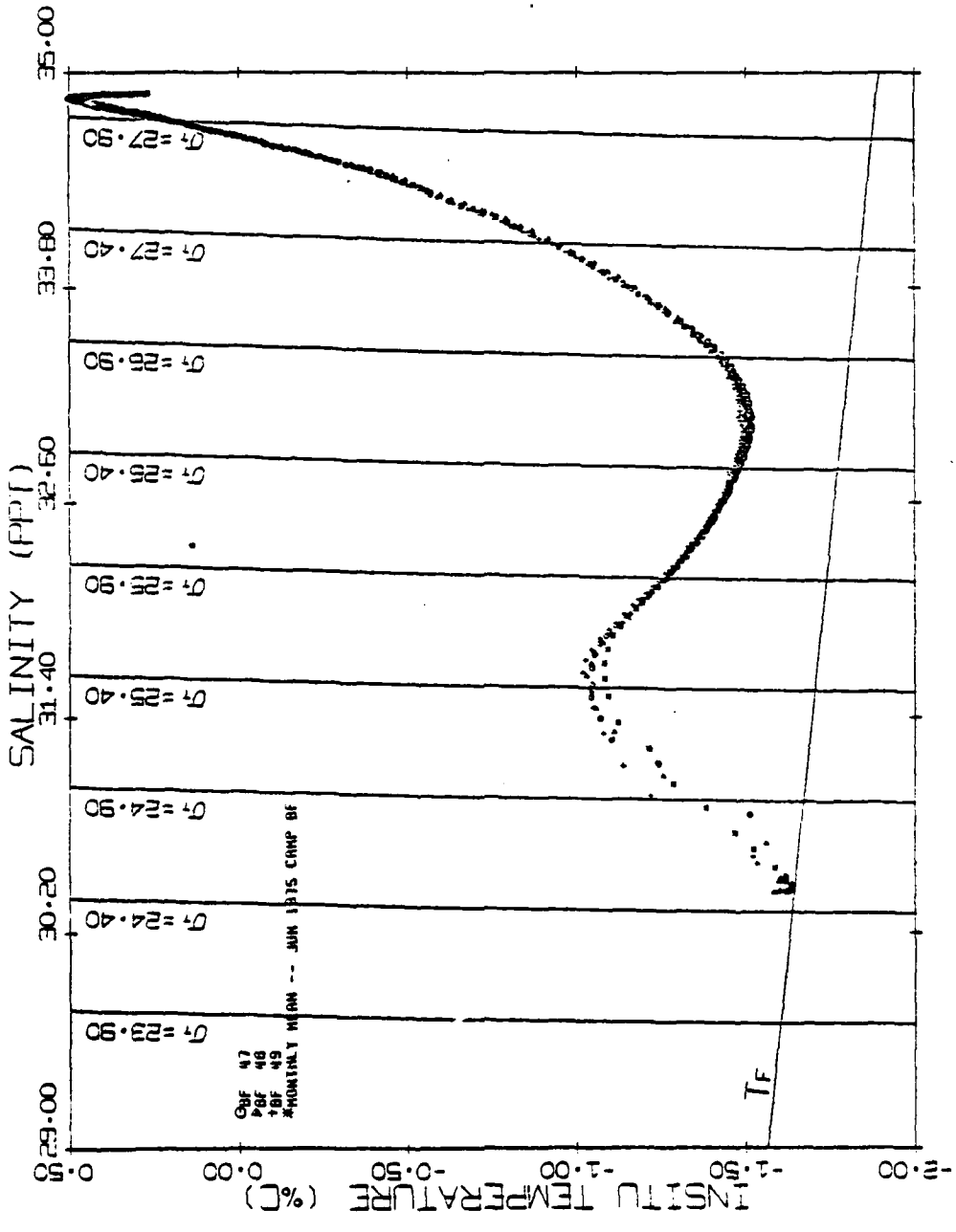

SALINITY (PPT)
35.00
33.60
32.80
32.00
31.40
30.20
29.00
σt =27.90
σt =27.40
σt =26.90
σt =26.40
σt =25.90
σt =25.40
σt =24.90
σt =24.40
σt =23.90
T_F
0.50
0.00
-0.50
-1.00
-1.50
-2.00
INSITU TEMPERATURE (°C)

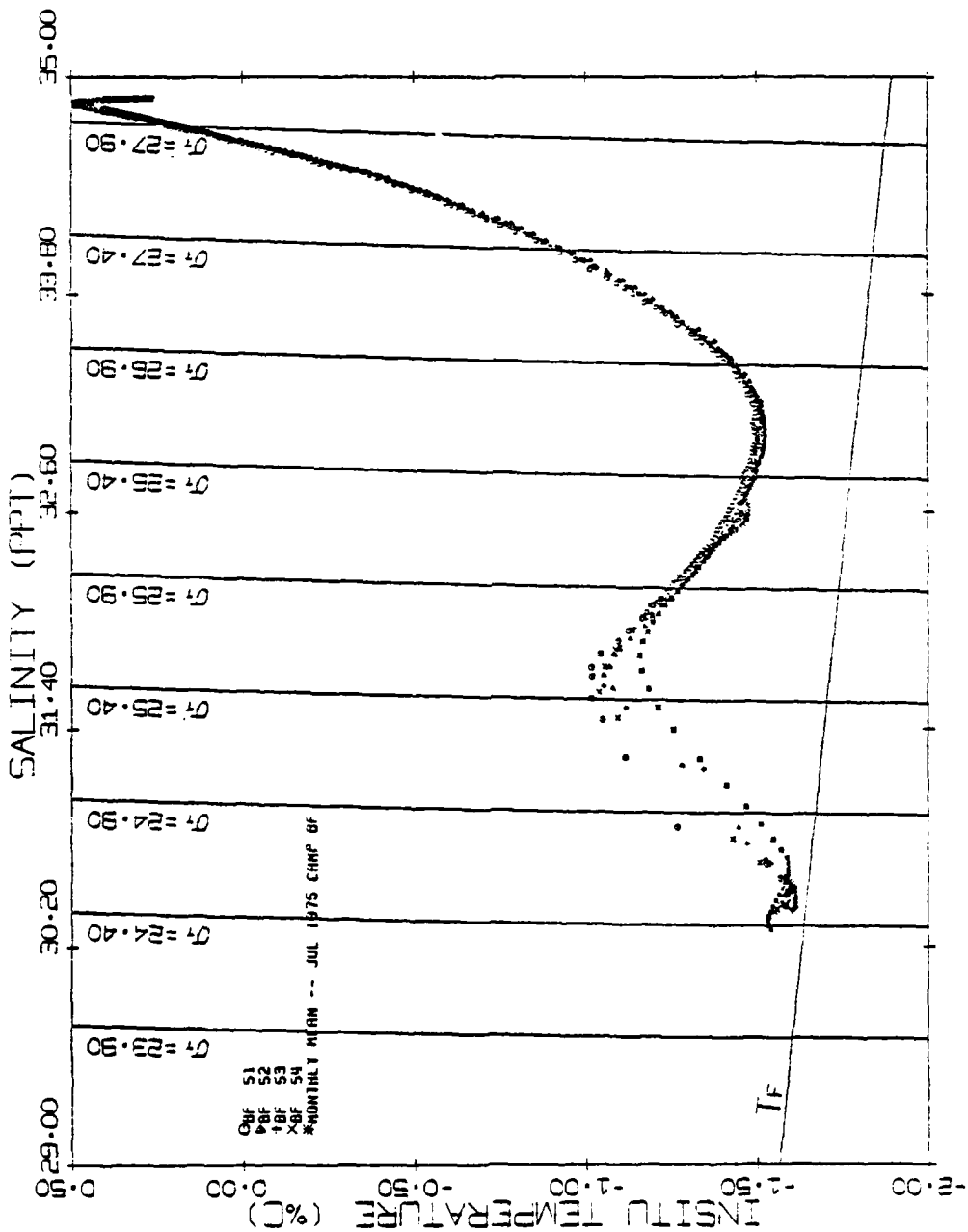

SALINITY (PPT)
35.00
33.80
32.60
31.40
30.20
29.00
INSITU TEMPERATURE (°C)
0.50
0.00
-0.50
-1.00
-1.50
-2.00
σt =27.90
σt =27.40
σt =26.90
σt =26.40
σt =25.90
σt =25.40
σt =24.90
σt =24.40
σt =23.90
Tf
Obs 19
Ref 20
Bf 21
MONTHLY MEAN -- NOT 1975 CHMP BF

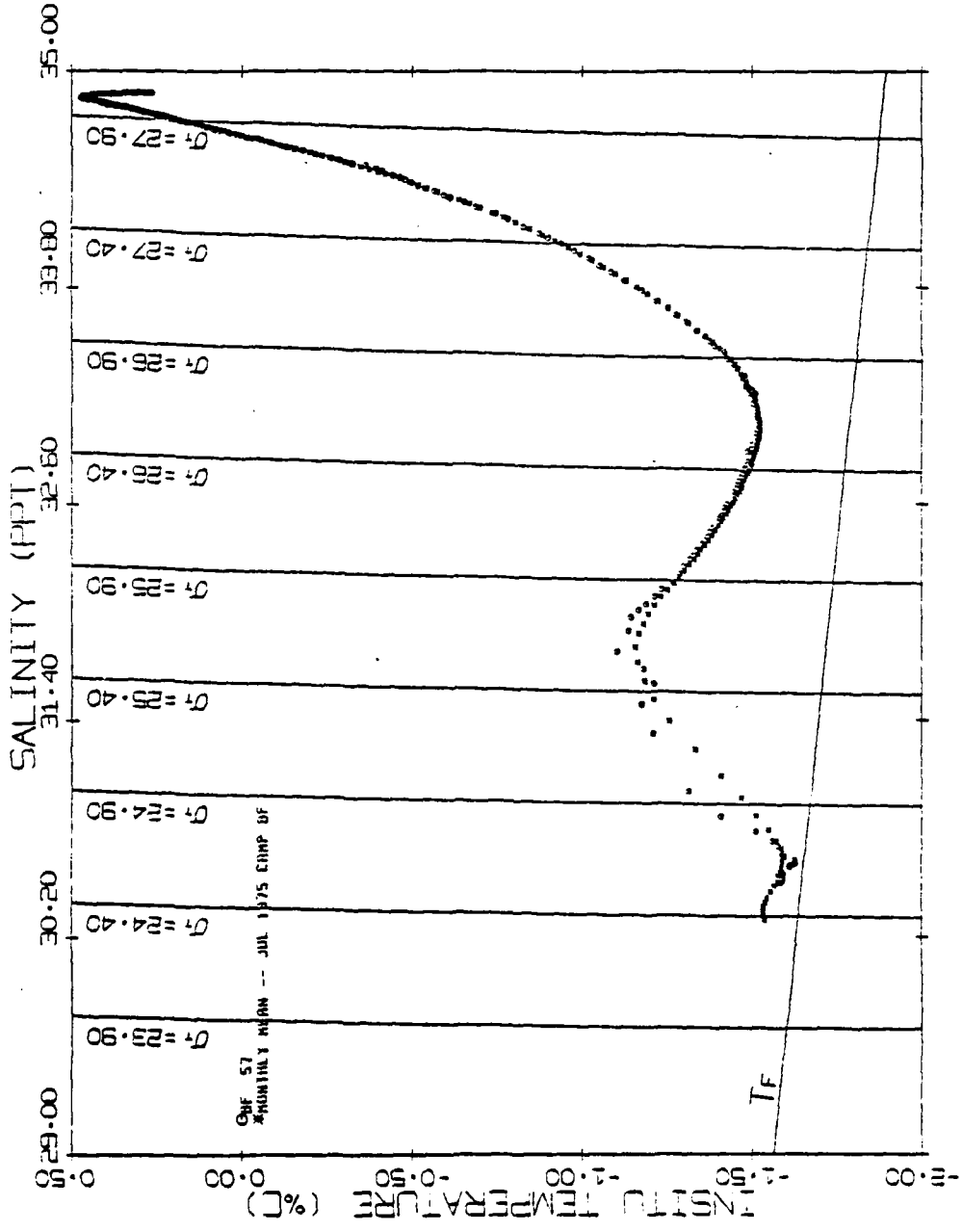

SALINITY (PPT)
35.00
33.00
31.60
31.40
30.20
29.00
σt =27.90
σt =27.40
σt =26.90
σt =26.40
σt =25.90
σt =25.40
σt =24.90
σt =24.40
σt =23.90
INSITU TEMPERATURE (°C)
0.50
0.00
-0.50
-1.00
-1.50
-2.00
T_F
ONF 22
ANF 23
XBF 24
XBF 25
MONTHLY MEAN -- JAN 1975 CORP MF

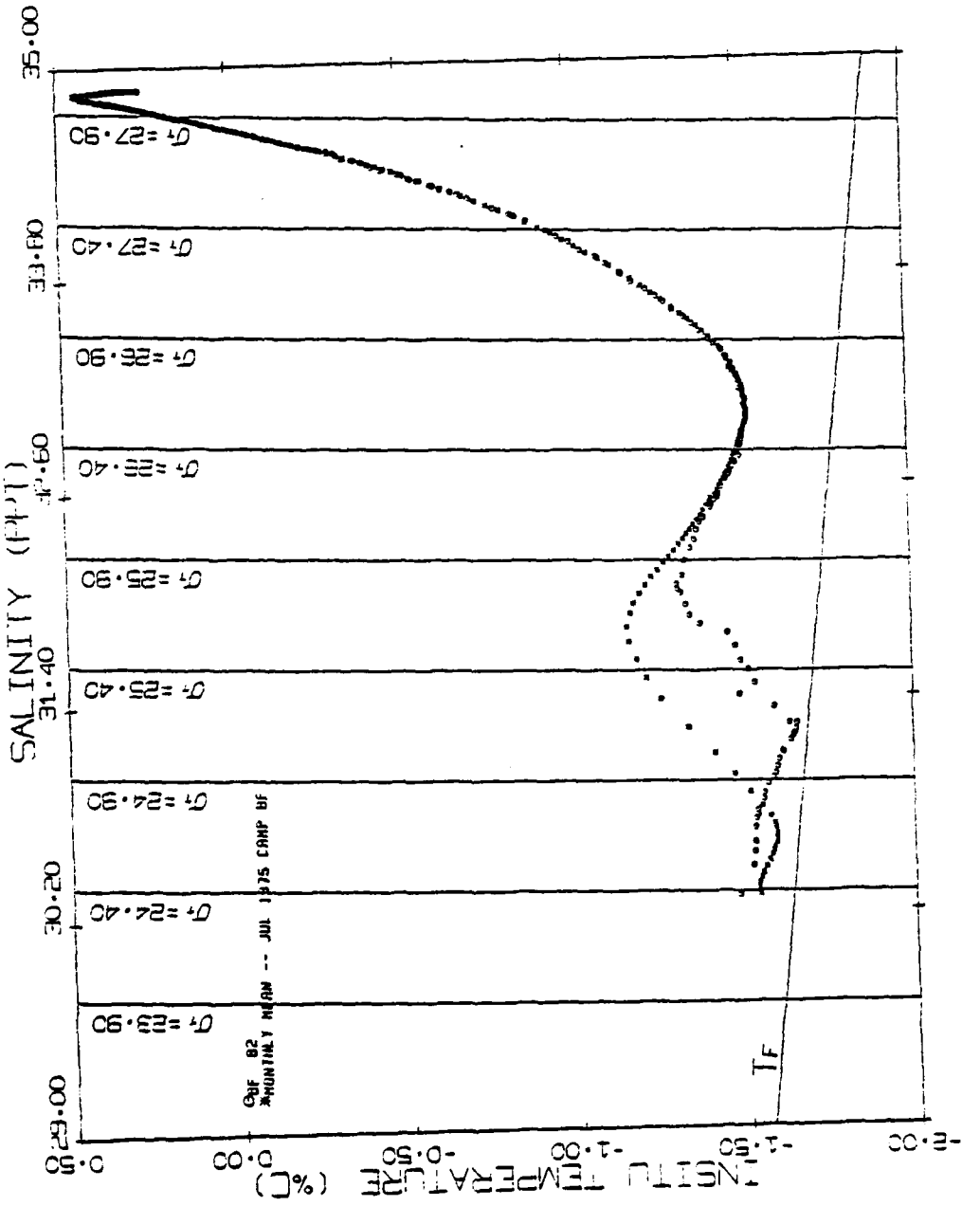

35.00
33.80
32.60
31.40
30.20
29.00
SALINITY (PPT)
σt =27.90
σt =27.40
σt =26.90
σt =26.40
σt =25.90
σt =25.40
σt =24.90
σt =24.40
σt =23.90
TF
0.50
0.00
-0.50
-1.00
-1.50
-2.00
INSITU TEMPERATURE (°C)
28 JUN 1975 CAMP BF
MONTHLY MEAN
BF 30
BF 29
BF 28

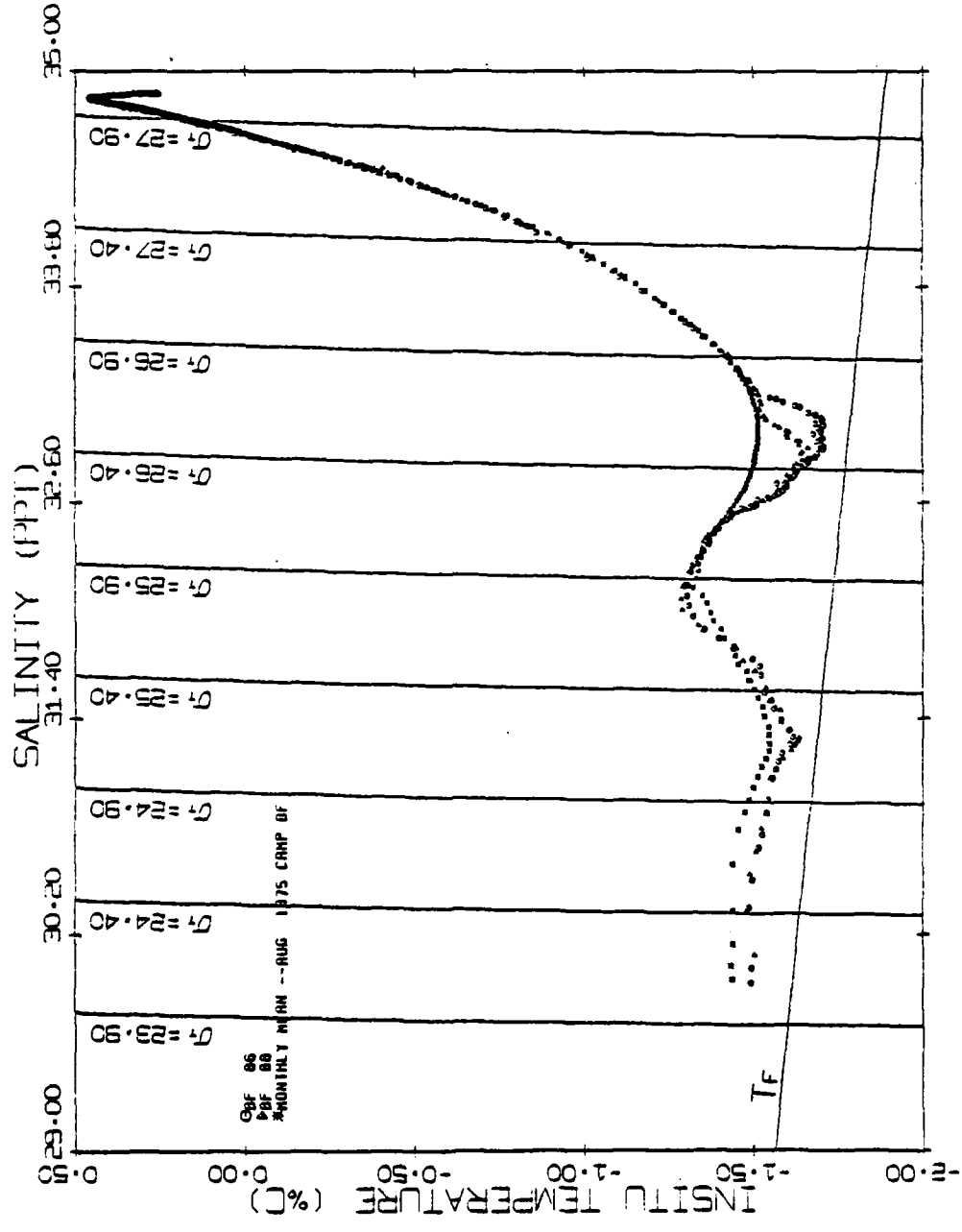

SALINITY (PPT)
INSITU TEMPERATURE (°C)
35.00
33.80
32.60
31.40
30.20
29.00
0.50
0.00
-0.50
-1.00
-1.50
-2.00
σt =27.90
σt =27.40
σt =26.90
σt =26.40
σt =25.90
σt =25.40
σt =24.90
σt =24.40
σt =25.90
TF
QBF 39
ΔBF 40
+BF 41
XBF 42
QBF 43
*MONTHLY MEAN -- JUN 1975 CAMP BF

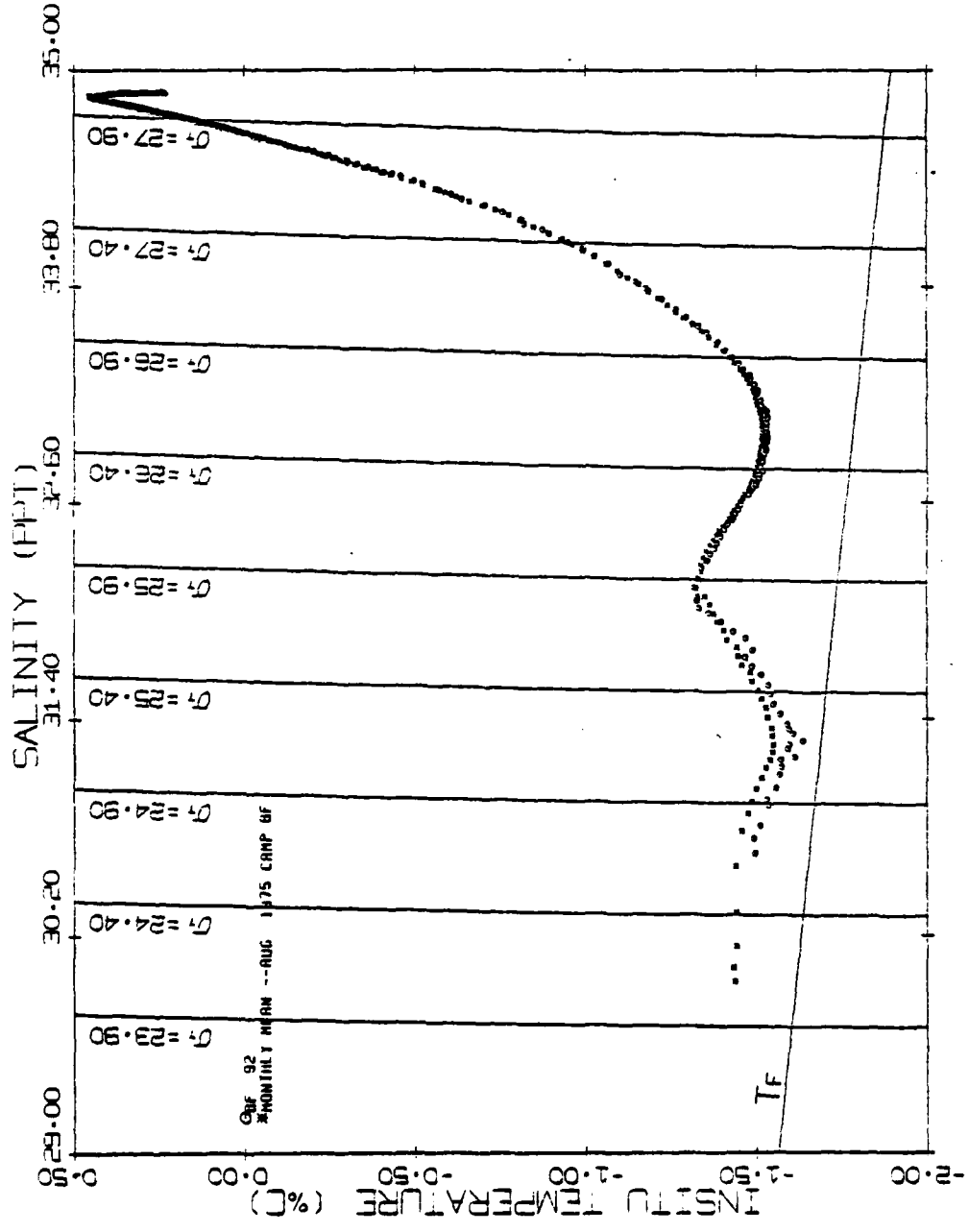

SALINITY (PPT)
IN SITU TEMPERATURE (°C)
35.00
33.80
32.60
31.40
30.20
29.00
0.50
0.00
-0.50
-1.00
-1.50
-2.00
σt =27.90
σt =27.40
σt =26.90
σt =26.40
σt =25.90
σt =25.40
σt =24.90
σt =24.40
σt =23.90
TF
BF 47
BF 48
BF 49
MONTHLY MEAN -- JAN 1975 CHNP BF

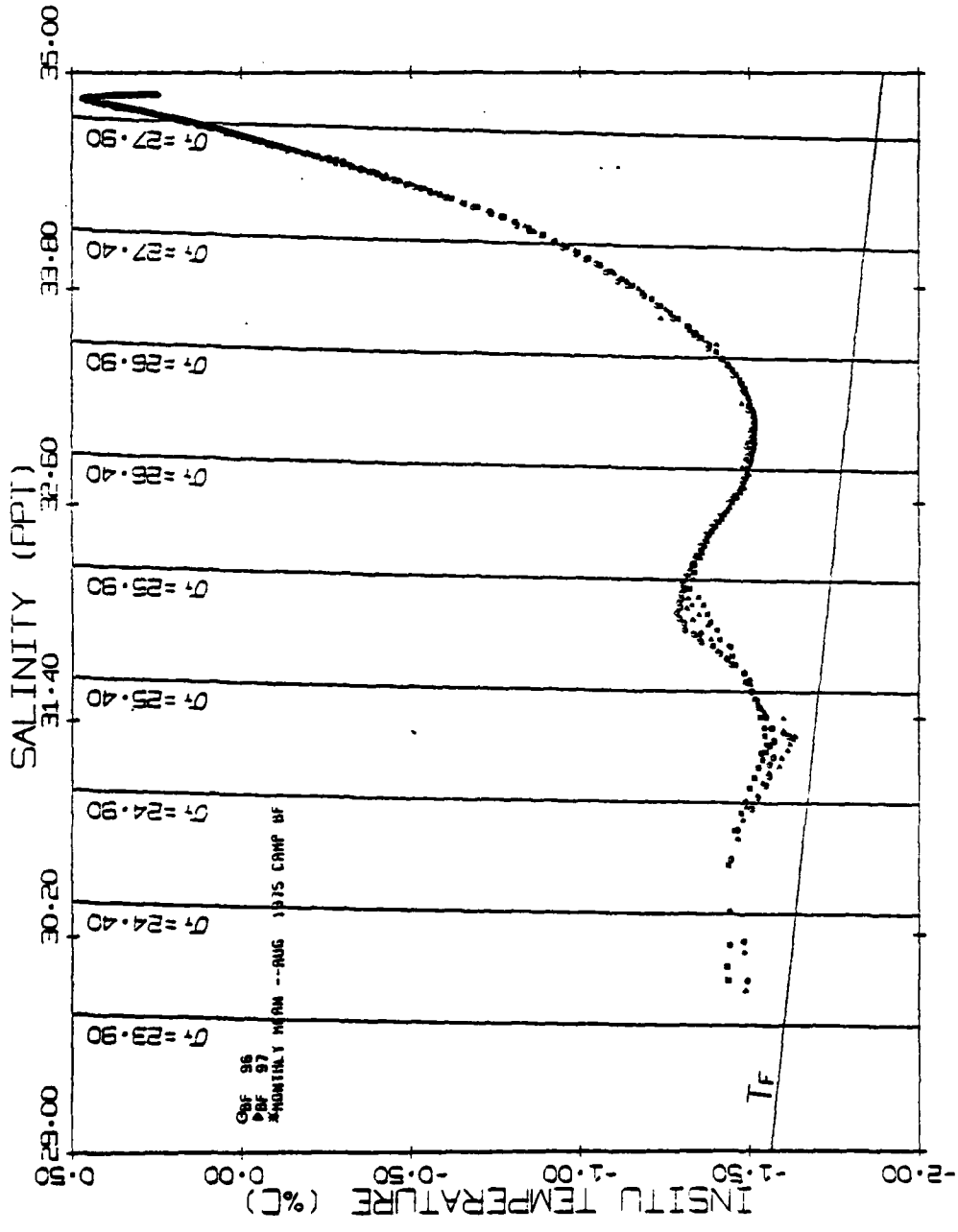

SALINITY (PPT)
35.00
33.80
32.60
31.40
30.20
29.00
σt =27.90
σt =27.40
σt =26.90
σt =26.40
σt =25.90
σt =25.40
σt =24.90
σt =24.40
σt =23.90
IN SITU TEMPERATURE (°C)
0.50
0.00
-0.50
-1.00
-1.50
-2.00
TF
□BF 51
▲BF 52
+BF 53
×BF 54
*MONTHLY MEAN -- JUL 1975 CHMP BF

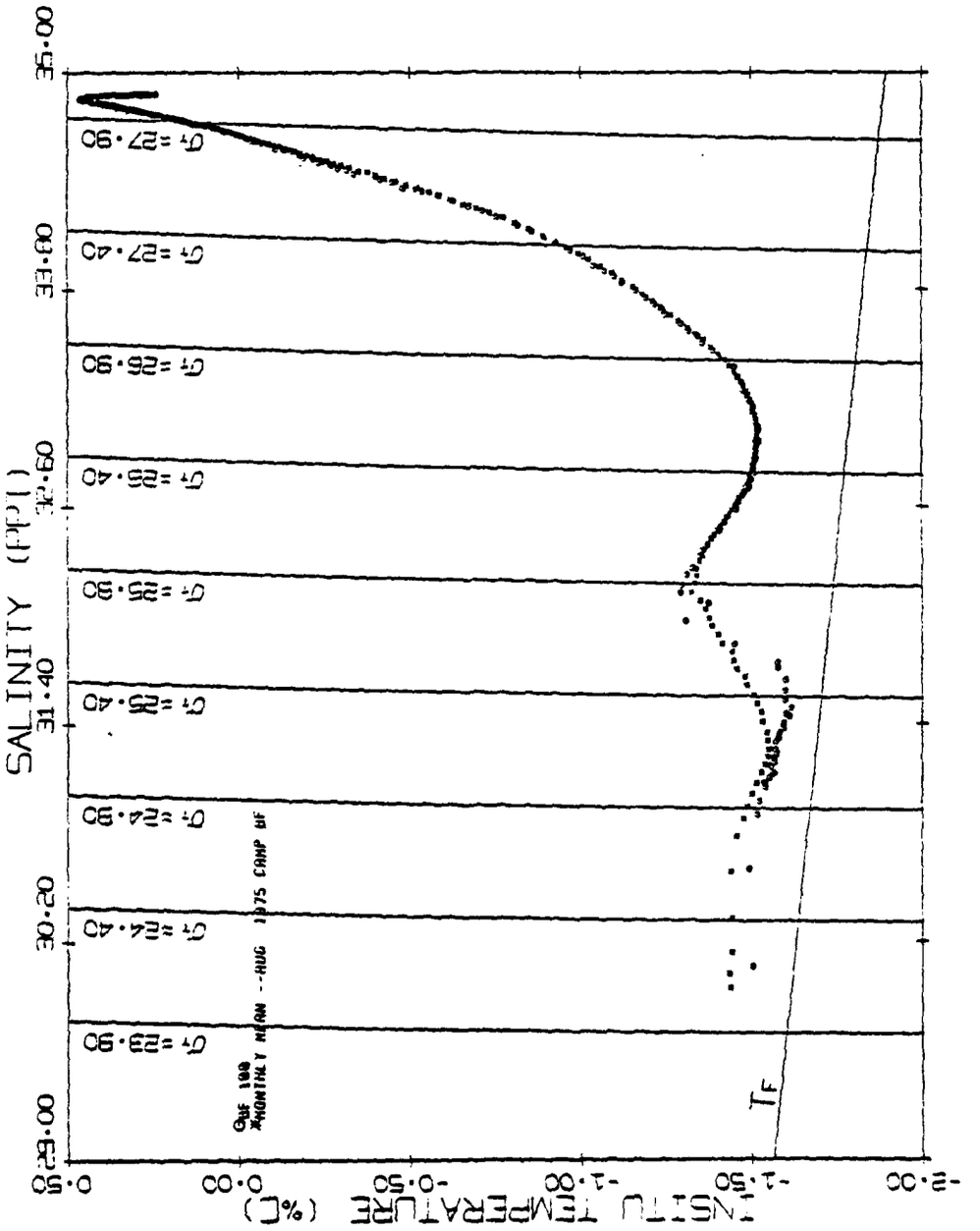

SALINITY (PPT)
POTENTIAL TEMPERATURE (°C)
σt =27.90
σt =27.40
σt =26.90
σt =26.40
σt =25.90
σt =25.40
σt =24.90
σt =24.40
σt =23.90
T_F
CBF 57
MONTHLY MEAN -- JUL 1975 CHNP BF

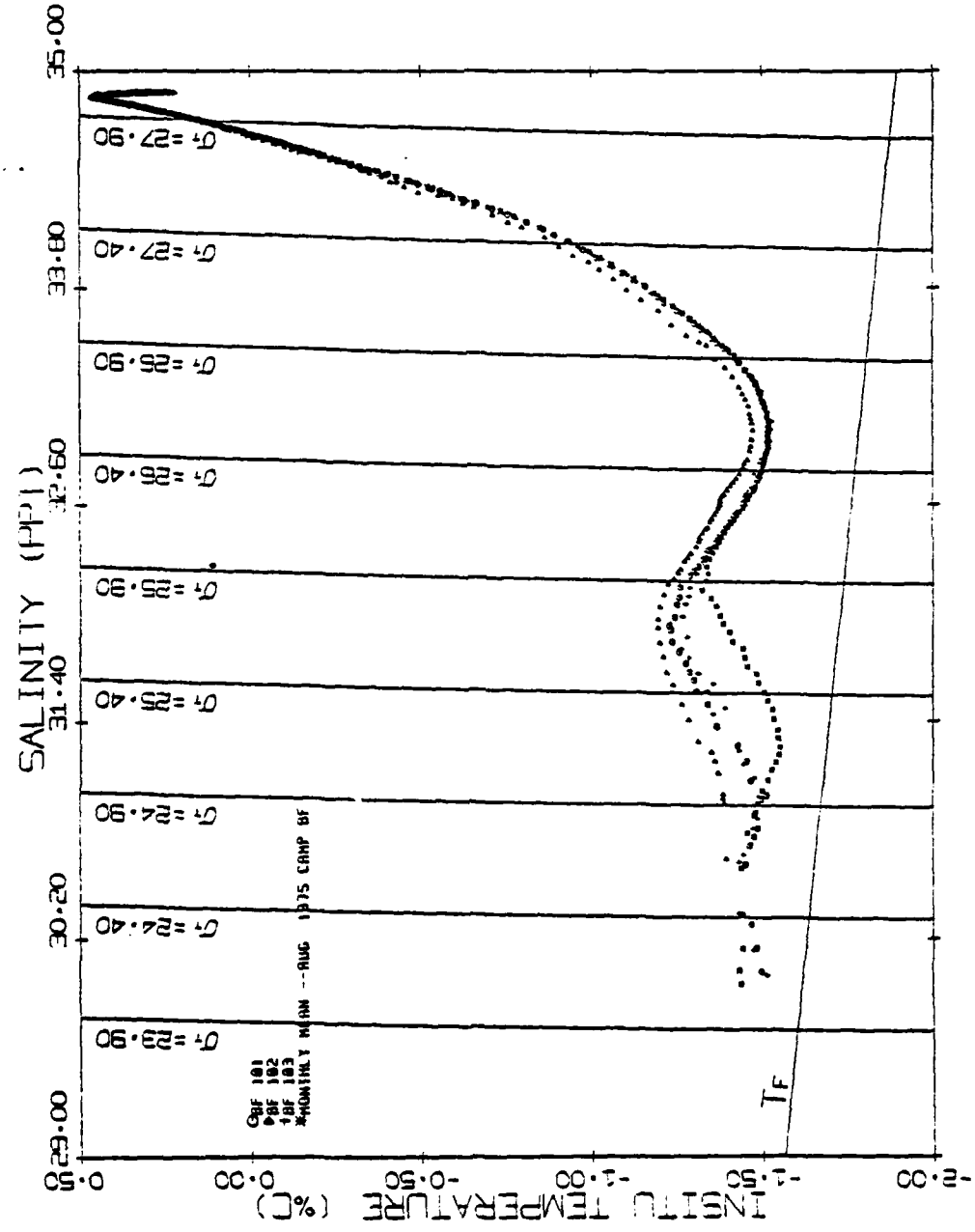

SALINITY (PPT)
35.00
34.60
34.20
33.80
33.40
33.00
32.60
32.20
31.80
31.40
31.00
30.60
30.20
29.80
29.40
29.00
σt =27.90
σt =27.40
σt =26.90
σt =26.40
σt =25.90
σt =25.40
σt =24.90
σt =24.40
σt =23.90
Tf
0.50
0.00
-0.50
-1.00
-1.50
-2.00
POTENTIAL TEMPERATURE (°C)
GOF 82
*MONTHLY MEAN -- JUL 1975 CAMP BF

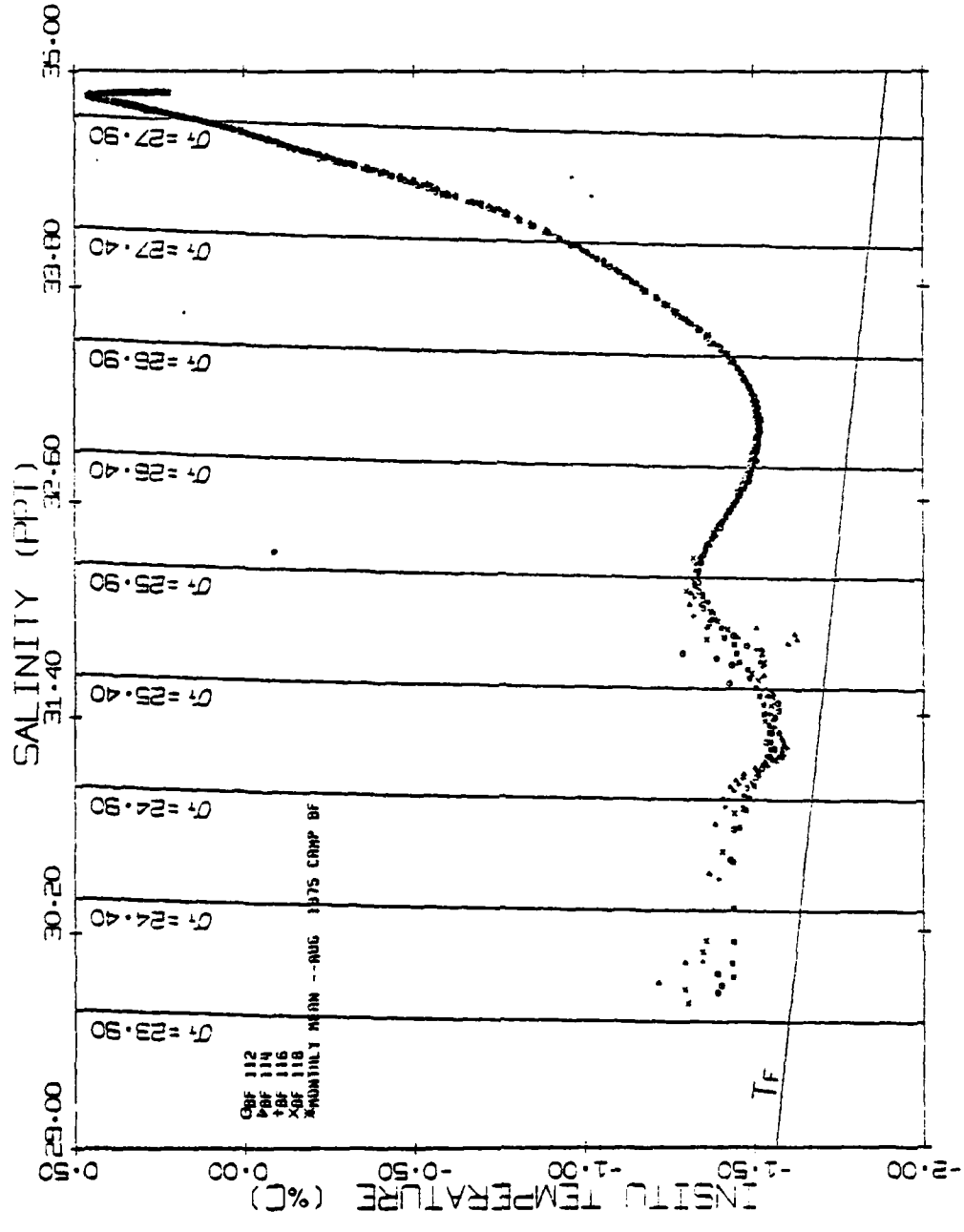

SALINITY (PPT)
IN SITU TEMPERATURE (°C)
σt =27.90
σt =27.40
σt =26.90
σt =26.40
σt =25.90
σt =25.40
σt =24.90
σt =24.40
σt =23.90
Tf
MONTHLY MEAN --RUG 1975 CRMP BF

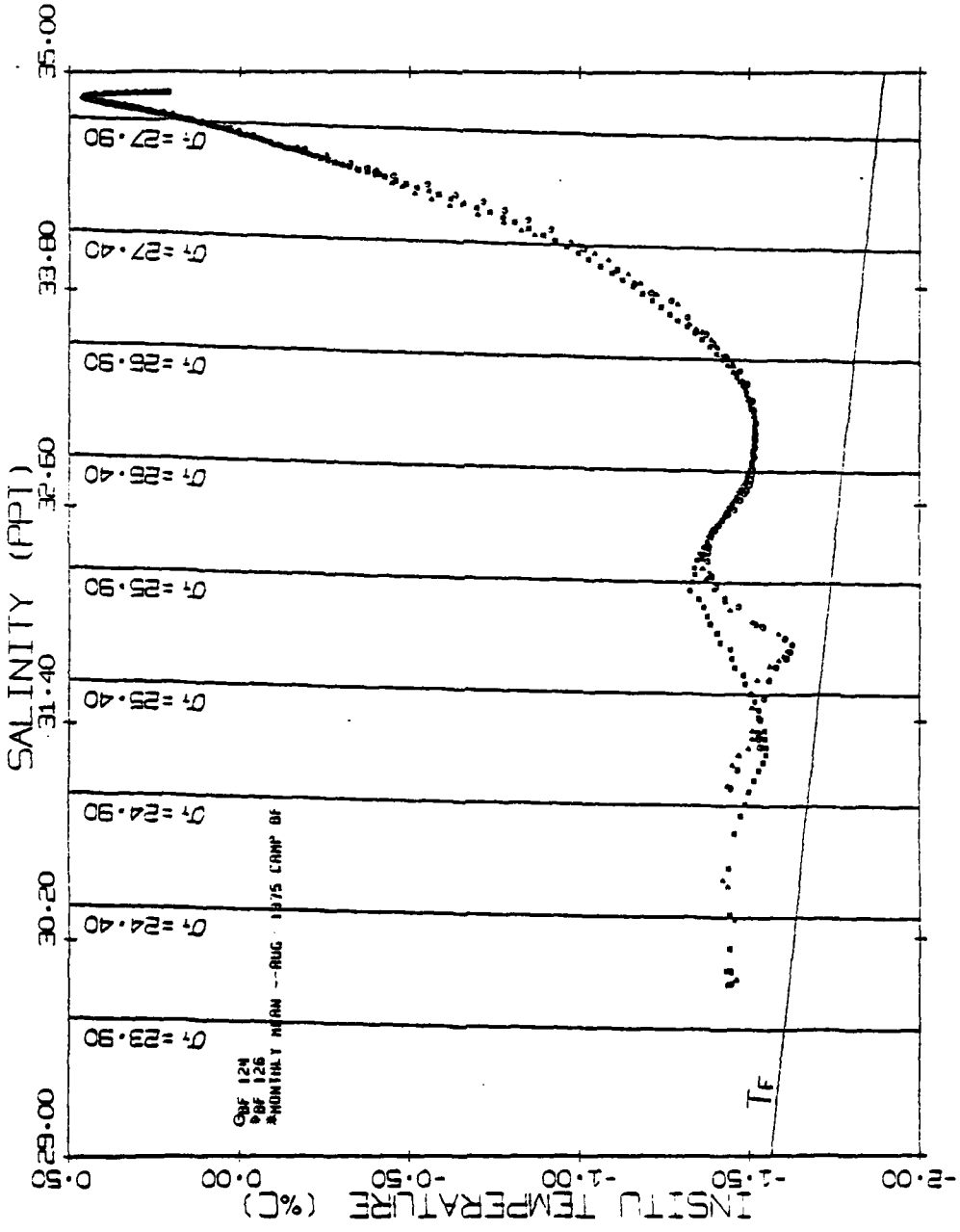

SALINITY (PPT)
35.00
33.80
32.60
31.40
30.20
29.00
σt =27.90
σt =27.40
σt =26.90
σt =26.40
σt =25.90
σt =25.40
σt =24.90
σt =24.40
σt =23.90
INSITU TEMPERATURE (°C)
0.50
0.00
-0.50
-1.00
-1.50
-2.00
T_F
MONTHLY MEAN --AUG 1975 CAMP 6F

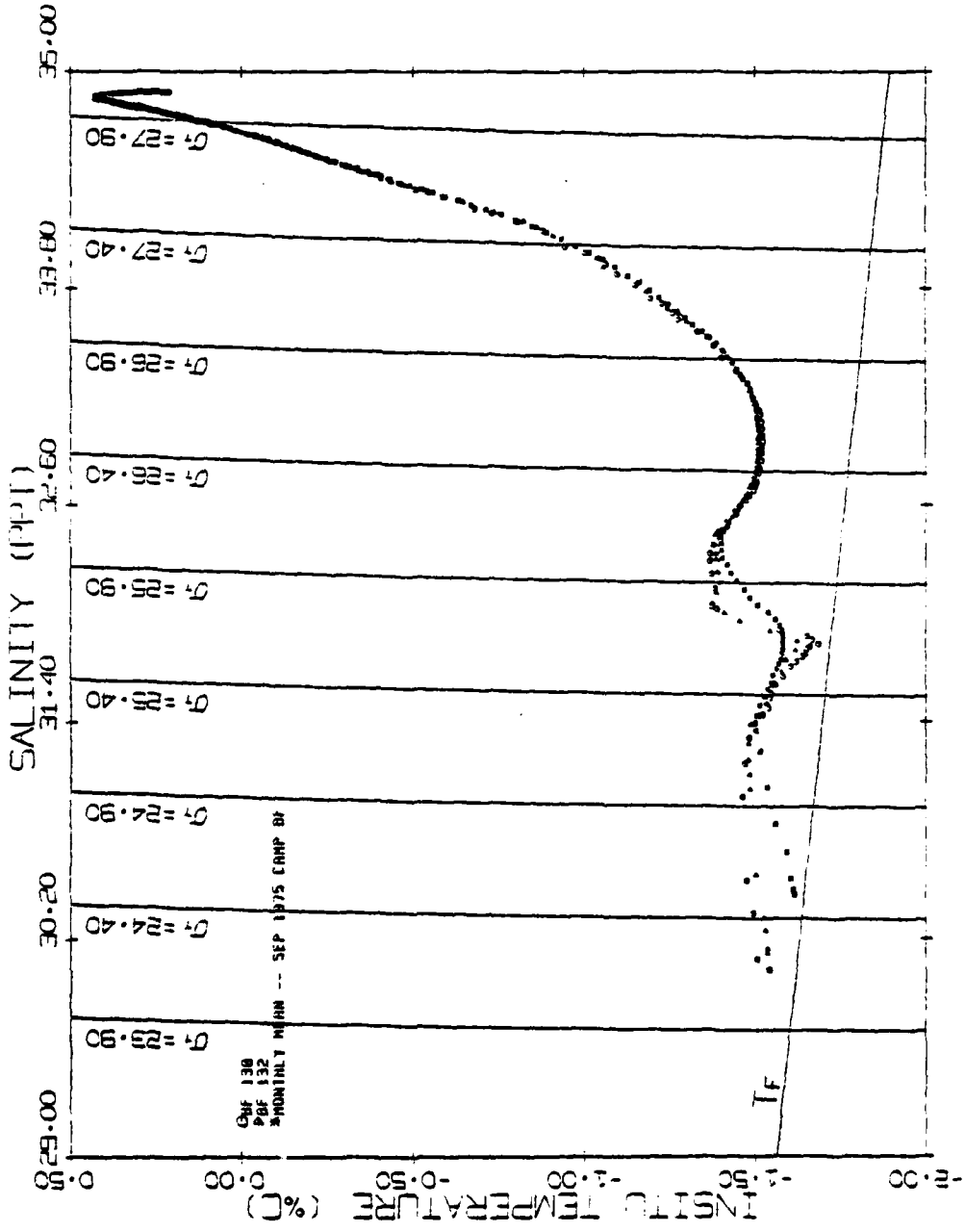

SALINITY (PPT)
35.00
33.80
32.60
31.40
30.20
29.00
σt =27.90
σt =27.40
σt =26.90
σt =26.40
σt =25.90
σt =25.40
σt =24.90
σt =24.40
σt =23.90
TF
0.50
0.00
-0.50
-1.00
-1.50
-2.00
IN SITU TEMPERATURE (°C)

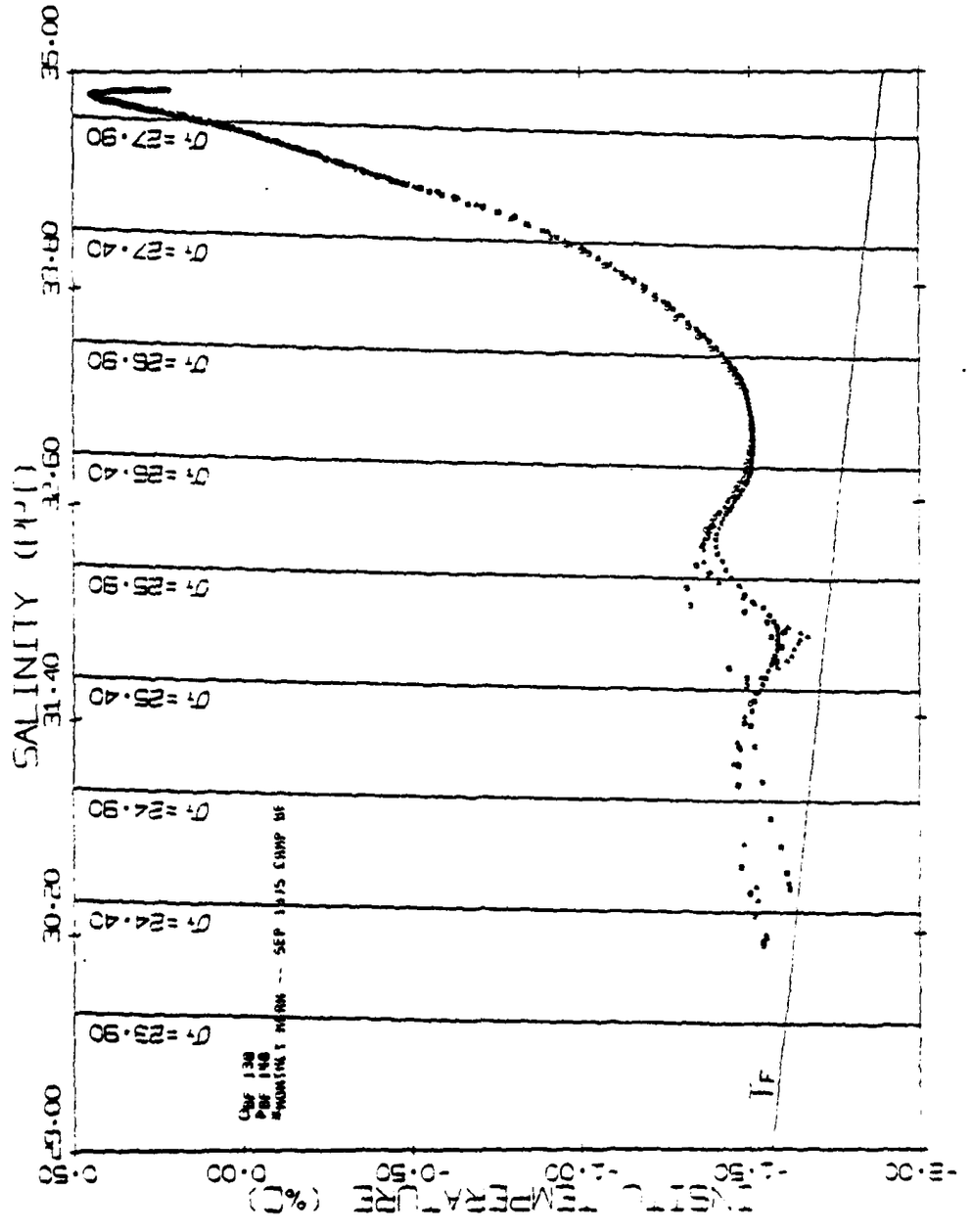

SALINITY (ppt)
35.00
34.80
34.60
34.40
34.20
34.00
σt =27.90
σt =27.40
σt =26.90
σt =25.40
σt =25.90
σt =25.40
σt =24.90
σt =24.40
σt =23.90
IN SITU TEMPERATURE (°C)
0.50
0.00
-0.50
-1.00
-1.50
-2.00
T_F
QUF 100
MONTHLY MEAN --HUG 1975 CAMP UF

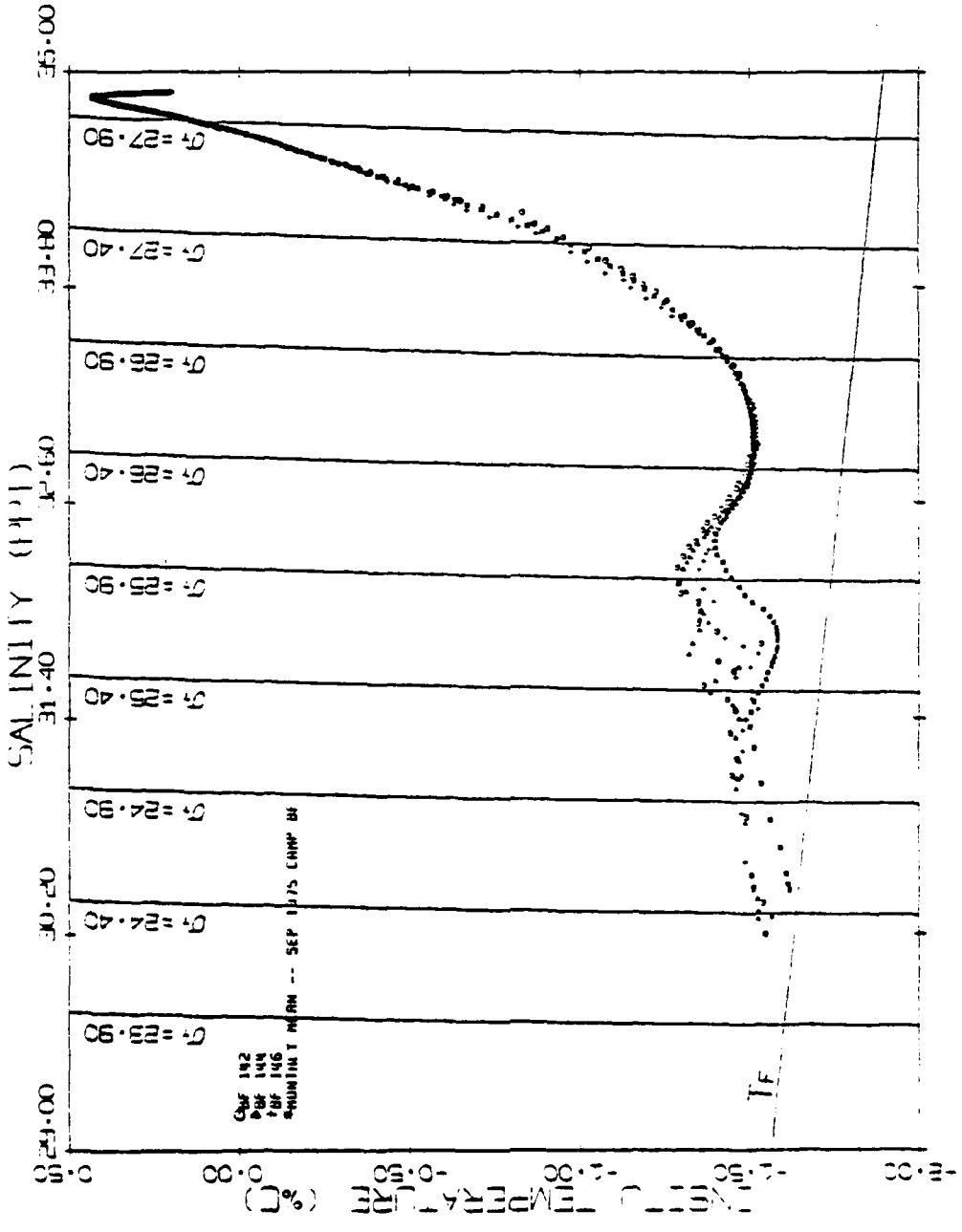

SALINITY (PPT)
35.00
33.80
32.60
31.40
30.20
29.00
σt =27.90
σt =27.40
σt =26.90
σt =26.40
σt =25.90
σt =25.40
σt =24.90
σt =24.40
σt =23.90
CBF 101
CBF 102
CBF 103
*MONTHLY MEAN --AUG 1975 CAMP BF
TF
INSITU TEMPERATURE (°C)
0.00
-0.50
-1.00
-1.50
-2.00

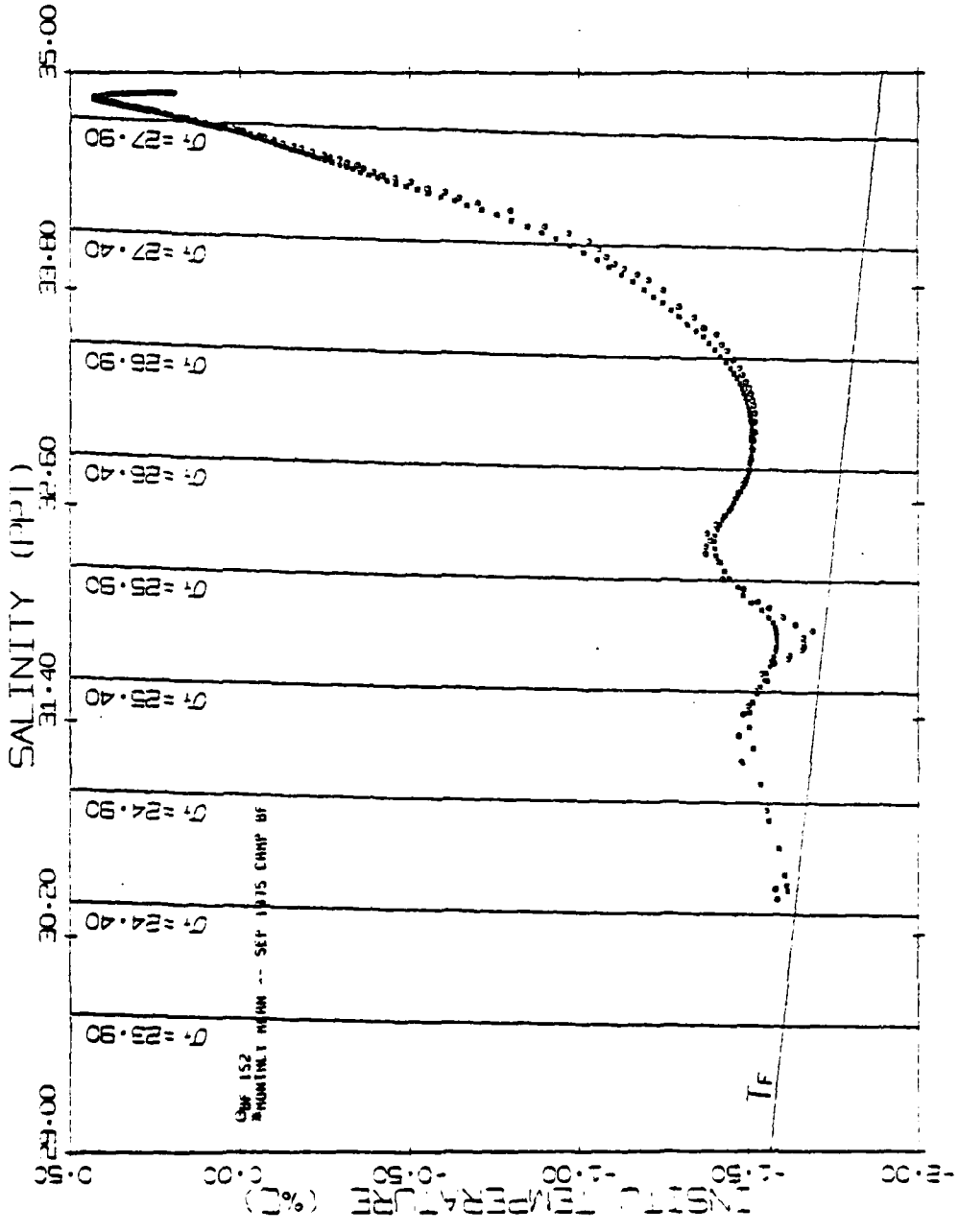

SALINITY (PPT)
INSITU TEMPERATURE (°C)
35.00
33.80
32.60
31.40
30.20
29.00
0.50
0.00
-0.50
-1.00
-1.50
-2.00
σt =27.90
σt =27.40
σt =26.90
σt =26.40
σt =25.90
σt =25.40
σt =24.90
σt =24.40
σt =23.90
CBF 112
CBF 114
CBF 116
CBF 118
MONTHLY MEAN --AUG 1975 CAMP BF
T_F

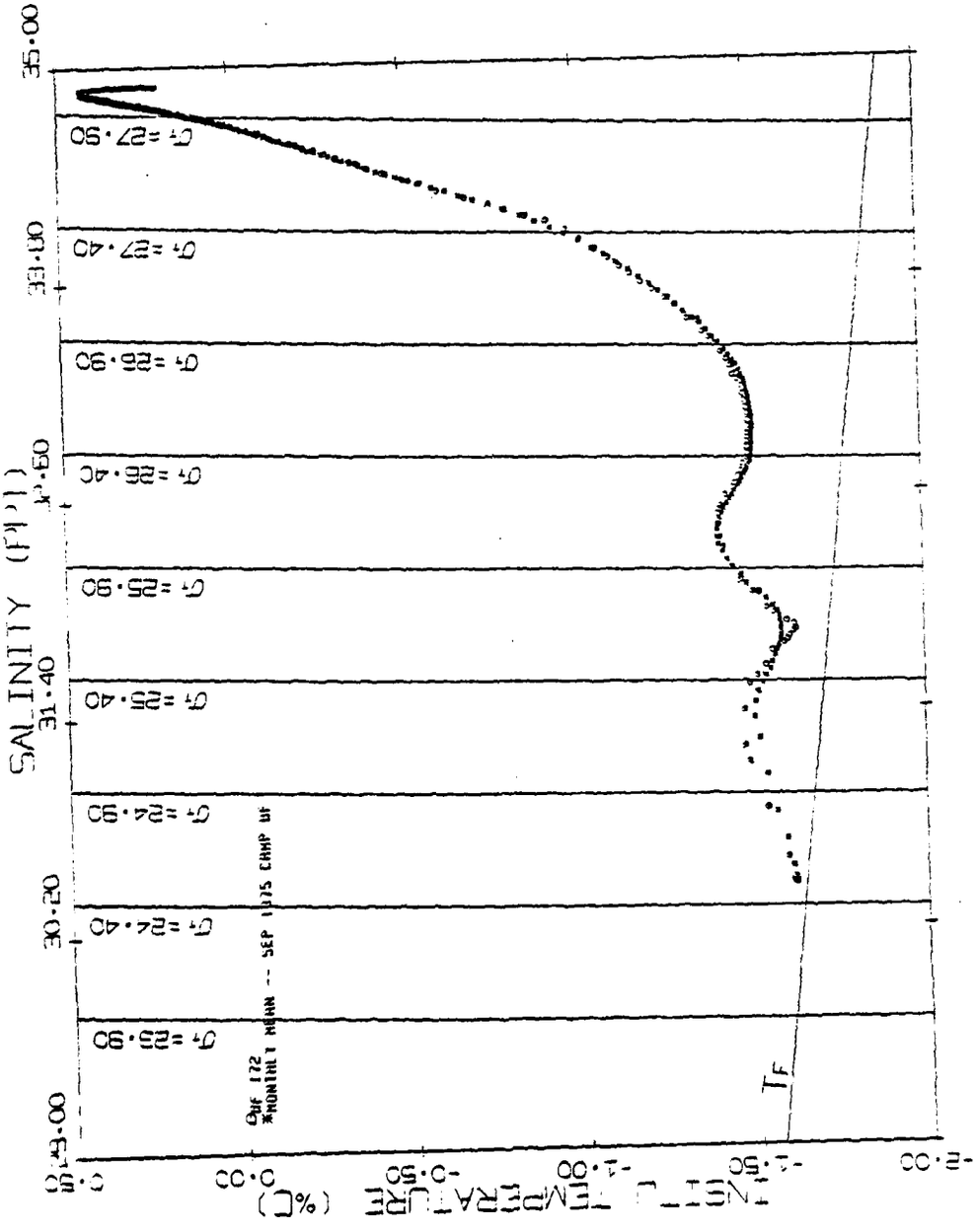

35.00
33.80
32.60
31.40
30.20
29.00
SALINITY (PPT)
σt =27.90
σt =27.40
σt =26.90
σt =26.40
σt =25.90
σt =25.40
σt =24.90
σt =24.40
σt =23.90
0.50
0.00
-0.50
-1.00
-1.50
-2.00
INSITU TEMPERATURE (°C)
T_F
CBF 124
BBF 126
MONTHLY MEAN --AUG 1975 CAMP BF

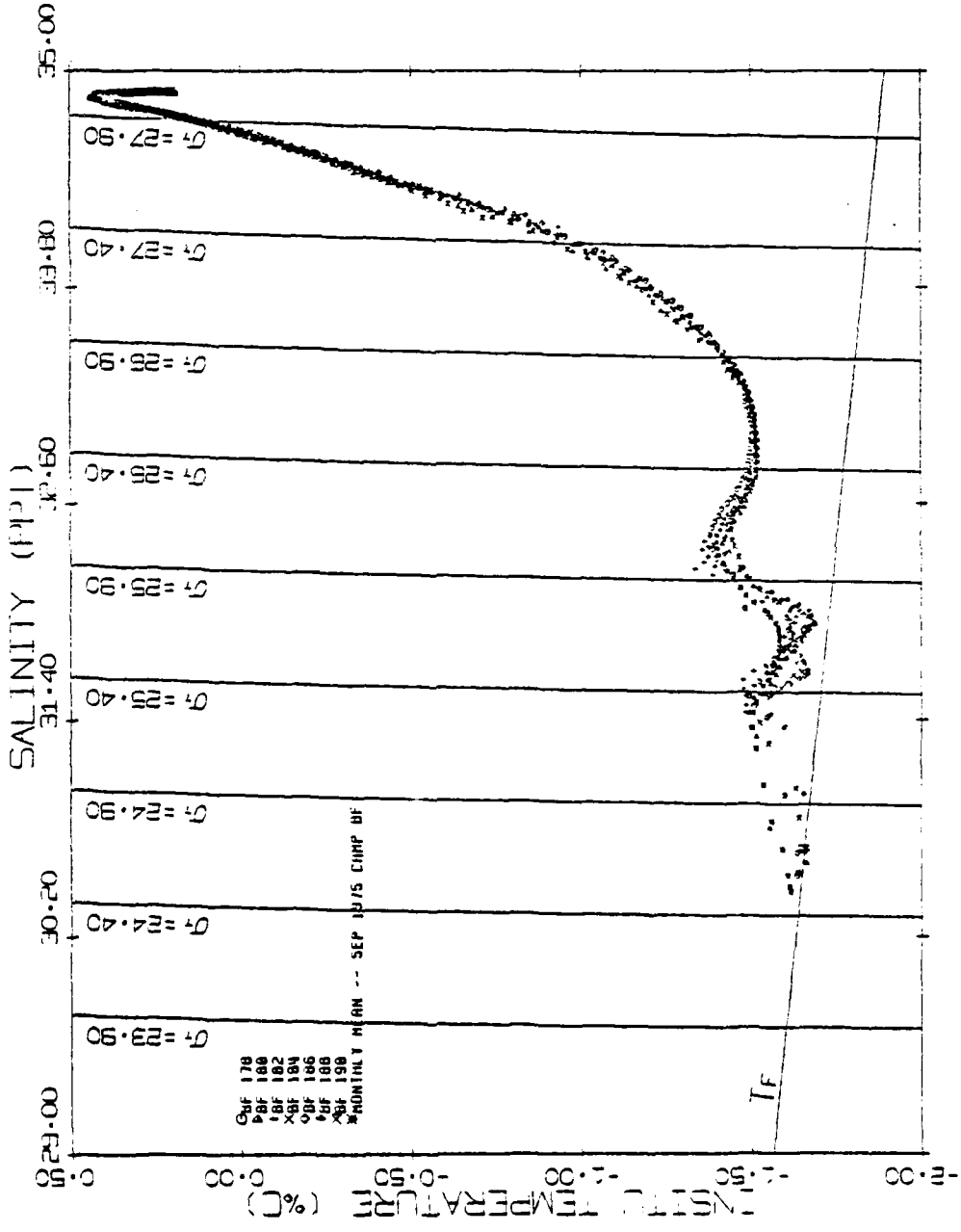

SALINITY (PPT)
35.00
33.80
32.60
31.40
30.20
29.00
σt =27.90
σt =27.40
σt =26.90
σt =26.40
σt =25.90
σt =25.40
σt =24.90
σt =24.40
σt =23.90
CNF 130
PBF 132
*MONTHLY MEAN -- SEP 1975 CAMP BA
T_F
INSITU TEMPERATURE (°C)
0.50
0.00
-0.50
-1.00
-1.50
-2.00

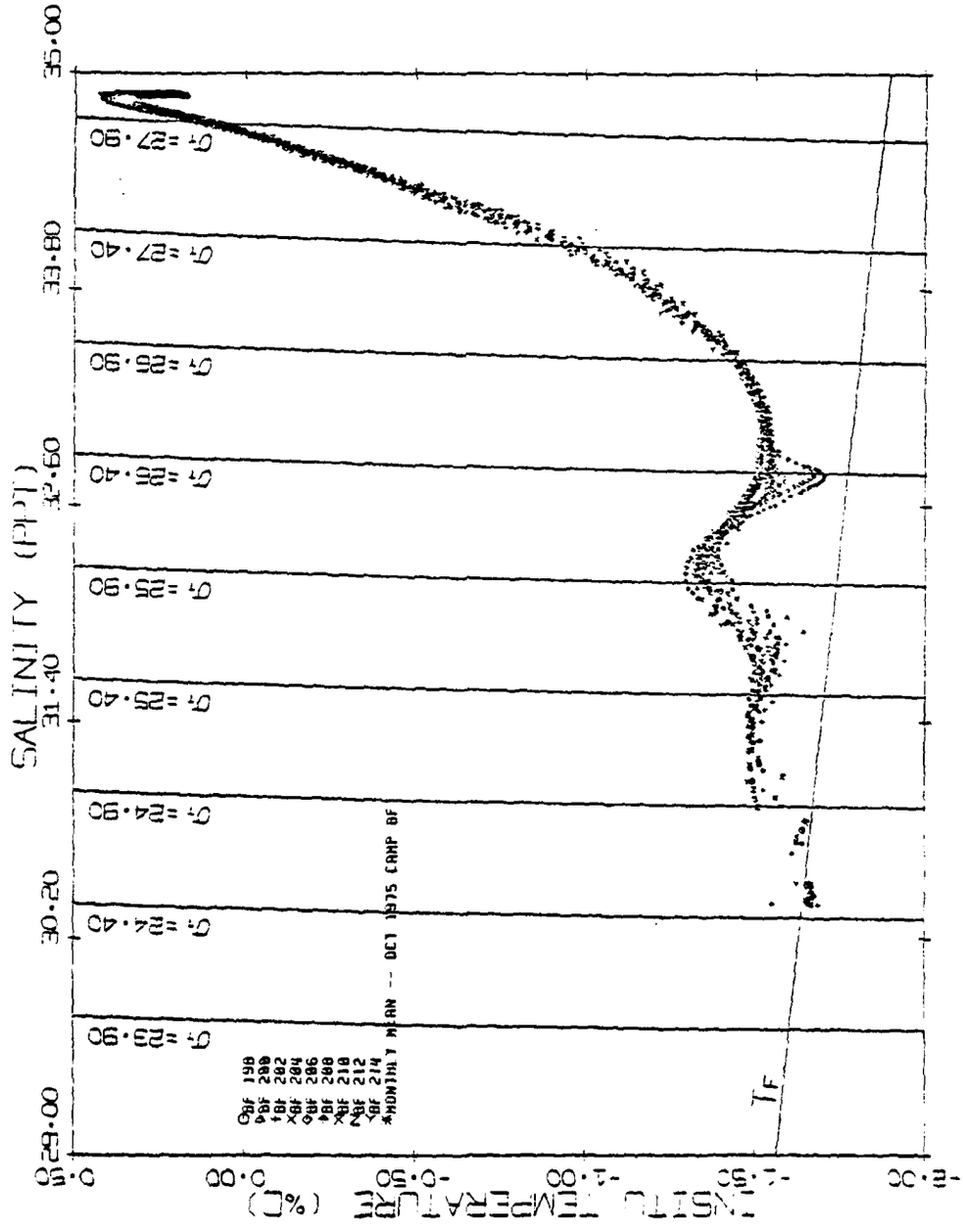

SALINITY (ppt)
35.00
34.40
33.80
33.20
32.60
32.00
31.40
30.80
30.20
29.60
29.00
σt =27.90
σt =27.40
σt =26.90
σt =26.40
σt =25.90
σt =25.40
σt =24.90
σt =24.40
σt =23.90
TF
0.50
0.00
-0.50
-1.00
-1.50
-2.00
POTENTIAL TEMPERATURE (°C)

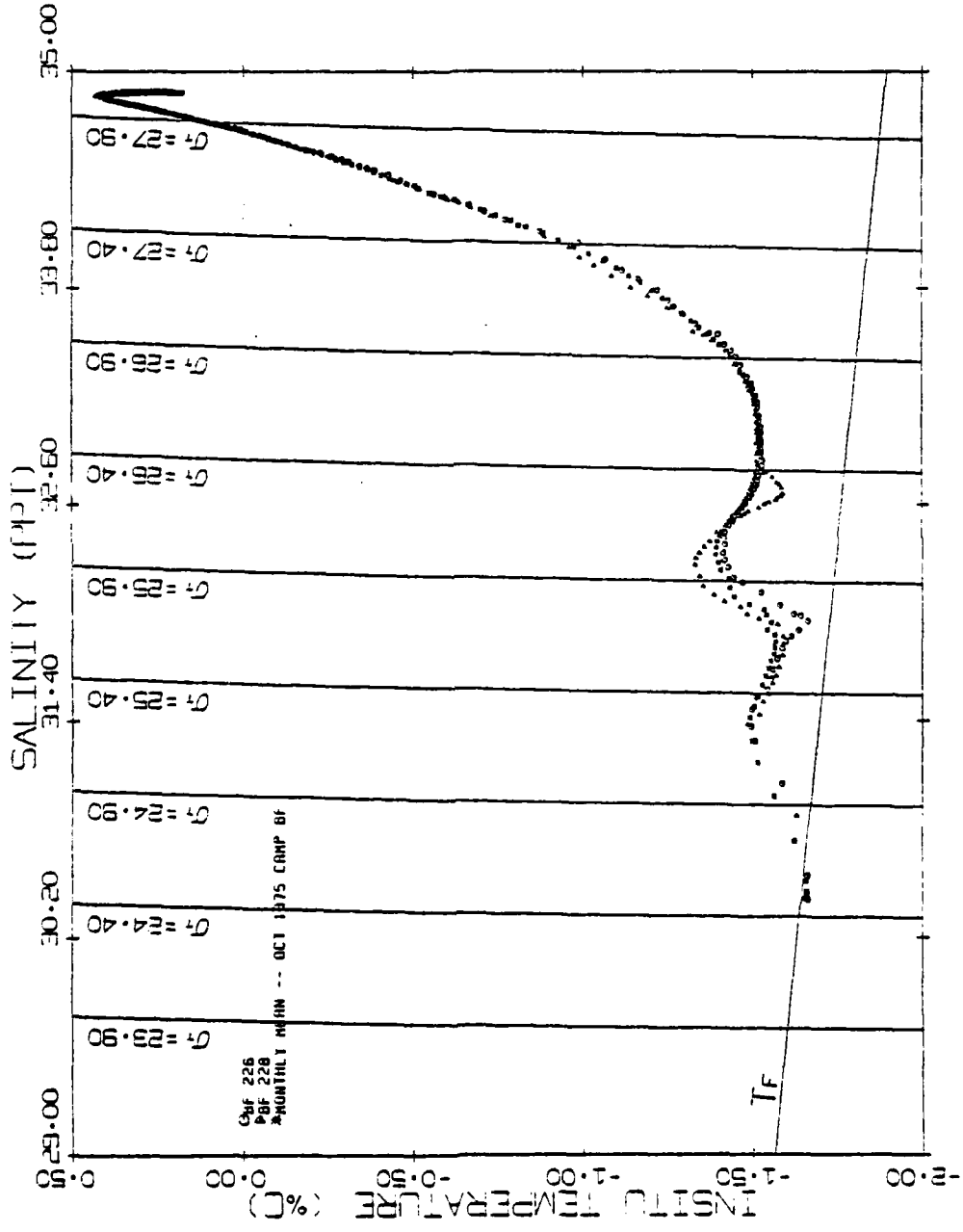

SALINITY (PPT)
35.00
34.40
33.80
33.20
σt = 27.90
σt = 27.40
σt = 26.90
σt = 26.40
σt = 25.90
σt = 25.40
σt = 24.90
σt = 24.40
σt = 23.90
0.00
-0.50
-1.00
-1.50
-2.00
TF

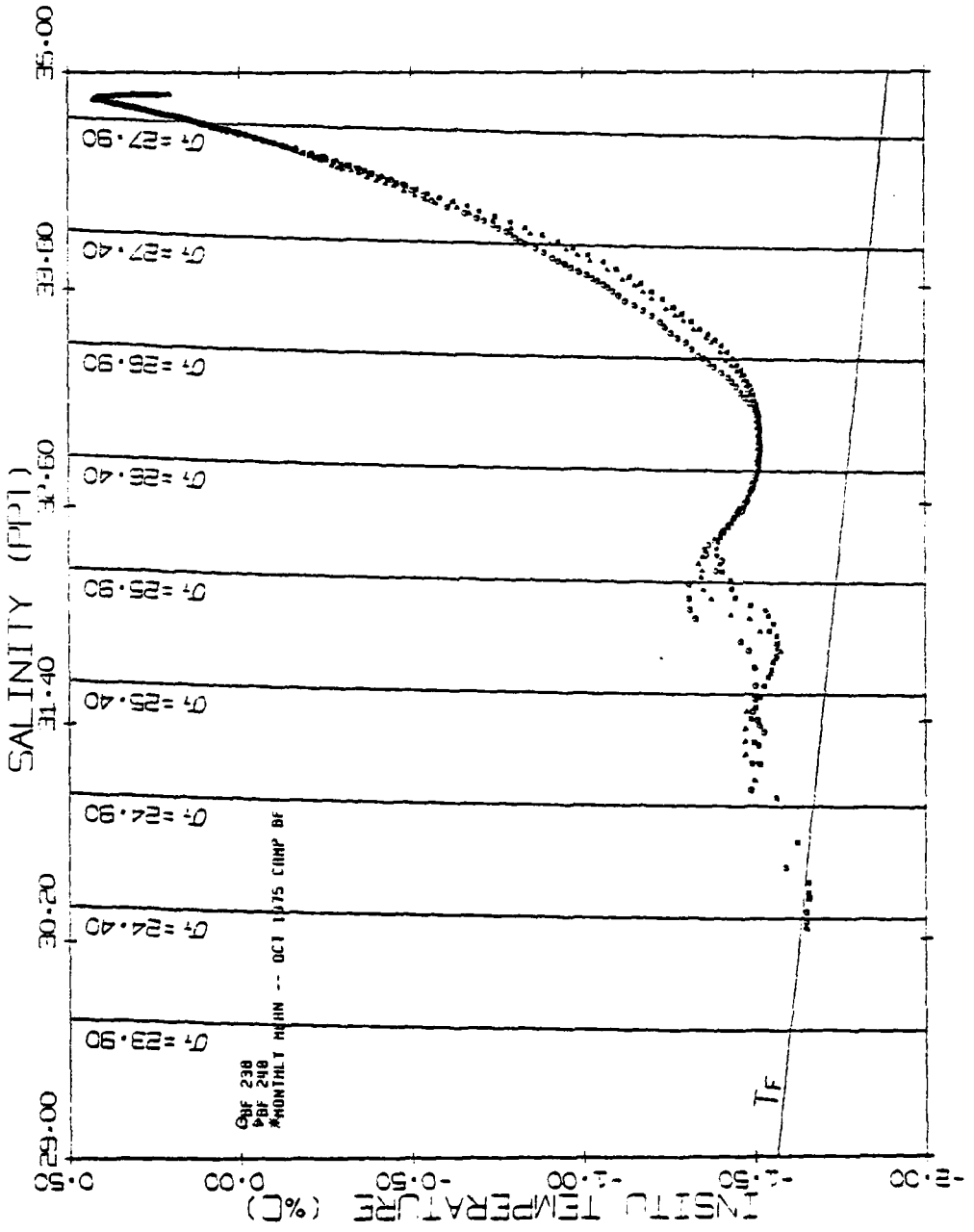

SALINITY (PPT)
POTENTIAL TEMPERATURE (°C)
35.00
33.80
32.60
31.40
30.20
29.00
σt =27.90
σt =27.40
σt =26.90
σt =26.40
σt =25.90
σt =25.40
σt =24.90
σt =24.40
σt =23.90
T_F

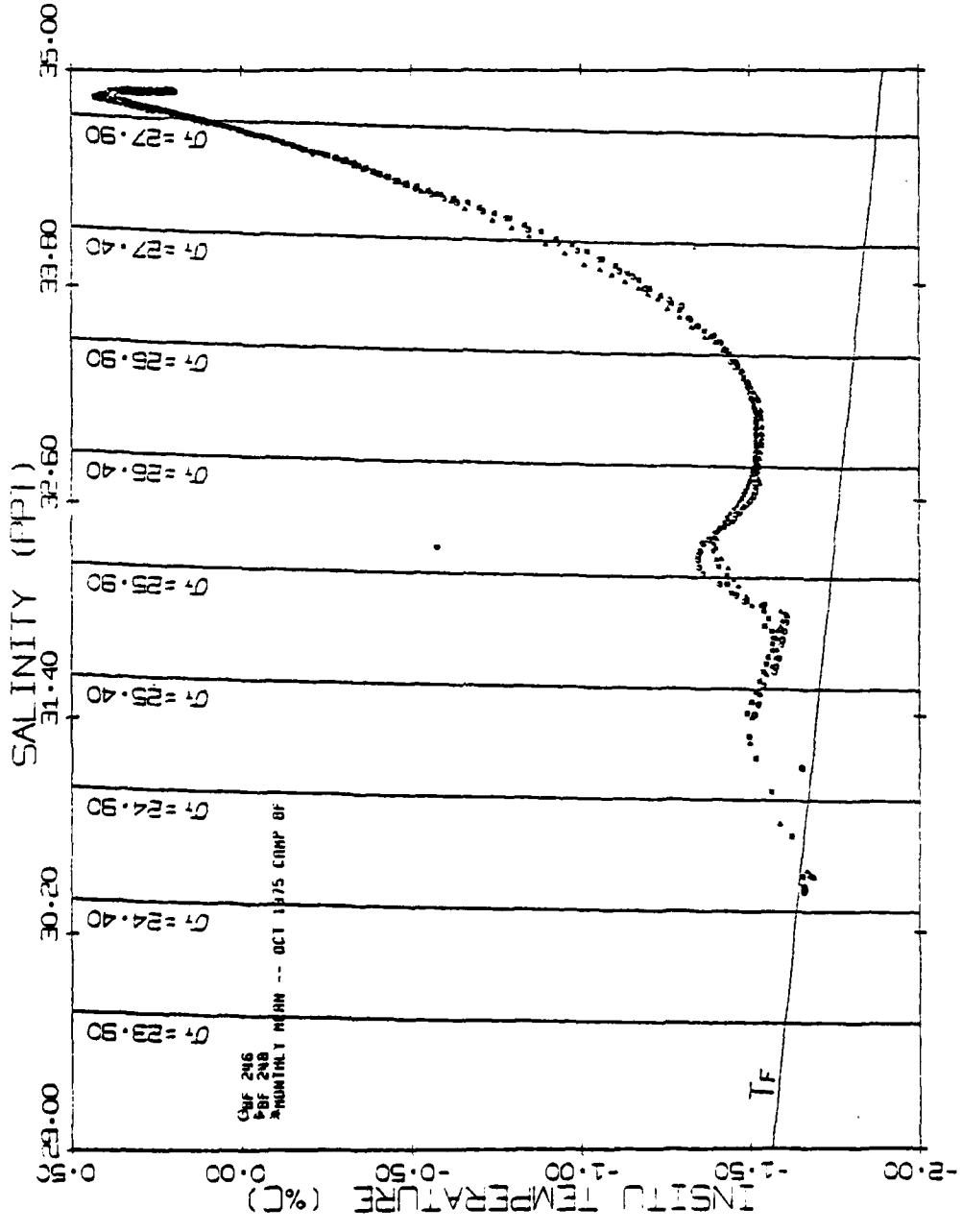

SALINITY (PPT)
POTENTIAL TEMPERATURE (°C)
35.00
33.80
32.60
31.40
30.20
29.00
0.50
0.00
-0.50
-1.00
-1.50
-2.00
σt =27.80
σt =27.40
σt =26.90
σt =26.40
σt =25.90
σt =25.40
σt =24.90
σt =24.40
σt =23.90
TF
ONR 122
*MONTHLY MEAN -- SEP 1975 CAMP WF

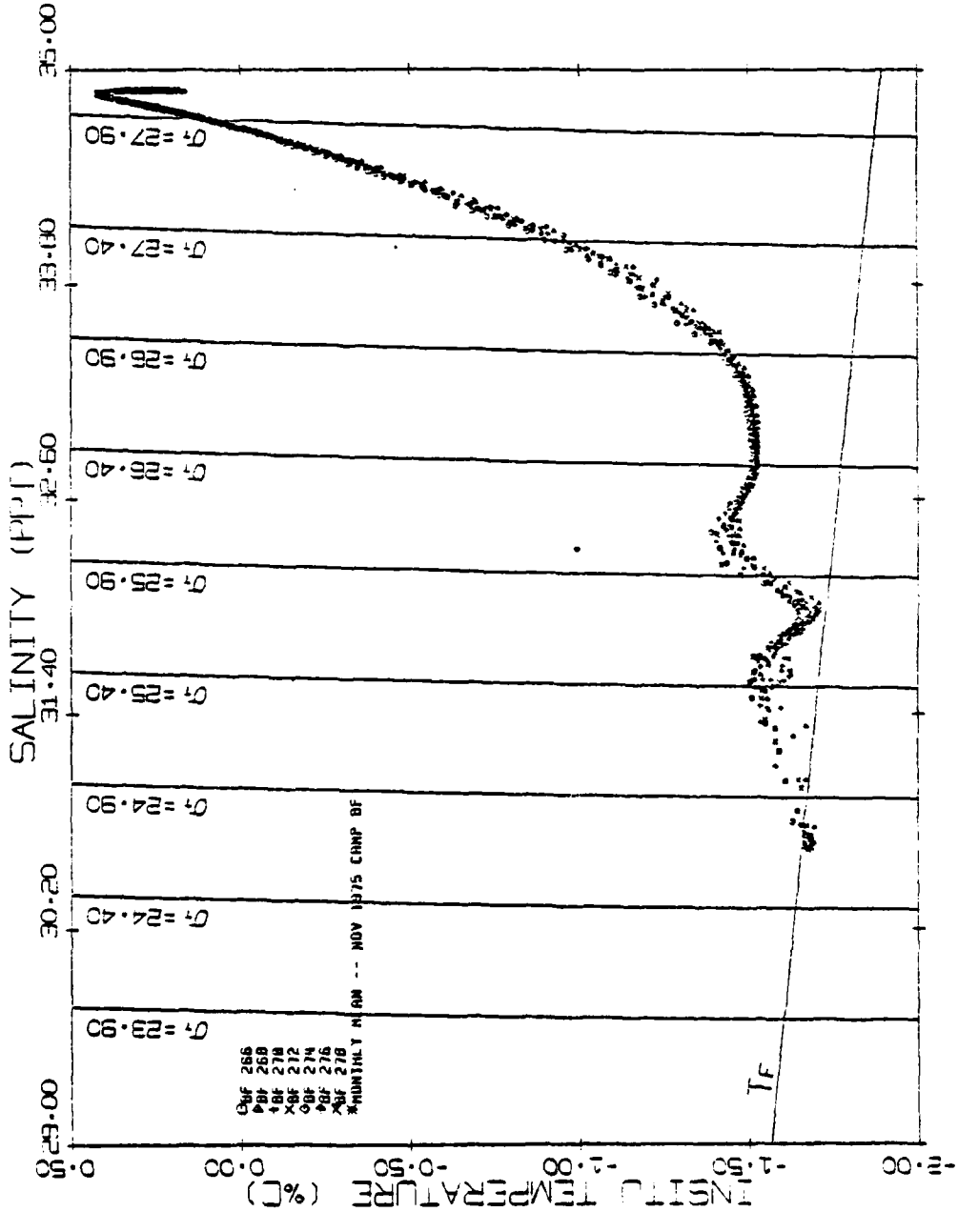

SALINITY (PPT)
POTENTIAL TEMPERATURE (°C)
35.00
33.80
32.60
31.40
30.20
29.00
0.50
0.00
-0.50
-1.00
-1.50
-2.00
σt =27.80
σt =27.40
σt =26.80
σt =26.40
σt =25.80
σt =25.40
σt =24.80
σt =24.40
σt =23.80
Tf
CTDF 178
BTDF 180
ATDF 182
XBF 184
OBF 186
+BF 188
XBF 190
*NOMINAL MEAN -- SEP 1975 CHMP BF

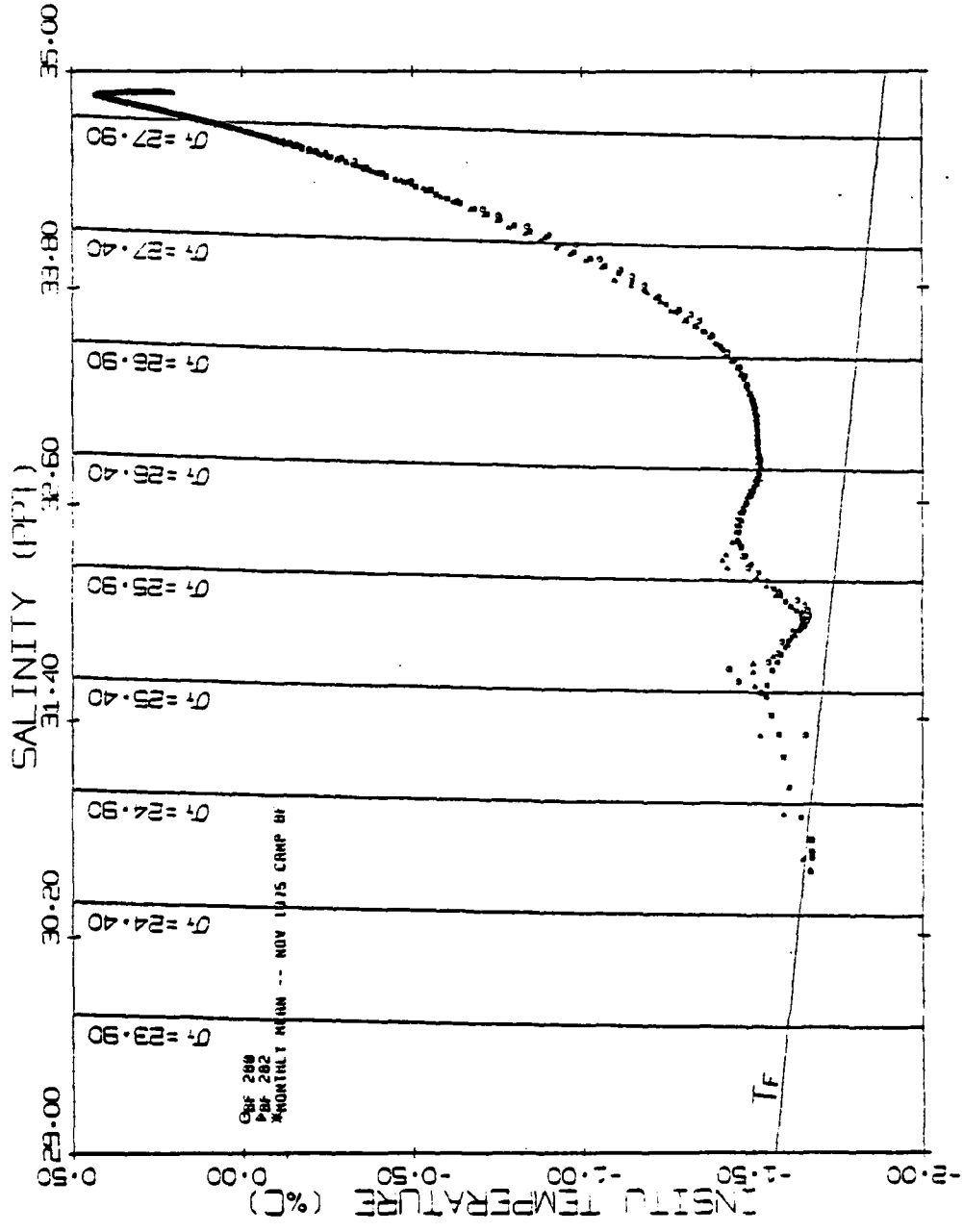

SALINITY (PPT)
POTENTIAL TEMPERATURE (°C)
σt =27.80
σt =27.40
σt =26.80
σt =26.40
σt =25.80
σt =25.40
σt =24.80
σt =24.40
σt =23.80
29.00
30.20
31.40
32.60
33.80
35.00
0.50
0.00
-0.50
-1.00
-1.50
-2.00
GBF 198
GBF 200
GBF 202
GBF 204
GBF 206
GBF 208
GBF 210
GBF 212
GBF 214
*MONTHLY MEANS -- OCT 1975 CAMP BF
T_F

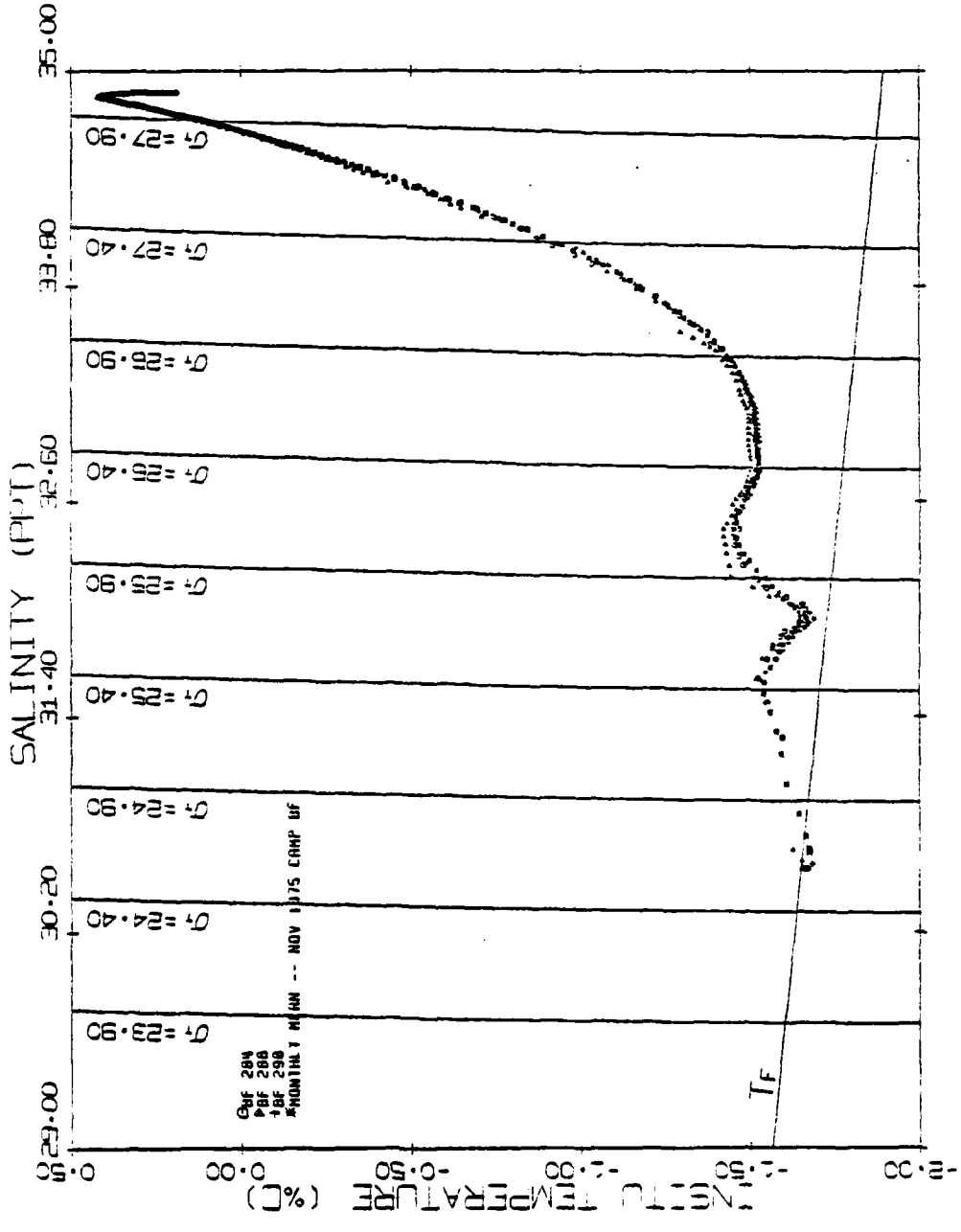

SALINITY (PPT)
35.00
33.80
32.60
31.40
30.20
29.00
σt =27.90
σt =27.40
σt =26.90
σt =26.40
σt =25.90
σt =25.40
σt =24.90
σt =24.40
σt =23.90
TF
INSITU TEMPERATURE (°C)
0.50
0.00
-0.50
-1.00
-1.50
-2.00
CBF 226
CBF 228
*MONTHLY MEAN -- OCT 1975 CAMP BF

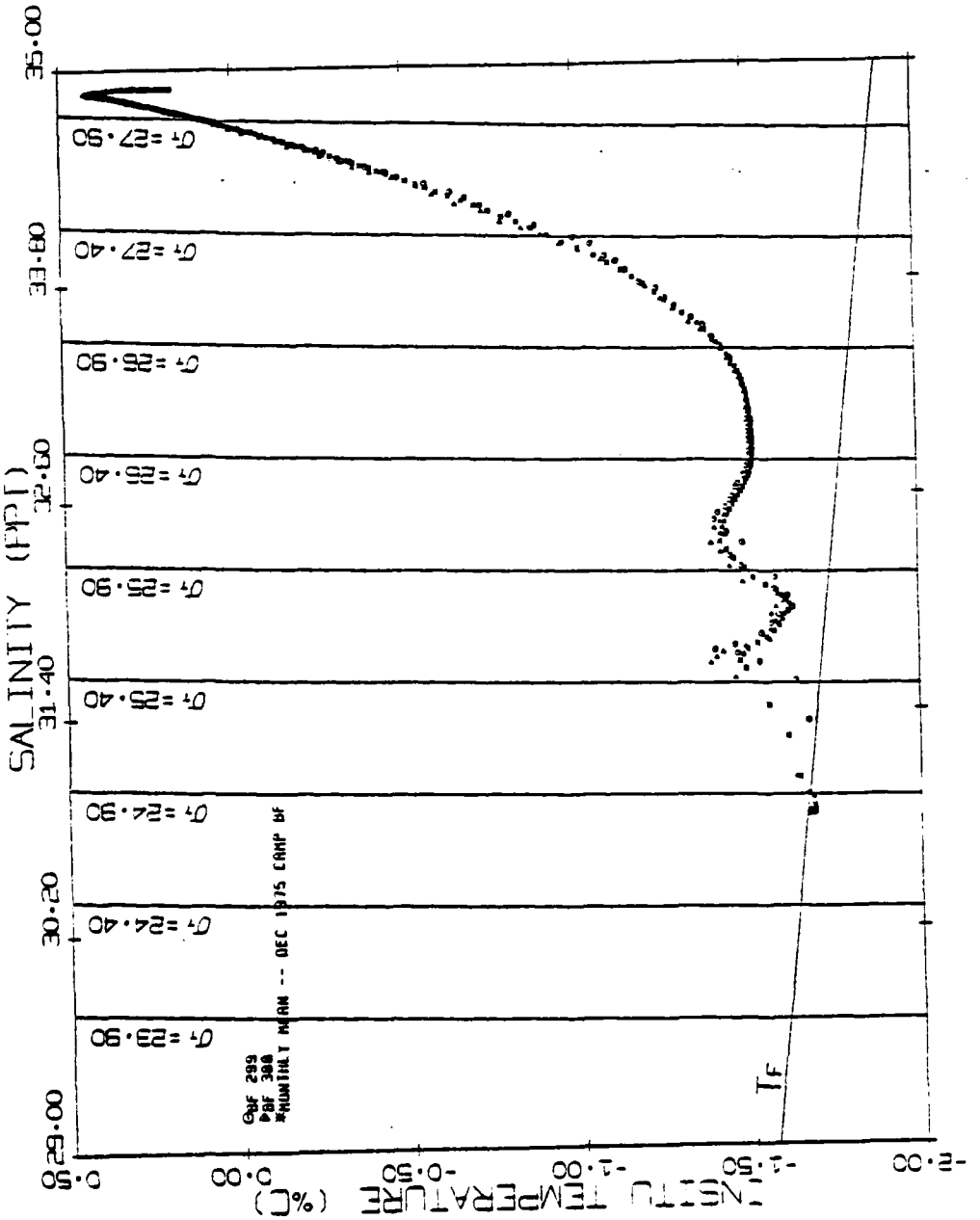

SALINITY (PPT)
35.00
34.60
34.20
33.80
33.40
33.00
32.60
32.20
31.80
31.40
31.00
30.60
30.20
29.80
29.00
σt =27.90
σt =27.40
σt =26.90
σt =26.40
σt =25.90
σt =25.40
σt =24.90
σt =24.40
σt =23.90
INSITU TEMPERATURE (°C)
0.50
0.00
-0.50
-1.00
-1.50
-2.00
-2.30
T_F
BF 238
BF 240
MONTHLY MEAN -- OCT 1975 CIMP BF

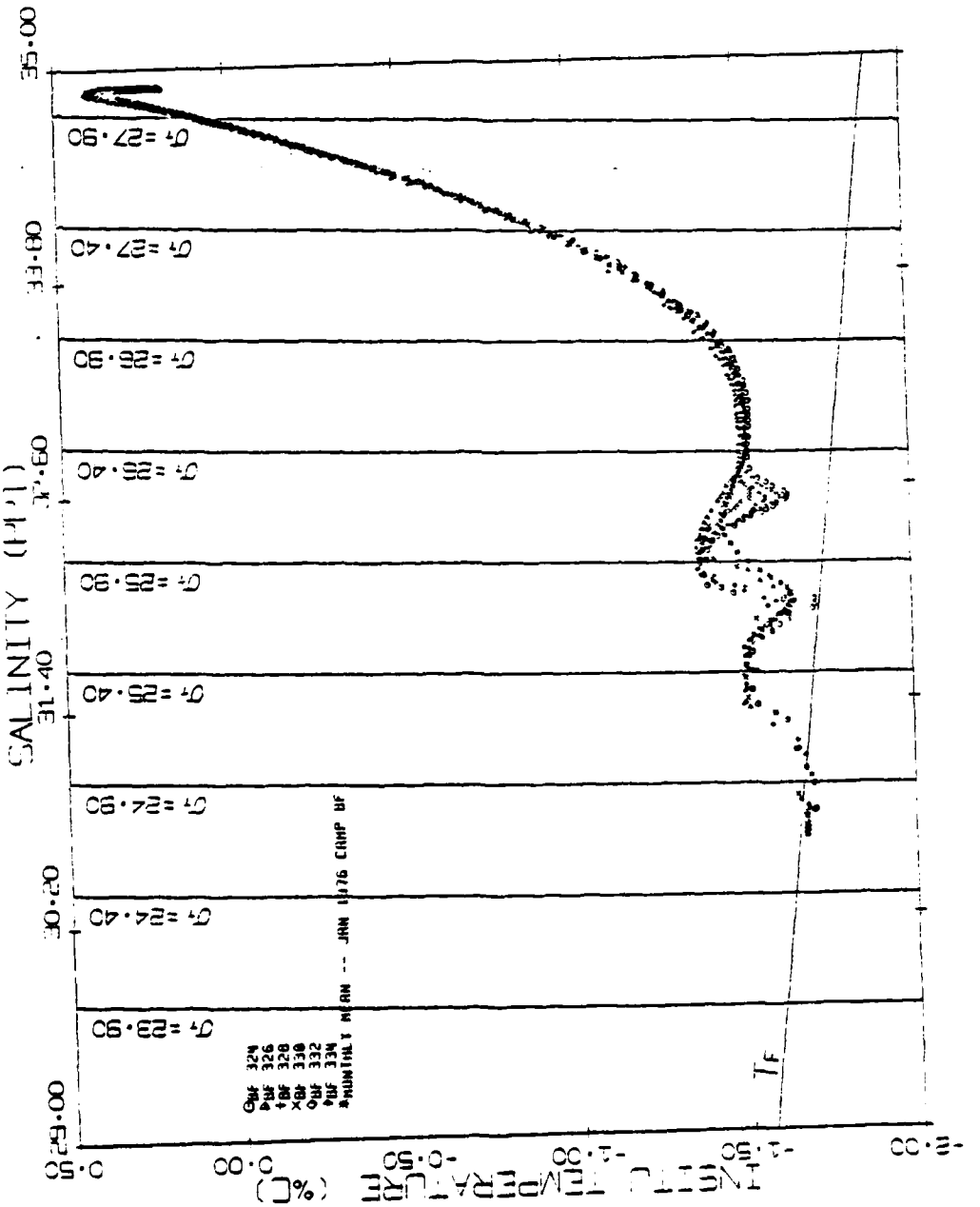

SALINITY (PPT)
35.00
33.80
32.60
31.40
30.20
29.00
σt =27.90
σt =27.40
σt =26.90
σt =26.40
σt =25.90
σt =25.40
σt =24.90
σt =24.40
σt =23.90
INSITU TEMPERATURE (°C)
0.50
0.00
-0.50
-1.00
-1.50
-2.00
T_F

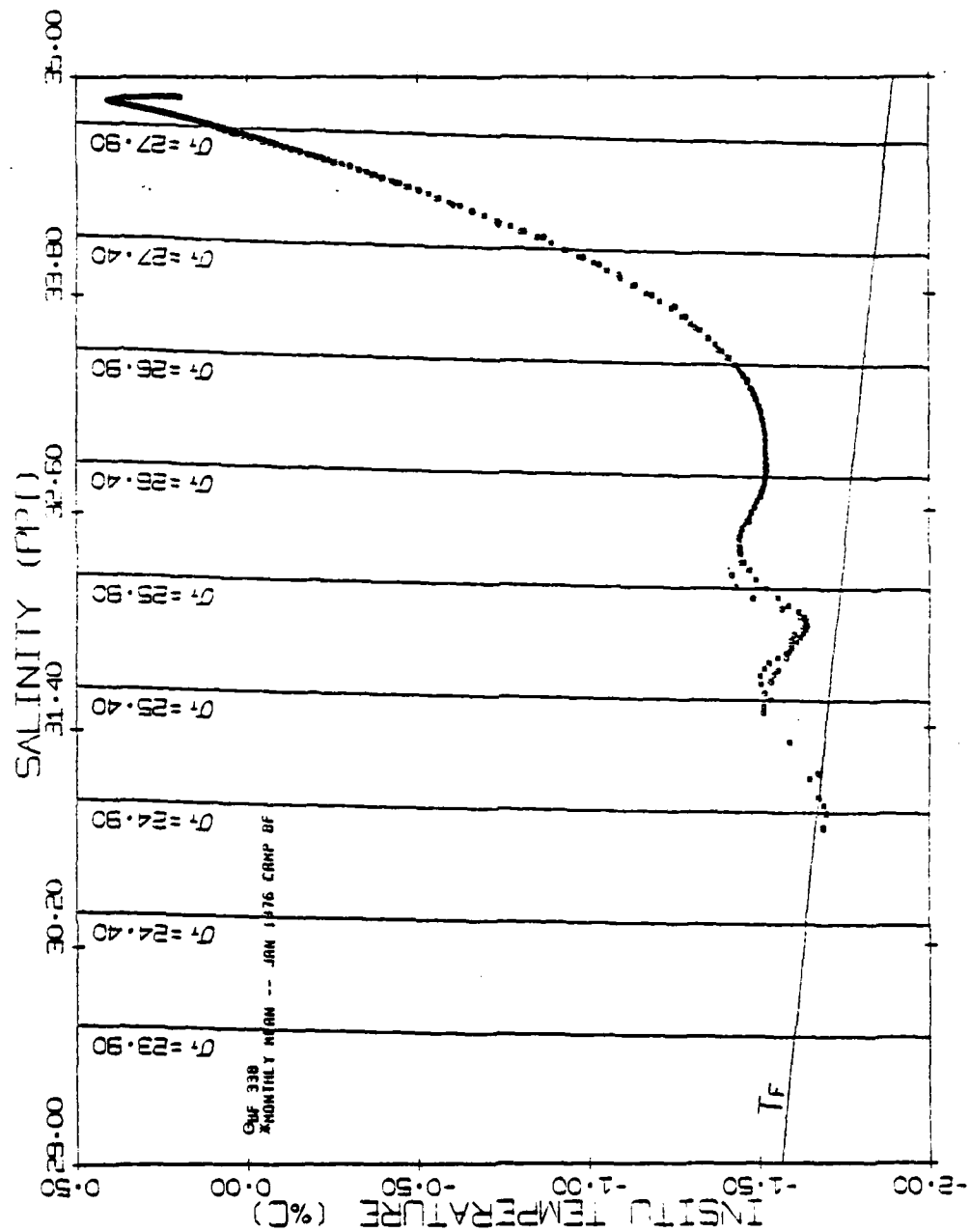

SALINITY (PPT)
35.00
33.00
32.60
31.40
30.20
29.00
σt =27.90
σt =27.40
σt =26.90
σt =26.40
σt =25.90
σt =25.40
σt =24.90
σt =24.40
σt =23.90
INSITU TEMPERATURE (°C)
0.50
0.00
-0.50
-1.00
-1.50
-2.00
T_F
*HUNTHLY MEAN -- NOV 1975 CHNP BF

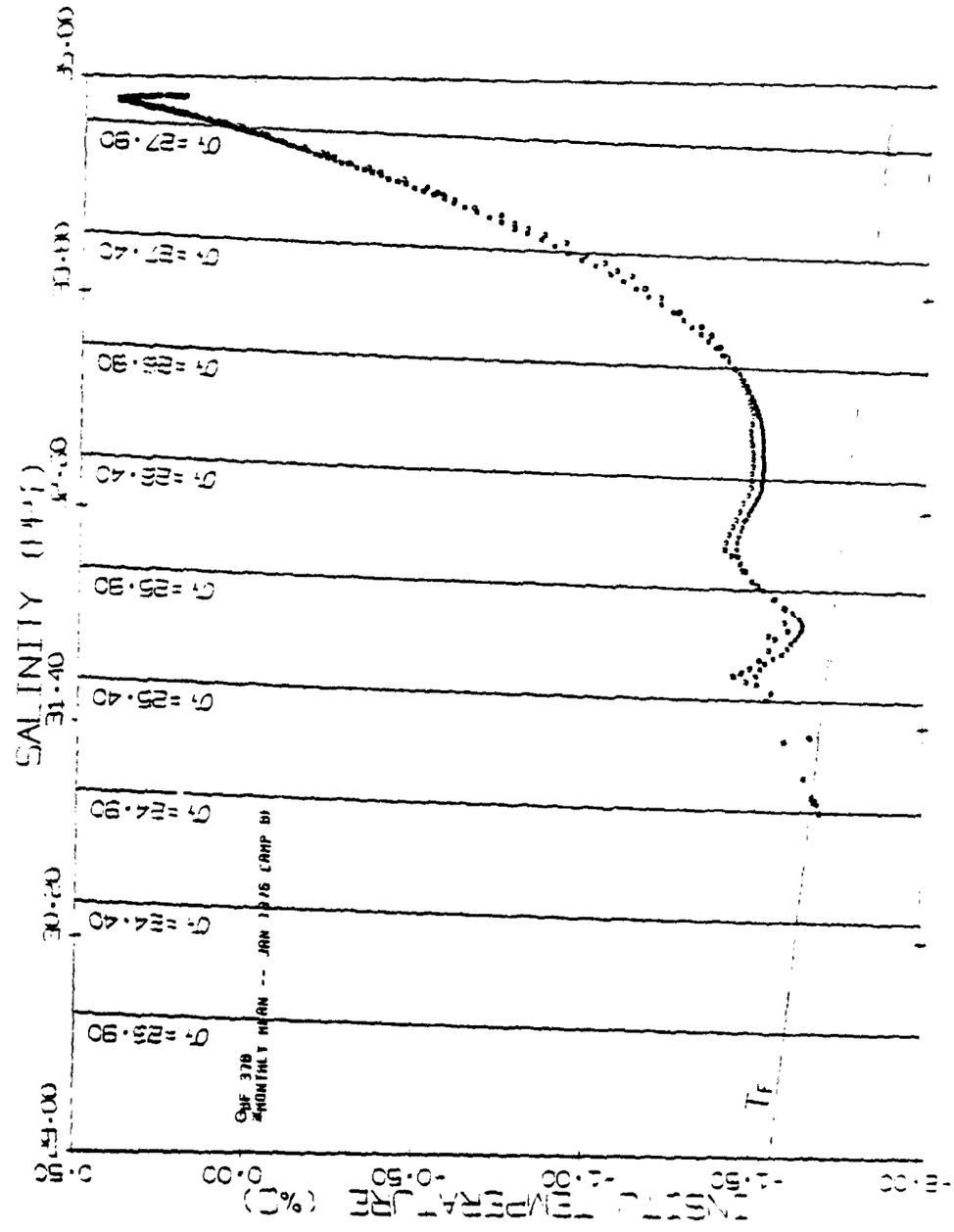

SALINITY (PPT)
35.00
33.80
32.60
31.40
30.20
29.00
σt =27.90
σt =27.40
σt =26.90
σt =26.40
σt =25.90
σt =25.40
σt =24.90
σt =24.40
σt =23.90
T_F
0.50
0.00
-0.50
-1.00
-1.50
-2.00
(°C)

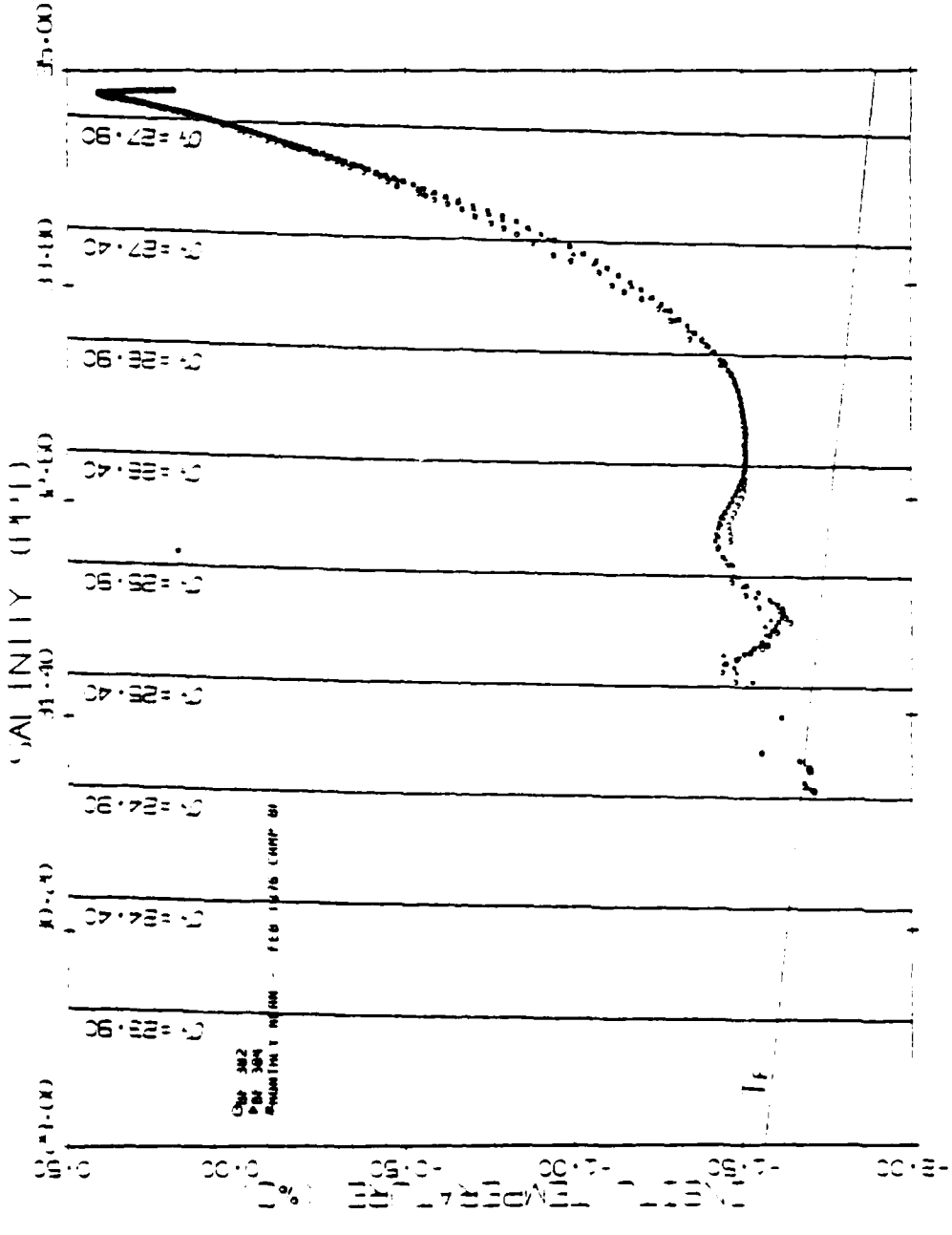

SALINITY (PPT)
POTENTIAL TEMPERATURE (°C)
35.00
33.80
32.60
31.40
30.20
29.00
0.50
0.00
-0.50
-1.00
-1.50
-2.00
σt =27.90
σt =27.40
σt =26.90
σt =26.40
σt =25.90
σt =25.40
σt =24.90
σt =24.40
σt =23.90
T_F
BF 284
BF 286
BF 298
MONTHLY MEAN -- NOV 1975 CAMP BF

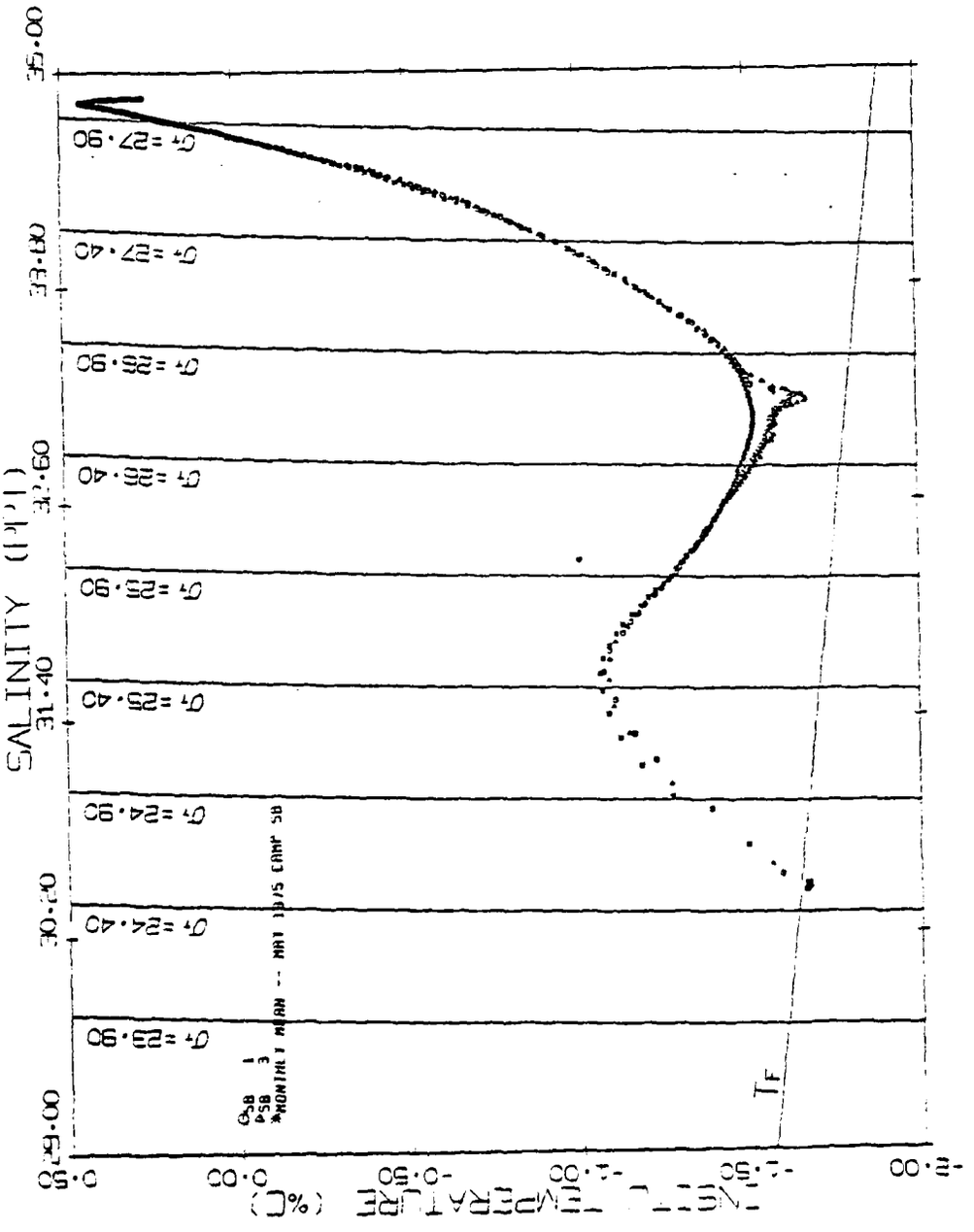

SALINITY (PPT)
35.00
33.80
32.60
31.40
30.20
29.00
σt =27.90
σt =27.40
σt =26.90
σt =25.40
σt =25.90
σt =25.40
σt =24.90
σt =24.40
σt =23.90
POTENTIAL TEMPERATURE (°C)
0.50
0.00
-0.50
-1.00
-1.50
-2.00
T_F
CRUISE 299
STA 388
MONTHLY MEAN -- DEC 1975 CAMP BF

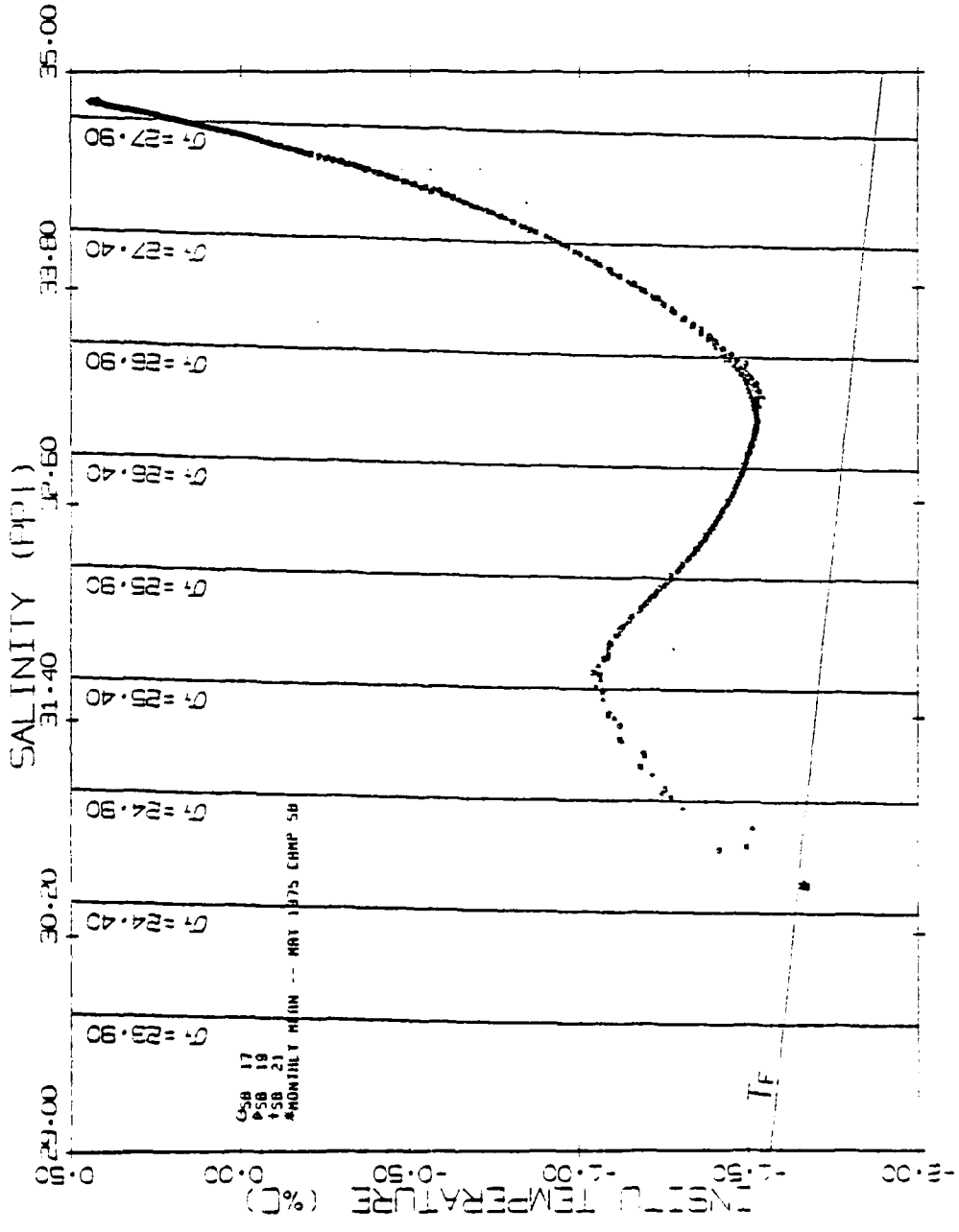

SALINITY (PPT)
35.00
34.60
34.20
33.80
33.40
33.00
σt =27.90
σt =27.40
σt =26.90
σt =26.40
σt =25.90
σt =25.40
σt =24.90
σt =24.40
σt =23.90
JAN 1976 CAMP BF
MEAN -- JAN 1976 CAMP BF
BF 324
BF 326
BF 328
BF 330
BF 332
BF 334
MONTHLY MEAN
POTENTIAL TEMPERATURE (°C)
0.50
0.00
-0.50
-1.00
-1.50
-2.00
T_f

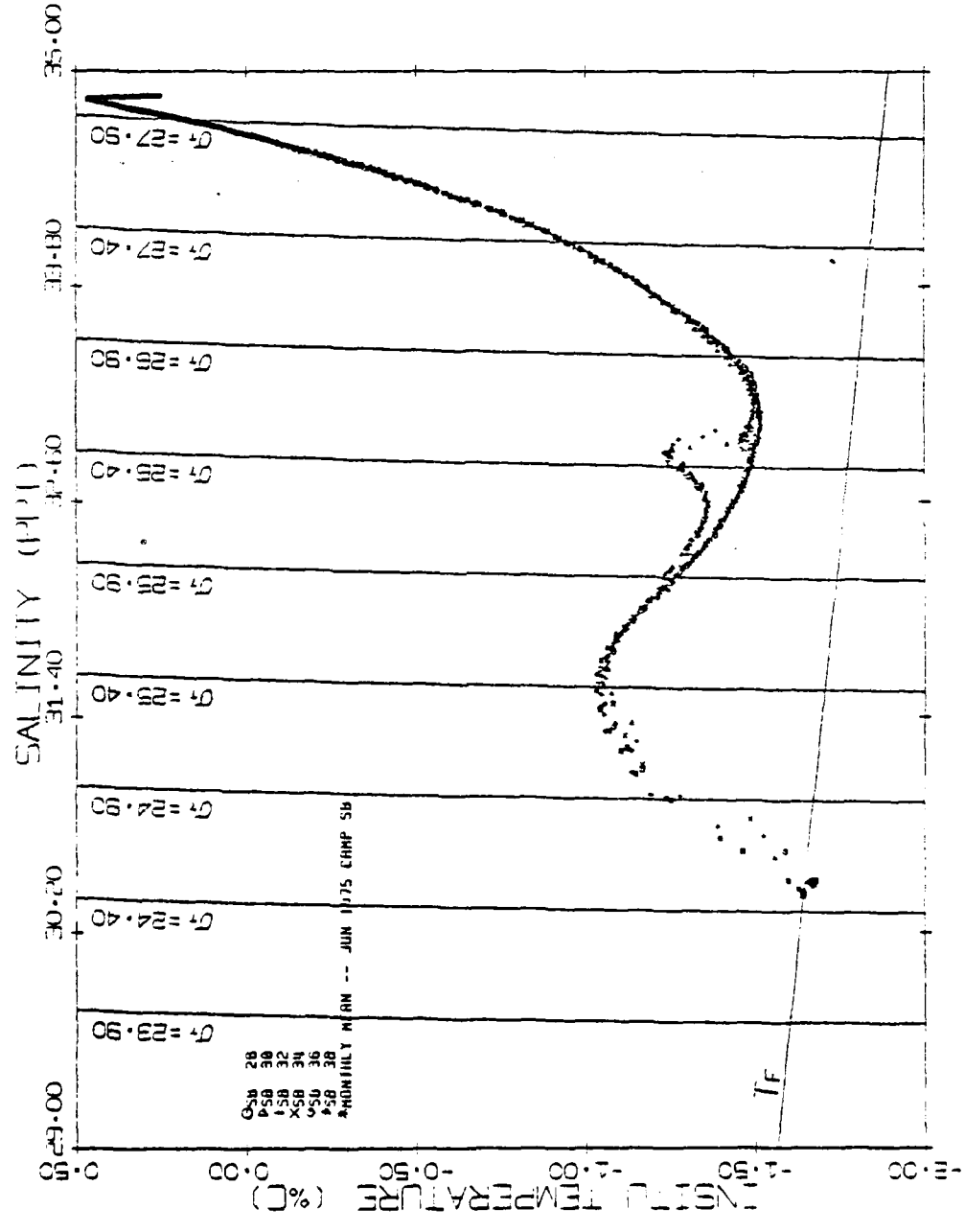

SALINITY (PPT)
POTENTIAL TEMPERATURE (°C)
σt =23.90
σt =24.40
σt =24.90
σt =25.40
σt =25.90
σt =26.40
σt =26.90
σt =27.40
σt =27.90
TF
GUF 338
MONTHLY MEAN -- JAN 1976 CAMP BF

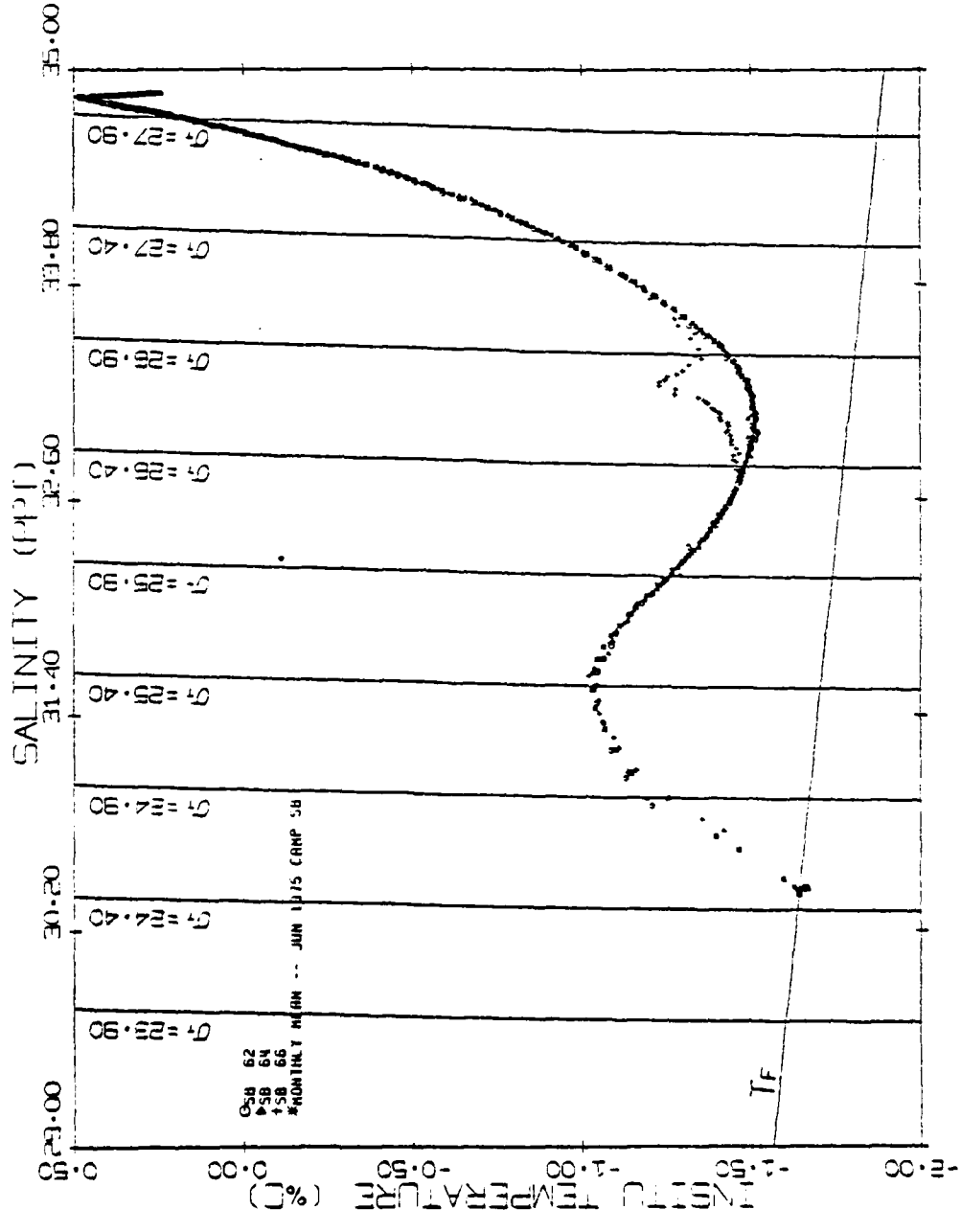

SALINITY (0/00)
31.00
31.20
31.40
σt =27.90
σt =27.40
σt =26.90
σt =26.40
σt =25.90
σt =25.40
σt =24.90
σt =24.40
σt =25.90
CHF 378
MONTHLY MEAN -- JAN 1976 CAMP 6
T_f
-2.00
-1.50
-1.00
-0.50
0.00
(°C)

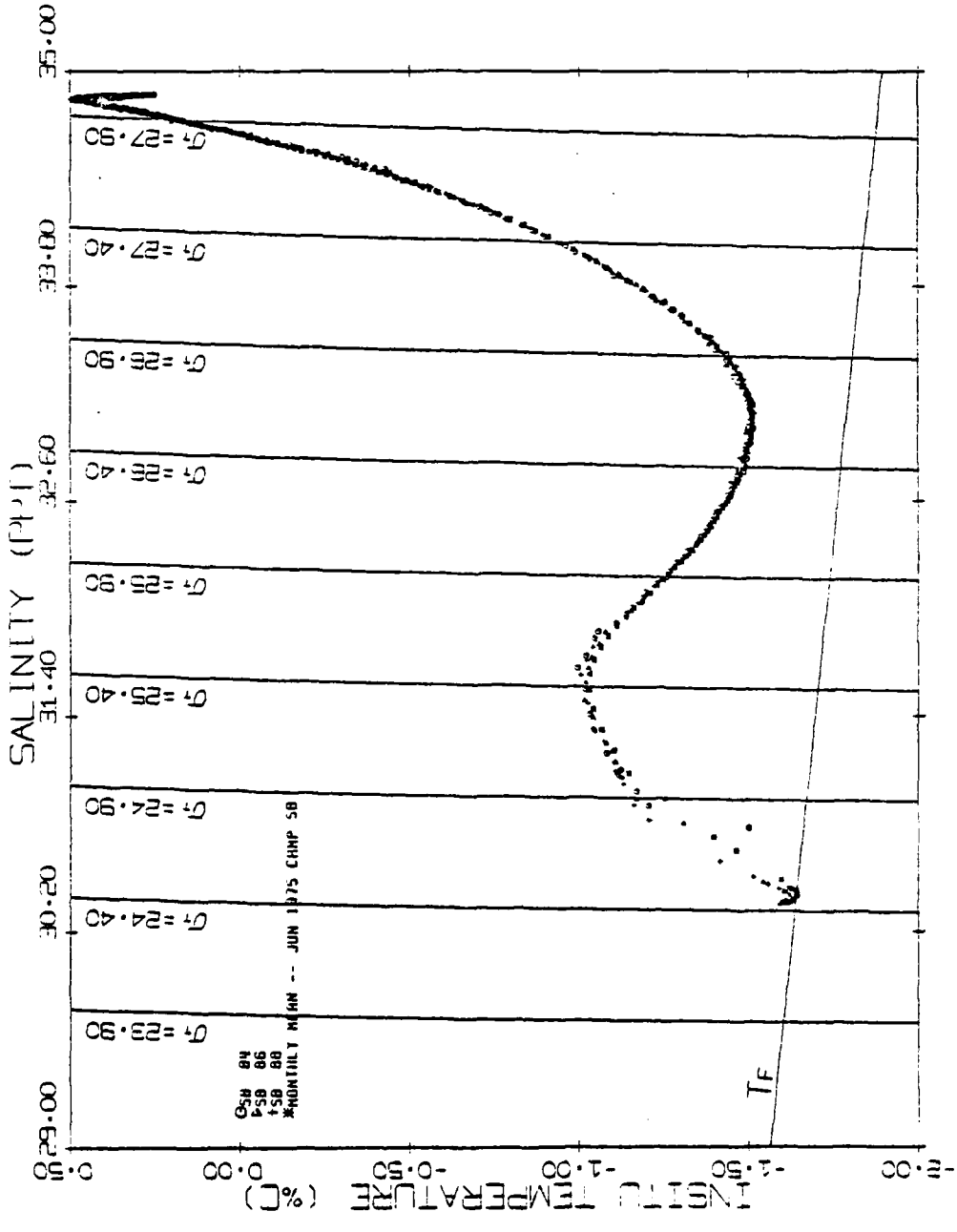


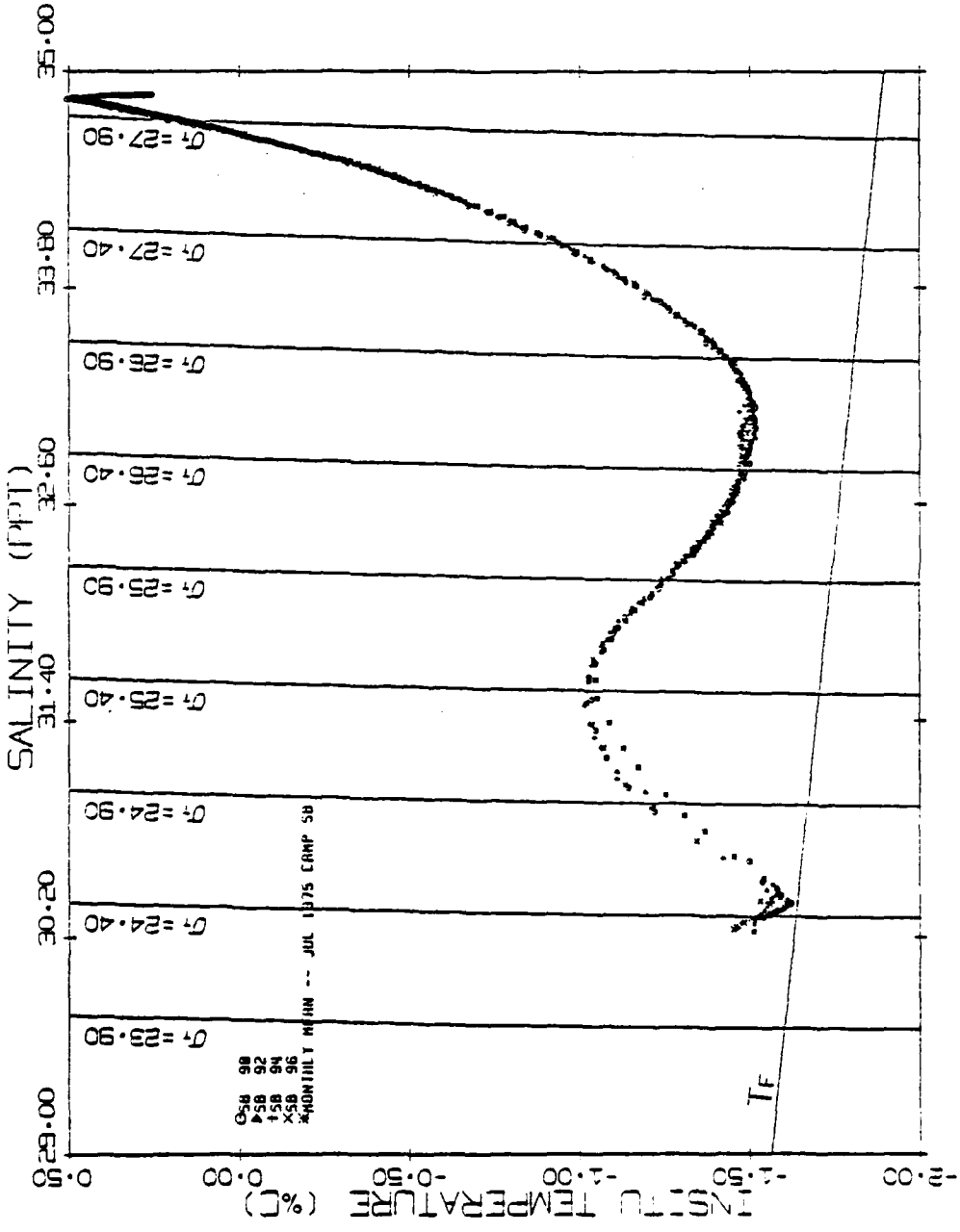

SALINITY (PPT)
35.00
33.80
32.60
31.40
30.20
29.00
σt =27.90
σt =27.40
σt =26.90
σt =26.40
σt =25.90
σt =25.40
σt =24.90
σt =24.40
σt =23.90
TF
0.50
0.00
-0.50
-1.00
-1.50
-2.00
(°C)

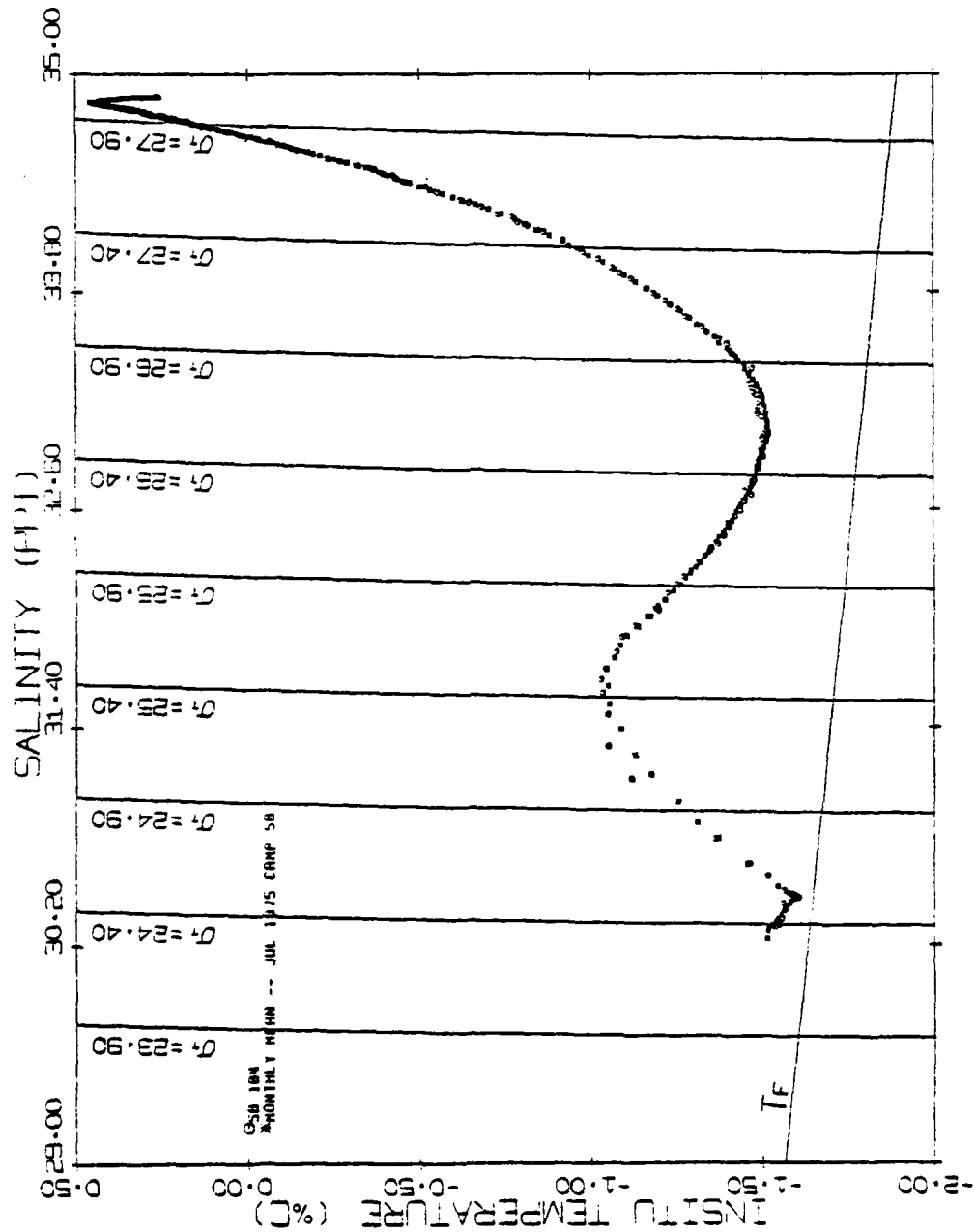

SALINITY (PPT)
35.00
33.80
32.60
31.40
30.20
29.00
σt =27.90
σt =27.40
σt =26.90
σt =26.40
σt =25.90
σt =25.40
σt =24.90
σt =24.40
σt =23.90
0.50
0.00
-0.50
-1.00
-1.50
-2.00
POTENTIAL TEMPERATURE (°C)
T_F

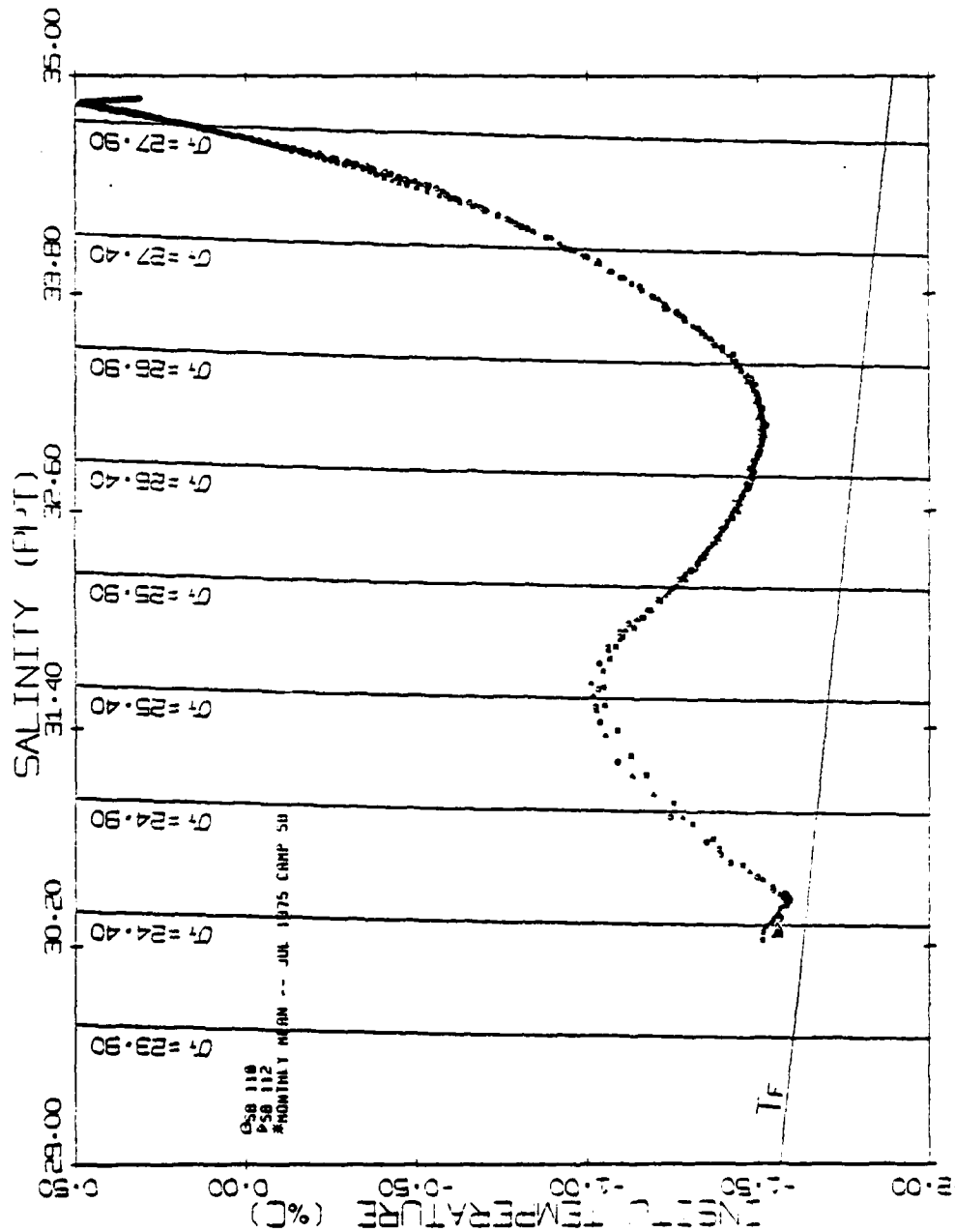

SALINITY (PPT)
POTENTIAL TEMPERATURE (°C)
σθ =27.90
σθ =27.40
σθ =26.90
σθ =26.40
σθ =25.90
σθ =25.40
σθ =24.90
σθ =24.40
σθ =23.90
35.00
33.80
32.60
31.40
30.20
29.00
0.0
-0.50
-1.00
-1.50
-2.00
TF
σθ 28
30
32
34
36
38
*MONTHLY MEAN -- JUN 1975 CAMP SB

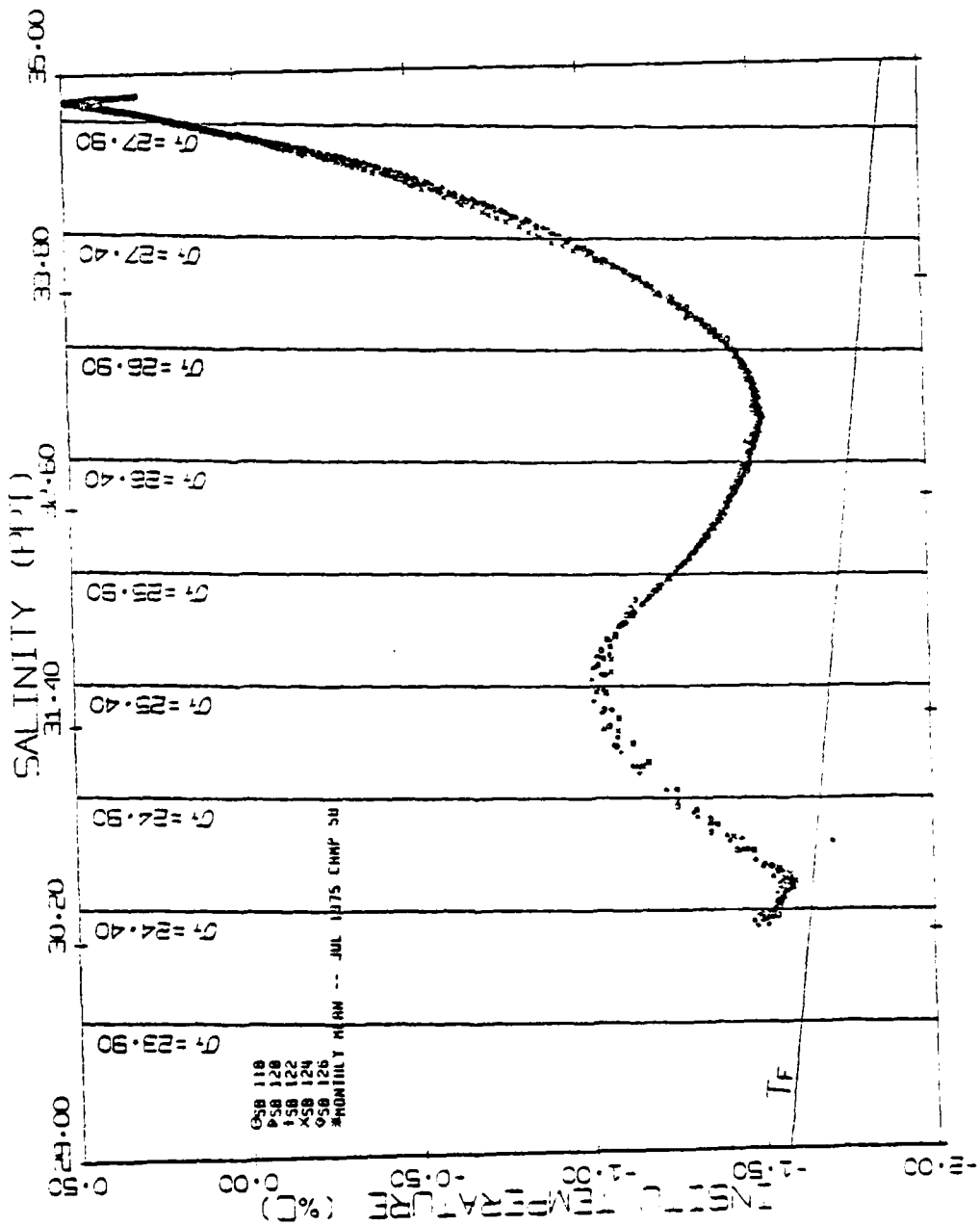

SALINITY (PPT)
35.00
33.80
32.60
31.40
30.20
29.00
σt =27.90
σt =27.40
σt =26.90
σt =26.40
σt =25.90
σt =25.40
σt =24.90
σt =24.40
σt =23.90
JUN 1975 CAMP 5B
62
64
66
MONTHLY MEAN
T_F
0.00
-0.50
-1.00
-1.50
-2.00
INSITU TEMPERATURE (°C)

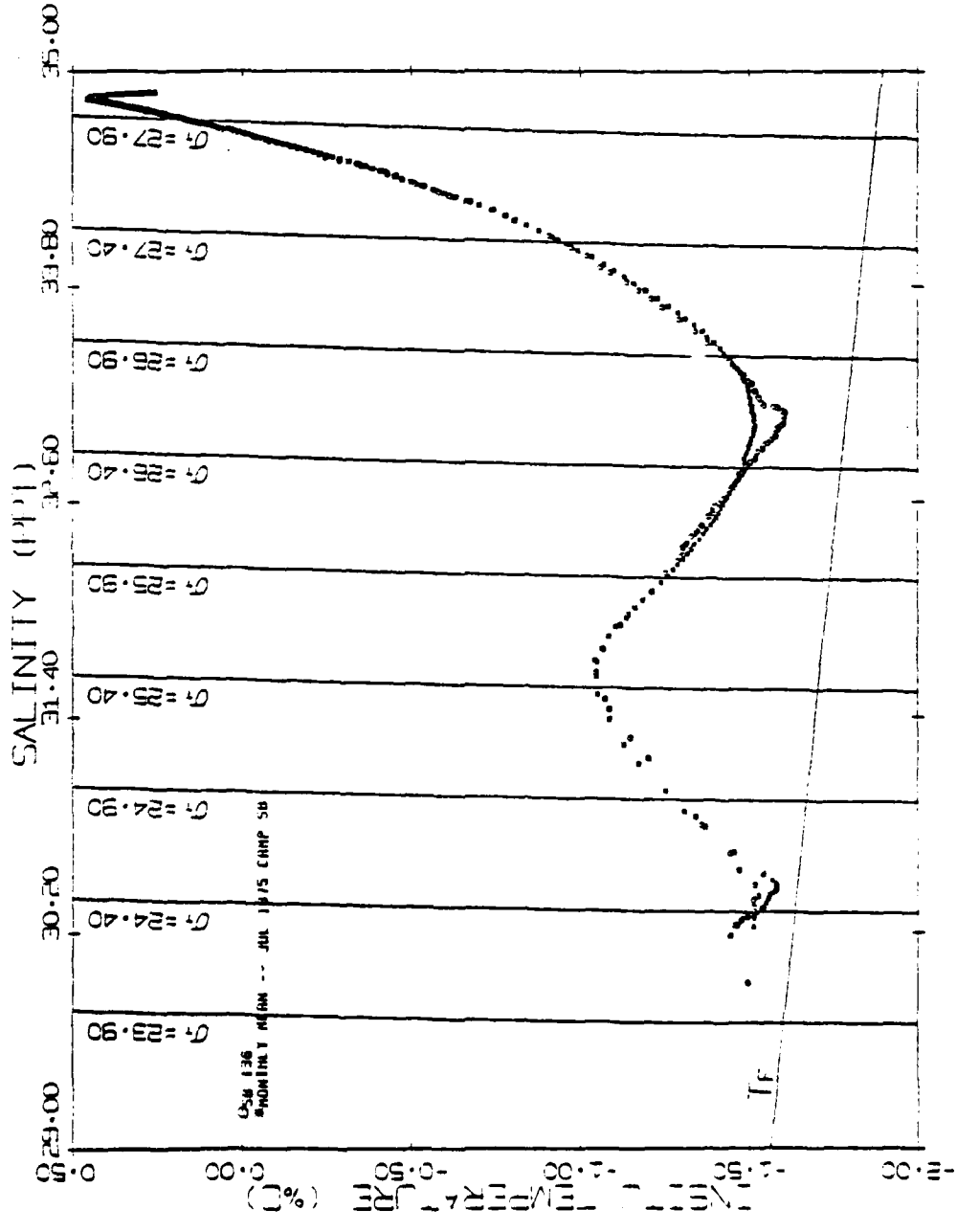

SALINITY (PPT)
INSITU TEMPERATURE (°C)
σt =27.90
σt =27.40
σt =26.90
σt =26.40
σt =25.90
σt =25.40
σt =24.90
σt =24.40
σt =23.90
T_F
MONTHLY MEAN -- JUN 1975 CHMP SB

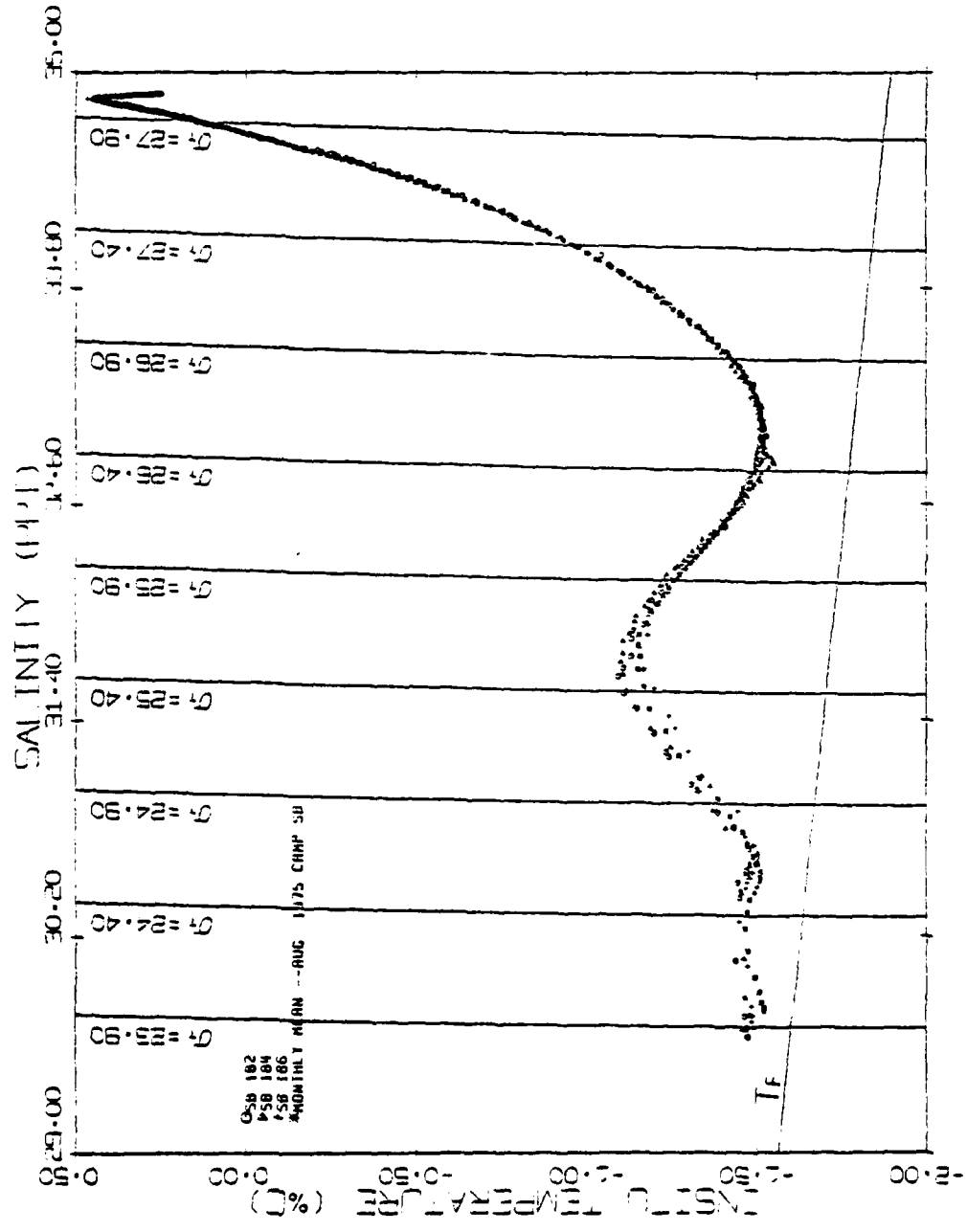

SALINITY (PPT)
IN SITU TEMPERATURE (°C)
σt =27.90
σt =27.40
σt =26.90
σt =26.40
σt =25.90
σt =25.40
σt =24.90
σt =24.40
σt =23.90
35.00
33.80
32.60
31.40
30.20
29.00
0.50
0.00
-0.50
-1.00
-1.50
-2.00
T_F
MONTHLY MEAN -- JUL 1975 CRMP SB
SB 90
SB 92
SB 94
SB 96

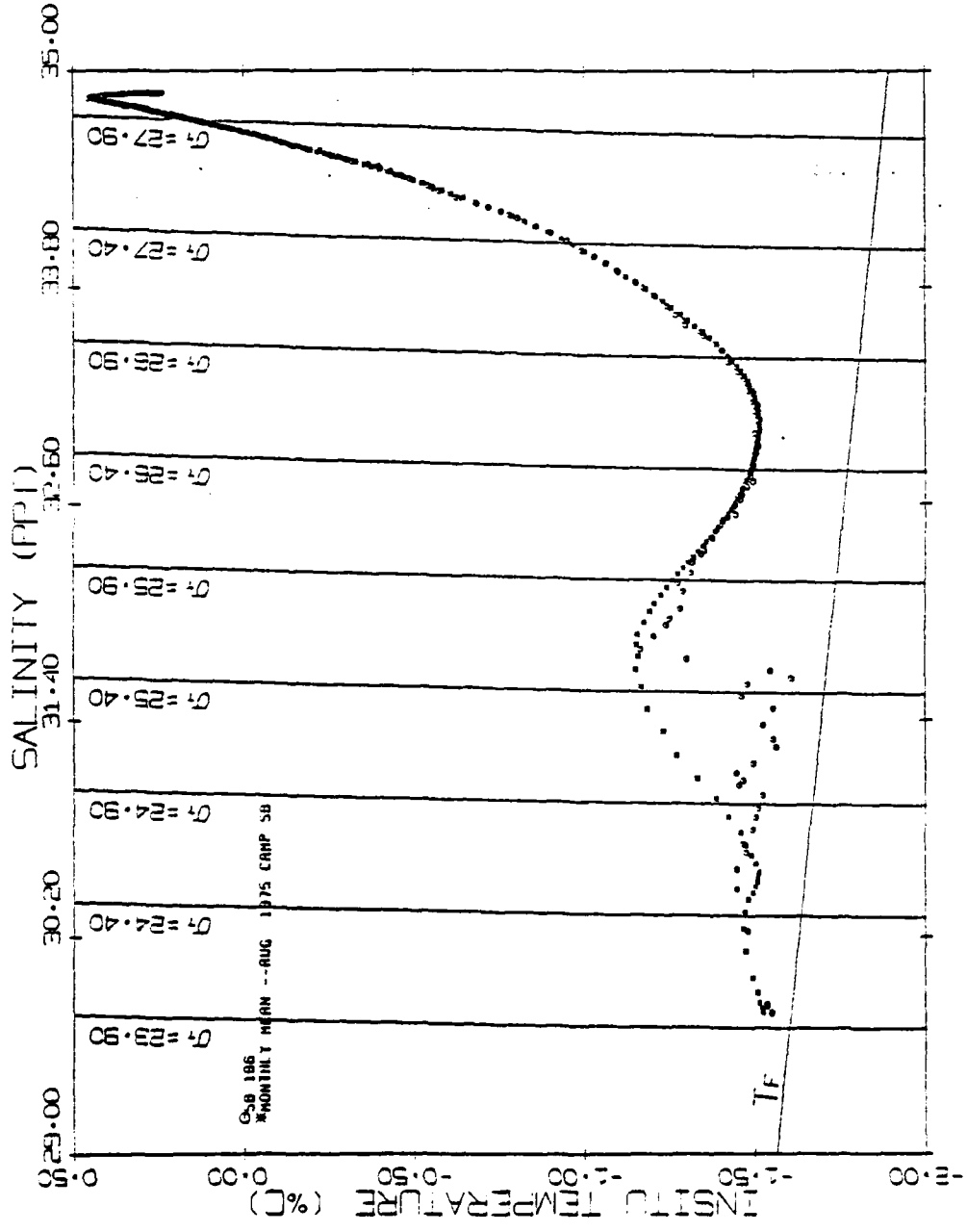

SALINITY (PPT)
35.00
33.80
32.60
31.40
30.20
29.00
σt =27.90
σt =27.40
σt =26.90
σt =26.40
σt =25.90
σt =25.40
σt =24.90
σt =24.40
σt =23.90
TF
INSITU TEMPERATURE (°C)
0.50
0.00
-0.50
-1.00
-1.50
-2.00

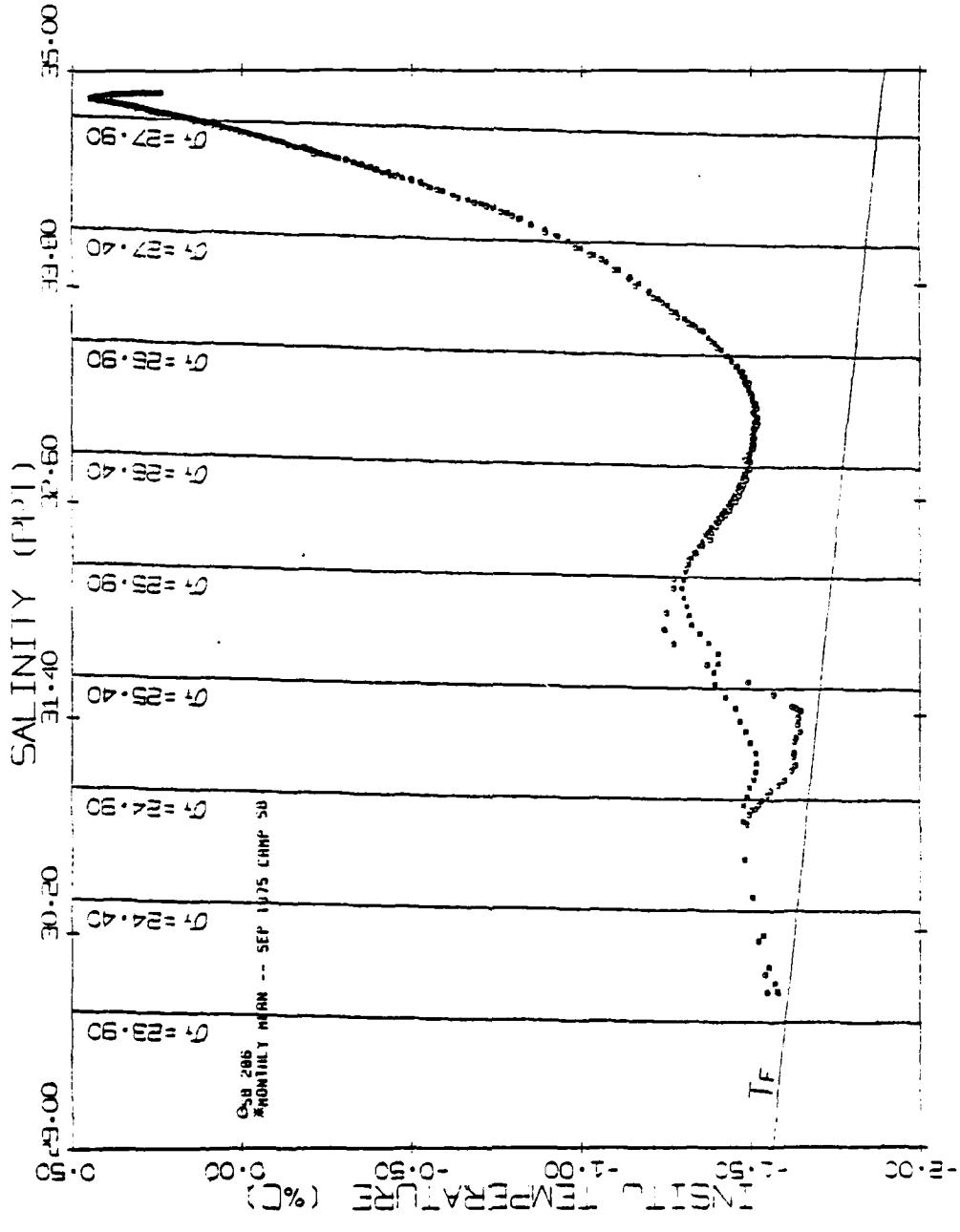

SALINITY (PPT)
POTENTIAL TEMPERATURE (°C)
σt =27.90
σt =27.40
σt =26.90
σt =26.40
σt =25.90
σt =25.40
σt =24.90
σt =24.40
σt =23.90
35.00
33.80
32.60
31.40
30.20
29.00
0.00
-0.50
-1.00
-1.50
-2.00
CSB 118
CSB 112
*MONTHLY MEAN -- JUL 1975 CAMP SU

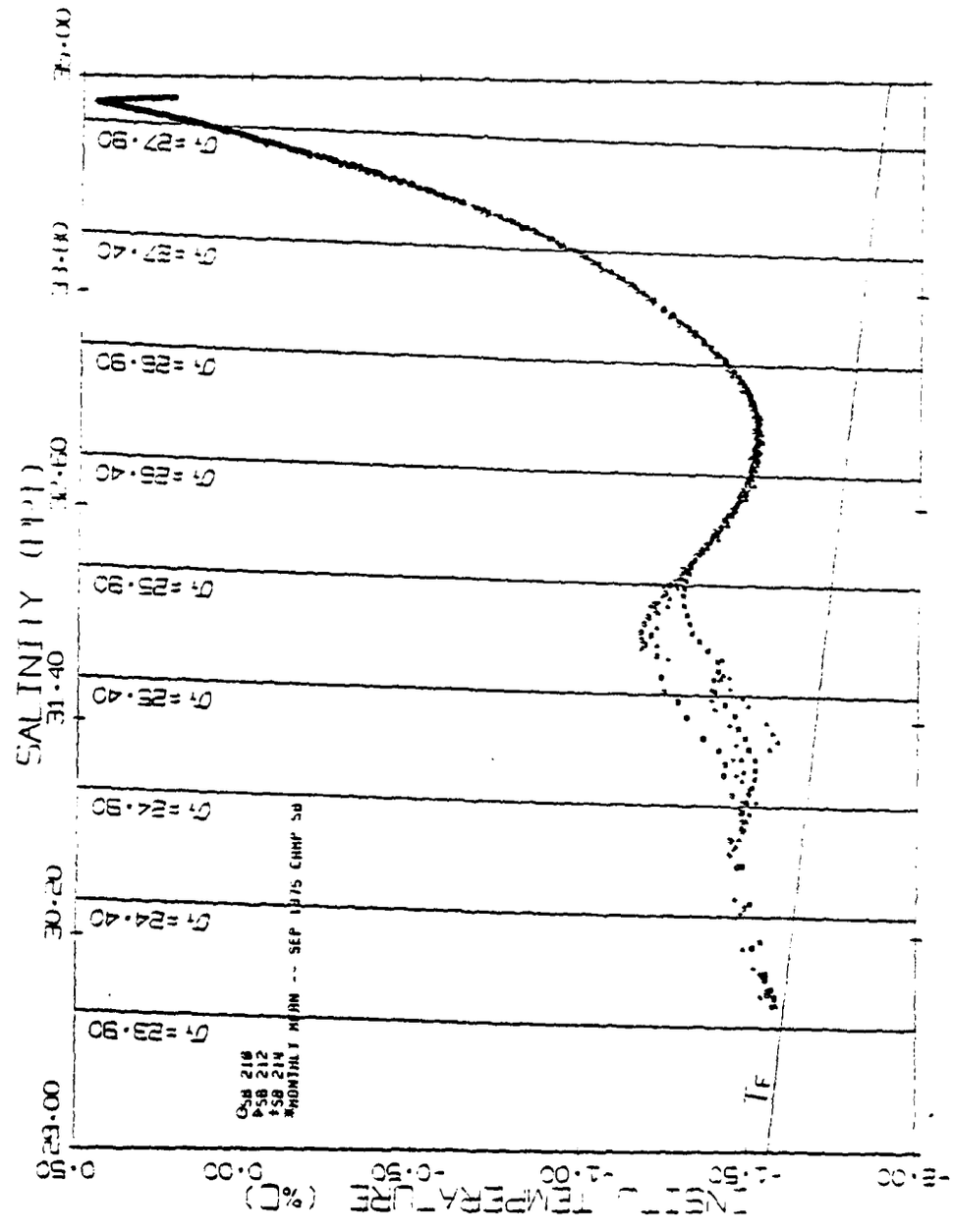

SALINITY (PPT)
35.00
34.80
34.60
34.40
34.20
34.00
σt =27.90
σt =27.40
σt =26.90
σt =26.40
σt =25.90
σt =25.40
σt =24.90
σt =24.40
σt =23.90
PSB 118
PSB 120
PSB 122
XSB 124
PSB 126
*HONOLULU MEAN -- JUL 1975 CHMP 30
T_F
0.50
0.00
-0.50
-1.00
-1.50
-2.00

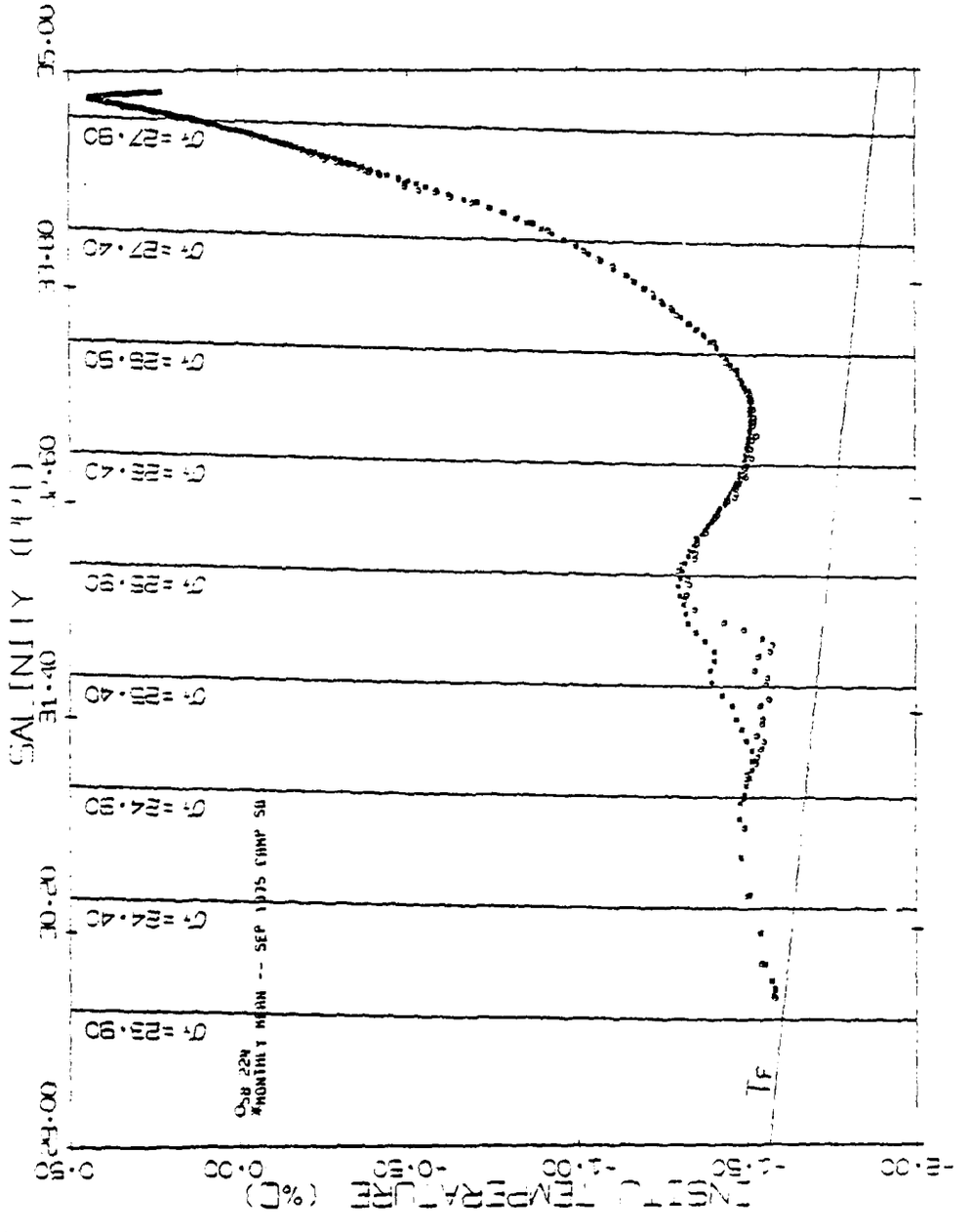

SALINITY (PPT)
35.00
33.80
32.60
31.40
30.20
29.00
σt =27.90
σt =27.40
σt =26.90
σt =26.40
σt =25.90
σt =25.40
σt =24.90
σt =24.40
σt =23.90
0.50
0.00
-0.50
-1.00
-1.50
-2.00
(°C)
Tf

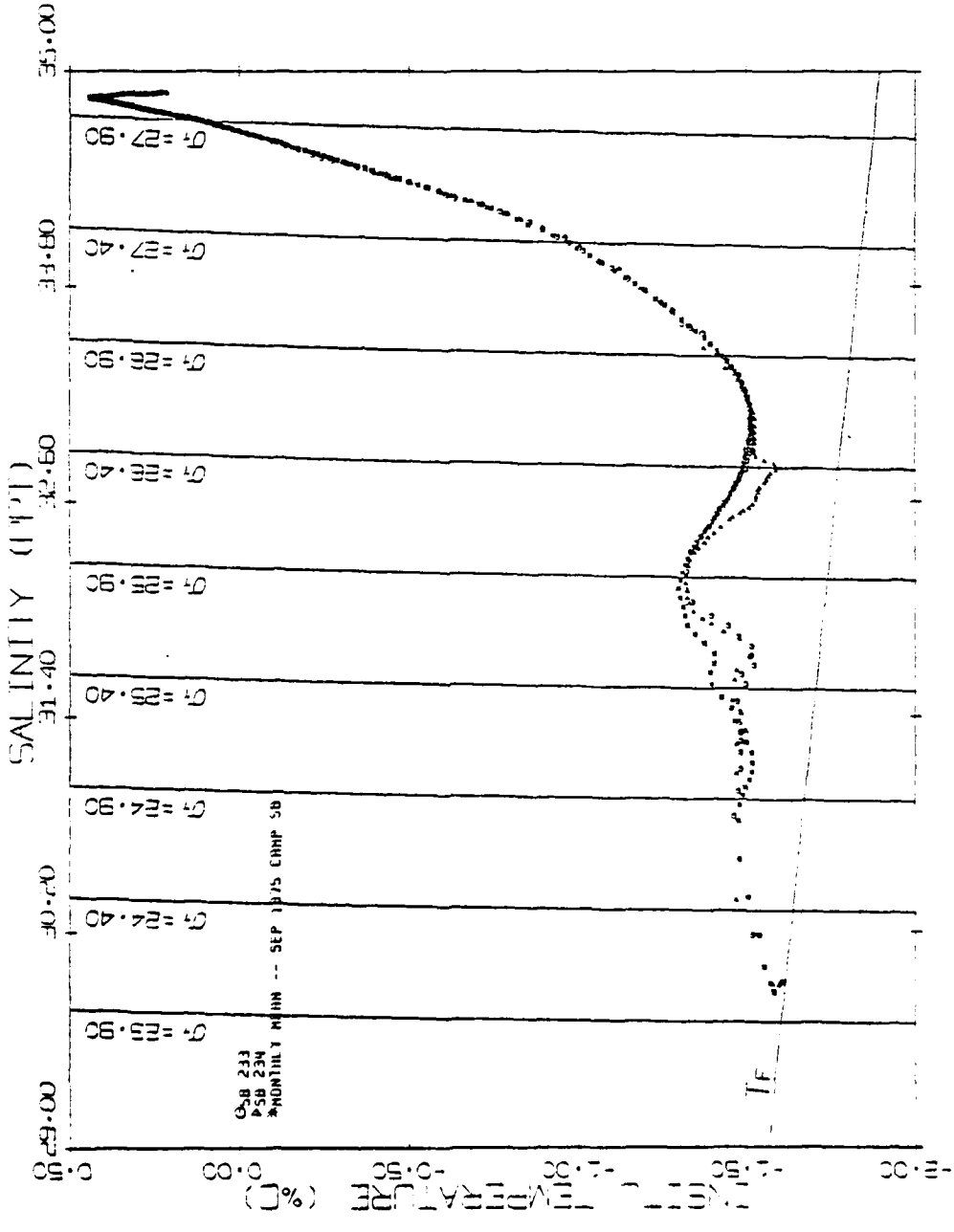

POTENTIAL TEMPERATURE (°C)
SALINITY (‰)
T_f
σθ = 27.90
σθ = 27.40
σθ = 26.90
σθ = 26.40
σθ = 25.90
σθ = 25.40
σθ = 24.90
σθ = 24.40
σθ = 23.90
MEAN --AUG 1975 CHAF SB
MONTHLY

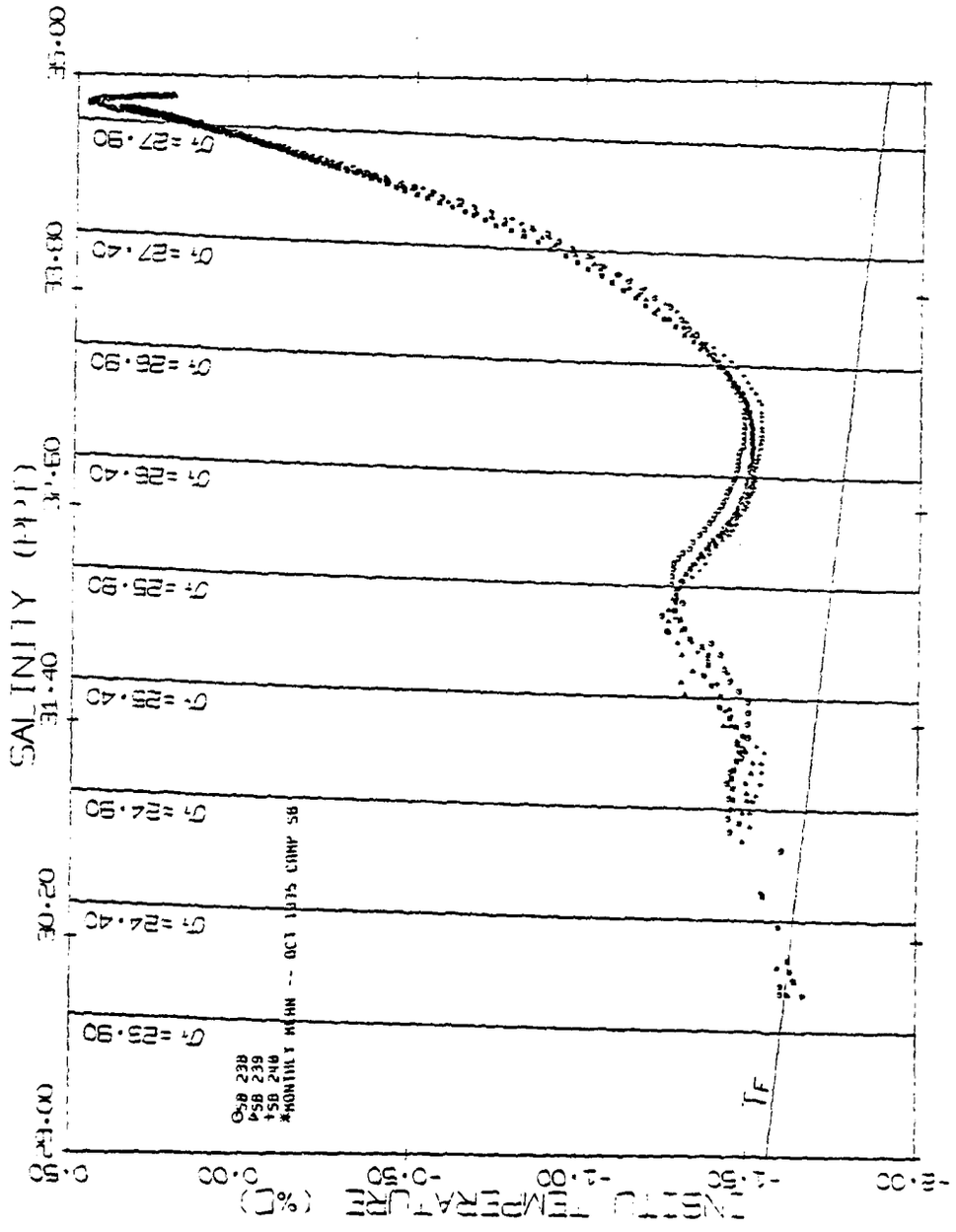

SALINITY (PPT)
35.00
33.80
32.60
31.40
30.20
29.00
σt =27.90
σt =27.40
σt =26.90
σt =26.40
σt =25.90
σt =25.40
σt =24.90
σt =24.40
σt =23.90
INSITU TEMPERATURE (°C)
0.50
0.00
-0.50
-1.00
-1.50
-2.00
T_F
CSB 186
*MONTHLY MEAN --AUG 1975 CAMP SB

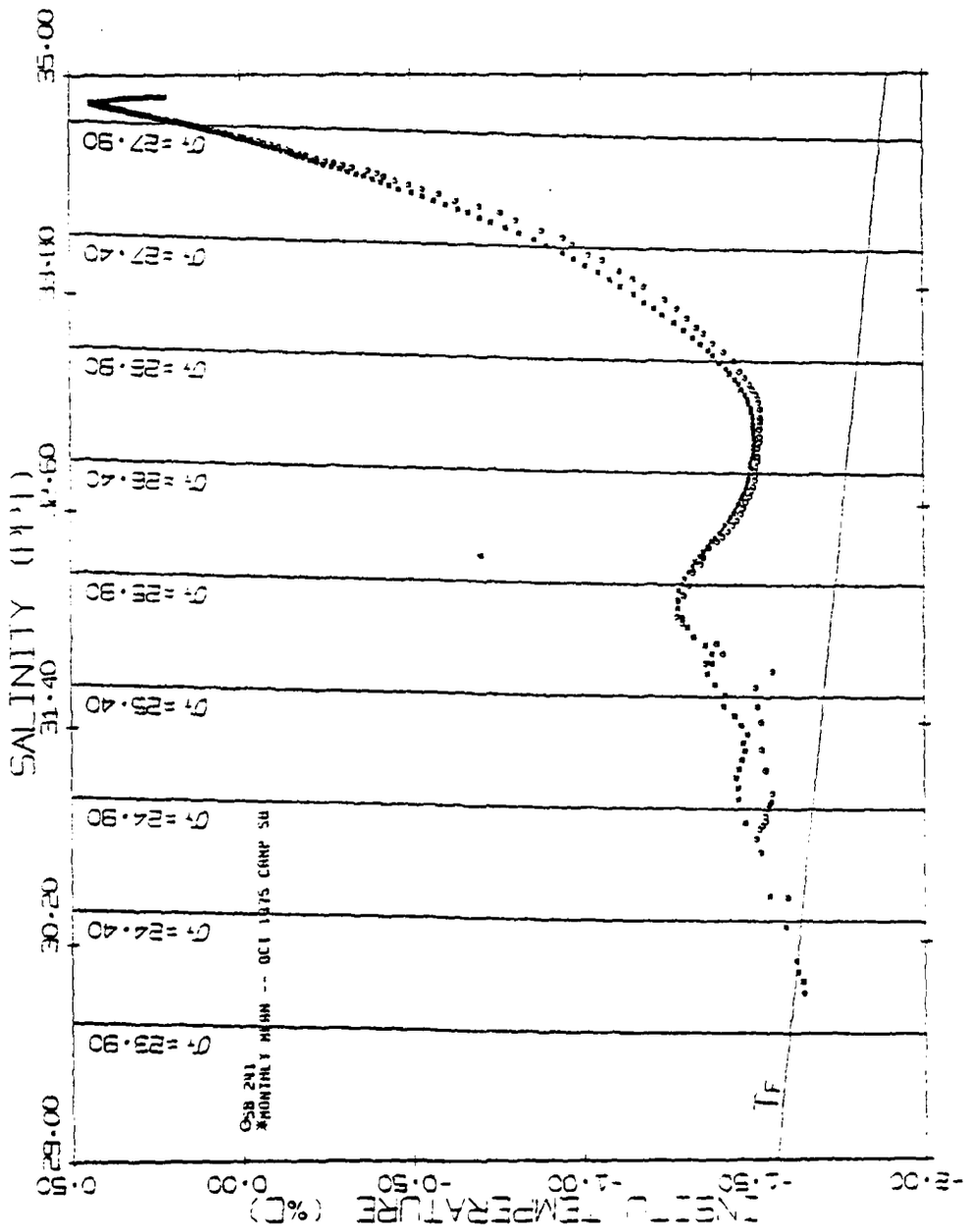

SALINITY (PPT)
35.00
33.80
32.60
31.40
30.20
29.00
σt =27.90
σt =27.40
σt =26.90
σt =26.40
σt =25.90
σt =25.40
σt =24.90
σt =24.40
σt =23.90
POTENTIAL TEMPERATURE (°C)
0.50
0.00
-0.50
-1.00
-1.50
-2.00
T_F
CSB 286
MONTHLY MEAN -- SEP 1975 CHNP SB

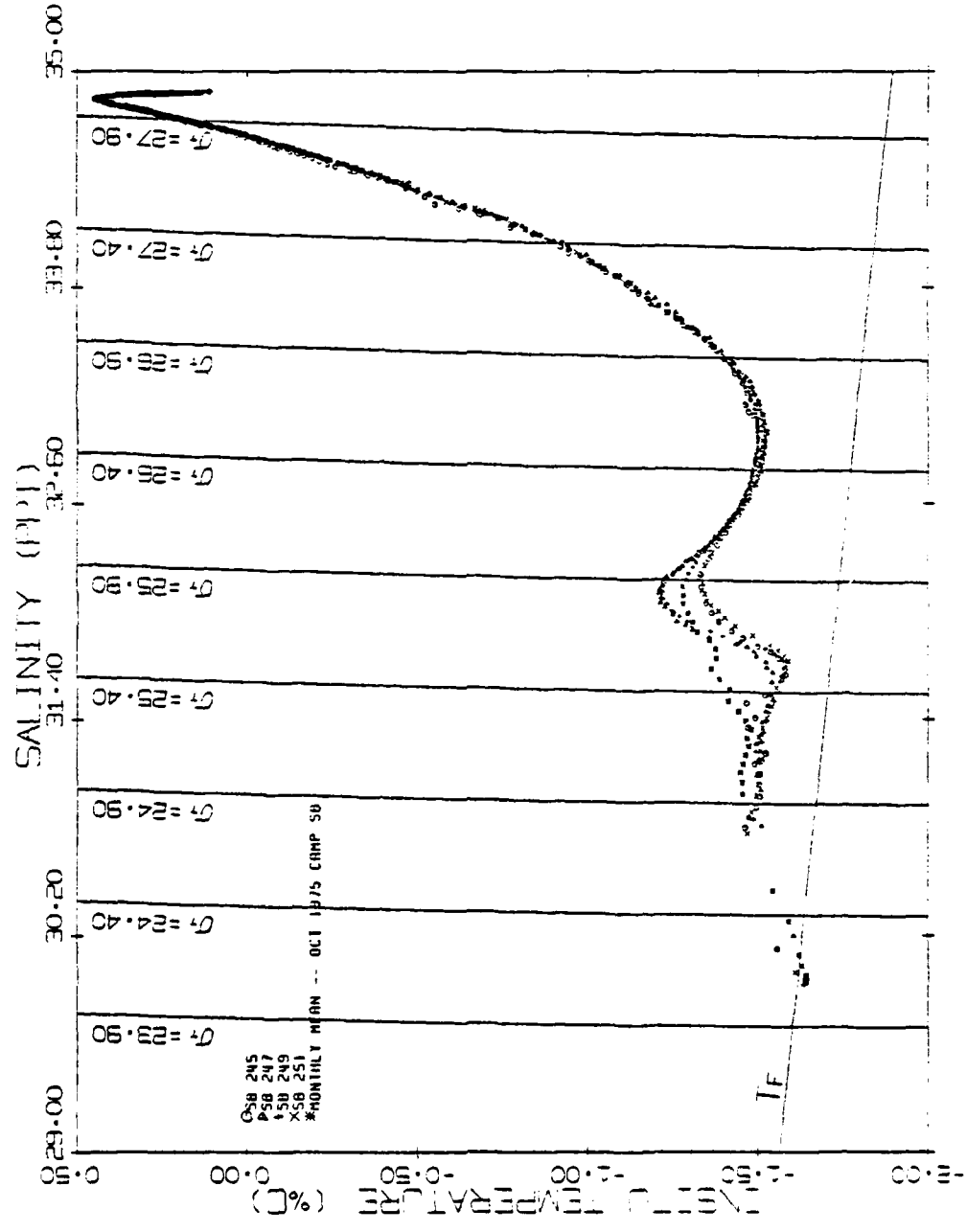

SALINITY (PPT)
31.40
30.20
σt =27.90
σt =27.40
σt =26.90
σt =26.40
σt =25.90
σt =25.40
σt =24.90
σt =24.40
σt =23.90
CSB 210
CSB 212
CSB 214
*MONTHLY MEAN -- SEP 1975 CNMP SB
POTENTIAL TEMPERATURE (°C)
0.00
-0.50
-1.00
-1.50

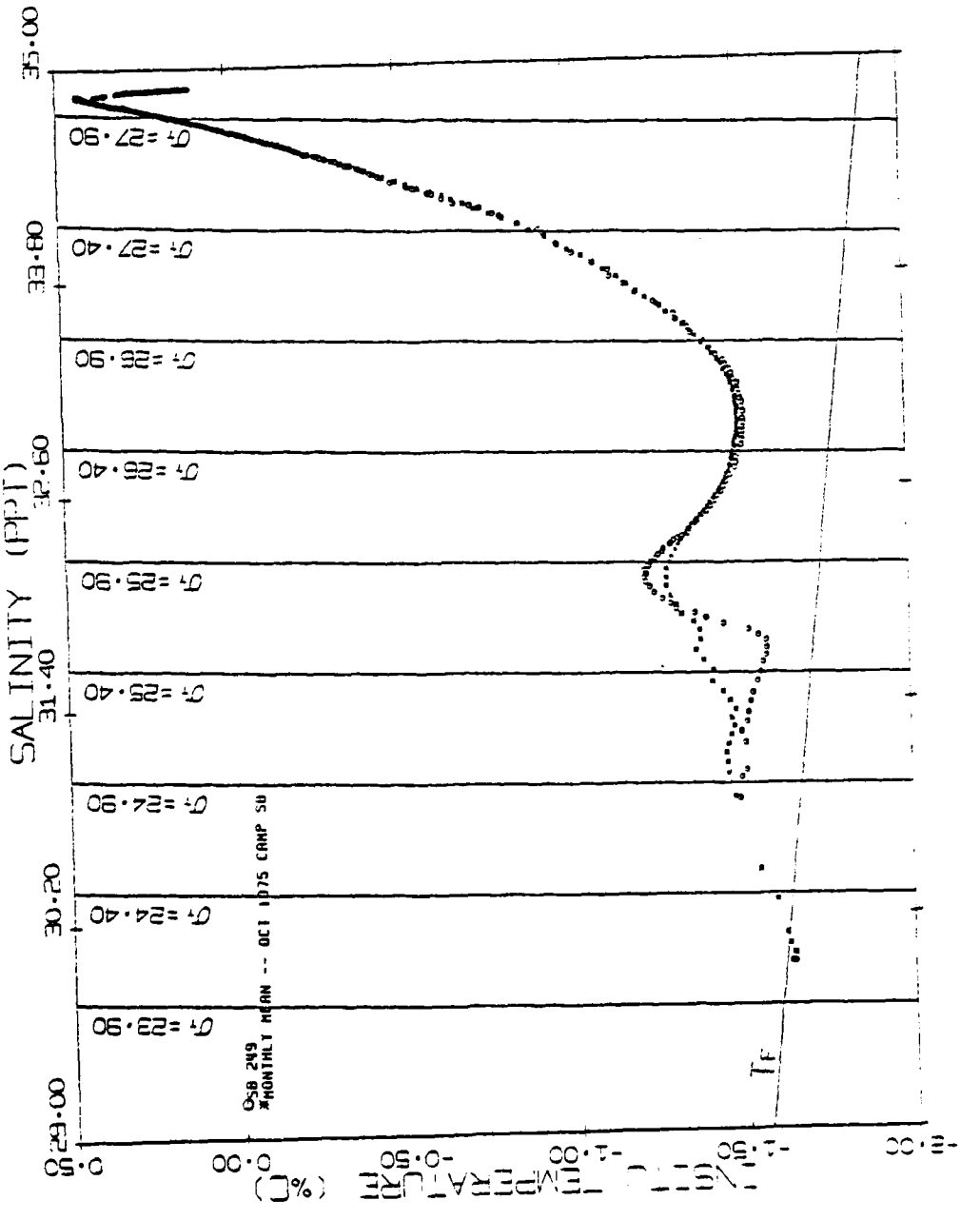

SALINITY (PPT)
35.00
34.80
34.60
34.40
34.20
34.00
σt =27.80
σt =27.40
σt =26.60
σt =26.40
σt =25.80
σt =25.40
σt =24.80
σt =24.40
σt =23.80
POTENTIAL TEMPERATURE (°C)
0.50
0.00
-0.50
-1.00
-1.50
-2.00
Tf
22N
NOMINAL MEAN -- SEP 1975 CHAP 58

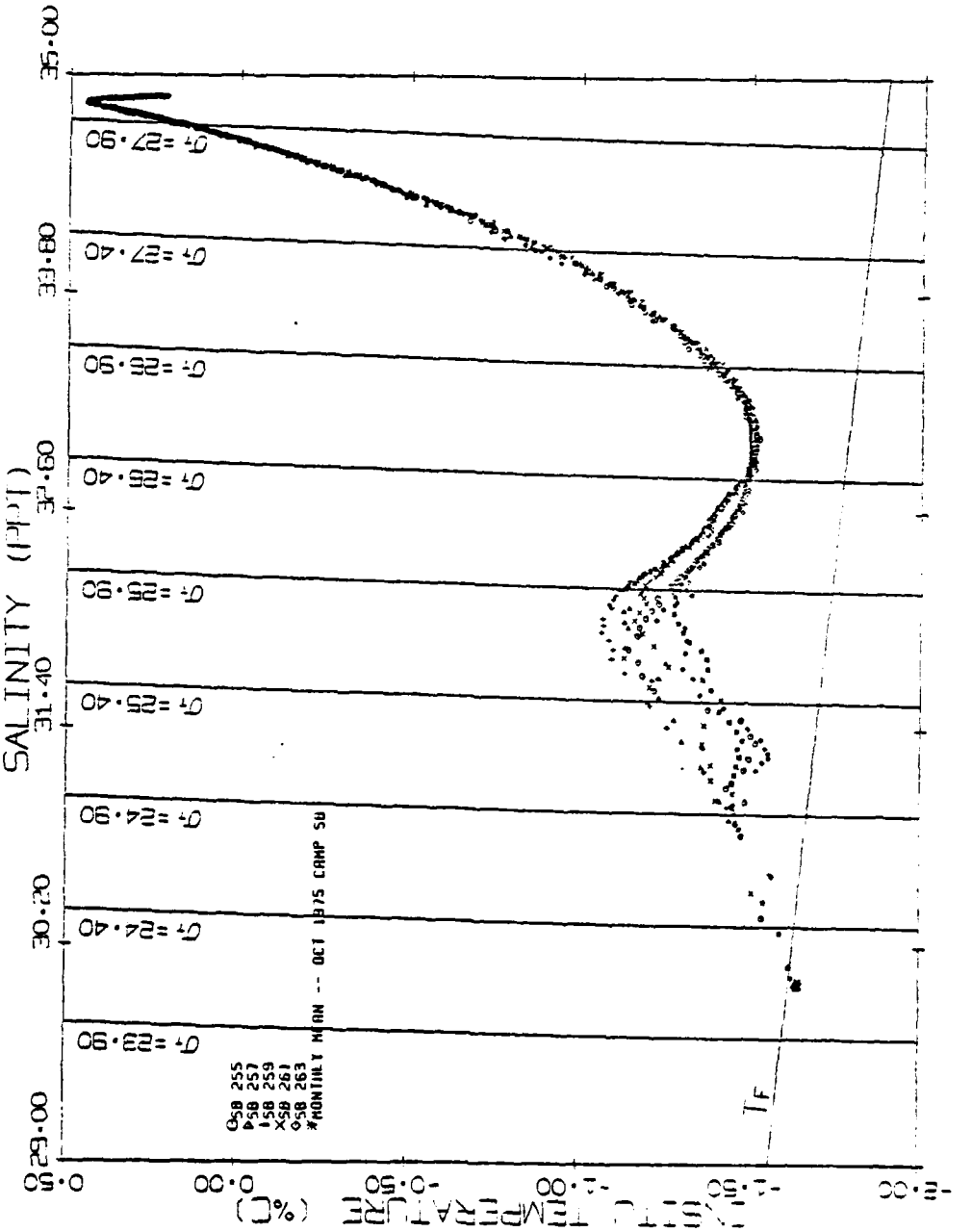

SALINITY (PPT)
35.00
34.80
32.60
31.40
30.20
29.00
σt =27.90
σt =27.40
σt =26.90
σt =26.40
σt =25.90
σt =25.40
σt =24.90
σt =24.40
σt =23.90
0.00
-0.50
-1.00
-1.50
-2.00
TEMPERATURE (°C)
Osb 233
Psb 234
*MONTHLY MEAN -- SEP 1975 CHMP 58

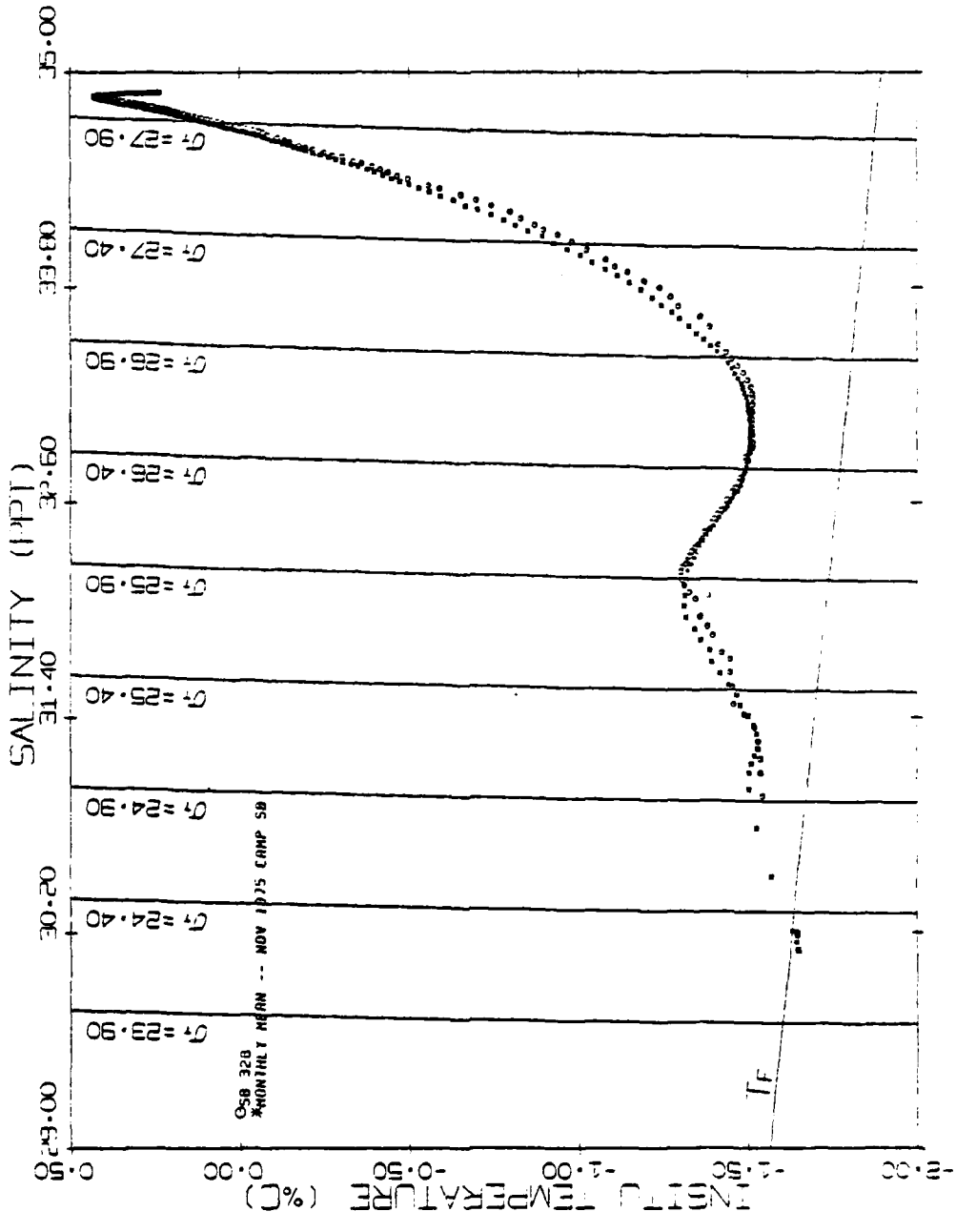

SALINITY (‰)
POTENTIAL TEMPERATURE (°C)
σt =27.90
σt =27.40
σt =26.90
σt =26.40
σt =25.90
σt =25.40
σt =24.90
σt =24.40
σt =25.90
TF
CTD 238
CTD 239
CTD 240


POTENTIAL TEMPERATURE (°C)
SALINITY (‰)
35.00
34.80
34.60
34.40
34.20
34.00
0.50
0.00
-0.50
-1.00
-1.50
-2.00
σt =27.80
σt =27.40
σt =26.80
σt =26.40
σt =25.80
σt =25.40
σt =24.80
σt =24.40
σt =23.80
OSB 241
*MONTHLY MEAN -- OCT 1975 CHNP SU
T_F

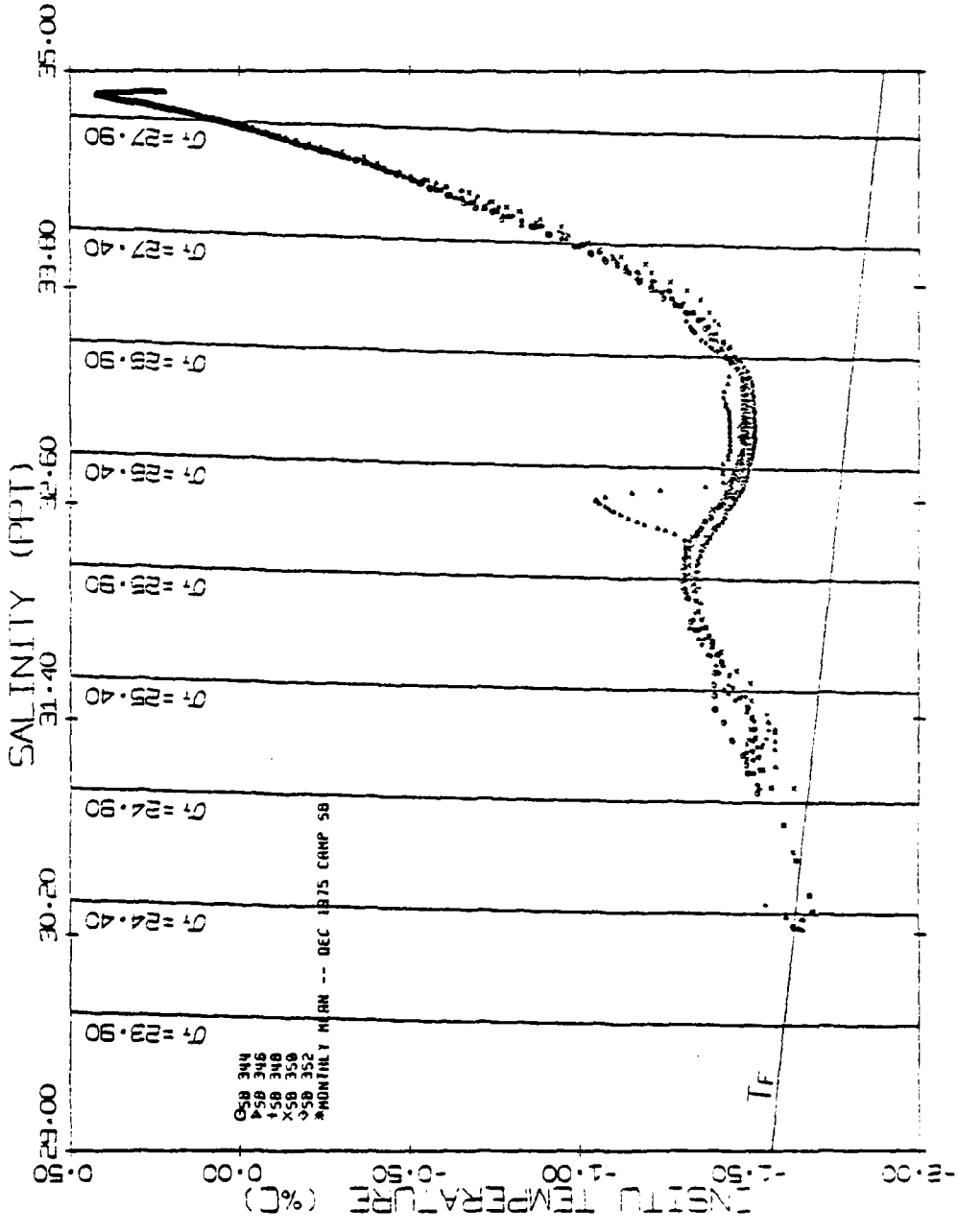

SALINITY (PPT)
POTENTIAL TEMPERATURE (°C)
35.00
33.80
32.60
31.40
30.20
29.00
0.50
0.00
-0.50
-1.00
-1.50
-2.00
σt = 27.80
σt = 27.40
σt = 26.80
σt = 26.40
σt = 25.80
σt = 25.40
σt = 24.80
σt = 24.40
σt = 23.80
CSB 245
PSB 247
ISB 249
XSB 251
*MONTHLY MEAN -- OCT 1975 CAMP SB

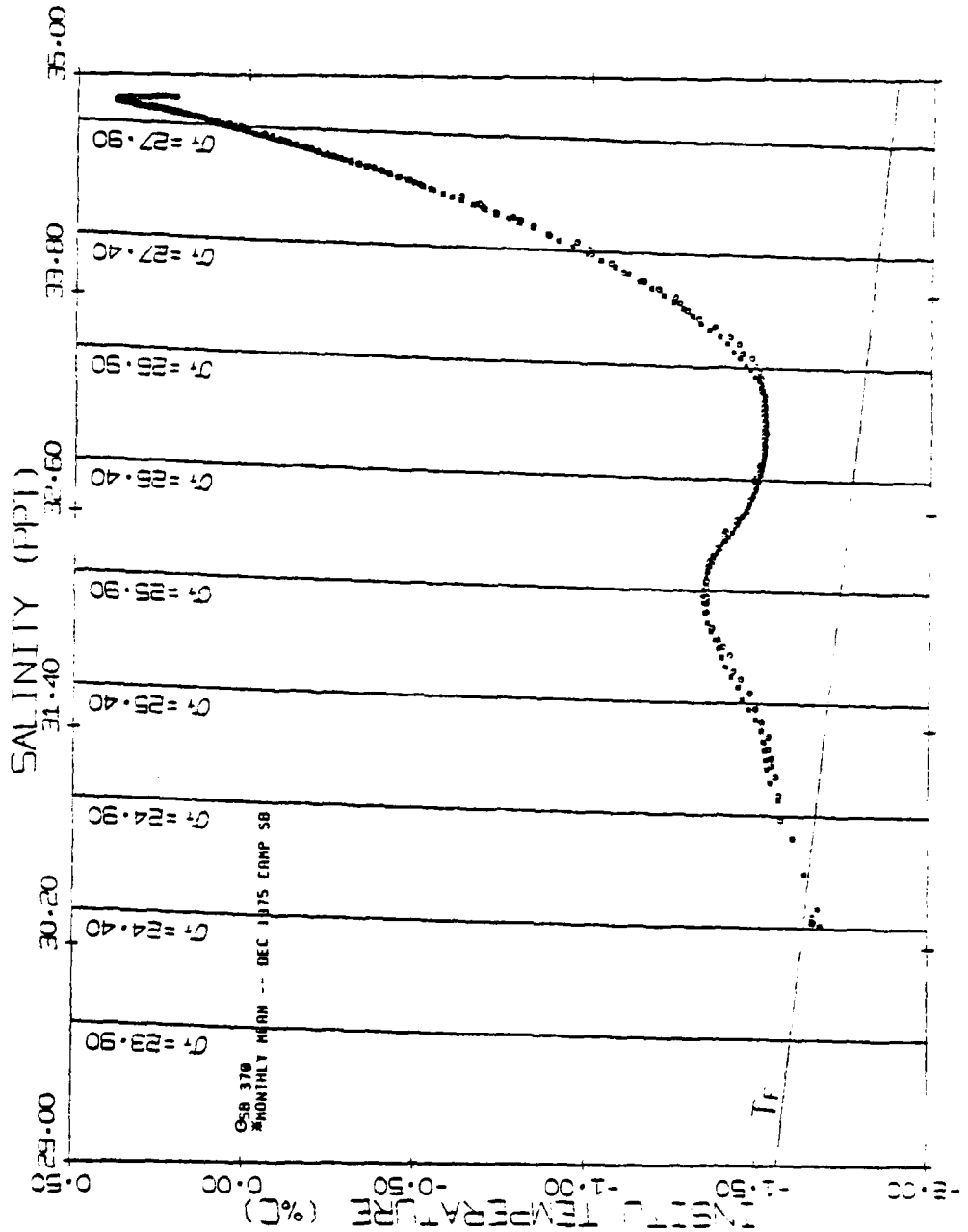

SALINITY (PPT)
35.00
33.80
32.60
31.40
30.20
29.00
σt =27.90
σt =27.40
σt =26.90
σt =26.40
σt =25.90
σt =25.40
σt =24.90
σt =24.40
σt =23.90
OSB 249
*MONTHLY MEAN -- OCT 1975 CAMP SU
TF
POTENTIAL TEMPERATURE (°C)
0.50
0.00
-0.50
-1.00
-1.50
-2.00

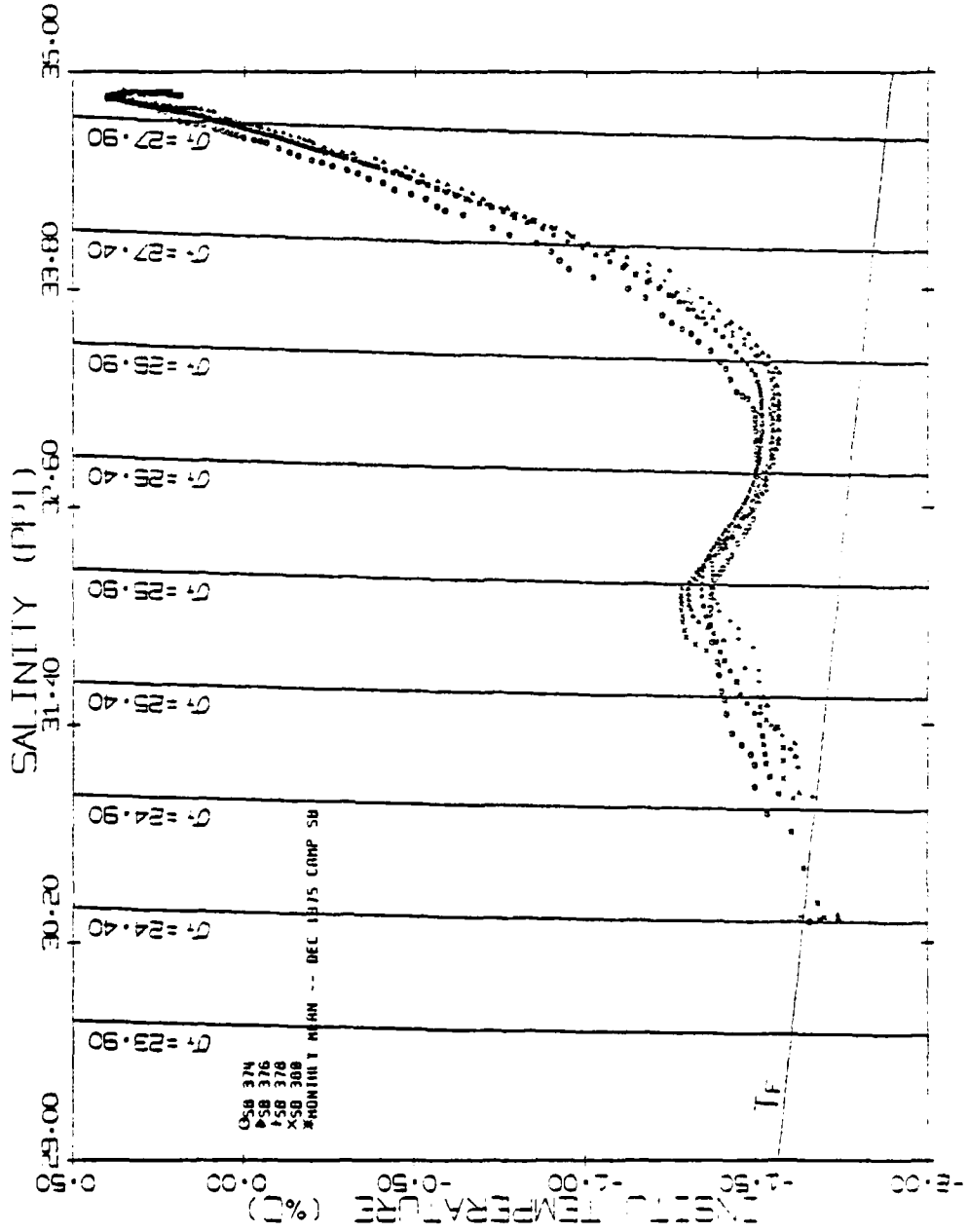

SALINITY (PPT)
POTENTIAL TEMPERATURE (°C)
σt =27.90
σt =27.40
σt =26.90
σt =26.40
σt =25.90
σt =25.40
σt =24.90
σt =24.40
σt =23.90
35.00
33.80
32.60
31.40
30.20
29.00
0.50
0.00
-0.50
-1.00
-1.50
-2.00
TF
*MONTHLY MEAN -- OCT 1975 CAMP SU
CSB 255
ΔSB 257
ISB 259
XSB 261
ΦSB 263

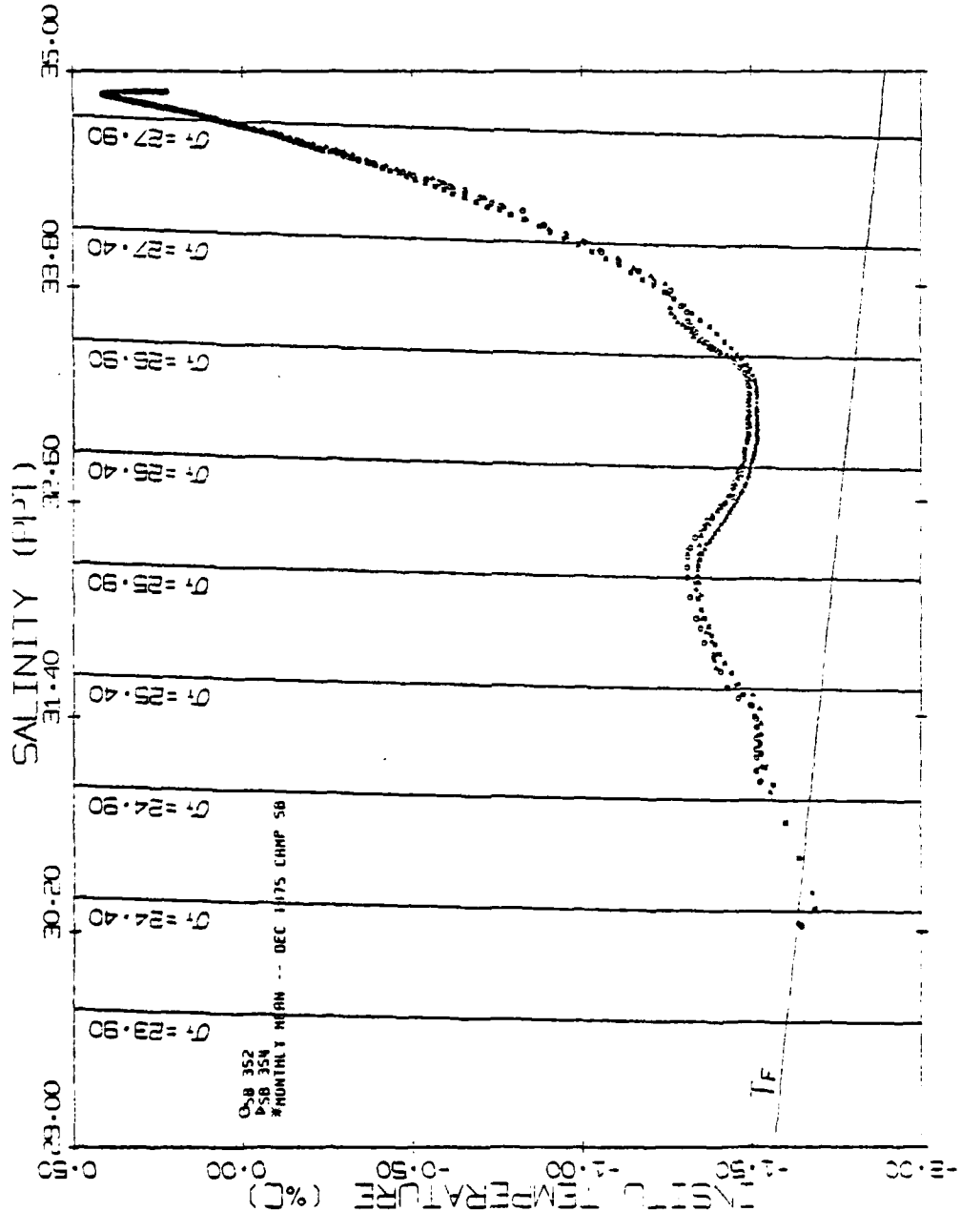


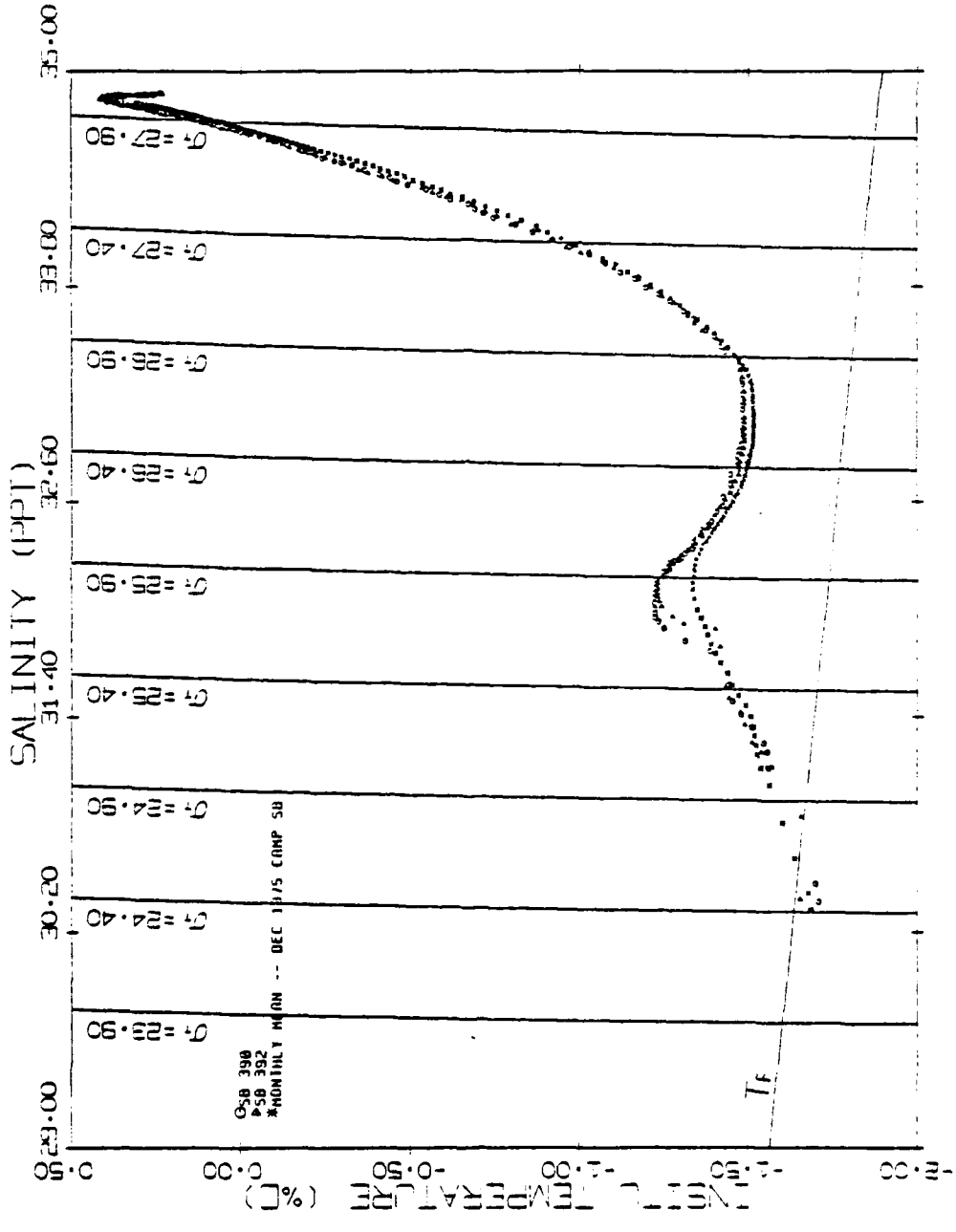
PRECEDING PAGE BLANK-NOT FILMED

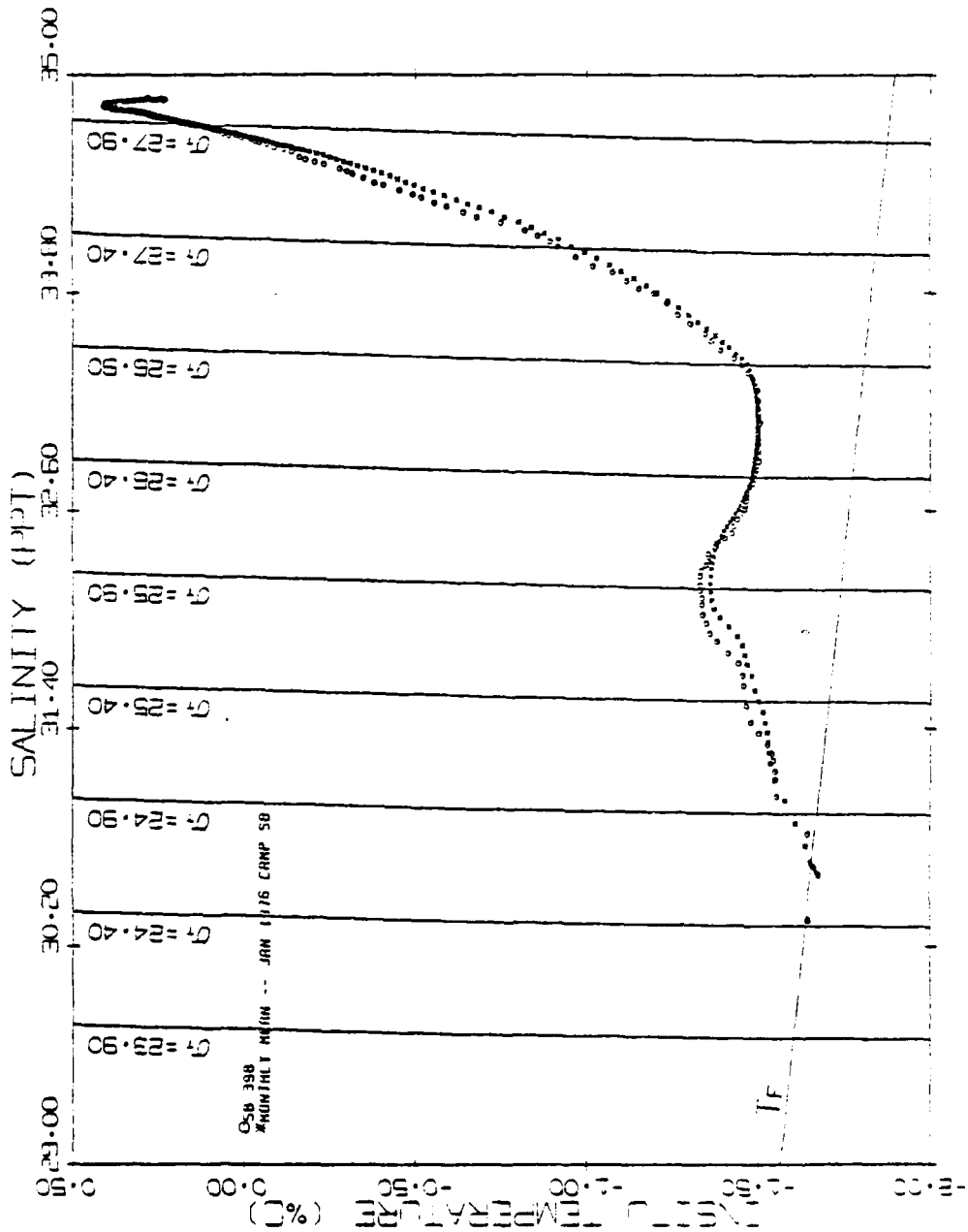

SALINITY (PPT)
35.00
33.00
32.60
31.40
30.20
29.00
σt =27.90
σt =27.40
σt =26.90
σt =26.40
σt =25.90
σt =25.40
σt =24.90
σt =24.40
σt =23.90
σsb 344
▲sb 346
+sb 348
×sb 350
◇sb 352
*MONTHLY MEAN -- DEC 1975 CAMP SB
T_F
INSITU TEMPERATURE (°C)
0.50
0.00
-0.50
-1.00
-1.50
-2.00

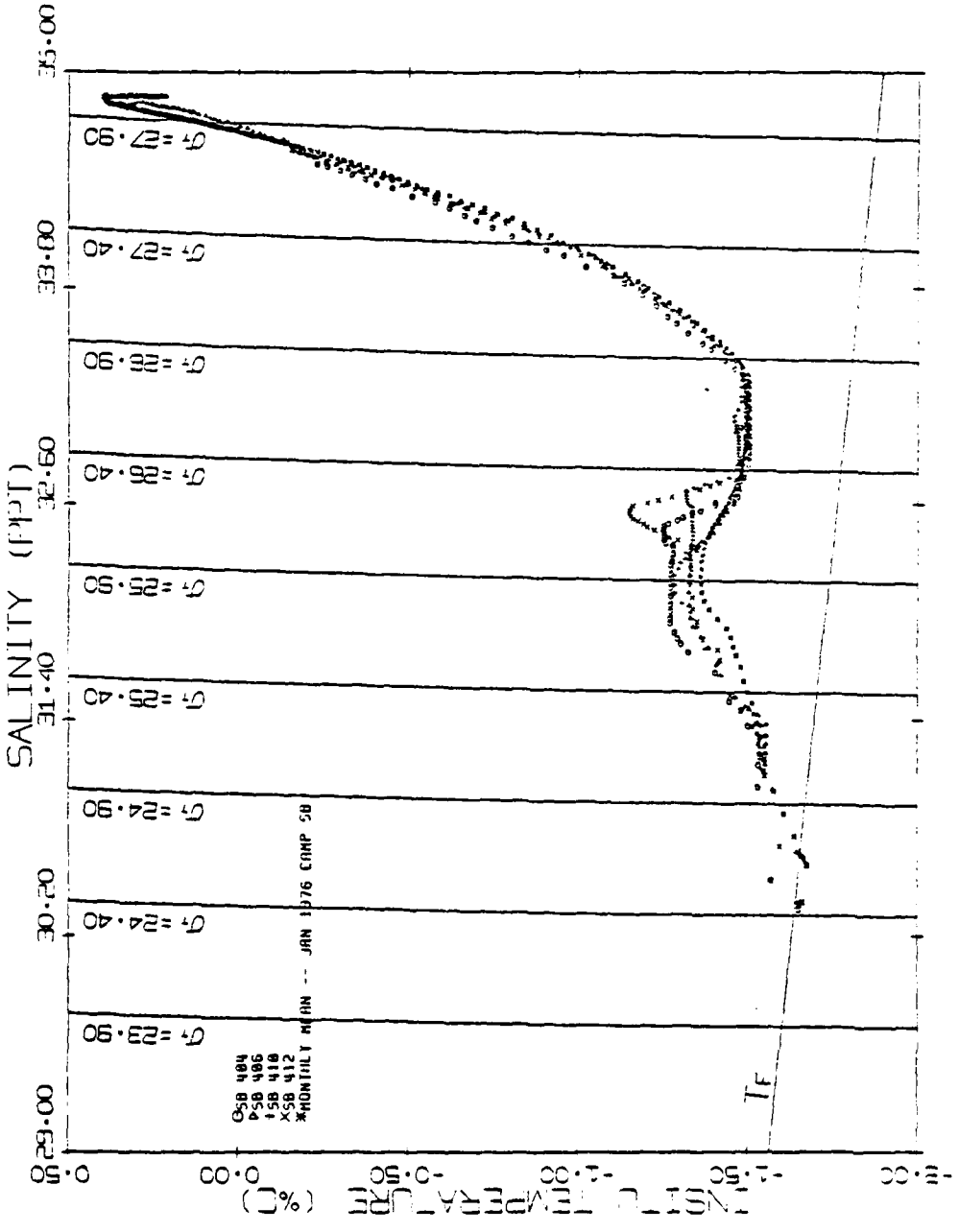

SALINITY (PPT)
35.00
34.80
34.60
34.40
34.20
34.00
σt =27.90
σt =27.40
σt =26.90
σt =26.40
σt =25.90
σt =25.40
σt =24.90
σt =24.40
σt =23.90
OSB 370
*MONTHLY MEAN -- DEC 1975 CAMP SB
Tf
POTENTIAL TEMPERATURE (°C)
0.00
-0.50
-1.00
-1.50
-2.00

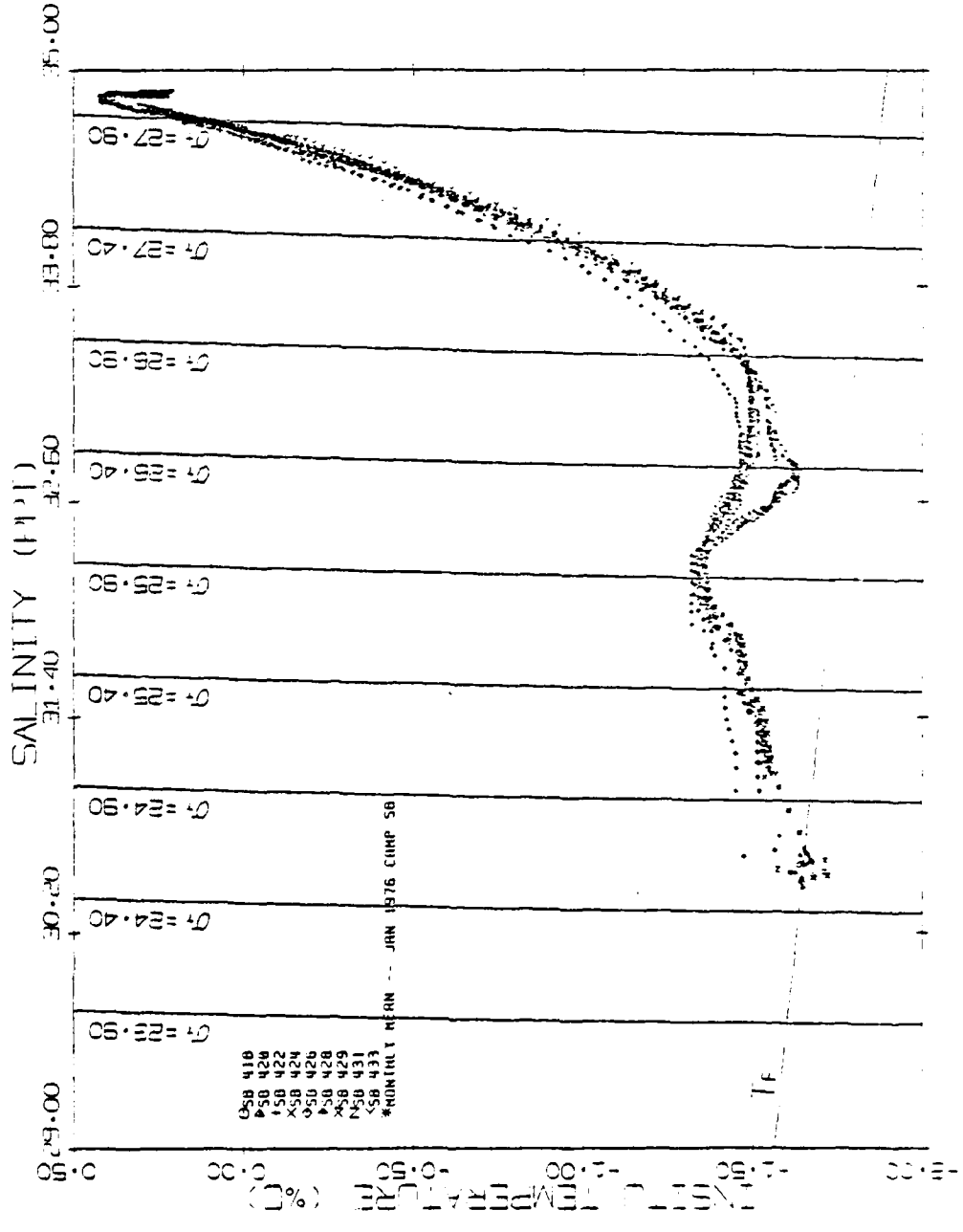

SALINITY (PPT)
POTENTIAL TEMPERATURE (°C)
σt =27.90
σt =27.40
σt =26.90
σt =26.40
σt =25.90
σt =25.40
σt =24.90
σt =24.40
σt =23.90
MONTHLY MEAN -- DEC 1975 CAMP SB
CSB 374
ΔSB 376
+SB 378
×SB 380

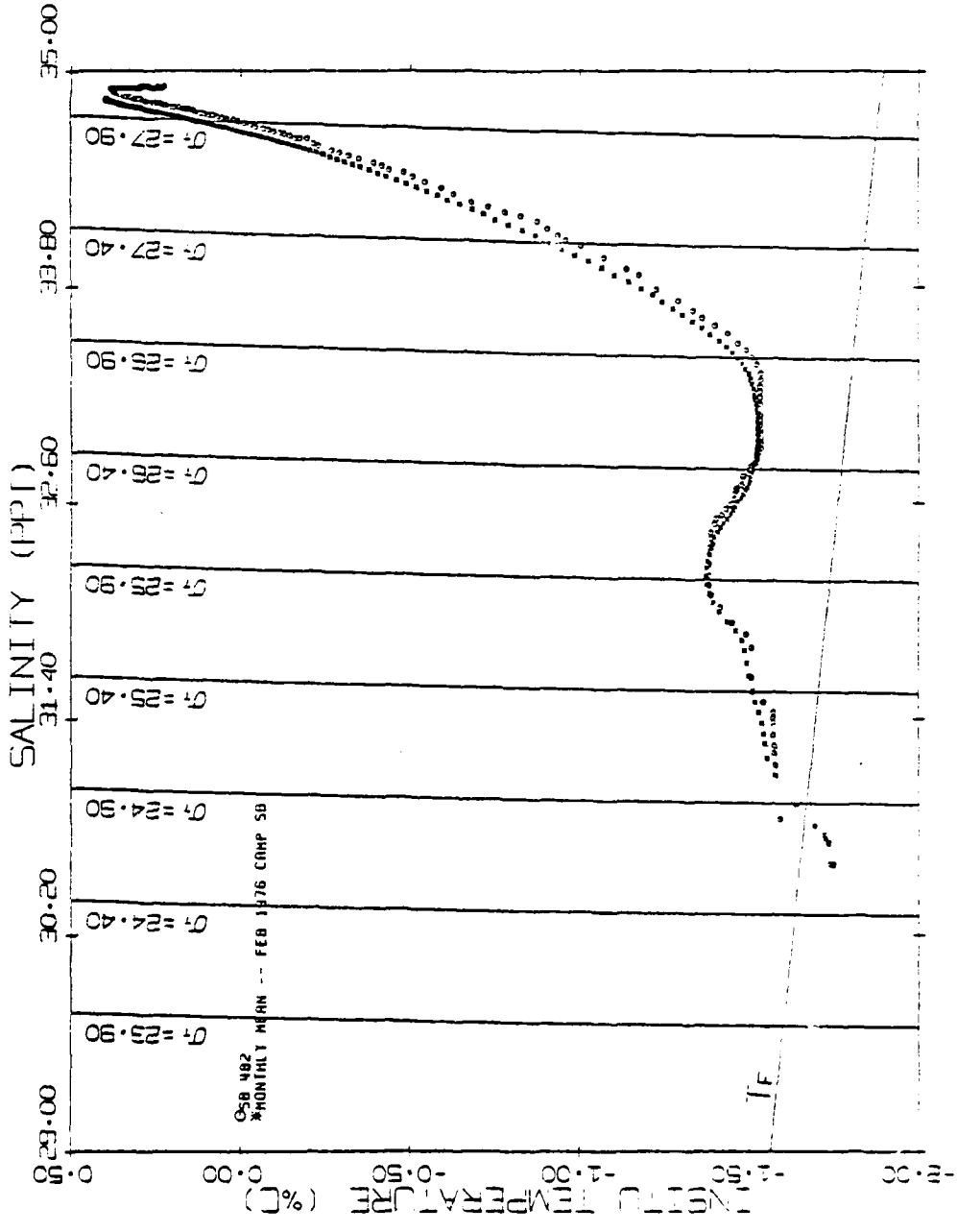

SALINITY (PPT)
35.00
33.80
32.60
31.40
30.20
29.00
σt =27.90
σt =27.40
σt =25.90
σt =25.40
σt =25.90
σt =25.40
σt =24.90
σt =24.40
σt =23.90
SB 352
SB 354
*MONTHLY MEAN -- DEC 1975 CHMP SB
T_F
INSITU TEMPERATURE (°C)
0.50
0.00
-0.50
-1.00
-1.50
-2.00

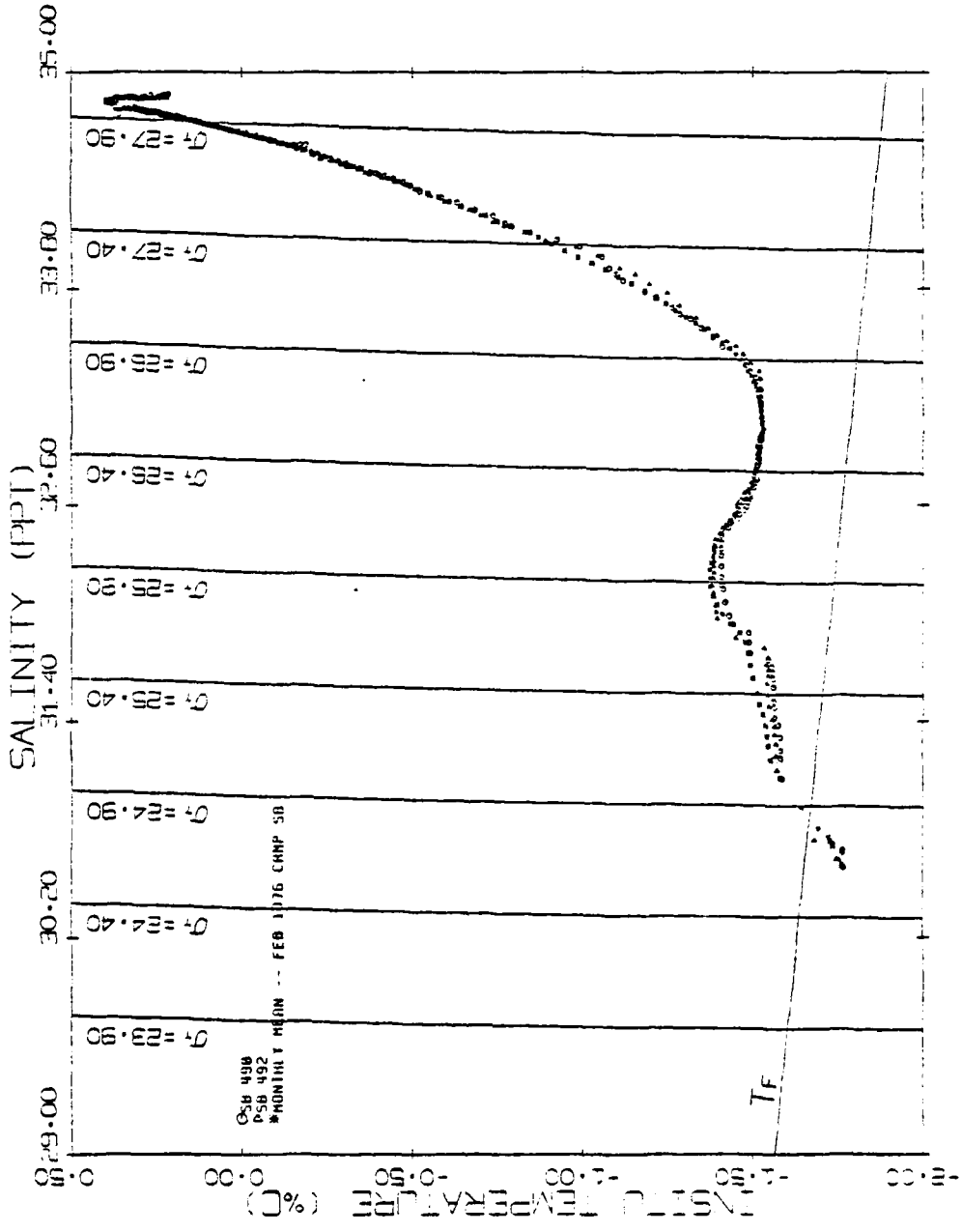

SALINITY (PPT)
30.00
30.20
30.40
30.60
30.80
31.00
σt =23.90
σt =24.40
σt =24.90
σt =25.40
σt =25.90
σt =26.40
σt =26.90
σt =27.40
σt =27.90
SB 390
SB 392
*MONTHLY MEAN -- DEC 1975 CAMP SB
POTENTIAL TEMPERATURE (°C)
-1.80
-1.60
-1.40
-1.20
-1.00
-0.80
-0.60
-0.40
-0.20
0.00
0.20
0.40
0.60
T_f

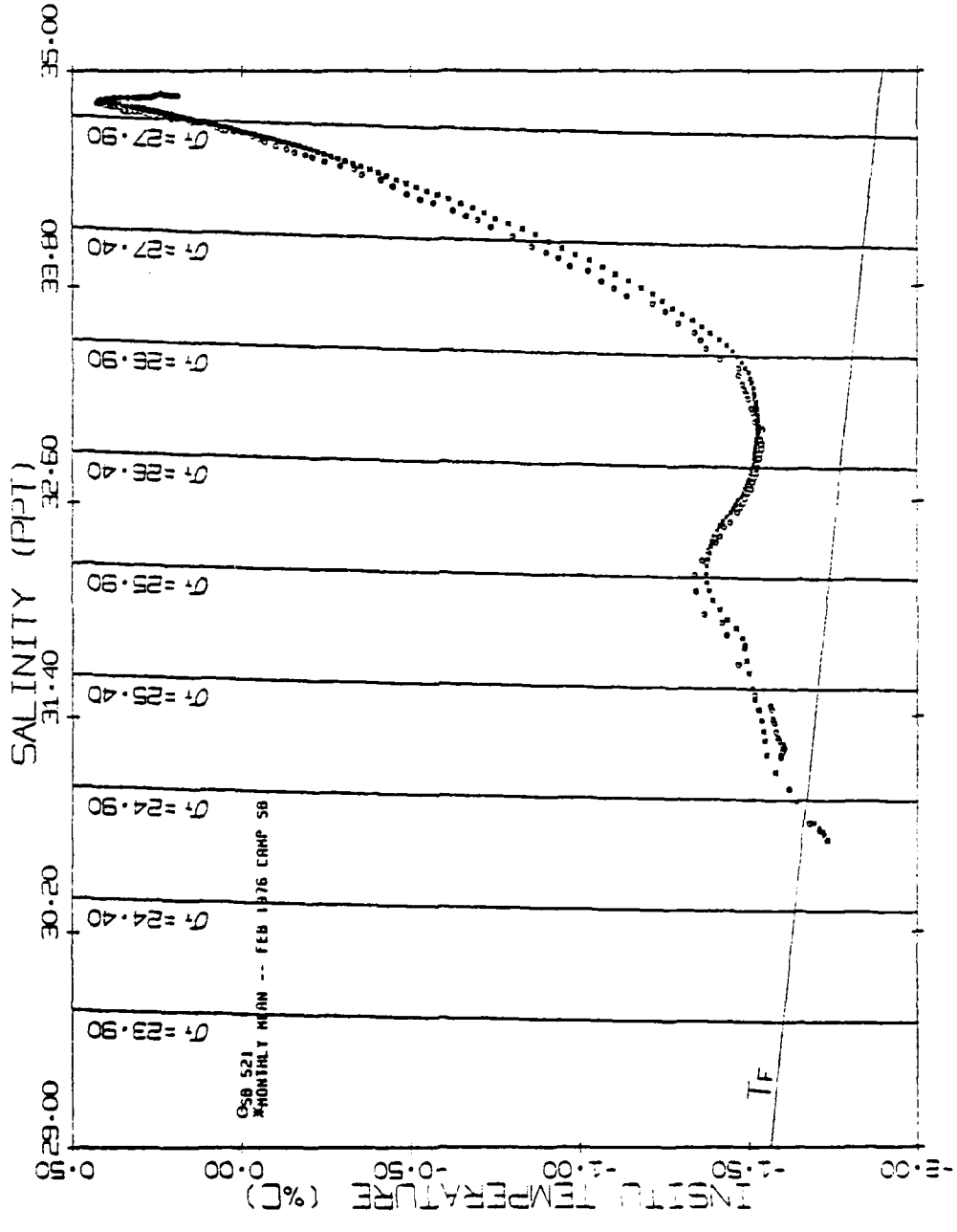

SALINITY (PPT)
35.00
33.80
32.60
31.40
30.20
29.00
σt =27.90
σt =27.40
σt =26.90
σt =26.40
σt =25.90
σt =25.40
σt =24.90
σt =24.40
σt =23.90
0.0
0.80
-0.50
-1.80
-3.00
(%C)
Tf
Os 398
*MONTHLY MEAN -- JAN 1976 CAMP 58

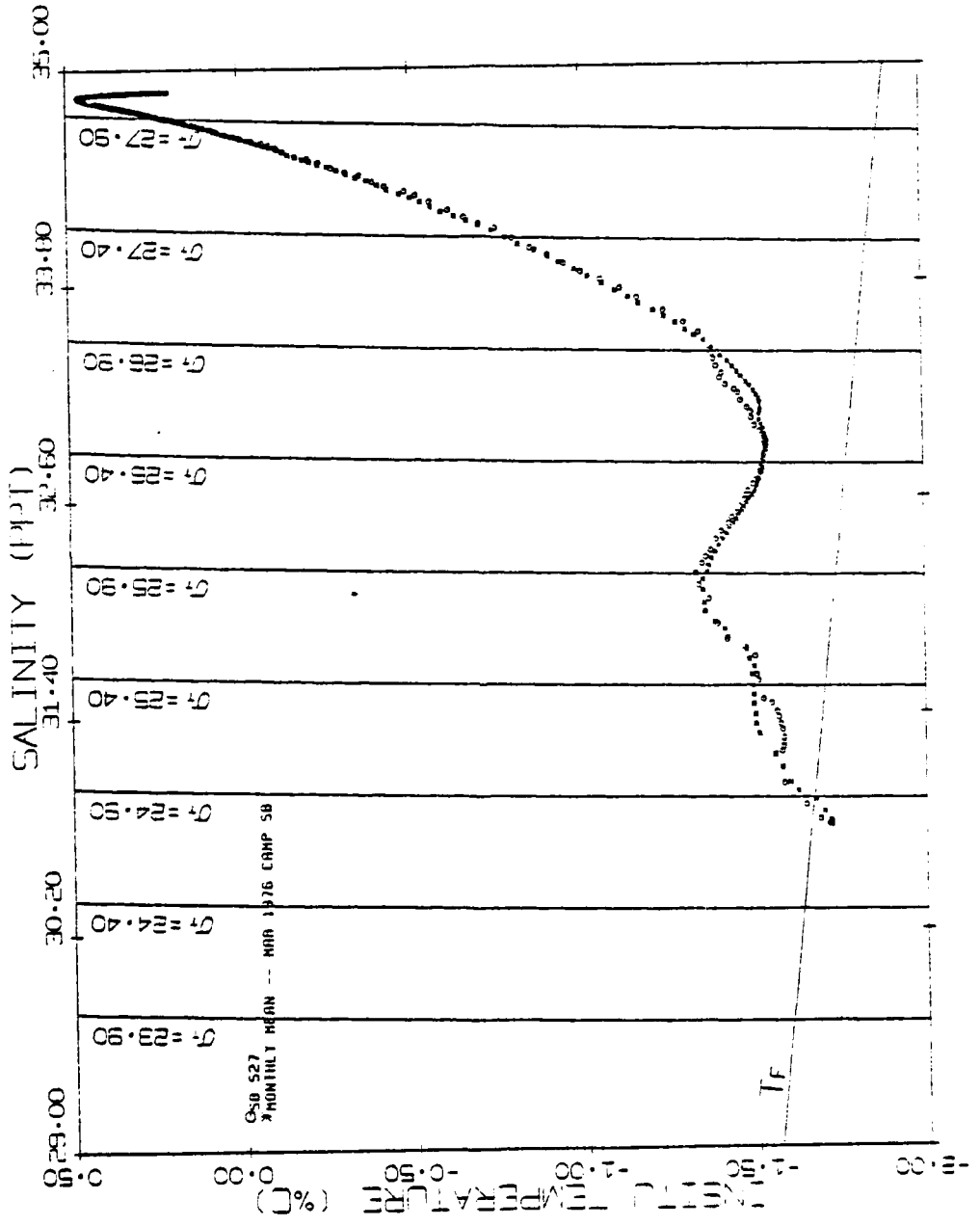

SALINITY (PPT)
POTENTIAL TEMPERATURE (°C)
σθ = 27.90
σθ = 27.40
σθ = 26.90
σθ = 26.40
σθ = 25.90
σθ = 25.40
σθ = 24.90
σθ = 24.40
σθ = 23.90
TF
MONTHLY MEAN -- JAN 1976 CAMP 5B

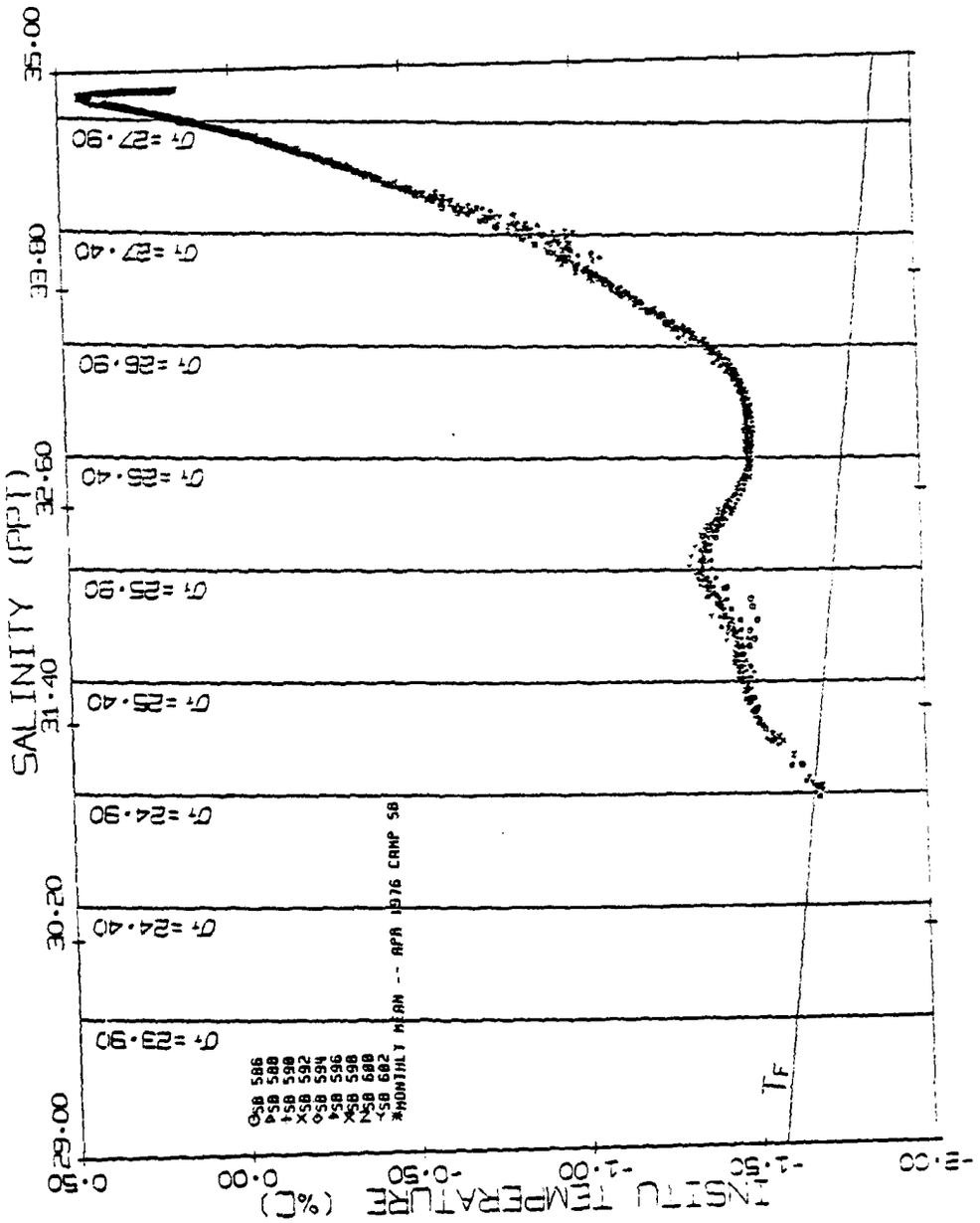

POTENTIAL TEMPERATURE (°C)
SALINITY (PPT)
σt =27.80
σt =27.40
σt =26.80
σt =26.40
σt =25.80
σt =25.40
σt =24.80
σt =24.40
σt =23.80
35.00
34.60
34.20
33.80
33.40
33.00
32.60
32.20
31.80
31.40
31.00
30.60
30.20
29.80
29.40
29.00
28.60
28.20
27.80
27.40
27.00
26.60
26.20
25.80
25.40
25.00
24.60
24.20
23.80
23.40
23.00
22.60
22.20
21.80
21.40
21.00
20.60
20.20
19.80
19.40
19.00
18.60
18.20
17.80
17.40
17.00
16.60
16.20
15.80
15.40
15.00
14.60
14.20
13.80
13.40
13.00
12.60
12.20
11.80
11.40
11.00
10.60
10.20
9.80
9.40
9.00
8.60
8.20
7.80
7.40
7.00
6.60
6.20
5.80
5.40
5.00
4.60
4.20
3.80
3.40
3.00
2.60
2.20
1.80
1.40
1.00
0.60
0.20
-0.20
-0.60
-1.00
-1.40
-1.80
JAN 1976 CHNP 58
*MONTHLY MEAN

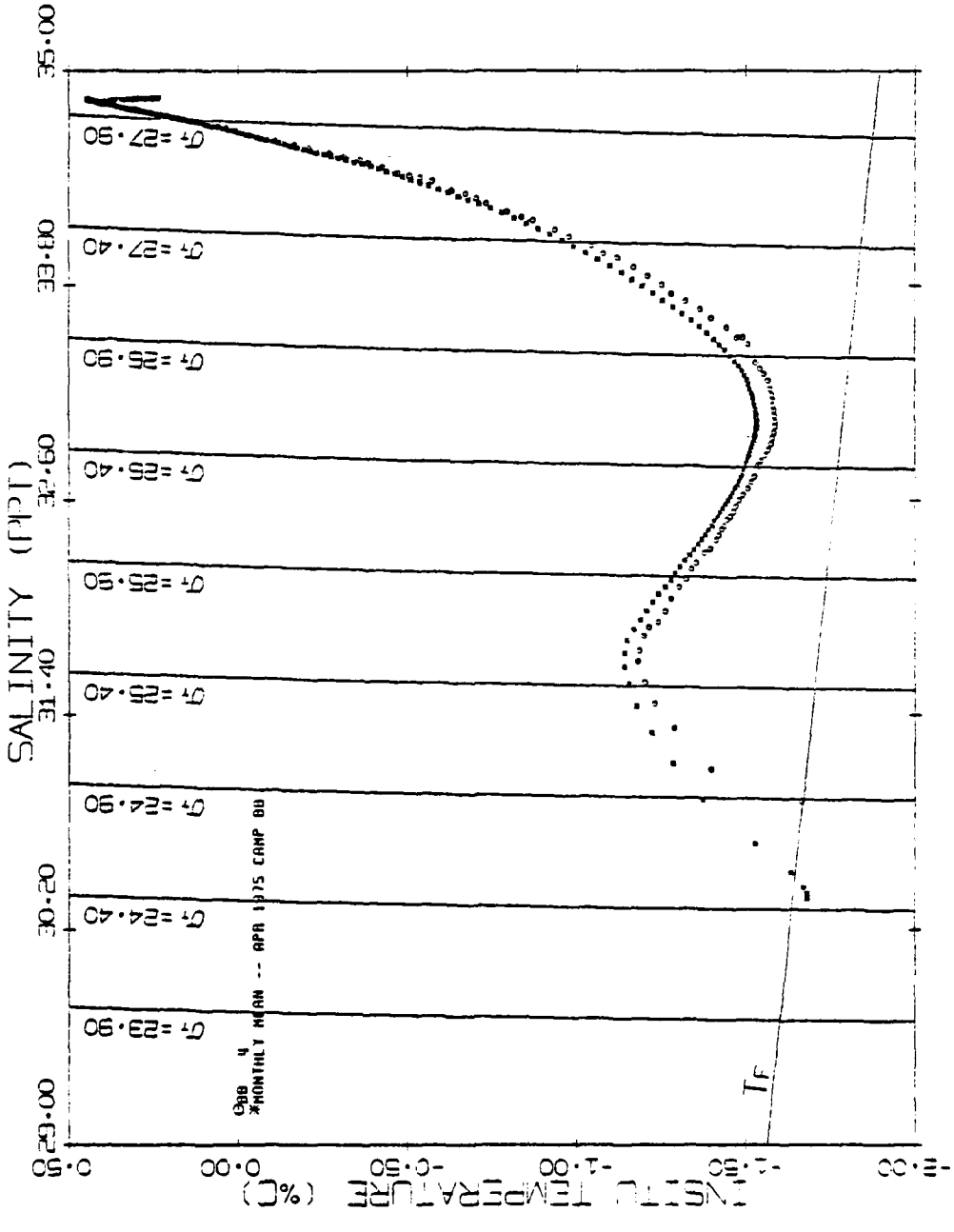

SALINITY (PPT)
35.00
33.80
32.60
31.40
30.20
29.00
σt =27.90
σt =27.40
σt =26.90
σt =26.40
σt =25.90
σt =25.40
σt =24.90
σt =24.40
σt =23.90
OSB 482
*MONTHLY MEAN -- FEB 1976 CNAP SB
POTENTIAL TEMPERATURE (°C)
0.50
0.00
-0.50
-1.00
-1.50
-2.00
TF

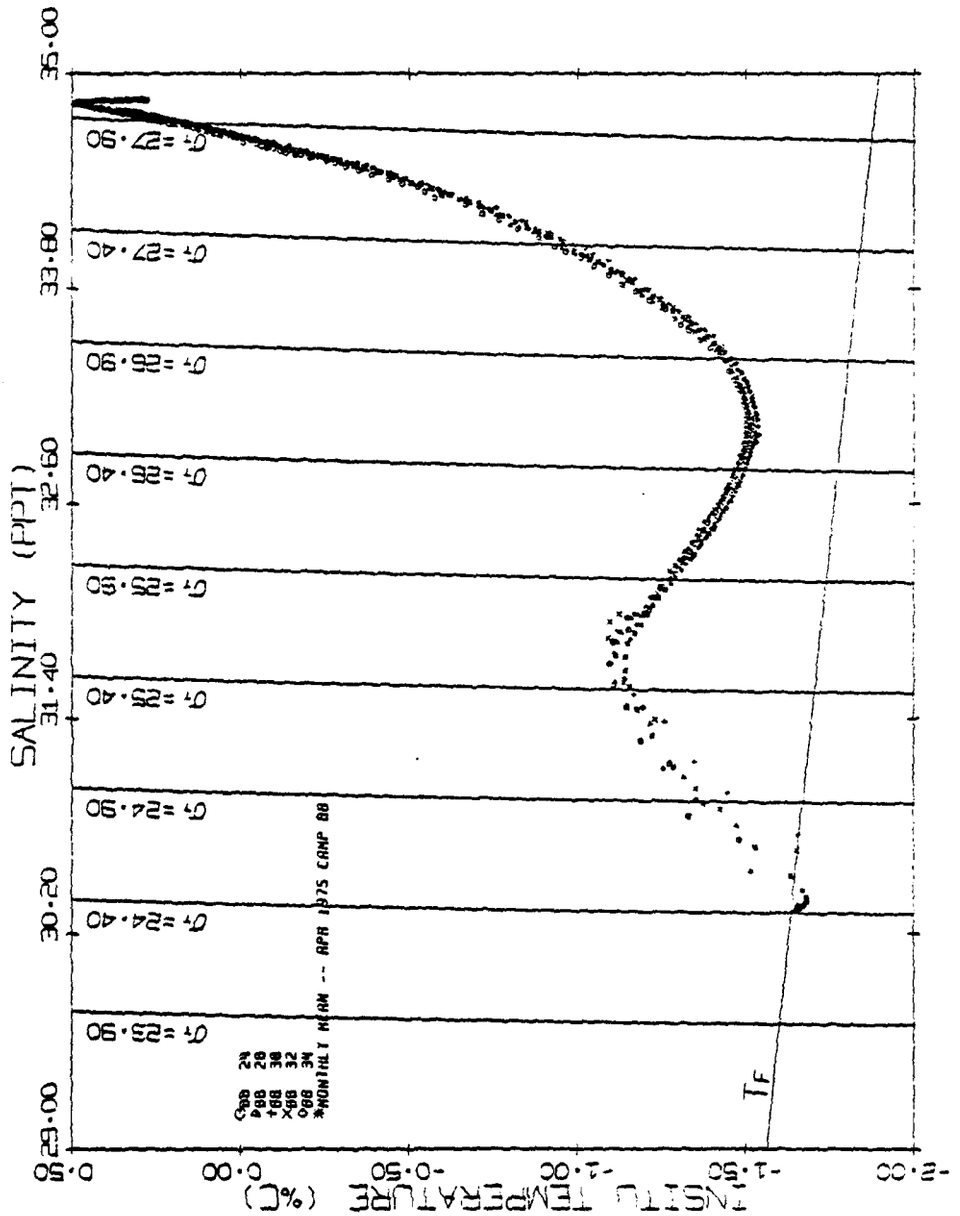

SALINITY (PPT)
35.00
33.00
32.00
31.40
30.20
29.00
σt =27.90
σt =27.40
σt =26.90
σt =26.40
σt =25.90
σt =25.40
σt =24.90
σt =24.40
σt =23.90
0.50
0.00
-0.50
-1.00
-1.50
-2.00
T_F
PSB 498
PSB 492
*MONTHLY MEAN -- FEB 1976 CHMP SB

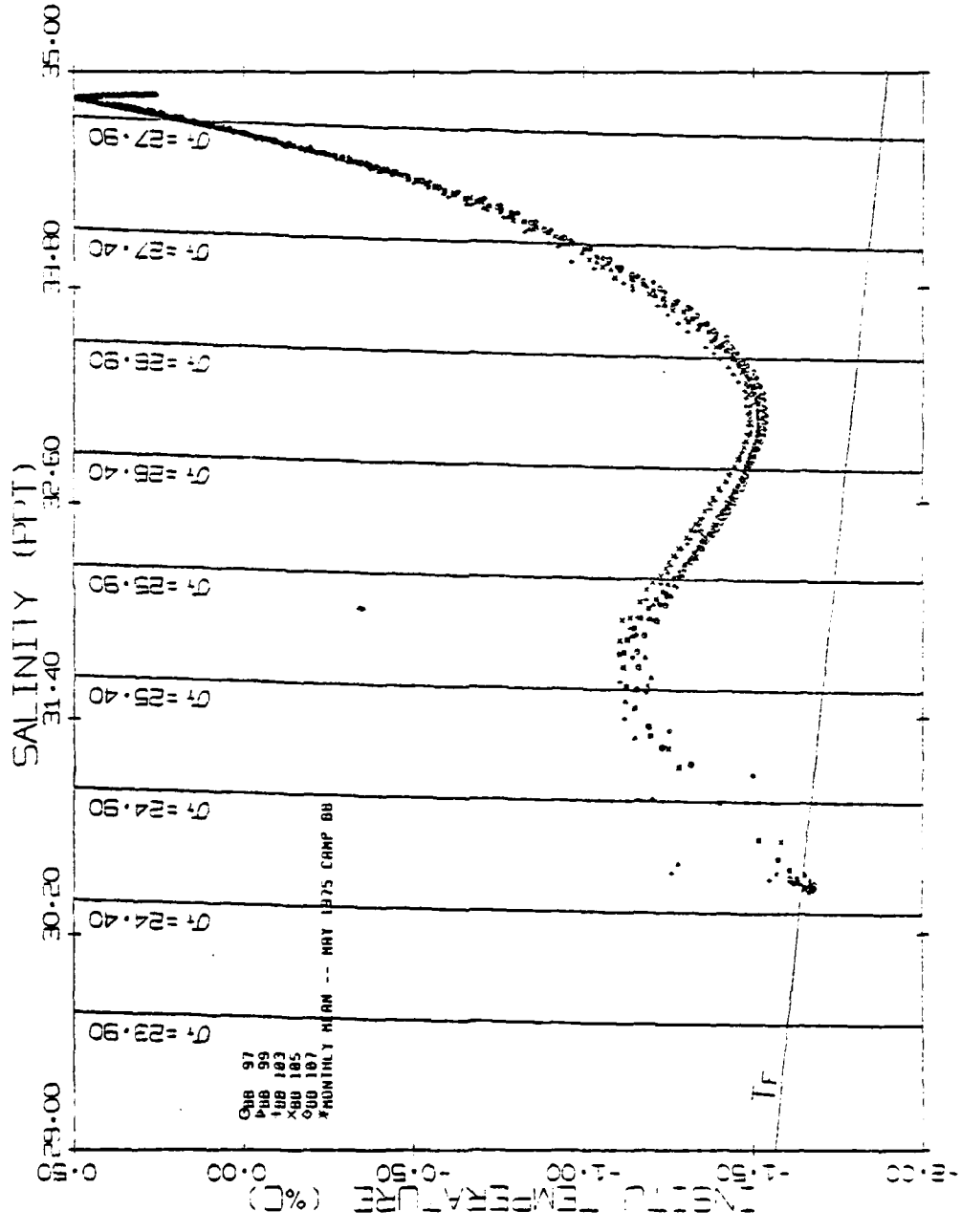

SALINITY (PPT)
INSITU TEMPERATURE (°C)
29.00
30.20
31.40
32.60
33.80
35.00
0.50
0.00
-0.50
-1.00
-1.50
-2.00
σθ =23.90
σθ =24.40
σθ =24.90
σθ =25.40
σθ =25.90
σθ =26.40
σθ =26.90
σθ =27.40
σθ =27.90
TF
OSB 521
*MONTHLY MEAN -- FEB 1976 CAMP SB

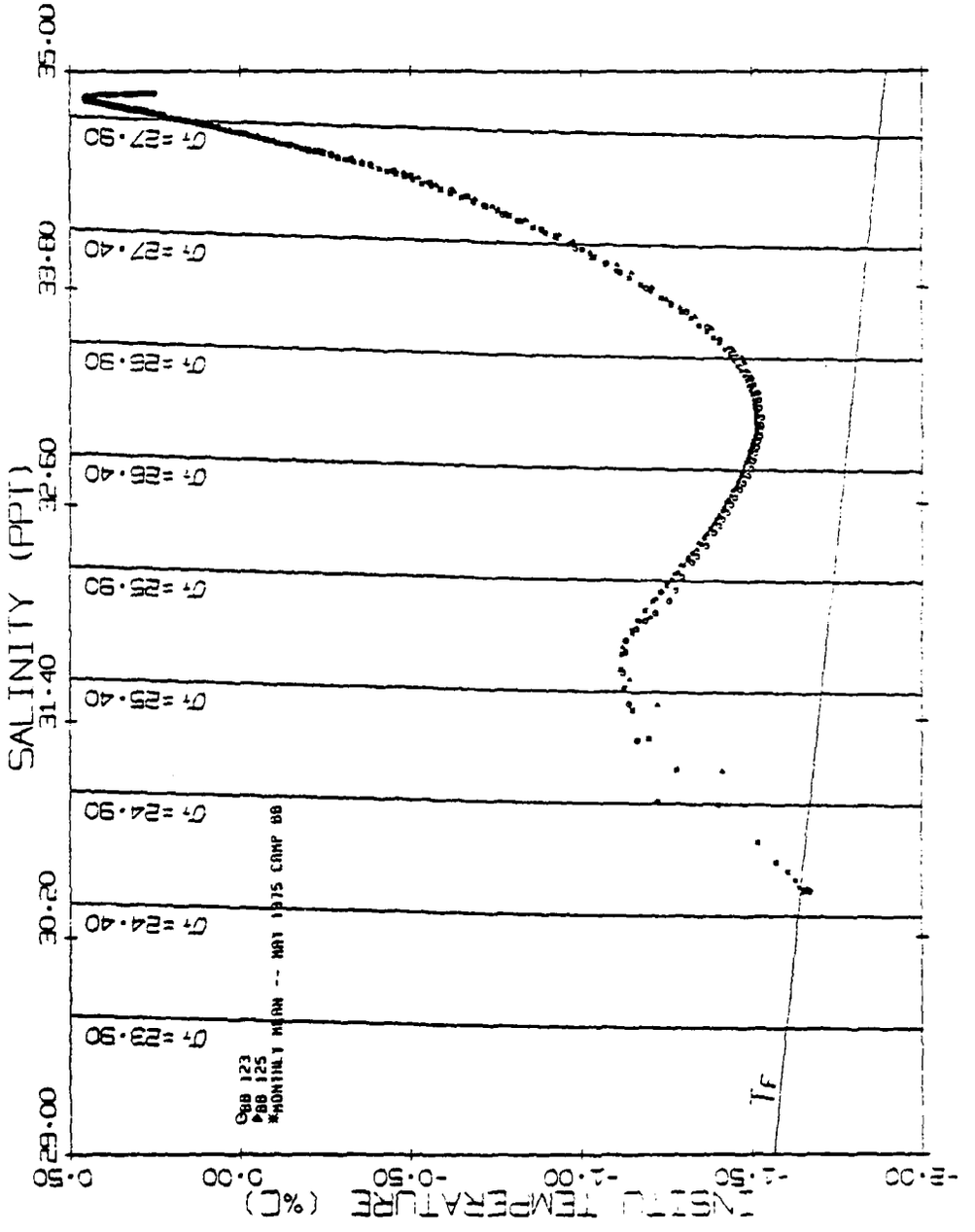

SALINITY (‰)
35.00
33.80
32.60
31.40
30.20
29.00
σt =27.90
σt =27.40
σt =26.90
σt =25.40
σt =25.90
σt =25.40
σt =24.90
σt =24.40
σt =23.90
0.50
0.00
-0.50
-1.00
-1.50
-2.00
(°C)
TF
SD 527
MONTHLY MEAN -- NOV 1976 CAMP SB

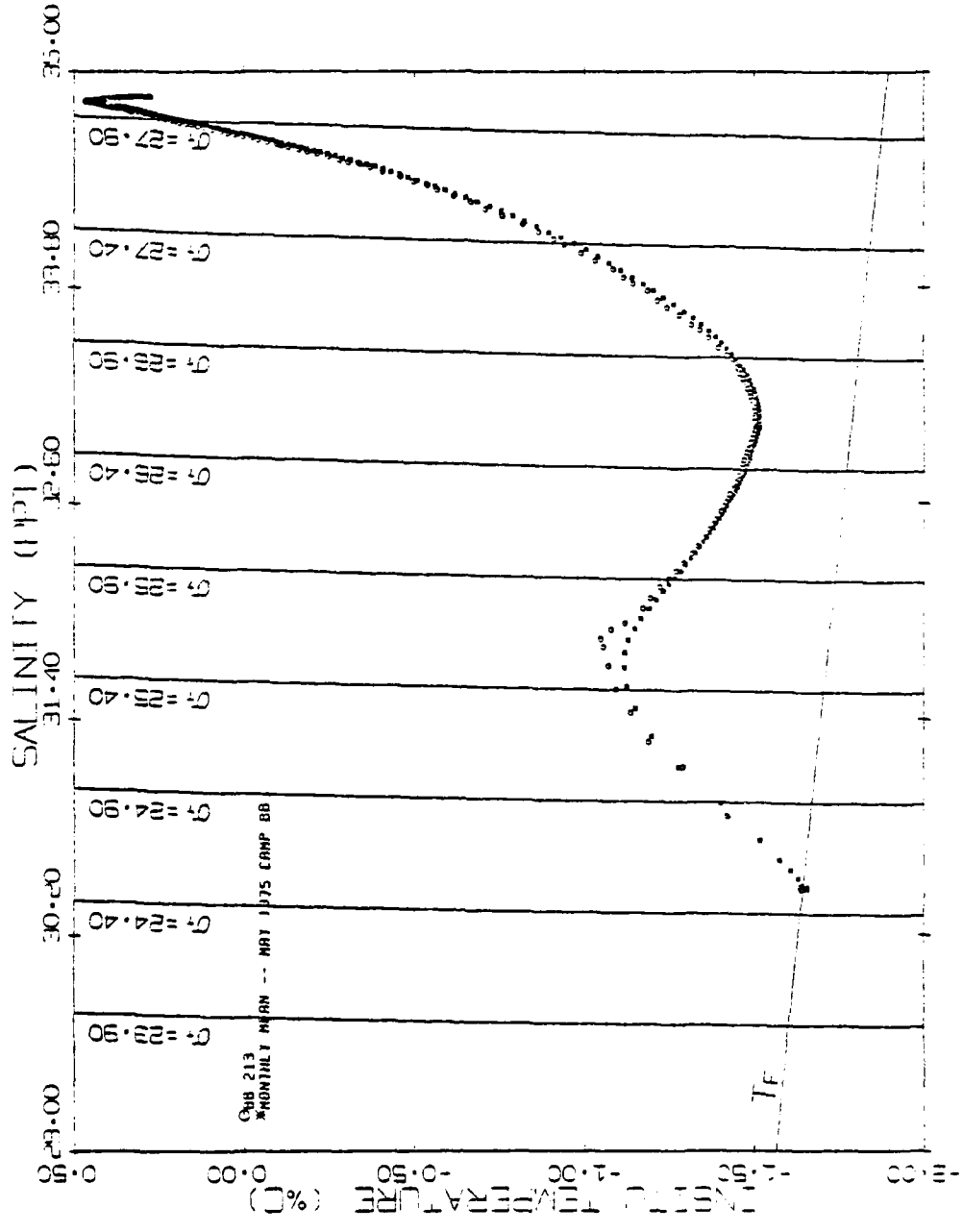

SALINITY (PPT)
35.00
33.80
32.60
31.40
30.20
29.00
σt =27.90
σt =27.40
σt =26.90
σt =26.40
σt =25.90
σt =25.40
σt =24.90
σt =24.40
σt =23.90
POTENTIAL TEMPERATURE (°C)
0.50
0.00
-0.50
-1.00
-1.50
-2.00
T_F
*MONTHLY MEAN -- APR 1976 CRNP 58
○58 586
▷58 588
+58 590
×58 592
◇58 594
*58 596
×58 598
▽58 600
◁58 602

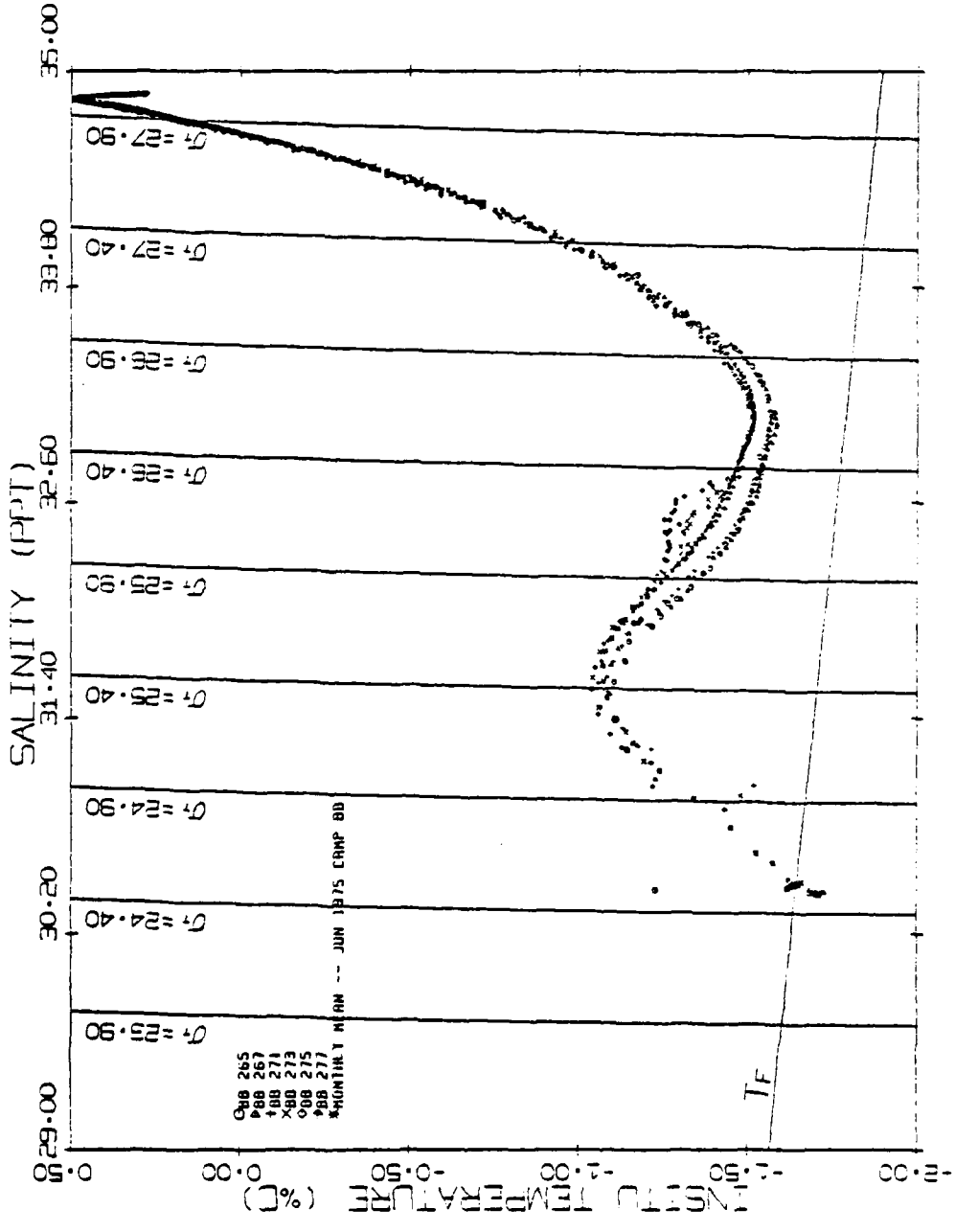

SALINITY (PPT)
35.00
33.80
32.60
31.40
30.20
29.00
σt =27.90
σt =27.40
σt =26.90
σt =26.40
σt =25.90
σt =25.40
σt =24.90
σt =24.40
σt =23.90
0.50
0.00
-0.50
-1.00
-1.50
-2.00
IN SITU TEMPERATURE (°C)
T_F
88 4
*MONTHLY MEAN -- APR 1975 CAMP 88

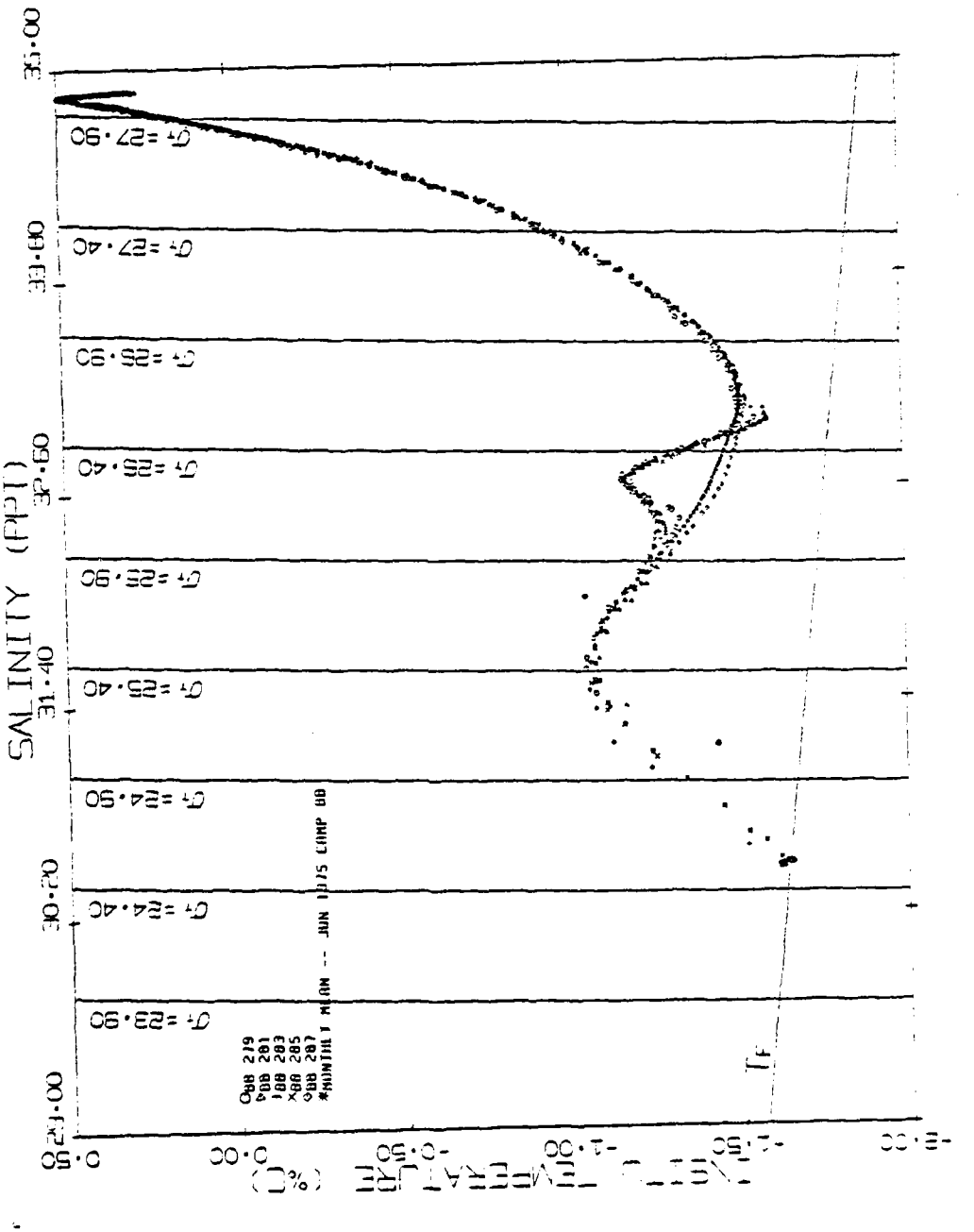

SALINITY (PPT)
35.00
33.80
32.60
31.40
30.20
29.00
σt =27.90
σt =27.40
σt =26.90
σt =26.40
σt =25.90
σt =25.40
σt =24.90
σt =24.40
σt =23.90
0.50
0.00
-0.50
-1.00
-1.50
-2.00
IN SITU TEMPERATURE (°C)
T_F
MONTHLY MEAN -- APR 1975 CANP 88
2N
2S
3S
3N

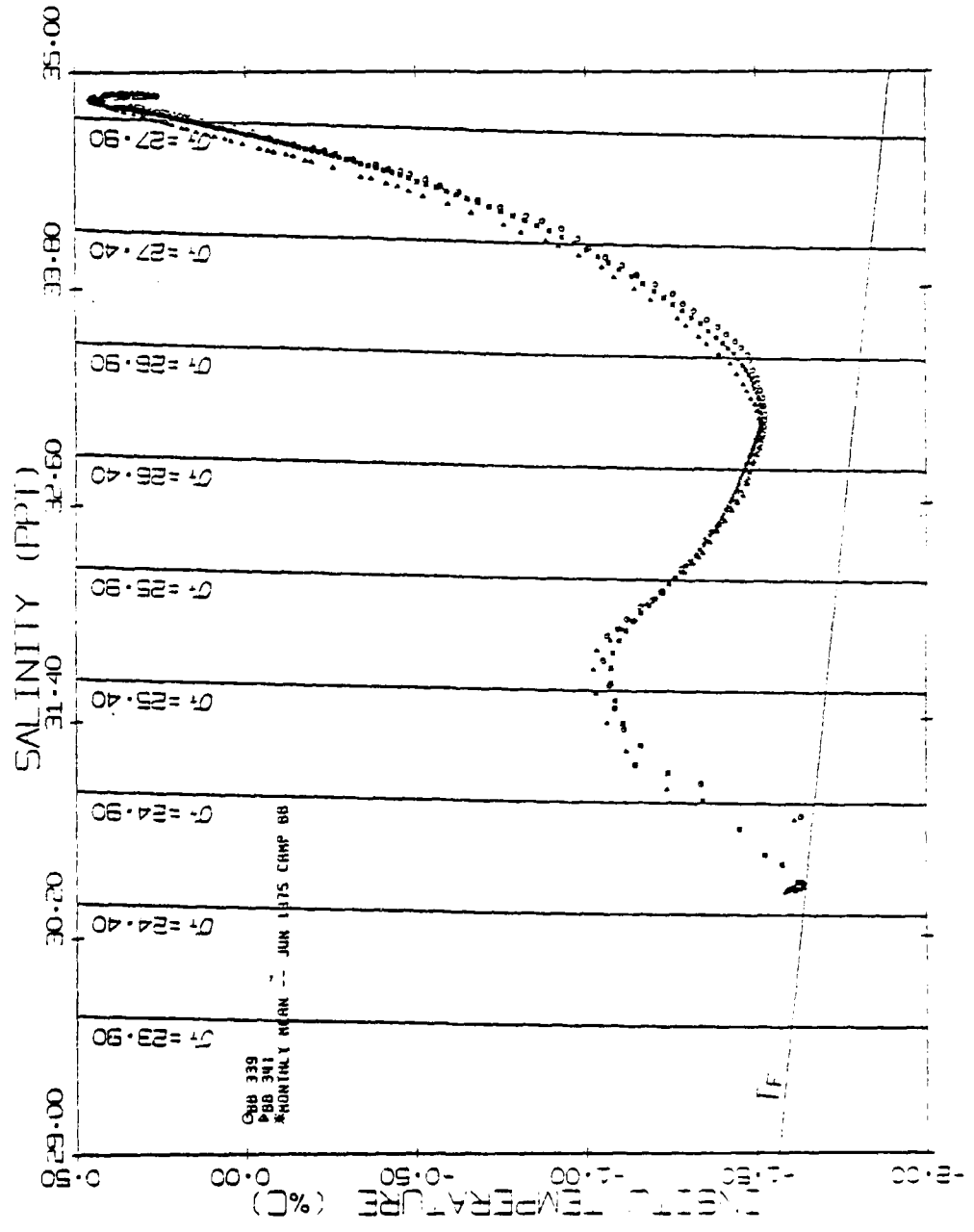

SALINITY (PPT)
POTENTIAL TEMPERATURE (°C)
σt =27.90
σt =27.40
σt =26.90
σt =26.40
σt =25.90
σt =25.40
σt =24.90
σt =24.40
σt =23.90
35.00
34.80
32.60
31.40
30.20
29.00
0.50
0.00
-0.50
-1.00
-1.50
-2.00
BB 97
BB 99
BB 103
BB 105
QUO 107
*MONTHLY MEAN -- MAY 1975 CAMP BB

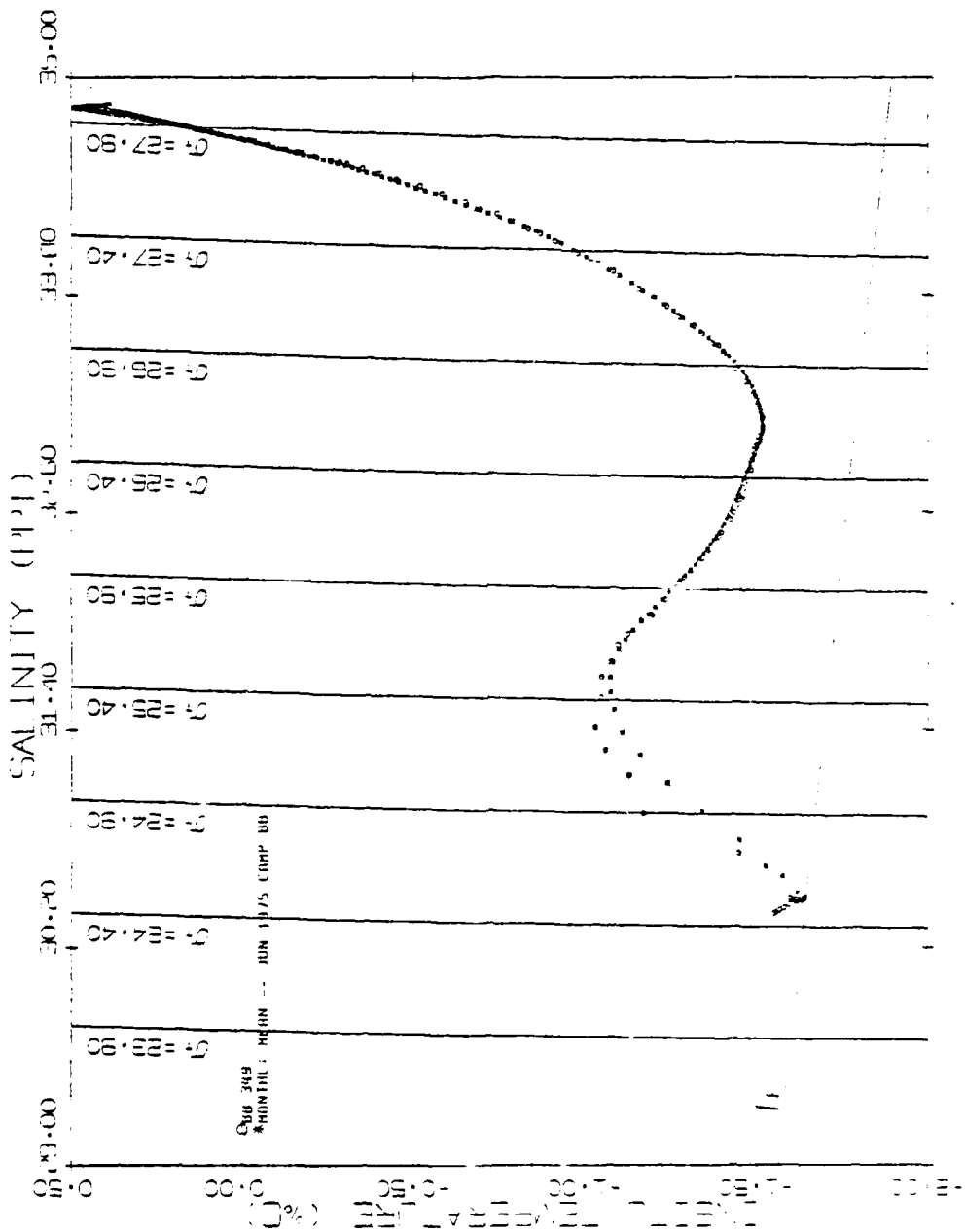

SALINITY (PPT)
35.00
33.80
32.60
31.40
30.20
29.00
σt =27.90
σt =27.40
σt =26.90
σt =26.40
σt =25.90
σt =25.40
σt =24.90
σt =24.40
σt =23.90
0.50
0.00
-0.50
-1.00
-1.50
-2.00
POTENTIAL TEMPERATURE (°C)
OBB 123
BB 125
MONTHLY MEAN -- MAY 1975 CAMP BB
T_F


SALINITY (PPT)
POTENTIAL TEMPERATURE (°C)
σθ = 23.90
σθ = 24.40
σθ = 24.90
σθ = 25.40
σθ = 25.90
σθ = 26.40
σθ = 26.90
σθ = 27.40
σθ = 27.90
30.00
30.40
30.80
31.20
31.60
32.00
32.40
32.80
33.20
33.60
34.00
34.40
34.80
35.00
0.50
0.00
-0.50
-1.00
-1.50
-2.00
-2.50
-3.00
T_F
QUB 213
*MONTHLY MEAN -- MAY 1975 CRNP BB


SALINITY (PPT)
35.00
33.80
32.60
31.40
30.20
29.00
σt =27.90
σt =27.40
σt =26.90
σt =26.40
σt =25.90
σt =25.40
σt =24.90
σt =24.40
σt =23.90
IN SITU TEMPERATURE (°C)
0.50
0.00
-0.50
-1.00
-1.50
-2.00
T_F
BB 265
BB 269
BB 271
BB 273
BB 275
BB 277
MEAN -- JUN 1975 CAMP BB

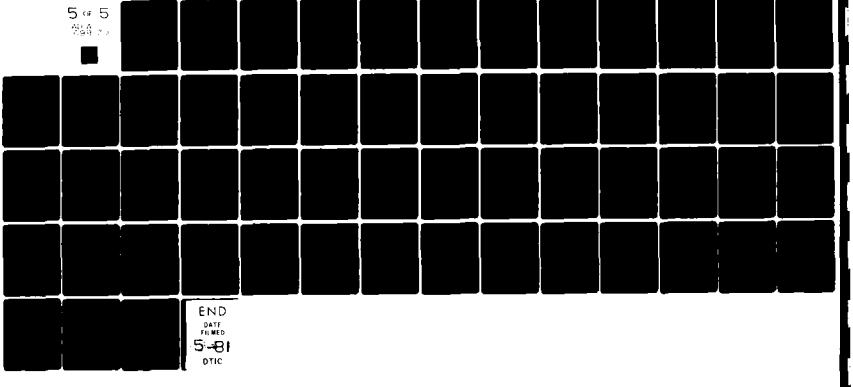

SALINITY (PPT)
POTENTIAL TEMPERATURE (°C)
σt =27.90
σt =27.40
σt =26.90
σt =26.40
σt =25.90
σt =25.40
σt =24.90
σt =24.40
σt =23.90
BB 219
BB 281
BB 283
BB 285
BB 287
MONTHLY MEAN -- JUN 1975 CHMP BB


POTENTIAL TEMPERATURE (°C)
SALINITY (ppt)
σt =23.90
σt =24.40
σt =24.90
σt =25.40
σt =25.90
σt =26.40
σt =26.90
σt =27.40
σt =27.90
BB 339
BB 341
*MONTHLY MEAN :: JUN 1975 CHMP BB

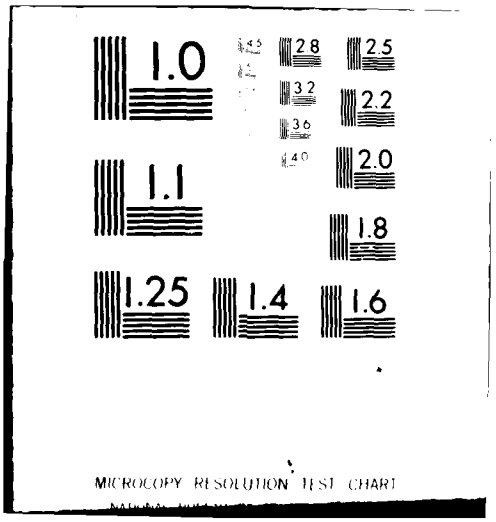

SALINITY (PPT)
σθ =27.80
σθ =27.40
σθ =26.80
σθ =26.40
σθ =25.80
σθ =25.40
σθ =24.80
σθ =24.40
σθ =23.80
35.00
34.40
33.80
33.20
32.60
32.00
31.40
30.80
30.20
29.60
29.00
0.00
-0.30
-0.60
-0.90
-1.20
-1.50
POTENTIAL TEMPERATURE (°C)
Obs 369
*MONTHLY MEAN -- JUN 1975 COMP 00

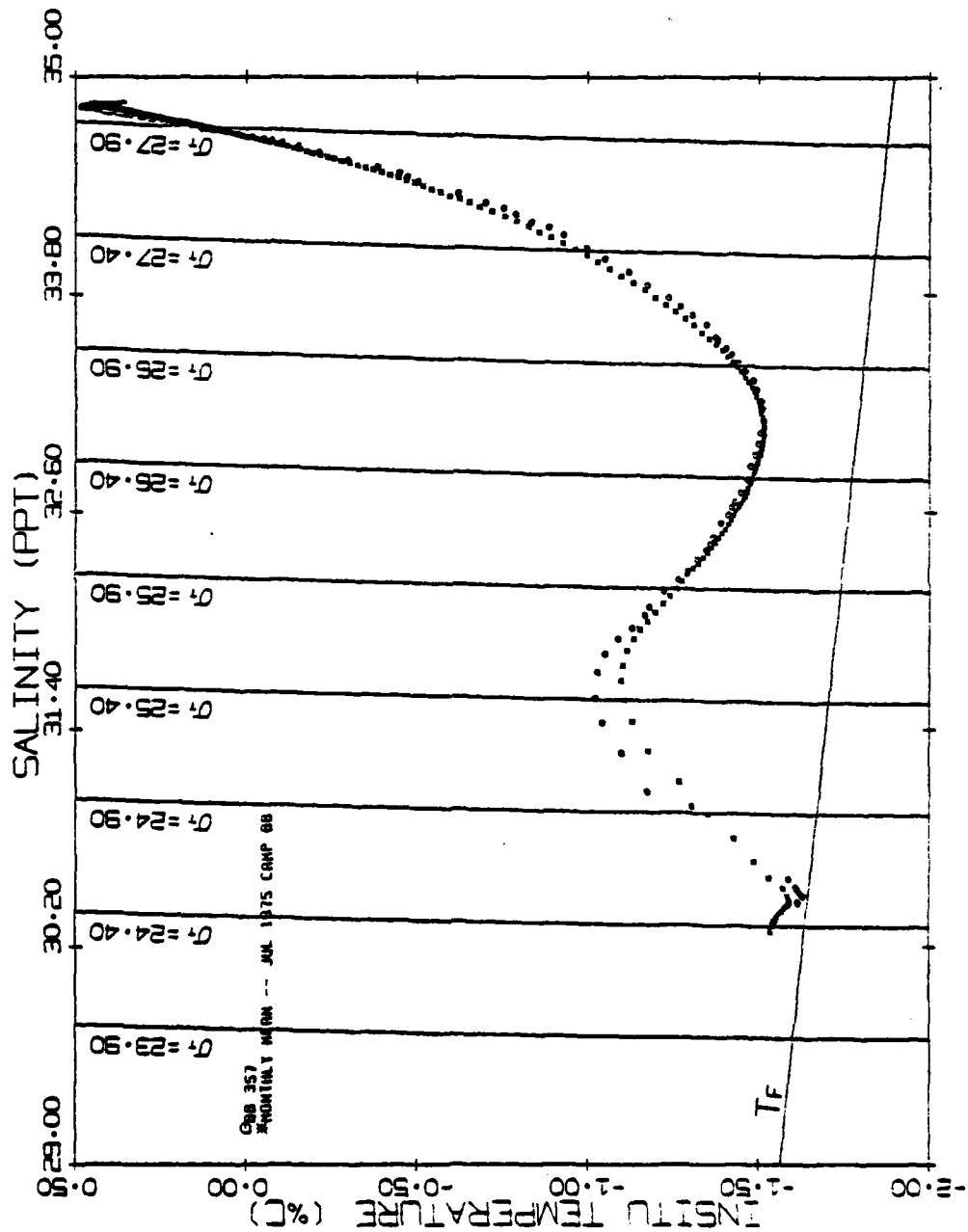
AD-A098 170 LAMONT-DOHERTY GEOLOGICAL OBSERVATORY PALISADES NY F/G 8/3
EDDIES OF THE WESTERN ARCTIC OCEAN - THEIR CHARACTERISTICS AND --ETC(U)
MAR 81 T O MANLEY N00014-76-C-0004
UNCLASSIFIED LDGO-CU-1-81 NL

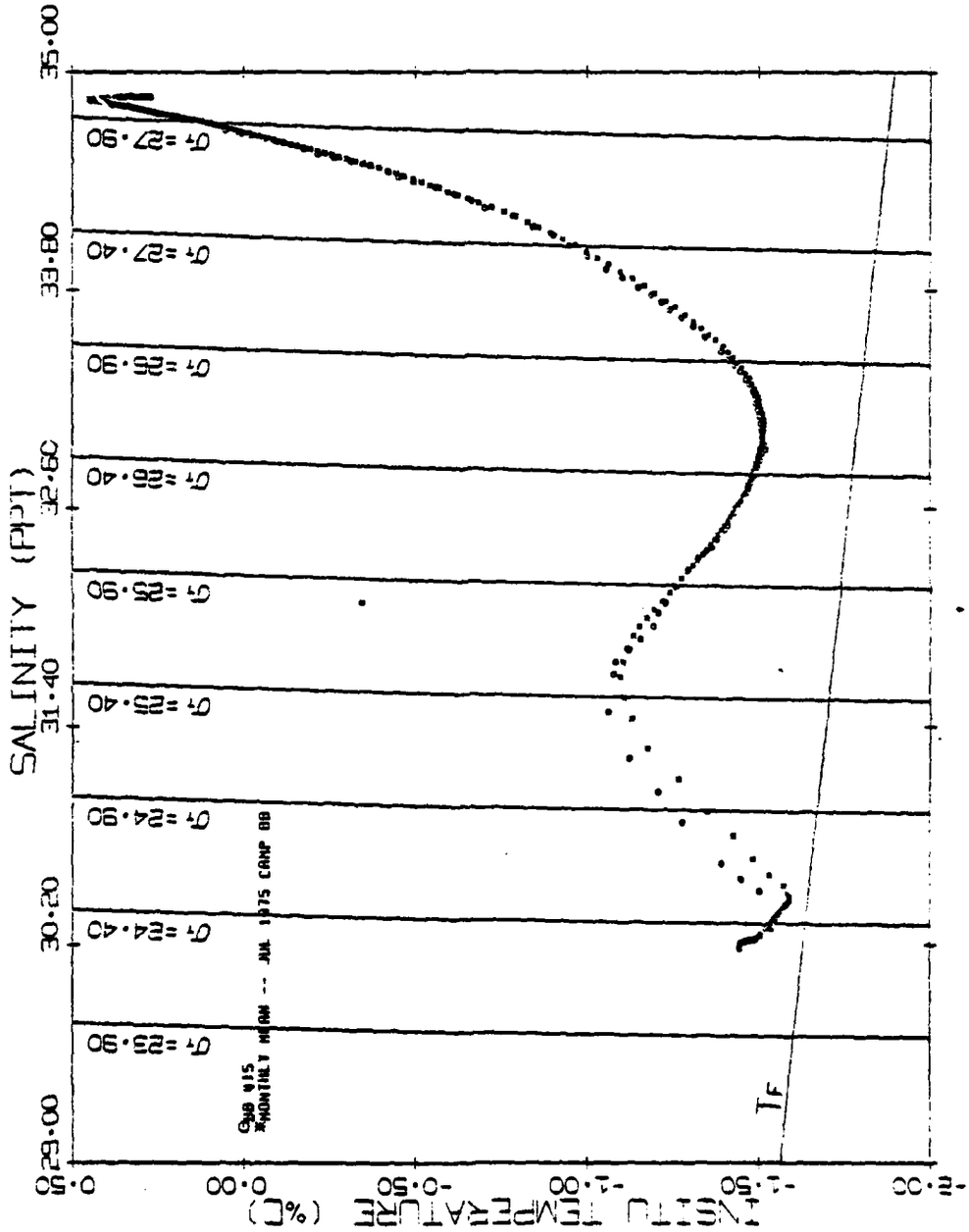
5 OF 5
AD A098 170

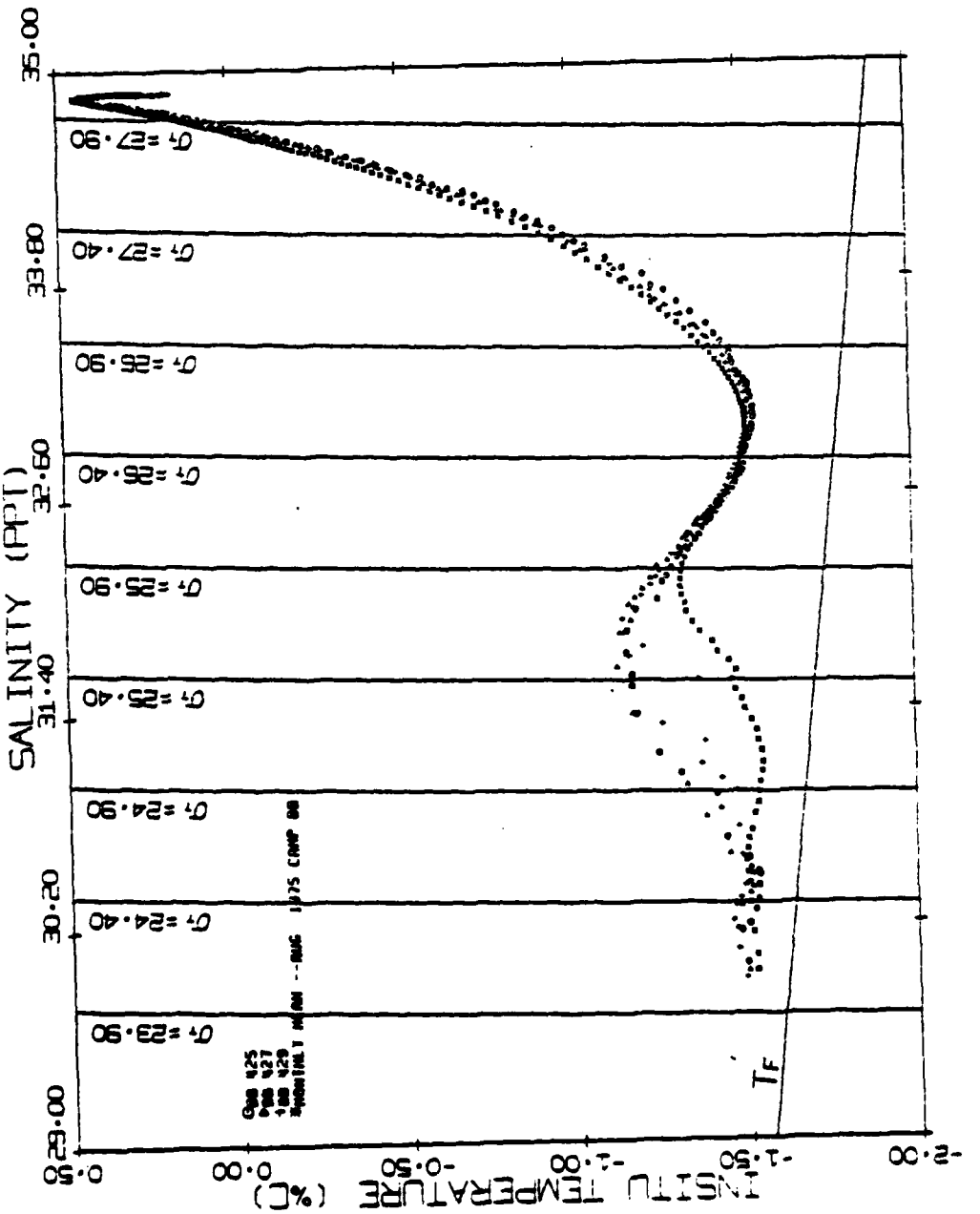


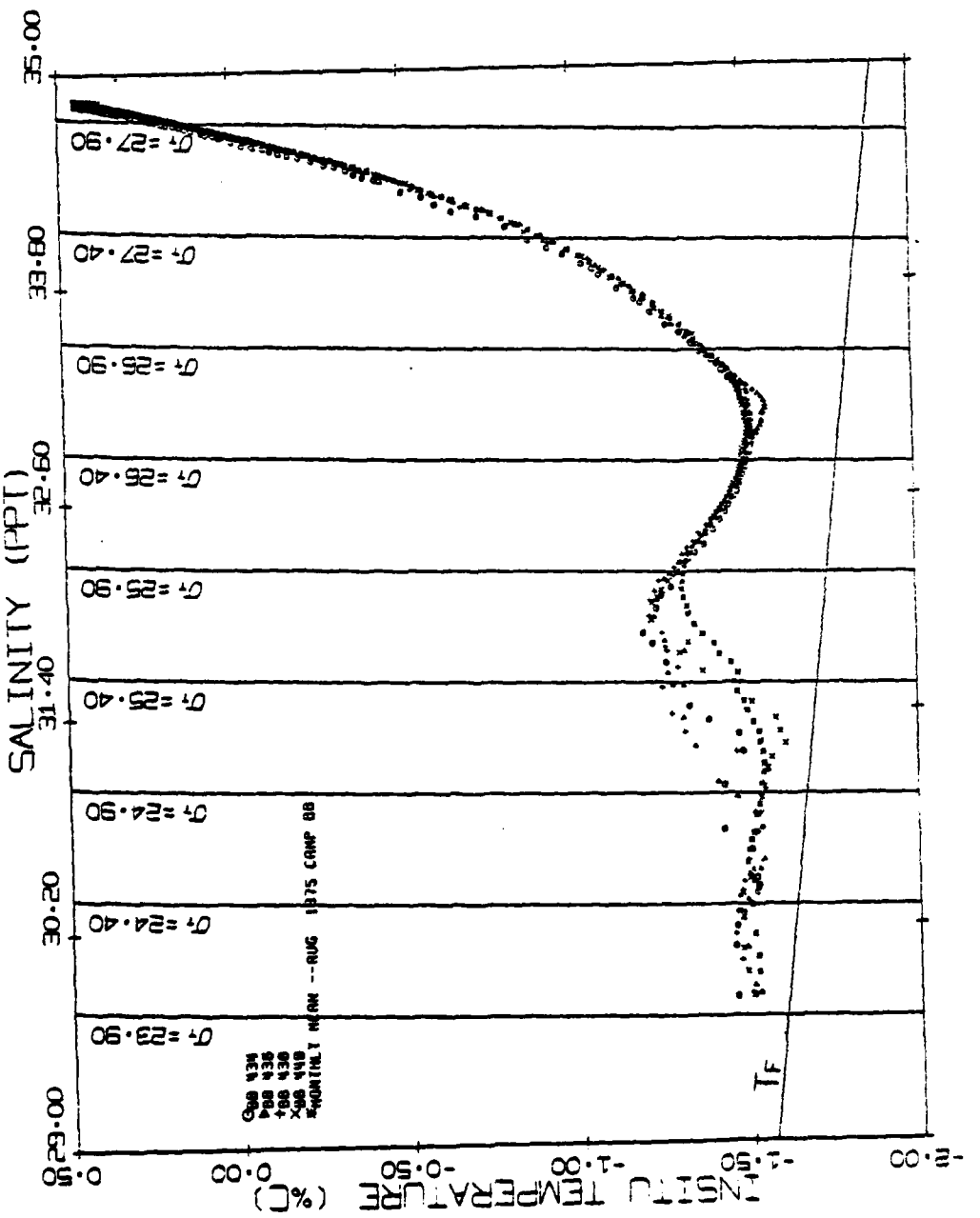
END
DATE FILMED
5-81
DTIC

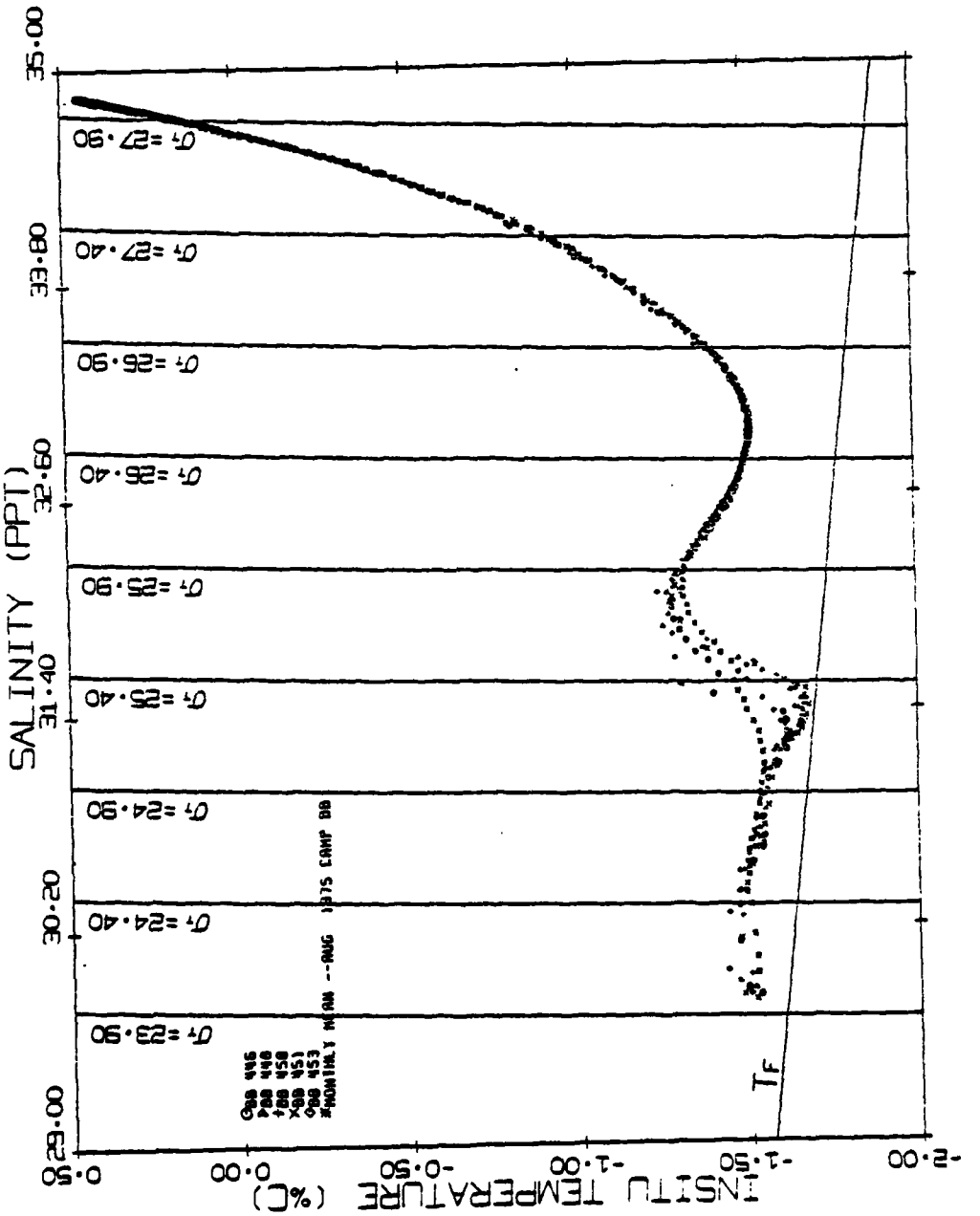

1.0
1.1
1.25
1.4
1.6
1.8
2.0
2.2
2.5
2.8
3.2
3.6
4.0
MICROCOPY RESOLUTION TEST CHART

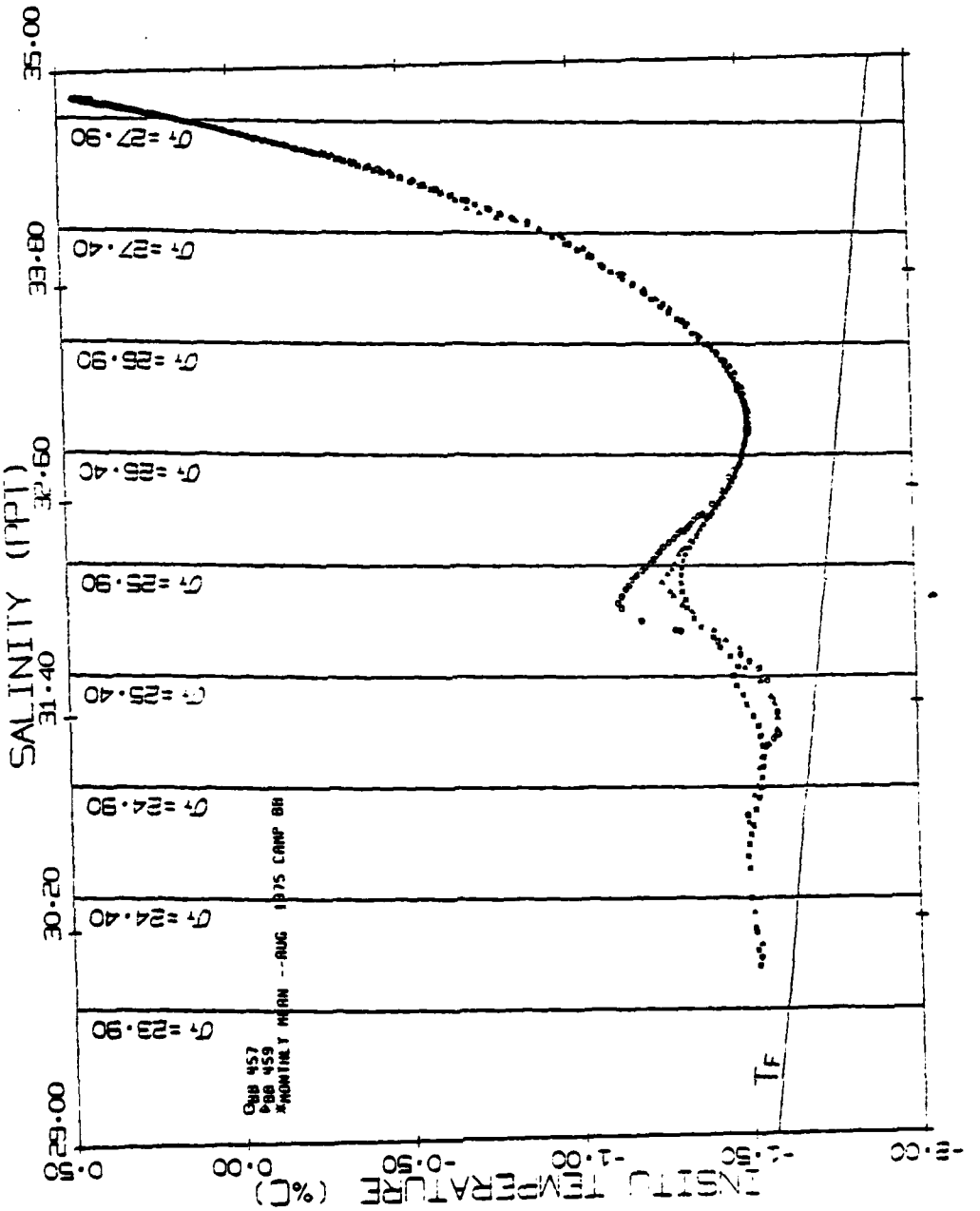

SALINITY (PPT)
35.00
33.80
32.60
31.40
30.20
29.00
σt =27.90
σt =27.40
σt =26.90
σt =26.40
σt =25.90
σt =25.40
σt =24.90
σt =24.40
σt =23.90
IN SITU TEMPERATURE (°C)
0.50
0.00
-0.50
-1.00
-1.50
-1.88
T_F
CRUISE 357
MONTHLY NORM -- JUL 1975 CANP 88

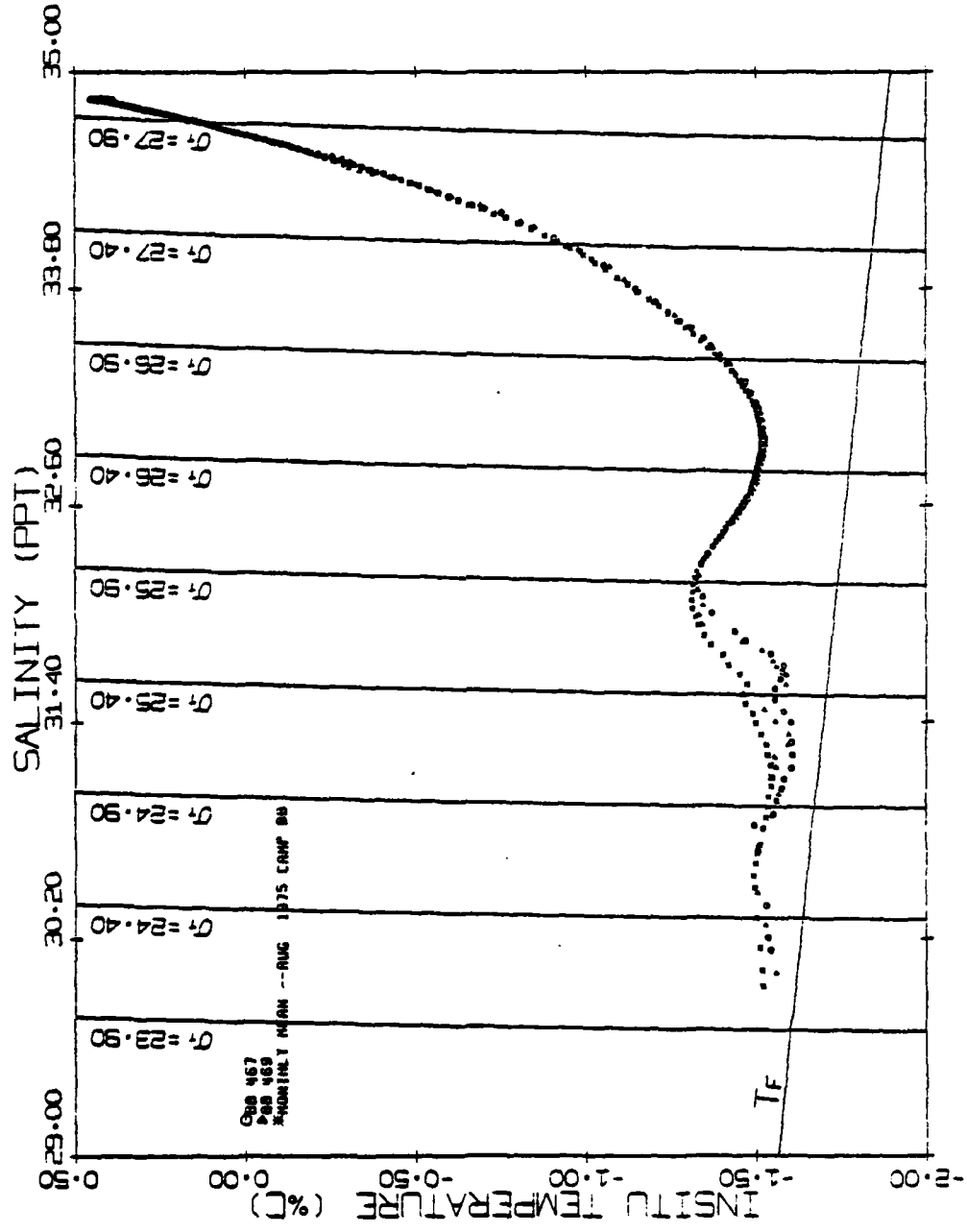

SALINITY (PPT)
35.00
33.80
32.60
31.40
30.20
29.00
σt =27.90
σt =27.40
σt =26.90
σt =26.40
σt =25.90
σt =25.40
σt =24.90
σt =24.40
σt =23.90
Tf
0.50
0.00
-0.50
-1.00
-1.50
-2.00
POTENTIAL TEMPERATURE (°C)

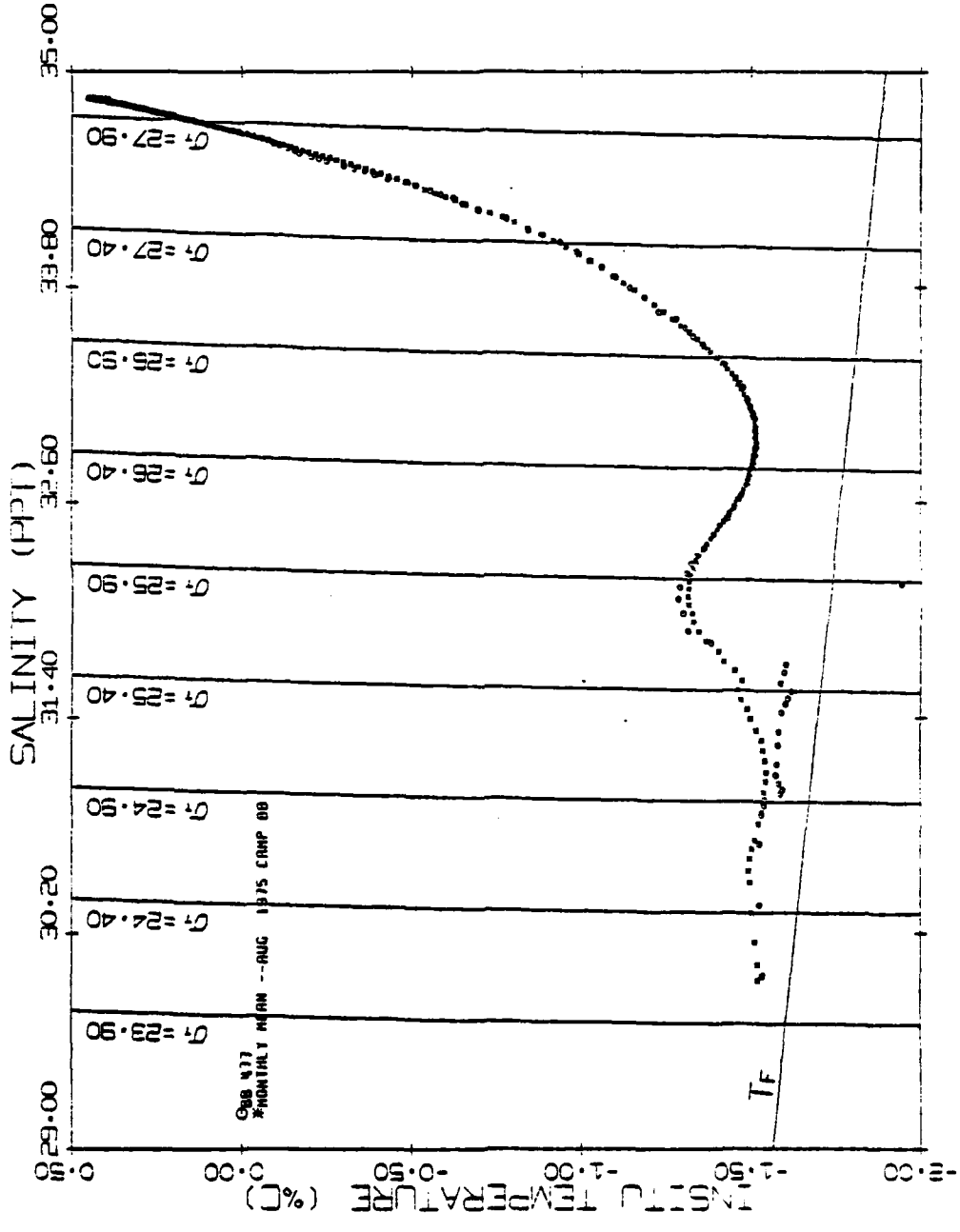

SALINITY (PPT)
35.00
33.80
32.60
31.40
30.20
29.00
σt =27.90
σt =27.40
σt =26.90
σt =26.40
σt =25.90
σt =25.40
σt =24.90
σt =24.40
σt =23.90
T_F
0.50
0.00
-0.50
-1.00
-1.50
-2.00
(°C)

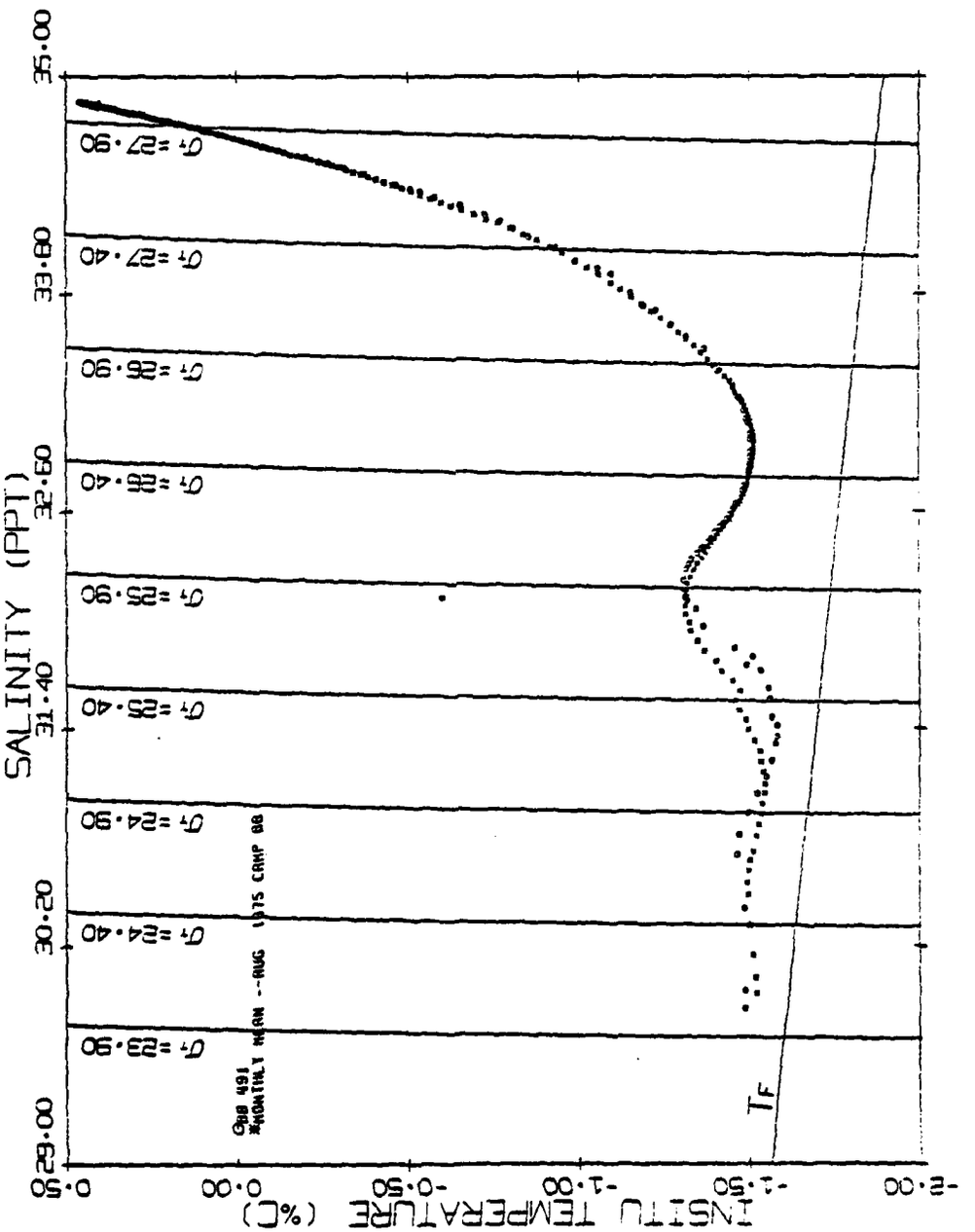

SALINITY (PPT)
35.00
33.80
32.60
31.40
30.20
29.00
σt =27.90
σt =27.40
σt =26.90
σt =26.40
σt =25.90
σt =25.40
σt =24.90
σt =24.40
σt =23.90
0.50
0.00
-0.50
-1.00
-1.50
-2.00
(°C)
T_F

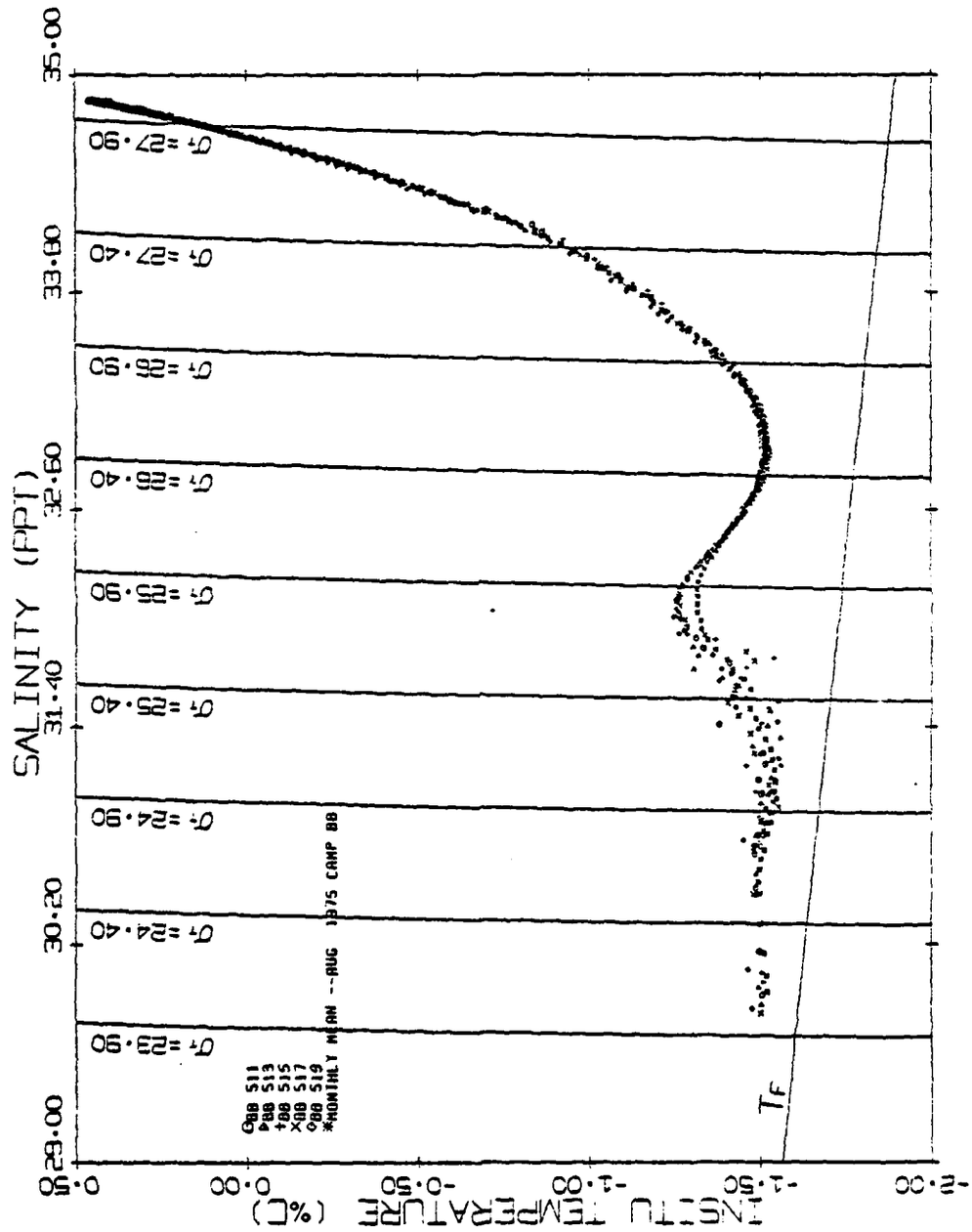

SALINITY (PPT)
35.00
33.80
32.60
31.40
30.20
29.00
σt =27.90
σt =27.40
σt =26.90
σt =26.40
σt =25.90
σt =25.40
σt =24.90
σt =24.40
σt =23.90
INSITU TEMPERATURE (°C)
0.50
0.00
-0.50
-1.00
-1.50
-2.00
T_F
MONTHLY MEAN --RMG 1975 CAMP BB

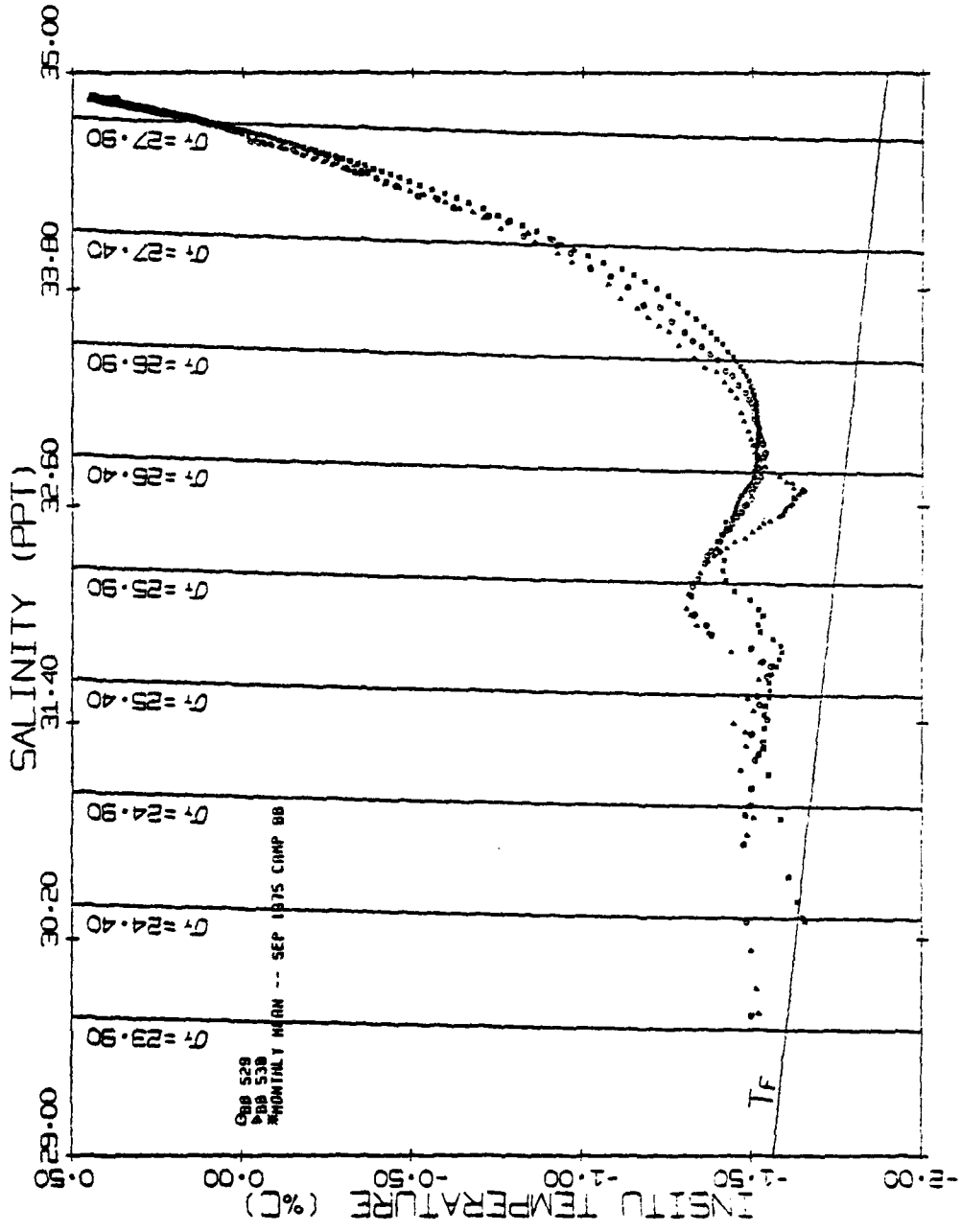

SALINITY (ppt)
35.00
33.80
32.60
31.40
30.20
29.00
σt =27.90
σt =27.40
σt =26.90
σt =26.40
σt =25.90
σt =25.40
σt =24.90
σt =24.40
σt =23.90
BB 457
BB 459
MONTHLY MEAN --AUG 1975 CAMP BB
0.50
0.00
-0.50
-1.00
-1.50
-2.00
INSITU TEMPERATURE (°C)
T_F

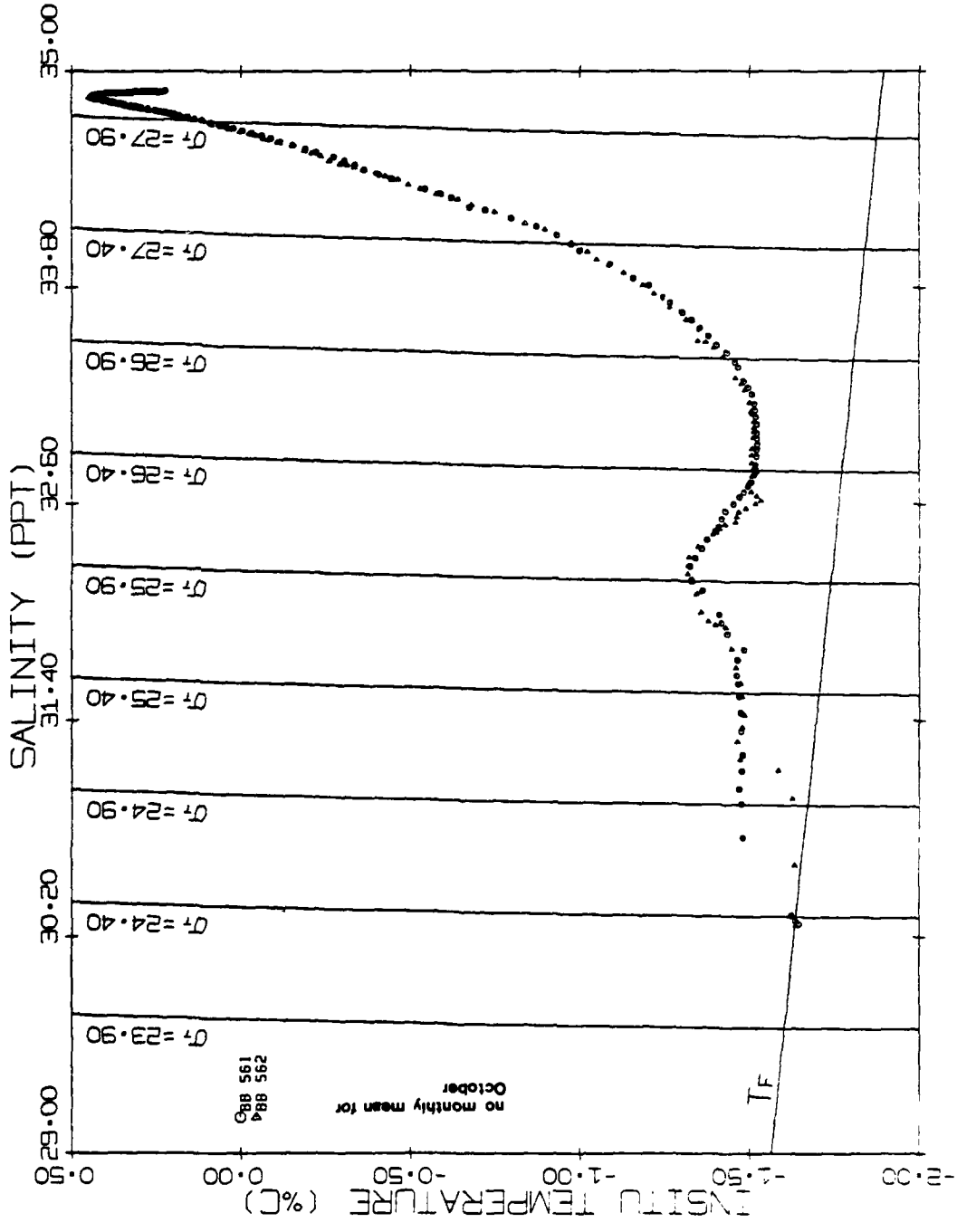

SALINITY (PPT)
35.00
33.80
32.60
31.40
30.20
29.00
σt =27.90
σt =27.40
σt =26.90
σt =26.40
σt =25.90
σt =25.40
σt =24.90
σt =24.40
σt =23.90
INSITU TEMPERATURE (°C)
0.50
0.00
-0.50
-1.00
-1.50
-2.00
T_F


SALINITY (PPT)
POTENTIAL TEMPERATURE (°C)
29.00
30.20
31.40
32.60
33.80
35.00
0.00
-0.50
-1.00
-1.50
-2.00
σθ =23.90
σθ =24.40
σθ =24.90
σθ =25.40
σθ =25.90
σθ =26.40
σθ =26.50
σθ =27.40
σθ =27.90
TF
σθ 417
*MONTHLY MEAN --AUG 1975 CAMP 08


SALINITY (PPT)
INSITU TEMPERATURE (°C)
σt =27.90
σt =27.40
σt =26.90
σt =26.40
σt =25.90
σt =25.40
σt =24.90
σt =24.40
σt =23.90
T_F


SALINITY (PPT)
35.00
33.80
32.60
31.40
30.20
29.00
σt =27.90
σt =27.40
σt =26.90
σt =26.40
σt =25.90
σt =25.40
σt =24.90
σt =24.40
σt =23.90
IN SITU TEMPERATURE (°C)
0.00
-0.50
-1.00
-1.50
-2.00
T_F
MEAN --AUG 1975 CAMP 88
*MONTHLY


SALINITY (PPT)
35.00
33.80
32.60
31.40
30.20
29.00
σt =27.90
σt =27.40
σt =26.90
σt =26.40
σt =25.90
σt =25.40
σt =24.90
σt =24.40
σt =23.90
IN SITU TEMPERATURE (°C)
0.50
0.00
-0.50
-1.00
-1.50
-2.00
T_F
BB 529
BB 538
*MONTHLY MEAN -- SEP 1975 COMP BB


SALINITY (PPT)
35.00
33.80
32.60
31.40
30.20
29.00
σt =27.90
σt =27.40
σt =26.90
σt =26.40
σt =25.90
σt =25.40
σt =24.90
σt =24.40
σt =23.90
IN SITU TEMPERATURE (°C)
0.50
0.00
-0.50
-1.00
-1.50
-2.00
BB 561
BB 562
no monthly mean for October
T_F

Section 3

Eddy Statistics

The following are defintions of the labels for this section:

IDYBGN - Date of first observation of eddy (AIDJEX DAYS)
IDYEND - Date of last observation of eddy (AIDJEX DAYS)
DEL - Total time that the eddy was observed (in decimal days)
PCM BGN - Beginning PCM station of observation
PCM END - Ending PCM station of observation
STD BGN - Beginning STD station of observation
STD END - Ending STD station of observation
STD CNTR - The STD station with the maximum vertical displacement of the isohalines
PCM MAX - The PCM station with the maximum observed absolute velocity
ROT - Rotation of eddy, CW(Clockwise), CCW(Counter-clockwise)
CLS - Classification label as defined in text
DAY OF MAXSPD - AIDJEX day of the maximum speed observed in the eddy
MAXSP - Maximum speed of the eddy in cm/sec
SPD DEP - Depth of maximum speed in meters

Section 3a

******** Information List for All Eddies Observed at Camp Caribou ********

- AIDJEX DAYS -			PCM		STD		STD	PCM			DAY OF		SPD
IDYBGN	IDYEND	DEL	BGN	END	BGN	END	CNTR	MAX	ROT	CLS	MAXSPD	MAXSP	DEP
145.76	147.75	2.0			023	027	027		CW	S			
149.75	149.75	.05			031	031	031		CW	S			
150.75	151.84	1.1			033	035	035		CW	S			
168.77	169.76	1.0			069	071	069		CW	S			
179.76	180.78	1.0			091	093	093		CW	S			
185.76	186.75	1.0			102	104	102		CW	S			
197.77	197.77	.05			124	124	124		CW	S			
202.75	202.75	.05			126	126	126		CW	S			
209.75	209.75	.05			140	140	140		CW	S			
216.76	218.80	2.0	001	001	154	158	156	001	CW	C	217.29	14.85	100
221.28	221.28	.05			163	163	163		CW	S			
222.78	222.96	0.2	007	007	167	167	167	007	CW	C	222.96	24.20	119
239.76	242.75	3.0			200	205	200		CW	S			
255.76	259.78	4.0			229	237	231		CW	S			
264.77	266.75	2.0			246	250	246		CW	S			
270.76	270.76	4.0			252	259	252		CW	S			
280.76	281.76	1.0			271	273	271		CW	S			
292.75	292.75	.05			289	289	289		CW	S			
302.35	302.35	.05	055	055				055		P	302.35	22.06	068
304.03	304.03	.05			300	300	300		CW	S			
310.17	314.79	4.6			309	322	314		UNK	D			
311.77	311.91	2.3	063	063	311	318	314	063	CW	C	311.91	17.62	062
320.10	320.81	0.7	074	075				075	CW	CSB	320.81	14.56	064
324.88	325.83	1.0	084	087				085	CW	CSB	325.83	15.00	090
327.21	331.28	4.1	090	098	371	388	382	096	CW	C	330.28	35.04	139
335.56	339.83	4.3	104	113				104	CW	CSB	335.56	31.79	167
340.27	345.32	5.1	114	126	426	440	432	122	CW	C	343.34	30.89	187
350.94	351.30	0.4	130	131				130		P	350.94	21.64	038
355.82	358.28	2.5	137	142	444	446	446	142	CW	C	358.28	17.29	187
366.25	368.80	2.6			468	478	474		CCW	S			
369.25	369.75	0.5	158	158	480	482	480	158	CW	C	369.27	31.80	180
374.05	375.92	1.9	168	169	500	502	500	169	CW	C	375.92	20.46	176
396.21	396.23	.05	185	185	559	559	559	185	CW	C	396.23	10.65	141
433.75	439.75	6.0	302	314	672	696	676	304	CW	C	434.96	23.66	079
467.25	467.35	0.1	377	377	804	804	804	377	CW	C	467.35	26.61	190

Section 3b

******** Information List for All Eddies Observed at Camp Blue Fox ********

- AIDJEX DAYS -			PCM		STD		STD	PCM			DAY OF		SPD
IDYBGN	IDYEND	DEL	BGN	END	BGN	END	CNTR	MAX	ROT	CLS	MAXSPD	MAXSP	DEP
148.75	151.23	2.5	042	047	019	021	020	044	CW	C	149.88	20.97	176
151.75	154.88	3.1	048	054	022	025	023	051	CW	C	153.24	32.57	099
157.75	158.87	1.1	061	062	028	030	029	061	CW	C	158.25	17.85	114
168.75	172.89	3.6	081	089	039	043	043	089	CW	C	172.89	29.31	078
173.23	173.23	.05	090	090				090		P	173.23	36.82	130
176.75	178.88	2.1	097	101				098	CW	CSB	177.31	18.32	113
179.26	180.24	1.0	102	104				103		P	179.88	29.63	190
180.75	184.24	3.5	105	112	051	054	054	109	CW	C	182.90	34.65	117
186.24	186.75	0.5	116	116	057	057	057	116	CW	C	186.24	20.00	047
211.88	212.23	0.4	167	168	082	082	082	168	CW	C	212.23	18.89	152
214.24	216.24	2.0	172	176	086	088	088	175	CW	C	215.88	25.48	139
218.18	218.28	0.1	179	179				179		P	218.28	18.45	187
218.75	220.89	2.1	180	184	094	097	096	182	CW	C	219.94	33.66	089
223.75	223.75	0.1			100	100	100		CW	S			
223.88	223.88	0.1	193	193				193		P	223.88	45.32	187
224.75	226.75	2.0	196	200	101	103	102	196	CW	C	224.88	39.15	128
234.75	237.76	4.0	224	226	112	118	114	226	CW	C	237.24	19.	050
240.25	242.03	2.2	232	235	124	126	124	234	CW	C	241.22	27.	100
240.75	240.90	0.2	233	233				233		P	240.90	28.25	189
243.75	244.75	1.0	241	241	130	132	130	241	CW	C	244.75	47.81	075
245.23	245.23	0.1	243	243				243		P	245.23	19.70	148
247.23	247.23	0.1	249	249				249		P	247.23	11.69	183
248.23	248.23	0.1	252	252				252		P	248.23	15.97	169
247.75	248.88	1.1	252	253	138	140	140	253	CW	C	248.88	15.	055
249.75	251.75	2.0	255	259	142	146	144	256	CW	C	250.25	29.71	115
251.88	253.24	1.4	260	263				260		P	251.88	35.13	180
254.75	255.24	0.5	266	267				266	CW	CSB	254.89	26.42	189
264.25	264.89	0.6	285	286				286	CW	CSB	264.89	47.94	122
267.77	273.75	6.0	296	296	178	190	184	296	CW	C	274.96	12.	55
270.98	270.98	0.1	298	298				298		P	270.98	13.	190
277.78	285.89	8.1	312	328	198	214	208	320	CW	C	281.90	28.75	134
291.75	292.98	1.2	340	342	226	228	228	342	CW	C	292.98	21.20	092
295.90	295.90	0.1	348	348				348		P	295.90	41.04	105
297.24	297.24	0.1	351	351				351		P	297.24	22.	082
297.75	298.88	1.1	352	353	238	240	238	352	CW	C	297.89	21.02	180
300.00	300.00	0.1	355	355				355		P	300.00	28.20	119
301.75	303.24	1.5	359	362	246	248	246	362	CW	C	303.24	33.	100
311.75	317.75	6.0	389	392	266	278	272	389	CW	C	316.86	12.	47
317.30	317.30	0.1	390	390				390		P	317.30	20.57	078
318.75	319.76	1.0			280	282	280		CW	S			
332.89	335.23	2.3	421	426				426		P	335.23	15.	125
369.30	375.30	6.0	485	497	324	334	324	485	CW	C	389.30	32.02	084
376.75	376.76	0.1			338	338	338		CW	S			
387.30	395.31	8.0	521	537				526		CSB	389.88	15.81	095
396.75	396.75	0.1			378	378	378		CW	S			
398.75	399.75	1.0			382	384	382		CW	S			
403.30	403.90	0.8	553	554				553		P	403.30	30.01	096

Section 3c

******** Information List for All Eddies Observed at Camp Snowbird ********

- AIDJEX DAYS -			PCM		STD		STD	PCM			DAY OF		SPD
IDYBGN	IDYEND	DEL	BGN	END	BGN	END	CNTR	MAX	ROT	CLS	MAXSPD	MAXSP	DEP
135.22	138.25	3.0	021	024	001	003	003	023	CW	C	137.27	51.75	158
143.87	146.75	2.9	035	040				036	CW	CSB	144.24	14.59	157
149.75	155.25	5.5	047	058	028	038	030	049	CW	C	150.86	58.23	135
165.86	169.24	3.4	079	086				085	CW	CSB	168.86	15.60	137
177.75	179.75	2.0			084	088	086		CW	S			
180.75	184.24	3.5	110	116	090	096	094	115	CW	C	183.88	28.96	149
186.87	187.76	0.9	120	122	104	104	104	122	CW	C	187.09	18.73	171
191.75	193.25	1.5			110	112	112		CW	CSB			
196.80	200.75	4.0	135	141	118	126	122	141	CW	C	200.25	24.01	196
211.75	212.29	0.5	147	147	136	136	136	147	CW	C	212.29	10.	090
235.75	237.75	2.0	206	211	182	186	184	210	CW	C	236.95	30.51	119
242.24	243.95	1.7	221	222				222	CW	CSB	243.95	31.87	065
247.59	248.09	0.5	238	238				238		P	247.59	16.69	055
248.75	249.24	0.5	241	241	206	206	206	241	CW	C	249.24	16.02	056
250.75	253.24	2.5	245	251				246	CCW	CSB	251.24	17.	120
258.24	259.24	1.0	261	263				262		P	258.93	14.17	077
267.77	268.95	1.2	280	282	233	234	234	280	CW	C	267.98	23.71	109
274.25	274.95	0.7	291	292				292		P	274.95	31.02	057
278.75	280.75	2.0			238	240	239			D			
281.75	282.24	0.5			241	241	241		CW	CSB			
284.75	288.24	3.5	308	313	245	251	247	310	CW	C	286.95	22.61	082
286.75	286.75	0.1			249	249	249		CCW	S			
289.75	294.24	3.5	316	324	255	263	257	321	CW	C	292.95	22.36	104
299.79	301.75	2.0	334	336	275	270	277	336	CW	C	301.25	24.87	055
326.02	327.24	1.2	380	382	328	328	328	380	CW	C	326.02	33.71	082
329.31	330.75	1.4	386	388	334	336	334	388	CW	C	330.29	26.43	113
334.75	339.24	4.5	396	405	344	352	346	398	CW	C	336.02	29.35	089
338.75	340.25	1.5	404	407	352	354	354	406	CW	C	339.95	11.00	200
342.95	344.31	1.4	412	415				412		P	342.95	16.69	105
351.83	352.41	0.6	429	429				429	CW	CSB	352.41	13.90	049
353.76	356.75	3.0			374	380	376		CW	S			
361.83	364.24	2.4	434	431	390	392	392	438	CW	C	363.88	21.47	076
366.27	367.26	1.0	443	445				445	CW	CSB	367.26	10.92	086
368.89	375.24	6.4	448	461	404	412	404	457	CW	C	372.27	31.43	089
377.71	383.29	5.6	464	473	418	433	418	467	CW	C	378.83	21.05	094
397.78	397.88	0.1	504	504	482	482	482	504	CW	C	397.88	16.58	139
402.76	403.76	1.0	506	507	490	492	492	507	CW	C	403.29	31.95	092
423.29	423.78	0.5	541	541				541	CW	CSB	423.29	16.	047
447.86	449.84	2.0	557	561				558		P	448.35	24.93	085
472.25	476.25	4.0	611	617	586	602	596	616	CW	C	475.06	20.23	097

Section 3d

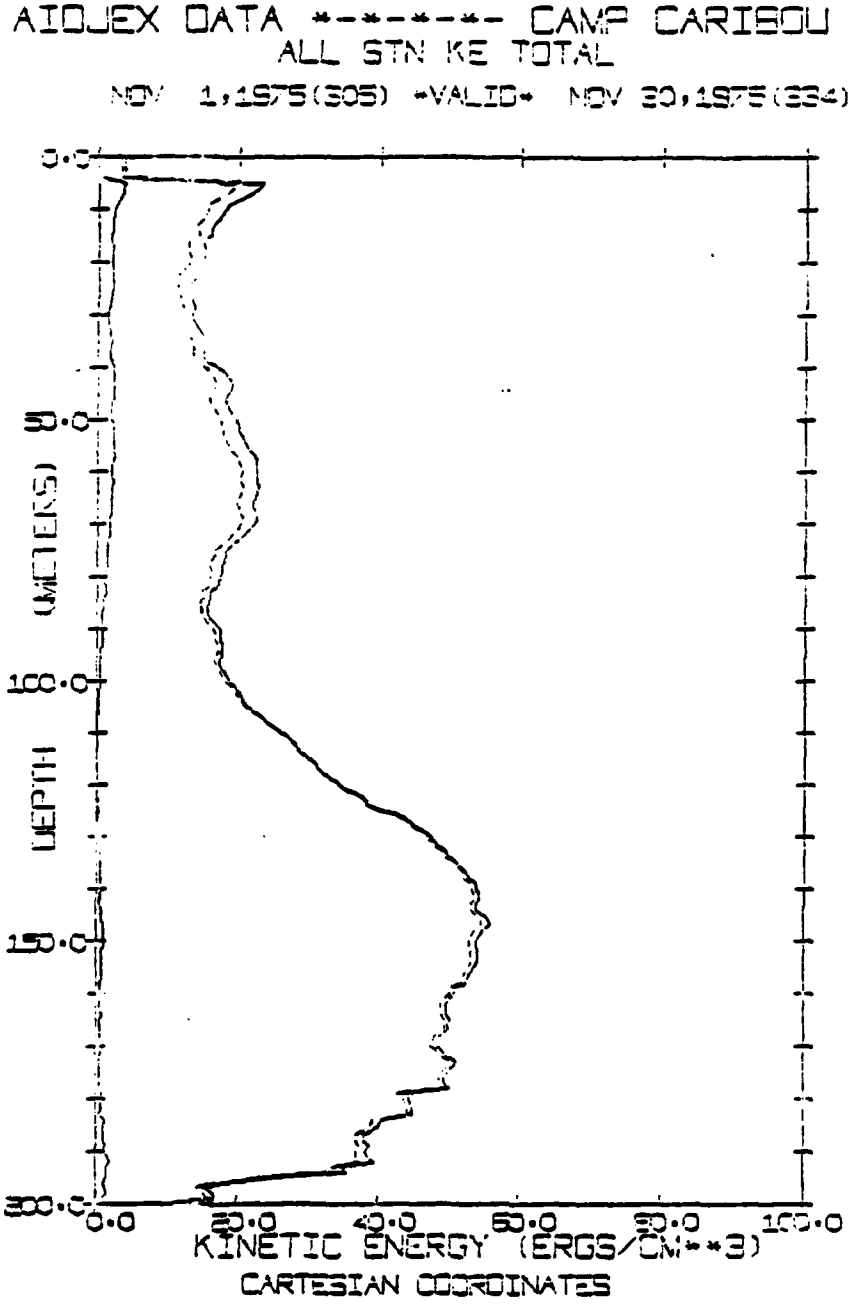
******** Information List for All Eddies Observed at Camp Big Bear ********

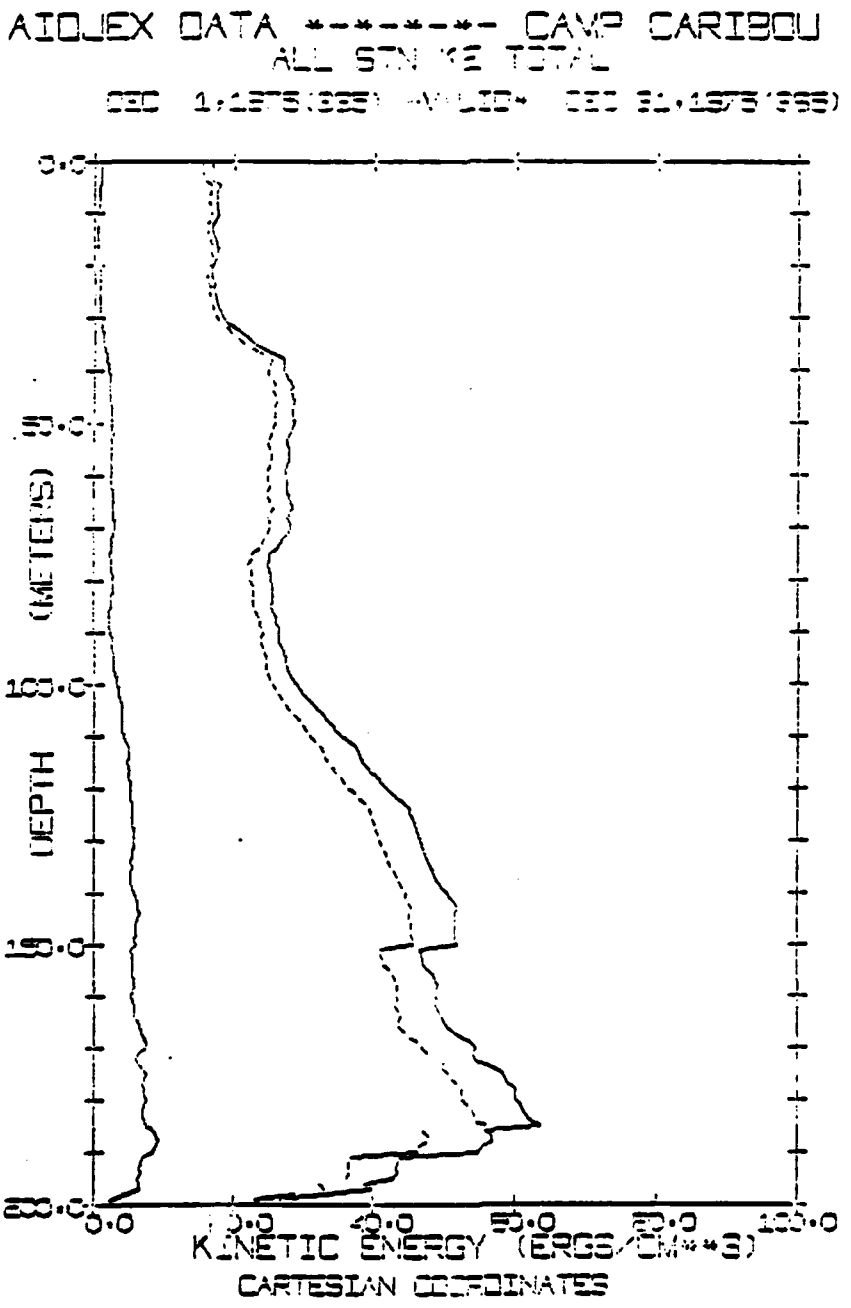
- AIDJEX DAYS -			PCM		STD		STD	PCM			DAY OF		SPD
IDYBGN	IDYEND	DEL	BGN	END	BGN	END	CNTR	MAX	ROT	CLS	MAXSPD	MAXSP	DEP
094.00	094.00				004	004	004		CW	S			
101.21	103.73	2.5			024	034	028		UNK	D			
119.74	122.81	3.1	048	055	097	107	105	050	CW	C	120.82	46.78	152
126.17	126.83	0.7	062	063				062	CW	CSB	126.28	10.08	140
148.23	150.93	2.7	102	111				105	CW	CSB	149.23	16.18	177
157.21	161.71	4.5	132	142	241	259	255	134	CW	C	158.73	45.79	131
163.21	168.71	5.5	145	168	285	297	291	168	CW	C	168.26	57.38	165
176.95	177.91	0.9	174	174				174	CW	CSB	176.95	15.69	086
181.21	181.21				349	349	349		CW	S			
183.21	183.21				357	357	357		CW	S			
196.68	197.25	0.6	242	244				244		P	197.25	12.75	064
207.67	208.67	1.0	276	278				278	CW	CSB	208.67	12.57	135
212.22	213.71	1.5	282	294	425	429	427	282	CW	C	212.67	26.32	113
215.23	217.21	2.0	287	291	434	440	436	291	CW	C	216.70	36.00	152
218.71	220.94	2.2	297	303	446	453	451	298	CW	C	219.72	17.10	062
221.23	222.23	1.0	304	412	452	459	457	307	CW	C	221.61	38.54	104
225.17	226.17	1.0	324	324	467	469	469	324	CW	C	225.70	19.45	070
227.26	229.23	2.0	327	331	477	477	477	327	CW	C	229.23	15.68	045
232.21	232.22		337	337	491	491	491	337	CW	C	232.21	28.41	105
237.79	239.73	2.0	349	349	511	519	513	349	CW	C	238.71	16.02	135
242.71	244.73	2.0	355	365	529	530	530	357	CW	C	243.72	26.97	117
243.22	244.16	0.9			529	530	530		CW	S			
256.21	256.73	0.5	389	390				389		P	256.21	18.45	040
259.23	260.76	1.5	395	398				396		P	259.72	15.73	042
263.74	264.21	1.5	404	405				404		P	263.74	19.27	038
268.24	269.80	1.6	413	416				415		P	269.23	20.75	060
273.76	274.23	0.5	424	425	561	562	562	424	CW	C	273.76	17.96	087

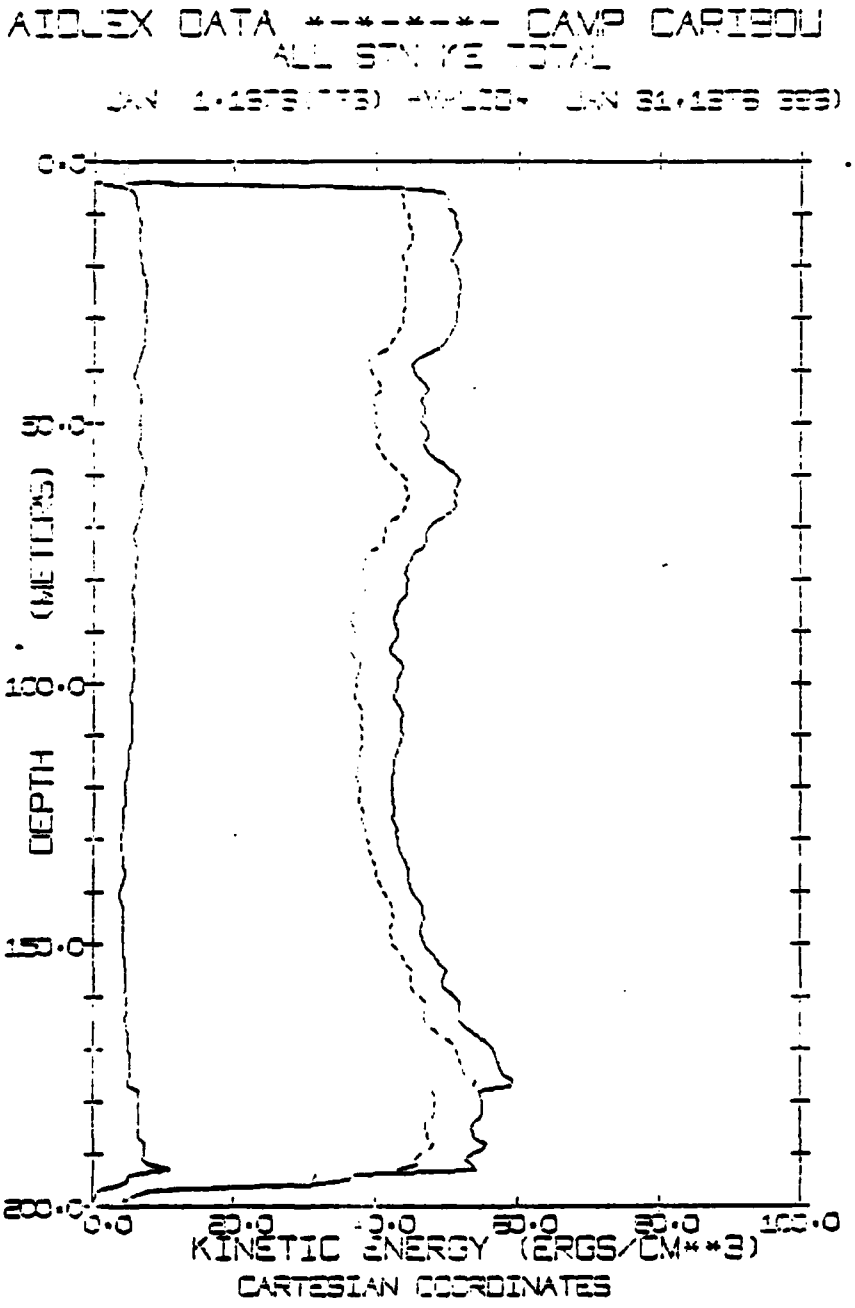
Section 4

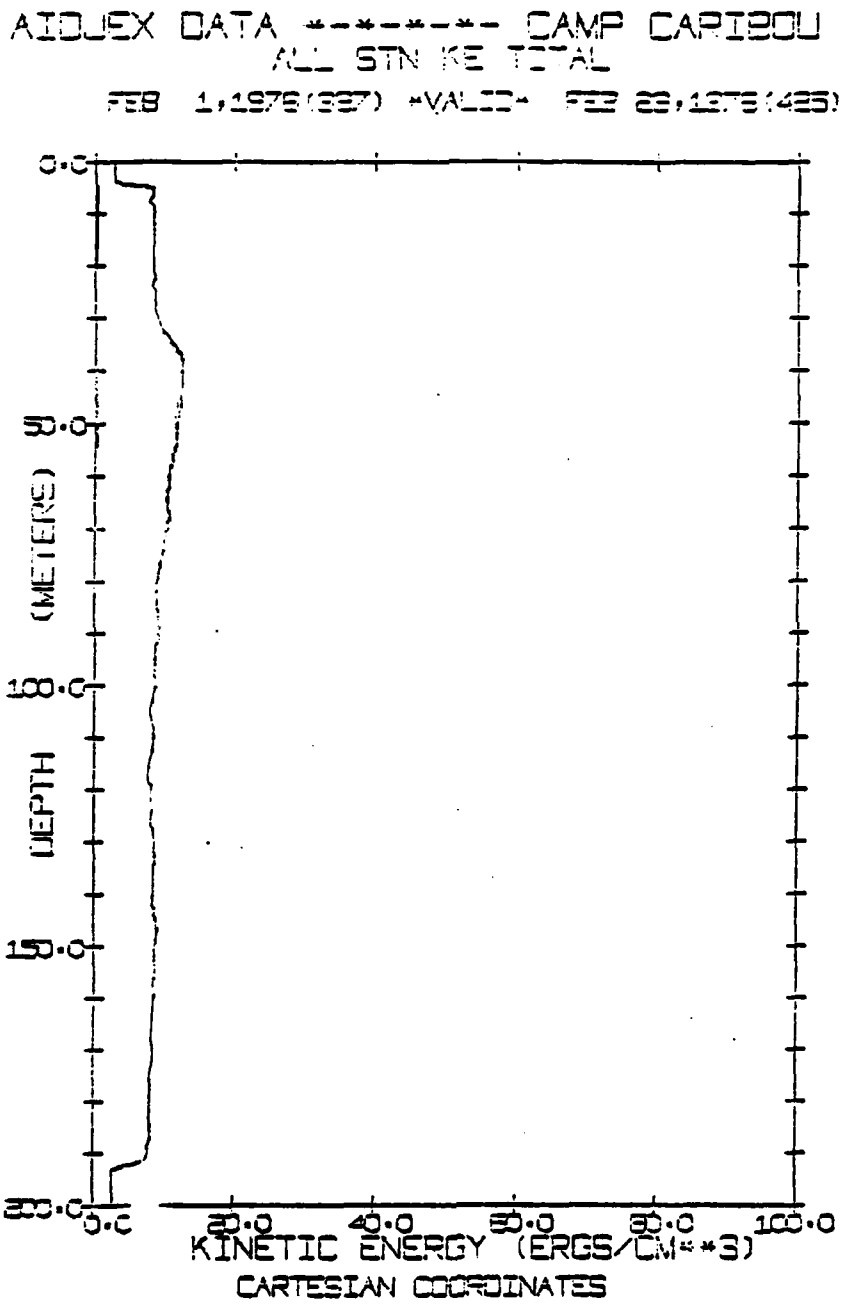
Monthly Mean Kinetic Energy

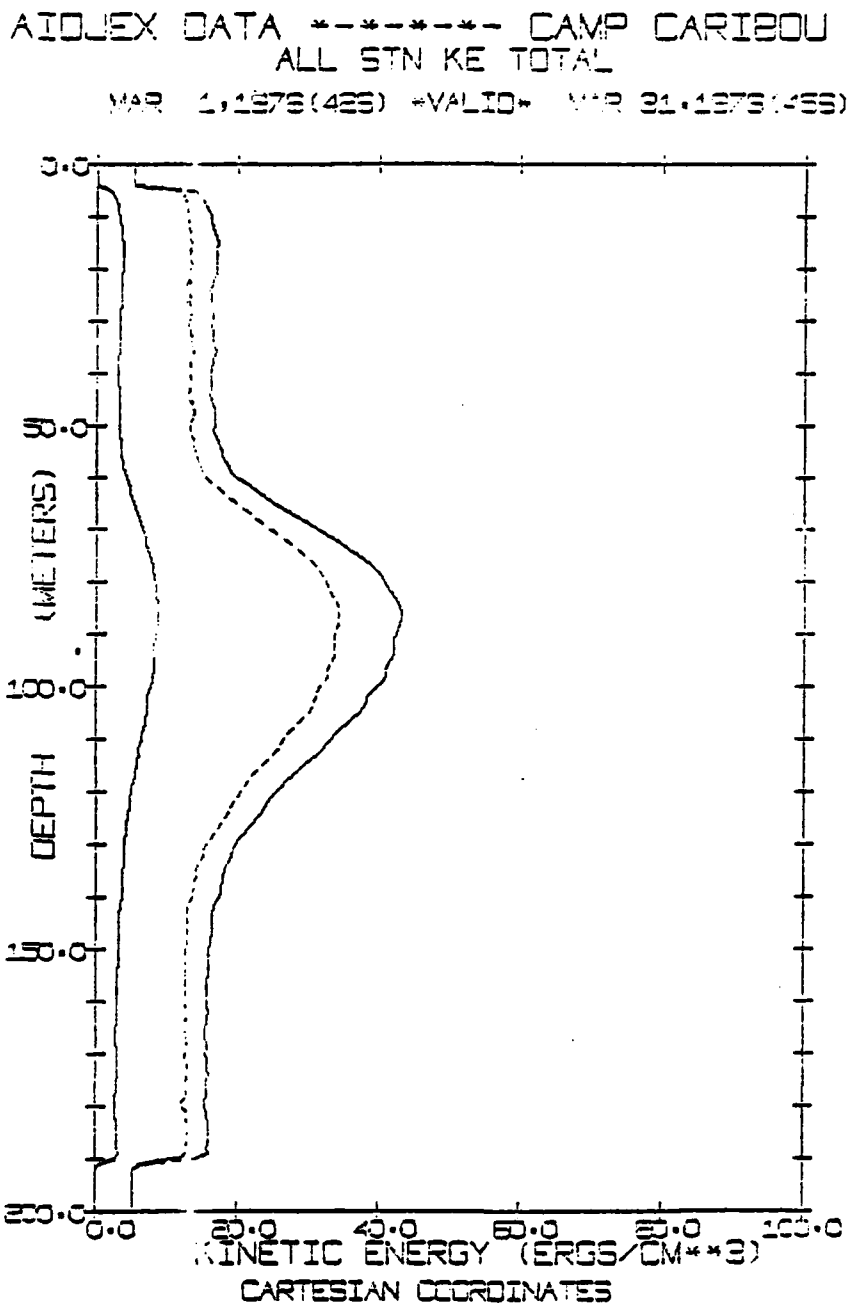
Note: Left most solid line is Mean Kinetic Energy.
Dashed line is Fluctuating Kinetic Energy.
Right most solid line is Total Kinetic Energy.

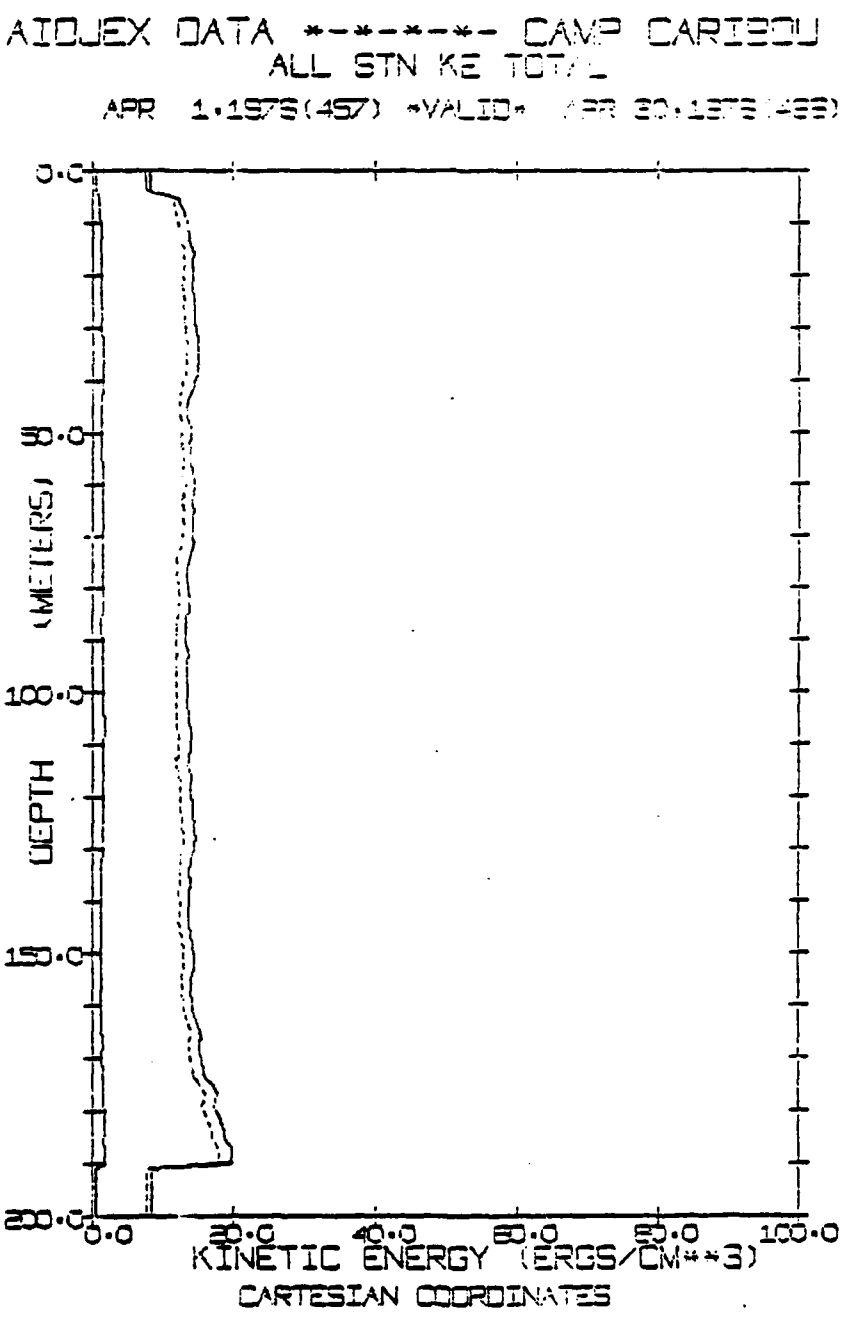

AIDJEX DATA **-**-**-** CAMP CARIBOU
ALL STN KE TOTAL
NOV 1,1975(305) *VALID* NOV 30,1975(334)
0.0
50.0
100.0
150.0
300.0
DEPTH (METERS)
0.0
20.0
40.0
60.0
80.0
100.0
KINETIC ENERGY (ERGS/CM**3)
CARTESIAN COORDINATES

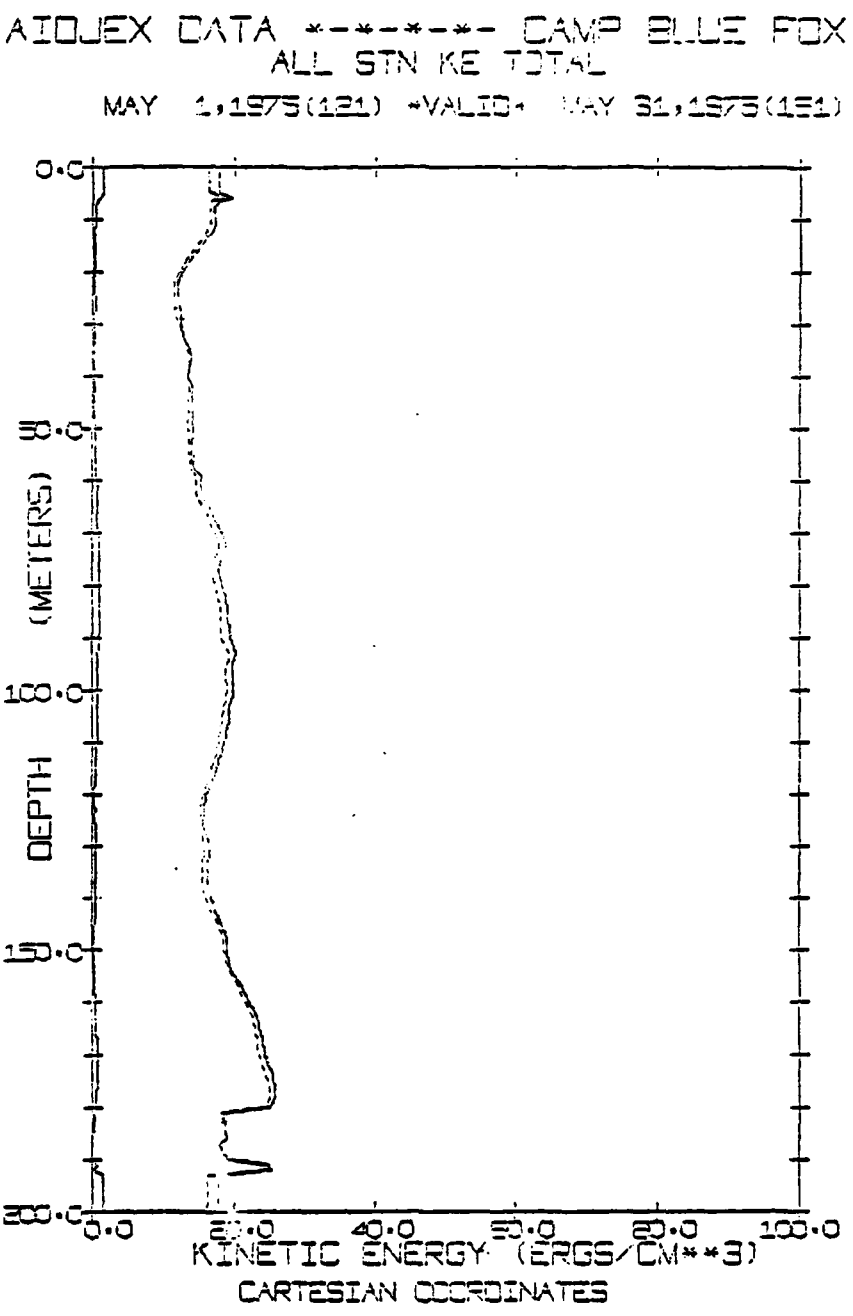

AIDJEX DATA *-*-*-*-*- CAMP CARIBOU
ALL STN KE TOTAL
DEPTH (METERS)
0.0
50.0
100.0
150.0
200.0
0.0
50.0
100.0
KINETIC ENERGY (ERGS/CM**3)
CARTESIAN COORDINATES

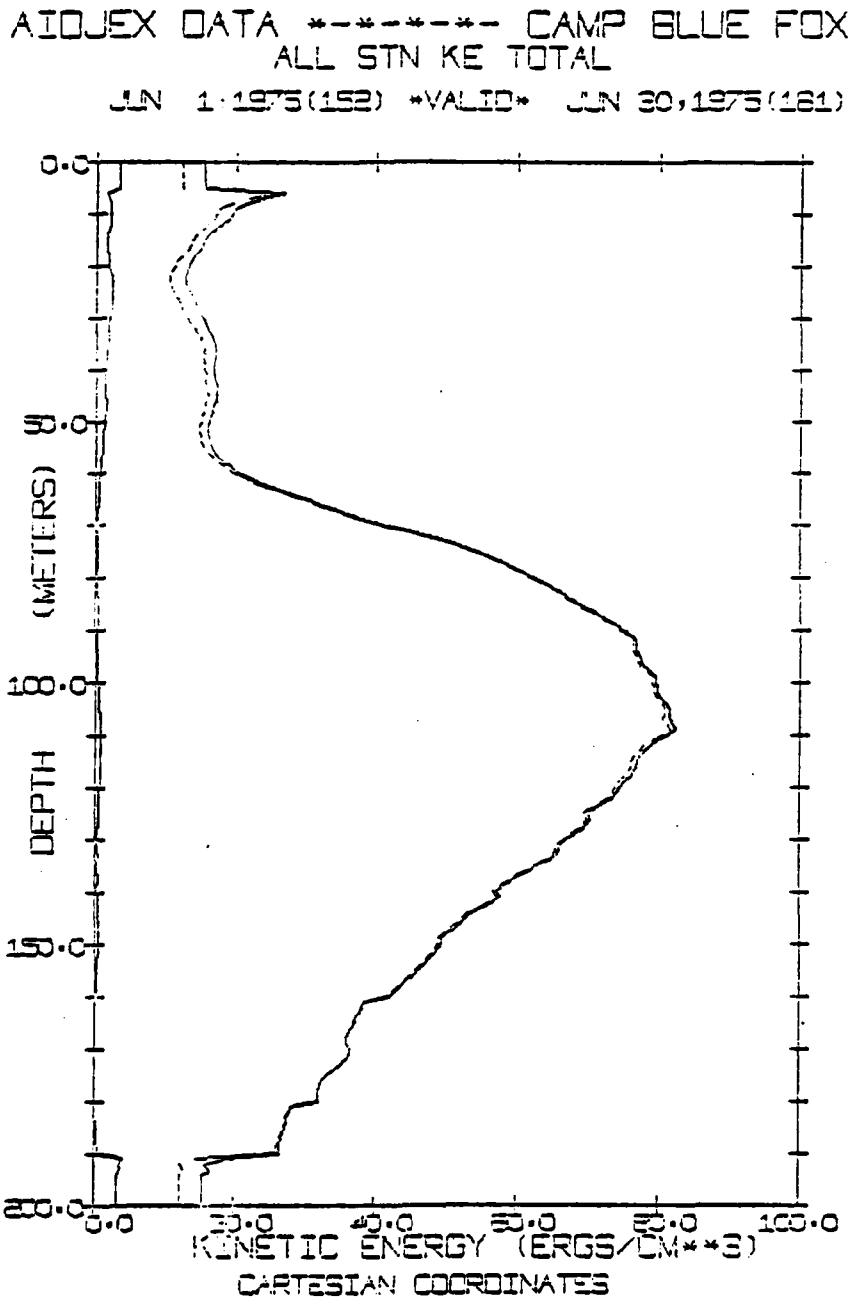

AIDJEX DATA *-*-*-*-*- CAMP CARIBOU
ALL STATE TOTAL
JAN 1,1975(??3) THRU JAN 31,1975 ???)
0.0
50.0
100.0
150.0
200.0
DEPTH (METERS) BY
0.0
20.0
40.0
60.0
80.0
100.0
KINETIC ENERGY (ERGS/CM**3)
CARTESIAN COORDINATES

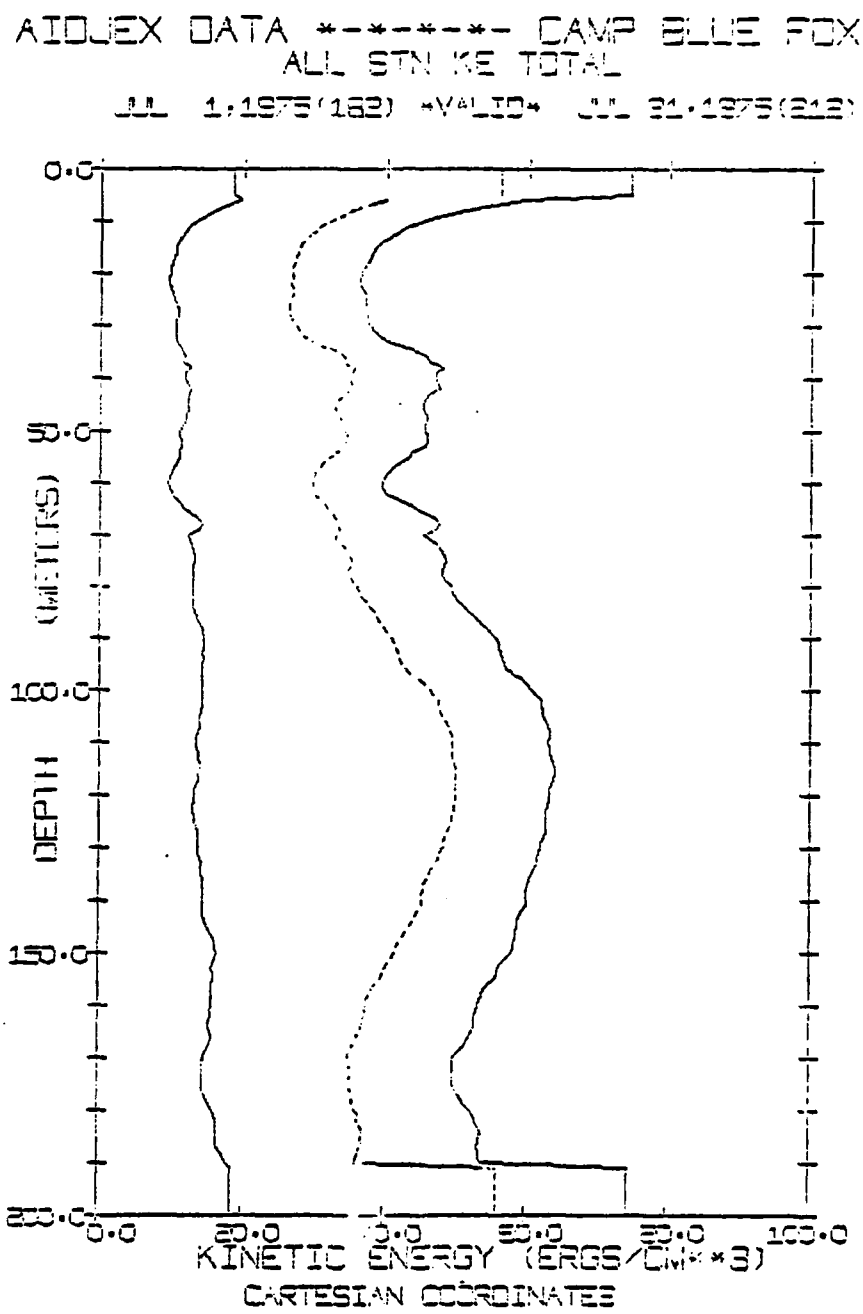

AIDJEX DATA *-*-*-*-*- CAMP CARIBOU
ALL STN KE TOTAL
FEB 1,1976(337) -VALID- FEB 28,1976(425)
0.0
50.0
100.0
150.0
200.0
DEPTH (METERS)
0.0
20.0
40.0
60.0
80.0
100.0
KINETIC ENERGY (ERGS/CM**3)
CARTESIAN COORDINATES

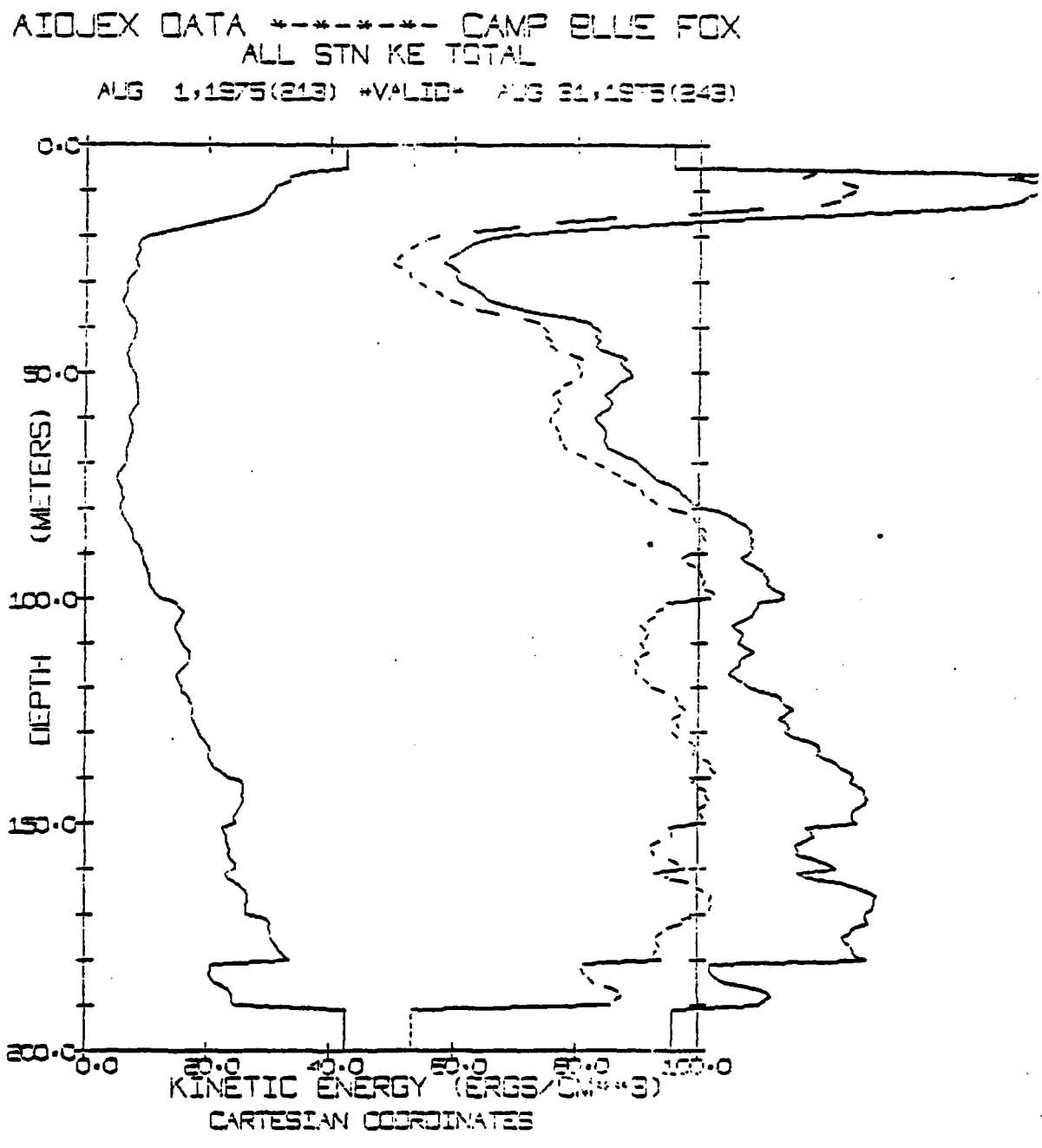

AIDJEX DATA *-*-*-*-*- CAMP CARIBOU
ALL STN KE TOTAL
MAR 1,1975(425) *VALID* MAR 31,1975(455)
0.0
50.0
100.0
150.0
200.0
DEPTH (METERS)
0.0
20.0
40.0
60.0
80.0
100.0
KINETIC ENERGY (ERGS/CM**3)
CARTESIAN COORDINATES

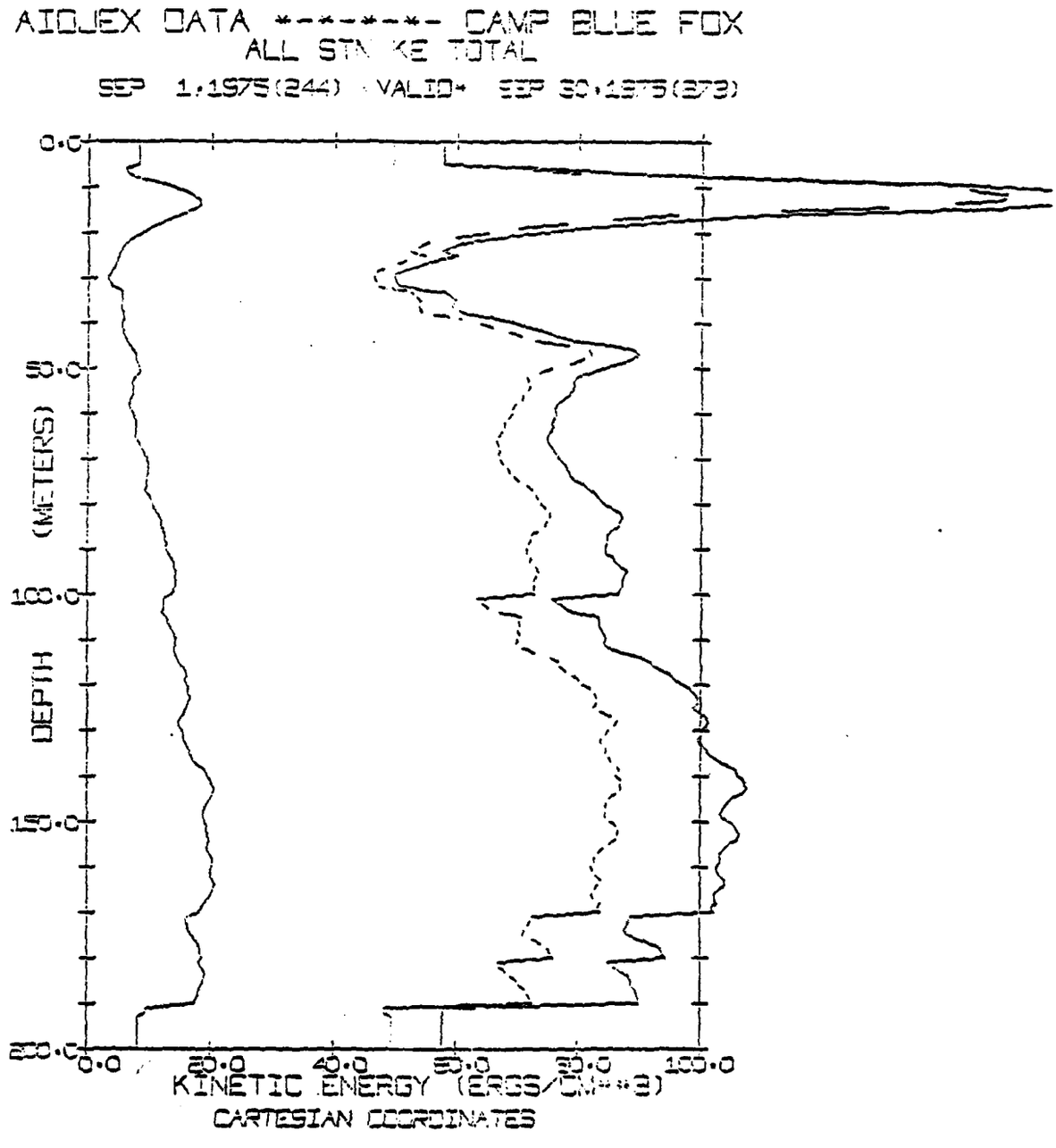

AIDJEX DATA *-*-*-*- CAMP CARIBOU
ALL STN KE TOTAL
APR 1.1975(457) *VALID* APR 30.1975(488)
0.0
8.0
18.0
15.0
20.0
DEPTH (METERS) B
0.0
20.0
40.0
60.0
80.0
100.0
KINETIC ENERGY (ERGS/CM**3)
CARTESIAN COORDINATES

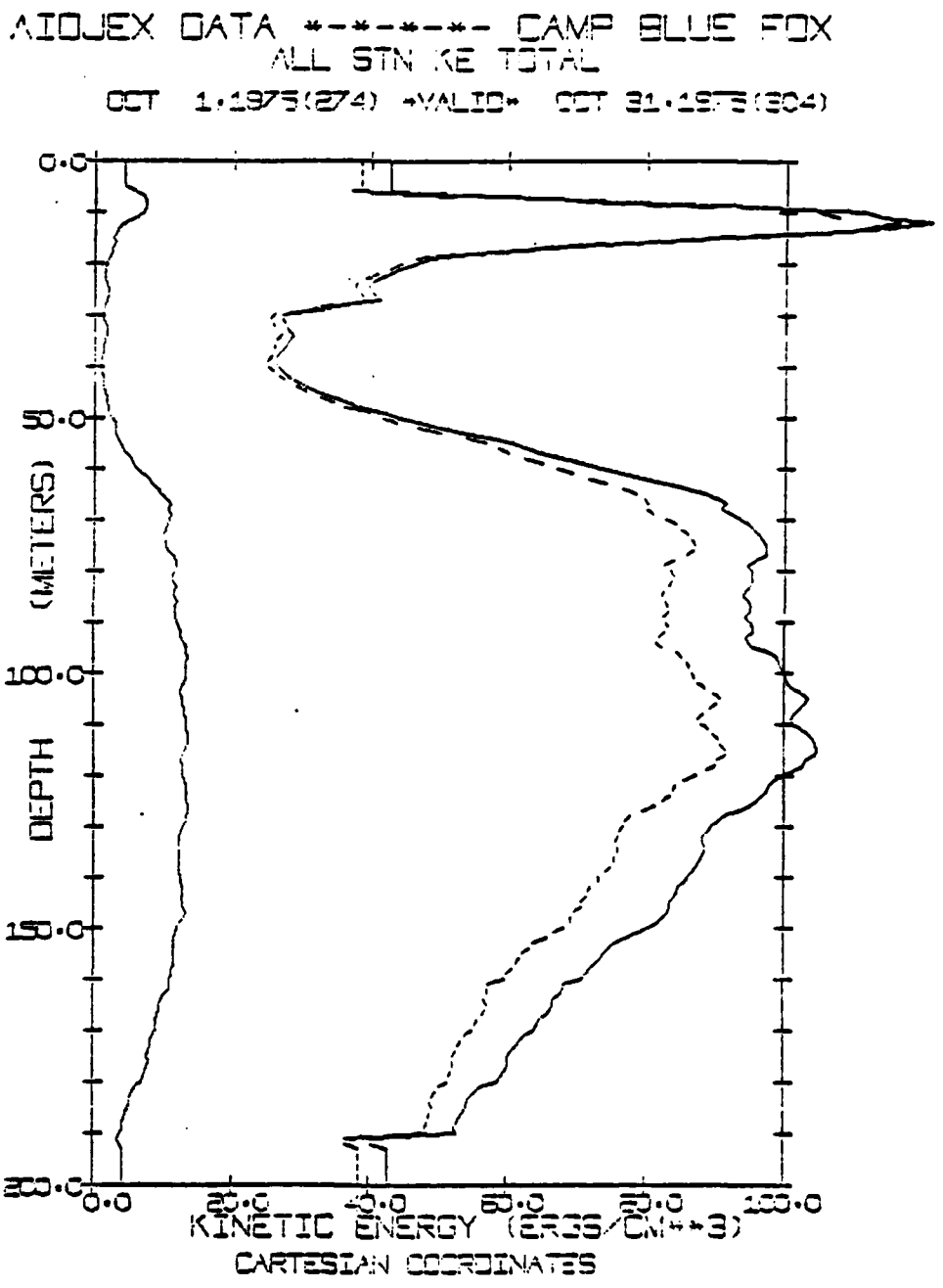

AIDJEX DATA *-*-*-*- CAMP BLUE FOX
ALL STN KE TOTAL
MAY 1,1975(121) *VALID* MAY 31,1975(151)
0.0
80.0
100.0
DEPTH (METERS)
KINETIC ENERGY (ERGS/CM**3)
CARTESIAN COORDINATES

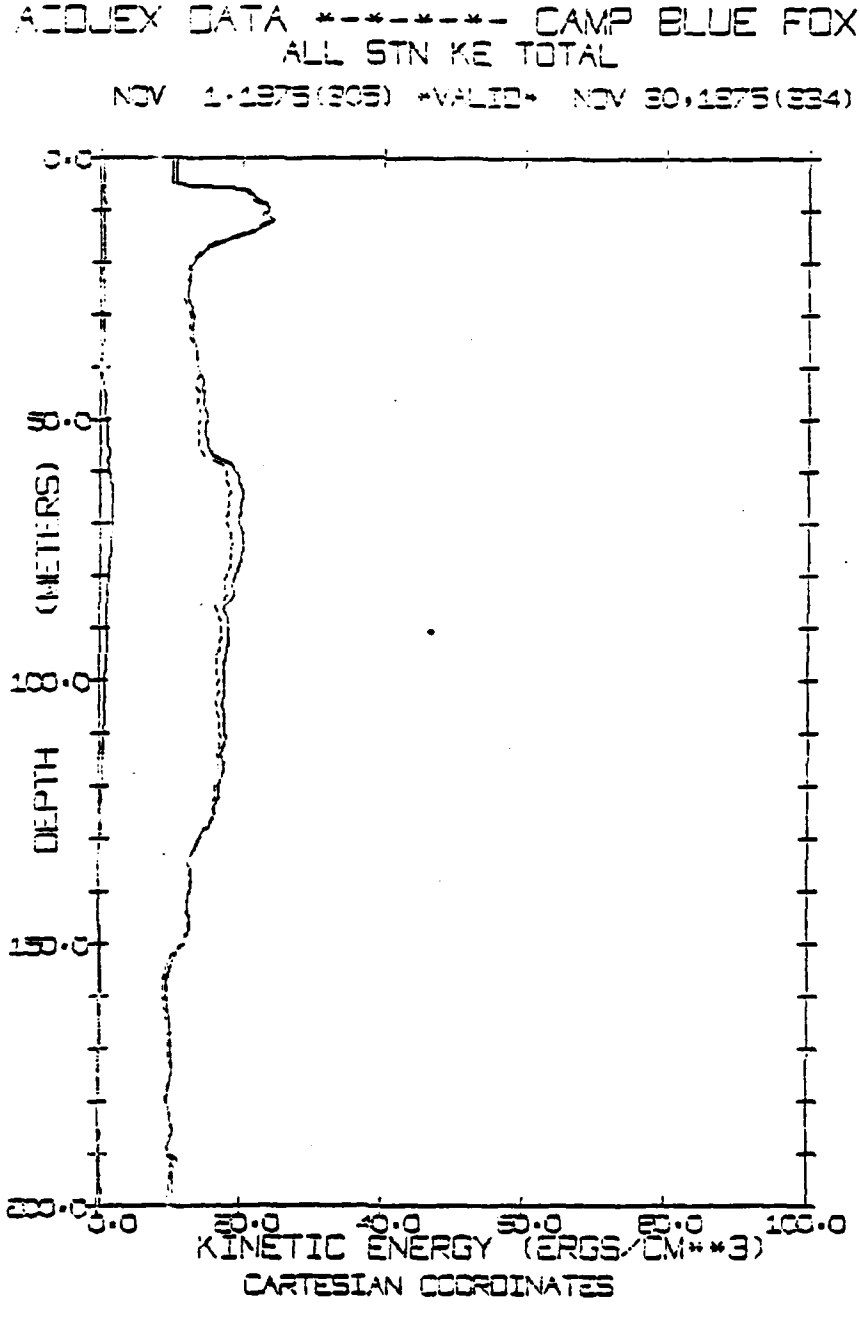

AIDJEX DATA *-*-*-*-*- CAMP BLUE FOX
ALL STN KE TOTAL
JUN 1,1975(152) *VALID* JUN 30,1975(181)
0.0
50.0
100.0
150.0
200.0
DEPTH (METERS)
0.0
20.0
40.0
60.0
80.0
100.0
KINETIC ENERGY (ERGS/CM**3)
CARTESIAN COORDINATES

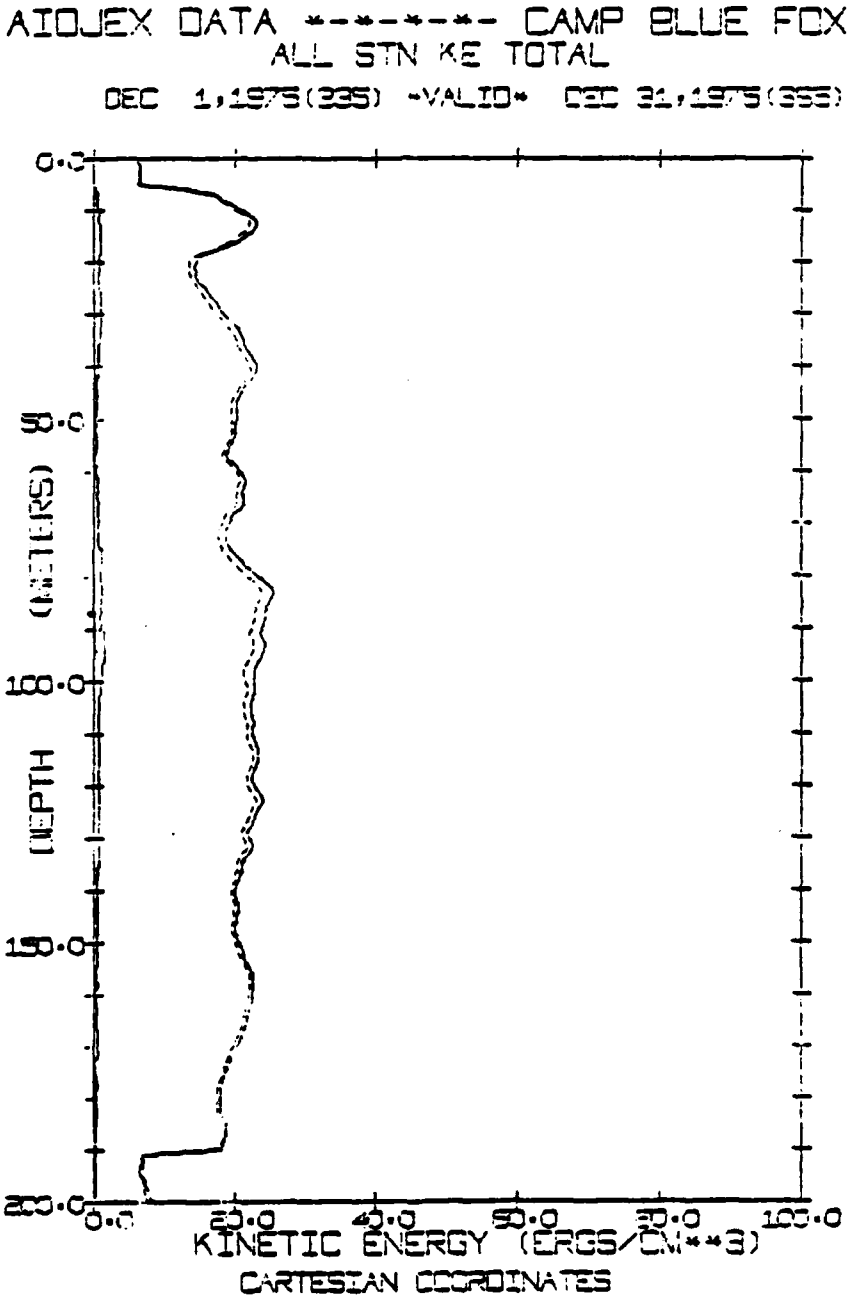

AIDJEX DATA *-*-*-*-*- CAMP BLUE FOX
ALL STN KE TOTAL
JUL 1,1975(182) *VALID* JUL 31,1975(212)
0.0
50.0
100.0
150.0
200.0
DEPTH (METERS)
0.0
20.0
40.0
60.0
80.0
100.0
KINETIC ENERGY (ERGS/CM**3)
CARTESIAN COORDINATES

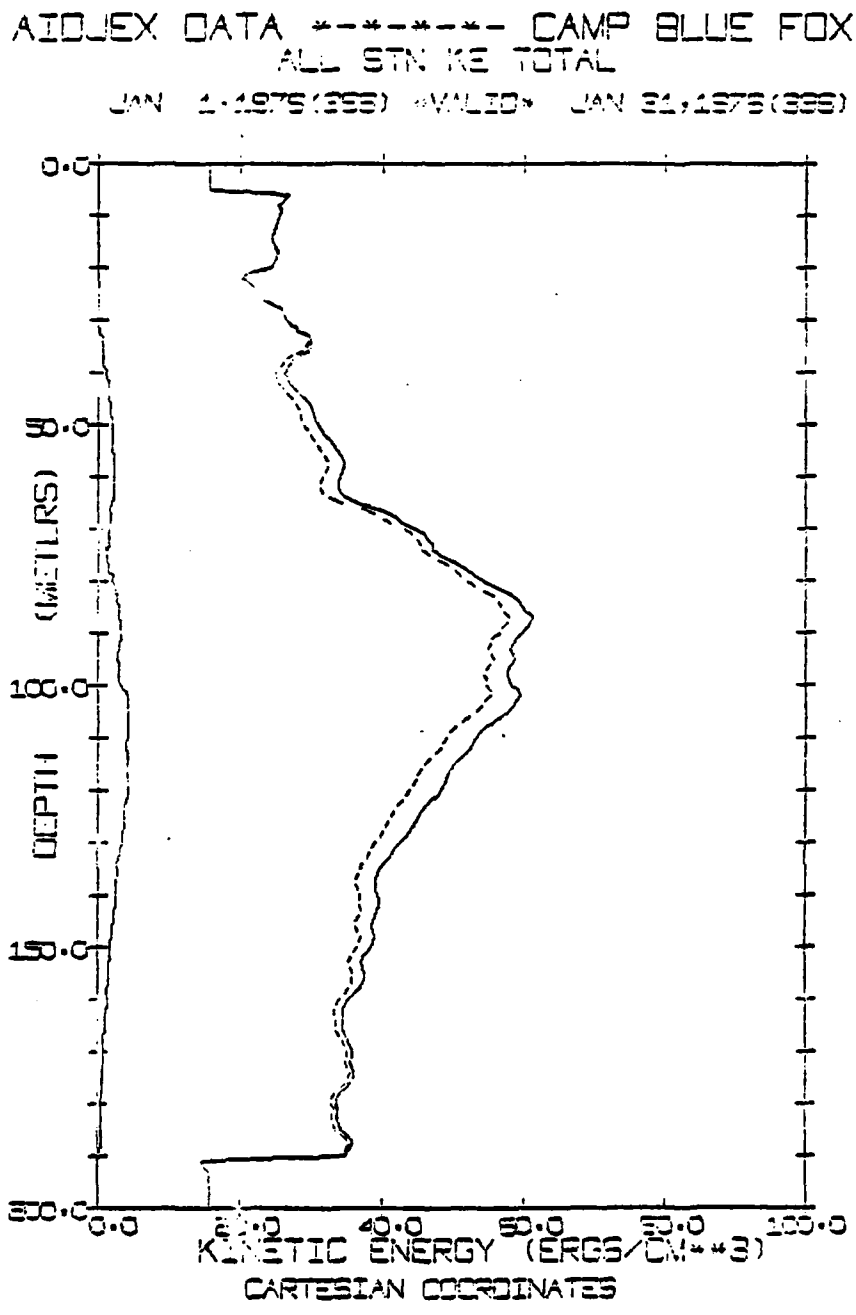

AIDJEX DATA *-*-*-*-*- CAMP BLUE FOX
ALL STN KE TOTAL
AUG 1,1975(213) *VALID* AUG 31,1975(243)
0.0
40.0
80.0
120.0
160.0
200.0
DEPTH (METERS)
0.0
20.0
40.0
60.0
80.0
100.0
KINETIC ENERGY (ERGS/CM**3)
CARTESIAN COORDINATES

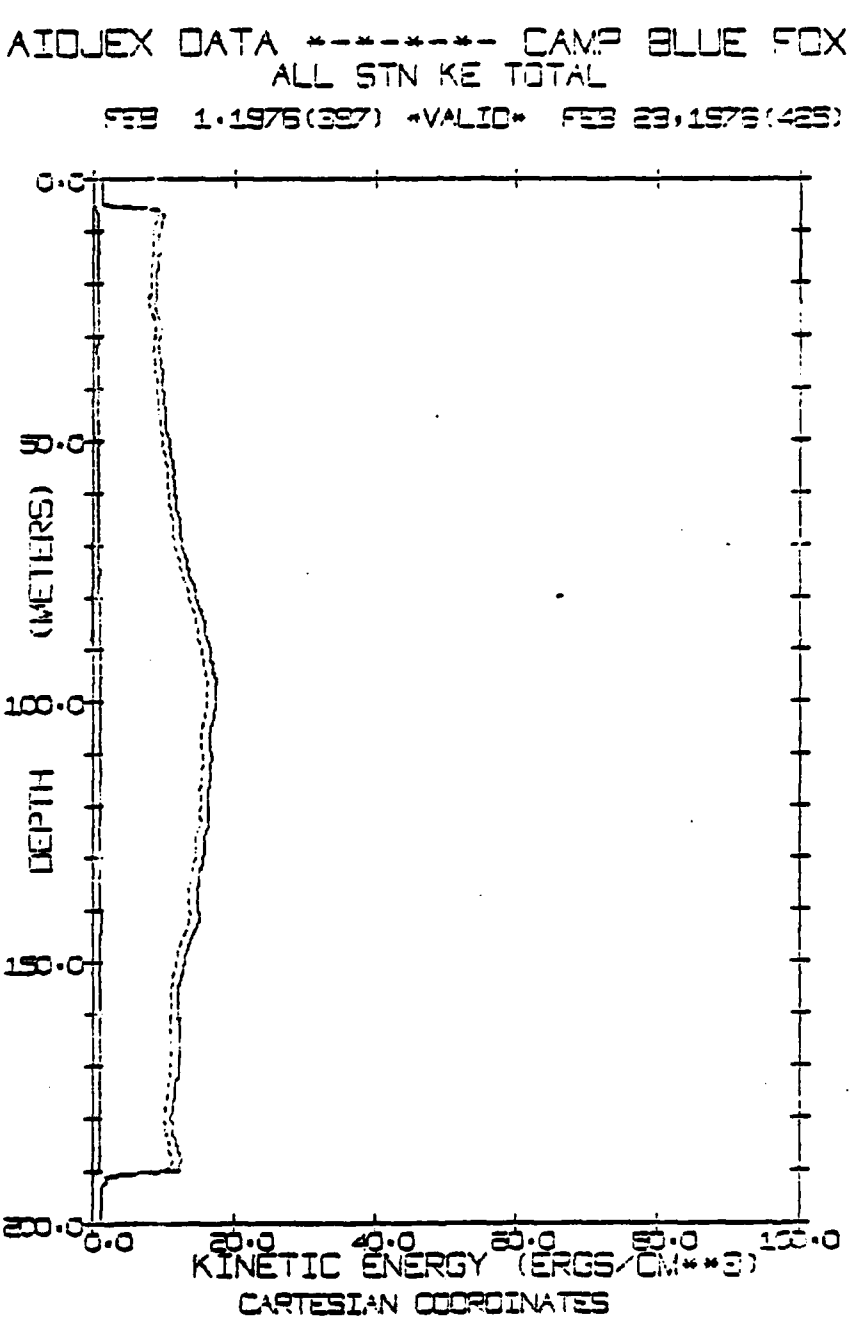

AIDJEX DATA *-*-*-*-*- CAMP BLUE FOX
ALL STN KE TOTAL
SEP 1,1975(244) VALID+ SEP 30,1975(273)
0.0
50.0
100.0
150.0
200.0
DEPTH (METERS)
0.0
20.0
40.0
60.0
80.0
100.0
KINETIC ENERGY (ERGS/CM**3)
CARTESIAN COORDINATES

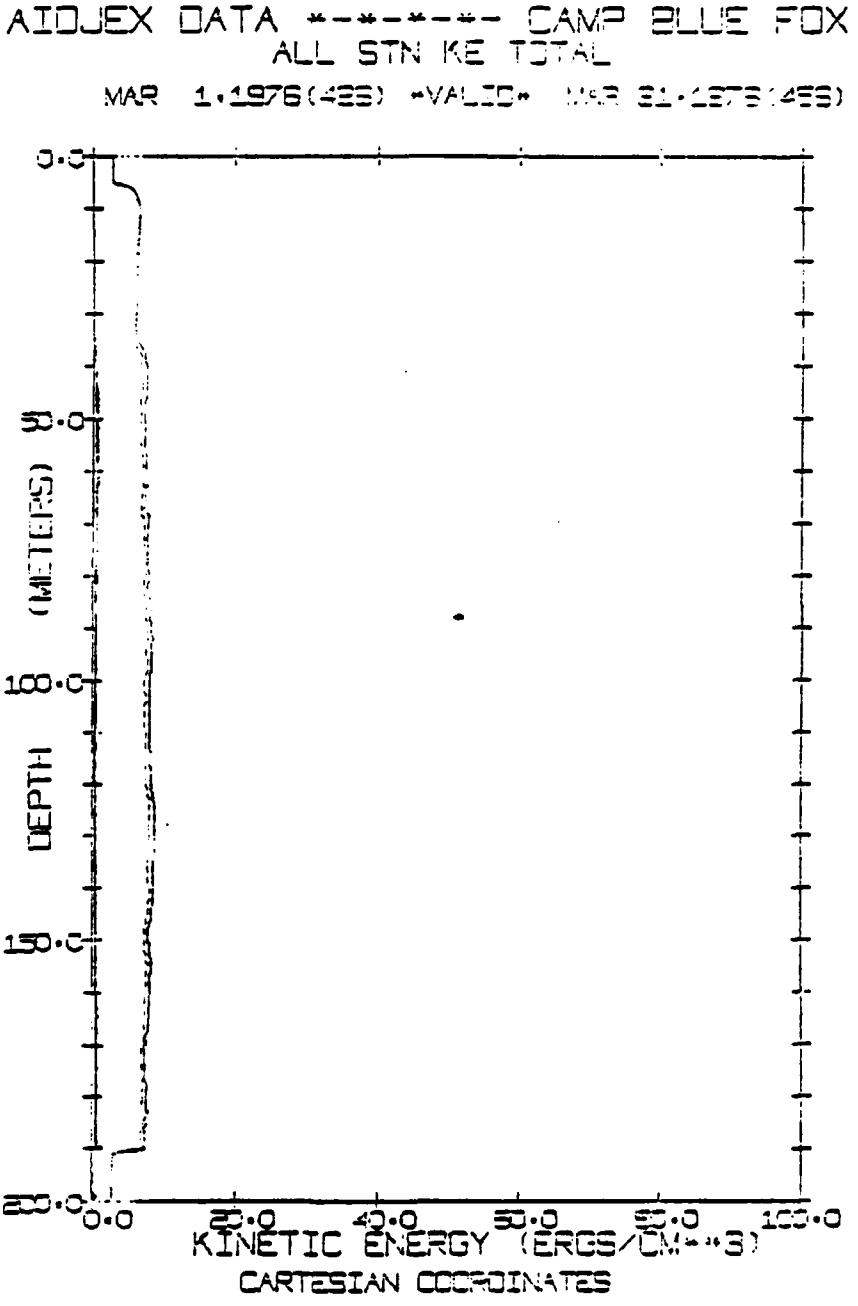

AIDJEX DATA *-*-*-*-*- CAMP BLUE FOX
ALL STN KE TOTAL
OCT 1,1975(274) *VALID* OCT 31,1975(304)
0.0
50.0
100.0
150.0
200.0
DEPTH (METERS)
0.0
20.0
40.0
60.0
80.0
100.0
KINETIC ENERGY (ERGS/CM**3)
CARTESIAN COORDINATES

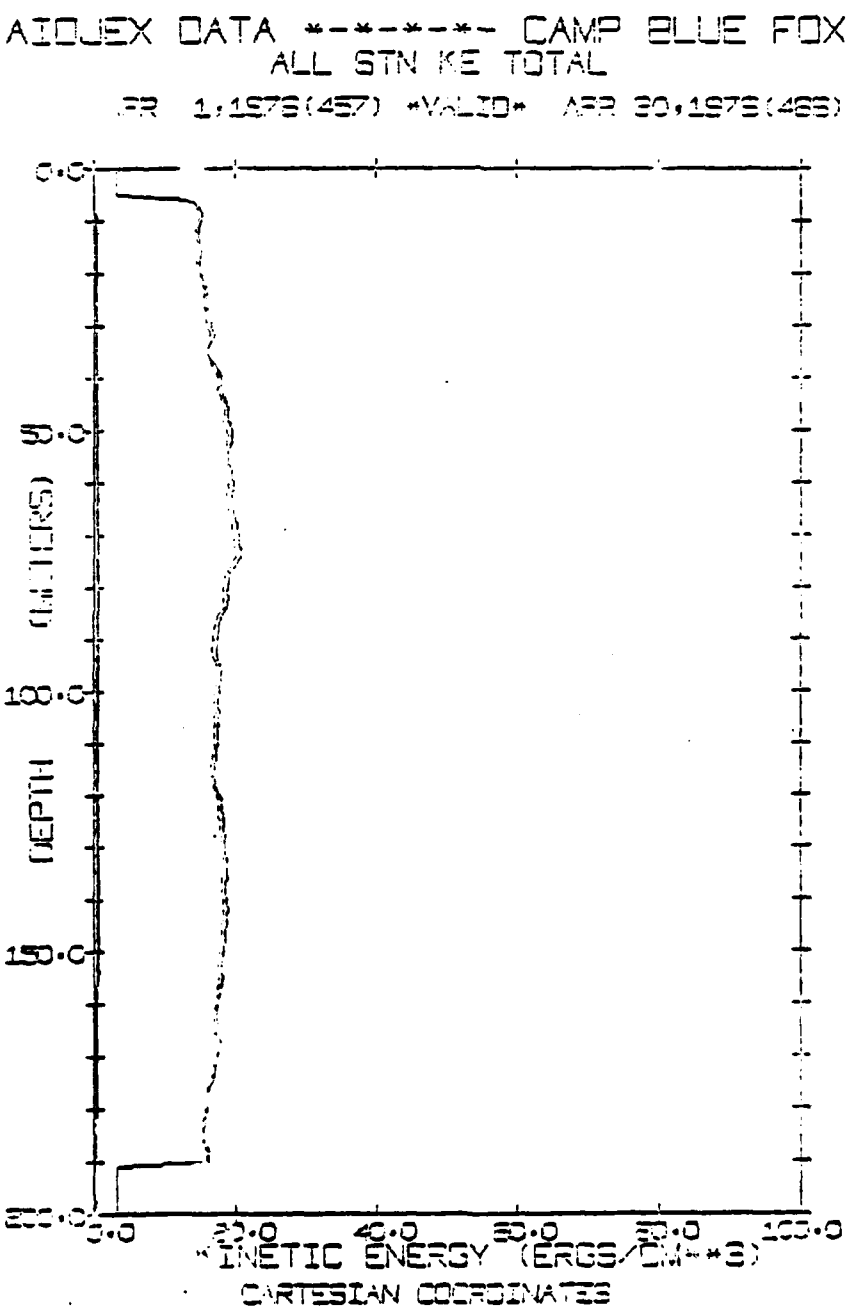

ACOJEX DATA *-*-*-*-*- CAMP BLUE FOX
ALL STN KE TOTAL
NOV 1,1975(305) *VALID* NOV 30,1975(334)
0.0
50.0
100.0
150.0
200.0
DEPTH (METERS)
0.0
20.0
40.0
60.0
80.0
100.0
KINETIC ENERGY (ERGS/CM**3)
CARTESIAN COORDINATES

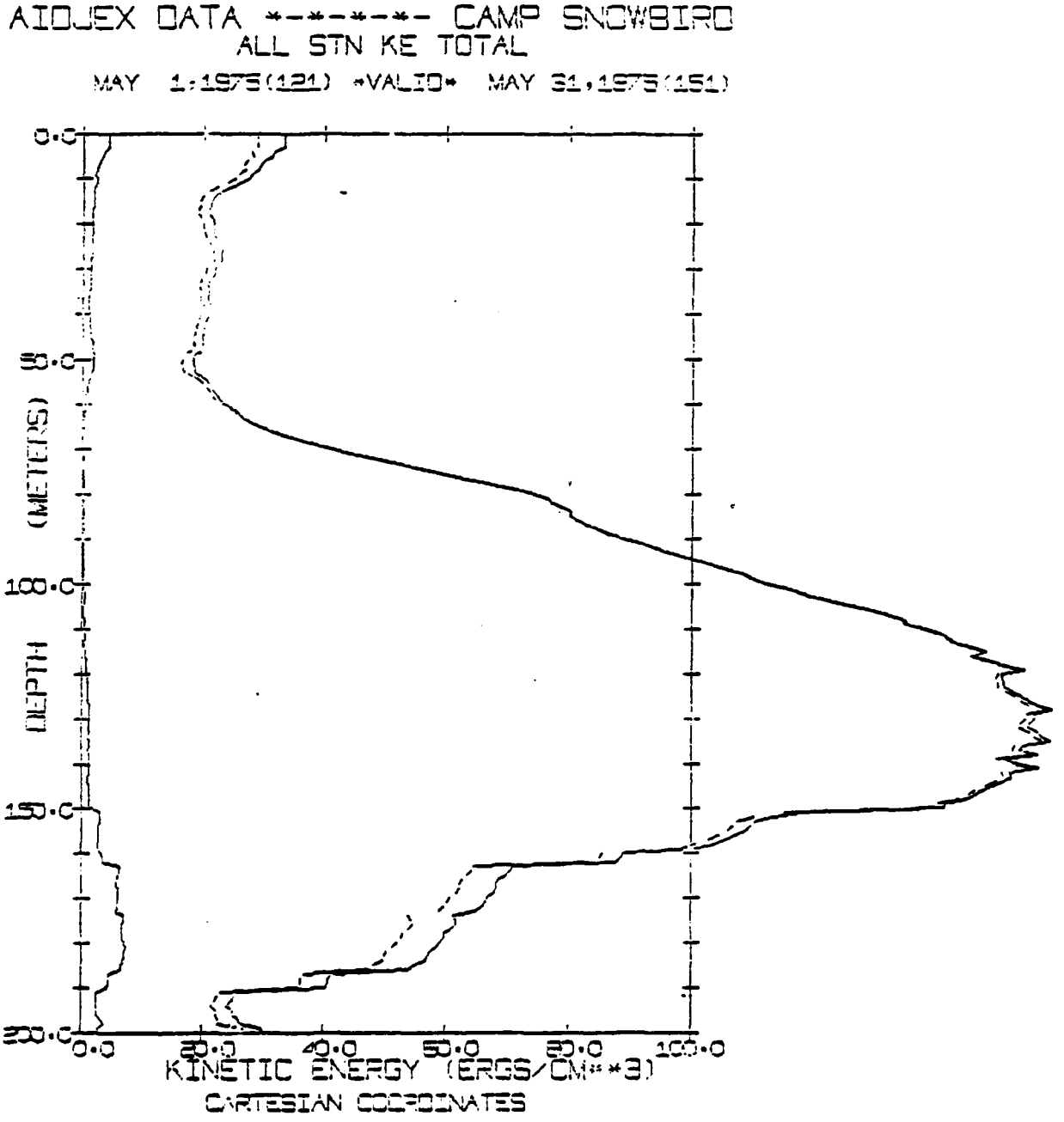

AIOJEX DATA *-*-*-*-*- CAMP BLUE FOX
ALL STN KE TOTAL
DEC 1,1975(335) -VALID- DEC 31,1975(365)
0.0
50.0
100.0
150.0
200.0
DEPTH (METERS)
0.0
20.0
40.0
60.0
80.0
100.0
KINETIC ENERGY (ERGS/CM**3)
CARTESIAN COORDINATES

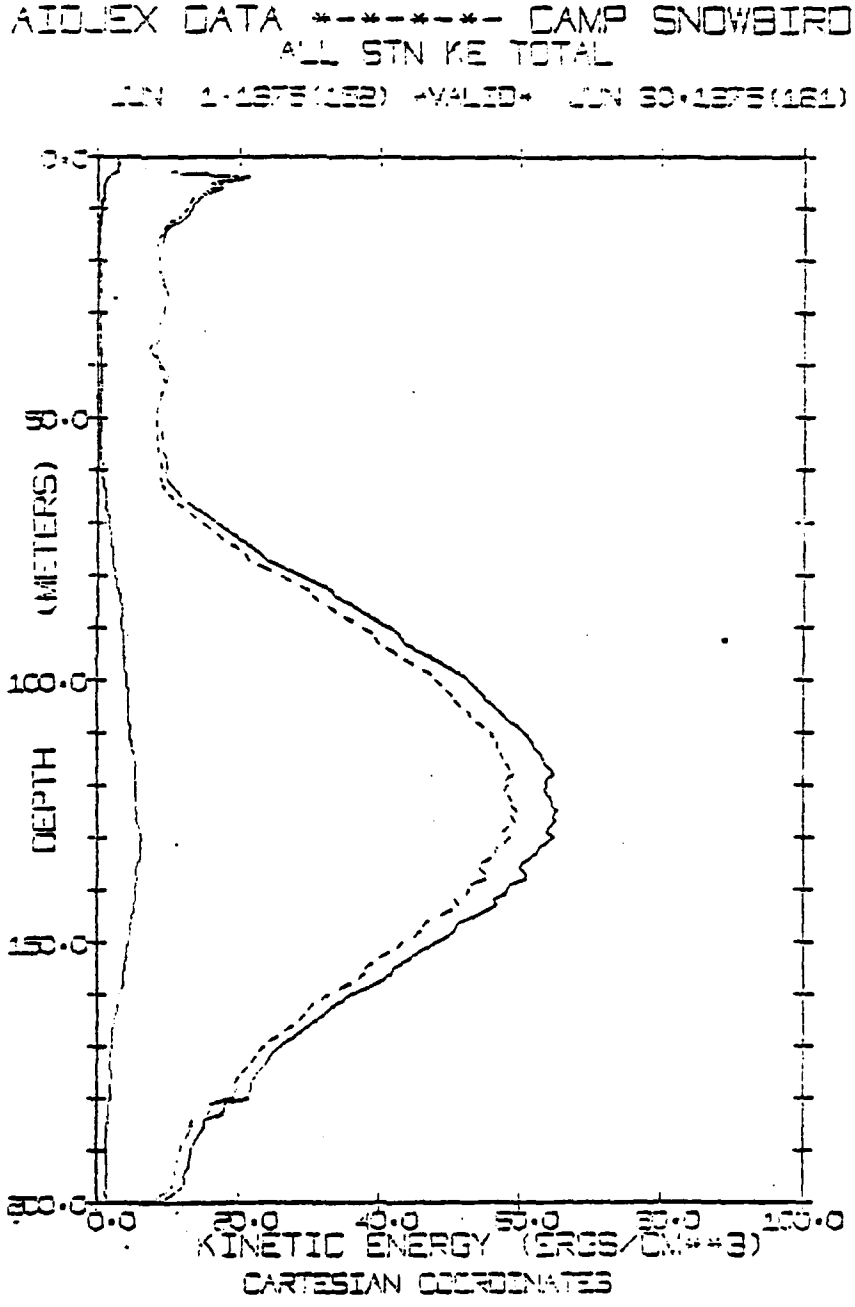

AIDJEX DATA *-*-*-*-*- CAMP BLUE FOX
ALL STN KE TOTAL
JAN 1,1975(365) *VALID* JAN 31,1975(365)
0.0
50.0
100.0
150.0
200.0
DEPTH (METERS)
0.0
20.0
40.0
60.0
80.0
100.0
KINETIC ENERGY (ERGS/CM**3)
CARTESIAN COORDINATES

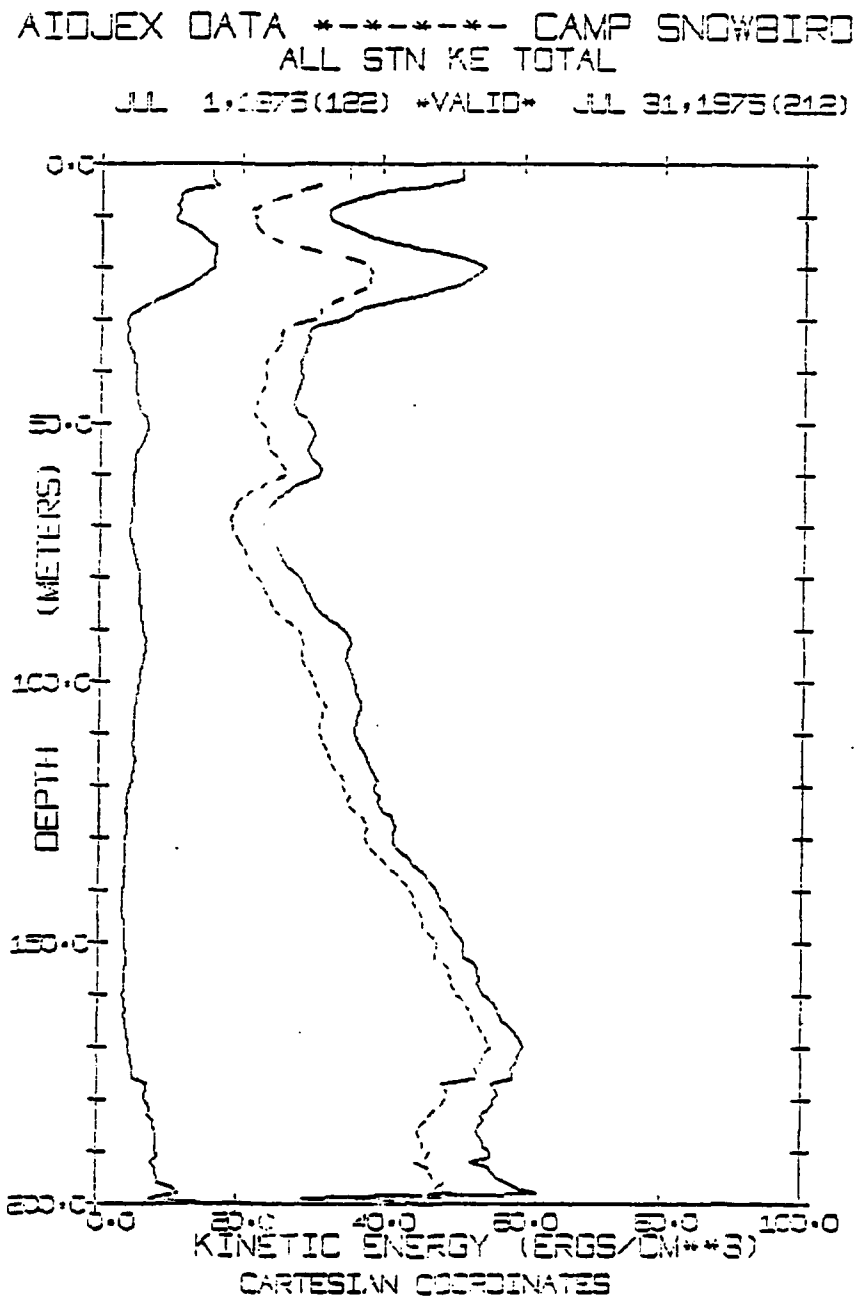

AIDJEX DATA *-*-*-*-*- CAMP BLUE FOX
ALL STN KE TOTAL
FEB 1,1976(397) *VALID* FEB 23,1976(425)
0.0
50.0
100.0
150.0
200.0
DEPTH (METERS)
0.0
20.0
40.0
60.0
80.0
100.0
KINETIC ENERGY (ERGS/CM**3)
CARTESIAN COORDINATES

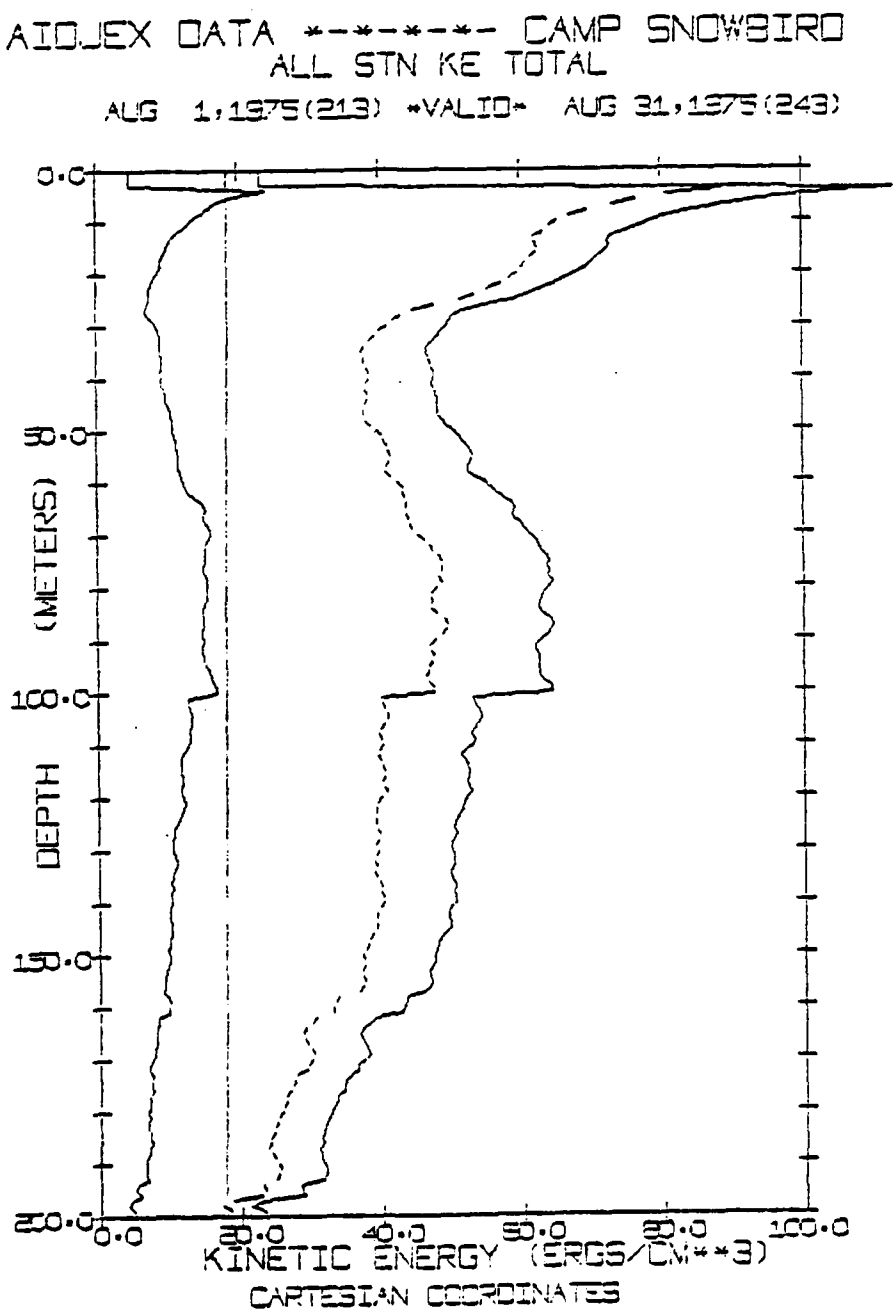

AIDJEX DATA *-*-*-*-*- CAMP BLUE FOX
ALL STN KE TOTAL
MAR 1,1976(433) *VALID* MAR 31,1976(459)
0.0
50.0
100.0
150.0
200.0
DEPTH (METERS) M
0.0
20.0
40.0
60.0
80.0
100.0
KINETIC ENERGY (ERGS/CM**3)
CARTESIAN COORDINATES

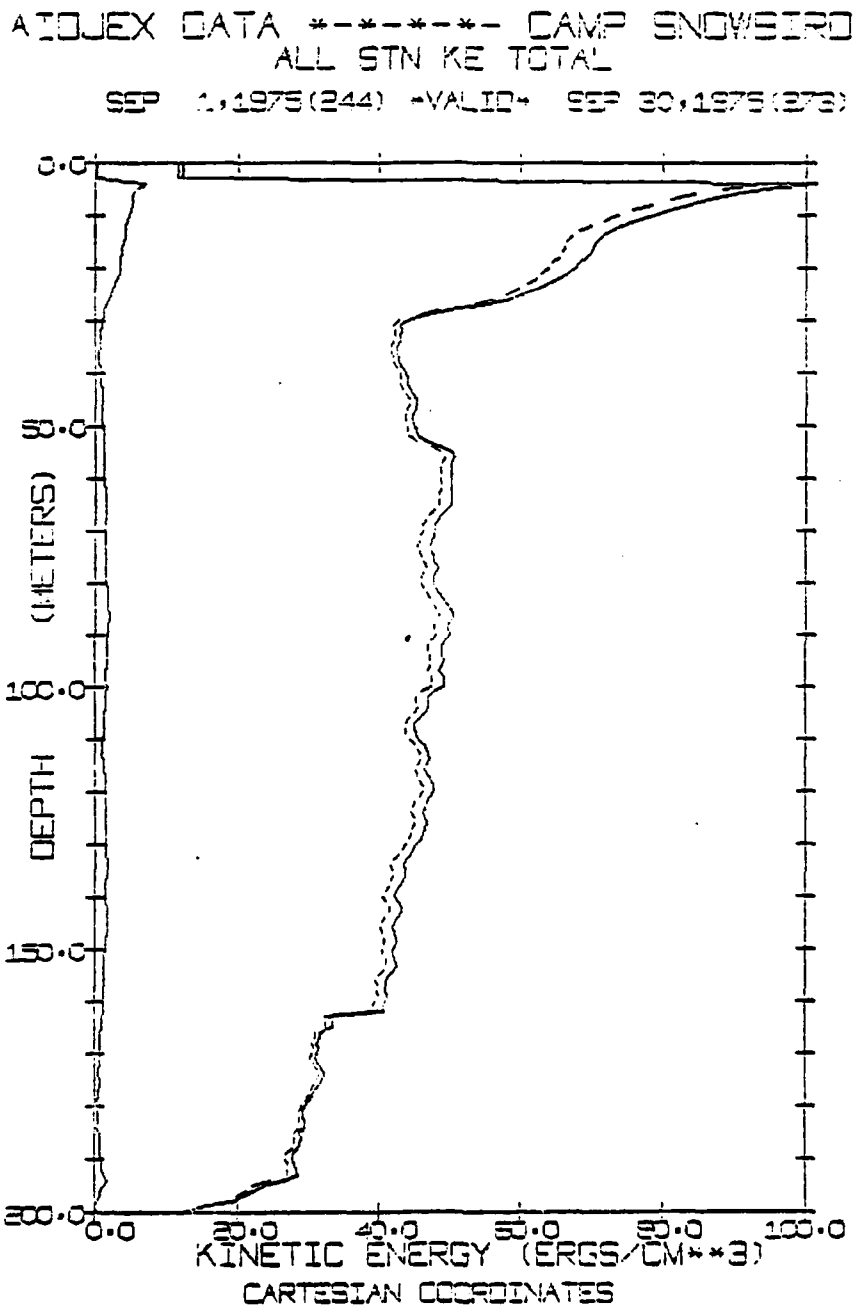

AIDJEX DATA *-*-*-*-*- CAMP BLUE FOX
ALL STN KE TOTAL
APR 1,1978(457) *VALID* APR 30,1978(486)
0.0
50.0
100.0
150.0
200.0
DEPTH (METERS)
0.0
20.0
40.0
60.0
80.0
100.0
KINETIC ENERGY (ERGS/CM**3)
CARTESIAN COORDINATES

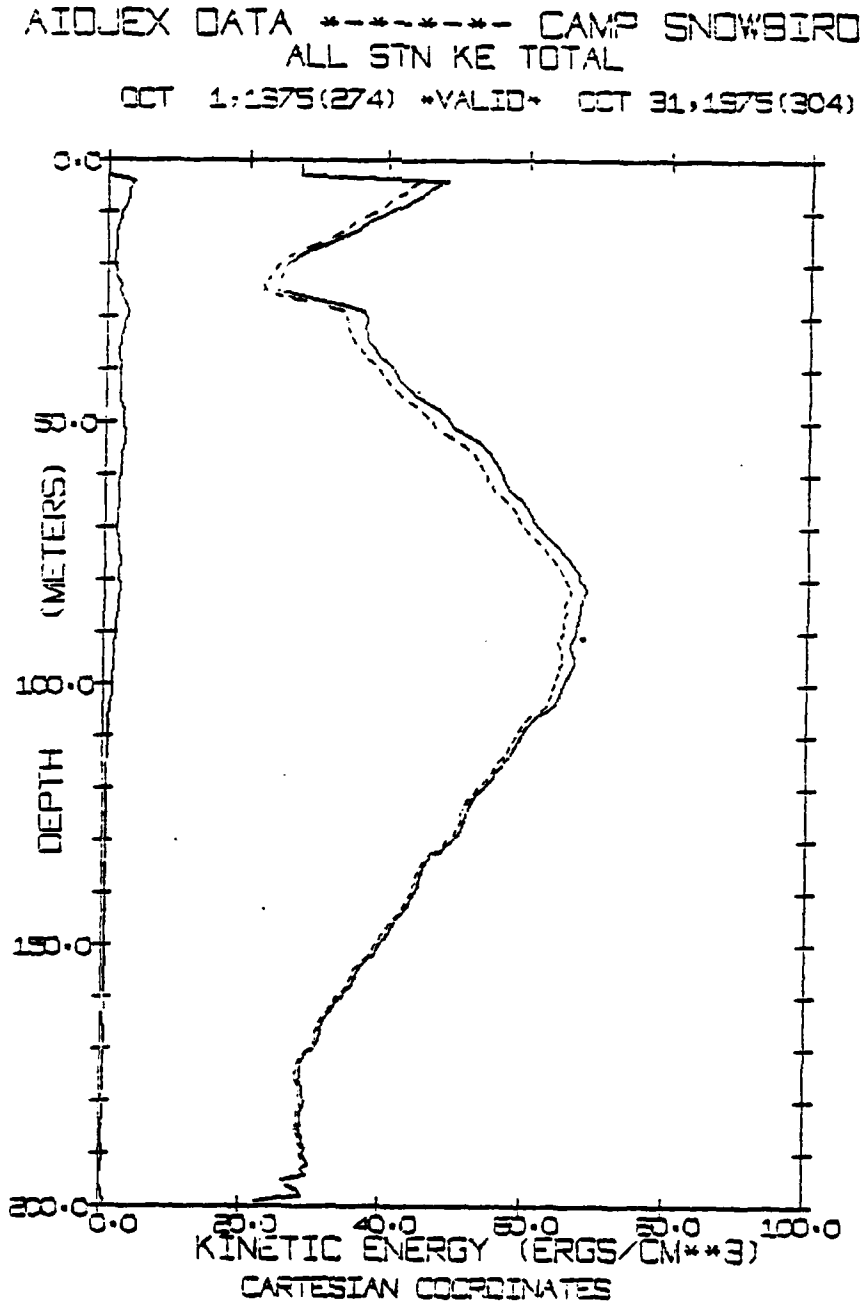

AIDJEX DATA *-*-*-*-*- CAMP SNOWBIRD
ALL STN KE TOTAL
MAY 1,1975(121) *VALID* MAY 31,1975(151)
0.0
50.0
100.0
150.0
200.0
DEPTH (METERS)
0.0
20.0
40.0
60.0
80.0
100.0
KINETIC ENERGY (ERGS/CM**3)
CARTESIAN COORDINATES

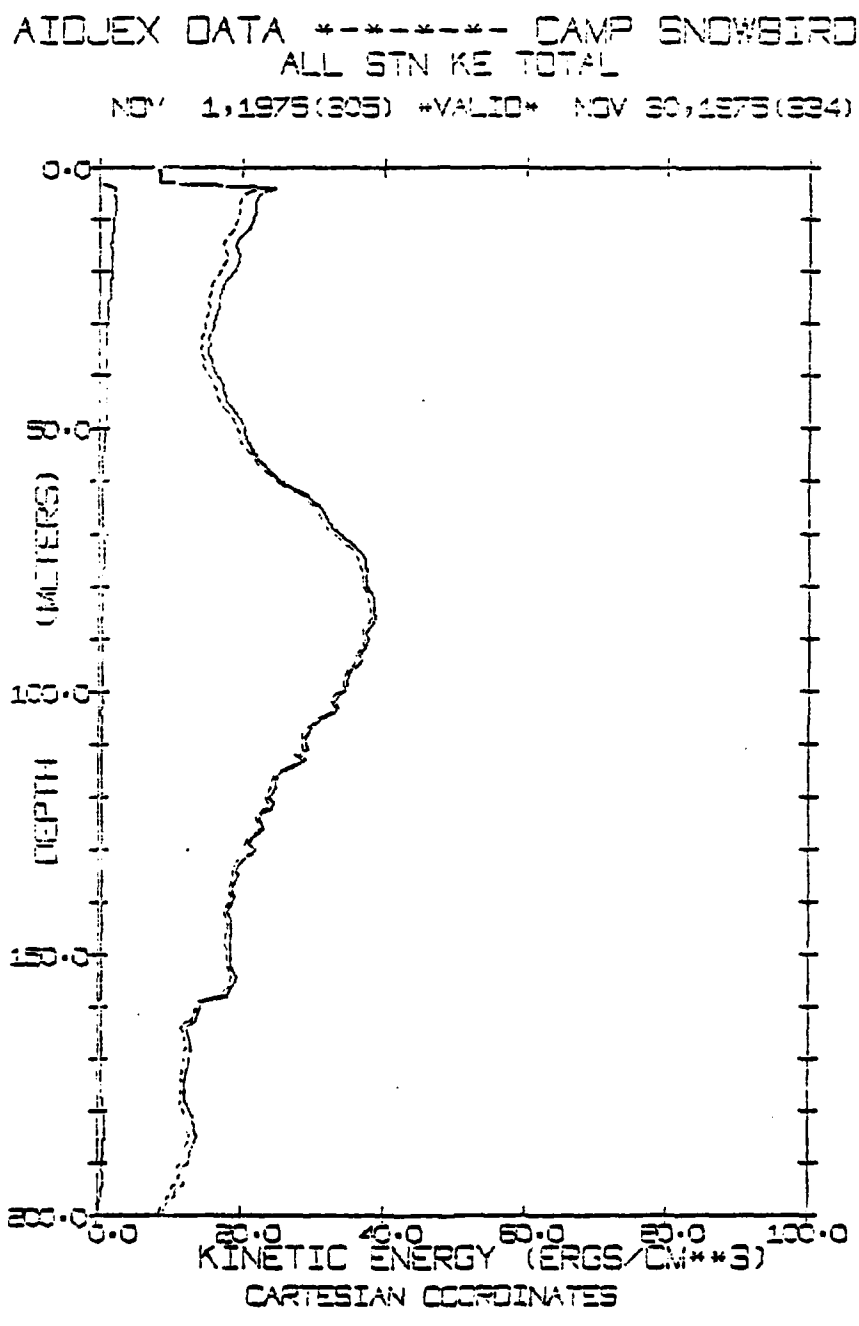

AIDJEX DATA *-*-*-*- CAMP SNOWBIRD
ALL STN KE TOTAL
JDN 1-1975(132) -VALID- JDN 30-1975(161)
0.0
50.0
100.0
150.0
200.0
DEPTH (METERS)
0.0
20.0
40.0
60.0
80.0
100.0
KINETIC ENERGY (ERGS/CM**3)
CARTESIAN COORDINATES

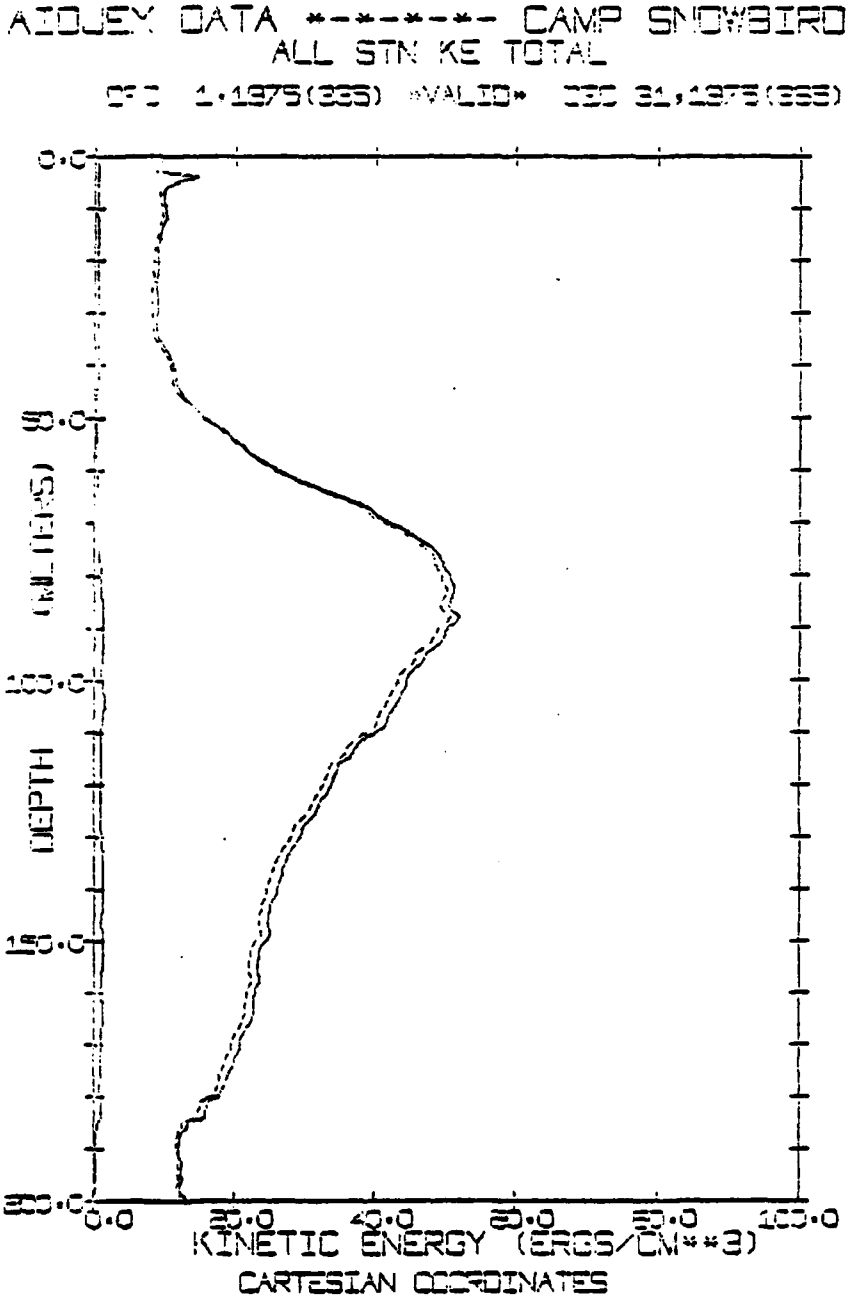

AIDJEX DATA *-*-*-*- CAMP SNOWBIRD
ALL STN KE TOTAL
JUL 1,1975(122) *VALID* JUL 31,1975(212)
0.0
50.0
100.0
150.0
200.0
DEPTH (METERS) W
0.0
20.0
40.0
60.0
80.0
100.0
KINETIC ENERGY (ERGS/CM**3)
CARTESIAN COORDINATES

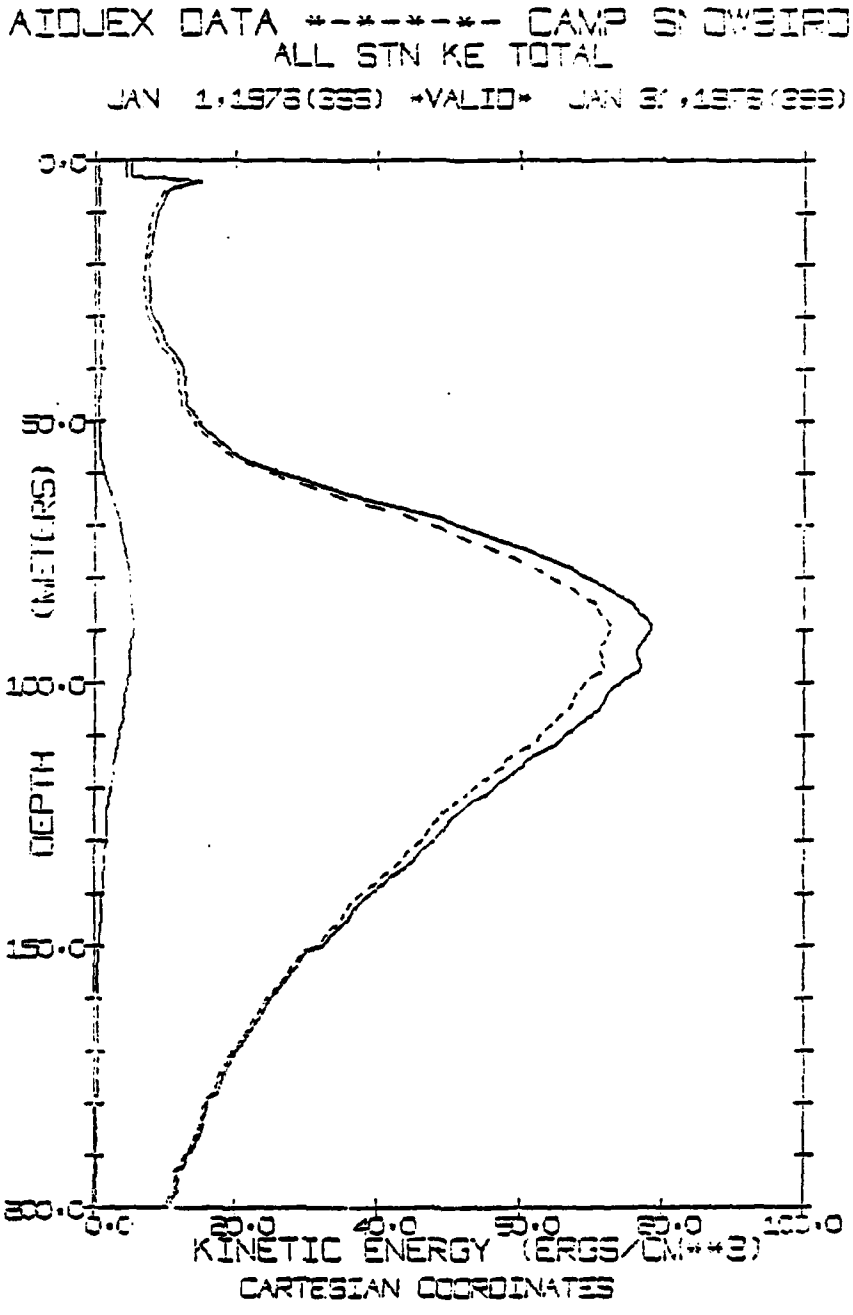

AIDJEX DATA *-*-*-*-*- CAMP SNOWBIRD
ALL STN KE TOTAL
AUG 1,1975(213) *VALID* AUG 31,1975(243)
0.0
50.0
100.0
150.0
200.0
DEPTH (METERS) M
0.0
20.0
40.0
60.0
80.0
100.0
KINETIC ENERGY (ERGS/CM**3)
CARTESIAN COORDINATES

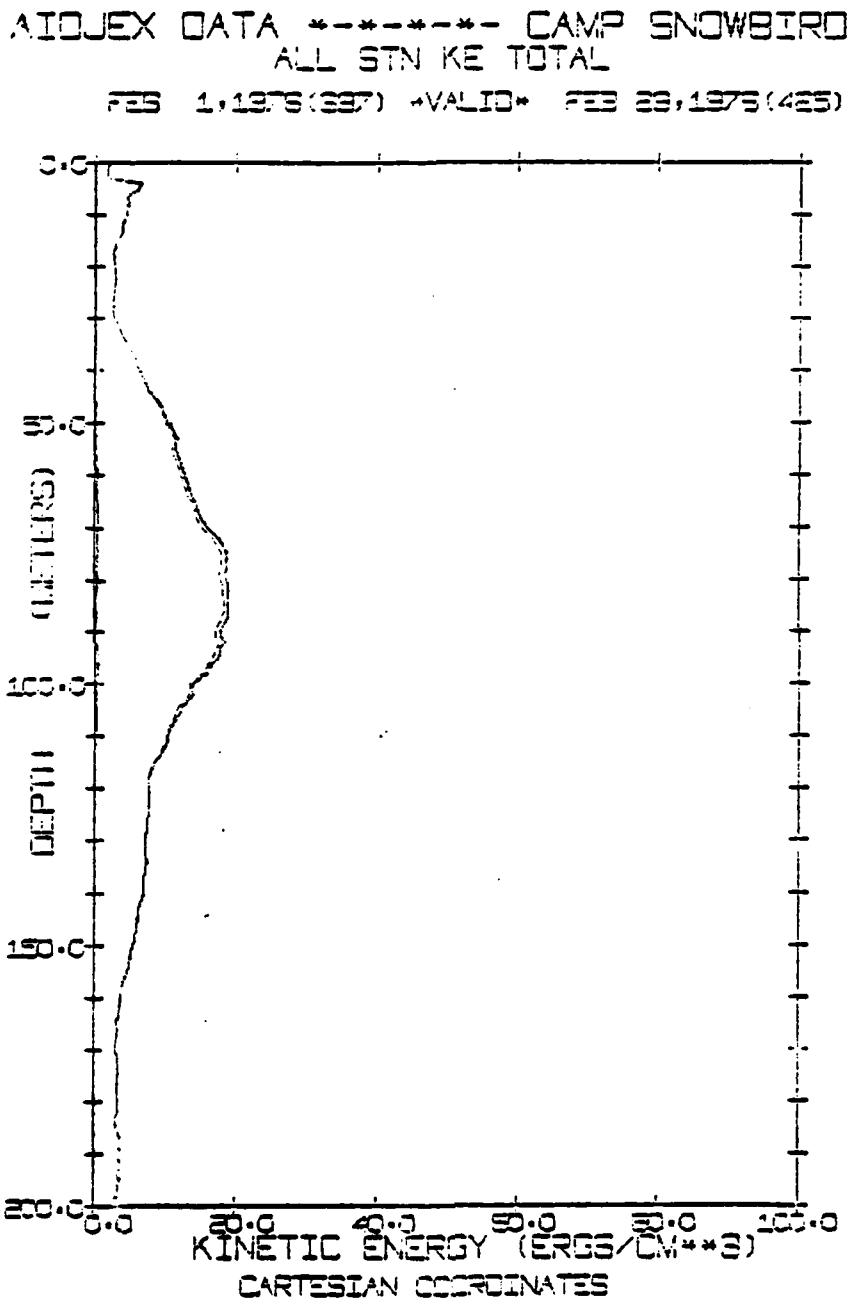

AIDJEX DATA *-*-*-*- CAMP SNOWBIRD
ALL STN KE TOTAL
SEP 1,1975(244) -VALID- SEP 30,1975(273)
0.0
50.0
100.0
150.0
200.0
DEPTH (METERS)
0.0
20.0
40.0
60.0
80.0
100.0
KINETIC ENERGY (ERGS/CM**3)
CARTESIAN COORDINATES

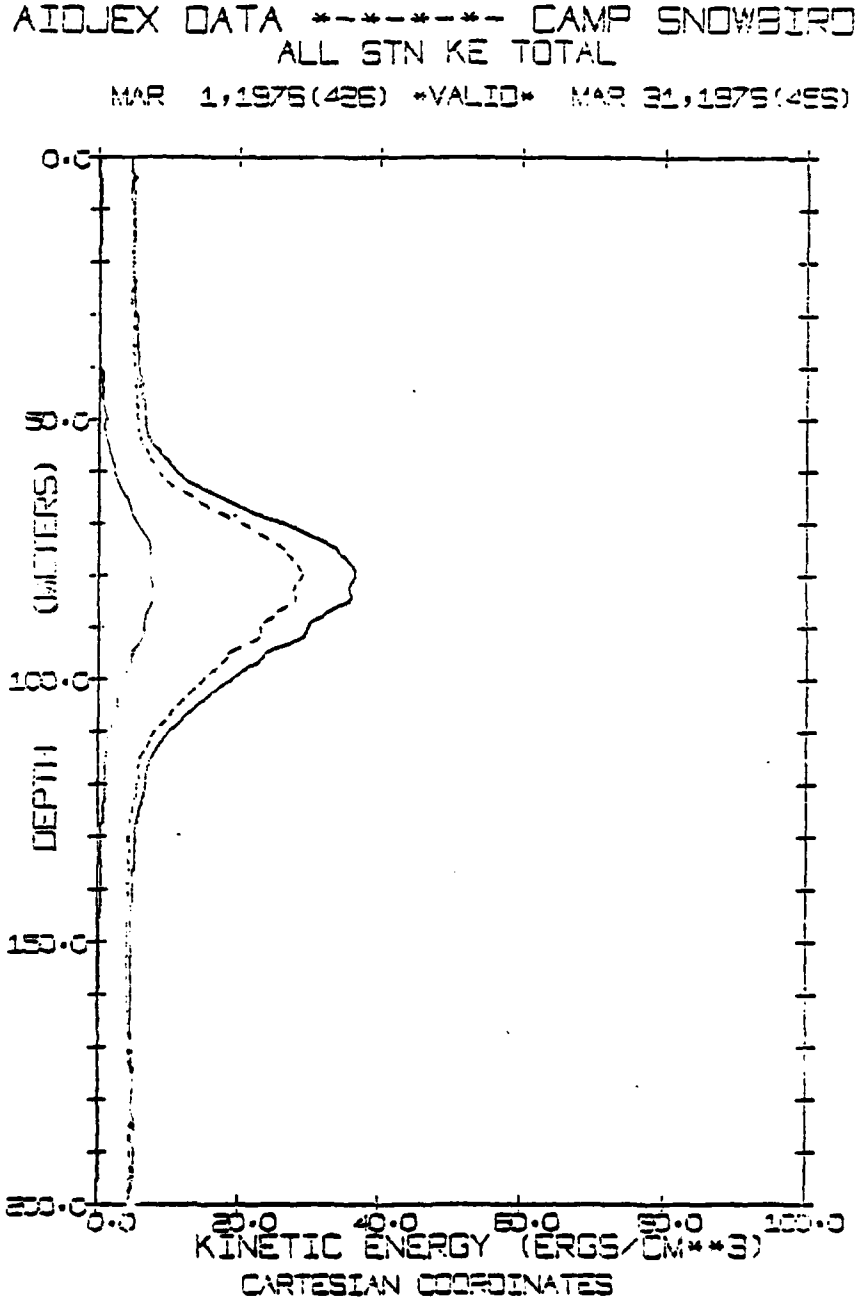

AIDJEX DATA *-*-*-*-*- CAMP SNOWBIRD
ALL STN KE TOTAL
OCT 1,1975(274) *VALID* OCT 31,1975(304)
0.0
50.0
100.0
150.0
200.0
DEPTH (METERS)
0.0
20.0
40.0
60.0
80.0
100.0
KINETIC ENERGY (ERGS/CM**3)
CARTESIAN COORDINATES

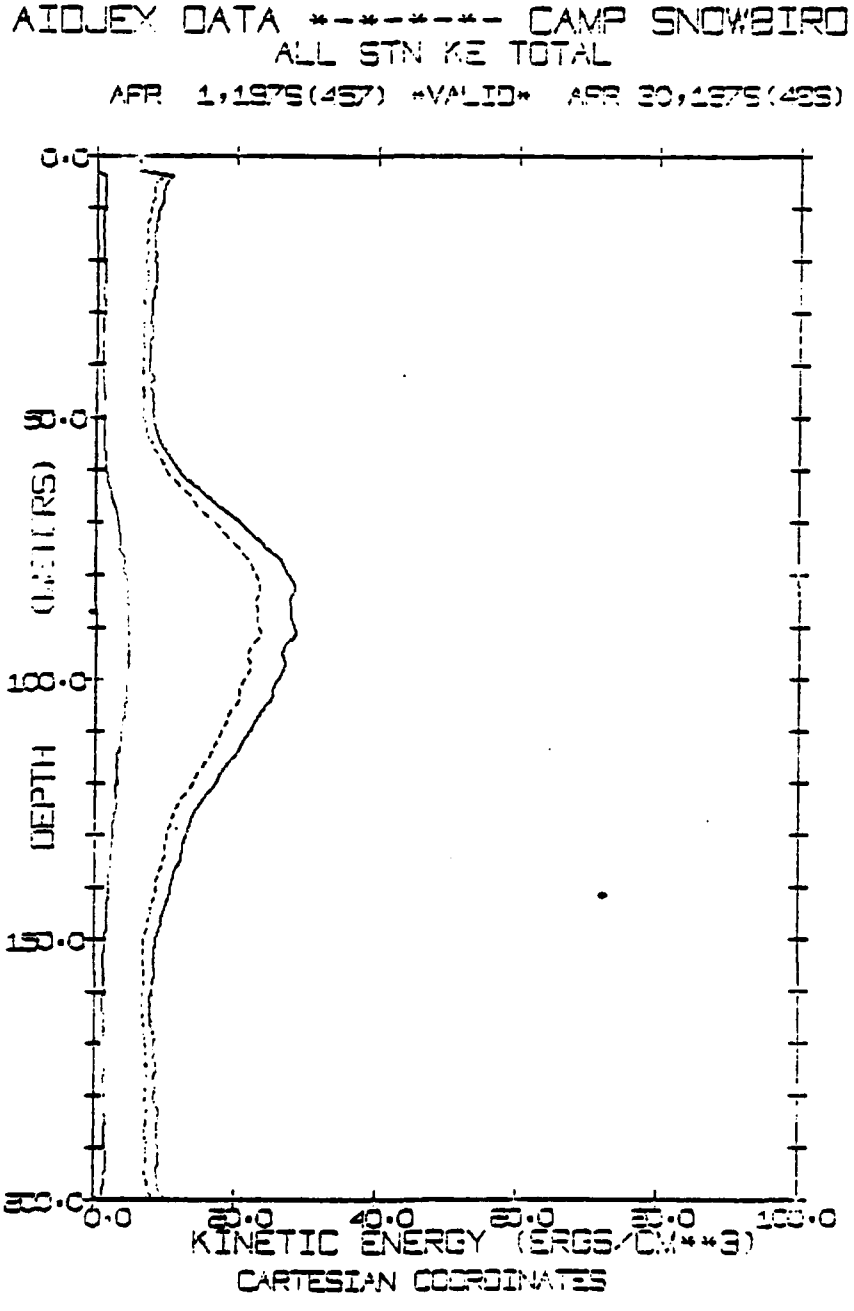

AIDJEX DATA *-*-*-*- CAMP SNOWBIRD
ALL STN KE TOTAL
NOV 1,1975(305) *VALID* NOV 30,1975(334)
0.0
50.0
100.0
150.0
200.0
DEPTH (METERS)
0.0
20.0
40.0
60.0
80.0
100.0
KINETIC ENERGY (ERGS/CM**3)
CARTESIAN COORDINATES

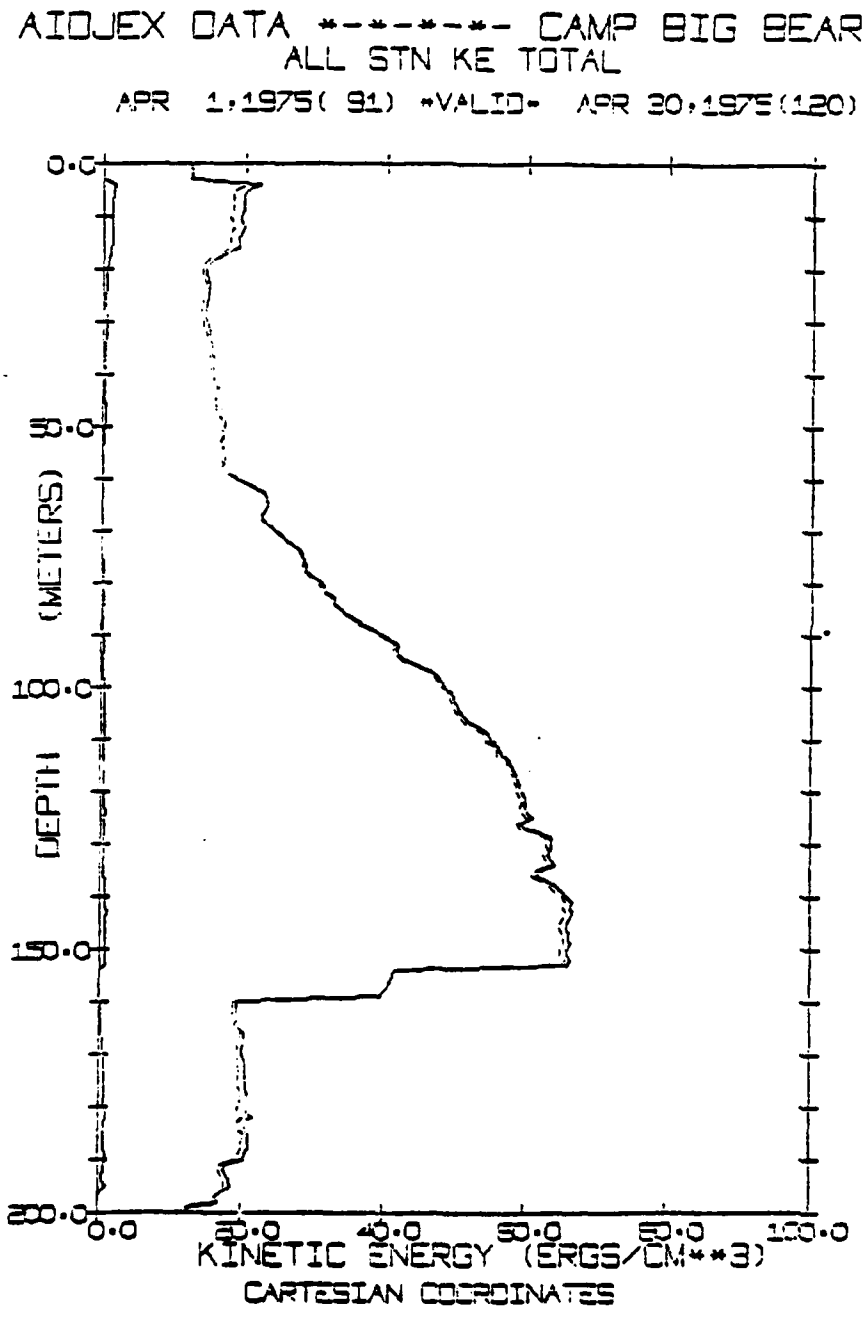

AIDJEX DATA *-*-*-*-*- CAMP SNOWBIRD
ALL STN KE TOTAL
DEC 1,1975(365) *VALID* DEC 31,1975(365)
0.0
50.0
100.0
150.0
200.0
DEPTH (METERS)
0.0
20.0
40.0
60.0
80.0
100.0
KINETIC ENERGY (ERGS/CM**3)
CARTESIAN COORDINATES

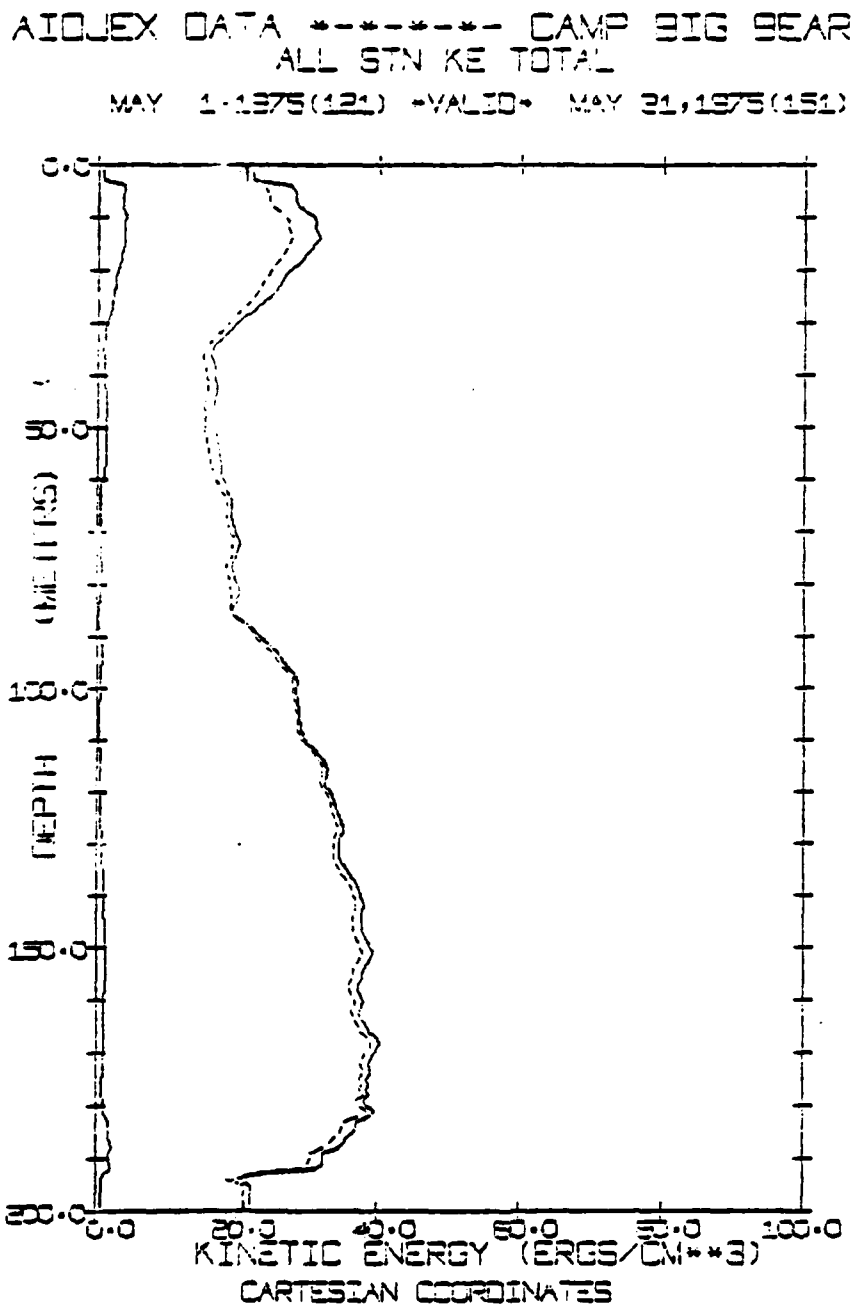

AIDJEX DATA *-*-*-*- CAMP SNOWBIRD
ALL STN KE TOTAL
JAN 1,1978(333) *VALID* JAN 3?,1978(333)
0.0
80.0
100.0
150.0
200.0
DEPTH (METERS)
0.0
20.0
40.0
60.0
80.0
100.0
KINETIC ENERGY (ERGS/CM**3)
CARTESIAN COORDINATES

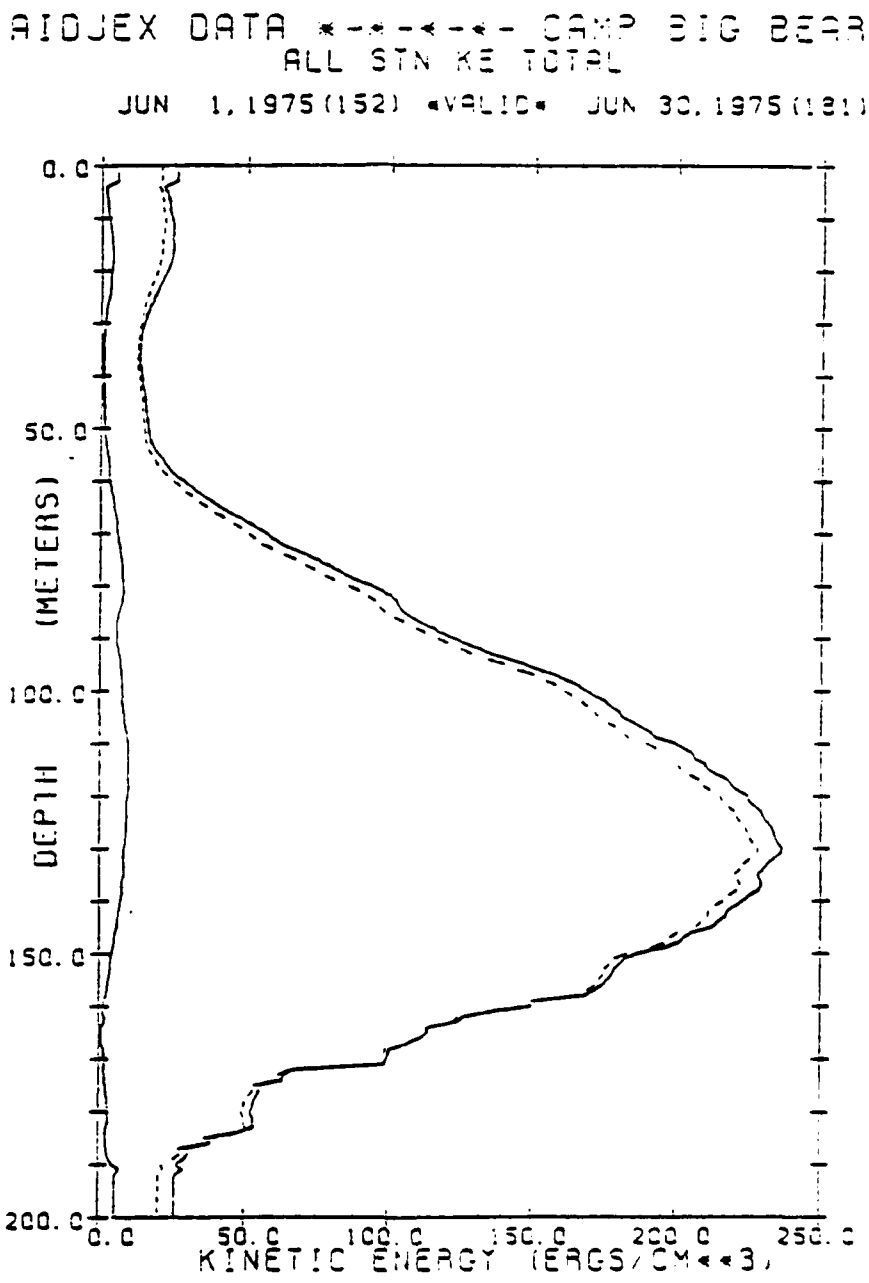

AIDJEX DATA *-*-*-*- CAMP SNOWBIRD
ALL STN KE TOTAL
FEB 1,1975(337) *VALID* FEB 23,1975(425)
0.0
50.0
100.0
150.0
200.0
DEPTH (METERS)
0.0
20.0
40.0
60.0
80.0
100.0
KINETIC ENERGY (ERGS/CM**3)
CARTESIAN COORDINATES

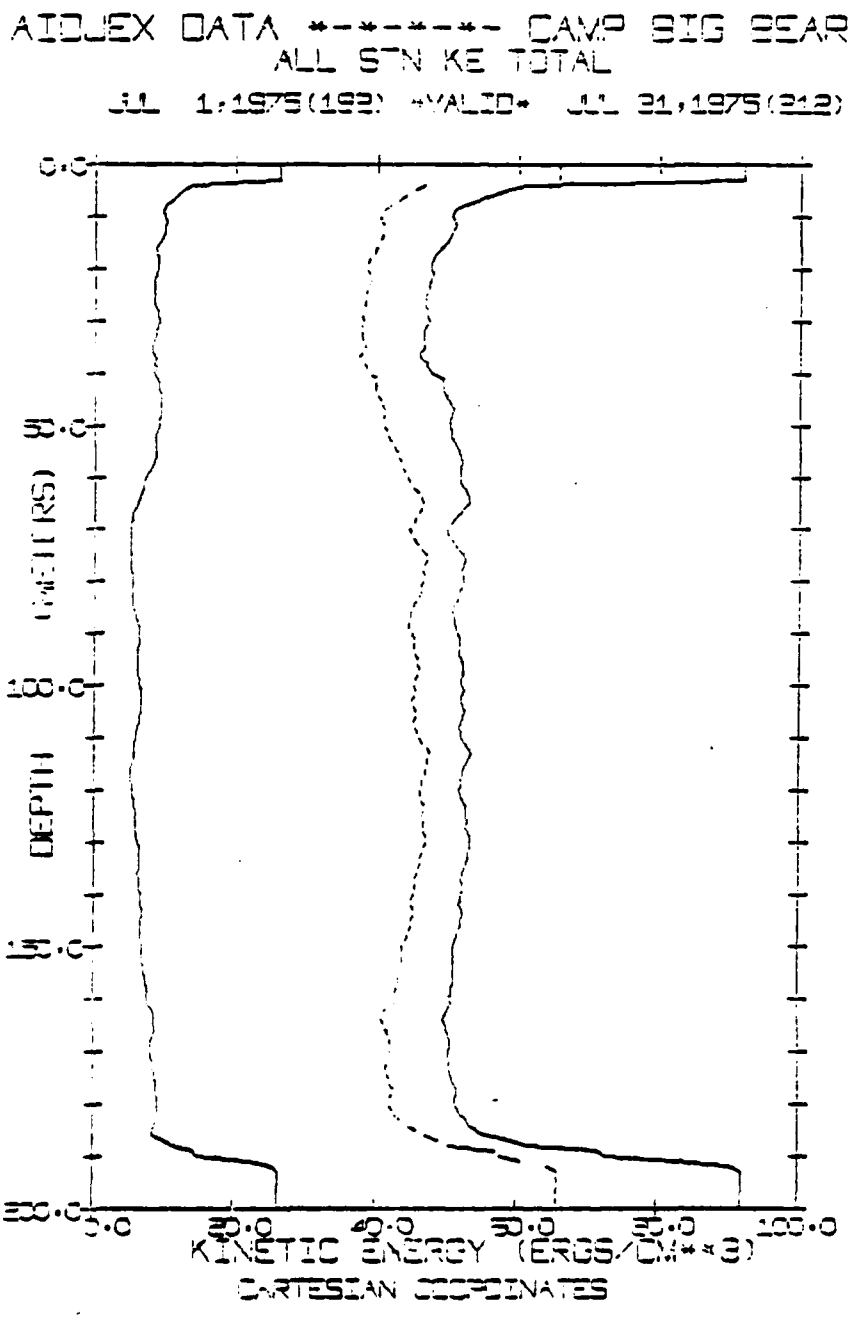

AIDJEX DATA *-*-*-*-*- CAMP SNOWBIRD
ALL STN KE TOTAL
MAR 1,1975(426) *VALID* MAR 31,1975(455)
0.0
50.0
100.0
150.0
200.0
DEPTH (METERS)
0.0
20.0
40.0
60.0
80.0
100.0
KINETIC ENERGY (ERGS/CM**3)
CARTESIAN COORDINATES

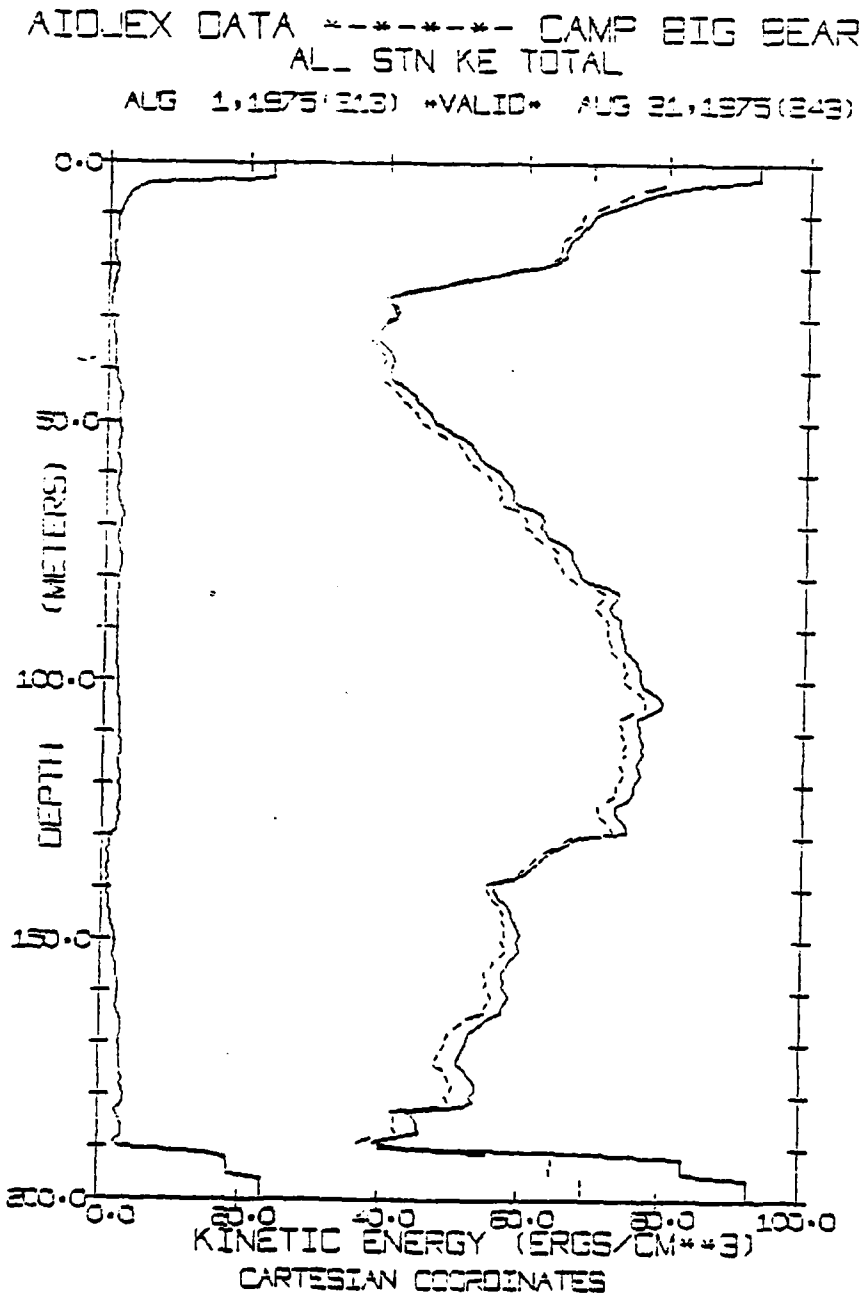

AIDJEX DATA *-*-*-*-*- CAMP SNOWBIRD
ALL STN KE TOTAL
APR 1,1975(457) *VALID* APR 30,1975(485)
0.0
50.0
100.0
150.0
200.0
DEPTH (METERS)
0.0
20.0
40.0
60.0
80.0
100.0
KINETIC ENERGY (ERGS/CM**3)
CARTESIAN COORDINATES

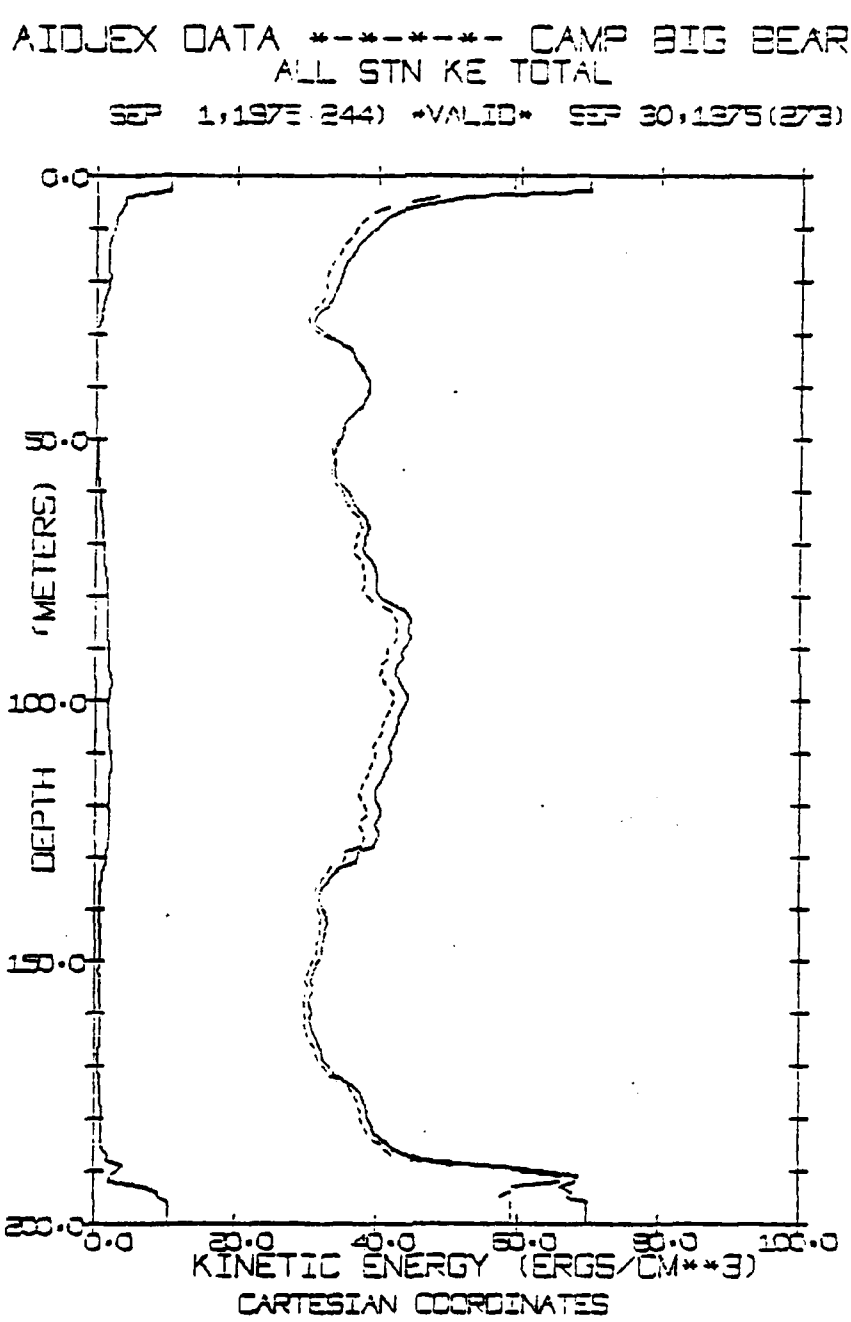

AIDJEX DATA *-*-*-*-*- CAMP BIG BEAR
ALL STN KE TOTAL
APR 1,1975(91) *VALID- APR 30,1975(120)
0.0
50.0
100.0
150.0
200.0
DEPTH (METERS) M
0.0
20.0
40.0
60.0
80.0
100.0
KINETIC ENERGY (ERGS/CM**3)
CARTESIAN COORDINATES


AIDJEX DATA *-*-*-*-*- CAMP BIG BEAR
ALL STN KE TOTAL
MAY 1-1975(121) -VALID- MAY 31,1975(151)
0.0
50.0
100.0
150.0
200.0
DEPTH (METERS)
0.0
20.0
40.0
60.0
80.0
100.0
KINETIC ENERGY (ERGS/CM**3)
CARTESIAN COORDINATES


AIDJEX DATA *-*-*-*-*- CAMP BIG BEAR
ALL STN KE TOTAL
JUN 1, 1975(152) *VALID* JUN 30, 1975(181)
0.0
50.0
100.0
150.0
200.0
DEPTH (METERS)
0.0
50.0
100.0
150.0
200.0
250.0
KINETIC ENERGY (ERGS/CM**3)


AIDJEX DATA *-*-*-*-*- CAMP BIG BEAR
ALL STN KE TOTAL
JUL 1,1975(182) *VALID* JUL 31,1975(212)
0.0
50.0
100.0
150.0
200.0
DEPTH (METERS)
0.0
20.0
40.0
60.0
80.0
100.0
KINETIC ENERGY (ERGS/CM**3)
CARTESIAN COORDINATES


AIDJEX DATA *-*-*-*- CAMP BIG BEAR
ALL STN KE TOTAL
AUG 1,1975(213) *VALID* AUG 31,1975(243)
0.0
80.0
160.0
240.0
DEPTH (METERS)
0.0
20.0
40.0
60.0
80.0
100.0
KINETIC ENERGY (ERGS/CM**3)
CARTESIAN COORDINATES


AIDJEX DATA *-*-*-*-*- CAMP BIG BEAR
ALL STN KE TOTAL
SEP 1,1975(244) *VALID* SEP 30,1975(273)
0.0
50.0
100.0
150.0
200.0
DEPTH (METERS)
0.0
20.0
40.0
60.0
80.0
100.0
KINETIC ENERGY (ERGS/CM**3)
CARTESIAN COORDINATES

MANDATORY
DISTRIBUTION LIST

FOR UNCLASSIFIED TECHNICAL REPORTS, REPRINTS, & FINAL REPORTS
PUBLISHED BY OCEANOGRAPHIC CONTRACTORS
OF THE OCEAN SCIENCE AND TECHNOLOGY DIVISION
OF THE OFFICE OF NAVAL RESEARCH

1 Director of Defense Research and
Engineering
Office of the Secretary of Defense
Washington, D. C. 20301
ATTN: Office, Assistant Director
(Research)

Office of Naval Research
Arlington, VA 22217
1 ATTN: (Code 102-C)
1 ATTN: (Code 200)
1 ATTN: (Code 460)
3 ATTN: (Code 480)

6 Director
Naval Research Laboratory
Washington, D. C. 20375
ATTN: Library, Code 2620

1 U. S. Naval Research Laboratory
Code 2627
Washington, D. C. 20375

2 Office of Naval Research - N.Y.
715 Broadway
New York, N. Y. 10003

12 Defense Documentation Center
Cameron Station
Alexandria, VA 22314

1 Commander
Naval Oceanographic Office
NSTL Station
Bay St. Louis, MS 39522
ATTN: Code 02

SECURITY CLASSIFICATION OF THIS PAGE (When Data Entered)

REPORT DOCUMENTATION PAGE	READ INSTRUCTIONS BEFORE COMPLETING FORM
1. REPORT NUMBER: Technical Report No. CU-1-81	2. GOVT ACCESSION NO.: AD-A098 170
	3. RECIPIENT'S CATALOG NUMBER
4. TITLE (and Subtitle): EDDIES OF THE WESTERN ARCTIC OCEAN -- Their Characteristics and Importance to the Energy, Heat, and Salt Balance	5. TYPE OF REPORT & PERIOD COVERED
	6. PERFORMING ORG. REPORT NUMBER
7. AUTHOR(s): Thomas Owen Manley	8. CONTRACT OR GRANT NUMBER(s): N00014-76-C-0004
9. PERFORMING ORGANIZATION NAME AND ADDRESS: Lamont-Doherty Geological Observatory of Columbia University, Palisades, NY 10964	10. PROGRAM ELEMENT, PROJECT, TASK AREA & WORK UNIT NUMBERS: NR 307-359
11. CONTROLLING OFFICE NAME AND ADDRESS: Dept. of Navy, Office of Naval Research Code 481, Arlington, VA 22217	12. REPORT DATE: March, 1981
	13. NUMBER OF PAGES
14. MONITORING AGENCY NAME & ADDRESS (if different from Controlling Office)	15. SECURITY CLASS. (of this report): Unclassified
	15a. DECLASSIFICATION/DOWNGRADING SCHEDULE

16. DISTRIBUTION STATEMENT (of this Report)

Approved for public release; distribution unlimited. Reproduction in whole or in part is permitted for any purpose of the United States Government.

17. DISTRIBUTION STATEMENT (of the abstract entered in Block 20, if different from Report)

18. SUPPLEMENTARY NOTES

19. KEY WORDS (Continue on reverse side if necessary and identify by block number)

Eddies, Arctic Ocean, AIDJEX, Beaufort Sea, mesoscale variability, kinetic energy, available potential energy

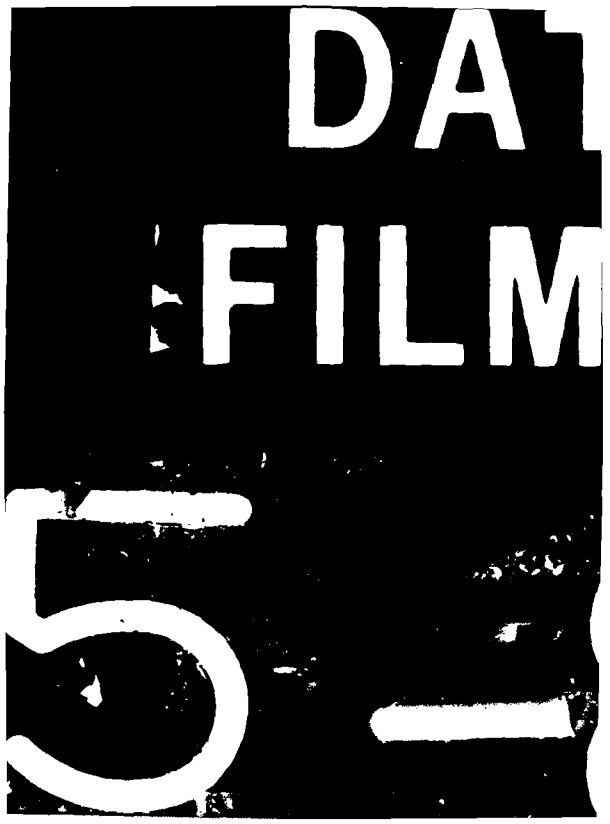
20. ABSTRACT (Continue on reverse side if necessary and identify by block number)

High speed transient undercurrents were first observed in the Arctic Ocean in 1937 however, it was not until 1974 that these high velocity jets were determined to be the instantaneous observations of small subsurface baroclinic eddies confined between the base of the mixed layer (50 m) and 300 meters. Typical dimensions of these eddies were estimated to be 10-20 km in diameter and roughly 200 meters in thickness.

DD FORM 1 JAN 73 1473 EDITION OF 1 NOV 65 IS OBSOLETE
S/N 0102-LF-014-6601

SECURITY CLASSIFICATION OF THIS PAGE (When Data Entered)

With the undertaking of the main 1975-76 AIDJEX experiment located in the central Beaufort Sea, four manned camps collected for one year the largest and most complete set of oceanographic data within the Arctic Ocean to this date. During this time, a total of 146 separate crossings of eddies were observed. Using T-S signatures, 31 of the 146 crossings are found to represent duplicate crossings of 12 individual eddies, making a total of 127 separate eddies observed during the one year. On the basis of the AIDJEX data set, arctic eddies have been found to 1) be prevalent in the Amerasia Basin and in particular the Beaufort Sea, 2) predominantly reside in the depth range of 50 to 300 meters although deeper eddies are also present, 3) contain more than half of the total amount of kinetic energy in the upper 200 m of the Beaufort Sea, 4) transfer kinetic energy to the mean flow, 5) be predominately anticyclonic in their rotational tendency, 6) apparently originate north of Point Barrow, Alaska as a result of instability in the eastward flowing Alaskan Coastal Current although there are a few eddies in which T-S data may indicate the possibility of local origin, 7) transfer fresher, less saline water into the deep Arctic Ocean from the Chukchi Sea, 8) transfer both warm and cold water into the deep Arctic Ocean in response to the seasonally changing shelf conditions, 9) translate in response to barotropic forcing over short time scales, although over longer time periods move with the mean geostrophic field, 10) decay in a clockwise pattern from their point of origin, which is consistent with the upper layer movement of the Beaufort Sea.


DA
FILM